

NASA SP-164

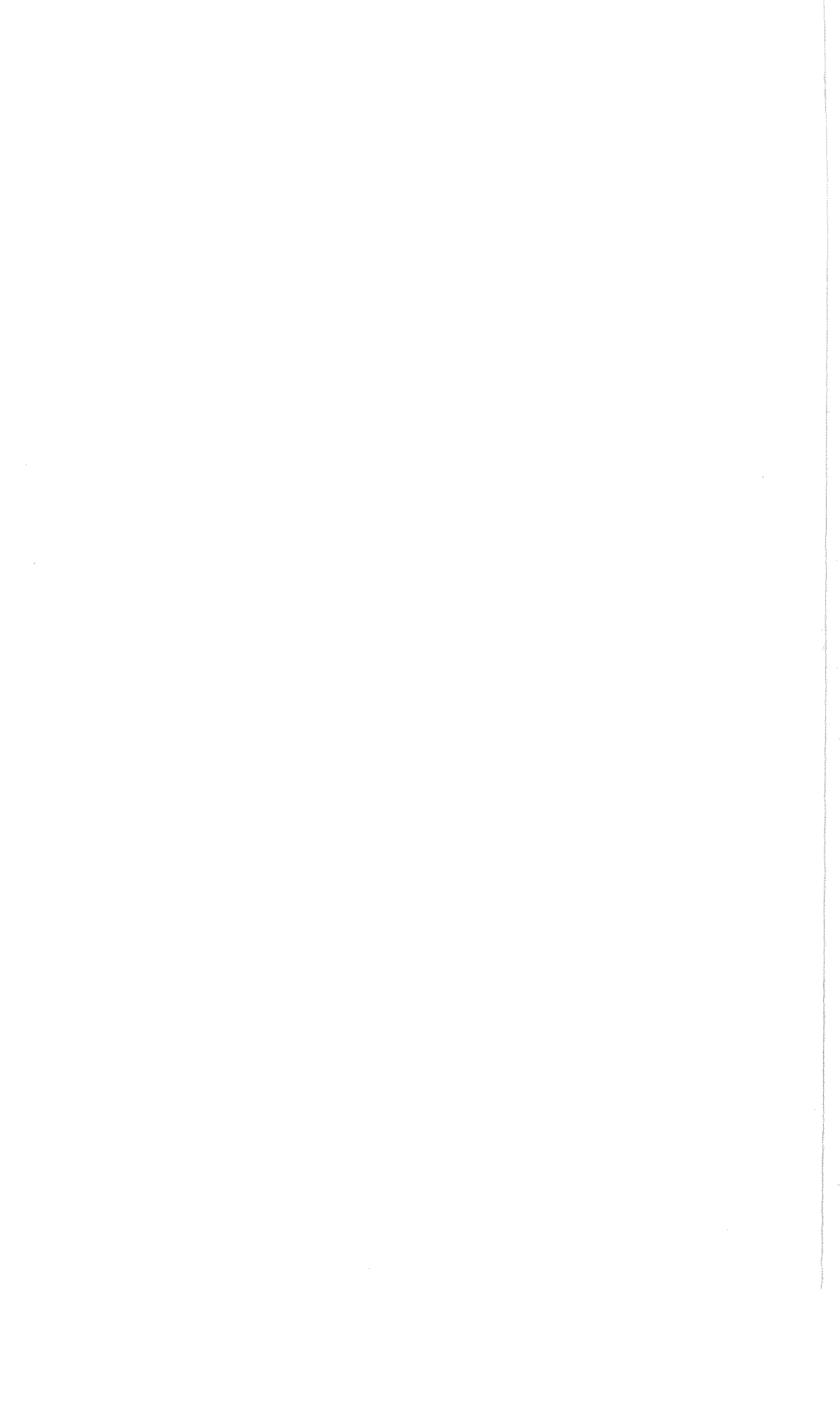
THERMAL RADIATION HEAT TRANSFER

Volume III

Radiation Transfer With Absorbing,
Emitting, and Scattering Media



NATIONAL AERONAUTICS AND SPACE ADMINISTRATION



THERMAL RADIATION HEAT TRANSFER

Volume III

Radiation Transfer With Absorbing,
Emitting, and Scattering Media

Robert Siegel and John R. Howell
Lewis Research Center
Cleveland, Ohio



Scientific and Technical Information Office 1971
NATIONAL AERONAUTICS AND SPACE ADMINISTRATION
Washington, D.C.

For sale by the Superintendent of Documents,
U.S. Government Printing Office, Washington, D.C. 20402
Price \$1.75
Library of Congress Catalog Card Number 67-62877

P R E F A C E

This is the third and final volume of the series "Thermal Radiation Heat Transfer" that is being published as the NASA Special Publication SP-164. The first and second volumes appeared in 1968 and 1969, respectively. As stated in the Preface to volume I, this publication is an outgrowth of a course in thermal radiation that has been given as part of an internal advanced study program at the NASA Lewis Research Center.

This volume contains nine chapters. The first discusses some of the fundamentals of absorption of radiation along a path in a medium, and emission by the medium. The important property of the radiation intensity is developed showing that along a path in a nonattenuating nonemitting medium the intensity is invariant with position. Thus the magnitudes of any attenuation or emission can be expressed in terms of the changes produced in the intensity with distance.

In chapter 2 the absorption, scattering, and emission effects along a path are combined to develop the equation of transfer. The solution of this equation gives the intensity within the medium. The intensity can then be used to obtain energy fluxes. These are related to the local temperature within the medium by means of the energy conservation equation. This provides the necessary relations to obtain energy transfers and temperature distributions in the medium.

Some methods for solving these equations are given in chapter 3. These methods include various approximate techniques, a very important one being the diffusion approximation. The boundary conditions and application of the diffusion method are considered in detail.

Before any radiation solution can be applied, the radiative properties must be known. Gas radiation properties vary considerably with wavelength. In chapter 4 some of the fundamentals of the radiative properties are discussed. These include line broadening mechanisms and band absorption correlations.

Chapter 5 considers the important situation of radiation from a gas that is well mixed so that it is isothermal. The method of analyzing heat transfer in a gas filled enclosure is developed by extending the net radiation method presented in volume II for enclosures containing a nonabsorbing medium. The very useful concept of radiative mean beam length is derived for use in gas energy exchange.

Chapters 6, 7, and 8 provide further development by discussing the Monte Carlo method, radiation combined with conduction and convection, and scattering. Finally, chapter 9 treats a number of specialized topics such as radiation in media with nonunity refractive index, and radiation from flames.

CONTENTS

CHAPTER		PAGE
1	FUNDAMENTALS OF RADIATION IN ABSORBING, EMITTING, AND SCATTERING MEDIA	1
	1.1 INTRODUCTION.....	1
	1.2 SYMBOLS.....	3
	1.3 PHYSICAL MECHANISMS OF ABSORPTION AND EMISSION.....	4
	1.4 SOME FUNDAMENTAL PROPERTIES OF THE RADIATION INTENSITY.....	8
	1.5 THE ATTENUATION OF ENERGY.....	12
	1.5.1 The Extinction Coefficient.....	13
	1.5.2 Radiation Mean Penetration Distance.....	14
	1.5.3 Optical Thickness.....	14
	1.5.4 The Absorption Coefficient.....	15
	1.5.5 True Absorption Coefficient.....	19
	1.5.6 The Scattering of Energy.....	20
	1.6 THE EMISSION OF ENERGY.....	21
	1.7 DEFINITIONS USED FOR ENGINEERING GAS PROPERTIES.....	24
	1.7.1 Absorptance.....	24
	1.7.2 Emittance.....	25
	1.7.3 Transmittance.....	29
	1.8 THE CONCEPT OF LOCAL THERMODYNAMIC EQUILIBRIUM.....	32
	1.9 CONCLUDING REMARKS.....	34
	REFERENCES.....	34
2	THE EQUATIONS OF TRANSFER FOR AN ABSORBING-EMITTING GAS	37
	2.1 INTRODUCTION.....	37
	2.2 SYMBOLS.....	37
	2.3 THE EQUATION OF TRANSFER.....	38
	2.3.1 Derivation.....	39
	2.3.2 Integration by Use of Integrating Factor.....	41
	2.4 ENERGY CONSERVATION WITHIN THE MEDIUM.....	43
	2.4.1 Radiative Equilibrium.....	45
	2.4.2 Some Mean Absorption Coefficients.....	45
	2.5 EQUATION OF TRANSFER FOR PLANE LAYER.....	46
	2.6 THE GRAY GAS.....	47
	2.6.1 Transfer Equations.....	48
	2.6.2 Plane Layer Between Black Plates.....	49
	2.6.3 Use of Exponential Integral Functions.....	55
	2.7 ENERGY RELATIONS BY USE OF PHOTON MODEL.....	56
	2.8 CONCLUDING REMARKS.....	59
	REFERENCES.....	59

CHAPTER	PAGE
3	<i>APPROXIMATE SOLUTIONS OF THE EQUATION OF TRANSFER</i> 61
3.1	INTRODUCTION..... 61
3.2	SYMBOLS..... 62
3.3	APPROXIMATE SOLUTIONS BY NEGLECTING TERMS IN THE EQUATION OF TRANSFER..... 64
3.3.1	The Transparent Gas Approximation..... 64
3.3.2	The Emission Approximation..... 67
3.3.3	The Cold Medium Approximation..... 70
3.4	DIFFUSION METHODS IN RADIATIVE TRANSFER..... 71
3.4.1	Simplified Derivation of the Diffusion Equation..... 72
3.4.2	The General Radiation Diffusion Equation..... 74
3.4.2.1	The Rosseland equation for local radiative flux..... 75
3.4.2.2	The emissive power jump as a boundary condition..... 79
3.4.2.3	The emissive power jump between two absorbing-emitting regions..... 82
3.4.2.4	Summary..... 83
3.4.3	Use of the Diffusion Solution..... 83
3.4.3.1	Gray stagnant gas between parallel plates..... 83
3.4.3.2	The discontinuity in emissive power between two gas regions..... 86
3.4.3.3	Other diffusion solutions for gray gases..... 89
3.4.4	Final Remarks..... 90
3.5	APPROXIMATIONS BY USING MEAN ABSORPTION COEFFICIENTS..... 93
3.5.1	Some Mean Absorption Coefficients..... 93
3.5.2	Approximate Solutions of the Transfer Equations Using Mean Absorption Coefficients..... 95
3.6	APPROXIMATE SOLUTION OF THE COMPLETE EQUATION OF TRANSFER..... 97
3.6.1	The Astrophysical Approximations..... 97
3.6.1.1	The Schuster-Schwarzschild approximation..... 97
3.6.1.2	The Milne-Eddington approximation..... 100
3.6.2	The Differential Approximation..... 102
3.6.2.1	Boundary conditions..... 106
3.6.2.2	Applications of the differential approximation..... 108
3.7	CONCLUDING REMARKS..... 110
	REFERENCES..... 111
4	<i>AN INTRODUCTION TO THE MICROSCOPIC BASIS FOR RADIATION IN GASES AND GAS PROPERTIES</i> 113
4.1	INTRODUCTION..... 113
4.2	SYMBOLS..... 113
4.3	SOME ELEMENTS OF QUANTUM THEORY..... 115
4.3.1	Bohr Model of Hydrogen Atom..... 115
4.3.2	Schrödinger Wave Equation..... 117
4.4	INDUCED EMISSION AND THE PLANCK DISTRIBUTION..... 121

CHAPTER	PAGE
4.5 THE EQUATION OF TRANSFER.....	125
4.6 THE ABSORPTION PROPERTIES OF GASES.....	128
4.6.1 Spectral Line Broadening.....	128
4.6.1.1 Natural broadening.....	131
4.6.1.2 Doppler broadening.....	131
4.6.1.3 Collision broadening.....	132
4.6.1.4 Stark broadening.....	134
4.6.2 Absorption or Emission by a Spectral Line.....	134
4.6.3 Continuum Absorption.....	137
4.6.3.1 Bound-free processes.....	137
4.6.3.2 Free-free processes.....	138
4.6.4 Band Absorption Correlations.....	138
4.7 CONCLUDING REMARKS.....	153
REFERENCES.....	153
5 THE ENGINEERING TREATMENT OF GAS RADIATION IN ENCLOSURES.....	157
5.1 INTRODUCTION.....	157
5.2 SYMBOLS.....	157
5.3 NET RADIATION METHOD FOR ENCLOSURE FILLED WITH ISOTHERMAL GAS—SPECTRAL RELATIONS... ..	159
5.3.1 Definitions of Spectral Transmission and Absorption Factors.....	164
5.3.2 Matrix of Enclosure Theory Equations.....	164
5.3.3 Heat Balance on Gas.....	166
5.4 EVALUATION OF SPECTRAL GEOMETRIC MEAN TRANSMITTANCE AND ABSORPTANCE FACTORS.....	168
5.4.1 Hemisphere to Differential Area at Center of Its Base.....	168
5.4.2 Top of Right Circular Cylinder to Center of Its Base.....	169
5.4.3 Side of Cylinder to Center of Its Base.....	171
5.4.4 Entire Sphere to Any Element on Its Surface or to Its Entire Surface.....	172
5.4.5 Infinite Plate to Area on Parallel Plate.....	173
5.4.6 Rectangle to a Directly Opposed Parallel Rectangle.....	174
5.5 THE MEAN BEAM LENGTH FOR RADIATION FROM AN ENTIRE GAS VOLUME TO ALL OR PART OF ITS BOUNDARY.....	175
5.5.1 Mean Beam Length for Gas Between Parallel Plates Radi- ating to Area on Plate.....	177
5.5.2 Mean Beam Length for Sphere of Gas Radiating to Any Area on Boundary.....	177
5.5.3 Radiation from Entire Gas Volume to Its Entire Boundary in Limit When Gas Is Optically Thin.....	178
5.5.4 Correction for Mean Beam Length When Gas Is Not Op- tically Thin.....	179
5.6 TOTAL RADIATION EXCHANGE IN BLACK ENCLOSURE BETWEEN ENTIRE GAS VOLUME AND ENCLOSURE BOUNDARY BY USE OF MEAN BEAM LENGTH.....	183
5.6.1 Radiation from Gas to All or Portion of Boundary.....	183
5.6.2 Exchange Between Entire Gas Volume and Boundary.....	187

CHAPTER		PAGE
	5.7 TOTAL RADIATION EXCHANGE IN ENCLOSURE BY INTEGRATION OF SPECTRAL EQUATIONS.....	188
	5.7.1 Band Equations.....	189
	5.7.2 Transmission and Absorption Factors.....	189
	5.8 RADIATION THROUGH NONISOTHERMAL GASES.....	201
	5.8.1 The Curtis-Godson Approximation	202
	5.8.2 The Zoning Method.....	207
	5.8.3 The Exchange Factor Approximation.....	211
	REFERENCES.....	219
6	<i>THE MONTE CARLO TECHNIQUE</i>	221
	6.1 INTRODUCTION.....	221
	6.2 SYMBOLS.....	221
	6.3 DISCUSSION OF THE METHOD.....	223
	6.4 RADIATION THROUGH GRAY GASES.....	229
	6.4.1 Infinite Parallel Planes.....	229
	6.4.2 Infinitely Long Concentric Cylinders.....	231
	6.4.3 Radiation Between Adjacent Gray Regions.....	233
	6.5 CONSIDERATION OF RADIATIVE PROPERTY VARIATIONS.....	234
	6.6 COUPLING WITH OTHER HEAT TRANSFER MODES.....	237
	6.7 TRANSIENT RADIATION PROBLEMS.....	237
	6.8 INCORPORATION OF SCATTERING PHENOMENA.....	238
	6.9 CONCLUDING REMARKS.....	238
	REFERENCES.....	238
7	<i>ENERGY TRANSFER BY RADIATION COMBINED WITH CONDUCTION AND/OR CONVECTION</i>	241
	7.1 INTRODUCTION.....	241
	7.2 SYMBOLS.....	241
	7.3 RADIATION WITH CONDUCTION.....	243
	7.3.1 The Conduction-Radiation Parameter.....	244
	7.3.2 Energy Balance.....	246
	7.3.3 Plane Layer Geometry.....	247
	7.3.4 Simple Addition of Radiation and Conduction Energy Transfers.....	251
	7.3.5 The Diffusion Method.....	254
	7.3.6 The Exchange Factor Approximation.....	260
	7.4 CONVECTION, CONDUCTION, AND RADIATION.....	264
	7.4.1 Boundary Layer Problems.....	265
	7.4.1.1 Optically thin thermal layer.....	266
	7.4.1.2 Optically thick thermal layer.....	268
	7.4.2 Channel Flows.....	270
	7.4.3 Other Multimode Problems.....	272
	7.5 CONCLUDING REMARKS.....	272
	REFERENCES.....	273

CHAPTER		PAGE
8	RADIATIVE TRANSFER IN SCATTERING AND ABSORBING MEDIA	277
	8.1 INTRODUCTION.....	277
	8.2 SYMBOLS.....	279
	8.3 SOME IMPORTANT QUANTITIES IN THE DESCRIPTION OF SCATTERING.....	280
	8.3.1 The Scattering Cross Section.....	280
	8.3.2 The Phase Function.....	284
	8.4 SCATTERING FROM VARIOUS TYPES OF PARTICLES.....	286
	8.4.1 A Cloud of Large Specularly Reflecting Spheres.....	286
	8.4.2 Reflection From a Diffuse Sphere.....	289
	8.4.3 Large Dielectric Sphere with Refractive Index Close to Unity.....	292
	8.4.4 Diffraction From a Large Sphere.....	292
	8.4.5 Rayleigh Scattering.....	294
	8.4.5.1 Scattering cross sections for Rayleigh scattering.....	295
	8.4.5.2 Phase function for Rayleigh scattering.....	298
	8.4.6 Mie Scattering Theory.....	299
	8.5 RADIATIVE TRANSFER IN SCATTERING MEDIA.....	302
	8.5.1 The Equation of Transfer in a Pure Scattering Atmosphere...	302
	8.5.2 Scattering in Absorbing-Emitting Media.....	306
	REFERENCES.....	312
9	SOME SPECIALIZED EFFECTS IN ABSORBING-RADIATING MEDIA	313
	9.1 INTRODUCTION.....	313
	9.2 SYMBOLS.....	313
	9.3 RADIATION PHENOMENA IN MEDIA WITH NONUNITY REFRACTIVE INDEX.....	315
	9.3.1 Media With Constant But Nonunity Refractive Index.....	315
	9.3.2 The Effect of Brewster's Angle.....	317
	9.3.3 Radiative Transfer Between Dielectrics Spaced Closely Together.....	322
	9.4 FLAMES, LUMINOUS FLAMES, AND PARTICLE RADIATION.....	324
	9.4.1 Theoretical Flame Temperature.....	325
	9.4.2 Radiation From Nonluminous Flames.....	329
	9.4.3 Radiation From and Through Luminous Flames.....	331
	9.4.3.1 Experimental correlation of soot spectral absorption.....	333
	9.4.3.2 Electromagnetic theory prediction of soot spectral absorption.....	335
	9.4.3.3 Total emittance of soot cloud.....	338
	9.4.4 Radiation From Gases Containing Luminous Particles.....	342
	9.5 LUMINESCENCE.....	343
	9.6 TRANSIENT RADIATION PROBLEMS.....	345
	REFERENCES.....	349
	APPENDIX	353
	INDEX	357

Chapter 1. Fundamentals of Radiation in Absorbing, Emitting, and Scattering Media

1.1 INTRODUCTION

The study of energy transfer through media that can absorb, emit, and scatter radiation has received increased attention in the past several years. This interest stems from the complicated and interesting phenomena associated with nuclear explosions, hypersonic shock layers, rocket propulsion, plasma generators for nuclear fusion, and ablating systems.

Although some of these applications are quite recent, the study of gas radiation has been of continuing interest for over 100 years. One of the early considerations was the absorption of radiation in the Earth's atmosphere. This has always plagued astronomers when observing on Earth the light from the Sun and more distant stars. Figure 1-1 shows the observed form of the solar spectrum recorded by Samuel Langley over a period of years beginning in 1880. The dashed curve shows the estimated solar emission curve (assumed to be a blackbody spectrum at 5600 K) and the solid curve shows the spectrum after atmospheric attenuation (ref. 1). The absorption occurs in specific wavelength regions, illustrating that gas radiation properties vary considerably with wavelength. The atmospheric absorption of solar radiation is chiefly by water vapor and carbon dioxide. Extensive discussions of absorption in the atmosphere are given by Goody (ref. 2) and Kondratyev (ref. 3).

Gas radiation has also been of interest to astrophysicists with regard

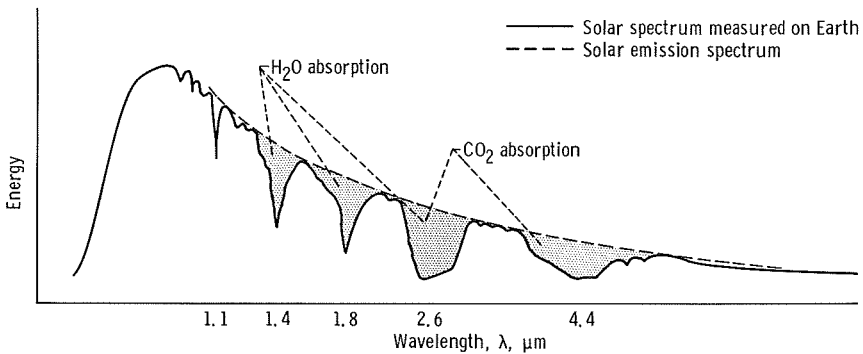


FIGURE 1-1. — Attenuation of solar spectrum by Earth's atmosphere as measured by Langley (ref. 1).

to the study of stellar structure. Models of stellar atmospheres, such as for the Sun, and the energy transfer processes within them have been constructed; then the emitted energy spectra calculated on the basis of the models are compared with observed stellar spectra.

In industry the importance of gas radiation was recognized in the 1920's in connection with heat transfer inside furnaces. The carbon dioxide and water vapor formed as products of combustion were found to be significant emitters and absorbers of radiant energy. Radiation can also be appreciable in engine combustion chambers where peak temperatures reach a few thousand degrees. The energy emitted from flames depends not only on the gaseous emission but also arises from the heated carbon (soot) particles that are formed within the flame.

Another interesting example of radiation within an absorbing-emitting medium is in a glass melting furnace. As described in reference 4, the temperature distribution measured within a deep tank of molten glass was found to be more uniform than that expected from heat conduction alone. It was thought that convection might account for the discrepancy, but experimental investigations did not indicate that this was the contributing heat transfer mode. In the late 1940's it became evident that radiative transfer by absorption and reemission within the glass provided a significant means of energy transport.

Two difficulties are encountered in studying radiation within absorbing, emitting, and scattering media that make these studies, to say the least, challenging. First, absorption and emission of energy are occurring not only at system boundaries, but at every local point within the medium. Scattering is also a local transfer process within the medium. A complete solution of the energy exchange problem therefore requires knowledge of the temperature and physical properties of the medium at every point within the system. The mathematics describing such a situation is inherently complex. A second difficulty is that spectral effects are often much more pronounced in gases than for solid surfaces. As a result a detailed spectrally dependent analysis may be required. When approximations are used based on spectrally averaged properties, special care must be taken. Most of the simplifications introduced in gas radiation problems are aimed at dealing with one or both of these two complexities.

A brief comment on the approach to radiation in gases used herein is in order. The astrophysical approach (i.e., the equation of transfer) is used for determining the local values of the radiation intensity within the medium. As will be defined in detail in section 1.4, the intensity is concerned with energy transport along a path in a single direction. By studying the variation of intensity along a path, a good understanding is obtained of how the individual processes of absorption, emission, and scattering enter into the radiative transfer. It is the most useful method

in problems dealing with atmospheric absorption, stellar structure, and others where the spectral intensity at some position is often a quantity of interest. Two excellent texts (refs. 5 and 6) deal in detail with this formulation as used in astrophysics.

The astrophysical approach however must be adapted for more convenient use by the engineer. The engineer is chiefly interested in energy fluxes and temperatures rather than radiation intensities. Also the astrophysical notation and nomenclature is foreign to most engineers and is often inconsistent within itself. For these reasons, although fundamental ideas are developed here on the basis of the intensity of the radiation, the change to terms of local energy flux and temperature is often made. This change aids in developing useful engineering solution methods and will also show how the engineering methods can be derived in a logical manner from the astrophysical relations.

1.2 SYMBOLS

A	area
a	absorption coefficient
C_i	concentration of gas in mixture
C_2	second constant in Planck's spectral energy distribution, hc_0/k
c	speed of light in medium other than vacuum
c_0	speed of light in vacuum
E	energy
E_i	ionization potential
e	emissive power
$F_{0-\lambda T}$	fraction of blackbody emissive power in spectral region $0-\lambda T$
h	Planck's constant
i	radiation intensity
K	extinction coefficient, $a + \sigma_s$
k	Boltzmann constant
l_m	extinction mean free path
n	simple refractive index
P	pressure
p	partial pressure of gas in mixture
Q	energy per unit time
q	energy flux, energy per unit area and time
R	radius of sphere
S	coordinate along path of radiation
T	absolute temperature
V	volume
α	absorptance

β	cone angle, angle from normal of area
ϵ	emittance
η	wave number
κ	optical thickness (eq. (1-17))
λ	wavelength in medium
ν	frequency
ρ	density
σ	Stefan-Boltzmann constant
σ_s	scattering coefficient
τ	transmittance
ω	solid angle

Subscripts:

a	absorbed
b	blackbody
e	emitted
g	gas
i	component i
m	mass coefficient; mean value
p	projected
s	source or scatter
η	wave number dependent
λ	wavelength dependent
ν	frequency dependent

Superscripts:

'	directional quantity
+	true value, not modified by addition of induced emission
*	dummy variable of integration

1.3 PHYSICAL MECHANISMS OF ABSORPTION AND EMISSION

Although this volume will be concerned with radiation in absorbing, emitting, and scattering media in general, it will almost always be gases that are used as examples. If the radiation properties of gases and opaque solids are compared, a difference in spectral behavior is quite evident. As shown by the plots of radiation properties in chapter 5 of reference 7 (which will be referred to from this point as vol. I), the property variations with wavelength for opaque solids are fairly smooth although in some instances the variation is somewhat irregular. Gas properties however exhibit very irregular wavelength dependencies. As a result the absorption or emission by gases is significant only in certain wavelength regions, especially at temperature levels below a few thousand degrees Kelvin.

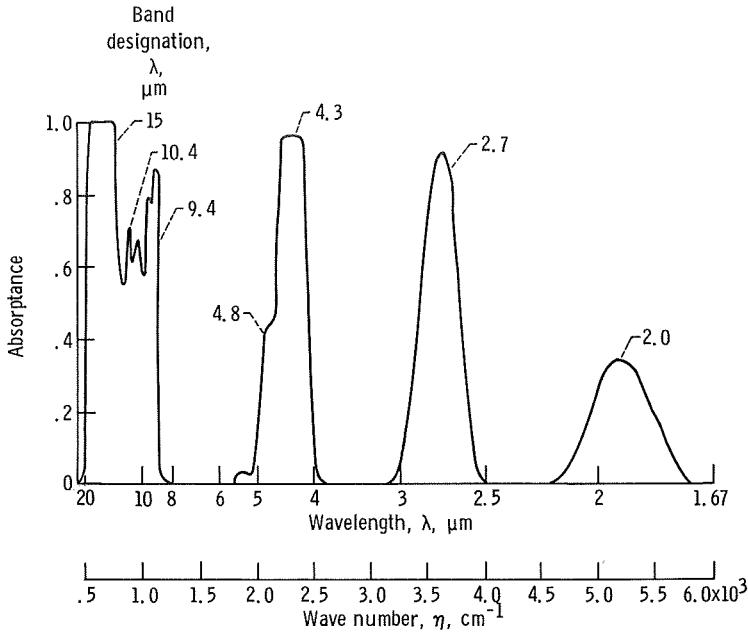


FIGURE 1-2.—Low-resolution spectrum of absorption bands for CO₂ gas at 830 K, 10 atm, and for path length through gas of 38.8 cm.

The absorbance of a gas layer as a function of wavelength typically looks as shown for carbon dioxide (CO₂) in figure 1-2.

The radiation emitted from a solid actually originates within the solid so the solid can be considered an absorbing and emitting medium like a gas; the physics of the radiation thus has a common basis for all media. The differences in spectra are caused by the various types of energy transitions that occur within the media. A gas has different types of transitions, a fact which leads to a less continuous spectrum than for a solid. The energy transitions that account for radiation emission and absorption will now be discussed.

A radiating gas can be composed of molecules, atoms, ions, and free electrons. These particles can have various energy levels associated with them. In a molecule, for example, the atoms form a dynamic system that has certain vibrational and rotational modes. These modes have specific energy levels associated with them. A schematic diagram of the energy levels for an atom, ion, or electron is shown in figure 1-3. (The levels for a molecule are diagramed in fig. 4-5.) The zero energy level is assigned to the ground state (lowest energy bound state) with the higher bound states being at positive energy levels. The energy E_I

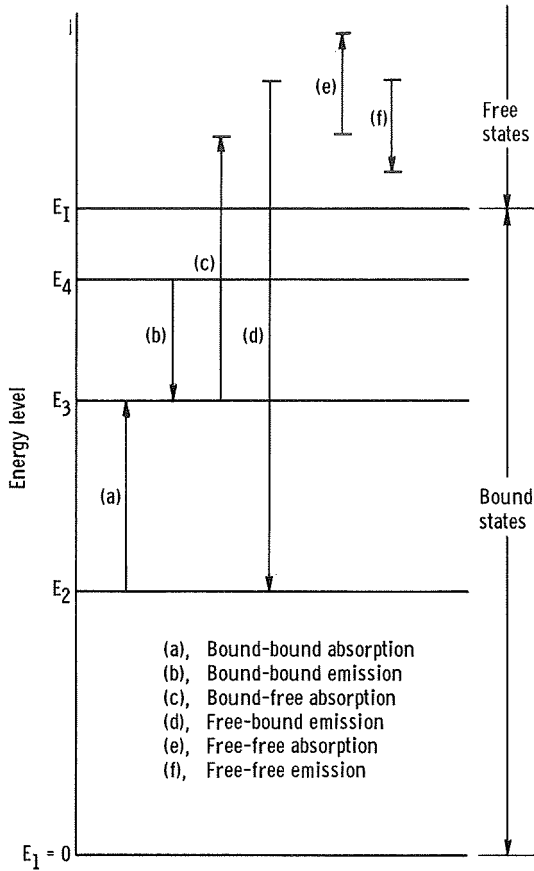


FIGURE 1-3. — Schematic diagram of energy states and transitions for atom, ion, or electron.

in figure 1-3 is the ionization potential, that is, the energy required to produce ionization from the ground state. Energies above E_1 denote that ionization has taken place and free electrons have been produced.

It will be convenient to discuss the radiation process by utilizing a photon or quantum point of view. The photon is the basic unit of radiative energy. Radiative emission will consist of the release of photons of energy, and absorption will be the capture of photons by a particle. When a photon is emitted or absorbed, the energy of the emitting or absorbing particle will be correspondingly decreased or increased. Figure 1-3 is a diagram of the three types of transitions that can occur. These are bound-bound, bound-free, and free-free; they will be discussed a little further on in more detail. In addition to emission and absorption processes, it is possible for a photon to transfer part of its energy in

certain inelastic scattering processes. These are of minor importance in engineering radiative transfer.

The magnitude of the energy transition is related to the frequency of the emitted or absorbed radiation. The energy of a photon is $h\nu$ where h is Planck's constant and ν is the frequency of the photon energy. For an energy transition, say from bound state E_3 down to bound state E_2 in figure 1-3, a photon is emitted with energy $E_3 - E_2 = h\nu$. The frequency of the emitted energy is then $\nu = (E_3 - E_2)/h$ so that a fixed frequency is associated with the transition from a specific energy level to another. Thus in the absence of any other effects, the radiation emitted will be in the form of a spectral line. Conversely in a transition between two bound states when a particle absorbs energy, the quantum nature of the process dictates that the absorption is such that the particle can only go to one of the discrete higher energy levels. Consequently, the frequency of the photon energy must have certain discrete values in order for the photon to be absorbed. For example, a particle in the ground state in figure 1-3 may absorb photons with frequencies $(E_2 - E_1)/h$, $(E_3 - E_1)/h$, or $(E_4 - E_1)/h$ and undergo a transition to a higher bound energy level. Photons with other frequencies in the range $0 < \nu < E_1/h$ cannot be absorbed.

When a photon is absorbed or emitted by an atom or molecule and there is no ionization or recombination of ions and electrons, the process is termed a *bound-bound* absorption or emission (see processes (a) and (b) in fig. 1-3). The atom or molecule moves from one quantized bound energy state to another. These states can be rotational, vibrational, or electronic in molecules, and electronic in atoms. Since the bound-bound energy changes are associated with specific energy levels, the absorption and emission coefficients will be sharply peaked functions of frequency in the form of a series of spectral lines. These lines do have a finite width from various broadening effects that will be discussed in section 4.6.1.

The vibrational energy modes are always coupled with rotational modes. The rotational spectral lines superimposed on the vibrational line give a band of closely spaced spectral lines. If these are averaged together into one continuous region, it becomes a *vibration-rotation* band (see section 4.6.4). Rotational transitions within a given vibrational state are associated with energies at long wavelengths, ~ 8 to $1000 \mu\text{m}$ (see fig. 1-2 of vol. I). Vibration-rotation transitions are at infrared energies of about 1.5 to $20 \mu\text{m}$. Electronic transitions are at short wavelengths in the visible region, 0.4 to $0.7 \mu\text{m}$, and at portions of the ultraviolet and infrared near the visible region. At industrial temperatures the radiation is principally from vibrational and rotational transitions; at high tempera-

tures (above several thousand °R), it is the electronic transitions that are important.

Process (c) in figure 1-3 is a *bound-free* absorption (photoionization). An atom absorbs a photon with sufficient energy to cause ionization. The resulting ion and electron are free to take on any kinetic energy; hence, the bound-free absorption coefficient is a continuous function of photon energy frequency ν as long as the photon energy $h\nu$ is sufficiently large to cause ionization. The reverse (process (d) in fig. 1-3) is free-bound emission (photorecombination). Here an ion and free electron combine, a photon of energy is released, and the energy of the resulting atom drops to that of a discrete bound state. The free-bound emission produces a continuous spectrum as the combining particles can have any initial kinetic energy.

In an ionized gas a free electron can pass near an ion and interact with its electric field. This can produce a *free-free* transition (often called Bremsstrahlung meaning "brake radiation"). The electron can absorb a photon (process (e) in fig. 1-3) thereby going to a higher kinetic energy, or it can emit a photon (process (f)) and drop to a lower free energy. Since the initial and final free energies can have any values, a continuous absorption or emission spectrum is produced. Bremsstrahlung can also be produced if an electron passes very close to a neutral atom since very close to an atom there can be an electric field. This process is much less probable than electron-positive ion interactions.

1.4 SOME FUNDAMENTAL PROPERTIES OF THE RADIATION INTENSITY

Radiation intensity is a convenient quantity for use in problems dealing with radiative transfer through absorbing-emitting and scattering media. This convenience is chiefly because of certain invariance properties. In chapter 2 of volume I, the radiation intensity in direction (β, θ) leaving a surface was defined as the energy leaving per unit time per unit of projected surface area normal to the (β, θ) direction and per unit elemental solid angle centered around direction (β, θ) . As a result of this definition, the intensity of emission from a blackbody did not vary with the direction of emission. This invariance was a useful characteristic in comparing the directional intensity of emission from nonblack surfaces with that from a black surface. This led to a convenient measure of the difference between the real surface behavior and the black surface behavior; the ratio of the two emissions was defined as the surface directional emissivity.

In the case of a transmitting medium, the intensity has to be considered in terms of a local area within the medium. The intensity is then defined in a manner consistent with the solid surface case (section

2.4.1 of vol I). It is as if the radiation traveling through an area within the medium originated at that area. *The intensity is then defined* (see fig. 1-4(a)) *as the radiation energy passing through the area per unit time, per unit of the projected area and per unit solid angle.* The projected area is formed by taking the area that the energy is passing through and projecting it *normal to the direction of travel.* The unit elemental solid angle is centered about the direction of travel and *has its origin at dA .* The spectral intensity is the intensity per unit small wavelength interval around a wavelength λ .

As stated previously, the emitted intensity from a blackbody is invariant with emission angle. Now a second invariant property of intensity will be examined. Consider radiation from a source dA_s traveling in an ideal medium that is nonabsorbing, nonemitting, and non-scattering and has constant properties. Suppose that an imaginary area element dA_1 is considered at distance S_1 from dA_s and that dA_1 is normal to S_1 as shown in figure 1-4(b). From the definition of spectral intensity $i'_{\lambda,1}$ as the rate of energy passing through dA_1 per unit projected area of dA_1 per unit solid angle and per unit wavelength interval, the energy from dA_s passing through dA_1 in the direction of S_1 is

$$d^3Q'_{\lambda,1} = i'_{\lambda,1} dA_1 d\omega_1 d\lambda \tag{1-1a}$$

where the third derivative notation d^3 emphasizes that there are three differential quantities on the right side of the equation. The solid angle $d\omega_1$ is equal to dA_s/S_1^2 so

$$d^3Q'_{\lambda,1} = i'_{\lambda,1} dA_1 \frac{dA_s}{S_1^2} d\lambda \tag{1-1b}$$

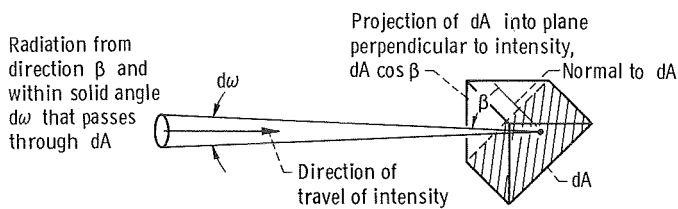
Suppose that dA_1 is now placed a distance S_2 from the source along the same direction as for the original position. The rate of energy passing through dA_1 in the new position is

$$d^3Q'_{\lambda,2} = i'_{\lambda,2} dA_1 d\omega_2 d\lambda = i'_{\lambda,2} dA_1 \frac{dA_s}{S_2^2} d\lambda \tag{1-2}$$

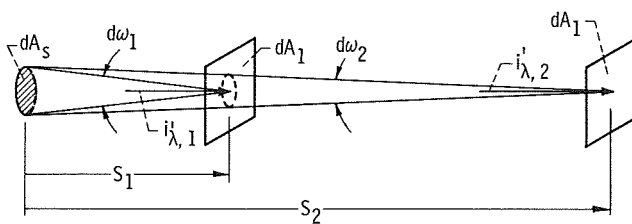
Dividing equation (1-1b) by equation (1-2) gives

$$\frac{d^3Q'_{\lambda,1}}{d^3Q'_{\lambda,2}} = \frac{i'_{\lambda,1} S_2^2}{i'_{\lambda,2} S_1^2} \tag{1-3}$$

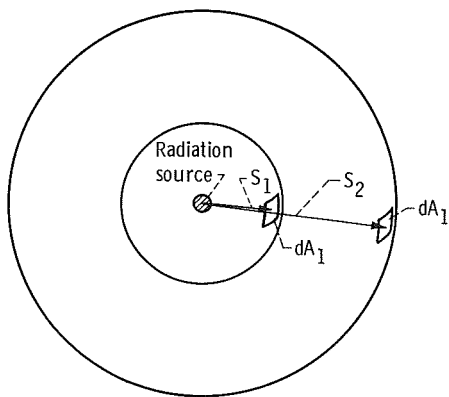
Now consider a differential source emitting energy equally in all



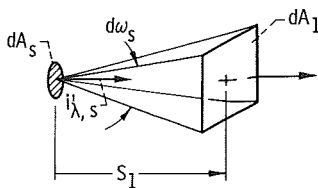
(a)



(b)



(c)



(d)

(a) Geometry for definition of intensity in medium.

(b) Intensity from source to area element.

(c) Variation of energy flux with distance from source.

(d) Intensity of emitted radiation.

FIGURE 1-4. — Derivations of intensity relations.

directions and draw two concentric spheres around it as in figure 1-4(c). If $d^2Q_{\lambda,s}$ is the entire spectral energy leaving the source, then the energy flux crossing the inner sphere is $d^2Q_{\lambda,s}/4\pi S_1^2$ and that crossing the outer sphere is $d^2Q_{\lambda,s}/4\pi S_2^2$. The ratio of the energies passing through the two elements dA_1 is

$$\frac{d^3Q'_{\lambda,1}}{d^3Q'_{\lambda,2}} = \frac{\frac{d^2Q_{\lambda,s}}{4\pi S_1^2} dA_1}{\frac{d^2Q_{\lambda,s}}{4\pi S_2^2} dA_1} = \frac{S_2^2}{S_1^2} \quad (1-4)$$

Substituting equation (1-4) for the left side of equation (1-3) gives the following important result:

$$i'_{\lambda,1} = i'_{\lambda,2} \quad (1-5)$$

Thus, *the intensity in a given direction in a nonattenuating and nonemitting medium with constant properties is independent of position along that direction.* Note that these intensities are based on the solid angles subtended by the source as viewed from dA_1 as in figure 1-4(b). As S is increased, the decrease in solid angle by which dA_1 views the source dA_s is accompanied by a comparable decrease in energy flux arriving at dA_1 . Thus the flux per unit solid angle, used in forming the intensity, remains constant.

The radiant energy passing through dA_1 can also be written in terms of the intensity leaving the source. Using figure 1-4(d) results in

$$d^3Q'_{\lambda,1} = i'_{\lambda,s} dA_s d\omega_s d\lambda = i'_{\lambda,s} dA_s \frac{dA_1}{S_1^2} d\lambda \quad (1-6)$$

Equating this with the energy rate passing through dA_1 as given by equation (1-1b) results in

$$i'_{\lambda,1} = i'_{\lambda,s} \quad (1-7)$$

This relation again shows the invariance of intensity with position in a nonattenuating and nonemitting medium.

The invariance of intensity when no attenuation or emission is present provides a convenient way of specifying the magnitudes of any attenuation or emission as these effects are given directly by the change of intensity with distance. By use of the foregoing intensity properties, the attenuation and emission of radiation within a medium can now be considered.

1.5 THE ATTENUATION OF ENERGY

Consider spectral radiation of intensity i'_λ impinging normally on a layer of material of thickness dS as in figure 1-5. The medium in the layer absorbs and scatters radiation. For the present it will be assumed that the layer is at low temperature so that its emitted energy is negligible. As the radiation passes through the layer, its intensity is reduced by absorption and scattering. The change in intensity has been found experimentally to depend on the magnitude of the local intensity. If a coefficient of proportionality K_λ which depends on the local properties of the medium is introduced, then the decrease is given by

$$di'_\lambda = -K_\lambda(S)i'_\lambda dS \quad (1-8)$$

This equation contains the assumption that no intensity is scattered from the radiation field into the direction of S .

The quantity K_λ is called the *extinction coefficient* of the material in the layer. The extinction coefficient is a physical property of the material and has the units of reciprocal length. It is in general a function of the temperature T , pressure P , composition of the material (specified here in terms of the concentration C_i of the i components), and the wavelength of the incident radiation so that

$$K_\lambda = K_\lambda(\lambda, T, P, C_i) \quad (1-9)$$

As will be shown later (see eq. (1-16)), the K_λ is inversely related to the mean penetration distance of radiation in an absorbing and scattering medium.

Integrating equation (1-8) over a path of length S gives the relation

$$\int_{i'_\lambda(0)}^{i'_\lambda(S)} \frac{di'_\lambda}{i'_\lambda} = - \int_0^S K_\lambda(S^*) dS^* \quad (1-10)$$

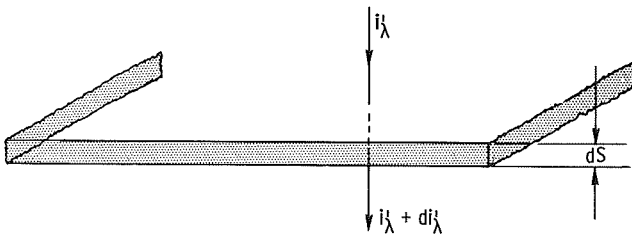


FIGURE 1-5. — Intensity incident normally on absorbing and scattering layer of thickness dS .

where $i'_\lambda(0)$ is the intensity entering the layer and S^* is a dummy variable of integration. Integrating equation (1-10) yields

$$\ln \left[\frac{i'_\lambda(S)}{i'_\lambda(0)} \right] = - \int_0^S K_\lambda(S^*) dS^* \quad (1-11)$$

or

$$i'_\lambda(S) = i'_\lambda(0) \exp \left[- \int_0^S K_\lambda(S^*) dS^* \right] \quad (1-12)$$

Equation (1-12) is known as Bouguer's law¹; it shows that, as a consequence of the proportionality in equation (1-8), the intensity of monochromatic radiation along a path is attenuated exponentially while passing through an absorbing-scattering medium. The exponent is equal to the integral of the local extinction coefficient over the path length traversed by the radiation.

1.5.1 The Extinction Coefficient

The extinction coefficient for thermal radiation K_λ is composed of two parts, an *absorption coefficient* $a_\lambda(\lambda, T, P)$ and a *scattering coefficient* $\sigma_{s\lambda}(\lambda, T, P)$. For simplicity the notation has been dropped showing dependence upon the relative concentration of the constituents of the gas. The coefficients are related by

$$K_\lambda(\lambda, T, P) = a_\lambda(\lambda, T, P) + \sigma_{s\lambda}(\lambda, T, P) \quad (1-13)$$

As noted previously, these coefficients have units of reciprocal length and are therefore called *linear coefficients*. Some researchers prefer to work with mass coefficients given by

$$K_{\lambda, m} = a_{\lambda, m} + \sigma_{s\lambda, m} = \frac{K_\lambda}{\rho} = \frac{a_\lambda}{\rho} + \frac{\sigma_{s\lambda}}{\rho} \quad (1-14)$$

where ρ is the local density of the absorbing-scattering species. The mass coefficients have units of area per unit mass and are directly related to the concept of a cross section in molecular physics (see section 8.3.1 for a discussion of scattering cross sections). Since the extinction coefficient K_λ increases as the density of the absorbing or scattering

¹ Named after Pierre Bouguer (1698 to 1758) who first showed on a quantitative basis how light intensities could be compared. Equation (1-12) is sometimes called Lambert's law, the Bouguer-Lambert law, or Beer's law. Beer's law is more properly a restricted form of equation (1-9) stating that the absorption of radiation depends only on the concentration of the absorbing species along the path. To avoid confusion with Lambert's cosine law, equation (1-12) will be referred to herein as Bouguer's law.

species is increased, the use of $K_{\lambda,m} = K_{\lambda}/\rho$ has the advantage that it tends to remain more constant than K_{λ} . However, the K_{λ} which will be used in this volume also has an advantage in that, when K_{λ} is constant, it can be interpreted as the reciprocal of the radiation mean penetration distance. This will now be shown.

1.5.2 Radiation Mean Penetration Distance

From equation (1-12) the fraction of the original radiation that travels through the path length S is

$$\frac{i_{\lambda}(S)}{i_{\lambda}(0)} = \exp \left[- \int_0^S K_{\lambda}(S^*) dS^* \right]$$

The fraction absorbed in the layer from S to $S + dS$ is

$$\frac{i_{\lambda}(S) - i_{\lambda}(S + dS)}{i_{\lambda}(0)} = - \frac{d \left[\frac{i_{\lambda}(S)}{i_{\lambda}(0)} \right]}{dS} = K_{\lambda}(S) \exp \left[- \int_0^S K_{\lambda}(S^*) dS^* \right] dS$$

The mean penetration distance of the radiation is obtained by multiplying the fraction absorbed at S by the distance S and then integrating over all path lengths from $S = 0$ to $S = \infty$; that is,

$$l_m = \int_{S=0}^{\infty} S K_{\lambda}(S) \exp \left[- \int_0^S K_{\lambda}(S^*) dS^* \right] dS \quad (1-15)$$

When K_{λ} is constant, carrying out the integral gives

$$l_m = K_{\lambda} \int_0^{\infty} S \exp (-K_{\lambda}S) dS = \frac{1}{K_{\lambda}} \quad (1-16)$$

demonstrating that the average penetration distance before absorption or scattering is the reciprocal of K_{λ} when K_{λ} does not vary along the path. Equation (1-16) provides a simple way of gaining some insight as to whether or not an absorbing-scattering medium is very opaque with regard to radiation traveling through it. This will now be further discussed in connection with the definition of optical thickness.

1.5.3 Optical Thickness

The exponential factor in equation (1-12) is often written in an alternate form by defining

$$\kappa_{\lambda}(S) \equiv \int_0^S K_{\lambda}(S^*) dS^* \quad (1-17)$$

so that equation (1-12) becomes

$$i'_{\lambda}(S) = i'_{\lambda}(0) \exp [-\kappa_{\lambda}(S)] \quad (1-18)$$

The quantity $\kappa_{\lambda}(S)$ is the *optical thickness* or *opacity* of the gas layer of thickness S and is a function of all the values of K_{λ} that lie between 0 and S . Because K_{λ} is a function of the local parameters P , T , and C_i , the optical thickness becomes a function of all these conditions along the path between 0 and S .²

The optical thickness is a measure of the ability of a given path length of gas to attenuate radiation of a given wavelength. A large optical thickness means large attenuation. The quantity κ_{λ} is a convenient dimensionless parameter that will occur in the solutions of radiative transfer problems.

For a gas that is of uniform composition and is at uniform temperature and pressure (a *uniform* gas) or for a gas with K_{λ} independent of T , P , and C_i , equation (1-17) becomes

$$\kappa_{\lambda}(S) = K_{\lambda}S \quad (1-19)$$

The optical thickness then depends directly on the extinction coefficient and the thickness of the absorbing-scattering layer.

1.5.4 The Absorption Coefficient

If scattering can be neglected (i.e., $\sigma_{s\lambda} \approx 0$), then $K_{\lambda} = a_{\lambda}$ and equation (1-12) becomes

$$i'_{\lambda}(S) = i'_{\lambda}(0) \exp \left[- \int_0^S a_{\lambda}(S^*) dS^* \right] \quad (1-20)$$

If, in addition, a_{λ} is not a function of position as is the case in a gas of uniform temperature, pressure, and composition, then

$$i'_{\lambda}(S) = i'_{\lambda}(0) \exp (-a_{\lambda}S) \quad (1-21)$$

²The notation for the optical thickness κ_{λ} should not be confused with the extinction coefficient for electromagnetic radiation κ used in equations (1-22) and (1-23) that follow. It is regrettable but true that the notation possibilities of the English and Greek alphabets reach saturation when such interdisciplinary fields as gas radiation are discussed.

In the electromagnetic theory of the propagation of radiant energy (see discussion following eq. (4-26) in vol. I), it is shown that the intensity of radiation is attenuated in conducting media according to the relation

$$\frac{i'_\lambda(S)}{i'_\lambda(0)} = \exp\left(\frac{-4\pi\kappa S}{\lambda}\right) \quad (1-22)$$

where κ is the extinction coefficient from electromagnetic theory and is related to the magnetic permeability, electrical resistivity, and electrical permittivity of the medium (eq. (4-23b) in vol. I). Thus, a_λ is related to κ by

$$a_\lambda = \frac{4\pi\kappa}{\lambda} \quad (1-23)$$

Such a relation provides some theoretical basis for Bouguer's law, which was originally based on experimental observations.

The absorption coefficient $a_\lambda(\lambda, T, P)$ usually has strong variations with wavelength and often varies substantially with temperature and pressure. Considerable analytical and experimental effort has been expended in the determination of a_λ for individual gases.

Analytical determinations of a_λ require detailed quantum mechanical calculations beyond the scope of this volume, although some of the concepts of these calculations are outlined in chapter 4. Except for the simplest gases such as atomic hydrogen, the calculations are very tedious and require many simplifying assumptions. For the methods used in calculation of a_λ , references 8 to 10 give detailed discussions.

The complexity of the calculations is presaged by examination of some measured solid and gas spectral absorption coefficients. In figure 1-6, a_λ is shown for pure diamond. Strong absorption peaks due to crystal lattice vibrations at certain wavelengths are evident. Figure 1-7 shows the calculated emission spectrum of hydrogen gas at 40 atm and 11 300 K for a path length through the gas of 50 cm. The variations in emission are closely related to variations in the absorption coefficient. The presence of "spikes" or strong emission lines is the result of transitions between bound energy states. The continuous part of the emission spectrum is due to various photodissociations, photoionization, and free electron-atom-photon interactions of other types. The lines and the continuous regions are common features of both emission and absorption spectra. Figure 1-8 shows the absorption coefficient of air at 1 atm and 12 000 K. In this case, there is a merging of the contributions from the many closely spaced lines produced by vibrational and rotational

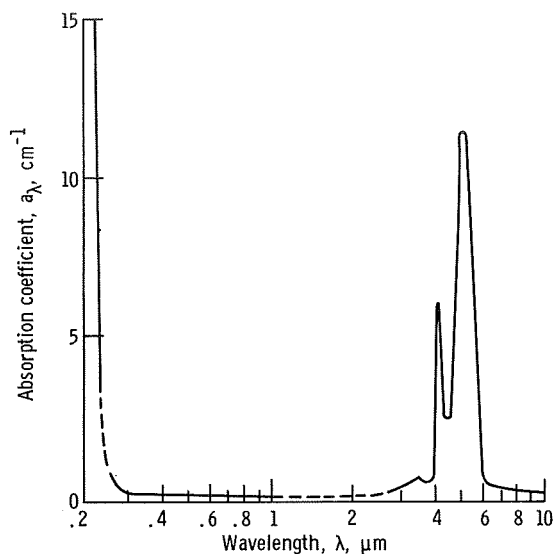


FIGURE 1-6.—Spectral absorption coefficient of diamond (from ref. 15).

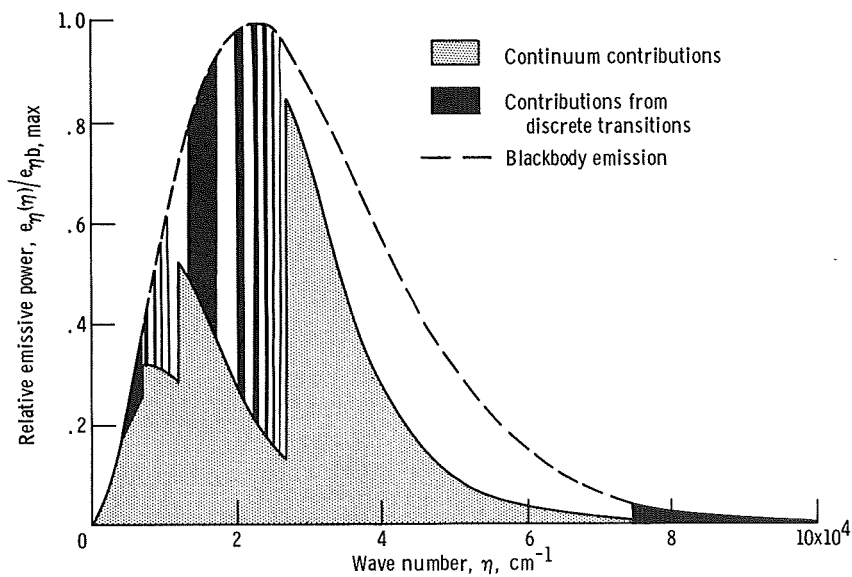


FIGURE 1-7.—Normalized emission spectrum of hydrogen at 11 300 K, 40 atm, and for path length of 50 cm (from ref. 16).

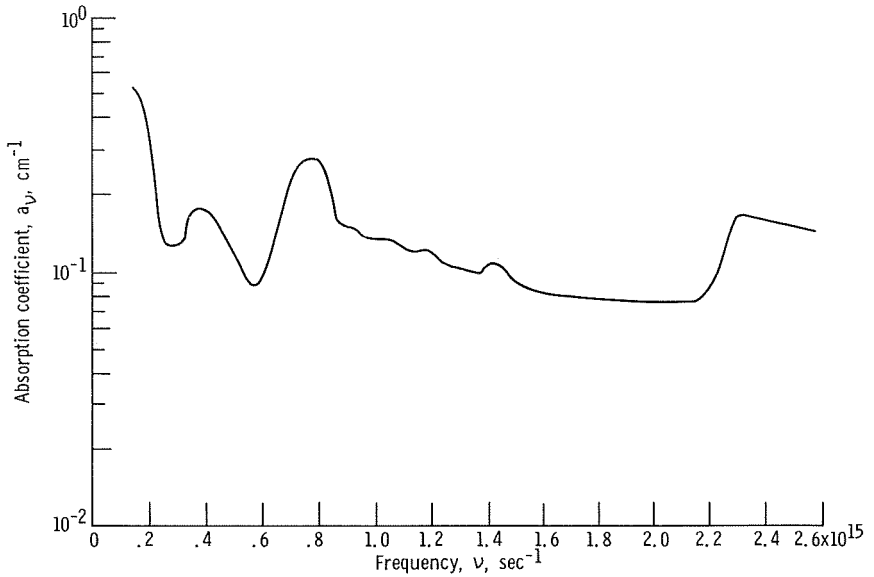


FIGURE 1-8.—Absorption coefficient of air at 12 000 K and 1 atm (from ref. 17).

transitions between energy states, and the absorption coefficient has the appearance of being continuous. Even when this merging is not complete, the resolution of experimental measurements causes the measured spectrum to appear continuous over these closely spaced lines.

It is noted that figures 1-6, 1-7, and 1-8 each have a different abscissa (i.e., wavelength, wave number, and frequency), emphasizing the lack of an accepted standard variable. When radiative properties of opaque surfaces were discussed in volume I of this series, it was found that the wavelength was generally used. In radiation from gases, however, the frequency is more common. It has the advantage that the frequency does not change when radiation passes from one medium into another with a different refractive index. The wavelength does change because of the change in propagation velocity.

Dealing with spectral line emission and absorption is one of the computational difficulties encountered in analyses of radiant energy transfer through gases. Incident radiation at wavelengths near the line center will be strongly absorbed, while radiation of only a slightly different wavelength may experience almost no attenuation. Integrating line absorption coefficients with respect to wavelength to obtain band or total absorption coefficients is generally tedious. These averaged coefficients are used in certain calculation methods of radiative transfer.

1.5.5 True Absorption Coefficient

Bouguer's law in the form of equation (1-20) gives the attenuation of a beam of radiation upon passing through a volume of nonemitting non-scattering gas along a path of length S as would be observed by detectors of incident and emerging radiation. Such observed information could be used in determining a_λ . Actually, as radiative energy passes through a gas, not only is it absorbed but there is an additional phenomenon in that its presence stimulates some of the gas atoms or molecules to emit energy. This is not the *ordinary* or *spontaneous* emission that will be discussed in section 1.6. The spontaneous emission is the result of the excited state of the gas being unstable and decaying spontaneously to a state of lower energy. The emission resulting from the presence of the radiation field is termed *stimulated* or *induced emission* and is in a sense a negative absorption.

Physically, the induced emission process can be pictured as follows: A photon of a certain frequency from the radiation field encounters a gas atom or molecule in an excited state, that is, an energy state above the ground state. There exists a certain probability that the incident photon will trigger a return of the gas particle to a lower energy state. If this occurs, the particle will emit a photon at the same frequency and in the same direction as the incident photon. Thus, the incident photon is not absorbed but is joined by a second identical photon. This process is often viewed as a negative absorption and is so treated in the equations of energy balance to be derived in chapter 2. More discussion of the induced emission process is given in section 4.4.

The induced emission constitutes a portion of the intensity that is observed in the beam emerging from the gas volume. Consequently, the amount of energy that was actually absorbed by the gas is greater than that found by taking the difference between the entering and leaving intensities. This is because the observed emerging intensity is the result of the actual absorption modified by the addition of induced emission along the path of the beam. The actual absorbed energy should be calculated using a true absorption coefficient $a_\lambda^\dagger(\lambda, T, P)$ which will be larger than the absorption coefficient $a_\lambda(\lambda, T, P)$ calculated by using observed attenuation data and Bouguer's law. The "true" law for absorption of energy along path S is then written as

$$i'_\lambda(S) = i'_\lambda(0) \exp \left[- \int_0^S a_\lambda^\dagger(S^*) dS^* \right] \quad (1-24)$$

Statistical mechanical considerations give the relation between $a_\lambda(\lambda, T, P)$ and $a_\lambda^\dagger(\lambda, T, P)$ for a gas with refractive index $n=1$ as

$$\begin{aligned}
 a_{\lambda}(\lambda, T, P) &= \left[1 - \exp\left(-\frac{hc_0}{k\lambda T}\right) \right] a_{\lambda}^{\dagger}(\lambda, T, P) \\
 &= \left[1 - \exp\left(-\frac{C_2}{\lambda T}\right) \right] a_{\lambda}^{\dagger}(\lambda, T, P) \quad (1-25)
 \end{aligned}$$

Examination of equation (1-25) shows that, because of the negative exponential term, a_{λ}^{\dagger} will always be larger than a_{λ} (hence the use of the superscript \dagger).

Because the induced emission depends on the incident radiation field, it is usually grouped together with the true absorption thereby yielding the absorption coefficient a_{λ} . The emission term in the equation of radiative transfer then includes only the spontaneous emission and consequently depends only on the local conditions of the gas. As will be shown in chapter 2, the grouping of induced emission into the absorption term simplifies the equations of radiative transfer.

The exponential term in equation (1-25) is small except at large values of λT . Thus a_{λ} and a_{λ}^{\dagger} are nearly equal except at large values of λT (long wavelengths and/or high temperatures). The values are within 1 percent for λT less than 3120 ($\mu\text{m})(\text{K})$ and within 5 percent for λT less than 4800 ($\mu\text{m})(\text{K})$.

When properties from the literature are used in calculations of radiative transfer in absorbing-emitting media, care must sometimes be exercised to determine whether the reported absorption coefficients include the effects of induced emission; usually it is a_{λ} that is given.

1.5.6 The Scattering of Energy

Scattering is taken here to be any encounter between a photon and one or more other particles during which the photon does not lose its *entire* energy. It may undergo a change in direction, and a partial loss or a gain of energy. In any of these cases, the photon is said to have been scattered.

The *scattering coefficient* $\sigma_{s\lambda}$ is the inverse of the mean free path that a photon of wavelength λ will travel before undergoing scattering. (This is strictly true only when $\sigma_{s\lambda}$ does not vary along the path.) The scattering can be characterized by four types of events: *elastic* scattering in which the energy (and, therefore, frequency and wavelength) of the photon is unchanged by the scattering, *inelastic* scattering in which the energy is changed, *isotropic* scattering in which scattering into any direction is equally likely, and *anisotropic* scattering in which there is a distribution of scattering directions. Elastic-isotropic scattering is most amenable to analysis without resorting to sophisticated analytical or

numerical techniques. Most scattering events of importance in engineering are elastic, or very nearly so.

For an elastic scattering process, there is no exchange of energy between the radiation field and the medium. Therefore, the local thermodynamic conditions of the gas are not affected by the radiation field, although the radiation field is affected by the gas conditions. Scattering calculations in this case become more tractable than for analogous absorption-emission effects where the internal energy of the gas and radiation field can interact strongly. Radiative transfer when scattering is present is treated in chapter 8. Until that point, attention will be restricted to cases involving only absorption and emission of radiation.

1.6 THE EMISSION OF ENERGY

Having considered the various definitions connected with attenuation within a medium, the emission of energy within the medium will now be discussed.

Consider an elemental volume dV of gas as shown in figure 1-9. The true absorption coefficient within dV is $a_{\lambda}^+(\lambda, T, P)$ and is considered constant over dV . Let dV be placed at the center of a large black hollow sphere of radius R at uniform temperature T . The space between dV and the sphere walls is filled with a nonparticipating material. The spectral intensity incident at the dA_s location on dV from an element dA on the surface of the enclosure is, by use of equation (1-7),

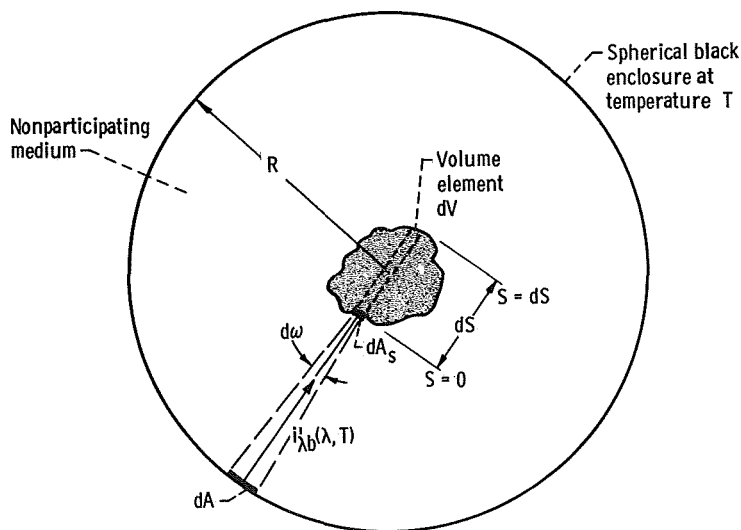


FIGURE 1-9.—Geometry for derivation of emission from volume of gas.

$$i'_\lambda(0) = i'_{\lambda b}(\lambda, T) \quad (1-26)$$

The intensity from this entering radiation that emerges from dV after passing through the path dS is given by Bouguer's law as

$$i'_\lambda(dS) = i'_\lambda(0) \exp(-a_\lambda^+ dS) \quad (1-27)$$

Since the true absorption coefficient has been used, the $i'_\lambda(dS)$ from equation (1-27) does not include any energy triggered by induced emission.

The change of the intensity as a result of true absorption in dV is the difference between equations (1-26) and (1-27); that is,

$$\begin{aligned} di'_\lambda &= i'_\lambda(dS) - i'_\lambda(0) = -i'_\lambda(0) [1 - \exp(-a_\lambda^+ dS)] \\ &= -i'_{\lambda b}(\lambda, T) [1 - \exp(-a_\lambda^+ dS)] \end{aligned} \quad (1-28)$$

This does not include induced emission. For very small values of $a_\lambda^+ dS$, note that

$$di'_\lambda = -i'_{\lambda b}(\lambda, T) [1 - \exp(-a_\lambda^+ dS)] \approx -i'_{\lambda b}(\lambda, T) a_\lambda^+ dS \quad (1-29)$$

which will apply since dS is a differential quantity. Equation (1-29) is also immediately evident from the differential form (eq. (1-8)). The energy absorbed by the volume $dS dA_s$ from this incident radiation is

$$d^4 Q'_{\lambda, a} = -di'_\lambda dA_s d\lambda d\omega \quad (1-30)$$

where $d\omega = dA/R^2$ and dA_s is a projected area normal to $i'_\lambda(0)$. Substituting equation (1-29) in equation (1-30) results in

$$d^4 Q'_{\lambda, a} = i'_{\lambda b}(\lambda, T) a_\lambda^+ dS dA_s d\lambda d\omega \quad (1-31)$$

The energy emitted by dA and absorbed by all of dV is found by integration over dV ; that is,

$$\begin{aligned} d^3 Q'_{\lambda, a} &= \int_{dV} d^4 Q'_{\lambda, a} = i'_{\lambda b}(\lambda, T) a_\lambda^+ d\lambda d\omega \int_{\substack{\text{projected area} \\ \text{of } dV \text{ normal} \\ \text{to path from } dA}} dA_s dS \\ &= a_\lambda^+ i'_{\lambda b}(\lambda, T) d\lambda d\omega dV \end{aligned} \quad (1-32)$$

where $d\omega$ is the solid angle subtended by dA when viewed from dV . To account for all energy incident upon dV from the entire spherical enclosure, integration is carried out over all such solid angles to give

$$\begin{aligned}
 d^2Q_{\lambda,a} &= \int_{\omega} d^3Q'_{\lambda,a} = a_{\lambda}^{\dagger} i'_{\lambda b}(\lambda, T) dV d\lambda \int_{4\pi} d\omega \\
 &= 4\pi a_{\lambda}^{\dagger} i'_{\lambda b}(\lambda, T) dV d\lambda \\
 &= 4a_{\lambda}^{\dagger} e_{\lambda b}(\lambda, T) dV d\lambda
 \end{aligned}
 \tag{1-33}$$

where $e_{\lambda b}$ is the blackbody spectral emissive power (eq. (2-12) in vol. I).

To maintain equilibrium in the enclosure, dV must emit an amount of energy equal to that absorbed. Hence, *the energy emitted by an isothermal volume element in equilibrium with its surroundings* is

$$d^2Q_{\lambda,e} = d^2Q_{\lambda,a} = 4a_{\lambda}^{\dagger}(\lambda, T, P) e_{\lambda b}(\lambda, T) dV d\lambda
 \tag{1-34}$$

This result includes both spontaneous emission and emission induced by the incident equilibrium radiation field. For only spontaneous emission, the coefficient a_{λ} would be used. The shape of the element dV is arbitrary; however, its size must be small enough to justify the approximation of equation (1-29) and also small enough so that energy emitted within dV escapes before reabsorption within dV . Further, the gas must be in thermodynamic equilibrium with respect to its internal energy, a restriction discussed more fully in section 1.8.

At this point an emission coefficient could be defined in a similar manner to the absorption coefficient. However, the radiation literature has other definitions of the emission coefficient³ which do not follow an analogy to the absorption coefficient definition, and there is no need to add confusion by defining a new coefficient here. Rather, equation (1-34) will be used directly as the relation for the emission of energy from an infinitesimal volume element of gas.

When the spontaneously emitted intensity is the same for all directions (isotropic spontaneous emission of energy), which is the condition for all cases discussed in this volume, the radiation intensity emitted spontaneously by a volume element into any direction is

$$i'_{\lambda,e}(\lambda, T) = \frac{d^2Q_{\lambda,e}}{4\pi dA_p d\lambda} = \frac{a_{\lambda}(\lambda, T, P) e_{\lambda b}(\lambda, T) dS}{\pi} = a_{\lambda}(\lambda, T, P) i'_{\lambda b}(\lambda, T) dS
 \tag{1-35}$$

³In the astrophysical literature (refs. 5 and 6), the emission coefficient is usually given the symbol j_{λ} defined by

$$j_{\lambda} = a_{\lambda} e_{\lambda b}$$

having units, therefore, of energy rate per unit volume per unit wavelength interval.

where dA_p is the projected area of dV normal to the direction of emission and dS is the mean thickness of dV parallel to the direction of emission (i.e., $dS = dV/dA_p$).

1.7 DEFINITIONS USED FOR ENGINEERING GAS PROPERTIES

It is desirable to make use of the extensive techniques in the engineering literature dealing with radiative interchange computations between surfaces (see ref. 11 (which will be referred to from this point as vol. II)) without intervening absorbing media. With this objective, analogous concepts and terminology will now be developed for problems involving participating gases. This is done through the concept of the emittance and absorptance of a gas volume. These gas property definitions are analogous to the emissivity and absorptivity of opaque bodies. Because the energies emitted or absorbed by a volume of gas depend on the *size* and *shape* of the volume in addition to its physical properties and temperature, the absorptance and emittance are *extensive* properties. The nomenclature used here will follow that of volume II of this series, where the "ance" suffix applies for extensive properties.

1.7.1 Absorptance

To be a reasonably simple engineering parameter, the absorptance should depend at most on the geometry, size, temperature, and physical properties of the volume for which it is evaluated. It is, therefore, defined for a volume with uniform conditions, so that no *gradients* in the physical conditions need be considered.

Consider energy of intensity $i'_\lambda(0)$ incident in the S direction on a uniform medium of projected area dA_p normal to S . The radiation passes through a thickness S as shown in figure 1-10. The amount of energy in solid angle $d\omega$ absorbed by the medium is

$$d^3Q'_{\lambda,a} = [i'_\lambda(0) - i'_\lambda(S)] dA_p d\omega d\lambda \quad (1-36)$$

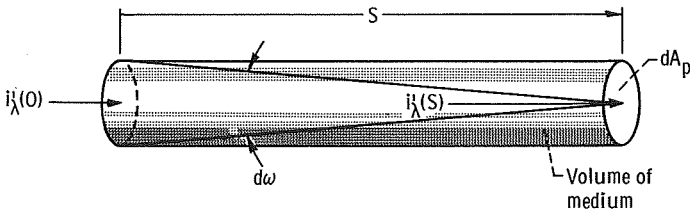


FIGURE 1-10.—Geometry for absorptance along path length S .

By substituting equation (1-21) for the attenuation of intensity by a uniform medium, this becomes

$$d^3Q'_{\lambda,a} = i'_\lambda(0) [1 - \exp(-a_\lambda S)] dA_p d\omega d\lambda \quad (1-37)$$

The energy incident upon dV in solid angle $d\omega$ is

$$d^3Q'_{\lambda,i} = i'_\lambda(0) dA_p d\omega d\lambda \quad (1-38)$$

If the absorptance for path length S in the volume is defined as the fraction of the incident energy in solid angle $d\omega$ that is absorbed while traversing S in the volume, then dividing equation (1-37) by equation (1-38) gives

Spectral absorptance for path length S in a uniform gas volume

$$\equiv \alpha'_\lambda(\lambda, T, P, S) = \frac{d^3Q'_{\lambda,a}}{d^3Q'_{\lambda,i}} = 1 - \exp(-a_\lambda S) \quad (1-39)$$

By substituting equation (1-39) into equation (1-21) the relation between intensities is obtained as

$$i'_\lambda(S) = i'_\lambda(0) [1 - \alpha'_\lambda(S)] \quad (1-40)$$

The $\alpha'_\lambda(S)$ is a directional spectral absorptance. The values of absorptance averaged over wavelength are also of use in engineering analyses. Integrating equations (1-37) and (1-38) over all wavelengths and then taking the ratio provides the relation

Total absorptance for path length S in a uniform gas volume

$$\begin{aligned} \equiv \alpha'(T, P, S) &= \frac{d^2Q'_a}{d^2Q'_i} = \frac{\int_0^\infty i'_\lambda(0) [1 - \exp(-a_\lambda S)] d\lambda}{\int_0^\infty i'_\lambda(0) d\lambda} \\ &= \frac{\int_0^\infty \alpha'_\lambda(\lambda, T, P, S) i'_\lambda(0) d\lambda}{\int_0^\infty i'_\lambda(0) d\lambda} \end{aligned} \quad (1-41)$$

1.7.2 Emittance

The directional emittance of a uniform gas volume is the ratio of the

energy emitted by the volume in a direction to that emitted by a blackbody at the same temperature. Because Kirchhoff's law holds without restriction for directional spectral absorptance values, as discussed in table 3-II of volume I, it immediately follows by use of equation (1-39) that

Directional spectral emittance for path length S in a uniform gas volume

$$\equiv \epsilon'_\lambda(\lambda, T, P, S) = 1 - \exp(-a_\lambda S) \quad (1-42)$$

The emittance is the ratio of emitted energy to that emitted by a blackbody. Consequently, the energy in wavelength interval $d\lambda$ arriving at dA_p at location S as a result of emission by the medium in solid angle $d\omega$ as shown in figure 1-10 is $i'_{\lambda b}[1 - \exp(-a_\lambda S)]dA_p d\omega d\lambda$. It follows by analogy to equation (1-41) that for total quantities

Directional total emittance for path length S in a uniform gas volume

$$\begin{aligned} \equiv \epsilon'(T, P, S) &= \frac{\int_0^\infty i'_{\lambda b}(\lambda, T)[1 - \exp(-a_\lambda S)]d\lambda}{\int_0^\infty i'_{\lambda b}(\lambda, T)d\lambda} \\ &= \frac{\int_0^\infty e_{\lambda b}(\lambda, T)[1 - \exp(-a_\lambda S)]d\lambda}{\sigma T^4} \\ &= \frac{\int_0^\infty \epsilon'_\lambda(\lambda, T, P, S)e_{\lambda b}(\lambda, T)d\lambda}{\sigma T^4} \end{aligned} \quad (1-43)$$

where by using σT^4 for the total blackbody emission it is assumed that the index of refraction of the medium is $n = 1$.

In figure 1-11, the directional total emittance of carbon dioxide is shown as a function of temperature, partial pressure of the CO_2 , and path length. This is an example of the extensive tabulations of such properties that are available for gases at conditions of importance in industrial design. The methods of using these properties in radiative exchange computations are developed in chapter 5, where more detailed charts of the radiative properties will be given.

Comparing equations (1-41) and (1-43) shows that Kirchhoff's law for directional total properties, which is

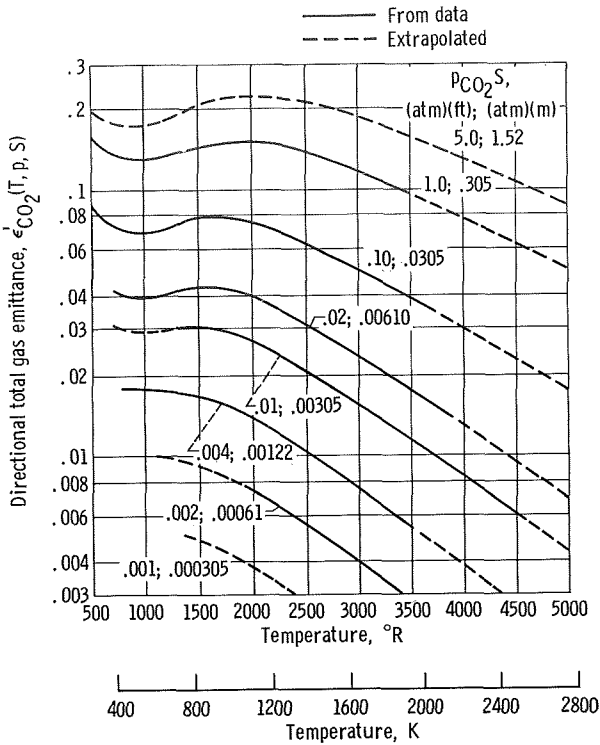


FIGURE 1-11.—Emittance of carbon dioxide in mixture with nonabsorbing gas at total pressure of 1 atm (ref. 18).

$$\alpha'(T, P, S) = \epsilon'(T, P, S) \tag{1-44}$$

holds only under the conditions that the incident spectral radiation for absorption is proportional to a blackbody spectrum at the gas temperature T , or the gas is gray, that is, $\alpha'_\lambda = \epsilon'_\lambda$ are independent of wavelength. The same restrictions apply for opaque bodies as discussed in volume I.

EXAMPLE 1-1: As a rough approximation, idealize the absorptance of CO_2 at $T_g = 1500^{\circ}R$ (830 K) and 10 atm as in figure 1-2 so that it consists of four bands having vertical boundaries at the values 1.8 and 2.2, 2.6 and 2.8, 4.0 and 4.6, and 9 and 19 μm . What is the total emittance of a very thick layer of gas at this temperature?

For a very thick layer of gas, equation (1-42) indicates that ϵ'_λ will go to unity in the absorbing regions. Hence, the gas will emit like a blackbody in the four spectral absorption bands. In the nonabsorbing regions

between the bands, ϵ'_λ will be zero. From equation (1-43) the total emittance becomes

$$\epsilon'(T_g, P, S) = \frac{\int_0^\infty \epsilon'_\lambda(\lambda, T_g, P, S) e_{\lambda b, g} d\lambda}{\sigma T_g^4} = \frac{\int_{\text{absorbing bands}} e_{\lambda b, g} d\lambda}{\sigma T_g^4}$$

The emittance is thus the fractional emission of a blackbody over the wavelength intervals of the absorbing bands which can be obtained from the $F_{0-\lambda T_g}$ factors in table V in the appendix of volume I. The required values are as follows:

λ , μm	λT_g , $(\mu\text{m})(^\circ\text{R})$	$F_{0-\lambda T_g}$
1.8	2 700	0.01285
2.2	3 300	.04338
2.6	3 900	.09478
2.8	4 200	.12665
4.0	6 000	.34734
4.6	6 900	.44977
9	13 500	.83435
19	28 500	.97302

Then the emittance is

$$\begin{aligned} \epsilon'(T_g, P, S) &= \int_{\text{absorbing bands}} [F_{(\lambda T_g)_{\text{lower}}} - (\lambda T_g)_{\text{upper}}]_{\text{band}} \\ &= \int_{\text{absorbing bands}} [F_{0 - (\lambda T_g)_{\text{upper}}} - F_{0 - (\lambda T_g)_{\text{lower}}}]_{\text{band}} \end{aligned}$$

Using the numerical values gives

$$\begin{aligned} \epsilon' &= (0.04338 - 0.01285) + (0.12665 - 0.09478) + (0.44977 - 0.34734) \\ &\quad + (0.97302 - 0.83435) = 0.304 \end{aligned}$$

EXAMPLE 1-2: What fraction of incident solar radiation will be absorbed by a very thick layer of CO_2 at 10 atm and 1500°R (830K)? Use the approximate absorption bands of example 1-1.

The effective radiating temperature of the Sun is about $T_s = 10\,000^\circ\text{R}$ (5600 K). The desired result is the fraction of the solar spectrum that lies within the four CO_2 bands as this is the only portion of the incident radiation that will be absorbed. Using the $F_{0-\lambda T_s}$ factors as in example 1-1, but using the solar temperature, gives the following values (using table V in the appendix of vol. I):

λ , μm	λT_s , ($\mu\text{m})(^\circ\text{R})$	$F_{0-\lambda T_s}$
1.8	18 000	0.91414
2.2	22 000	.94751
2.6	26 000	.96572
2.8	28 000	.97174
4.0	40 000	.98915
4.6	46 000	.99262
9	90 000	.99889
19	190 000	~ 1.0000

The fraction absorbed is then

$$\alpha' = \sum_{\substack{\text{absorbing} \\ \text{bands}}} [F_{0-(\lambda T_s)_{\text{upper}}} - F_{0-(\lambda T_s)_{\text{lower}}}]_{\text{band}}$$

$$= (0.94751 - 0.91414) + (0.97174 - 0.96572)$$

$$+ (0.99262 - 0.98915) + (1.00000 - 0.99889) = 0.044$$

Even though the gas layer is very thick, only 4.4 percent of the incident energy is absorbed since the gas is essentially transparent in the region between the absorption bands.

1.7.3 Transmittance

The *transmittance* of a gas volume is the fraction of the incident energy that passes through the gas volume. If it is assumed that no reflection or scattering of the incident radiation occurs, then the energy transmitted along a path is the incident energy minus the energy absorbed along the path; that is,

$$d^3Q'_{\lambda, t} = d^3Q'_{\lambda, i} - d^3Q'_{\lambda, a} \tag{1-45}$$

Rearranging gives the transmittance as

$$\frac{d^3 Q'_{\lambda, t}}{d^3 Q'_{\lambda, i}} = 1 - \frac{d^3 Q'_{\lambda, a}}{d^3 Q'_{\lambda, i}} \quad (1-46)$$

Substituting equation (1-39) gives

Spectral transmittance for path length S in a uniform gas volume

$$\equiv \tau'_{\lambda}(\lambda, T, P, S) = \frac{d^3 Q'_{\lambda, t}}{d^3 Q'_{\lambda, i}} = 1 - \alpha'_{\lambda}(\lambda, T, P, S) = \exp(-a_{\lambda} S) \quad (1-47)$$

From equation (1-40) the intensities (as shown in fig. 1-10) can then be related as

$$i'_{\lambda}(S) = i'_{\lambda}(0) \tau'_{\lambda}(S) \quad (1-48)$$

By analogous arguments, the directional total transmittance is given by (it is again assumed the reflectance of the gas volume is negligible) the following:

Directional total transmittance for path length S in a uniform gas volume $\equiv \tau'(T, P, S) = 1 - \alpha'(T, P, S)$

$$\begin{aligned} &= \frac{\int_0^{\infty} \tau'_{\lambda}(\lambda, T, P, S) i'_{\lambda}(0) d\lambda}{\int_0^{\infty} i'_{\lambda}(0) d\lambda} \\ &= \frac{\int_0^{\infty} i'_{\lambda}(0) \exp(-a_{\lambda} S) d\lambda}{\int_0^{\infty} i'_{\lambda}(0) d\lambda} \end{aligned} \quad (1-49)$$

EXAMPLE 1-3: Some types of nuclear explosions produce, at their peak, an emissive power spectrum like that of a blackbody at 6000 K. The Sun also emits very close to this spectrum. Consequently, the transmissivity of the atmosphere for solar radiation can be used to determine the attenuation of energy from a nuclear explosion.

When the Sun is directly overhead, the total transmittance of the atmosphere for solar radiation averages 35 percent throughout the fall and winter in the Great Lakes region. Assume that a 20-megaton weapon

is detonated at a height of 10 km and dissipates its energy uniformly over a period of 4 sec. Assume further that the fireball during this period is 1000 m in diameter and that 50 percent of the total energy is dissipated as thermal radiation. Calculate the radiant energy flux directly below the burst at ground level.

The total energy expended by the fireball per unit time is (1 megaton $\approx 10^{15}$ cal)

$$Q = \frac{20 \text{ megatons}}{4 \text{ sec}} = 5 \times 10^{15} \frac{\text{cal}}{\text{sec}}$$

For 50 percent of the energy going into thermal radiation, the emissive power of the fireball is

$$e = \frac{0.5Q}{A_{\text{fireball}}} = \frac{0.5Q}{4\pi R_{\text{fireball}}^2}$$

The intensity of radiation leaving the blackbody fireball is

$$i'(0) = \frac{e}{\pi}$$

and from equation (1-48) the intensity arriving at ground level is

$$i'(\text{ground}) = \tau' i'(0) = 0.35 \frac{e}{\pi} = \frac{0.35 \times 0.5Q}{4\pi^2 R_{\text{fireball}}^2}$$

To compute the energy arriving at the ground, the fireball is treated approximately as a differential area with projected area $dA_p = \pi R_{\text{fireball}}^2$ seen from the ground. Then the energy reaching the ground directly below the fireball per unit time is

$$dQ' = i'(\text{ground}) A_{\text{ground}} d\omega = \frac{0.175Q}{4\pi^2 R_{\text{fireball}}^2} A_{\text{ground}} \frac{\pi R_{\text{fireball}}^2}{S^2}$$

The energy flux at ground level directly below the fireball is

$$q = \frac{dQ'}{A_{\text{ground}}} = \frac{0.175Q}{4\pi S^2} = \frac{0.175 \times 5 \times 10^{15}}{4\pi \times 10^{12}} = \frac{69.5 \text{ cal}}{(\text{cm}^2)(\text{sec})}$$

Note that the result is independent of R_{fireball} .

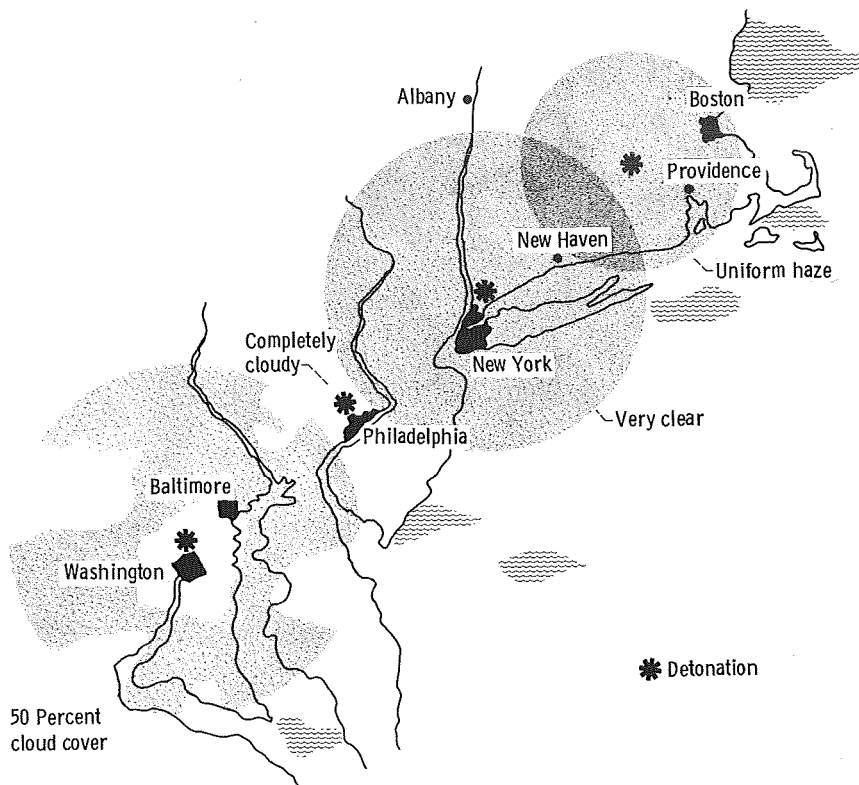


FIGURE 1-12.—Areas receiving $15 \text{ cal}/(\text{cm}^2)(\text{sec})$ or more of radiative flux as function of weather conditions during four large-yield high-altitude weapon detonations (ref. 12).

The rather grim result is that this flux applied over a few seconds is more than four times that required to ignite newspapers. A more complete approach to problems of this type is given in reference 12, where the slant angle to the ground is included. Higher altitude detonations than those of example 1-3 were studied. Figure 1-12 shows some results of reference 12 not recommended for the imaginative reader.

1.8 THE CONCEPT OF LOCAL THERMODYNAMIC EQUILIBRIUM

It was tacitly assumed in volume I of this series that opaque solids emit energy based solely on the temperature and physical properties of the body. The spectrum of emitted energy was assumed unaffected by the characteristics of any incident radiation. This is generally true because all the absorbed part of the energy incident on an opaque solid is quickly redistributed into internal energy states in an equilibrium distribution at

the temperature of the solid.

In a gas, the redistribution of absorbed energy occurs by various types of collisions between the atoms, molecules, electrons, and ions that comprise the gas. Under most engineering conditions, this redistribution occurs quite rapidly, and the energy states of the gas *will* be populated in equilibrium distributions at any given locality. When this is true, the Planck spectral distribution correctly describes the emission from a blackbody, and equation (1-34) correctly describes the emission from a gas volume element.

The assumption, that a gas will emit according to equation (1-34) regardless of the spectral distribution of intensity passing through and being absorbed by dV , is a consequence of the assumption of "local thermodynamic equilibrium" or LTE. When the condition of LTE is not present, the calculation of radiant transfer becomes much more complex.

Cases where the LTE assumption breaks down are occasionally encountered. Examples are in very rarefied gases, where the rate and/or effectiveness of interparticle collisions in redistributing absorbed radiant energy is low; when rapid transients exist so that the populations of energy states of the particles cannot adjust to new conditions during the transient; where very sharp gradients occur so that local conditions depend on particles that arrive from adjacent localities at widely different conditions and may emit before reaching equilibrium; and where extremely large radiative fluxes exist, so that absorption of energy and therefore population of higher energy states occur so strongly that collisional processes cannot repopulate the lower states to an equilibrium density. Under any of these conditions, the spectral distribution of emitted radiation is not given by equation (1-34). Then the populations must be determined by detailed examination of the relation between the collisional and radiation processes and their effect on the distribution of energy among the various possible states—a most formidable undertaking. It is, however, necessary in examination of shock phenomena (sharp gradients), stellar atmospheres (extreme energy flux and low density), nuclear explosions (transients, sharp gradients, and extreme fluxes), and high altitude and interplanetary gas dynamics (very low densities).

A gas with small optical thickness can have transmitted within it radiation from regions at widely different conditions. For this reason, a nearly transparent or "clear" gas is more likely to depart from LTE than is an optically thick gas of the same density.

A very prominent non-LTE effect is found in the laser. In this device, a material with a metastable energy state is excited by some external means. Because the excited state is metastable and is also chosen so that

no competing process is trying to depopulate it, its population can reach a value well above the equilibrium value. This condition is called a *population inversion*. The material is then exposed to radiation containing photons with the same frequency as the transition frequency from the excited to a lower state in the material. This radiation induces or stimulates the transition to the lower state. Consequently, a large number of photons with the transition frequency are emitted, thus amplifying the intensity of the incident radiation. This process leads to the acronym *light amplification by the stimulated emission of radiation*, or *laser*.

Such non-LTE problems are beyond the scope of this work. It will be assumed here that LTE always exists and that although the flux arriving at a volume element dV may come from localities at widely different temperatures, the emission from dV will be governed by equation (1-34).

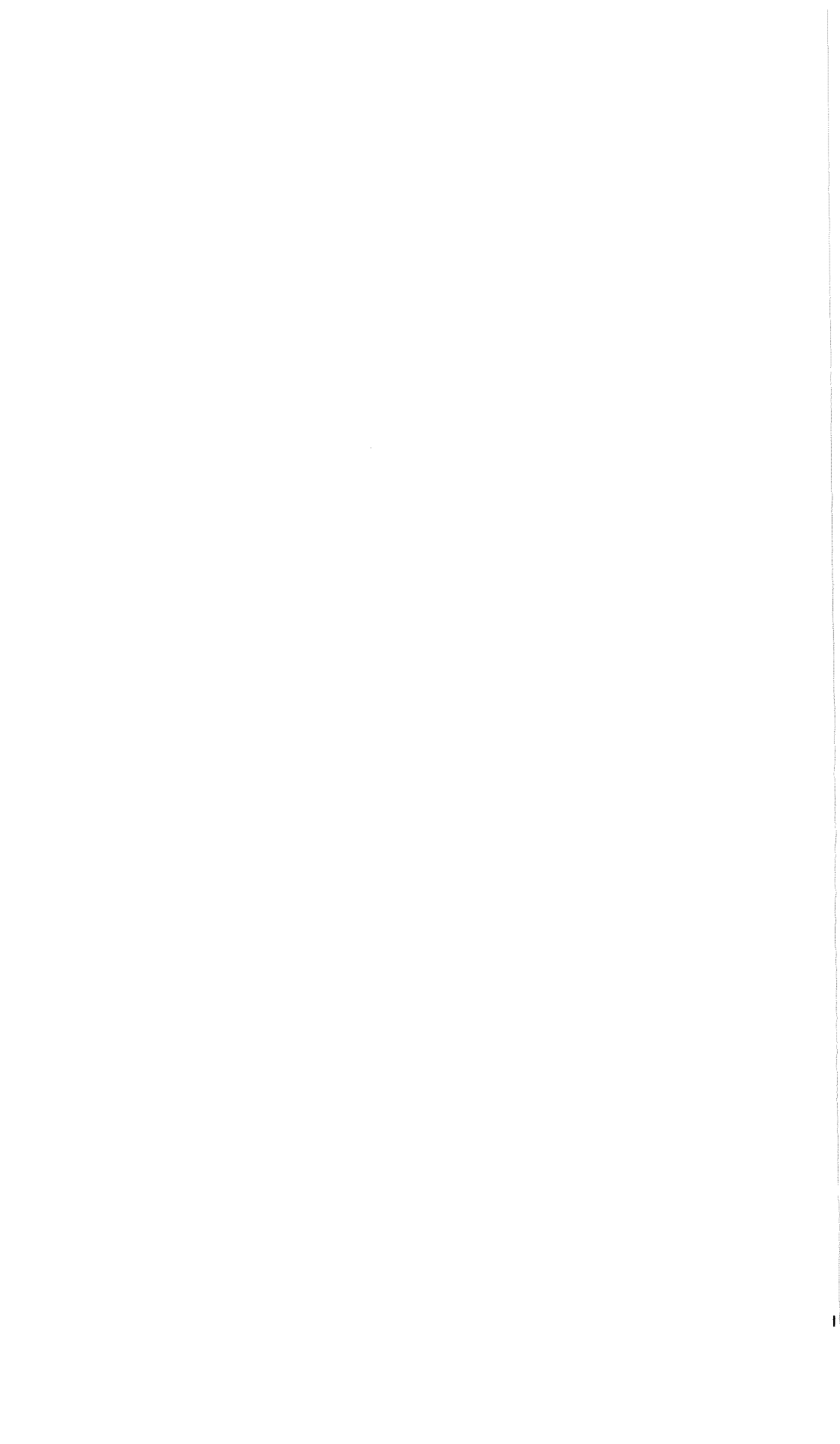
1.9 CONCLUDING REMARKS

In this chapter, some basic concepts and definitions in the theory and physics of gas radiation have been introduced. In succeeding chapters, application of these concepts will be made to the problem of radiant energy transfer in gases. The idea of induced emission has been introduced, and the method of accounting for this effect in the equation of transfer will be shown in chapter 2.

REFERENCES

1. LANGLEY, S. P.: Experimental Determination of Wave-Lengths in the Invisible Prismatic Spectrum. *Memoirs Nat. Acad. Sci.*, vol. 2, 1883, pp. 147-162.
2. GOODY, R. M.: *Atmospheric Radiation. Vol. 1-Theoretical Basis*. Clarendon Press, Oxford, 1964.
3. KONDRATYEV, K. YA.: *Radiation in the Atmosphere*. Academic Press, 1969.
4. GARDON, ROBERT: A Review of Radiant Heat Transfer in Glass. *J. Am. Cer. Soc.*, vol. 44, no. 7, July 1961, pp. 305-312.
5. CHANDRASEKHAR, S.: *Radiative Transfer*. Dover Publ., 1960.
6. KOURGANOFF, VLADIMIR: *Basic Methods in Transfer Problems; Radiative Equilibrium and Neutron Diffusion*. Dover Publ., 1963.
7. SIEGEL, ROBERT; AND HOWELL, JOHN R.: *Thermal Radiation Heat Transfer. I-The Blackbody, Electromagnetic Theory, and Material Properties*. NASA SP-164, 1968.
8. PENNER, S. S.: *Quantitative Molecular Spectroscopy and Gas Emissivities*. Addison-Wesley Publ. Co., 1959.
9. BOND, JOHN W., JR.; WATSON, KENNETH M.; AND WELCH, JASPER A., JR.: *Atomic Theory of Gas Dynamics*. Addison-Wesley Pub. Co., 1965.
10. BATES, DAVID R., ED.: *Atomic and Molecular Processes*. Academic Press, 1962.
11. HOWELL, JOHN R.; AND SIEGEL, ROBERT: *Thermal Radiation Heat Transfer. II-Radiation Exchange Between Surfaces and in Enclosures*. NASA SP-164, 1969.
12. ATLAS, REYNOLD; AND CHARLES, B. N.: *Atmospheric Attenuation of the Thermal Radiation from a High-Altitude Nuclear Detonation*. Paper 64-318, AIAA, June 1964.

13. KULANDER, JOHN L.: Non-Equilibrium Radiation. Rep. R64SD41, General Electric Co., June 1965. (Available from DDC as AD-617383.)
14. THOMAS, RICHARD N.: Some Aspects of Nonequilibrium Thermodynamics in the Presence of a Radiation Field. University of Colorado Press, 1965.
15. GARBUNY, MAX: Optical Physics. Academic Press, 1965.
16. AROESTE, HENRY; AND BENTON, WILLIAM C.: Emissivity of Hydrogen Atoms at High Temperatures. J. Appl. Phys., vol. 27, 1956, pp. 117-121.
17. MEYEROTT, R. E.; SOKOLOFF, J.; AND NICHOLLS, R. A.: Absorption Coefficients of Air. Rep. LMSD-288052. Lockheed Aircraft Corp. (AFCRC-TR-59-296), Sept. 1959.
18. HOTTEL, H. C.: Radiant-Heat Transmission. Heat Transmission. Third ed., William H. McAdams, McGraw-Hill Book Co., Inc., 1954, ch. 4.



Chapter 2. The Equations of Transfer for an Absorbing—Emitting Gas

2.1 INTRODUCTION

In chapter 1 some of the basic concepts and definitions were presented for intensity, emission, and absorption within a medium. The radiation traveling along a path within a medium is attenuated by absorption and scattering, and is enhanced by both spontaneous and induced emission and also by radiation scattered in from other directions. The fundamental processes of absorption and emission as discussed in chapter 1 will be employed to develop a differential equation governing the radiation intensity along a path through the absorbing and emitting medium. This equation is called the *equation of transfer*. The effects of scattering will be neglected in this chapter and in chapters 3 to 7; scattering will be considered in chapter 8.

When obtaining a solution to the equation of transfer, a constant of integration will be introduced; the evaluation of this constant introduces the intensity at the origin of the radiation path being considered. Because the origin is usually at the boundary of the radiating medium, the radiation at the boundaries is thereby coupled into the radiation distribution within the medium.

The intensity gives the radiation that is traveling in a single direction, per unit solid angle, and that is crossing a unit area normal to the direction of travel. To obtain the net *energy* crossing an area, an integration must be made that includes the contributions of the intensities crossing in all directions. This results in an equation for radiative flux which will be used in the formation of heat balances within the medium.

2.2 SYMBOLS

A	area
a	absorption coefficient
c	speed of light in a medium
D	spacing between parallel plates or diameter ratio
E_n	exponential integral function, eq. (2-45)
e	emissive power
f	photon distribution function
h	Planck's constant
i	radiation intensity

i, j, k	unit vectors in x, y, z coordinate directions
n	unit normal vector
P	pressure
Q	energy per unit time
q	energy flux, energy per unit area and time
r	position vector
S	coordinate along path of radiation
s	unit vector in S direction
T	absolute temperature
U	radiant energy density
V	volume
x, y, z	coordinates in Cartesian system
β	cone angle, angle from normal of area
θ	circumferential angle
κ	optical thickness
κ_D	optical thickness for path of length D
λ	wavelength
ν	frequency
σ	Stefan-Boltzmann constant
ω	solid angle

Subscripts:

a	absorbed
b	blackbody
e	emitted
i	incident mean value, eq. (2-21)
P	Planck mean value, eq. (2-20)
λ, ν	spectrally dependent
+	along directions having positive $\cos \beta$
-	along directions having negative $\cos \beta$
1, 2	surface 1 or 2

Superscripts:

'	directional quantity
+	true value, not modified by addition of induced emission
*	dummy variable of integration
-	averaged over all incident solid angles

2.3 THE EQUATION OF TRANSFER

The equation of transfer in a nonscattering medium will now be derived. As stated in section 2.1, this will describe the intensity of

radiation at any position along its path through an absorbing-emitting medium.

2.3.1 Derivation

Bouguer's law, equation (1-12), in a nonscattering medium accounts only for attenuation by absorption. The equation of transfer is an extension of Bouguer's law to include the contribution to the radiation intensity of energy emission along the path.

Consider radiation of intensity $i'_\lambda(S)$ within a region of absorbing-emitting medium as shown in figure 2-1. Attention will now be directed to the change of intensity as the radiation passes through a distance dS . Not including the gas emission for a moment, the intensity at $S + dS$ for a nonscattering gas is equal to the intensity at S plus the change caused by absorption in dS ; that is,

$$i'_\lambda(S + dS) = i'_\lambda(S) + di'_{\lambda, a}$$

Using equation (1-8) with $K_\lambda = a_\lambda$ in this case gives

$$i'_\lambda(S + dS) = i'_\lambda(S) - a_\lambda(S)i'_\lambda(S)dS = i'_\lambda(S)[1 - a_\lambda(S)]dS \quad (2-1)$$

Note that a_λ has been used in equation (2-1) rather than the "true" absorption coefficient a_λ^* . Thus the intensity $i'_\lambda(S + dS)$ is the result

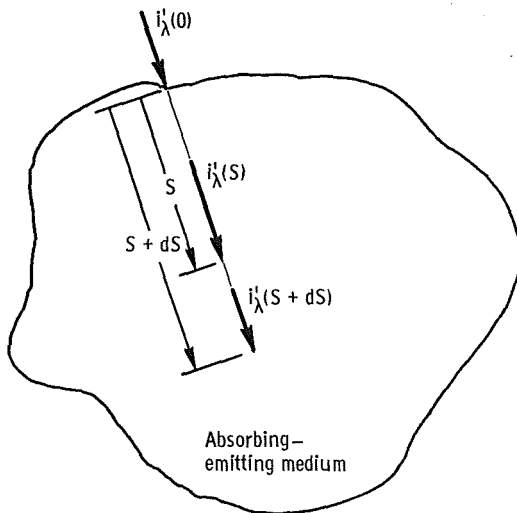


FIGURE 2-1.—Geometry for derivation of equation of transfer.

not only of true absorption, but also includes the contribution of induced emission as discussed in section 1.5.5.

Assuming the radiation along the path is in local thermodynamic equilibrium, the spontaneous emission contribution by the gas along the path length dS to the intensity in the S direction is given by equation (1-35) as

$$di'_{\lambda, e} = a_{\lambda}(S) i'_{\lambda b}(S) dS \quad (2-2)$$

Adding equations (2-1) and (2-2) gives the intensity of the radiation $i'_{\lambda}(S + dS)$ as

$$\begin{aligned} i'_{\lambda}(S + dS) &= i'_{\lambda}(S) + di'_{\lambda, a} + di'_{\lambda, e} \\ &= i'_{\lambda}(S) [1 - a_{\lambda}(S) dS] + a_{\lambda}(S) i'_{\lambda b}(S) dS \end{aligned} \quad (2-3)$$

where $i'_{\lambda}(S + dS)$ now includes all emission from the gas as well as the contribution of the attenuated incident intensity. The change in intensity di'_{λ} of the incident radiation as a result of passing through dS is then

$$di'_{\lambda} = i'_{\lambda}(S + dS) - i'_{\lambda}(S) = a_{\lambda}(S) [i'_{\lambda b}(S) - i'_{\lambda}(S)] dS \quad (2-4)$$

A form of equation (2-4) in astrophysical texts and which is often more convenient to work with is obtained by combining $a_{\lambda} dS$ into a single quantity, that is,

$$d\kappa_{\lambda} = a_{\lambda}(S) dS \quad (2-5)$$

which takes into account the absorption coefficient and the differential path through which the radiation is traveling. The $d\kappa_{\lambda}$ is called the *optical differential thickness*. By integrating equation (2-5) as in equation (1-17) the *optical thickness* or *optical depth* is obtained for a layer of thickness S or a path of length S

$$\kappa_{\lambda}(S) = \int_0^S a_{\lambda}(S^*) dS^* \quad (2-6)$$

Using the optical differential thickness results in equation (2-4) taking the form

$$\frac{di'_{\lambda}}{d\kappa_{\lambda}} + i'_{\lambda}(\kappa_{\lambda}) = i'_{\lambda b}(\kappa_{\lambda}) \quad (2-7)$$

Equation (2-7) is the *equation of transfer* for an absorbing-emitting gas.

There is a basic advantage for including the induced emission in the absorption coefficient. The induced emission as discussed in section 1.5.5 is in the same direction as the transmitted radiation. The spontaneous emission, however, is uniform over all directions. Thus by combining the induced emission with the "true" absorption to form a_λ (and κ_λ), the quantities depending on the direction of the incident radiation have been brought together. The resulting emission term in the equation of transfer contains only spontaneous emission and hence does not depend on direction.

2.3.2 Integration by Use of Integrating Factor

Equation (2-7) is a first-order linear differential equation and a general solution can be obtained by use of an integrating factor. Multiplying through by the factor $\exp(\kappa_\lambda)$ gives

$$\begin{aligned} \exp(\kappa_\lambda) \left(\frac{di'_\lambda}{d\kappa_\lambda} \right) + i'_\lambda(\kappa_\lambda) \exp(\kappa_\lambda) \\ = \frac{d}{d\kappa_\lambda} [i'_\lambda(\kappa_\lambda) \exp(\kappa_\lambda)] = i'_{\lambda b}(\kappa_\lambda) \exp(\kappa_\lambda) \end{aligned} \quad (2-8)$$

Integrating over an optical thickness from $\kappa_\lambda = 0$ to $\kappa_\lambda(S)$ gives

$$i'_\lambda(\kappa_\lambda) \exp(\kappa_\lambda) - i'_\lambda(0) = \int_0^{\kappa_\lambda} i'_{\lambda b}(\kappa_\lambda^*) \exp(\kappa_\lambda^*) d\kappa_\lambda^* \quad (2-9)$$

or

$$i'_\lambda(\kappa_\lambda) = i'_\lambda(0) \exp(-\kappa_\lambda) + \int_0^{\kappa_\lambda} i'_{\lambda b}(\kappa_\lambda^*) \exp[-(\kappa_\lambda - \kappa_\lambda^*)] d\kappa_\lambda^* \quad (2-10)$$

where κ_λ^* is a dummy variable of integration.

Equation (2-10) is interpreted physically as the intensity at optical depth κ_λ being composed of two terms. The first is the attenuated incident radiation arriving at κ_λ (including, however, the contribution of induced emission along the path), and the second is the intensity resulting from spontaneous emission in the S direction by all thickness elements along the path and reduced by exponential attenuation between the point of emission κ_λ^* and the location κ_λ . Equation (2-10) is the *integrated form of the equation of transfer*. As derived, this equation

applies to the *spectral* intensity traveling in the positive κ_λ direction.

Although equation (2-10) is a general solution to the equation of transfer, the intensity cannot be obtained directly from it unless the temperature distribution is known. The temperature will determine the blackbody emission term $i'_{\lambda b}(\kappa_\lambda)$ in the integral on the right side. Also the temperature distribution is needed to determine the absorption coefficient $a_\lambda(S)$ so that the local optical depth $\kappa_\lambda(S)$ can be computed from equation (2-6) and the physical coordinate S thereby related to the optical coordinate κ_λ . The temperature distribution depends on conservation of energy within the medium which in turn depends on the total absorbed radiation in each volume element along the path. This total energy quantity will be obtained in the next section by utilizing the intensity passing through a location and integrating over all incident solid angles and all wavelengths. The energy equation and equation (2-10) yield the necessary relations from which compatible temperature and radiation intensity distributions can be found.

EXAMPLE 2-1: A black surface element dA is 10 cm from an element of gas dV (fig. 2-2). The gas element is a part of a gas volume V that is isothermal and at the same temperature T as dA . If the gas has an absorption coefficient a_λ of 0.1 cm^{-1} at wavelength $1 \mu\text{m}$, what is the spectral intensity at $\lambda = 1 \mu\text{m}$ that arrives at dV along the path S from dA to dV ?

Because element dA is black and at temperature T , the intensity at $S=0$ is $i'_\lambda(0) = i'_{\lambda b}(T)$. Since the gas is isothermal, the emitted blackbody intensity in the gas is $i'_{\lambda b}(\kappa_\lambda) = i'_{\lambda b}(T)$. Substituting into the integrated equation of transfer (eq. (2-10)) gives

$$i'_\lambda(\kappa_\lambda) = i'_{\lambda b}(T) \exp(-\kappa_\lambda) + i'_{\lambda b}(T) \exp(-\kappa_\lambda) \int_0^{\kappa_\lambda} \exp(\kappa_\lambda^*) d\kappa_\lambda^*$$

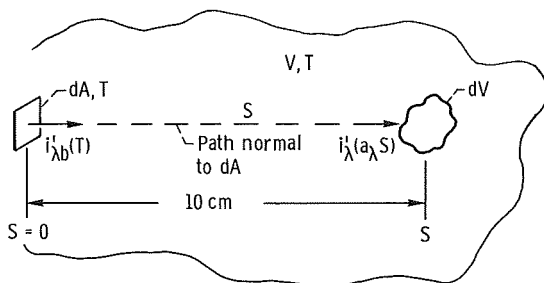


FIGURE 2-2. — Geometry for example 2-1.

After carrying out the integral, this reduces to

$$i'_\lambda(\kappa_\lambda) = i'_{\lambda b}(T)$$

The $i'_{\lambda b}(T)$ is given by equation (2-11a) of volume I for a gas with refractive index $n=1$. The intensity arriving at dV along an isothermal path from a black surface element at the same temperature as the gas is thus equal to the blackbody intensity emitted by the wall and does not depend on a_λ or S . The attenuation by the gas of the intensity emitted by the wall was exactly compensated by emission from the gas along the path from dA to dV .

2.4 ENERGY CONSERVATION WITHIN THE MEDIUM

Equation (2-10) is concerned with the energy at only a single wavelength traveling in only a single direction within the medium. The temperature distribution within the medium is governed by conservation of energy which depends on the energy arriving at a volume element in all wavelength regions and from all incident directions. Since equation (2-10) depends on $i'_{\lambda b}$ which is a function of local temperature, the intensity equation is coupled to the energy conservation equation to obtain the radiation intensity and temperature distributions.

To derive the energy conservation equation consider the energy absorbed by a volume element dV within a medium as shown in figure 2-3. The energy absorbed from the incident intensity $i'_\lambda(\lambda, \omega, \kappa_\lambda)$ that

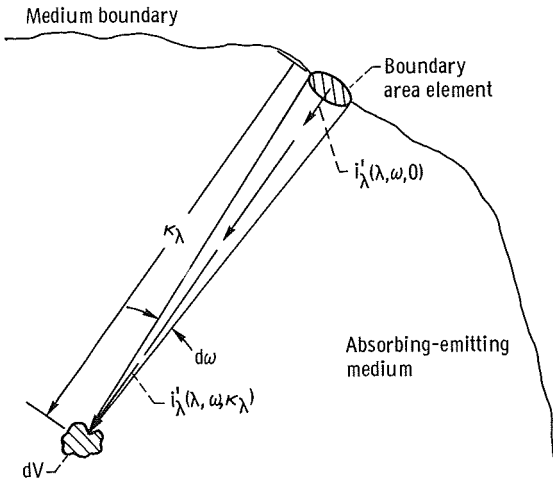


FIGURE 2-3. — Geometry for derivation of energy conservation relation.

arrives within the incremental solid angle $d\omega$ is, by analogy with equation (1-32)

$$d^3Q'_{\lambda, a} = a_\lambda(dV)i'_\lambda(\lambda, \omega, \kappa_\lambda) dV d\lambda d\omega \quad (2-11)$$

The incident intensity $i'_\lambda(\lambda, \omega, \kappa_\lambda)$ is given by the equation of transfer (eq. (2-10)) as

$$i'_\lambda(\lambda, \omega, \kappa_\lambda) = i'_\lambda(\lambda, \omega, 0) \exp(-\kappa_\lambda) + \int_0^{\kappa_\lambda} i'_{\lambda b}(\kappa_\lambda^*) \exp[-(\kappa_\lambda - \kappa_\lambda^*)] d\kappa_\lambda^* \quad (2-12)$$

where $i'_\lambda(\lambda, \omega, 0)$ is the spectral intensity directed toward dV from the system boundary in the direction of $d\omega$.

The energy absorbed ("true" absorption reduced by induced emission) by dV from all incident directions is found by integrating equation (2-11) with respect to ω

$$d^2Q_{\lambda, a} = \int_{\omega=0}^{4\pi} d^3Q'_{\lambda, a} = a_\lambda(dV) dV d\lambda \int_{\omega=0}^{4\pi} i'_\lambda(\lambda, \omega, \kappa_\lambda) d\omega \quad (2-13)$$

For convenience in writing the equations a little more compactly a mean incident intensity $\bar{i}_{\lambda, i}(\lambda)$ can be defined by

$$4\pi\bar{i}_{\lambda, i}(\lambda) \equiv \int_0^{4\pi} i'_\lambda(\lambda, \omega, \kappa_\lambda) d\omega \quad (2-14)$$

Then equation (2-13) becomes

$$d^2Q_{\lambda, a} = 4\pi a_\lambda(dV) \bar{i}_{\lambda, i}(\lambda) dV d\lambda \quad (2-15)$$

By integrating equation (2-15) over all wavelengths, the total energy absorbed by dV from the radiation field is obtained as

$$dQ_a = \int_{\lambda=0}^{\infty} d^2Q_{\lambda, a} = 4\pi dV \int_0^{\infty} a_\lambda(dV) \bar{i}_{\lambda, i}(\lambda) d\lambda \quad (2-16)$$

The total energy emitted spontaneously from dV is obtained by using a_λ in equation (1-34) and integrating over all wavelengths; the result is

$$dQ_e = \int_0^\infty d^2Q_{\lambda, e} = 4dV \int_0^\infty a_\lambda(dV)e_{\lambda b}(\lambda, T)d\lambda \quad (2-17)$$

This equation contains the assumption that dV is so small that all the energy emitted by dV escapes before any can be reabsorbed within dV .

2.4.1 Radiative Equilibrium

For situations when all energy exchange mechanisms such as conduction and convection are negligible compared with radiation and no transients in local temperature are occurring, the total emitted energy from dV is equal to the total absorbed energy. This is termed *radiative equilibrium* and is simply a statement of steady-state energy conservation in absence of any other exchange mechanism but radiation. Using equations (2-16) and (2-17) radiative equilibrium gives

$$dQ_e = dQ_a$$

or

$$\int_0^\infty a_\lambda(\lambda, T, P)e_{\lambda b}(\lambda, T)d\lambda = \pi \int_0^\infty a_\lambda(\lambda, T, P)\bar{i}_{\lambda, i}(\lambda)d\lambda \quad (2-18)$$

2.4.2 Some Mean Absorption Coefficients

As a result of the emission integral on the left of equation (2-18) it is convenient to define the *Planck mean absorption coefficient* $a_P(T, P)$ as

$$a_P(T, P) \equiv \frac{\int_0^\infty a_\lambda(\lambda, T, P)e_{\lambda b}(\lambda, T)d\lambda}{\int_0^\infty e_{\lambda b}(\lambda, T)d\lambda} = \frac{\int_0^\infty a_\lambda(\lambda, T, P)e_{\lambda b}(\lambda, T)d\lambda}{\sigma T^4} \quad (2-19)$$

The a_P is the mean of the spectral coefficient when weighted by the blackbody emission spectrum. It will prove useful when considering *emission* from a volume, and in certain limiting cases of radiative transfer.

Substituting equation (2-19) into equation (2-18) results in energy conservation in the form

$$a_P(T, P)\sigma T^4 = \pi \int_0^\infty a_\lambda(\lambda, T, P)\bar{i}_{\lambda, i}(\lambda)d\lambda \quad (2-20)$$

Thus, if $\bar{i}_{\lambda, i}(\lambda)$ is known at a position within the gas, equation (2-20) can

be solved for T at that location. The Planck mean a_P is convenient since it depends only on the properties at dV . It can be tabulated readily and is especially useful where the pressure is constant over the geometry of the system.

As a result of the absorption integral on the right side of equation (2-20), another type of mean absorption coefficient can be defined. This is the *incident mean* (or *modified Planck mean*) absorption coefficient $a_i(T, P)$ given by

$$a_i(T, P) = \frac{\int_0^\infty a_\lambda(\lambda, T, P) \bar{i}_{\lambda, i}(\lambda) d\lambda}{\int_0^\infty \bar{i}_{\lambda, i}(\lambda) d\lambda} \quad (2-21)$$

However, such a definition for general use has little value. A tabulation of a_i would have to be carried out for all combinations of incident spectral distributions and spectral variations of local absorption coefficients. Except in certain very limited special cases, the work involved in such a tabulation would not be warranted. Further discussion of the physical interpretation of various mean absorption coefficients is given in section 3.5.1.

2.5 EQUATION OF TRANSFER FOR PLANE LAYER

In order to evaluate the influence of some of the many variables in gas radiation problems, it is sometimes convenient to consider a simple geometry. A plane layer is often used and there is a considerable literature for this geometry in both engineering and astrophysical publications. The astrophysical interest (refs. 1 and 2) stems from the fact that the atmosphere of the Earth and the outer radiating layers of the Sun can be approximated as a plane layer.

The plane layer is illustrated in figure 2-4. The temperature and

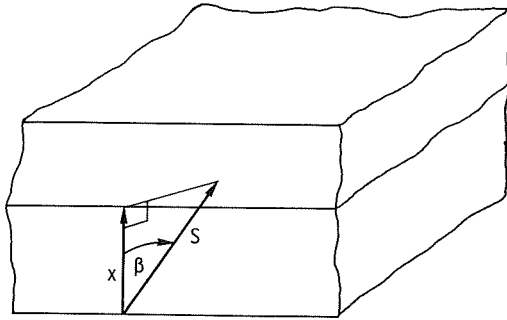


FIGURE 2-4. — Plane layer geometry.

properties of the gas vary only along the x coordinate. An arbitrary path S within the gas is at angle β to the x direction. The optical depth $\kappa(x)$ is now defined *along the x coordinate* as

$$\kappa(x) = \int_0^x adx^* \quad (2-22)$$

The relation between optical positions along the S and x directions is given by

$$\kappa(S) = \int_0^S adS^* = \int_0^{x/\cos\beta} ad\left(\frac{x^*}{\cos\beta}\right) = \frac{1}{\cos\beta} \int_0^x adx^* = \frac{\kappa(x)}{\cos\beta} \quad (2-23)$$

The equation of transfer (eq. (2-7)) is written along any path S and thus the κ in equation (2-7) are $\kappa(S)$. By use of equation (2-23), the transfer equation is written in terms of $\kappa(x)$ as

$$\cos\beta \frac{\partial i'_\lambda}{\partial \kappa_\lambda(x)} + i'_\lambda[\kappa_\lambda(x), \beta] = i'_{\lambda b}[\kappa_\lambda(x)] \quad (2-24)$$

A partial derivative is used to emphasize that i'_λ depends on $\kappa_\lambda(x)$ and β . The equation of transfer in integrated form, equation (2-10), becomes

$$i'_\lambda(\kappa_\lambda, \beta) = i'_\lambda(0) \exp\left(\frac{-\kappa_\lambda}{\cos\beta}\right) + \int_0^{\kappa_\lambda} i'_{\lambda b}(\kappa_\lambda^*) \exp\left[\frac{-(\kappa_\lambda - \kappa_\lambda^*)}{\cos\beta}\right] \frac{d\kappa_\lambda^*}{\cos\beta} \quad (2-25)$$

where all the κ in equation (2-25) are $\kappa(x)$. A convenient substitution that is often used is to let $\mu = \cos\beta$. Then equation (2-25) becomes

$$i'_\lambda(\kappa_\lambda, \mu) = i'_\lambda(0) \exp\left(\frac{-\kappa_\lambda}{\mu}\right) + \int_0^{\kappa_\lambda} i'_{\lambda b}(\kappa_\lambda^*) \exp\left[\frac{-(\kappa_\lambda - \kappa_\lambda^*)}{\mu}\right] \frac{d\kappa_\lambda^*}{\mu} \quad (2-26)$$

2.6 THE GRAY GAS

A gas having an absorption coefficient that is independent of wavelength is called a *gray gas*. From the discussion of gas property spectral

variations such as in connection with figure 1-2, it is evident that gases are usually far from being gray. However, there are some instances when gases may be considered gray over a portion of the spectrum. In other cases such as when particles of soot or other material are present or are injected into a gas to enhance its absorption or emission of radiation, the absorption coefficient of the gas-particle mixture may act as if the mixture were nearly a gray gas. In addition, examination of the radiative behavior of a gray gas provides an understanding of many of the features of a real gas without some of the complicating features that real gas effects introduce. The gray gas is thus of some practical and theoretical interest and has consequently received a great deal of attention in the literature. The equation for local intensity and temperature will now be written for a gray gas.

2.6.1 Transfer Equations

For a gray gas, κ_λ is independent of wavelength and will be called κ for simplicity. Then the local total intensity in the gas can be found by integrating equation (2-10) over all wavelengths to give

$$\int_0^\infty i'_\lambda(\kappa) d\lambda = \exp(-\kappa) \int_0^\infty i'_\lambda(0) d\lambda + \int_0^\kappa \left[\{ \exp[-(\kappa - \kappa^*)] \} \right. \\ \left. \times \int_0^\infty i'_{\lambda b}(\kappa^*) d\lambda \right] d\kappa^* \quad (2-27)$$

Using the definition of total intensity, which is

$$i' = \int_0^\infty i'_\lambda(\lambda) d\lambda$$

results in equation (2-27) becoming

$$i'(\kappa) = i'(0) \exp(-\kappa) + \int_0^\kappa \exp[-(\kappa - \kappa^*)] i'_b(\kappa^*) d\kappa^* \quad (2-28)$$

For a gray gas a_λ is independent of λ and equation (2-19) gives $a_p = a_\lambda$. The condition for radiative equilibrium as given by equation (2-20) reduces to the following equality at any optical depth within the medium:

$$\sigma T^4(\kappa) = \pi \bar{i}_i(\kappa) \quad (2-29)$$

As was defined in equation (2-14), the relation between \bar{i}_i in equation (2-29) and i' in equation (2-28) is an integration over all incident solid

angles,

$$4\pi\bar{i}_i(\kappa) = \int_{\omega=0}^{4\pi} i'(\omega, \kappa) d\omega \quad (2-30)$$

so equation (2-29) becomes

$$\sigma T^4(\kappa) = \frac{1}{4} \int_{\omega=0}^{4\pi} i'(\omega, \kappa) d\omega \quad (2-31)$$

Equations (2-28) and (2-31) give a set of relations coupling $i'(\kappa)$ and $T(\kappa)$ that may be used to determine the temperature distribution within the gas when boundary conditions are prescribed. The boundary conditions are needed to supply $i'(0)$ in equation (2-28) for each path. In the following section the relations given here will be applied to a plane layer of gray gas between infinite parallel black plates.

2.6.2 Plane Layer Between Black Plates

Consider two black infinite parallel plates that are separated by a gray gas with absorption coefficient $a(T, P)$. The gas is in radiative equilibrium. As shown in figure 2-5, the lower plate is at temperature

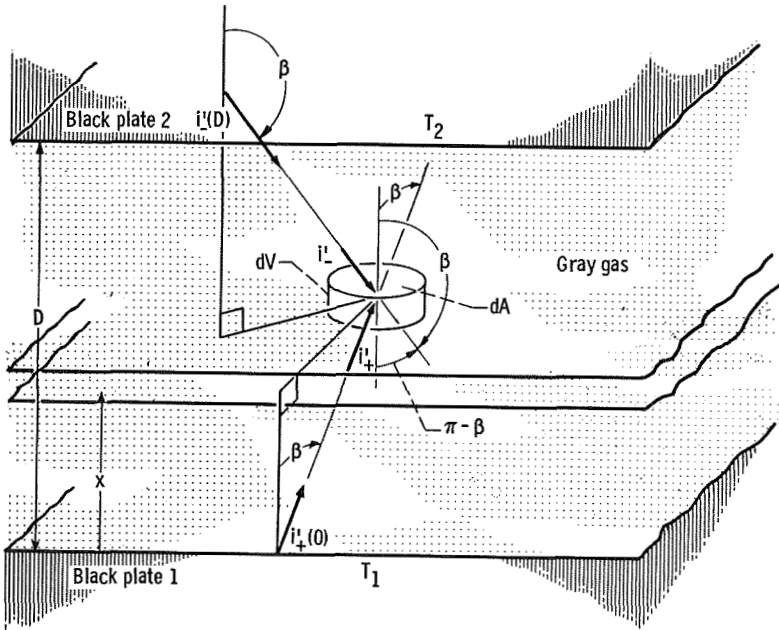


FIGURE 2-5. — Geometry for finding distribution of temperature in gray gas.

T_1 , and the upper plate is at T_2 . The plates are separated by a distance D . It is desired to obtain expressions for the temperature distribution in the gas and the energy transfer between the plates.

Since the geometry is a plane layer, all the κ in what follows are $\kappa(x)$ as defined in equation (2-22). The temperature distribution is found from equation (2-31). The integration of i' over ω is conveniently expressed in two parts for intensities i'_+ approaching dV from directions with positive $\cos \beta$ (from plate 1 in this case, $0 \leq \beta \leq 90^\circ$) and i'_- approaching from negative $\cos \beta$ directions (from plate 2 in this case, $90^\circ \leq \beta \leq 180^\circ$). These intensities are shown in figure 2-5 and it is noted that β is measured from the positive x direction. Then equation (2-31) can be written as

$$\sigma T^4(\kappa) = \frac{1}{4} \int_{\Delta} i'_+(\omega, \kappa) d\omega + \frac{1}{4} \int_{\square} i'_-(\omega, \kappa) d\omega \quad (2-32)$$

where the notation $\int_{\Delta} d\omega$ denotes integration over all solid angles in the hemisphere in directions from surface 1 and $\int_{\square} d\omega$ denotes integration over the hemisphere in directions from surface 2.

The intensities in equation (2-32) are obtained from equation (2-25). This gives for radiation traveling from wall 1 at angle β and in the direction of positive $\cos \beta$

$$i'_+(\kappa) = i'_+(0) \exp\left(\frac{-\kappa}{\cos \beta}\right) + \int_0^{\kappa} i'_b(\kappa^*) \exp\left[\frac{-(\kappa - \kappa^*)}{\cos \beta}\right] \frac{d\kappa^*}{\cos \beta} \quad (2-33)$$

The $i'_+(0)$ is the total intensity leaving wall 1; and since wall 1 is black,

$$i'_+(0) = \frac{\sigma T_1^4}{\pi}$$

The total intensity under the integral is related to the local gas temperature by

$$i'_b(\kappa^*) = \frac{\sigma T^4(\kappa^*)}{\pi}$$

Substituting this into equation (2-33) gives

$$i'_+(\kappa) = \frac{1}{\pi} \left\{ \sigma T_1^4 \exp\left(\frac{-\kappa}{\cos \beta}\right) + \frac{\sigma}{\cos \beta} \int_0^{\kappa} T^4(\kappa^*) \exp\left[\frac{-(\kappa - \kappa^*)}{\cos \beta}\right] d\kappa^* \right\} \quad (2-34)$$

where $0 \leq \beta \leq 90^\circ$. By a similar analysis, the intensity at angle β ($90^\circ \leq \beta \leq 180^\circ$) reaching optical depth κ from the direction of plate 2 is (note that $\cos \beta$ is negative in this range)

$$i'_-(\kappa) = \frac{1}{\pi} \left[\sigma T_{\frac{1}{2}} \exp \left(\frac{\kappa_D - \kappa}{\cos \beta} \right) - \frac{\sigma}{\cos \beta} \int_{\kappa}^{\kappa_D} T^4(\kappa^*) \exp \left(\frac{\kappa^* - \kappa}{\cos \beta} \right) d\kappa^* \right] \quad (2-35)$$

where $\kappa_D = \int_0^D a(x) dx$.

The intensities in equations (2-34) and (2-35) are substituted into equation (2-32) to yield the following integral equation for $T^4(\kappa)$:

$$\begin{aligned} T^4(\kappa) = & \frac{1}{2} \int_0^{\pi/2} \sin \beta \left\{ T_1^4 \exp \left(\frac{-\kappa}{\cos \beta} \right) \right. \\ & + \frac{1}{\cos \beta} \int_0^{\kappa} T^4(\kappa^*) \exp \left[\frac{-(\kappa - \kappa^*)}{\cos \beta} \right] d\kappa^* + T_{\frac{1}{2}} \exp \left[\frac{-(\kappa_D - \kappa)}{\cos \beta} \right] \\ & \left. + \frac{1}{\cos \beta} \int_{\kappa}^{\kappa_D} T^4(\kappa^*) \exp \left[\frac{-(\kappa^* - \kappa)}{\cos \beta} \right] d\kappa^* \right\} d\beta \quad (2-36) \end{aligned}$$

where the substitution $d\omega = 2\pi \sin \beta d\beta$ has also been made. Solutions giving the temperature distribution will be discussed later.

The radiative energy flux in the positive x direction crossing the plane at x in figure 2-5 is found in two parts, one from the i'_+ and one from the i'_- . Since intensity represents energy crossing an area normal to the direction of i' , the projection of the area dA must be considered normal to either i'_+ or i'_- . The flux in the positive x direction from the i'_+ is

$$q_+(\kappa) = \int_{\beta=0}^{\pi/2} i'_+(\kappa) \cos \beta 2\pi \sin \beta d\beta \quad (2-37a)$$

The flux in the negative x direction from the i'_- is

$$\begin{aligned} q_-(\kappa) &= \int_{\pi-\beta=0}^{\pi-\beta=\pi/2} i'_-(\kappa) \cos(\pi-\beta) 2\pi \sin(\pi-\beta) d(\pi-\beta) \\ q_-(\kappa) &= -2\pi \int_{\beta=\pi/2}^{\pi} i'_-(\kappa) \cos \beta \sin \beta d\beta \quad (2-37b) \end{aligned}$$

The net flux in the positive x direction is

$$q(\kappa) = q_+(\kappa) - q_-(\kappa) \quad (2-38)$$

Substituting equations (2-37) into equation (2-38) gives

$$q(\kappa) = 2\pi \left[\int_{\beta=0}^{\pi/2} i'_+(\kappa) \cos \beta \sin \beta \, d\beta + \int_{\pi/2}^{\pi} i'_-(\kappa) \cos \beta \sin \beta \, d\beta \right] \quad (2-39)$$

The intensities from equations (2-34) and (2-35) are substituted into equation (2-39) and the integrals combined to yield

$$\begin{aligned} q(\kappa) = & 2 \int_0^{\pi/2} \sin \beta \cos \beta \left\{ \sigma T_1^4 \exp\left(\frac{-\kappa}{\cos \beta}\right) \right. \\ & + \frac{\sigma}{\cos \beta} \int_0^{\kappa} T^4(\kappa^*) \exp\left[\frac{-(\kappa - \kappa^*)}{\cos \beta}\right] d\kappa^* - \sigma T_2^4 \exp\left[\frac{-(\kappa_D - \kappa)}{\cos \beta}\right] \\ & \left. - \frac{\sigma}{\cos \beta} \int_{\kappa}^{\kappa_D} T^4(\kappa^*) \exp\left[\frac{-(\kappa^* - \kappa)}{\cos \beta}\right] d\kappa^* \right\} d\beta \end{aligned} \quad (2-40)$$

For energy transfer only by radiation (radiative equilibrium) in the geometry being considered here, $q(\kappa)$ must be independent of κ because there are no energy sources or sinks in the gas. Evaluating q at the convenient location $\kappa=0$ then gives the heat flux flowing from wall 1 to wall 2,

$$\begin{aligned} q = & 2 \int_0^{\pi/2} \sin \beta \cos \beta \left[\sigma T_1^4 - \sigma T_2^4 \exp\left(\frac{-\kappa_D}{\cos \beta}\right) \right. \\ & \left. - \frac{\sigma}{\cos \beta} \int_0^{\kappa_D} T^4(\kappa^*) \exp\left(\frac{-\kappa^*}{\cos \beta}\right) d\kappa^* \right] d\beta \\ = & \sigma T_1^4 - 2 \int_0^{\pi/2} \sin \beta \cos \beta \left[\sigma T_2^4 \exp\left(\frac{-\kappa_D}{\cos \beta}\right) \right. \\ & \left. + \frac{\sigma}{\cos \beta} \int_0^{\kappa_D} T^4(\kappa^*) \exp\left(\frac{-\kappa^*}{\cos \beta}\right) d\kappa^* \right] d\beta \end{aligned} \quad (2-41)$$

This can be evaluated after $T^4(\kappa)$ is found from equation (2-36).

For the limiting case as the absorption of the medium between the plates becomes very small $\kappa_D \rightarrow 0$, equation (2-41) reduces to

$$q|_{\kappa_D \rightarrow 0} = \sigma(T_1^4 - T_2^4)$$

which is the correct solution for black infinite parallel plates separated by a transparent medium. In addition for this limit equation (2-36) yields

$$T^4(\kappa) \Big|_{\kappa \rightarrow 0} = \frac{T_1^4 + T_2^4}{2}$$

so that a nearly transparent gray medium approaches a temperature to the fourth power equal to the average of fourth powers of the boundary temperatures.

Solutions for the temperature distribution in a gray gas with temperature-independent properties contained between infinite parallel plates have been obtained by many researchers. Some of the solution methods will be discussed in succeeding chapters. Heaslet and Warming (ref. 3) have presented solutions accurate to four significant figures for the quantities $[T^4(\kappa) - T_2^4]/(T_1^4 - T_2^4)$ and $q/[\sigma(T_1^4 - T_2^4)]$. Their results for the black boundary case are shown in figure 2-6.

The temperature distributions of figure 2-6(a) show that a discontinuity exists between the wall temperature and the gas temperature at the wall. This phenomenon is called the temperature "slip" or "jump." If the slip were not present, the curves would all go to 1 at $\kappa/\kappa_D = 0$ and 0 at $\kappa/\kappa_D = 1$. The slip disappears when heat conduction is included in the analysis. To determine the magnitude of the slip, the gas temperature is evaluated at $\kappa = 0$. This gives by using equation (2-36)

$$T^4(\kappa=0) = \frac{1}{2} \int_0^{\pi/2} \sin \beta \left[T_1^4 + T_2^4 \exp\left(\frac{-\kappa_D}{\cos \beta}\right) + \frac{1}{\cos \beta} \int_0^{\kappa_D} T^4(\kappa^*) \exp\left(\frac{-\kappa^*}{\cos \beta}\right) d\kappa^* \right] d\beta$$

which can be written as

$$\frac{T_1^4 - T^4(\kappa=0)}{T_1^4 - T_2^4} = \frac{T_1^4}{2(T_1^4 - T_2^4)} - \frac{1}{2} \int_0^{\pi/2} \sin \beta \left[\frac{T_2^4}{T_1^4 - T_2^4} \exp\left(\frac{-\kappa_D}{\cos \beta}\right) - \frac{1}{\cos \beta} \int_0^{\kappa_D} \frac{T^4(\kappa^*)}{T_1^4 - T_2^4} \exp\left(\frac{-\kappa^*}{\cos \beta}\right) d\kappa^* \right] d\beta \quad (2-42)$$

Again it is seen that as κ_D approaches zero, equation (2-42) reduces to

$$\frac{T_1^4 - T^4(\kappa=0)}{T_1^4 - T_2^4} \Big|_{\kappa_D \rightarrow 0} = \frac{1}{2}$$

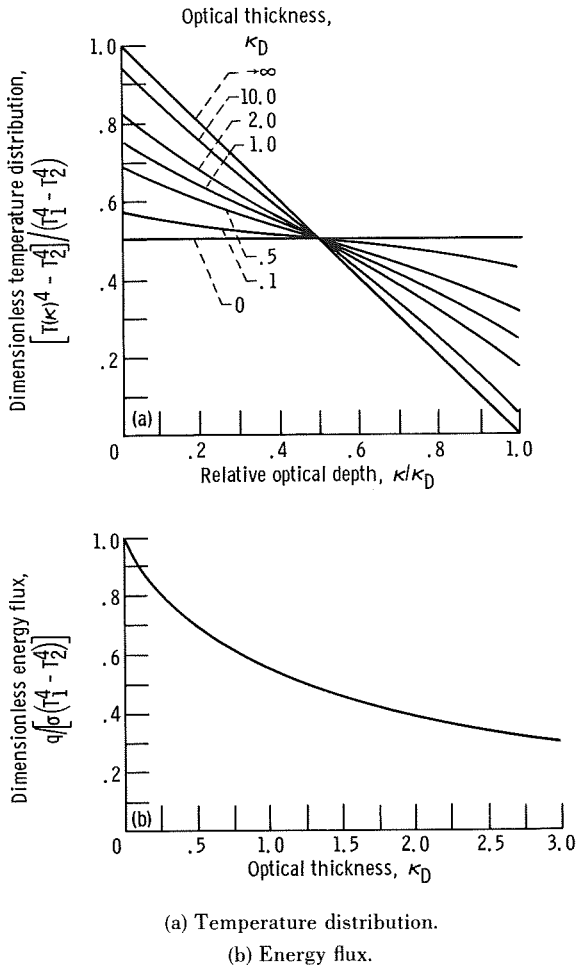


FIGURE 2-6.—Temperature distribution and energy flux in gray gas contained between infinite black parallel plates (ref. 3).

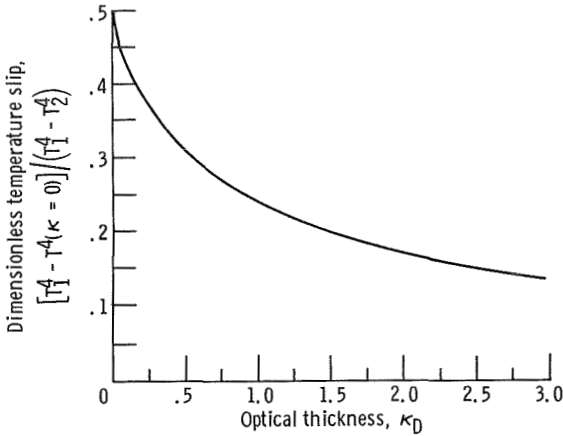


FIGURE 2-7.—Discontinuity at wall between gray gas and black wall temperatures (ref. 3).

The magnitude of the slip for a gray gas with constant absorption coefficient is shown in figure 2-7 as a function of the optical thickness of the layer. (Note that from symmetry $T_1^4 - T^4(\kappa = 0) = T^4(\kappa = \kappa_D) - T_2^4$.)

2.6.3 Use of Exponential Integral Functions

There are some mathematical substitutions that are useful in dealing with the results derived from the equation of transfer for plane layers. By letting $\mu = \cos \beta$, equations (2-36) and (2-41) become

$$\begin{aligned}
 T^4(\kappa) = & \frac{1}{2} \int_0^1 \left\{ T_1^4 \exp\left(\frac{-\kappa}{\mu}\right) \right. \\
 & + \frac{1}{\mu} \int_0^\kappa T^4(\kappa^*) \exp\left[\frac{-(\kappa - \kappa^*)}{\mu}\right] d\kappa^* + T_2^4 \exp\left[\frac{-(\kappa_D - \kappa)}{\mu}\right] \\
 & \left. + \frac{1}{\mu} \int_\kappa^{\kappa_D} T^4(\kappa^*) \exp\left[\frac{-(\kappa^* - \kappa)}{\mu}\right] d\kappa^* \right\} d\mu \quad (2-43)
 \end{aligned}$$

$$\begin{aligned}
 q = \sigma T_1^4 - 2 \int_0^1 \mu \left[\sigma T_2^4 \exp\left(\frac{-\kappa_D}{\mu}\right) \right. \\
 \left. + \frac{\sigma}{\mu} \int_0^{\kappa_D} T^4(\kappa^*) \exp\left(\frac{-\kappa^*}{\mu}\right) d\kappa^* \right] d\mu \quad (2-44)
 \end{aligned}$$

The exponential integral function can now be introduced. This function is defined as

$$E_n(\xi) = \int_0^1 \mu^{n-2} \exp\left(\frac{-\xi}{\mu}\right) d\mu \quad (2-45)$$

Then equation (2-43) can be written as

$$T^4(\kappa) = \frac{1}{2} \left[T_1^4 E_2(\kappa) + \int_0^\kappa T^4(\kappa^*) E_1(\kappa - \kappa^*) d\kappa^* \right. \\ \left. + T_2^4 E_2(\kappa_D - \kappa) + \int_\kappa^{\kappa_D} T^4(\kappa^*) E_1(\kappa^* - \kappa) d\kappa^* \right] \quad (2-46)$$

and equation (2-44) becomes

$$q = \sigma T_1^4 - 2 \left[\sigma T_2^4 E_3(\kappa_D) + \sigma \int_0^{\kappa_D} T^4(\kappa^*) E_2(\kappa^*) d\kappa^* \right] \quad (2-47)$$

The exponential integral functions are discussed in detail by Kourganoff (ref. 1) and Chandrasekhar (ref. 2). For convenient use by the reader some of the important relations are given in the appendix.

2.7 ENERGY RELATIONS BY USE OF PHOTON MODEL

The radiation field and transfer of radiation in a medium can also be expressed in terms of a photon model. This is sometimes helpful in providing a physical picture of the transport and is also useful in Monte Carlo methods as will be considered in chapter 6. Since photon energy is related to the frequency of the radiation, frequency will be used in this section rather than wavelength.

When considering the radiation as a collection of photons the conditions at any location in the medium are given by the photon distribution function f . Let

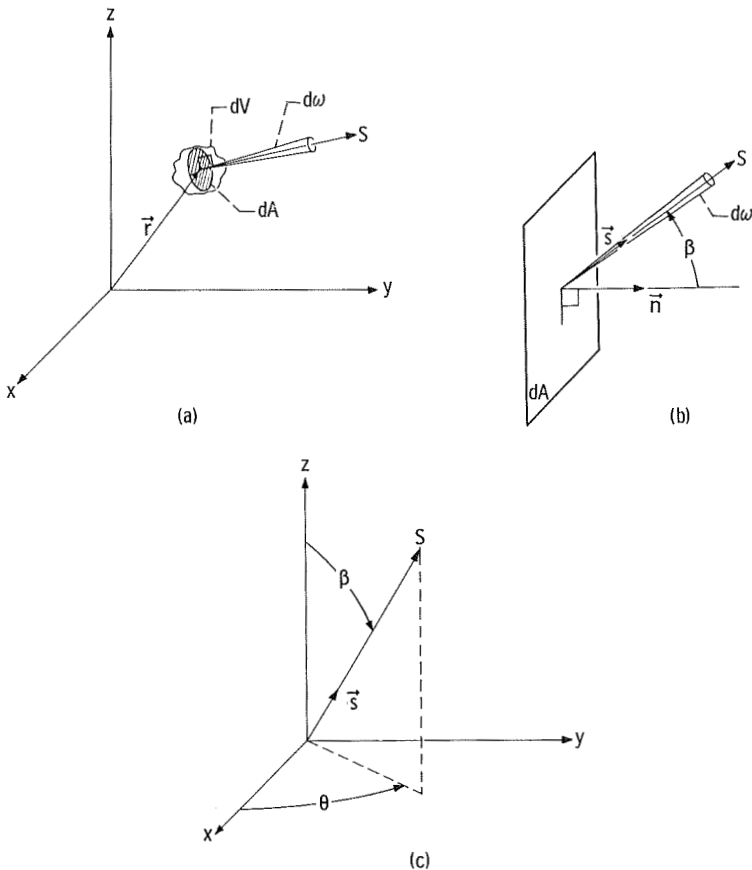
$$f(\nu, \vec{r}, S) d\nu dV d\omega \quad (2-48)$$

be the number of photons traveling in direction S in frequency interval $d\nu$ centered about ν , in volume dV at position \vec{r} , and within solid angle $d\omega$ about the direction S (see fig. 2-8(a)). Each photon has energy $h\nu$. The energy per unit volume per unit frequency interval is then $h\nu f d\omega$ integrated over all solid angles. This is called the spectral radiant energy density

$$U_\nu(\nu, \vec{r}) = h\nu \int_{\omega=0}^{4\pi} f(\nu, \vec{r}, S) d\omega \quad (2-49)$$

To obtain the intensity, the energy flux in the S direction is needed across the area dA in figure 2-8(a) which is normal to the S direction. The photons have velocity c , and the particle density traveling in the normal direction across dA is $fdv d\omega$. The number of particles crossing dA per unit time is then $cf dv d\omega dA$. The energy carried by these particles is $h\nu cf dv d\omega dA$. The spectral intensity is the energy per unit time, unit frequency interval, and unit solid angle crossing a unit area normal to the direction of the intensity. This gives the intensity at location \vec{r} and in direction S as

$$i'_\nu = h\nu c f(\nu, \vec{r}, S) \quad (2-50)$$



(a) Quantities in intensity derivation.

(b) Quantities in flux derivation.

(c) Spherical coordinate system for radiative flux vector.

FIGURE 2-8.—Geometries used in derivations of radiative energy quantities.

The energy density and the intensity can then be related by using equation (2-50) to eliminate f from equation (2-49), that is,

$$U_\nu(\nu, \bar{r}) = \frac{1}{c} \int_{\omega=0}^{4\pi} i'_\nu d\omega \quad (2-51)$$

This integral was encountered in equation (2-31).

Now consider the energy flux crossing an area within a medium. As shown in figure 2-8(b) let dA be an arbitrary element whose unit normal vector is \bar{n} . Energy passes through dA from all directions; a typical direction is the S direction at angle β to \bar{n} . This energy is given by $h\nu c f d\nu d\omega dA \cos \beta$. To obtain the net energy flux crossing dA integrate over all incident solid angles. The energy per unit of dA moving across dA in the direction of increasing \bar{n} is then (note that $\cos \beta$ becomes negative for $\beta > \pi/2$ so that the sign of the portion of the energy flux traveling in the direction opposite to the positive \bar{n} direction is automatically included)

$$dq_\nu = h\nu c d\nu \int_{\omega=0}^{4\pi} f \cos \beta d\omega = d\nu \int_{\omega=0}^{4\pi} i'_\nu \cos \beta d\omega \quad (2-52)$$

The latter form of equation (2-52) was obtained by use of equation (2-50).

Let \bar{s} be a unit vector in the direction S of the photons. Then $\cos \beta = \bar{s} \cdot \bar{n}$ and equation (2-52) can be written as

$$dq_\nu = d\nu \int_{\omega=0}^{4\pi} i'_\nu \bar{s} \cdot \bar{n} d\omega \quad (2-53)$$

Thus dq_ν is the component in the \bar{n} direction of a flux vector given by

$$d\vec{q}_\nu = d\nu \int_{\omega=0}^{4\pi} i'_\nu \bar{s} d\omega \quad (2-54)$$

that is, $dq_\nu = \bar{n} \cdot d\vec{q}_\nu$.

To further reveal the vector nature of $d\vec{q}_\nu$, consider a spherical coordinate system as shown in figure 2-8(c). The unit vector \bar{s} can then be written as

$$\bar{s} = \bar{i} \cos \theta \sin \beta + \bar{j} \sin \theta \sin \beta + \bar{k} \cos \beta \quad (2-55)$$

Substituting \bar{s} and $d\omega = \sin \beta d\beta d\theta$ into equation (2-54) gives the vector $d\vec{q}_\nu$ in terms of its three components,

$$\begin{aligned}
 d\vec{q}_v = d\nu \vec{i} \left[\int_{\theta=0}^{2\pi} \int_{\beta=0}^{\pi} i'_v(\beta, \theta) \cos \theta \sin^2 \beta \, d\beta d\theta \right. \\
 + \vec{j} \int_{\theta=0}^{2\pi} \int_{\beta=0}^{\pi} i'_v(\beta, \theta) \sin \theta \sin^2 \beta \, d\beta d\theta \\
 \left. + \vec{k} \int_{\theta=0}^{2\pi} \int_{\beta=0}^{\pi} i'_v(\beta, \theta) \cos \beta \sin \beta \, d\beta d\theta \right] \quad (2-56)
 \end{aligned}$$

2.8 CONCLUDING REMARKS

The equation of transfer has been derived which gives the variation of intensity for radiation traveling in a fixed direction through an absorbing-emitting medium. The equation expresses how the intensity is attenuated by absorption and strengthened by emission; scattering has been neglected. The equation of transfer was integrated so that the intensity can be found along a path if an initial intensity is known; the initial intensity would usually be that leaving a boundary. Since the intensity involves the emission along a path, and the emission depends on temperature, the temperature distribution in the gas is required to evaluate the intensity solution.

The gas temperature distribution is found from the energy conservation equation. The energy terms are obtained from the total radiation fluxes which are found by integrating the energy carried by spectral intensities over wavelength and direction. Thus the solution of the equation of transfer is coupled to the energy equation and it was found that the temperature distribution is governed by an integral equation.

Chapter 3 will consider in detail various approximate solutions that have been obtained by use of the equation of transfer.

REFERENCES

1. KOURGANOFF, VLADIMIR: *Basic Methods in Transfer Problems*. Dover Publications, Inc., 1963.
2. CHANDRASEKHAR, SUBRAHMANYAN: *Radiative Transfer*. Dover Publications, Inc., 1960.
3. HEASLET, MAX A.; AND WARMING, ROBERT F.: *Radiative Transport and Wall Temperature Slip in an Absorbing Planar Medium*. *Int. J. Heat Mass Transfer*, vol. 8, July 1965, pp. 979-994.

Chapter 3. Approximate Solutions of the Equation of Transfer

3.1 INTRODUCTION

Exact solutions to the radiative transfer equations to yield temperature distributions and heat flows in an absorbing-emitting medium require considerable effort in most practical cases. Two approaches can be taken to circumvent this complexity. In the first, the equation of transfer may be simplified either by neglecting one or more terms when justified or by transforming it into a diffusion equation. In the second, the complete equation of transfer is used but approximate solutions are obtained to it.

The equation of transfer was derived and integrated in chapter 2 to give the variation of intensity along a direction of propagation in an absorbing-emitting medium. The assumptions used in chapter 2, that will also be retained here, are that there is no scattering, no heat conduction or convection, and that the gas is in local thermodynamic equilibrium. The expression for the spectral intensity was given by equation (2-10). This showed that the intensity along a path depends on the intensity at the origin of the path, for example at a boundary, and on the temperature distribution along the path.

There are three approximate solution methods that involve neglecting terms in the transfer equation: the transparent, emission, and cold medium approximations. They are summarized in table 3-I and will be treated in section 3.3 of this chapter.

The last approximation in table 3-I is the diffusion approximation. This is not obtained by neglecting a term in the equation of transfer, but rather is derived by transforming the integral equations for the radiative energy balance into a diffusion equation. The details of the derivation, the approximations that are involved, and the solution of the resulting diffusion equation form the second main portion of the chapter, section 3.4.

The remainder of the chapter will deal with approximate solutions of the complete equation of transfer. These are methods such as the Milne-Eddington approximation and the differential approximation.

TABLE 3-I.—APPROXIMATIONS TO EQUATION OF TRANSFER

Approximation	Form of equation of transfer	Conditions
Strong transparent	$i'_\lambda(S) = i'_\lambda(0)$	The medium has such a low absorption coefficient that an intensity does not change by absorption or emission while traveling within the medium.
Emission	$i'_\lambda(S) = \int_0^S a_\lambda(S^*) i'_{\lambda b}(S^*) dS^*$	No energy is incident from the boundaries, and the gas is relatively transparent so that emitted energy from the gas passes within the system without significant attenuation.
Cold medium	$i'_\lambda(S) = i'_\lambda(0) \exp \left[- \int_0^S a_\lambda(S^*) dS^* \right]$	Emitted radiation from medium is negligible compared to that incident from boundaries or external sources.
Diffusion	$-\frac{4\pi}{3a_\lambda} \frac{\partial i'_{\lambda b}}{\partial S} = q_\lambda(S)$	The optical depth of the gas is sufficiently large, and the temperature gradients sufficiently small so that the local intensity results only from local emission.

3.2 SYMBOLS

A	area
A_i^n	coefficients in eq. (3-105)
a	absorption coefficient
C_1, C_2	constants in Planck's spectral energy distribution
D	spacing between parallel planes, or diameter
E	ratio, $(1 - \epsilon)/\epsilon$
e	emissive power
G	volumetric energy generation rate
H	length over which temperature changes significantly
I	mean absorption value defined by eq. (3-50)
i	radiation intensity

l_j, l_k	direction cosines
l_m	absorption mean free path, $1/a_\lambda$
P	pressure
P_l^m	spherical harmonics, eq. (3-107)
Q	energy per unit time
q	energy flux, energy per unit area and time
R	sphere radius
r	radial coordinate
\vec{r}	position vector
S	coordinate along path of radiation
\vec{s}	unit vector in S direction
T	absolute temperature
V	volume
x, y, z x_1, x_2, x_3 }	distances measured along Cartesian coordinates
Y_l^m	functions of angle in eq. (3-105)
β	cone angle, angle from normal of area
Γ	Gamma function
δ_{kj}	Kronecker delta
ϵ	hemispherical emissivity
θ	circumferential angle in fig. 3-3(b)
κ	optical depth
κ_D	optical thickness for path length D
λ	wavelength
σ	Stefan-Boltzmann constant
φ	temperature ratio, tables 3-II and 3-III
ψ	dimensionless heat flux, tables 3-II and 3-III
Ω	function defined by eq. (3-34)
ω	solid angle

Subscripts:

b	blackbody
D	mean absorption coefficient in eq. (3-49)
e	emitted
$g-g$	evaluated at interface between gas regions 1 and 2
i	incident
P	Planck mean value
R	Rosseland mean value in eq. (3-39)
r	net value in r direction
s	sphere
w	evaluated on the wall
z	net value in the z direction
$+z, -z$	propagating in positive or negative z direction, respectively

λ	spectrally dependent
$\Delta\lambda$	value integrated over wavelength interval $\Delta\lambda$
0	evaluated at point of origin, initial value
1, 2	boundary 1 or 2, respectively, or region 1 or 2, respectively
+, -	propagating in positive or negative direction
Superscripts:	
'	directional quantity
*, **	dummy variable of integration
-	average over all incident solid angles
(0), (1), (2)	zeroth-, first-, or second-order term or moment

3.3 APPROXIMATE SOLUTIONS BY NEGLECTING TERMS IN THE EQUATION OF TRANSFER

In chapter 2 the equation of transfer was integrated to give the intensity variation along the optical path κ (eq. (2-10)). For use in the present discussion this equation is repeated here in terms of the actual distance S along the path

$$i'_\lambda(S) = i'_\lambda(0) \exp \left[- \int_0^S a_\lambda(S^*) dS^* \right] + \int_0^S a_\lambda(S^*) i'_{\lambda b}(S^*) \exp \left[- \int_{S^*}^S a_\lambda(S^{**}) dS^{**} \right] dS^* \quad (3-1)$$

The intensity $i'_\lambda(S)$ as given by equation (3-1) depends on the intensity $i'_\lambda(0)$ leaving the boundary at $S=0$, and on the temperature distribution since the local temperature governs the variation of $i'_{\lambda b}$ and a_λ . As given by equation (2-20), the energy conservation equation needed to obtain the temperature distribution involves an integration of incident intensities from all solid angles. This results in a coupling of the energy conservation and transfer equations which can become quite complex. It is often possible to use some approximations that provide considerable simplification. Three of these approximations as summarized by the first three entries in table 3-I will now be discussed.

3.3.1 The Transparent Gas Approximation

When the optical depth along a path in the gas is small, the integrated form of the equation of transfer can be simplified as the two exponential attenuation terms in equation (3-1) each approach unity. The intensity equation (3-1) then reduces to

$$i'_\lambda(S) = i'_\lambda(0) + \int_0^S a_\lambda(S^*) i'_{\lambda b}(S^*) dS^* \quad (3-2)$$

There is no attenuation along the path of either the energy emitted in the gas or the energy that enters at $S=0$. In some instances, an even stronger assumption can be made. If the absorption coefficient is sufficiently small and the $i'_\lambda(0)$ is finite, the emission from the gas as given by the integral in equation (3-2) becomes negligible compared with the intensity at $S=0$ and equation (3-2) reduces simply to

$$i'_\lambda(S) = i'_\lambda(0) \quad (3-3)$$

This is the strong transparent approximation listed in table 3-I. An incident intensity is thus essentially unchanged as it travels through the gas. The local energy balances based on this simple intensity relation are obviously much easier to carry out than those involving the complete equation of transfer. The use of the strong transparent approximation will now be demonstrated.

EXAMPLE 3-1: Two infinite parallel black plates at temperatures T_1 and T_2 as in figure 2-5 are separated by a small distance D , and the space between them filled with a gas of absorption coefficient a_λ . Assuming that the strong transparent approximation holds, derive an expression for the gas temperature as a function of position between the plates. It is assumed the gas is in local thermodynamic equilibrium although this assumption can sometimes break down in a thin gas as mentioned in section 1.8.

Equation (2-20) is the general expression for local radiative equilibrium in the gas. For the present case, it gives

$$a_P(T, P) \sigma T^4 = \pi \int_0^\infty a_\lambda(\lambda, T, P) \bar{i}_{\lambda, i}(\lambda) d\lambda \quad (3-4)$$

As in equation (2-32) and from the definition (eq. (2-30)), $\bar{i}_{\lambda, i}$ is given by the contributions approaching a volume element from above and below, that is,

$$4\pi \bar{i}_{\lambda, i}(\lambda) = \int_0^{4\pi} i'_\lambda(\lambda, \omega) d\omega = \int_{\square} i'_{\lambda+}(\lambda, \omega) d\omega + \int_{\square} i'_{\lambda-}(\lambda, \omega) d\omega \quad (3-5)$$

Since the walls are black, the strong transparent approximation gives

$$i'_{\lambda+}(\lambda, \omega) = i'_{\lambda b}(\lambda, T_1)$$

and

$$i'_{\lambda-}(\lambda, \omega) = i'_{\lambda b}(\lambda, T_2)$$

Then since the black intensity is independent of angle, equation (3-5) gives

$$\begin{aligned} 4\pi \bar{i}_{\lambda, i}(\lambda) &= 2\pi i'_{\lambda b}(\lambda, T_1) \int_0^{\pi/2} \sin \beta \, d\beta + 2\pi i'_{\lambda b}(\lambda, T_2) \int_0^{\pi/2} \sin \beta \, d\beta \\ &= 2\pi [i'_{\lambda b}(\lambda, T_1) + i'_{\lambda b}(\lambda, T_2)] \end{aligned} \quad (3-6)$$

Substituting equation (3-6) into equation (3-4) gives at any x position between the plates

$$\sigma T^4(x) = \frac{\pi}{2a_p(x)} \int_0^\infty a_\lambda(\lambda, x) [i'_{\lambda b}(\lambda, T_1) + i'_{\lambda b}(\lambda, T_2)] d\lambda \quad (3-7)$$

Equation (3-7) can be solved iteratively for $T(x)$. The necessity for an iterative solution arises because a_λ depends on local temperature.

If a_λ does not depend on gas temperature, then using equation (2-19) results in

$$\begin{aligned} \int_0^\infty a_\lambda(\lambda) i'_{\lambda b}(\lambda, T_1) d\lambda &= \frac{a_p(T_1) \sigma T_1^4}{\pi} \\ \int_0^\infty a_\lambda(\lambda) i'_{\lambda b}(\lambda, T_2) d\lambda &= \frac{a_p(T_2) \sigma T_2^4}{\pi} \end{aligned}$$

and

$$a_p[T(x)] = \frac{\int_0^\infty a_\lambda(\lambda) e_{\lambda b}[T(x)] d\lambda}{\sigma T^4(x)}$$

Then equation (3-7) reduces to

$$T^4(x) = \frac{1}{2a_p[T(x)]} [a_p(T_1) T_1^4 + a_p(T_2) T_2^4] \quad (3-8)$$

The local temperature solution, although still requiring an iterative solution on $T(x)$ and $a_p[T(x)]$, is relatively easily found by use of tabulated values of $a_p(T)$. Note further that for a gray gas with temperature-independent properties, a_p is a constant and equation (3-8) reduces still further to

$$T^4(x) = \frac{T_1^4 + T_2^4}{2} \quad (3-9)$$

Hence, the entire gas approaches a fourth-power temperature that is the average of the fourth powers of the boundary temperatures. This limit was also found in section 2.6.2 following equation (2-41).

3.3.2 The Emission Approximation

In the strong transparent approximation, the gas was optically thin and the local intensity was dominated by the intensity incident at the gas boundary. In the emission approximation the gas is again optically thin but there is also negligible incoming energy at the gas boundary from external sources. For these conditions, in equation (3-1) the exponential attenuation terms both become unity as a_λ is small, and $i'_\lambda(0)$ is zero. This gives

$$i'_\lambda(S) = \int_0^S a_\lambda(S^*) i'_{\lambda b}(S^*) dS^* \quad (3-10)$$

Thus the only important term is the emission which is of order $a_\lambda i'_{\lambda b}$. Reabsorption of emitted energy along a path is of order $a_\lambda (a_\lambda i'_{\lambda b})$ and is negligible because a_λ is very small. The intensity $i'_\lambda(S)$ in equation (3-10) is consequently the integrated contribution of all the emission along a path as the emitted energy travels through the gas without attenuation.

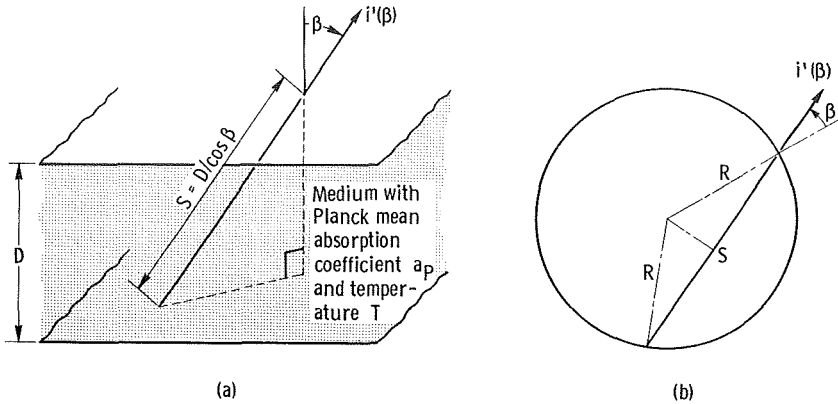
Equation (3-10) can be integrated over all wavelengths to give the total intensity

$$i'(S) = \int_0^\infty i'_\lambda(S) d\lambda = \int_0^S \left[\int_0^\infty a_\lambda(S^*) i'_{\lambda b}(S^*) d\lambda \right] dS^*$$

The definition of a_P (eq. (2-19)) is now applied to give

$$i'(S) = \int_0^S a_P(S^*) \frac{\sigma T^4(S^*)}{\pi} dS^* \quad (3-11)$$

The fact that equation (3-11) contains the Planck mean absorption coefficient and was derived for optically thin conditions has sometimes led to the statement that the Planck mean absorption coefficient is applicable *only* in optically thin situations. However, the Planck mean was defined in general for the *emission* from a volume element in connection with equation (2-18), and hence can be applied for the emission term in a gas of *any* optical thickness.



(a) Slab geometry for example 3-2.

(b) Emission from spherical gas-filled satellite with transparent skin.

FIGURE 3-1.—Examples for emission approximation.

EXAMPLE 3-2: Find the flux emerging from an isothermal slab of gas with Planck mean absorption coefficient 0.010 cm^{-1} and thickness $D=1 \text{ cm}$ if the slab is bounded by transparent nonradiating walls (fig. 3-1(a)).

If $i'(\beta)$ is the emerging total intensity in direction β , the emerging flux is

$$q = \int_{\omega=0}^{2\pi} i'(\beta) \cos \beta \, d\omega = 2\pi \int_{\beta=0}^{\pi/2} i'(\beta) \cos \beta \sin \beta \, d\beta$$

Since the slab is isothermal with constant a_p , equation (3-11) can be integrated over any path $D/\cos \beta$ through the slab to yield

$$i'(\beta) = a_p \frac{\sigma T^4}{\pi} \frac{D}{\cos \beta}$$

Then

$$q = 2 \int_0^{\pi/2} a_p \sigma T^4 D \sin \beta \, d\beta = 2a_p \sigma T^4 D \quad (3-12)$$

Substituting the numerical values gives

$$q = 0.02\sigma T^4$$

It should be realized that equation (3-12) is really not a precise result even though the slab is optically thin in the sense that the optical thickness based on D is $a_p D = 0.01 \ll 1$. This is because some of the radi-

tion reaching the slab boundary has passed through the thickness $D/\cos \beta$. Because for large β directions this path length becomes *infinite*, the emission approximation cannot hold. A more accurate solution of the equation of transfer including the proper path lengths gives

$$q = 1.8a_p\sigma T^4 D \quad (3-13)$$

which is 10 percent less than equation (3-12).

EXAMPLE 3-3: An inflated spherical balloon satellite of radius R is in orbit in the Earth's shadow. The satellite has a perfectly transparent wall and is filled with a gray gas of constant absorption coefficient a , such that $aR \ll 1$. Neglecting radiant exchange with the Earth, derive a relation for the initial rate of energy loss from the satellite if the initial temperature of the gas in the balloon is T_0 .

From the emission approximation equation (3-11), figure 3-1(b) shows that the following can be written for the intensity at the surface:

$$i'(\beta) = \int_0^S \frac{a\sigma T_0^4}{\pi} dS = \frac{a\sigma T_0^4}{\pi} S$$

since a and T_0 are constants. From the geometry

$$S = 2R \cos \beta$$

Then q , the flux leaving the surface, is

$$\begin{aligned} q &= 2\pi \int_0^{\pi/2} i'(\beta) \cos \beta \sin \beta d\beta \\ &= 4a\sigma T_0^4 R \int_0^{\pi/2} \cos^2 \beta \sin \beta d\beta \\ &= \frac{4}{3} a\sigma T_0^4 R \end{aligned}$$

To obtain the energy loss Q per unit time from the entire sphere, multiply through by the surface area of the sphere

$$Q = \frac{4}{3} a\sigma T_0^4 R (4\pi R^2) = 4a\sigma T_0^4 V_s \quad (3-14)$$

where V_s is the volume of the sphere. This is what is expected—it was found that *any* isothermal gas volume radiates according to this formula (see section 1.6) so long as there is no internal absorption; the emission approximation gives a compatible solution.

3.3.3 The Cold Medium Approximation

The final approximate form of the equation of transfer to be discussed in this section is found when the local blackbody emission within the medium is very small. Such a situation might arise in considering radiative transfer within a cold medium such as an absorbing cryogenic fluid. The integrated equation of transfer (3-1) reduces to

$$i'_\lambda(S) = i'_\lambda(0) \exp \left[- \int_0^S a_\lambda(S^*) dS^* \right] \quad (3-15)$$

The local intensity thus consists only of the attenuated incident intensity.

EXAMPLE 3-4: 100 watts of radiant energy leave a spherical light bulb enclosed in a fixture having a flat glass plate as shown in figure 3-2. If the glass is 2 cm thick and has a gray absorption coefficient of 0.05 cm^{-1} , find the intensity leaving the fixture at an angle of 60° to the bulb axis. (Assume the bulb diameter is 10 cm.)

An integration of equation (3-15) over λ and S results in the total intensity

$$i'(\beta) = i'(0) \exp(-aS)$$

To obtain $i'(0)$, consider the light bulb a diffuse sphere. The energy flux (emissive power) at the surface of the sphere is 100 watts (W) divided by the sphere area. The intensity is this diffuse emissive power divided by π . Then

$$i'(0) = \frac{100 \text{ W}}{\pi 10^2 \text{ cm}^2 \pi \text{ sr}} = 0.101 \frac{\text{W}}{(\text{cm}^2)(\text{sr})}$$

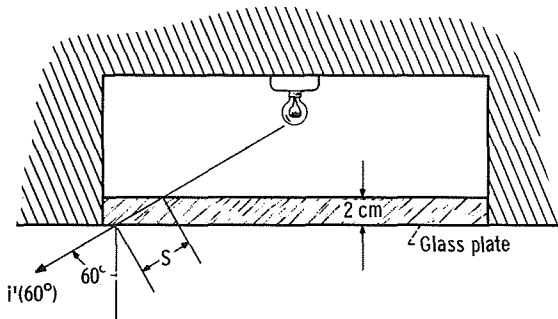


FIGURE 3-2.—Intensity of beam from light fixture (example 3-4).

Then

$$i'(\beta) = 0.101 \exp\left(-0.05 \times \frac{2}{\cos 60^\circ}\right) = 0.0818 \frac{\text{W}}{(\text{cm}^2)(\text{sr})}$$

Note that this problem has involved only a simple attenuated transmission solution. The cold-material approximation is just that, a neglect of emission along the path of transmission. In this problem it was assumed that emission from the glass plate is small, so that only the intensity originating at the source needed to be considered.

3.4 DIFFUSION METHODS IN RADIATIVE TRANSFER

When a medium is optically dense, the radiation within it can travel only a short distance before being absorbed. Consider the situation where this radiation penetration distance is small compared with the distance over which significant temperature changes occur. Then a local intensity will be the result of radiation coming only from nearby locations where the temperature is close to that of the location under consideration. Radiation emitted by locations where the temperature is appreciably different will be greatly attenuated before reaching the location being considered.

For these conditions it will be shown that it is possible to transform the integral-type equations that result from the radiative energy balance into a diffusion equation. The diffusion equation is like a heat conduction equation. The energy transfer depends only on the conditions in the immediate vicinity of the position being considered and can be described in terms of the gradient of the conditions at that position. The use of the diffusion approximation leads to a very great simplification in treating many problems of radiative transfer. Standard techniques, including well-developed finite difference schemes, can be used for solving the resulting diffusion differential equations. Such methods for differential equations are developed to a much higher degree and are more familiar to most engineers, for example in the solution of heat conduction problems, than are the methods of solution for the corresponding integral equations.

As will be shown in the derivations that follow, the diffusion approximation requires that the intensity within the medium be nearly isotropic. This can occur well within an optically thick medium with small temperature gradients but cannot be valid near certain types of boundaries. For example, at a boundary adjacent to a vacuum at absolute zero temperature radiation will leave the medium but there will be none incident from the vacuum. As a result of this large nonisotropy, the diffusion approximation will not be valid near this type of boundary. The ability

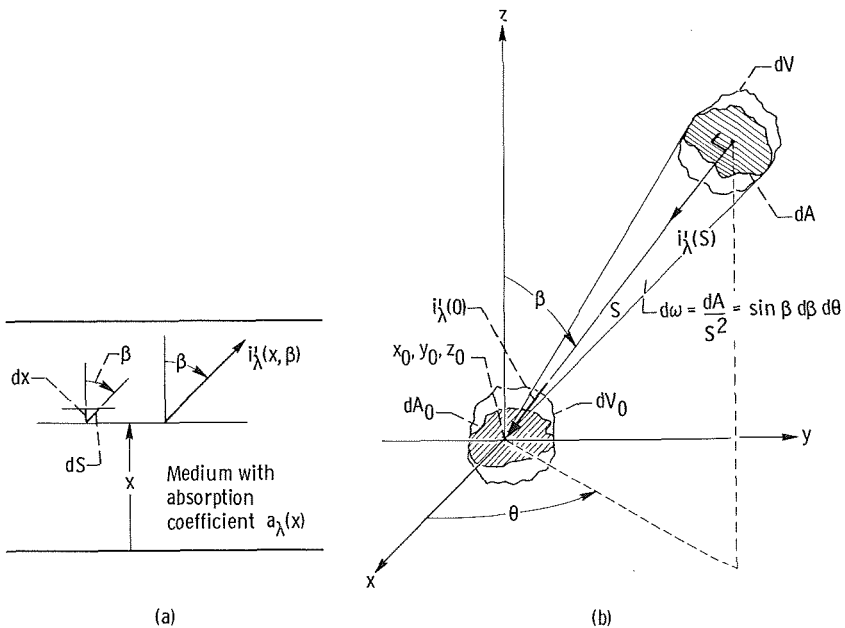
to apply diffusion methods at the interfaces between regions has been improved recently by the introduction of so-called "radiation slip" or "jump" boundary conditions.

For real gases there are wavelength regions that are essentially transparent. The diffusion approach can only be applied at specific wavelengths or in wavelength bands for which the optical thickness of the medium is greater than about two; the fact that some *mean* optical thickness meets this criterion is not sufficient. Wavelength band-type applications of the diffusion method can be made in the optically thick regions.

3.4.1 Simplified Derivation of the Diffusion Equation

First, a simplified derivation of radiation diffusion in a one-dimensional layer will be carried out to give the spirit of the diffusion approximation. The diffusion assumption is made that the medium in question has an absorption coefficient sufficiently large so that the absorption mean free penetration distance $1/a_\lambda$ is small compared with the distances over which significant temperature changes occur.

Consider the layer of gas shown in figure 3-3(a). The equation of transfer from equation (2-7) is



(a) One-dimensional plane gas layer.

(b) General three-dimensional region.

FIGURE 3-3.—Geometry for derivation of diffusion equations.

$$\frac{1}{a_\lambda} \frac{di'_\lambda}{dS} + i'_\lambda(S) = i'_{\lambda b}(S) \quad (3-16)$$

By using the relation $dS = dx/\cos \beta$, the equation of transfer giving the change of i'_λ with x for a fixed β is written as

$$-\frac{\cos \beta}{a_\lambda} \frac{\partial i'_\lambda(x, \beta)}{\partial x} = i'_\lambda(x, \beta) - i'_{\lambda b}(x) \quad (3-17)$$

where the blackbody intensity does not depend on angle. Let H be a length over which the temperature changes by a significant amount. Then nondimensionalize equation (3-17) using H and let $1/a_\lambda = l_m$ from equation (1-16)

$$-\frac{l_m}{H} \cos \beta \frac{\partial i'_\lambda(x, \beta)}{\partial \left(\frac{x}{H}\right)} = i'_\lambda(x, \beta) - i'_{\lambda b}(x) \quad (3-18)$$

We now proceed to obtain a solution to equation (3-18) in the form of a series. The diffusion approximation states that the penetration distance is small compared to the length over which the temperature changes appreciably. Hence $l_m/H \ll 1$ and the intensity can be written as a series of functions $i'_\lambda^{(n)}$ multiplied by powers of l_m/H

$$i'_\lambda = i'_\lambda^{(0)} + \frac{l_m}{H} i'_\lambda^{(1)} + \left(\frac{l_m}{H}\right)^2 i'_\lambda^{(2)} + \dots \quad (3-19)$$

Substituting into equation (3-18) gives (up to terms in first power of l_m/H)

$$-\frac{l_m}{H} \cos \beta \frac{\partial i'_\lambda^{(0)}}{\partial \left(\frac{x}{H}\right)} - \dots = i'_\lambda^{(0)} + \frac{l_m}{H} i'_\lambda^{(1)} + \dots - i'_{\lambda b} \quad (3-20)$$

Equating the zeroth-order terms gives

$$i'_\lambda^{(0)} = i'_{\lambda b} \quad (3-21)$$

Equating the terms in l_m/H and then using equation (3-21) to eliminate $i'_\lambda^{(0)}$ gives

$$i'_\lambda^{(1)} = -\cos \beta \frac{di'_{\lambda b}}{d\left(\frac{x}{H}\right)} \quad (3-22)$$

Equations (3-21) and (3-22) are substituted into the series solution equation (3-19) to yield (up to terms in l_m/H)

$$i'_\lambda = i'_{\lambda b} - \frac{l_m}{H} \cos \beta \frac{di'_{\lambda b}}{d\left(\frac{x}{H}\right)}$$

or

$$i'_\lambda = i'_{\lambda b} - \frac{\cos \beta}{a_\lambda} \frac{di'_{\lambda b}}{dx} \quad (3-23)$$

This result reveals the important feature that *in the diffusion solution the local intensity depends only on the magnitude and gradient of the local blackbody intensity.*

The local spectral energy flux at x flowing in the x direction is found by multiplying i'_λ by $\cos \beta d\lambda$ and integrating over all solid angles as in equation (2-39)

$$\begin{aligned} \frac{dq_\lambda(x)}{d\lambda} &= 2\pi \int_{\beta=0}^{\pi} i'_\lambda(x, \beta) \cos \beta \sin \beta d\beta \\ &= 2\pi \int_{\cos \beta = -1}^1 i'_\lambda(x, \cos \beta) \cos \beta d(\cos \beta) \end{aligned} \quad (3-24)$$

Using equation (3-23) in equation (3-24) gives, after noting that $i'_{\lambda b}$ does not depend on β ,

$$\begin{aligned} \frac{dq_\lambda(x)}{d\lambda} &= 2\pi i'_{\lambda b}(x) \int_{\cos \beta = -1}^1 \cos \beta d(\cos \beta) \\ &\quad - \frac{2\pi}{a_\lambda} \frac{di'_{\lambda b}}{dx} \int_{\cos \beta = -1}^1 \cos^2 \beta d(\cos \beta) \\ &= -\frac{4\pi}{3a_\lambda(x)} \frac{di'_{\lambda b}}{dx} = -\frac{4}{3a_\lambda(x)} \frac{de_{\lambda b}}{dx} \end{aligned} \quad (3-25)$$

Equation (3-25) is an important result known as the *Rosseland diffusion equation*. This equation relates the local energy flux to local conditions only; it does not involve integrals of contributions from other regions and thus provides a considerable simplification over the exact formulation of the equation of transfer.

3.4.2 The General Radiation Diffusion Equation

In the previous section the diffusion equation was derived for a simpli-

fied case. Only first-order terms were retained in the series of equation (3-19) and an unbounded region of gas was considered. The general equations used in radiation diffusion will now be derived including the second-order terms. Boundary conditions will be introduced into the theory so that the diffusion equations can be applied to finite regions. As shown by the solution in section 3.4.3.1, the boundary conditions must account for a jump in emissive power between the wall and the gas at the wall for a situation where there is radiative transfer only. The derivation follows the general outline of that of Deissler (ref. 1). The intermediate equations in the following derivation become somewhat complex because of their general form. The final equations however are relatively simple and are very useful.

3.4.2.1 *The Rosseland equation for local radiative flux.*—Consider the geometry in figure 3-3(b). There is a volume element dV_0 at x_0, y_0, z_0 having cross-sectional area dA_0 in the x, y plane. The energy flux crossing dA_0 originates from all surrounding volume elements such as dV . If the emission from dV produces an intensity $i'_\lambda(S)$, then the intensity reaching dV_0 is given by equation (1-21) as

$$i'_\lambda(0) = i'_\lambda(S) \exp [-a_\lambda(\lambda)S] \quad (3-26)$$

This accounts for attenuation along S but does not include emission along S which will be accounted for later by integrating the contributions of equation (3-26) from all elements of the volume. Note that a spatially constant a_λ has been used. This is not restrictive here as in the diffusion approximation the gas temperature does not change significantly over the region contributing significant radiation to a location. The solid angle subtended by dV when viewed from dA_0 is dA/S^2 where dA is the projected area of dV normal to S . The energy per unit time incident on dA_0 as a result of the intensity in equation (3-26) is then

$$d^3Q_{\lambda,i}(0) = i'_\lambda(S) \exp [-a_\lambda(\lambda)S] \frac{dA}{S^2} dA_0 \cos \beta d\lambda \quad (3-27)$$

From equation (1-35), the spectral energy emitted spontaneously by dV per unit time is

$$i'_{\lambda,e}(S) = a_\lambda(\lambda, T, P) i'_{\lambda,b}(\lambda, T) dS \quad (3-28)$$

Substituting equation (3-28) into equation (3-27) gives

$$d^3Q_{\lambda,i}(0) = a_\lambda(\lambda) i'_{\lambda,b}(\lambda, T) dS \exp [-a_\lambda(\lambda)S] \frac{dA}{S^2} dA_0 \cos \beta d\lambda \quad (3-29)$$

If as a result of the gas being optically dense, the radiation field at dV_0 originates only from locations close to dV_0 , then $i'_{\lambda b}(\lambda, T)$ in equation (3-29) can be expanded in a three-dimensional Taylor series about the origin $S=0$ in the hope that truncation of the series after a few terms will give an adequate representation of the $i'_{\lambda b}$ distribution near dV_0 . The general Taylor series in three dimensions can be written as

$$i'_{\lambda b}(\lambda, T) = \sum_{n=0}^{\infty} \left\{ \frac{1}{n!} \left[(z-z_0) \left(\frac{\partial}{\partial z} \right)_0 + (y-y_0) \left(\frac{\partial}{\partial y} \right)_0 + (x-x_0) \left(\frac{\partial}{\partial x} \right)_0 \right]^n i'_{\lambda b}(\lambda, T) \right\} \quad (3-30)$$

This general series will be carried for the next several steps and will then be truncated to a few terms. By applying the binomial theorem twice to expand the factor in square brackets, equation (3-30) becomes

$$i'_{\lambda b}(\lambda, T) = \sum_{n=0}^{\infty} \sum_{v=0}^n \sum_{s=0}^v \frac{(z-z_0)^{n-v} (y-y_0)^{v-s} (x-x_0)^s}{(n-v)! (v-s)! s!} \times \left(\frac{\partial^n i'_{\lambda b}}{\partial z^{n-v} \partial y^{v-s} \partial x^s} \right)_0 \quad (3-31)$$

This relation is substituted into equation (3-29), which is then integrated over the half space encompassing positive z values. This gives all energy traveling in the negative z direction that is incident on dA_0 as

$$\begin{aligned} \frac{d^2 Q_{\lambda, -z}}{d\lambda} &= a_{\lambda}(\lambda) dA_0 \sum_{n=0}^{\infty} \sum_{v=0}^n \sum_{s=0}^v \frac{1}{(n-v)! (v-s)! s!} \\ &\times \left(\frac{\partial^n i'_{\lambda b}}{\partial z^{n-v} \partial y^{v-s} \partial x^s} \right)_0 \int_{\theta=0}^{2\pi} \int_{\beta=0}^{\pi/2} \int_{s=0}^{\infty} (S \cos \beta)^{n-v} \\ &\times (S \sin \theta \sin \beta)^{v-s} (S \sin \beta \cos \theta)^s \cos \beta \sin \beta \\ &\times \exp [-a_{\lambda}(\lambda) S] dS d\beta d\theta \end{aligned} \quad (3-32)$$

where the integral and summation signs have been interchanged and spherical coordinates of the following form have been introduced:

$$\begin{aligned} x-x_0 &= S \sin \beta \cos \theta \\ y-y_0 &= S \sin \beta \sin \theta \\ z-z_0 &= S \cos \beta \end{aligned}$$

The solid angle dA/S^2 has also been replaced by $\sin \beta d\beta d\theta$. Note that the

following assumptions have been used in the integration over the entire half space in equation (3-32): (1) the a_λ is constant within the region that contributes significantly to the energy flux at dA_0 , and (2) there are no bounding surfaces that contribute significant radiation energy at dA_0 . Otherwise, the a_λ would have to be retained as a variable in the integration, and the integration would have to be over a finite region with a specified intensity along the boundaries.

Carrying out the integration of equation (3-32) gives

$$\frac{d^2 Q_{\lambda, -z}}{d\lambda} = \frac{dA_0}{4} \sum_{n=0}^{\infty} \sum_{v=0}^n \sum_{s=0}^v \Omega(n, v, s) \frac{1}{a_\lambda^n} \left(\frac{\partial^n i'_{\lambda b}}{\partial z^{n-v} \partial y^{v-s} \partial x^s} \right)_0 \quad (3-33)$$

where

$$\Omega(n, v, s) = \frac{[1 + (-1)^{v-s}][1 + (-1)^s] n! \Gamma\left(\frac{n-v+2}{2}\right) \Gamma\left(\frac{v-s+1}{2}\right) \Gamma\left(\frac{s+1}{2}\right)}{(n-v)!(v-s)!s! \Gamma\left(\frac{n+4}{2}\right)} \quad (3-34)$$

and Γ is the gamma function.

A similar derivation for the energy incident on dA_0 from below, that is, energy traveling in the positive z direction, gives

$$\frac{d^2 Q_{\lambda, +z}}{d\lambda} = \frac{dA_0}{4} \sum_{n=0}^{\infty} \sum_{v=0}^n \sum_{s=0}^v (-1)^{n-v} \Omega(n, v, s) \frac{1}{a_\lambda^n} \left(\frac{\partial^n i'_{\lambda b}}{\partial z^{n-v} \partial y^{v-s} \partial x^s} \right)_0 \quad (3-35)$$

The net energy flux passing through dA_0 in the positive z direction is then

$$\begin{aligned} \frac{dq_{\lambda, z}}{d\lambda} &= \frac{d^2 Q_{\lambda, +z} - d^2 Q_{\lambda, -z}}{dA_0 d\lambda} \\ &= -\frac{1}{4} \sum_{n=0}^{\infty} \sum_{v=0}^n \sum_{s=0}^v [1 - (-1)^{n-v}] \Omega(n, v, s) \frac{1}{a_\lambda^n} \\ &\quad \times \left(\frac{\partial^n i'_{\lambda b}}{\partial z^{n-v} \partial y^{v-s} \partial x^s} \right)_0 \end{aligned} \quad (3-36)$$

Similar relations can be derived for the x and y directions.

In the diffusion approximation a region is being considered where temperature changes slowly with optical depth. Hence derivatives such

as $(1/a_\lambda^n)(\partial^n i'_{\lambda b}/\partial z^n)$ become small as n is increased and the series in equation (3-36) can be truncated. *Retaining only terms through the second derivative* causes the formidable looking equation (3-36) to reduce to

$$\frac{dq_{\lambda,z}}{d\lambda} = -\frac{4\pi}{3a_\lambda} \left(\frac{\partial i'_{\lambda b}}{\partial z} \right)_0 = -\frac{4}{3a_\lambda} \left(\frac{\partial e_{\lambda b}}{\partial z} \right)_0 \quad (3-37)$$

This is the general relation for local energy flux in terms of the emissive power gradient and is in agreement with equation (3-25); it is the *Rosseland diffusion equation* for radiative energy transfer. Retaining only first-order derivatives, as in the derivation of equation (3-25), also gives this same equation because the second-order terms have been found to cancel. Note that equation (3-37) has the same form as the Fourier law of heat conduction. This allows solution of some radiation problems by analogy with heat conduction methods.

To obtain the energy flux in a wavelength range, integrate equation (3-37) over the wavelength band $\Delta\lambda$ (the parentheses and 0 subscript will be dropped for simplicity)

$$\begin{aligned} q_{\Delta\lambda,z} &= \int_{\Delta\lambda} -\frac{4}{3a_\lambda} \frac{\partial e_{\lambda b}}{\partial z} d\lambda \equiv -\frac{4}{3a_{R,\Delta\lambda}} \int_{\Delta\lambda} \frac{\partial e_{\lambda b}}{\partial z} d\lambda \\ &= -\frac{4}{3a_{R,\Delta\lambda}} \frac{\partial}{\partial z} \int_{\Delta\lambda} e_{\lambda b} d\lambda = -\frac{4}{3a_{R,\Delta\lambda}} \frac{\partial e_{\Delta\lambda b}}{\partial z} \end{aligned} \quad (3-38)$$

This defines the mean absorption coefficient $a_{R,\Delta\lambda}$ as

$$\frac{1}{a_{R,\Delta\lambda}} = \frac{\int_{\Delta\lambda} \frac{1}{a_\lambda} \frac{\partial e_{\lambda b}}{\partial z} d\lambda}{\int_{\Delta\lambda} \frac{\partial e_{\lambda b}}{\partial z} d\lambda}$$

By multiplying the numerator and denominator by $\partial z/\partial e_b$, this can be written as

$$\frac{1}{a_{R,\Delta\lambda}} = \frac{\int_{\Delta\lambda} \frac{1}{a_\lambda} \frac{\partial e_{\lambda b}}{\partial e_b} d\lambda}{\int_{\Delta\lambda} \frac{\partial e_{\lambda b}}{\partial e_b} d\lambda} \quad (3-39)$$

The a_R is called the *Rosseland mean absorption coefficient* after S. Rosseland who first made use of the diffusion theory in studying radiation effects in astrophysics (ref. 2). The $\partial e_{\lambda b}/\partial e_b$ can be found by differentiating

Planck's law (eq. (2-11b), vol. I) after letting $T = (e_b/\sigma)^{1/4}$

$$\begin{aligned} \frac{\partial e_{\lambda b}}{\partial e_b} &= \frac{\partial \left(\frac{2\pi C_1}{\lambda^5 \left\{ \exp \left[\frac{C_2}{\lambda} \left(\frac{\sigma}{e_b} \right)^{1/4} \right] - 1 \right\}} \right)}{\partial e_b} \\ &= \frac{\pi C_1 C_2 \sigma^{1/4}}{2 \lambda^6 e_b^{5/4}} \left(\frac{\exp \left[\frac{C_2}{\lambda} \left(\frac{\sigma}{e_b} \right)^{1/4} \right]}{\left\{ \exp \left[\frac{C_2}{\lambda} \left(\frac{\sigma}{e_b} \right)^{1/4} \right] - 1 \right\}^2} \right) \end{aligned} \quad (3-40)$$

3.4.2.2 *The emissive power jump as a boundary condition.*—Up to now the position considered in the gas was sufficiently far from any boundary so that the effect of the boundary did not enter the diffusion relations. Now the interaction of the radiating gas with a diffuse wall will be considered. Let the wall bounding the gas from above as shown in figure 3-4 have a hemispherical spectral emissivity $\epsilon_{\lambda w2}$. All quantities pertaining to the wall itself will have the subscript w to differentiate them from quantities *in the gas* at the wall which will have no w subscript. Consider an area dA_2 *in the gas* parallel to the wall and immediately adjacent to the wall. The spectral energy passing through dA_2 in the negative z direction is

$$(d^2Q_{\lambda, -z})_2 = \epsilon_{\lambda w2} e_{\lambda b w2} d\lambda dA_2 + (1 - \epsilon_{\lambda w2}) (d^2Q_{\lambda, +z})_2 \quad (3-41)$$

where the terms on the right account for the emitted and reflected energy from wall 2, respectively. The net spectral flux across dA_2 in the positive z direction is then

$$\begin{aligned} (dq_{\lambda, z})_2 &= \frac{(d^2Q_{\lambda, +z})_2 - (d^2Q_{\lambda, -z})_2}{dA_2} \\ &= \epsilon_{\lambda w2} \left[\frac{(d^2Q_{\lambda, +z})_2}{dA_2} - \epsilon_{\lambda b w2} d\lambda \right] \end{aligned} \quad (3-42)$$

This can be placed in the form

$$-e_{\lambda b w2} = \frac{(dq_{\lambda, z})_2}{\epsilon_{\lambda w2} d\lambda} - \frac{(d^2Q_{\lambda, +z})_2}{dA_2 d\lambda} \quad (3-43)$$

Now equation (3-35) is substituted for $(d^2Q_{\lambda, +z})_2$. The first term of equation (3-35) for $n=0$ and $dA_0 = dA_2$ is

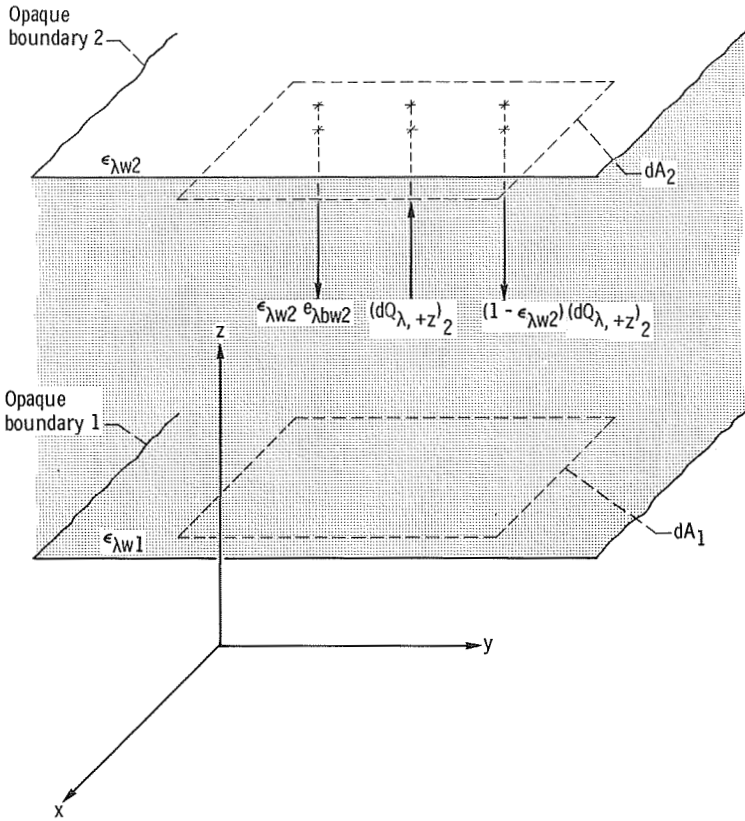


FIGURE 3-4. — Geometry for derivation of energy jump condition at opaque boundary.

$$\frac{dA_2}{4} 4\pi i'_{\lambda b2} = dA_2 e_{\lambda b2}$$

Then equation (3-43) becomes at dA_2 in the gas adjacent to the wall

$$e_{\lambda b2} - e_{\lambda bw2} = \frac{(dq_{\lambda, z})_2}{\epsilon_{\lambda w2} d\lambda} - \frac{1}{4\pi} \sum_{n=1}^{\infty} \sum_{v=0}^n \sum_{s=0}^v (-1)^{n-v} \Omega(n, v, s) \frac{1}{a_{\lambda}^n} \times \left(\frac{\partial^n e_{\lambda b}}{\partial z^{n-v} \partial y^{v-s} \partial x^s} \right)_2 \quad (3-44)$$

Retaining only terms through second order and using equation (3-37) to remove the first derivatives in terms of the spectral energy flux result in the following relation for the jump in emissive power at dA_2

$$e_{\lambda b2} - e_{\lambda bw2} = \left(\frac{1}{\epsilon_{\lambda w2}} - \frac{1}{2} \right) \frac{(dq_{\lambda, z})_2}{d\lambda} - \frac{1}{2a_{\lambda}^2} \left(\frac{\partial^2 e_{\lambda b}}{\partial z^2} + \frac{1}{2} \frac{\partial^2 e_{\lambda b}}{\partial y^2} + \frac{1}{2} \frac{\partial^2 e_{\lambda b}}{\partial x^2} \right)_2 \quad (3-45)$$

All the quantities that do not have a w subscript are evaluated at dA_2 which is *in the gas* adjacent to the wall. The quantities with a w subscript are evaluated on wall 2 and $dq_{\lambda, z}$ is the net flux in the positive z direction.

In a similar fashion, the jump in emissive power at dA_1 in figure 3-4 is

$$e_{\lambda bw1} - e_{\lambda b1} = \left(\frac{1}{\epsilon_{\lambda w1}} - \frac{1}{2} \right) \frac{(dq_{\lambda, z})_1}{d\lambda} + \frac{1}{2a_{\lambda}^2} \left(\frac{\partial^2 e_{\lambda b}}{\partial z^2} + \frac{1}{2} \frac{\partial^2 e_{\lambda b}}{\partial y^2} + \frac{1}{2} \frac{\partial^2 e_{\lambda b}}{\partial x^2} \right)_1 \quad (3-46)$$

where the quantities with a w subscript are on wall 1, and those without a w are *in the gas* adjacent to wall 1.

Equations (3-45) and (3-46) are boundary conditions that relate the emissive power in the gas immediately adjacent to the wall $e_{\lambda b}$ to the wall emissive power $e_{\lambda bw}$. It is evident that there is a jump in emissive power in passing from the gas to the wall at each boundary. Some applications to clarify the use of these relations will be given in section 3.4.3. The use of equation (3-35) in the derivation of these boundary relations *assumes that the proportionality between local radiative flux and emissive power gradient in the gas holds even at points in the gas very near to a bounding surface*. Although this is not strictly true, the use of the jump boundary conditions corrects to a good approximation for the wall effects.

To apply the diffusion equation (3-38) in a wavelength interval, the jump boundary conditions (eqs. (3-45) and (3-46)) must also be integrated over an increment of wavelength $\Delta\lambda$. The wall emissivities are assigned average values in this range, and the integration is carried out as in reference 1 to yield

$$e_{\Delta\lambda b2} - e_{\Delta\lambda bw2} = \left(\frac{1}{\epsilon_{w2}} - \frac{1}{2} \right) (q_{\Delta\lambda, z})_2 - \left\{ \frac{1}{2a_{D, \Delta\lambda}^2} \left(\frac{\partial^2 e_{\Delta\lambda b}}{\partial z^2} + \frac{1}{2} \frac{\partial^2 e_{\Delta\lambda b}}{\partial y^2} + \frac{1}{2} \frac{\partial^2 e_{\Delta\lambda b}}{\partial x^2} \right) + \frac{I_{\Delta\lambda}}{2} \left[\left(\frac{\partial e_{\Delta\lambda b}}{\partial z} \right)^2 + \frac{1}{2} \left(\frac{\partial e_{\Delta\lambda b}}{\partial y} \right)^2 + \frac{1}{2} \left(\frac{\partial e_{\Delta\lambda b}}{\partial x} \right)^2 \right] \right\}_2 \quad (3-47)$$

$$\begin{aligned}
e_{\Delta\lambda b w_1} - e_{\Delta\lambda b 1} &= \left(\frac{1}{\epsilon_{w_1}} - \frac{1}{2} \right) (q_{\Delta\lambda, z})_1 \\
&+ \left\{ \frac{1}{2a_{D, \Delta\lambda}^2} \left(\frac{\partial^2 e_{\Delta\lambda b}}{\partial z^2} + \frac{1}{2} \frac{\partial^2 e_{\Delta\lambda b}}{\partial y^2} + \frac{1}{2} \frac{\partial^2 e_{\Delta\lambda b}}{\partial x^2} \right) \right. \\
&+ \left. \frac{I_{\Delta\lambda}}{2} \left[\left(\frac{\partial e_{\Delta\lambda b}}{\partial z} \right)^2 + \frac{1}{2} \left(\frac{\partial e_{\Delta\lambda b}}{\partial y} \right)^2 + \frac{1}{2} \left(\frac{\partial e_{\Delta\lambda b}}{\partial x} \right)^2 \right] \right\}_1 \quad (3-48)
\end{aligned}$$

where $q_{\Delta\lambda} = \int_{\Delta\lambda} dq_{\lambda}$.

In these equations, two mean coefficients are given as originally derived in reference 1

$$\frac{1}{a_{D, \Delta\lambda}^2} = \frac{\int_{\Delta\lambda} \frac{1}{a_{\lambda}^2} \frac{\partial e_{\lambda b}}{\partial e_b} d\lambda}{\int_{\Delta\lambda} \frac{\partial e_{\lambda b}}{\partial e_b} d\lambda} \quad (3-49)$$

$$I_{\Delta\lambda} = \frac{\int_{\Delta\lambda} \frac{1}{a_{\lambda}^2} \frac{\partial^2 e_{\lambda b}}{\partial e_b^2} d\lambda}{\left(\int_{\Delta\lambda} \frac{\partial e_{\lambda b}}{\partial e_b} d\lambda \right)^2} \quad (3-50)$$

The $I_{\Delta\lambda}$ has units of length to the fourth power times inverse energy rate.

3.4.2.3 *The emissive power jump between two absorbing-emitting regions.*—When internal sources or sinks for energy are present in absorbing-emitting media, it is possible in the absence of energy conduction to have a discontinuity in emissive power at the interface of two such adjacent media. This is obtained by considering a volume element at the interface between two regions. The lower region has absorption coefficient $a_{\lambda 1}$ and the upper $a_{\lambda 2}$. Then the net flux passing through the element per unit area normal to z is by use of equations (3-33) and (3-35) in media 2 and 1, respectively,

$$\begin{aligned}
\frac{(dq_{\lambda, z})_{g-g}}{d\lambda} &= \frac{(d^2 Q_{\lambda, +z})_1 - (d^2 Q_{\lambda, -z})_2}{dA d\lambda} \\
&= \frac{1}{4\pi} \sum_{n=0}^{\infty} \sum_{v=0}^n \sum_{s=0}^v \Omega(n, v, s) \left[\frac{(-1)^{n-v}}{a_{\lambda 1}^n} \left(\frac{\partial^n e_{\lambda b}}{\partial z^{n-v} \partial y^{v-s} \partial x^s} \right)_1 \right. \\
&\quad \left. - \frac{1}{a_{\lambda 2}^n} \left(\frac{\partial^n e_{\lambda b}}{\partial z^{n-v} \partial y^{v-s} \partial x^s} \right)_2 \right]_{g-g} \quad (3-51)
\end{aligned}$$

Neglecting terms of order higher than two gives the emissive power jump as

$$\begin{aligned}
 (e_{\lambda b2} - e_{\lambda b1})_{g-g} = & -\frac{(dq_{\lambda,z})_{g-g}}{d\lambda} + \left\{ -\frac{2}{3} \left[\frac{1}{a_{\lambda 1}} \left(\frac{\partial e_{\lambda b}}{\partial z} \right)_1 + \frac{1}{a_{\lambda 2}} \left(\frac{\partial e_{\lambda b}}{\partial z} \right)_2 \right] \right. \\
 & + \frac{1}{2a_{\lambda 1}^2} \left(\frac{\partial^2 e_{\lambda b}}{\partial z^2} + \frac{1}{2} \frac{\partial^2 e_{\lambda b}}{\partial y^2} + \frac{1}{2} \frac{\partial^2 e_{\lambda b}}{\partial x^2} \right)_1 \\
 & \left. - \frac{1}{2a_{\lambda 2}^2} \left(\frac{\partial^2 e_{\lambda b}}{\partial z^2} + \frac{1}{2} \frac{\partial^2 e_{\lambda b}}{\partial y^2} + \frac{1}{2} \frac{\partial^2 e_{\lambda b}}{\partial x^2} \right)_2 \right\}_{g-g} \quad (3-52)
 \end{aligned}$$

The integrated form of equation (3-52) for a wavelength interval is given in reference 3.

As will be shown in section 3.4.3.2, the value of the jump $e_{\lambda b2} - e_{\lambda b1}$ from this equation will be nonzero under certain conditions.

3.4.2.4 *Summary.*—The general radiation diffusion equation, given at a single wavelength by equation (3-36) or (3-37) and for a wavelength band by equation (3-38), has now been derived. The general boundary conditions at solid boundaries with normals into the gas in the negative and positive coordinate directions are given at a single wavelength by equations (3-45) and (3-46), respectively, and for a wavelength band by equations (3-47) and (3-48). Finally, a boundary condition for use at the interface between two absorbing-emitting media in the absence of heat conduction is given by equation (3-52).

3.4.3 Use of the Diffusion Solution

When the diffusion equation is utilized, it is assumed to apply throughout the entire medium including the region adjacent to a boundary. The effect of the boundary is imposed on the solution by utilizing a jump boundary condition.

If a real gas is considered, three coefficients must be evaluated as given by equations (3-39), (3-49), and (3-50). However, each of these depends only on local conditions so that they can be tabulated.

3.4.3.1 *Gray stagnant gas between parallel plates.*—Most gases have strong variations of properties with wavelength and it is necessary to solve the diffusion equation in a number of wavelength regions. For illustrative purposes here it is not feasible to consider an involved spectral solution. There are some limited situations such as soot filled flames and high temperature uranium gas where a gray gas approximation can be made. The equations presented in section 3.4.2 reduce considerably in this case. Let us examine then, for illustrative purposes, the case of a gray gas contained between infinite parallel plates at different temperatures (fig. 3-5). For simplicity let both plates have the

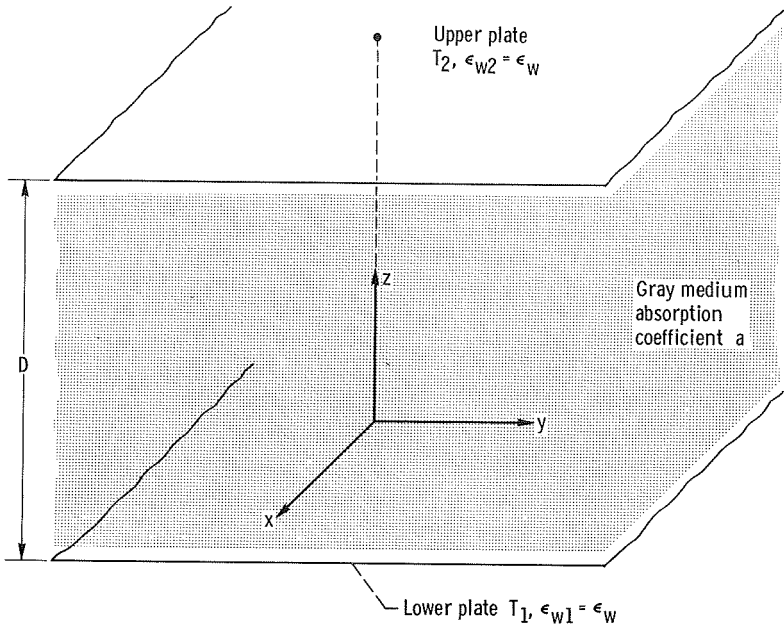


FIGURE 3-5.—Radiant interchange between infinite parallel plates enclosing gray medium.

same emissivity so that $\epsilon_{w1} = \epsilon_{w2} = \epsilon_w$.

For a gray gas the absorption coefficient a_λ is independent of wavelength. Then the wavelength range for integration of equations (3-39), (3-49), and (3-50) can be $0 \rightarrow \infty$. Letting $a_\lambda = a$, which can be taken out of the integrals, gives

$$\frac{1}{a_R} = \frac{1}{a_D} = \frac{1}{a}$$

and

$$I = \frac{\frac{1}{a^2} \frac{\partial^2}{\partial e_b^2} \int_0^\infty e_{\lambda b} d\lambda}{\left(\frac{\partial}{\partial e_b} \int_0^\infty e_{\lambda b} d\lambda \right)^2} = \frac{\frac{1}{a^2} \frac{\partial^2 e_b}{\partial e_b^2}}{\left(\frac{\partial e_b}{\partial e_b} \right)^2} = 0 \quad (3-53)$$

Equation (3-38) reduces to

$$q_z = -\frac{4}{3a} \frac{\partial}{\partial z} \int_0^\infty e_{\lambda b} d\lambda = -\frac{4}{3a} \frac{de_b}{dz}$$

This can be integrated directly because, with no sources or sinks in the gas, q_z is a constant in this geometry. Then, with the additional assump-

tion that a does not depend on temperature and is therefore independent of z , the result is

$$e_b(z) - e_{b1} = -\frac{3a}{4} q_z z \quad (3-54)$$

Evaluating equation (3-54) at $z=D$ yields

$$\frac{e_{b2} - e_{b1}}{q_z} = -\frac{3aD}{4} \quad (3-55)$$

The e_{b1} and e_{b2} are *in the gas* at the walls. To connect these quantities with the wall conditions, the jump boundary conditions are applied. Differentiating equation (3-54) twice with respect to z shows that the second derivative terms are zero in the boundary condition equations (3-47) and (3-48). Equations (3-47) and (3-48) then become

$$\frac{e_{b2} - e_{bw2}}{q_z} = \frac{1}{\epsilon_w} - \frac{1}{2} \quad (3-56)$$

and

$$\frac{e_{bw1} - e_{b1}}{q_z} = \frac{1}{\epsilon_w} - \frac{1}{2} \quad (3-57)$$

To eliminate the unknown gas emissive powers e_{b1} and e_{b2} , add equations (3-56) and (3-57) to obtain

$$\frac{e_{bw1} - e_{bw2}}{q_z} + \frac{e_{b2} - e_{b1}}{q_z} = \frac{2}{\epsilon_w} - 1$$

Then substitute $e_{b2} - e_{b1}$ from equation (3-55) to give

$$\frac{e_{bw1} - e_{bw2}}{q_z} = \frac{2}{\epsilon_w} - 1 + \frac{3aD}{4} \quad (3-58)$$

or taking the reciprocal

$$\frac{q_z}{e_{bw1} - e_{bw2}} = \frac{1}{\frac{3aD}{4} + \frac{2}{\epsilon_w} - 1} = \frac{1}{\frac{3\kappa_D}{4} + \frac{2}{\epsilon_w} - 1} \quad (3-59)$$

Equation (3-59) gives the radiative energy transfer through a gray gas layer as a function of the gas absorption coefficient, plate spacing, and plate emissivity. It is ratioed to the difference in the black emissive

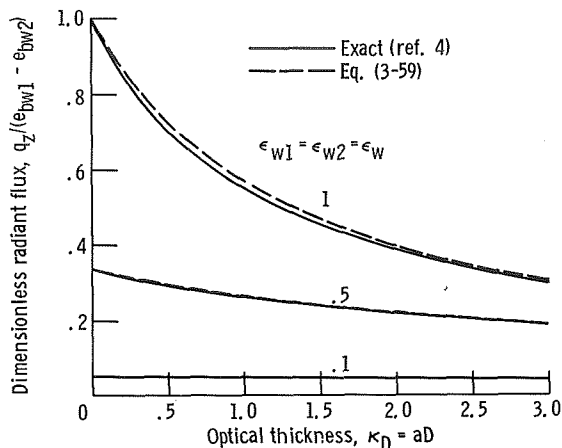


FIGURE 3-6.—Validity of diffusion solution for energy transfer through gray gas between parallel plates.

powers of the plates, which is the maximum possible energy transfer between black plates with no intervening gas. A comparison of this diffusion solution with the exact analytical solution of the same gray gas problem by solution of the integral equations (ref. 4) is shown in figure 3-6. Agreement is seen to be excellent for all optical thicknesses in this geometry.

3.4.3.2 *The discontinuity in emissive power between two gas regions.*— Consider now two semi-infinite regions adjacent to one another (fig. 3-7). Let us determine the discontinuity in emissive power, if any, that might occur at the interface between the regions in the absence of heat conduction. First, consider the media in the two regions to have no internal heat sources or sinks. Both media are gray and stagnant; the lower region has a constant absorption coefficient a_1 , and the upper has a_2 . The emissive power jump at the interface between the two media is found by integrating equation (3-52) over all wavelengths. Noting that $a_{\lambda 1} = a_1$ and $a_{\lambda 2} = a_2$ and that derivatives with respect to x and y are zero for the one-dimensional layer being considered gives

$$(e_{b2} - e_{b1})_{g-g} = - (q_z)_{g-g} - \frac{2}{3} \left[\frac{1}{a_1} \left(\frac{\partial e_b}{\partial z} \right)_1 + \frac{1}{a_2} \left(\frac{\partial e_b}{\partial z} \right)_2 \right]_{g-g} \quad (3-60)$$

Second derivatives with z have been taken to be zero by noting that in either region equation (3-38) gives

$$q_z = - \frac{4}{3a} \frac{\partial e_b}{\partial z} \quad (3-61)$$

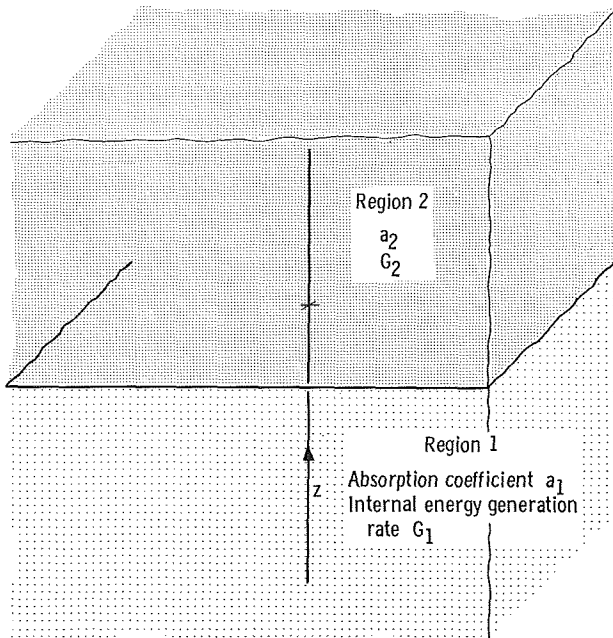


FIGURE 3-7.—Geometry for derivation of interface emissive power discontinuity.

The q_z must be constant since no heat sources or sinks are present. Therefore, in either region,

$$\frac{\partial^2 e_b}{\partial z^2} = 0 \quad (3-62)$$

Also, q_z must be the same in either region because the radiative flux will be continuous across the interface. Therefore, equation (3-61) can be substituted for the first derivatives in equation (3-60) to give

$$(e_{b2} - e_{b1})_{g-g} = - (q_z)_{g-g} - \frac{2}{3} \left[\frac{1}{a_1} \left(-\frac{3a_1}{4} \right) q_z + \frac{1}{a_2} \left(-\frac{3a_2}{4} \right) q_z \right]_{g-g} \quad (3-63)$$

This reduces to

$$(e_{b2} - e_{b1})_{g-g} = - (q_z)_{g-g} + (q_z)_{g-g} = 0 \quad (3-64)$$

so that no discontinuity in emissive power exists in this case.

Consider now the presence of uniform volumetric energy sources of magnitude G_1 and G_2 in regions 1 and 2, respectively. Now the flux gradient in the z direction is given in either region by

$$\frac{\partial q_z}{\partial z} = G = -\frac{4}{3a} \left(\frac{\partial^2 e_b}{\partial z^2} \right) \quad (3-65)$$

In this case, then, the second derivatives of the e_b with z are obviously not zero. Equation (3-52) then becomes

$$(e_{b2} - e_{b1})_{g-g} = - (q_z)_{g-g} + \left\{ -\frac{2}{3} \left[\frac{1}{a_1} \left(\frac{\partial e_b}{\partial z} \right)_1 + \frac{1}{a_2} \left(\frac{\partial e_b}{\partial z} \right)_2 \right] + \frac{1}{2} \left[\frac{1}{a_1^2} \left(\frac{\partial^2 e_b}{\partial z^2} \right)_1 - \frac{1}{a_2^2} \left(\frac{\partial^2 e_b}{\partial z^2} \right)_2 \right] \right\}_{g-g} \quad (3-66)$$

Again, equation (3-61) must hold in either region. At the interface between the two media, since the flux is continuous,

$$q_{z, g-g} = -\frac{4}{3a_1} \left(\frac{\partial e_b}{\partial z} \right)_{1, g-g} = -\frac{4}{3a_2} \left(\frac{\partial e_b}{\partial z} \right)_{2, g-g} \quad (3-67)$$

Substituting equations (3-65) and (3-67) into equation (3-66) to eliminate the first and second derivatives of e_b gives

$$(e_{b2} - e_{b1})_{g-g} = - (q_z)_{g-g} + \left\{ -\frac{2}{3} \left[\frac{1}{a_1} \left(-\frac{3a_1}{4} q_z \right) + \frac{1}{a_2} \left(-\frac{3a_2}{4} q_z \right) \right] + \frac{1}{2} \left[\frac{1}{a_1^2} \left(-\frac{3a_1}{4} G_1 \right) - \frac{1}{a_2^2} \left(-\frac{3a_2}{4} G_2 \right) \right] \right\}_{g-g}$$

which reduces to

$$(e_{b1} - e_{b2})_{g-g} = \frac{3}{8} \left(\frac{G_1}{a_1} - \frac{G_2}{a_2} \right) \quad (3-68)$$

The discontinuity in emissive power is seen to exist whenever there is energy generation in either region unless the ratios G_1/a_1 and G_2/a_2 are equal.

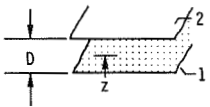
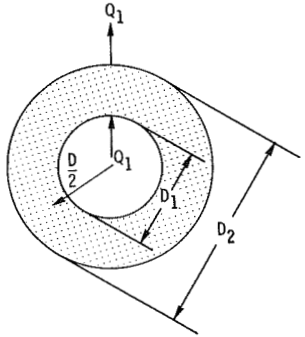
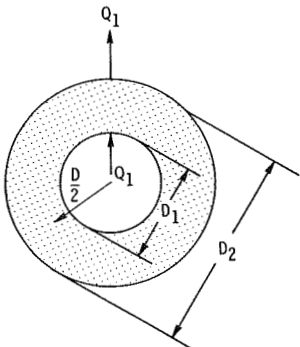
For this situation, formulation in terms of integral equations (ref. 5) gives

$$(e_{b1} - e_{b2})_{g-g} = \frac{1}{4} \left(\frac{G_1}{a_1} - \frac{G_2}{a_2} \right) \quad (3-69)$$

The diffusion solution, although giving the correct functional dependence of the emissive power discontinuity in terms of the a and G values, does differ from the exact solution by a factor of 3/2.

3.4.3.3 *Other diffusion solutions for gray gases.* — In table 3-II, solutions for the temperature distributions and energy transfer in simple

TABLE 3-II. — DIFFUSION THEORY PREDICTIONS OF ENERGY TRANSFER AND TEMPERATURE DISTRIBUTIONS FOR A GRAY GAS BETWEEN GRAY SURFACES

Geometry	Relations ^a
<p>Infinite parallel plates</p> 	$\psi = \frac{1 + \epsilon_1}{\frac{3aD}{4} + \epsilon_1 + \epsilon_2 + 1}$ $\varphi(z) = \frac{\psi}{1 + \epsilon_1} \left[\frac{3a}{4} (D - z) + \epsilon_2 + \frac{1}{2} \right]$
<p>Infinitely long concentric cylinders</p> 	$\psi = \frac{1 + \epsilon_1}{\frac{3}{8} \left[aD_1 \ln \left(\frac{D_2}{D_1} \right) + \frac{1 - \frac{D_1^2}{D_2^2}}{aD_1} \right] + \left(\epsilon_1 + \frac{1}{2} \right) + \frac{D_1}{D_2} \left(\epsilon_2 + \frac{1}{2} \right)}$ $\varphi \left(\frac{D}{2} \right) = \frac{\psi}{1 + \epsilon_1} \left\{ -\frac{3}{8} \left[aD_1 \ln \left(\frac{D}{D_2} \right) + \frac{D_1}{aD_2^2} \right] + \left(\epsilon_2 + \frac{1}{2} \right) \frac{D_1}{D_2} \right\}$
<p>Concentric spheres</p> 	$\psi = \frac{1 + \epsilon_1}{\frac{3}{8} \left[aD_1 \left(1 - \frac{D_1}{D_2} \right) + 2 \frac{1 - \frac{D_1^3}{D_2^3}}{aD_1} \right] + \left(\epsilon_1 + \frac{1}{2} \right) + \frac{D_1^2}{D_2^2} \left(\epsilon_2 + \frac{1}{2} \right)}$ $\varphi \left(\frac{D}{2} \right) = \frac{\psi}{1 + \epsilon_1} \left\{ \frac{3}{8} \left[aD_1 \left(\frac{D_1}{D_2} - \frac{D_1}{D} \right) + \frac{2D_1^2}{aD_2^3} \right] + \left(\epsilon_2 + \frac{1}{2} \right) \frac{D_1^2}{D_2^2} \right\}$

^aDefinitions: $\epsilon_N = (1 - \epsilon_{wN})/\epsilon_{wN}$, $\psi = Q_1/[\epsilon_{w1}A_1\sigma(T_{w1}^4 - T_{w2}^4)]$, $\varphi(\xi) = [T^4(\xi) - T_{w2}^4]/(T_{w1}^4 - T_{w2}^4)$.

geometries involving gray gases contained between gray walls are gathered. These equations are derived from the diffusion equations, and caution is advised in their application since real gases are usually not gray nor optically thick in all wavelength regions. Agreement with exact solutions is sometimes not as good for cylindrical or spherical geometries as for the infinite parallel plate case. Agreement has been found to be excellent in cylindrical and spherical geometries for all parametric variations so long as the optical thickness is greater than about seven, with better agreement as wall emissivity becomes lower and diameter ratios (D_{inner}/D_{outer}) become larger. A comparison for the cylindrical geometry will be discussed later in connection with figure 3-11.

3.4.4 Final Remarks

The diffusion solution, because of its usefulness in treating difficult problems by standard analytical techniques, is a powerful method and is recommended for use whenever the assumptions used in the derivation are justified.

The most stringent assumption is that of "optically thick conditions," which usually is the assumption limiting application of the method. Because most gases have line spectra, they are optically thick within the wavelengths encompassed by the lines. Here the radiation absorption mean free path is quite small, and the assumption that only local conditions affect the spectral radiant flux is quite good. At other wavelengths the gas can often be considered transparent and diffusion methods are then not justified. Care must be taken, then, in applying the diffusion equation only in geometrical and spectral regions where the assumption of an optically thick gas is valid.

The Rosseland mean absorption coefficient should not be used as the criterion for optical thickness. It may have a large value itself, but the spectral absorption coefficient used in calculating a_R may be very small in certain spectral regions. Use of the Rosseland mean in such cases may lead to large errors. The remedy is to use wavelength bands in which the spectral absorption coefficient is everywhere large and evaluate a Rosseland mean for each of these regions.

Howell and Perlmutter (ref. 6) have applied the diffusion solution to a real gas situation and have compared the results to those from an exact formulation by the Monte Carlo method. The agreement was generally not as good as for gray gases.

EXAMPLE 3-5: The space between two diffuse-gray spheres (fig. 3-8) is filled with an optically dense stagnant medium having constant absorp-

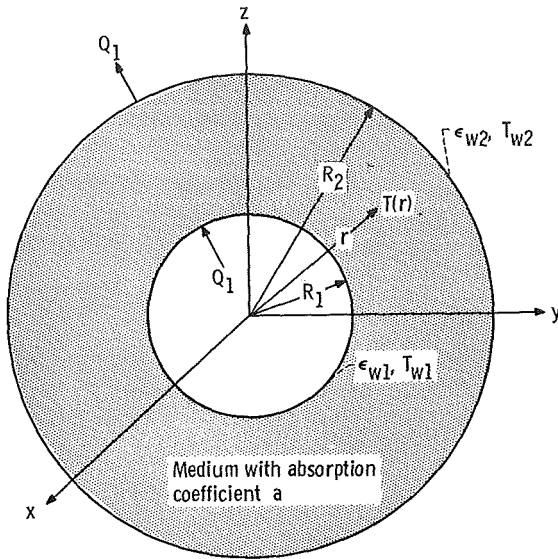


FIGURE 3-8.—Radiation across gap between concentric spheres with intervening medium of constant absorption coefficient.

tion coefficient a . Compute the heat flow Q_1 across the gap from sphere 1 to sphere 2 and the temperature distribution $T(r)$ in the gas using the diffusion method with jump boundary conditions.

For a gray medium with constant a , equation (3-37) gives the heat flux in the positive r direction

$$q_r = -\frac{4}{3a} \frac{de_b}{dr} \quad (3-70)$$

The q_r varies with r according to $q_r = Q_1/4\pi r^2$. Substitute into equation (3-70) and integrate from R_1 to R_2 to obtain

$$\frac{Q_1}{4\pi} \int_{R_1}^{R_2} \frac{dr}{r^2} = -\frac{4}{3a} \int_{e_{b1}}^{e_{b2}} de_b \quad (3-71)$$

$$\frac{Q_1}{4\pi} \left(\frac{1}{R_2} - \frac{1}{R_1} \right) = \frac{4}{3a} (e_{b2} - e_{b1}) \quad (3-72)$$

The e_{b1} and e_{b2} are *in the gas* at the boundaries and the jump boundary conditions are needed to express these quantities in terms of wall values. The jump boundary conditions are given by equations (3-47) and (3-48) and involve second derivatives which will now be found. By

integrating equation (3-71) from R_1 to r , there is obtained

$$e_b(r) - e_{b1} = \frac{3aQ_1}{16\pi} \left(\frac{1}{r} - \frac{1}{R_1} \right) \quad (3-73)$$

Substitute $r = (x^2 + y^2 + z^2)^{1/2}$ and differentiate twice with respect to x to obtain

$$\frac{\partial^2 e_b(r)}{\partial x^2} = -\frac{3aQ_1}{32\pi} \frac{2(x^2 + y^2 + z^2)^{3/2} - 6x^2(x^2 + y^2 + z^2)^{1/2}}{(x^2 + y^2 + z^2)^3} \quad (3-74)$$

Similarly for the y and z directions.

In the boundary condition (eq. (3-47)) the point 2 can be conveniently taken on figure 3-8 at $x = y = 0$ and $z = R_2$. This gives

$$\left[\frac{\partial^2 e_b(r)}{\partial x^2} \right]_2 = \left[\frac{\partial^2 e_b(r)}{\partial y^2} \right]_2 = -\frac{3aQ_1}{16\pi} \frac{1}{R_2^3}$$

$$\left[\frac{\partial^2 e_b(r)}{\partial z^2} \right]_2 = \frac{3aQ_1}{8\pi} \frac{1}{R_2^3}$$

Also $(q_z)_2 = Q_1/4\pi R_2^2$. Substituting into equation (3-47) gives

$$e_{b2} - e_{bw2} = \left(\frac{1}{\epsilon_{w2}} - \frac{1}{2} \right) \frac{Q_1}{4\pi R_2^2} - \frac{3Q_1}{32a\pi} \frac{1}{R_2^3} \quad (3-75)$$

Similarly at the inner sphere boundary from equation (3-48)

$$e_{bw1} - e_{b1} = \left(\frac{1}{\epsilon_{w1}} - \frac{1}{2} \right) \frac{Q_1}{4\pi R_1^2} + \frac{3Q_1}{32a\pi} \frac{1}{R_1^3} \quad (3-76)$$

Adding equation (3-75) and (3-76) gives

$$e_{b2} - e_{b1} = e_{bw2} - e_{bw1} + \frac{Q_1}{4\pi} \left[\frac{1}{R_2^2} \left(\frac{1}{\epsilon_{w2}} - \frac{1}{2} \right) + \frac{1}{R_1^2} \left(\frac{1}{\epsilon_{w1}} - \frac{1}{2} \right) + \frac{3}{8a} \left(\frac{1}{R_1^3} - \frac{1}{R_2^3} \right) \right]$$

After substituting this into the right side of equation (3-72), the result is solved for Q_1 to give the ψ in the last entry in table 3-II.

To obtain the temperature distribution, integrate equation (3-71) from R_2 to r to give

$$e_b(r) - e_{b2} = \frac{3aQ_1}{16\pi} \left(\frac{1}{r} - \frac{1}{R_2} \right)$$

Add equation (3-75) to eliminate e_{b2}

$$e_b(r) - e_{bw2} = \frac{3aQ_1}{16\pi} \left(\frac{1}{r} - \frac{1}{R_2} \right) + \left(\frac{1}{\epsilon_{w2}} - \frac{1}{2} \right) \frac{Q_1}{4\pi R_2^2} - \frac{3Q_1}{32a\pi} \frac{1}{R_2^3} \quad (3-77)$$

This gives the last expression for φ in table 3-II.

3.5 APPROXIMATIONS BY USING MEAN ABSORPTION COEFFICIENTS

Before continuing to discuss solution methods in radiative transfer, some comments are warranted on the use of mean absorption coefficients that have been formed by an integration over all wavelengths. Using a mean absorption coefficient avoids the need to carry out a spectral analysis and then integrate over all wavelengths to obtain total energy quantities. The question is whether it is possible to decide in advance what mean absorption coefficient will yield an accurate solution for a particular problem. Let us now examine in detail the mean coefficients that have been defined thus far and the relations between these coefficients.

3.5.1 Some Mean Absorption Coefficients

To this point, three general types of mean absorption coefficient have been defined. In equations (2-19) and (2-21) were defined the Planck mean

$$a_P(T, P) = \frac{\int_0^\infty a_\lambda(\lambda, T, P) e_{\lambda b}(\lambda, T) d\lambda}{\sigma T^4} \quad (3-78)$$

and the incident mean

$$a_i(T, P) = \frac{\int_0^\infty a_\lambda(\lambda, T, P) \bar{i}_{\lambda, i}(\lambda) d\lambda}{\int_0^\infty \bar{i}_{\lambda, i}(\lambda) d\lambda} \quad (3-79)$$

In connection with the diffusion solution, the Rosseland mean absorption coefficient was defined in equation (3-39); thus,

$$a_R(T, P) = \frac{\int_0^\infty \frac{\partial e_{\lambda b}(\lambda, T)}{\partial e_b(T)} d\lambda}{\int_0^\infty \frac{1}{a_\lambda(\lambda, T, P)} \frac{\partial e_{\lambda b}(\lambda, T)}{\partial e_b(T)} d\lambda} \quad (3-80)$$

It is instructive to examine these various mean absorption coefficients and their relations to each other.

The incident mean absorption coefficient can be conveniently utilized only under certain restrictive conditions when the incident intensity has a spectral form that remains fixed so that the a_i can be evaluated and tabulated. For example, the situation of the incident energy being a solar spectrum occurs sufficiently often that the a_i could be tabulated for this case. The a_i is useful for the transparent gas approximation when the spectral intensity leaving the boundaries is known, as this spectrum will remain unchanged while traveling through the gas. If the mean spectral intensity $\bar{i}_{\lambda, i}$ is proportional to a blackbody spectrum at the temperature of the position for which $a_{\lambda}(\lambda, T, P)$ is evaluated, that is, $\bar{i}_{\lambda, i} \propto i'_{\lambda b}(\lambda, T)$ then the incident mean becomes

$$a_i(T, P) = \frac{\int_0^{\infty} a_{\lambda}(\lambda, T, P) i'_{\lambda b}(\lambda, T) d\lambda}{\int_0^{\infty} i'_{\lambda b}(\lambda, T) d\lambda} = a_P(T, P) \quad (3-81)$$

In this special case only, a_i becomes equal to a_P .

At first glance, the Rosseland mean as defined by equation (3-80) appears to be entirely different in character from a_P and a_i which are weighted by spectral distributions of energy or intensity. However, let us take equation (3-37) and write, for a one-dimensional diffusion case,

$$\frac{dq_{\lambda, z}}{d\lambda} = -\frac{4}{3a_{\lambda}} \frac{de_{\lambda b}(\lambda, T)}{dz} = -\frac{4}{3a_{\lambda}} \left(\frac{\partial e_{\lambda b}}{\partial T} \frac{dT}{dz} + \frac{\partial e_{\lambda b}}{\partial \lambda} \frac{d\lambda}{dz} \right) \quad (3-82)$$

But $d\lambda/dz$ is zero since λ and z are independent variables so that, for the diffusion case only,

$$\frac{\partial e_{\lambda b}}{\partial T} = \frac{-3a_{\lambda} \frac{dq_{\lambda, z}}{d\lambda}}{\frac{dT}{dz}} \quad (3-83)$$

Substituting equation (3-83) into equation (3-80) gives

$$a_R(T, P) = \frac{\int_0^{\infty} a_{\lambda} dq_{\lambda, z}}{\int_0^{\infty} dq_{\lambda, z}} \quad (3-84)$$

The Rosseland mean is thus seen to be an average value of a_λ weighted by the local spectral energy flux $dq_{\lambda, z}$ through the assumption that the local flux depends only on the local gradient of emissive power and the local a_λ .

For a gray gas the absorption coefficient is independent of wavelength, $a_\lambda(\lambda, T, P) = a(T, P)$, and equations (3-78) to (3-80) reduce to

$$a_p(T, P) = a_i(T, P) = a_R(T, P) = a(T, P)$$

as would be expected.

Determination of any of the mean coefficients from spectral absorption coefficients usually requires tedious detailed numerical integrations. Even so, if appropriate mean values can be successfully applied to yield reasonably accurate solutions, the time involved in solution of many radiation problems can be considerably decreased.

3.5.2 Approximate Solutions of the Transfer Equations Using Mean Absorption Coefficients

In this section are reviewed some of the references where mean absorption coefficients have been used in radiative transfer calculations. Solving the transfer equations is considerably simplified when a mean absorption coefficient is present or assumed because the integrations over wavelength are not needed. This is contrasted with exact solutions for real gases which require that these integrations be performed during each solution. It would be impossible to perform all the required integrations in advance so that they would not be needed during each calculation. For example, the incident energy absorbed at each location depends on the incident mean absorption coefficient a_i which is weighted according to the incident spectrum. Since this spectrum can have an infinite variety of forms, the a_i cannot be conveniently tabulated in advance. Also the a_λ present in the exponential attenuation terms in equation (3-1) for example cannot be conveniently averaged over wavelength.

To avoid having to carry out spectral calculations and then integrating over wavelength, certain approximations are often made. The simplifying assumption most often used is that the *gray* gas equation of transfer (2-28) can be used for a *real* gas by substituting an appropriate mean absorption coefficient in place of the a for the gray gas. In section 2.4.2 it was already shown that, although the Planck mean may indeed be used in *part* of the energy balance equation (i.e., the term dealing with local emission), the use of the same mean coefficient in the absorption and attenuation terms is invalid except in special cases. Patch (refs. 7 and 8) has shown, by examination of 40 cases, that simple substitution of the Planck

mean in the gray gas equations leads to errors in total intensities that varied from -43 to 881 percent from the solutions using spectral properties in the equation of transfer and then integrating the spectral solution. Reductions in error were found by dividing the intensity into two or more spectral bands and using a Planck mean for each individual band.

In an effort to improve this situation, a number of other mean absorption coefficients have been introduced. Sampson (ref. 9) synthesizes a coefficient that varies from the Planck mean to the Rosseland mean as the optical depth increases along a given path. He finds agreement within a factor of two to exact solutions for various example problems. Abu-Romia and Tien (ref. 10) apply a weighted Rosseland mean over optically thick portions of the spectrum, and a Planck mean over optically thin regions and obtain relations for energy transfer between bounding surfaces. Planck and Rosseland mean absorption coefficients for carbon dioxide, carbon monoxide, and water vapor are also given as an aid to such computations.

Patch (refs. 7 and 8) defines an *effective mean absorption coefficient* as

$$a_e(S, T, P) = \frac{\int_0^\infty a_\lambda(\lambda, T, P) i'_{\lambda b}(\lambda, T) \exp[-a_\lambda(\lambda, T, P)S] d\lambda}{\int_0^\infty i'_{\lambda b}(\lambda, T) \exp[-a_\lambda(\lambda, T, P)S] d\lambda} \quad (3-85)$$

The values of $a_e(S, T, P)$ can be tabulated as a function of temperature and pressure as for the other mean absorption coefficients. In addition a_e depends on the path length S and must be tabulated as a function of this additional variable. For S small, a_e approaches a_p . For very large S , the exponential term in the integrals causes a_e to approach the minimum value of a_λ in the spectrum considered. In the radiative transfer calculations the approximation is made that the real gas with T, P variable along S is replaced along any path by an effective uniform gas with absorption coefficient a_e . The computations are then performed using a_e in the gray gas equation of transfer. The a_e value used is found by equating $a_e S$ at the T, P of the point to which S is measured, to the optical depth of that point in the real gas. For 40 cases Patch (refs. 7 and 8) shows agreement within -25 to 28 percent of the integrated spectral solutions, as compared with the -43 to 881 percent agreement using a_p as discussed previously in this section. This method has value in computer-oriented solutions where the tabulated values of $a_e(S, T, P)$ can be effectively manipulated.

Other methods of using mean coefficients are given in references 11 to 15.

3.6 APPROXIMATE SOLUTION OF THE COMPLETE EQUATION OF TRANSFER

In section 3.3, it was found that in certain situations it is possible to neglect one or more terms in the equation of transfer. Solutions using the resulting simplified equation are of course much easier than solving the entire equation.

In this section some analytical methods are presented that account for *all* terms in the equation of transfer. However, only approximate solutions of the complete equation will be sought so that, while some accuracy may be lost in obtaining the solution, the ability will be gained to obtain closed-form analytical solutions in many cases. This makes it possible to gain insight into the important governing factors of the radiative transfer, in addition to obtaining answers that are often of acceptable accuracy.

3.6.1 The Astrophysical Approximations

As mentioned in the first chapter of this volume, much work has been done in the study of stellar structure by analysis of the observed radiation. Quite early in the twentieth century, astrophysicists considered the mathematical properties of the equation of transfer and applied some approximations which remain useful today. However, these approximations were developed for one-dimensional layers of an atmosphere which is the case most useful in astrophysics, and the extensions to multidimensional problems is not always obvious or possible. In this section, two of these approximations will be examined briefly. For more detailed treatments, see references 16 and 17.

3.6.1.1 *The Schuster-Schwarzschild approximation.*—The simplest approximation is to assume that, in the one-dimensional equation of transfer, the intensity in the positive direction is isotropic and that in the negative direction has a different value but is also isotropic. This is illustrated in figure 3-9.

The equation of transfer is written for the intensity in each hemisphere as

$$-\frac{\cos \beta}{a_\lambda} \frac{\partial i'_{\lambda,+}(\beta, x)}{\partial x} = i'_{\lambda,+}(\beta, x) - i'_{\lambda b}(x) \quad (3-86a)$$

$$-\frac{\cos \beta}{a_\lambda} \frac{\partial i'_{\lambda,-}(\beta, x)}{\partial x} = i'_{\lambda,-}(\beta, x) - i'_{\lambda b}(x) \quad (3-86b)$$

These equations are now integrated over their respective hemispheres to give

$$-\frac{1}{2a_\lambda} \frac{di'_{\lambda,+}(x)}{dx} = i'_{\lambda,+}(x) - i'_{\lambda b}(x) \quad (3-88a)$$

$$\frac{1}{2a_\lambda} \frac{di'_{\lambda,-}(x)}{dx} = i'_{\lambda,-}(x) - i'_{\lambda b}(x) \quad (3-88b)$$

Equations (3-88) with appropriate boundary conditions can be solved by use of an integrating factor as was done in section 2.3.2 for the equation of transfer. For the geometry of figure 3-5, if $i'_{\lambda,+}(0)$ and $i'_{\lambda,-}(D)$ are the spectral intensities at the walls for a gas layer between parallel planes, the $i'_{\lambda,+}(x)$ and $i'_{\lambda,-}(x)$ are (letting $\kappa_\lambda = a_\lambda x$)

$$i'_{\lambda,+}(\kappa_\lambda) = i'_{\lambda,+}(0) \exp(-\kappa_\lambda) + \int_0^{\kappa_\lambda} i'_{\lambda b}(\kappa_\lambda^*) \exp(\kappa_\lambda^* - \kappa_\lambda) d\kappa_\lambda^* \quad (3-89a)$$

$$i'_{\lambda,-}(\kappa_\lambda) = i'_{\lambda,-}(\kappa_{\lambda D}) \exp(\kappa_\lambda - \kappa_{\lambda D}) + \int_{\kappa_\lambda}^{\kappa_{\lambda D}} i'_{\lambda b}(\kappa_\lambda^*) \exp(\kappa_\lambda - \kappa_\lambda^*) d\kappa_\lambda^* \quad (3-89b)$$

From equation (2-39), the net spectral heat flux in the positive x direction is (with the assumption that $i'_{\lambda,+}$ and $i'_{\lambda,-}$ are isotropic)

$$\begin{aligned} q_\lambda(\kappa) &= 2\pi \left[i'_{\lambda,+}(\kappa) \int_0^{\pi/2} \cos \beta \sin \beta d\beta + i'_{\lambda,-}(\kappa) \int_{\pi/2}^\pi \cos \beta \sin \beta d\beta \right] \\ &= \pi [i'_{\lambda,+}(\kappa) - i'_{\lambda,-}(\kappa)] \end{aligned} \quad (3-90)$$

For the simplified case of a gray gas between parallel plates with no internal heat sources, the q is a constant and $i'_{\lambda b}(\kappa) = \sigma T^4(\kappa)/\pi$. Then $dq/d\kappa = 0$ giving

$$\frac{di'_+(\kappa)}{d\kappa} = \frac{di'_-(\kappa)}{d\kappa}$$

Substituting equations (3-89) yields

$$\begin{aligned} -i'_+(0) \exp(-\kappa) - \int_0^\kappa i'_b(\kappa^*) \exp(\kappa^* - \kappa) d\kappa^* + i'_b(\kappa) \\ = i'_-(\kappa_D) \exp(\kappa - \kappa_D) + \int_\kappa^{\kappa_D} i'_b(\kappa^*) \exp(\kappa - \kappa^*) d\kappa^* - i'_b(\kappa) \end{aligned}$$

or

$$\begin{aligned} \pi i'_b(\kappa) = \sigma T^4(\kappa) = & \frac{1}{2} \left[\pi i'_+(0) \exp(-\kappa) \right. \\ & + \int_0^\kappa \sigma T^4(\kappa^*) \exp(\kappa^* - \kappa) d\kappa^* + \pi i'_-(\kappa_D) \exp(\kappa - \kappa_D) \\ & \left. + \int_\kappa^{\kappa_D} \sigma T^4(\kappa^*) \exp(\kappa - \kappa^*) d\kappa^* \right] \end{aligned} \quad (3-91)$$

This is an integral equation for the temperature distribution in the gas layer and is analogous to the exact formulation in equation (2-46).

Chandrasekhar (ref. 17) has extended this method as originally developed by Schuster (ref. 18) and Schwarzschild (ref. 19) by dividing the intensity into mean portions from discrete directions, terming this the "discrete ordinate" method. The discrete ordinate method has been shown to be equivalent to the differential approximation or moment method which will be described in section 3.6.2 (ref. 20).

3.6.1.2 *The Milne-Eddington approximation.*—With respect to the intensity, the approximation made independently by Eddington (ref. 21) and Milne (ref. 22) is the same as that of Schuster and Schwarzschild. It is that all the intensity traveling along all paths crossing a unit area oriented normal to the x direction with positive components in x has a constant value with angle, and all intensity with a negative x component has a different constant value; that is, the radiation in each direction can be considered isotropic (fig. 3-9). However, the approximation is made one step later in the heat flux equation than in the Schuster-Schwarzschild method.

Start with the one-dimensional equation of transfer (2-24). Then multiply by $d\omega$ and by $\cos \beta d\omega$ to obtain the two equations

$$-\frac{\cos \beta}{a_\lambda} \frac{\partial i'_\lambda}{\partial x} d\omega = (i'_\lambda - i'_{\lambda b}) d\omega \quad (3-92a)$$

$$-\frac{\cos^2 \beta}{a_\lambda} \frac{\partial i'_\lambda}{\partial x} d\omega = \cos \beta (i'_\lambda - i'_{\lambda b}) d\omega \quad (3-92b)$$

The reason for doing this is that $i'_\lambda \cos \beta$ is related to the heat flux, and equations (3-92) will thus yield a pair of equations involving q_λ . If equations (3-92) are integrated over all solid angles, the result is

$$-\frac{1}{a_\lambda} \frac{dq_\lambda}{dx} = -\frac{1}{a_\lambda} \int_{\omega=4\pi} \cos \beta \frac{\partial i'_\lambda(\beta, x)}{\partial x} d\omega = \int_{\omega=4\pi} i'_\lambda(\beta, x) d\omega - 4\pi i'_{\lambda b} \quad (3-93a)$$

$$-\frac{1}{a_\lambda} \int_{\omega=4\pi} \cos^2 \beta \frac{\partial i'_\lambda(\beta, x)}{\partial x} d\omega = \int_{\omega=4\pi} i'_\lambda(\beta, x) \cos \beta d\omega = q_\lambda \quad (3-93b)$$

The assumption is now introduced that the i'_λ is isotropic in each hemisphere. Then

$$-\frac{1}{a_\lambda} \frac{dq_\lambda}{dx} = i'_{\lambda,+} \int_0^{\pi/2} 2\pi \sin \beta d\beta + i'_{\lambda,-} \int_{\pi/2}^\pi 2\pi \sin \beta d\beta - 4\pi i'_{\lambda b} \quad (3-94a)$$

$$q_\lambda = -\frac{1}{a_\lambda} \left[\frac{di'_{\lambda,+}}{dx} \int_0^{\pi/2} 2\pi \cos^2 \beta \sin \beta d\beta + \frac{di'_{\lambda,-}}{dx} \int_{\pi/2}^\pi 2\pi \cos^2 \beta \sin \beta d\beta \right] \quad (3-94b)$$

Integrating gives

$$-\frac{1}{a_\lambda} \frac{dq_\lambda}{dx} = 4\pi \left(\frac{i'_{\lambda,+} + i'_{\lambda,-}}{2} - i'_{\lambda b} \right) \quad (3-95a)$$

$$q_\lambda = -\frac{2\pi}{a_\lambda} \frac{d}{dx} \left(\frac{i'_{\lambda,+} + i'_{\lambda,-}}{3} \right) \quad (3-95b)$$

Eliminating $i'_{\lambda,+} + i'_{\lambda,-}$ between these two expressions gives

$$\frac{1}{a_\lambda^2} \frac{d^2 q_\lambda(x)}{dx^2} = 3q_\lambda(x) + \frac{4\pi}{a_\lambda} \frac{di'_{\lambda b}(x)}{dx} \quad (3-96)$$

or

$$\frac{d^2 q_\lambda}{d\kappa_\lambda^2} = 3q_\lambda(\kappa_\lambda) + 4 \frac{de_{\lambda b}}{d\kappa_\lambda} \quad (3-97)$$

For the situation of a gray gas layer with no internal heat sources, equation (3-97) is integrated over all wavelengths and $d^2 q/d\kappa^2 = 0$ giving

$$q(\kappa) = -\frac{4}{3} \frac{de_b}{d\kappa} \quad (3-98)$$

This is the same relation as for the diffusion approximation used to obtain equation (3-54).

3.6.2 The Differential Approximation

The *differential* approximation reduces the integral equations of radiative transfer in absorbing-emitting media to differential equations by approximating the equation of transfer with a finite set of moment equations. The moments are generated by multiplying the equation of transfer by powers of the cosine between the coordinate direction and the direction of the intensity. This is a generalization of the method of Milne and Eddington as equations (3-92a) and (3-92b) have been multiplied by $(\cos \beta)^0$ and $(\cos \beta)^1$, respectively. As will be discussed, the first three moment equations have a definite physical significance so that developing a solution method by this technique has some physical basis. The development will be given in a three-dimensional coordinate system so that general geometries can be treated. The treatment due to Cheng (refs. 23 and 24) will be followed here. Other pertinent references are 20 and 25 to 29.

A rectangular coordinate system with coordinates x_1, x_2, x_3 is shown in figure 3-10(a). The variation in the intensity at position \vec{r} along the S direction in the direction of the unit vector \vec{s} is given by the equation of transfer (2-4)

$$\frac{di'_\lambda}{dS} = a_\lambda(S) [i'_{\lambda b}(S) - i'_\lambda(S)]$$

Let a_λ be assumed constant and integrate over all wavelengths to obtain

$$\frac{di'}{dS} = a [i'_b(S) - i'(S)] \quad (3-99)$$

It should be emphasized that, although the simplified notation $i'(S)$ is used, the intensity is a function of position and angular direction vectors $i'(\vec{r}, \vec{s})$ as shown in figure 3-10(a). In terms of a three-dimensional coordinate system x_1, x_2, x_3 , equation (3-99) can be written as
 (note that $\frac{di'}{dS} = \frac{\partial i'}{\partial x_1} \frac{\partial x_1}{\partial S} + \frac{\partial i'}{\partial x_2} \frac{\partial x_2}{\partial S} + \frac{\partial i'}{\partial x_3} \frac{\partial x_3}{\partial S}$)

$$\sum_{j=1}^3 l_j \frac{\partial i'(\vec{r}, \vec{s})}{\partial x_j} = a [i'_b(\vec{r}) - i'(\vec{r}, \vec{s})] \tag{3-100}$$

where the l_j 's are the direction cosines (fig. 3-10(a)), $l_1 = \cos \beta$, $l_2 = \cos \delta$, and $l_3 = \cos \gamma$.

The moments of i' are generated by multiplying i' by powers of the l_i and integrating over all solid angles. Some new notation is introduced to designate the moments

$$\left. \begin{aligned} i'^{(0)}(\vec{r}) &\equiv \int_{\omega=4\pi} i'(\vec{r}, \vec{s}) d\omega \\ i'_j{}^{(1)}(\vec{r}) &\equiv \int_{4\pi} l_j i'(\vec{r}, \vec{s}) d\omega \\ i'_{kj}{}^{(2)}(\vec{r}) &\equiv \int_{4\pi} l_k l_j i'(\vec{r}, \vec{s}) d\omega \\ &\vdots \\ i'_{k^{n-1}j}{}^{(n)}(\vec{r}) &= \int_{4\pi} l_k^{n-1} l_j i'(\vec{r}, \vec{s}) d\omega \\ &\vdots \\ i'_{k^n}{}^{(n)}(\vec{r}) &= \int_{\omega=4\pi} l_k^n i'(\vec{r}, \vec{s}) d\omega \end{aligned} \right\} \tag{3-101}$$

Also

The zeroth-order moment $i'^{(0)}$ has the physical significance that dividing it by the speed of light gives the radiation energy density as shown by equation (2-51). The first moment $i'_j{}^{(1)}$ is the radiative energy flux in the j coordinate direction as shown in equation (2-52). The second moment $i'_{kj}{}^{(2)}$ divided by the speed of light can be shown to be the radiation stress and pressure tensor. The higher moments have no specific physical significance associated with them and are generated by analogy with the first three.

The moment equations are obtained by multiplying equation (3-100) by powers of the l_i and integrating the result over all solid angles ω . The zeroth-order moment equation is the integral of equation (3-100) itself, or noting that i'_b is independent of angle and applying the definitions of $i'^{(0)}$ and $i'^{(1)}$

$$\sum_{j=1}^3 \frac{\partial i'_j{}^{(1)}(\vec{r})}{\partial x_j} = a [4\pi i'_b{}^{(1)}(\vec{r}) - i'^{(0)}(\vec{r})] \tag{3-102}$$

Multiplying equation (3-100) by l_k and integrating give the first-order moment equation

$$\sum_{j=1}^3 \int_{4\pi} l_k l_j \frac{\partial i'}{\partial x_j} d\omega = a \left[i'_b \int_{4\pi} l_k d\omega - \int_{4\pi} l_k i' d\omega \right]$$

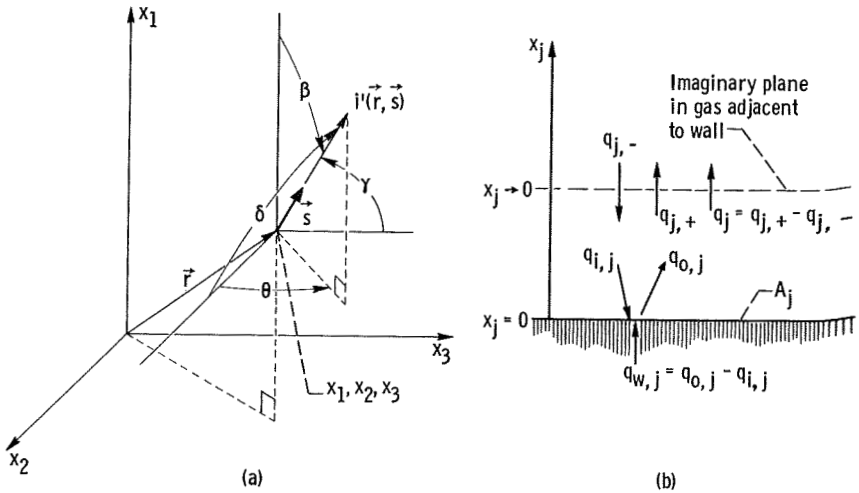
which can be written as ($k=1, 2, 3$)

$$\sum_{j=1}^3 \frac{\partial i'_{kj}{}^{(2)}(\vec{r})}{\partial x_j} = -a i'_{k'}{}^{(1)}(\vec{r}) \tag{3-103}$$

This procedure is continued to generate for example the n^{th} -order moment equation of the form

$$\sum_{j=1}^3 \frac{\partial i'_{kn}{}^{(n+1)}(\vec{r})}{\partial x_j} = -a i'_{kn}{}^{(n)}(\vec{r}) \tag{3-104}$$

By continuing the process used to obtain equations (3-102) to (3-104), an infinite set of moment equations can be generated as $n \rightarrow \infty$.



(a) Coordinate system showing intensity as a function of position and angle for differential approximation.

(b) Heat fluxes in boundary condition.

FIGURE 3-10.—Differential approximation.

The next step is to approximate the infinite set of moment equations by a finite set. When such a truncation is carried out, there will in general be n equations in $n + 1$ unknowns. The additional equation needed to relate the moments and provide a determinate set is obtained by representing the unknown angular distribution of i' as a series of spherical harmonics and then truncating this series after a finite number of terms. This whole procedure becomes quite complicated and will only be briefly treated. It is the final differential approximation obtained in equation (3-112) that is of most importance here.

The series expansion used to represent i' is

$$i'(\vec{r}, \vec{s}) = \sum_{l=0}^{\infty} \sum_{m=-l}^{+l} A_l^m(\vec{r}) Y_l^m(\omega) \tag{3-105}$$

where $A_l^m(\vec{r})$ are coefficients to be determined and

$$Y_l^m(\omega) = \left[\frac{2l+1}{4\pi} \frac{(l-m)!}{(l+m)!} \right]^{1/2} e^{im\theta} P_l^m(\cos \beta) \tag{3-106}$$

The $P_l^m(\cos \beta)$ are associated Legendre spherical harmonics (ref. 30), defined by

$$P_l^m(\cos \beta) = \frac{2^{m+1}}{\pi^{1/2}} (\sin \beta)^m \frac{\Gamma(l+m+1)}{\Gamma\left(l+\frac{3}{2}\right)} \sum_{k=0}^{\infty} \frac{\left(m+\frac{1}{2}\right)_k (l+m+1)_k}{k! \left(l+\frac{3}{2}\right)_k} \times \sin [(l+m+2k+1)\beta] \tag{3-107}$$

where $\Gamma(\xi)$ is the Gamma function, and the notation $(\alpha)_k$ signifies

$$(\alpha)_0 = 1 \quad \alpha \neq 0$$

$$(\alpha)_k = \alpha(\alpha+1)(\alpha+2) \dots (\alpha+k-1)$$

Equations (3-106) and (3-107) are substituted into equation (3-105) and the resulting series is truncated by setting $A_l^m(\vec{r}) = 0$ for $l \geq 2$. This gives an equation for $i'(\vec{r}, \vec{s})$ which is substituted into the first three moment equations to give

$$i'^{(0)}(\vec{r}) = 2\pi^{1/2} A_0^0(\vec{r}) \tag{3-108}$$

$$i'_{kj}^{(2)}(\vec{r}) = \frac{2}{3} \pi^{1/2} A_0^0(\vec{r}) \delta_{kj} \tag{3-109}$$

where δ_{kj} is the Kronecker delta. The form of these equations has been considerably simplified by applying the orthogonality relations for spherical harmonics (ref. 31). Further, note that the first moment of i' is shown by equation (2-52) to be the energy flux, or for the j direction

$$i_j^{(1)}(\vec{r}) = \int_{\omega=4\pi} i'(\vec{r}, \vec{s}) l_j d\omega = q_j(\vec{r}) \quad (3-110)$$

Eliminating $A_0^0(\vec{r})$ by combining equations (3-108) and (3-109) gives

$$\delta_{kj} i'^{(0)}(\vec{r}) = 3i_k'^{(2)}(\vec{r}) \quad (3-111)$$

Then take equation (3-111) and substitute equations (3-102), (3-103), and (3-110) to eliminate $i'^{(0)}$, $i'^{(2)}$, and $i'^{(1)}$, respectively. This results after letting $\sigma T^4 = \pi i_b'$ in the *first differential approximation to the equation of transfer* ($k=1, 2, 3$)

$$\frac{\partial}{\partial x_k} \left(\frac{1}{a} \sum_{j=1}^3 \frac{\partial q_j}{\partial x_j} \right) - 4\sigma \frac{\partial T^4}{\partial x_k} - 3aq_k = 0 \quad (3-112)$$

As mentioned by Cheng (ref. 23), equation (3-111) is equivalent to the assumption that the radiation pressure is isotropic, which in turn is equivalent to assuming radiative equilibrium in the gas.

The derivation briefly presented here by use of the moment equations can be developed in a more mathematically rigorous form by use of the spherical harmonic method, as was done in reference 24. The spherical harmonic method requires considerably more algebraic manipulation and results in the same equations developed here.

It is interesting that for $a \gg 1$, equation (3-112) reduces to the diffusion approximation as given by equation (3-37). For $a \ll 1$, equation (3-112) reduces to

$$\sum_{j=1}^3 \frac{\partial q_j}{\partial x_j} = 4a\sigma T^4 + C \quad (3-113)$$

where C is a constant of integration. As pointed out by Cess (ref. 25), equation (3-113) is the correct optically thin limit only in certain cases.

3.6.2.1 Boundary conditions.—Consider a gray boundary A_j which is perpendicular to the x_j direction as shown in figure 3-10(b). The net radiative flux leaving A_j in the positive x_j direction is

$$q_{o,j} = \epsilon_j \sigma T_j^4 + (1 - \epsilon_j) q_{i,j} \quad (3-114)$$

where q_0 and q_i are the outgoing and incoming radiation fluxes. The $q_{i,j}$ however is equal to the radiation flux in the gas traveling in the negative direction at the wall (fig. 3-10(b))

$$q_{i,j} = q_{j,-}(x_j \rightarrow 0)$$

The net flux in the gas in the positive x direction is $q_j = q_{j,+} - q_{j,-}$ so that $q_{i,j} = -q_j(x_j \rightarrow 0) + q_{j,+}(x_j \rightarrow 0)$. Now note that $q_{j,+}(x_j \rightarrow 0)$ is equal to the outgoing flux from the wall $q_{o,j}$ so that

$$q_{i,j} = -q_j(x_j \rightarrow 0) + q_{o,j}$$

Substituting into equation (3-114) gives the boundary condition

$$q_{o,j} = \epsilon_j \sigma T_j^4 + (1 - \epsilon_j) [-q_j(x_j \rightarrow 0) + q_{o,j}] \quad (3-115)$$

The outgoing flux can also be written in terms of the intensity leaving A_j as

$$q_{o,j} = \int_{\Omega} l_j i'_j d\omega \quad (3-116)$$

where l_j is the cosine of the angle between i'_j and the x_j direction.

A general form for the intensity is now found by substituting equations (3-106) and (3-107) into equation (3-105) and truncating as before. The moment equations are used to determine the $A_l^m(\vec{r})$ and after considerable manipulation the equation for $i'(\vec{r}, \vec{s})$ is found to be

$$i'(\vec{r}, \vec{s}) = \frac{1}{4\pi} [i^{(0)}(\vec{r}) + 3q_3 \sin \theta \sin \beta + 3q_1 \cos \beta + 3q_2 \cos \theta \sin \beta] \quad (3-117)$$

As a specific case, assume the boundary surface is normal to the x_1 direction. Then equation (3-117) is substituted into equation (3-116) to give

$$q_{o,1} = \int_0^{2\pi} \int_0^{\pi/2} \frac{1}{4\pi} [i^{(0)}(\vec{r}) + 3q_3 \sin \theta \sin \beta + 3q_1 \cos \beta + 3q_2 \cos \theta \sin \beta]_{x_1=0} \cos \beta \sin \beta d\beta d\theta$$

which reduces to

$$q_{o,1} = \frac{i^{(0)}(x_1 \rightarrow 0)}{4} + \frac{q_1(x_1 \rightarrow 0)}{2} \quad (3-118)$$

where $q_1(x_1 \rightarrow 0)$ is the net heat flux in the x_1 direction in the gas adjacent to the wall. The $i^{(0)}$ can be eliminated by using equation (3-102) and then $i^{(1)}$ is eliminated by using equation (3-110). This gives

$$q_{o,1} = \left(\sigma T^4 - \frac{1}{4a} \sum_{j=1}^3 \frac{\partial q_j}{\partial x_j} + \frac{q_1}{2} \right)_{x_1=0} \quad (3-119)$$

Combining equations (3-119) and (3-115) written for $j=1$ to eliminate $q_{o,1}$ gives the boundary condition

$$\left(\frac{1}{\epsilon_1} - \frac{1}{2} \right) q_1(x_1 \rightarrow 0) - \frac{1}{4a} \sum_{j=1}^3 \frac{\partial q_j}{\partial x_j} \Big|_{x_1 \rightarrow 0} = \sigma [T_1^4 - T^4(x_1 \rightarrow 0)] \quad (3-120)$$

Equations (3-112) and (3-120) comprise the governing equation and boundary condition for the differential approximation to radiative transfer. Stone and Gaustad (ref. 26) give a formulation for nongray gases for the astrophysical boundary condition of zero incident flux at one boundary.

3.6.2.2 Applications of the differential approximation.— Consider the case of infinite parallel gray plates (as in fig. 3-5) with emissivities ϵ_{w1} and ϵ_{w2} , at temperatures T_{w1} and T_{w2} , separated by a distance D and having a gray gas between them. The heat flux traveling through the gas is independent of x and y and by conservation of energy is constant with z so all $\partial q_j / \partial x_j = 0$. Then the differential equation of transfer (3-112) reduces to

$$q_z = -\frac{4\sigma}{3a} \frac{\partial T^4}{\partial z} \quad (3-121)$$

The boundary condition at $z=0$ becomes from equation (3-120)

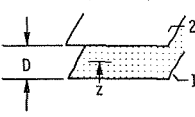
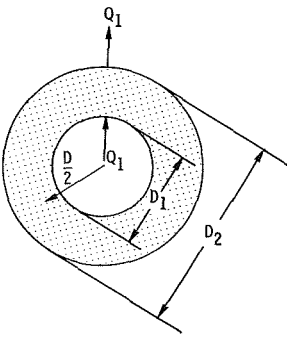
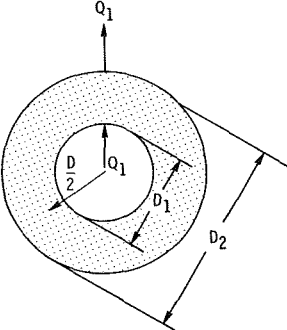
$$\left(\frac{1}{\epsilon_{w1}} - \frac{1}{2} \right) q_z = \sigma [T_{w1}^4 - T_g^4(z \rightarrow 0)] \quad (3-122)$$

where the subscript g is used in T_g to emphasize that this temperature is in the gas. At $z=D$,

$$-\left(\frac{1}{\epsilon_{w2}} - \frac{1}{2} \right) q_z = \sigma [T_{w2}^4 - T_g^4(z \rightarrow D)] \quad (3-123)$$

the negative sign in equation (3-123) arising because the normal direction from the surface into the gas is in the negative z direction. These are precisely the equations found for the parallel plate case in section

TABLE 3-III.—DIFFERENTIAL APPROXIMATIONS FOR ENERGY TRANSFER AND TEMPERATURE DISTRIBUTION FOR A GRAY GAS BETWEEN GRAY SURFACES

Geometry	Relations ^a
<p>Infinite parallel plates</p> 	$\psi = \frac{1 + E_1}{\frac{3aD}{4} + E_1 + E_2 + 1}$ $\varphi(z) = \frac{\psi}{1 + E_1} \left[\frac{3a}{4} (D - z) + E_2 + \frac{1}{2} \right]$
<p>Infinitely long concentric cylinders</p> 	$\psi = \frac{1 + E_1}{\frac{3}{8} \left[aD_1 \ln \left(\frac{D_2}{D_1} \right) + \frac{4}{3} \frac{D_1^2}{aD_1} \right] + \left(E_1 + \frac{1}{2} \right) + \frac{D_1}{D_2} \left(E_2 + \frac{1}{2} \right)}$ $\varphi \left(\frac{D}{2} \right) = \frac{\psi}{1 + E_1} \left\{ -\frac{3}{8} \left[aD_1 \ln \left(\frac{D}{D_2} \right) + \frac{4}{3} \frac{D_1}{aD_2^2} \right] + \left(E_2 + \frac{1}{2} \right) \frac{D_1}{D_2} \right\}$
<p>Concentric spheres</p> 	$\psi = \frac{1 + E_1}{\frac{3}{8} \left[aD_1 \left(1 - \frac{D_1}{D_2} \right) + \frac{8}{3aD_1} \left(1 - \frac{D_1^3}{D_2^3} \right) \right] + \left(E_1 + \frac{1}{2} \right) + \frac{D_1^2}{D_2^2} \left(E_2 + \frac{1}{2} \right)}$ $\varphi \left(\frac{D}{2} \right) = \frac{\psi}{1 + E_1} \left\{ -\frac{3}{8} \left[aD_1 \left(\frac{D_1}{D_2} - \frac{D_1}{D} \right) + \frac{8D_1^2}{3aD_2^2} \right] + \left(E_2 + \frac{1}{2} \right) \frac{D_1^2}{D_2^2} \right\}$

^aDefinitions: $E_N = (1 - \epsilon_{WN})/\epsilon_{WN}$, $\psi = Q_1/[\epsilon_{W1}A_1\sigma(T_{W1}^4 - T_{W2}^4)]$, $\varphi(\xi) = [T^4(\xi) - T_{W2}^4]/(T_{W1}^4 - T_{W2}^4)$.

3.4.3.1 by use of the diffusion approximation. Thus for infinite parallel plates the predicted temperature distributions and heat transfer by the differential approximation will be the same as for the diffusion approximation. In table 3-III are also shown the differential predictions

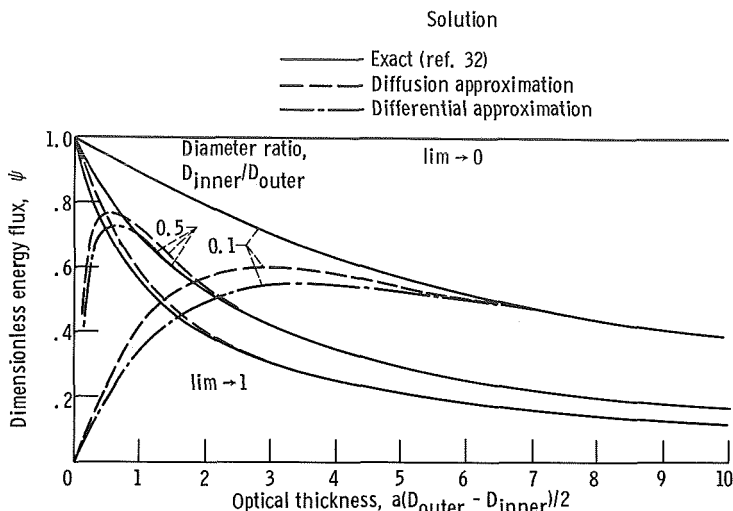


FIGURE 3-11.—Comparison of solutions for energy transfer between infinitely long concentric black cylinders enclosing gray gas.

for concentric cylinders and spheres. Comparison with table 3-II for the diffusion approximation with second-order slip shows that for these geometries the results by the two methods differ only by constant factors that have little effect on the predictions in most cases. A comparison with the exact numerical solution of reference 32 is shown in figure 3-11 for the case of black concentric cylinders. Note that agreement with the exact solution is better in some ranges for the diffusion approximation, and in others for the differential approximation.

3.7 CONCLUDING REMARKS

This chapter is an attempt to survey briefly the most important of the many approximation techniques that are used for solution of the equation of transfer. The transparent, emission, and cold material approximations are valuable in certain simplified cases; the diffusion solution with slip boundary conditions is easy to use and accurate when the limitations are satisfied. The astrophysical approximations for one-dimensional layers are of interest chiefly from a historical standpoint, although they are still sometimes useful. The equations resulting from the differential approximation are becoming widely used because of their simplicity and accuracy. The gray gas equation using mean absorption coefficients is often applied, but can produce large errors in some cases.

REFERENCES

1. DESSLER, R. G.: Diffusion Approximation for Thermal Radiation in Gases with Jump Boundary Condition. *J. Heat Transfer*, vol. 86, no. 2, May 1964, pp. 240-246.
2. ROSSELAND, S.: *Theoretical Astrophysics; Atomic Theory and the Analysis of Stellar Atmospheres and Envelopes*. Clarendon Press, Oxford, 1936.
3. HOWELL, JOHN R.: Radiative Interactions Between Absorbing-Emitting and Flowing Media with Internal Energy Generation. NASA TN D-3614, 1966.
4. HEASLET, MAX A.; AND WARMING, ROBERT F.: Radiative Transport and Wall Temperature Slip in an Absorbing Planar Medium. *Int. J. Heat Mass Transfer*, vol. 8, no. 7, July 1965, pp. 979-994.
5. HOWELL, JOHN R.: On the Radiation Slip Between Absorbing-Emitting Regions with Heat Sources. *Int. J. Heat Mass Transfer*, vol. 10, no. 3, Mar. 1967, pp. 401-402.
6. HOWELL, JOHN R.; AND PERLMUTTER, MORRIS: Monte Carlo Solution of Radiant Heat Transfer in a Nongray Nonisothermal Gas with Temperature Dependent Properties. *AIChE J.*, vol. 10, no. 4, June 1964, pp. 562-567.
7. PATCH, R. W.: Effective Absorption Coefficients for Radiant Energy Transport in Nongray, Nonscattering Gases. *J. Quant. Spectrosc. Radiat. Transfer*, vol. 7, no. 4, 1967, pp. 611-637.
8. PATCH, R. W.: Approximation for Radiant Energy Transport in Nongray, Nonscattering Gases. NASA TN D-4001, 1967.
9. SAMPSON, DOUGLAS H.: Choice of an Appropriate Mean Absorption Coefficient for Use in the General Grey Gas Equations. *J. Quant. Spectrosc. Radiat. Transfer*, vol. 5, no. 1, 1965, pp. 211-225.
10. ABU-ROMIA, M. M.; AND TIEN, C. L.: Appropriate Mean Absorption Coefficients for Infrared Radiation in Gases. *J. Heat Transfer*, vol. 89, no. 4, Nov. 1967, pp. 321-327.
11. GRANT, IAN P.: On the Representation of Frequency Dependence in Non-Grey Radiative Transfer. *J. Quant. Spectrosc. Radiat. Transfer*, vol. 5, no. 1, 1965, pp. 227-243.
12. STEWART, JOHN C.: Non-Grey Radiative Transfer. *J. Quant. Spectrosc. Radiat. Transfer*, vol. 4, no. 5, 1964, pp. 723-729.
13. THOMAS, M.; AND RICDON, W. S.: A Simplified Formulation for Radiative Transfer. *AIAA J.*, vol. 2, no. 11, Nov. 1964, pp. 2052-2054.
14. LICK, WILBERT: Energy Transfer by Radiation and Conduction. *Proceedings of the 1963 Heat Transfer and Fluid Mechanics Institute*. Anatol Roshko, Bradford Sturtevant, and D. R. Bartz, eds., Stanford Univ. Press, 1963, pp. 14-26.
15. HOWE, JOHN T.; AND SHEAFFER, YVONNE S.: Spectral Radiative Transfer Approximations for Multicomponent Gas Mixtures. *J. Quant. Spectrosc. Radiat. Transfer*, vol. 7, no. 4, 1967, pp. 695-701.
16. KOURGANOFF, VLADIMIR: *Basic Methods in Transfer Problems; Radiative Equilibrium and Neutron Diffusion*. Dover Publications, 1963.
17. CHANDRASEKHAR, SUBRAHMANYAN: *Radiative Transfer*. Dover Publications, 1960.
18. SCHUSTER, A.: Radiation Through a Foggy Atmosphere. *Astrophys. J.*, vol. 21, Jan. 1905, pp. 1-22.
19. SCHWARZSCHILD, K.: Equilibrium of the Sun's Atmosphere. *Gesell. Wiss. Göttingen, Nachr., Math.-Phys. Klasse*, vol. 1, 1906, pp. 41-53.
20. KROOK, MAX: On the Solution of Equations of Transfer. I. *Astrophys. J.*, vol. 122, no. 3, Nov. 1955, pp. 488-497.
21. EDDINGTON, A. S.: *The Internal Constitution of the Stars*. Dover Publications, 1959.
22. MILNE, E. A.: *Thermodynamics of the Stars*. *Handbuch der Astrophysik*, vol. 3. J. Springer, Berlin, 1930, pp. 65-255.
23. CHENG, PING: Two-Dimensional Radiating Gas Flow by a Moment Method. *AIAA J.*, vol. 2, no. 9, Sept. 1964, pp. 1662-1664.

24. CHENG, PING: Dynamics of a Radiating Gas With Application to Flow Over a Wavy Wall. *AIAA J.*, vol. 4, no. 2, Feb. 1966, pp. 238-245.
25. CESS, ROBERT D.: On the Differential Approximation in Radiative Transfer. *Zeit. f. Angew. Math. Phys.*, vol. 17, 1966, pp. 776-781.
26. STONE, PETER H.; AND GAUSTAD, JOHN E.: The Application of a Moment Method to the Solution of Non-Gray Radiative-Transfer Problems. *Astrophys. J.*, vol. 134, no. 2, 1961, pp. 456-468.
27. TRAUGOTT, S. C.: A Differential Approximation for Radiative Transfer with Application to Normal Shock Structure. *Proceedings of the 1963 Heat Transfer and Fluid Mechanics Institute*. Anatol Roshko, Bradford Sturtevant, and D. R. Bartz, eds., Stanford Univ. Press, 1963, pp. 1-13.
28. ADRIANOV, V. N.; AND POLYAK, G. L.: Differential Methods for Studying Radiant Heat Transfer. *Int. J. Heat Mass Transfer*, vol. 6, no. 5, May 1963, pp. 355-362.
29. TRAUGOTT, S. C.; AND WANG, K. C.: On Differential Methods for Radiant Heat Transfer. *Int. J. Heat Mass Transfer*, vol. 7, no. 2, Feb. 1964, pp. 269-273.
30. ABRAMOWITZ, MILTON A.; AND STEGUN, IRENE A., EDS.: *Handbook of Mathematical Functions with Formulas, Graphs, and Mathematical Tables*. Appl. Math. Ser. 55, Nat. Bur. Standards, 1965.
31. WYLIE, CLARENCE R., JR.: *Advanced Engineering Mathematics*. Second ed., McGraw-Hill Book Co., Inc., New York, 1960.
32. PERLMUTTER, M.; AND HOWELL, J. R.: Radiant Transfer Through a Gray Gas Between Concentric Cylinders Using Monte Carlo. *J. Heat Transfer*, vol. 86, no. 2, May 1964, pp. 169-179.

Chapter 4. An Introduction to the Microscopic Basis for Radiation in Gases and Gas Properties

4.1 INTRODUCTION

In earlier chapters, the treatment of thermal radiative transfer through absorbing, emitting, and scattering media has been chiefly from a macroscopic viewpoint. The atomic and molecular processes that govern the macroscopic effects have been only briefly described in chapter 1. Since the physical phenomena are understood on atomic and molecular levels, much of the macroscopic material can be developed or at least interpreted on a fundamental basis. In this chapter, the nomenclature of some of the atomic and molecular processes is introduced and a qualitative discussion is given to relate these processes to the macroscopic approach. Little is done to give methods of quantitative analysis; rather, it is intended that for further information the reader will consult more specialized literature, having gained some knowledge of the background material from this chapter.

The analytical expressions are generally given in terms of *angular frequency* $\Omega = 2\pi\nu = 2\pi c/\lambda$ (rad/sec) rather than wavelength λ or frequency ν . This is done because Ω is the most common cyclical quantity employed in the literature related to this chapter and it is advisable for the reader to become familiar with it. By use of Ω some of the equations have a shorter form resulting from the elimination of 2π factors. In a few places the wave number $\eta = 1/\lambda$ is employed because certain correlations in the literature have been given in terms of this variable.

4.2 SYMBOLS

A	area
\bar{A}	effective line or band width
A_{ij}	Einstein coefficient for spontaneous emission
a	absorption coefficient
B_{ij}	Einstein coefficient for absorption or induced emission
b	line shape parameter
c	speed of light in a medium
c_0	speed of light in a vacuum
D	diameter of colliding particles
E	energy
e	electronic charge

f	oscillator strength, eq. (4-49)
h	Planck's constant
\hbar	modified Planck's constant, $h/2\pi$
i	radiation intensity
k	Boltzmann's constant
l	separation constant in solution for ψ
M	mass of molecule or nucleus
m_e	mass of electron
m_l	separation constant in solution for ψ
m_p	mass of particle
n	number density, particles per unit volume; separation constant in solution for ψ ; an integer
P	total pressure
p	partial pressure; momentum of photon
Q	energy per unit time
R_e	equilibrium distance between atoms
R_y	Rydberg constant
r	radial coordinate
r_e	radius of electron orbit
r_o	classical electron radius
S	coordinate along path of radiation
S_{ij}	integrated line absorption
T	absolute temperature
T_0	reference temperature of 100 K in table 4-III
t	time
V	potential energy; volume
v	velocity
X	mass path length, ρS
x, y, z	coordinates in Cartesian system
β	pressure broadening parameter in table 4-II
Δ	"full" half-width of spectral line
δ	average spacing between lines of absorption band
ϵ	emittance
η	wave number
λ	wavelength
μ	reduced mass
ν	frequency
ρ	density of gas
τ	time-dependent portion of Ψ
Ψ	time-dependent wave function
ψ	time-independent wave function
Ω	angular frequency
ω	solid angle

Subscripts:

a	absorbed
b	blackbody
c	for collisional broadening
D	for Doppler broadening
e	electron; equilibrium; emitted
i, j	energy state i or j
l	l^{th} band
N_2	nitrogen
n	allowable particle orbits; for natural broadening
p	projected; photon
ν	dependent upon frequency
Ω	dependent upon angular frequency

Superscripts:

'	directional quantity
+	true value, not modified by addition of induced emission
*	complex conjugate

4.3 SOME ELEMENTS OF QUANTUM THEORY

4.3.1 Bohr Model of Hydrogen Atom

Classical physics is unable to account for the line emission spectrum of gases. To account for the line emission, Bohr in 1913 introduced his theory of the atom, and in so doing departed radically from the classical picture. Bohr's atom is constructed in its most simple form by considering the hydrogen atom and making three basic postulates:

(1) An electron moves in a circular orbit without decay of energy, and the orbit is subject to a balance of dynamic and electrostatic forces.

(2) Only stable orbits exist such that the angular momentum of the electron is *quantized*; that is, the angular momentum of the electron takes on only discrete values.

(3) The difference in energy for electrons present in different stable orbits is equal to the energy of a photon required to produce a change in orbit.

To write these postulates in mathematical form, consider an electron of mass m_e and negative charge e in a circular orbit of radius r_e around a stationary hydrogen nucleus. The Coulomb force of attraction on the electron exerted by the nucleus is e^2/r_e^2 , while the outward force from centripetal acceleration is $m_e r_e \Omega_e^2$ where Ω_e is the orbital angular frequency of the *electron*. This yields the force balance

$$\frac{e^2}{r_e^2} = m_e r_e \Omega_e^2 \quad (4-1)$$

The energy of the electron consists of potential (see eq. (4-19)) and kinetic energy, giving

$$E = -\frac{e^2}{r_e} + \frac{m_e r_e^2 \Omega_e^2}{2} \quad (4-2)$$

By use of equation (4-1) this can be written as

$$E = -\frac{e^2}{2r_e} \quad (4-3)$$

so that the electron energy has a reference level of zero as r_e becomes infinite.

Since the electron is accelerating, classical electrodynamic theory would dictate that it should radiate energy and consequently slow down and spiral into the nucleus. To provide radiation in the form of spectral lines, however, Bohr considered that the radiative energy loss must occur in finite steps so that the energy given by equation (4-3) would consist of a series of discrete levels. It was postulated that the allowable states would be those for which the electron angular momentum is a multiple of Planck's constant. Thus,

$$m_e r_{e,n}^2 \Omega_{e,n} = n\hbar \quad n = 1, 2, 3, \dots i, j, \dots \quad (4-4)$$

Equation (4-1) written for the n^{th} orbit is combined with equation (4-4) to eliminate $\Omega_{e,n}$. This gives the allowable radii of the electron orbits as

$$r_{e,n} = \frac{n^2 \hbar^2}{m_e e^2} \quad (4-5)$$

Equation (4-5) is used for the radius in equation (4-3) to yield the discrete energy states as

$$E_n = -\frac{e^4 m_e}{2n^2 \hbar^2} \quad (4-6)$$

Now consider the transition between two energy states. The difference in energy between the j^{th} and i^{th} states is obtained from equation (4-6) as

$$E_j - E_i = \frac{e^4 m_e}{2\hbar^2} \left(\frac{1}{i^2} - \frac{1}{j^2} \right) \quad (4-7)$$

The energy of the photon required to produce a transition of the electron between the two stable orbits i and j is equal to $\hbar\Omega_{ij}$ where Ω_{ij} is the *photon* angular frequency. Then equation (4-7) can be written as

$$E_j - E_i = \hbar\Omega_{ij} = Ry \left(\frac{1}{i^2} - \frac{1}{j^2} \right) \quad (4-8)$$

where Ry is the Rydberg constant,

$$Ry = \frac{e^4 m_e}{2\hbar^2} \quad (4-9)$$

and has units of energy. If the transition is considered between the lowest energy orbit (ground state, $i = 1$) and the highest energy orbit ($j = \infty$), it is seen that

$$E_\infty - E_1 = Ry \quad (4-10)$$

This is the energy required to remove the electron from the atom, and Ry is considered to be the *ionization potential* for the hydrogen atom. Equation (4-8) is found to predict exactly the frequencies of the spectral line series of atomic hydrogen. However, for other atoms the prediction of line frequencies is not accurate, and in many cases fails completely. For atoms with a single electron in the outer shell, the theory can be patched up to yield adequate results.

4.3.2 Schrödinger Wave Equation

Because the Bohr theory is a rather curious mixture of classical and quantum ideas, and because the predictions of the theory are not adequate, a better formulation is required. This formulation is given by modern quantum theory. The price we pay for the more adequate predictions is a loss of the clear physical picture presented by the Bohr atom.

In 1924, Louis deBroglie suggested that matter could have wave properties associated with it in much the same way that a photon can be assigned a mass. The momentum of a *photon* is given by

$$p = \frac{\hbar\Omega}{c} = \frac{h}{\lambda} \quad (4-11)$$

Then by analogy, for a particle of mass m_p and velocity v , an associated wavelength can be found by letting $m_p v = h/\lambda$ giving the wavelength associated with the particle as

$$\lambda = \frac{h}{m_p v} \quad (4-12)$$

The idea that a particle of matter can have an associated wavelength seemed to be useless—however, experimental confirmation came in the form of diffraction patterns produced by the scattering of electrons from crystals. The patterns which are wave phenomena were predictable if the electrons (assumed to be particles of matter) were given the wavelength predicted by equation (4-12).

If matter indeed has the properties of waves, then some form of equation should predict the behavior of these waves. Where the waves interfere constructively, we expect to find a particle and we expect this interference to occur over relatively small regions of space. The equation that is found to provide this behavior for the waves was derived by Schrödinger in 1926 and is known as the *Schrödinger wave equation*. In the *time-dependent form* it is for a particle

$$\frac{-\hbar^2}{2m_p} \nabla^2 \Psi + V\Psi = \frac{-\hbar}{i} \frac{\partial \Psi}{\partial t} \quad (4-13)$$

where V is the time-dependent potential energy of the particle in the coordinates of ∇^2 and i is the imaginary root $i = \sqrt{-1}$. Equation (4-13) cannot be derived from a physical model as can the classical wave equation in chapter 4 of volume I. Rather, the justification for this form is that it predicts observable effects. We are left with constructing physical models to fit the mathematical equation if we desire them, rather than the usual process of fitting an equation to the physical model.

Schrödinger showed that the *wave function* Ψ has certain boundary conditions that are physically meaningful; it is single valued, finite, continuous, and vanishes at infinity. When these constraints on Ψ are observed, it is found that the solutions to equation (4-13) are eigenvalue-eigenfunction solutions. It is this fact that imposes quantization on a system through the mathematics: quantization is not *assumed*, but is a *result* of the boundary conditions on the Schrödinger equation.

The function Ψ has no direct physical interpretation. It corresponds in some ways to the amplitude in the classical wave equation. A more useful interpretation is to consider Ψ as a probability density. However, since Ψ is in general a complex function, it is more convenient to treat the real quantity $\Psi\Psi^* = |\Psi|^2$ as the probability density where Ψ^* is the complex conjugate of Ψ . The square of the magnitude of the wave function $|\Psi|^2$ then gives the probability density at any instant of finding a particle of matter in a given location.

To satisfy the boundary conditions, it is possible to obtain a solution

to the time-dependent Schrödinger equation by separation of variables if the potential energy V does not depend on time. The separated product has the form

$$\Psi(x, y, z, t) = \psi(x, y, z)\tau(t) \quad (4-14)$$

Inserting this into equation (4-13) gives the two equations

$$\nabla^2\psi + \frac{2m_p}{\hbar^2}(\epsilon - V)\psi = 0 \quad (4-15)$$

and

$$\frac{d\tau}{dt} + \frac{\epsilon i}{\hbar}\tau = 0 \quad (4-16)$$

where ϵ is the separation constant.

Equation (4-16) has the solution (within an arbitrary multiplying constant)

$$\tau = \exp\left(-i\frac{\epsilon}{\hbar}t\right) = \cos\left(\frac{\epsilon}{\hbar}t\right) + i\sin\left(\frac{\epsilon}{\hbar}t\right) \quad (4-17)$$

and therefore by substituting into equation (4-14)

$$\Psi = \psi(x, y, z) \exp\left(-i\frac{\epsilon}{\hbar}t\right) \quad (4-18)$$

(Note that the i in equations (4-17) and (4-18) is the imaginary number, not the i^{th} energy state.) We now need to find ψ , the solution to the time-independent form of Schrödinger's wave equation (eq. (4-15)) to determine the complete wave function Ψ .

The wave equation will be considered here specifically for determining energy of an electron around the nucleus of the hydrogen atom. The potential energy of the electron is (based on zero potential energy at $r \rightarrow \infty$)

$$V = \int_{\infty}^{r_e} F dr = \int_{\infty}^{r_e} \frac{e^2}{r^2} dr = \frac{-e^2}{r_e} \quad (4-19)$$

where F is the Coulomb force between the electron and the nucleus. Using V from equation (4-19) results in the time-independent Schrödinger equation (4-15) becoming (the subscript of r_e is dropped for simplicity)

$$\nabla^2\psi + \frac{2\mu}{\hbar^2}\left(\epsilon + \frac{e^2}{r}\right)\psi = 0 \quad (4-20)$$

where the particle mass has been replaced by μ , the reduced mass of

the nucleus-electron system,

$$\mu = \frac{Mm_e}{M + m_e}$$

where M is the mass of the nucleus. The use of μ accounts in the dynamics of the electron nucleus system for the slight motion of the nucleus around the center of mass, an effect that was neglected in equation (4-1).

In spherical coordinates, equation (4-20) is

$$\begin{aligned} \frac{1}{r^2} \frac{\partial}{\partial r} \left(r^2 \frac{\partial \psi}{\partial r} \right) + \frac{1}{r^2 \sin \theta} \frac{\partial}{\partial \theta} \left(\sin \theta \frac{\partial \psi}{\partial \theta} \right) \\ + \frac{1}{r^2 \sin^2 \theta} \frac{\partial^2 \psi}{\partial \varphi^2} + \frac{2\mu}{\hbar^2} \left(\epsilon + \frac{e^2}{r} \right) \psi = 0 \end{aligned} \quad (4-21)$$

A separation of variables can be applied to obtain ψ as a function of r , θ , and φ , where θ is the cone angle,

$$\psi = R(r)\Theta(\theta)\Phi(\varphi) \quad (4-22)$$

Substituting into equation (4-21) results in the three separated equations

$$\frac{-1}{\Phi} \frac{d^2 \Phi}{d\varphi^2} = m_l^2 \quad (4-23)$$

$$\frac{1}{R} \frac{d}{dr} \left(r^2 \frac{dR}{dr} \right) + \frac{2\mu}{\hbar^2} \left(\epsilon + \frac{e^2}{r} \right) r^2 = l(l+1) \quad (4-24)$$

$$\frac{-1}{\Theta \sin \theta} \frac{d}{d\theta} \left(\sin \theta \frac{d\Theta}{d\theta} \right) = l(l+1) - \frac{m_l^2}{\sin^2 \theta} \quad (4-25)$$

where m_l and l are separation constants which are specified as $m_l = 0, \pm 1, \pm 2, \dots, \pm l$; $l = 0, 1, 2, \dots, n-1$; and $n = 1, 2, \dots, \infty$. The solution to equation (4-23) that is used is

$$\Phi = A \exp(im_l \varphi) \quad (4-26)$$

Equation (4-24) has solutions for R in terms of Laguerre polynomials that involve the arbitrary constant n , and equation (4-25) has solutions for Θ in terms of Legendre polynomials. The solution for ψ thus depends on the three constants, n , l , and m_l , each of which has discrete values. These constants are called the *quantum numbers*, and they define the possible discrete forms of ψ .

If the radii are found for which the wave function has a large expectation value, these should correspond to the positions at which electrons are found with a high probability. These radii are found by the usual spatial averaging techniques

$$r_n = \frac{\int_{\text{all space}} \psi_n r \psi_n^* dV}{\int_{\text{all space}} \psi_n \psi_n^* dV} = \int_{\text{all space}} \psi_n r \psi_n^* dV \quad (4-27)$$

where the denominator is unity by virtue of ψ being normalized as a probability density function. When this integration is carried out, the radii for various integer values of n are found to be exactly those predicted by Bohr (eq. 4-5). It is again emphasized that the discrete values of r are imposed by the mathematics of the Schrödinger equation, and not by assumption as in the Bohr theory.

Each of the linearly independent solutions for ψ specifies a *quantum state* of the electron. The energy of the electron in the hydrogen atom is found to be independent of the quantum numbers l and m_l . Thus there are a large number of quantum states corresponding to the various l and m_l that have the same energy. Such states are called degenerate. By summing the number of such states that are present for a given energy, it is found that there are $2n^2$ degenerate states per energy level E_n . (Actually, the treatment given here predicts n^2 degenerate states; the inclusion of electron spin provides the factor of 2.)

In statistical mechanics, it is assumed that every quantum state in the atom is equally likely. Because there are $2n^2$ quantum states in a given energy level E_n , the factor $2n^2$ is called the *statistical weight* or *multiplicity* of energy level n in the hydrogen atom. Other atoms will have other statistical weights. Knowing the statistical weight allows us to treat the total number of transitions per unit time occurring between two energy levels in terms of an average transition rate for all the states in that level times the statistical weight. Detailed examination of each degenerate state is unnecessary.

4.4 INDUCED EMISSION AND THE PLANCK DISTRIBUTION

The concept of induced emission was introduced in section 1.5.5. It was noted there that measuring the attenuation of a radiant beam traveling through a medium gives no distinct information about induced emission. This is because physically the induced emission combines with the true absorption to produce an effective absorption smaller than the true absorption. As far as radiation attenuation measurements are concerned, the true absorption and induced emission effects cannot be

separated. Einstein (refs. 1 and 2) showed, however, that induced emission must exist. Einstein's relatively simple arguments will now be given, employing induced emission in the course of a derivation of Planck's blackbody spectral distribution. Without induced emission certain rules that are now available in statistical mechanics are also violated, although statistical mechanics will not be discussed here.

Consider bound-bound transitions in an absorbing medium exposed to incident radiation having spectral intensity i'_Ω . For simplicity let the system be a collection of noninteracting atoms. Since blackbody radiation is desired, let the medium be in a black isothermal enclosure at uniform temperature—this is the condition for blackbody equilibrium (section 2.3.2 of vol. I). An atom in the medium can absorb incident energy and thereby undergo a transition from energy state i to energy state j . State j will consequently have a larger energy than i , or in other words j is an "excited" state relative to i . The rate at which the transitions from i to j occur will depend on the intensity of the incident radiation field and the population of state i . Let n_i be the number of atoms per unit volume in state i . The Einstein coefficient B_{ij} is now introduced. This is defined as the probability per unit time and volume of a transition occurring from state i to state j as a result of the incident energy flux per unit solid angle and is a function only of the particular atomic system being considered.⁴ Then the number of transitions per unit time, considering the effect of incident energy from all directions, is

$$\left(\frac{dn_i}{dt}\right)_{i \rightarrow j} = B_{ij}n_i \int_{\omega=4\pi} i'_\Omega d\omega \quad (4-28)$$

Since the Einstein coefficient depends only on the states i and j for the particular atomic system, it is taken out of the integral over solid angle.

The rate at which transitions will occur from the excited state j to the initial state i depends on two factors. These factors are *spontaneous emission* which depends on the population n_j in the excited state, and *induced emission* which depends on the population n_j and on the radiation field intensity. Thus introduce A_{ji} as the probability for a transition by spontaneous emission into a unit solid angle, and let B_{ji} be the transition probability for induced emission. Then the rate of transitions from j to i is

$$\left(\frac{dn_j}{dt}\right)_{j \rightarrow i} = 4\pi n_j A_{ji} + n_j B_{ji} \int_{\omega=4\pi} i'_\Omega d\omega \quad (4-29)$$

⁴ Other texts include or exclude various factors of 2 and π in the definitions. Sometimes the transition rate is written as proportional to the spectral energy density $(1/c) \int_{\omega=4\pi} i'_\Omega d\omega$ rather than the intensity.

Since on the average for a collection of randomly oriented emitting atoms in equilibrium the spontaneous emission is isotropic, $4\pi A_{ji}$ is the probability of transition from j to i by spontaneous emission into all directions.

For a system in equilibrium, the principle of *detailed balancing* must hold (ref. 3). This principle states that the transition rates upward and downward between any two energy states must be equal when all transition processes are included. Using this principle, the dn/dt from equations (4-28) and (4-29) are equated giving

$$B_{ij}n_i \int_{\omega=4\pi} i'_{\Omega b} d\omega = 4\pi n_j A_{ji} + n_j B_{ji} \int_{\omega=4\pi} i'_{\Omega b} d\omega \quad (4-30)$$

where at equilibrium in the assumed isothermal black enclosure the intensity becomes the blackbody intensity $i'_{\Omega b}$. For blackbody equilibrium conditions the incident intensity is also isotropic so that

$$\int_{\omega=4\pi} i'_{\Omega b} d\omega = 4\pi i'_{\Omega b}$$

Then solving equation (4-30) for $i'_{\Omega b}$ gives

$$i'_{\Omega b} = \frac{A_{ji}}{\frac{n_i}{n_j} B_{ij} - B_{ji}} \quad (4-31)$$

At thermal equilibrium the populations of the energy states are related according to the Boltzmann distribution (ref. 3). If E_i and E_j are the energies of the states, then the Boltzmann distribution gives

$$\frac{n_i}{n_j} = \exp \left[\frac{-(E_i - E_j)}{kT} \right] \quad (4-32)$$

where k is the Boltzmann constant. As discussed in section 1.3 and in connection with equation (4-8), the energy difference $E_j - E_i$ is equal to the energy of the photon either absorbed to produce the transition from E_i to E_j or emitted when there is a transition from E_j to E_i . Then, in terms of angular frequency

$$E_j - E_i = \hbar\Omega_{ij} \quad (4-33)$$

so that equation (4-32) becomes

$$\frac{n_i}{n_j} = \exp \left(\frac{\hbar\Omega_{ij}}{kT} \right) \quad (4-34)$$

When equation (4-34) is applied to a system, the statistical weights discussed at the end of section 4.3.2 must also be included in order to account for all the degenerate states in each energy level.

When equation (4-34) is substituted into equation (4-31), the result is

$$i'_{\Omega b} = \frac{A_{ji}}{B_{ij} \left(e^{\hbar\Omega_{ij}/kT} - \frac{B_{ji}}{B_{ij}} \right)} \quad (4-35)$$

The Planck blackbody spectral intensity is given by equation (2-11b) of volume I as

$$i'_{\nu b} = \frac{e_{\nu b}}{\pi} = \frac{2C_1\nu^3}{c_0^4(e^{C_2\nu/c_0T} - 1)}$$

which becomes the following after using $C_1 = hc_0^2$, $C_2 = hc_0/k$, $h = 2\pi\hbar$, and $\nu = \Omega_{ij}/2\pi$:

$$i'_{\Omega b} = \frac{\hbar\Omega_{ij}^3}{2\pi^2c_0^2(e^{\hbar\Omega_{ij}/kT} - 1)} \quad (4-36)$$

Equation (4-35) has the same basic form as equation (4-36), and equating these two expressions for $i'_{\Omega b}$ gives the following relations between the Einstein coefficients (in absence of degenerate states):

$$B_{ij} = B_{ji} \quad (4-37)$$

and

$$\frac{A_{ji}}{B_{ji}} = \frac{\hbar\Omega_{ij}^3}{2\pi^2c_0^2} \quad (4-38)$$

Although at the time of the derivation induced emission had not been discerned by experiment, the analysis outlined in equations (4-28) to (4-38) gave strong evidence that it existed. If the induced emission term of equation (4-29) is not included and the analysis is then carried through, the resulting equation by the Einstein approach is

$$i'_{\Omega b} = \frac{A_{ji}}{B_{ij}e^{\hbar\Omega_{ij}/kT}} \quad (4-39)$$

To make equation (4-39) conform to Planck's distribution, the ratio of the Einstein coefficients must be, by comparison with equation (4-36) and by use of equation (4-34),

$$\frac{A_{ji}}{B_{ij}} = \frac{\hbar\Omega_{ij}^3}{2\pi^2c_0^2} \frac{e^{\hbar\Omega_{ij}/kT}}{(e^{\hbar\Omega_{ij}/kT} - 1)} = \frac{\hbar\Omega_{ij}^3}{2\pi^2c_0^2} \frac{n_i}{n_i - n_j}$$

or

$$A_{ji} = \frac{\hbar\Omega_{ij}^3}{2\pi^2c_0^2} \frac{n_i}{n_i - n_j} B_{ij} \quad (4-40)$$

This relation would make A_{ji} dependent on the populations n_i and n_j of the i and j states. Because the transition probabilities A_{ji} and B_{ij} for a particular atomic system should depend only on the particular states i and j and not the populations of these states, equation (4-40) cannot be valid.

Suppose the properly specified Einstein coefficients given by equations (4-37) and (4-38) are substituted in equation (4-39) in which induced emission has been omitted. This will show what deviation should be expected from Planck's distribution as a result of not accounting for induced emission. Making this substitution gives

$$i'_{\Omega b} = \frac{\hbar\Omega_{ij}^3}{2\pi^2c_0^2 e^{\hbar\Omega_{ij}/kT}} \quad (4-41)$$

But (see eq. (2-13) in vol. I) this is Wien's distribution! A comparison of Planck's and Wien's spectral distribution in terms of wavelength is shown in figure 2-7 of volume I, and this comparison is thus a measure of the effect of induced emission on the spectral energy distribution. Wien's curve is slightly below the Planck curve as a result of omitting induced emission. It is evident that neglecting induced emission would introduce only a small error in most cases of engineering interest.

Note that this, and indeed any, derivation of the Planck blackbody distribution depends on the assumption of thermodynamic equilibrium. Also, it is seen that Planck's distribution will not be obtained by the foregoing arguments unless the existence of induced emission is postulated.

4.5 THE EQUATION OF TRANSFER

The equation of transfer was derived in section 2.3. It will now be considered from a microscopic view by using the concepts of the previous section. Consider a beam of radiation of intensity i'_Ω traveling through a gas along a path S . Let the gas atoms (or molecules) be in one of the two energy states i and j , with j being an excited state relative to state i , that is $E_j > E_i$. Let the volume concentration of atoms in these states be n_i and n_j , respectively. Along a path distance dS , the change in the intensity of the beam will be governed by the energy added or lost in the dS interval. Neglecting scattering, the gains or losses are due to spontaneous emission, induced emission, and absorption. By use of the

photon model discussed in section 2.7, and considering only transitions between two energy states, the intensity added to the beam by spontaneous emission is

$$\begin{aligned} \left(\frac{di'_{\Omega}}{dS}\right)_{\text{spontaneous emission}} &= \left(\frac{\text{rate of transitions}}{\text{particle - solid angle}}\right) \left(\frac{\text{number of particles}}{\text{volume}}\right) \left(\frac{\text{energy}}{\text{transition}}\right) \\ &= A_{ji}n_j\hbar\Omega_{ij} \end{aligned} \quad (4-42)$$

Similar relations are derived for induced emission and absorption. The equation of transfer becomes

$$\frac{di'_{\Omega}}{dS} = A_{ji}n_j\hbar\Omega_{ij} + B_{ji}i'_{\Omega}n_j\hbar\Omega_{ij} - B_{ij}i'_{\Omega}n_i\hbar\Omega_{ij} \quad (4-43)$$

This can be arranged into

$$\frac{di'_{\Omega}}{dS} = B_{ij}n_i\hbar\Omega_{ij} \left[\frac{A_{ji}}{B_{ij}} \frac{n_j}{n_i} + \left(\frac{B_{ji}n_j}{B_{ij}n_i} - 1 \right) i'_{\Omega} \right] \quad (4-44)$$

Although the system here is not in blackbody equilibrium, the Einstein coefficients can be used as previously obtained as they depend only on the energy states and particular atomic system being considered. From equation (4-35) (noting that $B_{ij} = B_{ji}$ from eq. (4-37))

$$\frac{A_{ji}}{B_{ij}} = i'_{\Omega b} (e^{\hbar\Omega_{ij}/kT} - 1)$$

Substituting this and equations (4-34) and (4-37) into equation (4-44) gives

$$\frac{di'_{\Omega}}{dS} = B_{ij}n_i\hbar\Omega_{ij} [i'_{\Omega b} (e^{\hbar\Omega_{ij}/kT} - 1) e^{-\hbar\Omega_{ij}/kT} + (e^{-\hbar\Omega_{ij}/kT} - 1) i'_{\Omega}]$$

which simplifies to

$$-\frac{di'_{\Omega}}{dS} = B_{ij}n_i\hbar\Omega_{ij} (1 - e^{-\hbar\Omega_{ij}/kT}) (i'_{\Omega} - i'_{\Omega b}) \quad (4-45)$$

Noting that $\hbar\Omega/kT = hc_0/k\lambda T$, the quantity multiplying the i'_{Ω} on the right side of equation (4-45) is compared with equation (1-25). The true absorption coefficient is thus found to be

$$a_{\Omega}^{\dagger} = B_{ij}n_i\hbar\Omega_{ij} \quad (4-46)$$

and the absorption coefficient including induced emission is

$$a_{\Omega} = a_{\Omega}^{\dagger}(1 - e^{-\hbar\Omega_{ij}/kT}) = B_{ij}n_i\hbar\Omega_{ij}(1 - e^{-\hbar\Omega_{ij}/kT}) \quad (4-47)$$

Equation (4-45) becomes

$$\frac{1}{a_{\Omega}} \frac{di'_{\Omega}}{dS} = i'_{\Omega b} - i'_{\Omega} \quad (4-48)$$

This is the form given for the equation of transfer by the macroscopic derivation (eq. (2-4)).

Thus the equation of transfer and, earlier, the form of Planck's distribution have been derived from consideration of microscopic processes. The true absorption coefficient a_{Ω}^{\dagger} is shown by equation (4-46) to be directly related to the Einstein coefficient B_{ij} . Rather than using the Einstein coefficient, it is customary to give the transition rate between bound electronic energy states in terms of a parameter called the oscillator strength or f -number. This is related to B_{ij} by

$$f_{ij} = \frac{\hbar m_e c_0 \Omega_{ij}}{\pi e^2} B_{ij} \quad (4-49)$$

where m_e is the mass of the electron and e is the electronic charge. Substituting equation (4-49) into equation (4-46) gives a_{Ω}^{\dagger} in terms of the oscillator strength as

$$a_{\Omega}^{\dagger} = \frac{\pi e^2}{m_e c_0} f_{ij} n_i = \pi r_o c_0 f_{ij} n_i \quad (4-50)$$

where r_o is the classical electron radius (see table I in the appendix).

From equation (4-50), it is seen that the true absorption coefficient is directly proportional to two factors. These are n_i , the population of the initial state of the absorbing species, and f_{ij} , which through its connection with B_{ij} , is related to the probability per unit time for transitions to occur from state i to j . Calculation of the population n_i , at least in the case of local thermodynamic equilibrium, is a problem in statistical mechanics. It is possible to derive f -numbers for many electronic transitions by quantum mechanics and thus derive a_{Ω}^{\dagger} from first principles.

The determination of the spectral absorption coefficient by means of statistical and quantum mechanics requires a knowledge of the transition

processes that can occur. In complicated atoms and molecules so many transitions are possible that calculations must either be restricted to only the important transitions, or else statistical or simplified models must be tried. Some discussion of the form of the spectral absorption coefficients for various types of transitions is given in the next section.

4.6 THE ABSORPTION PROPERTIES OF GASES

A gas can absorb energy by a variety of microscopic mechanisms. Each of these mechanisms involves adding the energy of the absorbed photon to the internal energy of a gas atom or molecule. A preliminary discussion of the types of absorption processes was given in section 1.3.

4.6.1 Spectral Line Broadening

If the gas is not dissociated or ionized, then the internal energy (not including translational energy) of the gas is contained in discrete vibrational, rotational, and electronic energy states of its atoms or molecules. The absorption of a photon can cause a transition of some state of the atom or molecule to a state of higher energy. Because only discrete energy states are involved in these transitions, photons of only certain energies can be absorbed. If the energies of the upper and lower discrete states are E_j and E_i , respectively, then only photons of energy $E_p = E_j - E_i$ can cause a transition. As discussed in sections 1.3 and 4.3.1, the energy of a photon is related to its frequency through the relation

$$E_p = E_j - E_i = h\nu_{ij} = \hbar\Omega_{ij} \quad (4-51)$$

Consequently the discrete transitions result in the absorption of photons of only very definite frequencies causing the appearance of dark lines in the absorption spectrum. Hence this process is termed *line absorption*. Because both the initial and final states of the atom or molecule are discrete bound states, these energy changes between states are called *bound-bound* transitions. The rates at which these transitions occur are available in tabular form for some molecules and atoms (refs. 4 and 5). The relations for the transition rates are often given by the semi-classical results describing radiating atoms multiplied by a modifying factor, called the *Gaunt factor*, that provides the correction for quantum mechanical effects.

Equation (4-51) would predict that very little energy could be absorbed from the entire incident spectrum by any given absorption line, because only those photons having a single frequency could be absorbed. Other effects, however, cause the line to be broadened and consequently have a

finite frequency span around the transition frequency Ω_{ij} of equation (4-51). The frequency span of the broadened spectral range, and the variation within it of the absorption ability, depends on the physical mechanism causing the broadening of the spectral line. Some of the important line broadening mechanisms are called natural broadening, Doppler broadening, collision broadening, and Stark broadening. For most engineering conditions involving infrared radiation, collision broadening is the most important.

The variation within the broadened spectral line of the absorption coefficient with frequency is called the *shape* of the spectral line. These shapes are important as they are related to the basic trends of the gas absorption with temperature, pressure, and path length through the gas. The shape of a typical spectral line is illustrated by figure 4-1(a). The $a_{\Omega,ij}(\Omega)$ is the variation of absorption coefficient within the line broadened about the frequency Ω_{ij} , which is the transition frequency obtained from equation (4-51). The *integrated absorption coefficient* S_{ij} for a single line is found as the integral under the entire $a_{\Omega,ij}(\Omega)$ curve

$$S_{ij} = \int_0^{\infty} a_{\Omega,ij}(\Omega) d\Omega \quad (4-52)$$

The $a_{\Omega,ij}(\Omega)$ will be essentially zero except for Ω close to Ω_{ij} . The regions away from Ω_{ij} , where $a_{\Omega,ij}$ becomes small, are called the "wings" of the line. The magnitude of S_{ij} will depend on the number of molecules in energy level i and hence will depend on the gas density.

The *line shape parameter* is defined as

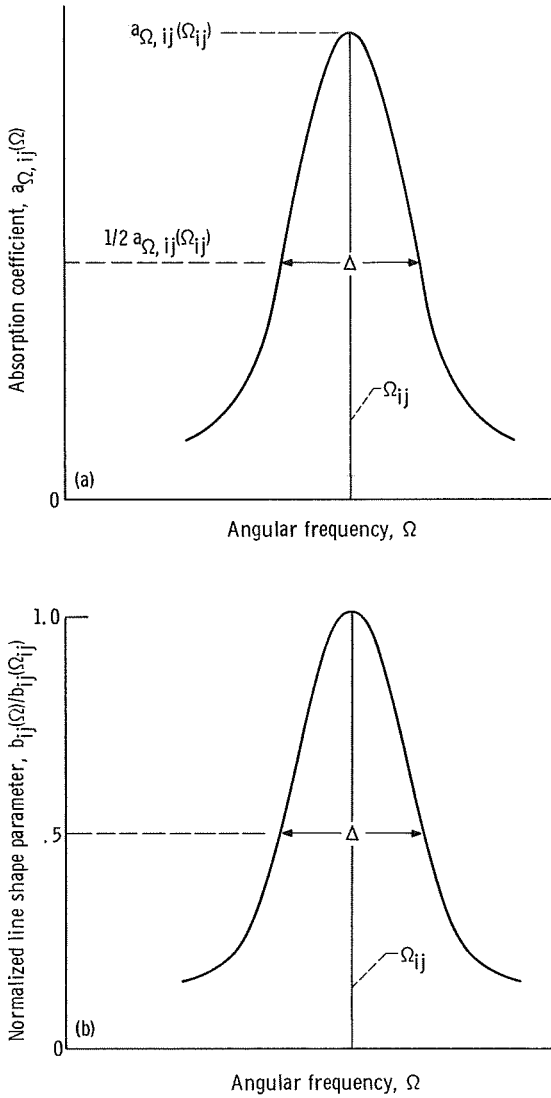
$$b_{ij}(\Omega) = \frac{a_{\Omega,ij}(\Omega)}{S_{ij}} \quad (4-53)$$

so that the S_{ij} is used as a normalizing factor. If equation (4-53) is integrated over the range $0 \leq \Omega \leq \infty$, then substitution of equation (4-52) shows that $b_{ij}(\Omega)$ is normalized such that

$$\int_0^{\infty} b_{ij}(\Omega) d\Omega = 1 \quad (4-54)$$

By dividing $b_{ij}(\Omega_{ij})$ the line shape parameter can be given as a function extending from 0 to 1 as in figure 4-1(b). Note that from the definitions there is the simple equality

$$\frac{b_{ij}(\Omega)}{b_{ij}(\Omega_{ij})} = \frac{a_{\Omega,ij}(\Omega)}{a_{\Omega,ij}(\Omega_{ij})}$$



(a) Absorption coefficient.

(b) Normalized line shape parameter.

FIGURE 4-1.—Broadened spectral line for transition between energy levels i and j .

The form of the spectral line depends on the governing line broadening phenomenon. One characteristic of the line shape is often expressed in terms of a parameter Δ called the “full” half-width of the line. The Δ is the width of the line (in units of angular frequency for the present discussion) evaluated at half the maximum line height as shown in figure

4-1.⁵ This provides a definite width dimension to help describe the line. Since $a_{\Omega,ij}$ goes to zero asymptotically as $|\Omega - \Omega_{ij}|$ increases, it is not possible to define a line width in terms of frequencies at which $a_{\Omega,ij}$ becomes zero.

Four phenomena that cause line broadening will now be discussed along with the resulting line shapes.

4.6.1.1 *Natural broadening.*—A perfectly stationary emitter unperturbed by all external effects is observed to emit energy over a finite spectral interval about a single transition frequency. This *natural line broadening* results from the uncertainty in the exact levels E_i and E_j of the transition energy states, which is related to the Heisenberg uncertainty principle. The natural line broadening produces a line shape parameter of the form

$$b_{ij}(\Omega) = \frac{\frac{\Delta_n}{2\pi}}{\frac{\Delta_n^2}{4} + (\Omega - \Omega_{ij})^2} \quad (4-55)$$

where Δ_n is the “full” half-width of the line for natural broadening. This form of b_{ij} is called a resonance or Lorentz profile. In units of frequency, it provides a profile that is symmetric about Ω_{ij} and that depends on Δ_n and the transition frequency Ω_{ij} . Equation (4-55) conforms with the various definitions imposed on it. When $\Omega = \Omega_{ij}$, the maximum b_{ij} is $b_{ij}(\Omega_{ij}) = 2/\pi\Delta_n$ so that $(1/2)b_{ij}(\Omega_{ij})$ is $1/\pi\Delta_n$. This is the b_{ij} obtained when $\Omega - \Omega_{ij}$ is set equal to $\Delta_n/2$, as expected from the definition of Δ_n . The integral

$$2 \int_{\Omega_{ij}}^{\infty} \frac{\frac{\Delta_n}{2\pi}}{\frac{\Delta_n^2}{4} + (\Omega - \Omega_{ij})^2} d\Omega = 1$$

in conformity with equation (4-54).

For engineering applications the half-width produced by natural broadening is usually quite small compared with that caused by other line broadening mechanisms. Natural line broadening is therefore usually neglected.

4.6.1.2 *Doppler broadening.*—The atoms or molecules of an absorbing or emitting gas are not stationary, but have a distribution of velocities

⁵ Sometimes a quantity equal to $\Delta/2$ is used which would be called here a “half” half-width. The reader must be careful to be sure which line width is being used as the terminology varies in the literature.

associated with their thermal energy. If an atom or molecule is emitting at the frequency Ω_{ij} and at the same time is moving at velocity v toward an observer, the waves will arrive at the observer at an increased frequency Ω given by

$$\Omega = \Omega_{ij} \left(1 + \frac{v}{c} \right) \quad (4-56)$$

If the emitter is moving away from the observer, the v will be negative and the observed frequency will be less than Ω_{ij} . An example of such a frequency decrease is the “red shift” of the radiation detected from galaxies in the universe. This provides evidence that the galaxies are moving away from Earth thereby indicating that the universe is expanding.

In thermal equilibrium the gas molecules will have a Maxwell-Boltzmann distribution of velocities. If an observer is detecting radiation along one coordinate direction, then the velocities of interest are those along the single direction either toward or away from the observer. The fraction of molecules moving in that direction within a velocity range between v and $v + dv$ is

$$\frac{dn}{n} = \sqrt{\frac{M}{2\pi kT}} \exp\left(-\frac{Mv^2}{2kT}\right) dv \quad (4-57)$$

where M is the mass of a molecule of the radiating gas and k is the Boltzmann constant. Using equation (4-56) in equation (4-57) to eliminate v gives the fractional number of molecules providing radiation in each differential frequency interval as a result of Doppler broadening. The result is a spectral line shape having a Gaussian distribution; that is,

$$b_{ij}(\Omega) = \frac{2\sqrt{\ln 2}}{\sqrt{\pi}\Delta_D} \exp\left[-4(\Omega - \Omega_{ij})^2\left(\frac{\ln 2}{\Delta_D^2}\right)\right] \quad (4-58)$$

where Δ_D is the “full” half-width of the line for Doppler broadening. The line shape parameter $b_{ij}(\Omega)$ depends only on Δ_D and the transition frequency Ω_{ij} . The Doppler “full” half-width, however, is given by

$$\Delta_D = \frac{2\Omega_{ij}}{c} \left(\frac{2kT}{M} \ln 2 \right)^{1/2} \quad (4-59)$$

thus depending on Ω_{ij} , T , and M . The dependency of Δ_D on $T^{1/2}$ shows that Doppler broadening is important at high temperatures.

4.6.1.3 *Collision broadening.*—As the pressure of a gas is increased,

the collision rate experienced by any given atom or molecule of the gas is also increased. The collisions can perturb the energy states of the atoms or molecules resulting in collision broadening of the spectral lines. For noncharged particles, the line takes on a Lorentz profile (ref. 4); that is,

$$b_{ij}(\Omega) = \frac{\frac{\Delta_c}{2\pi}}{\frac{\Delta_c^2}{4} + (\Omega - \Omega_{ij})^2} \tag{4-60}$$

which is the same shape as for natural broadening.

The collision “full” half-width Δ_c is determined by the collision rate and an approximate value can be found from kinetic theory. The Δ_c is given by

$$\Delta_c = \frac{8\sqrt{\pi}D^2P}{(MkT)^{1/2}} \tag{4-61}$$

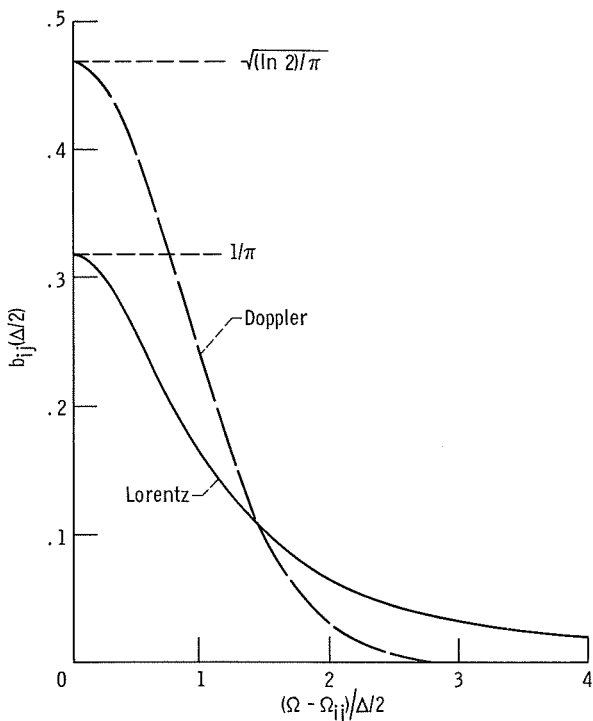


FIGURE 4-2.—Line shape parameter for Doppler and Lorentz broadened spectral lines (areas under two curves are equal).

where D is the diameter of the atoms or molecules and P is the gas pressure for the single component gas. Equation (4-61) shows that collision broadening becomes important at high pressures and low temperatures.

Collision broadening is often the chief contributor to line broadening for engineering infrared conditions, and the other line broadening mechanisms can usually be neglected. The shapes of the Doppler and Lorentz broadened lines are compared in figure 4-2 for the same half-width and area under the curves. The Lorentz profile is lower at the line center, but remains of appreciable size further out in the wings of the line than the Doppler profile. Even when Doppler broadening is dominant near the line center, collision broadening is often the important mechanism far from the center.

4.6.1.4 Stark broadening. — When strong electrical fields are present, the energy levels of the radiating gas particles can be greatly perturbed. This is the *Stark effect* and can result in very large line broadening. It is often observed in ionized gases where radiating particle interactions with the electrons and protons give large Stark broadening effects. Calculation of the line shapes must be approached through quantum mechanics and the resulting line shapes are quite unsymmetrical and complicated.

Stark and collision broadening are often lumped under the general heading of “pressure broadening.” Both effects depend on the pressure of the broadening component of the gas. When two or more broadening effects simultaneously contribute to the line broadening, calculation of the resulting line shape becomes more difficult. References 4, 6, 7, and 8 can be consulted for additional information.

Broadening has been discussed here under the assumption that only one atomic or molecular species is present in the gas. If the gas consists of more than one component, then collision broadening in the radiation absorbing gas is caused by collisions with like molecules (self-broadening) and by collisions with other species. Both collision processes must be included in calculating line shapes.

4.6.2 Absorption or Emission by a Spectral Line

By integrating equation (1-37) over the entire spectrum, the total energy absorbed along a path S per unit solid angle and projected area can be found within a uniform gas. As shown in figure 1-10, this is the energy absorbed when radiation with an incident intensity $i'_{\lambda}(0)$ travels through the shaded solid angle and reaches dA_p

$$\frac{d^2 Q'_a}{dA_p d\omega} = \int_0^{\infty} i'_{\lambda}(0) [1 - \exp(-a_{\lambda} S)] d\Omega \quad (4-62a)$$

where $i'_{\Omega}(0)$ is the incident spectral intensity at the origin of path S . Similarly, from the analogous forms of equations (1-41) and (1-43), the energy can be found that is emitted to dA_p by a uniform gas in the region of solid angle $d\omega$ and length S of figure 1-10. Per unit solid angle and per unit of the projected area, this is

$$\frac{d^2Q'_e}{dA_p d\omega} = \int_0^{\infty} i'_{\Omega b} [1 - \exp(-a_{\Omega} S)] d\Omega \tag{4-62b}$$

The integrals in equations (4-62) can be evaluated for a_{Ω} variations corresponding to a broadened spectral line, but first some simplifications can be made. Consider a spectral line having the transition frequency Ω_{ij} . The line absorption coefficient $a_{\Omega, ij}(\Omega)$ will be essentially zero except in a narrow frequency range surrounding Ω_{ij} . Hence unless S is large the integrands in equations (4-62) will be of appreciable magnitude only within this narrow frequency region and the integration need be performed only over this narrow range. Within this range the $i'_{\Omega}(0)$ or $i'_{\Omega b}$ can be approximated as being constant, and since the largest absorption is at Ω_{ij} , the $i'_{\Omega}(0)$ and $i'_{\Omega b}$ are ordinarily taken at that frequency. Then equations (4-62) become for the spectral line

$$\frac{d^2Q'_a}{dA_p d\omega} = i'_{\Omega}(0, \Omega_{ij}) \int_0^{\infty} \{1 - \exp[-a_{\Omega, ij}(\Omega) S]\} d\Omega \tag{4-63a}$$

$$\frac{d^2Q'_e}{dA_p d\omega} = i'_{\Omega b}(\Omega_{ij}) \int_0^{\infty} \{1 - \exp[-a_{\Omega, ij}(\Omega) S]\} d\Omega \tag{4-63b}$$

The absorbed and emitted energies for the line thus both involve the same integral. This integral will be called the *effective line width* \bar{A}_{ij} so that

$$\bar{A}_{ij}(S) \equiv \int_0^{\infty} \{1 - \exp[-a_{\Omega, ij}(\Omega) S]\} d\Omega \tag{4-64}$$

The \bar{A}_{ij} is a function of path length S , and has units of the spectral variable which is Ω in this instance. By considering a spectral line within which the gas is perfectly absorbing ($a_{\Omega, ij} \rightarrow \infty$), and having no absorption outside this line, it is found from equation (4-64) that \bar{A}_{ij} can be interpreted as the width of a black line centered about Ω_{ij} that produces the same emission as the actual line.

The evaluation of \bar{A}_{ij} will now be considered for two important limiting cases. First consider the situation where the optical path length $a_{\Omega, ij}(\Omega) S$ is small ($a_{\Omega, ij}(\Omega) S \ll 1$). The exponential term in equation (4-64) can be expanded in a series yielding

$$1 - \exp(-a_{\Omega, ij}S) = a_{\Omega, ij}S - \frac{(a_{\Omega, ij}S)^2}{2!} + \dots$$

and then only the first term retained. By using equation (4-64), the \bar{A}_{ij} becomes

$$\bar{A}_{ij}(S) = S \int_0^\infty a_{\Omega, ij} d\Omega$$

By use of equation (4-52) this yields

$$\bar{A}_{ij}(S) = SS_{ij} \quad (4-65)$$

where S_{ij} is the integrated absorption coefficient and should not be confused with S which is the path length. The effective line width is thus linear with path length S in the limit when $a_{\Omega, ij}(\Omega)S \ll 1$ regardless of the line shape. A line with this linear behavior is called a *weak line*.

Next to be considered is the situation where the optical path $a_{\Omega, ij}(\Omega)S$ is large. This will be done for the Lorentz line shape equation (4-60) for collision broadening, as this is the most important type of broadening for engineering applications in the infrared region. From equation (4-53) the line absorption coefficient as a function of frequency Ω is

$$a_{\Omega, ij}(\Omega) = S_{ij}b_{ij}(\Omega)$$

where $b_{ij}(\Omega)$ is the line shape parameter. Using the Lorentz line shape equation (4-60) for b_{ij} gives

$$a_{\Omega, ij}(\Omega) = \frac{S_{ij}}{2\pi} \frac{\Delta_c}{\frac{\Delta_c^2}{4} + (\Omega - \Omega_{ij})^2} \quad (4-66)$$

Now substitute this into equation (4-64) to obtain \bar{A}_{ij} for the spectral line as

$$\bar{A}_{ij}(S) = \int_0^\infty \left\{ 1 - \exp \left[-\frac{S_{ij}}{2\pi} \frac{\Delta_c S}{\frac{\Delta_c^2}{4} + (\Omega - \Omega_{ij})^2} \right] \right\} d\Omega \quad (4-67)$$

For a line that is very strongly absorbing at its center, the collision "full" half-width Δ_c is small and can be neglected compared with $|\Omega - \Omega_{ij}|$ except in the small region where Ω is very close to Ω_{ij} . In the region where Ω is close to Ω_{ij} , the exponential term in the integrand is small and hence its accuracy is not important. As a result for a strong line, equation

(4-67) can be approximated as

$$\bar{A}_{ij}(S) = \int_0^\infty \left\{ 1 - \exp \left[-\frac{S_{ij}}{2\pi} \frac{\Delta_c S}{(\Omega - \Omega_{ij})^2} \right] \right\} d\Omega \quad (4-68)$$

Since it is a single line that is being considered in equation (4-68), the integrand becomes very small as $|\Omega - \Omega_{ij}|$ becomes large. For a Lorentz profile the line shape is symmetric about Ω_{ij} so that the integral can be written as

$$\bar{A}_{ij}(S) = 2 \int_{\Omega_{ij}}^\infty \left\{ 1 - \exp \left[-\frac{S_{ij}}{2\pi} \frac{\Delta_c S}{(\Omega - \Omega_{ij})^2} \right] \right\} d\Omega \quad (4-69)$$

To carry out the integral, let the variable γ be defined as

$$\gamma \equiv \frac{S_{ij} \Delta_c S}{2\pi(\Omega - \Omega_{ij})^2}$$

Then equation (4-69) can be written as

$$\bar{A}_{ij}(S) = \left(\frac{S_{ij} \Delta_c S}{2\pi} \right)^{1/2} \int_0^\infty \frac{1 - \exp(-\gamma)}{\gamma^{3/2}} d\gamma \quad (4-70)$$

This can be integrated to give

$$\bar{A}_{ij}(S) = \sqrt{2S_{ij} \Delta_c S} \quad (4-71)$$

Equation (4-71) shows that, for a *strong Lorentz line*, the absorptance varies as the *square root* of the path length. This is in contrast to the results for any *weak line*, equation (4-65), where the absorptance varies *linearly* with path length. Experimental results bear out these functional dependencies.

4.6.3 Continuum Absorption

Certain energy transition processes can result in the absorption of photons having a wide range of energies as opposed to the relatively small range of energies that line absorption can encompass. The *continuum absorption processes* can be divided into two categories, *bound-free processes* and *free-free processes*. These processes were previously discussed in section 1.3 and are briefly reviewed here. Continuum absorption can also result from solid particles suspended in the gas which will be discussed in chapter 9.

4.6.3.1 *Bound-free processes*.—Consider when a molecule absorbs a photon of sufficient energy to cause dissociation or ionization. A photon of *any* energy greater than the minimum necessary for these proc-

esses can be absorbed, giving rise to a continuous absorption spectrum. To produce ionization, ejection of an electron from a *bound* to a *free* state occurs upon absorption of a photon.

4.6.3.2 *Free-free processes.*—A photon can be absorbed by a free electron as a result of an interaction of the electron with the electric field that exists in the vicinity of a positive ion. The energy of the absorbed photon is added to the kinetic energy of the absorbing electron, which remains in the free state. Since the initial and final states are not quantized, a continuous absorption spectrum results.

4.6.4 Band Absorption Correlations

The gases that are commonly encountered in engineering calculations are diatomic or polyatomic, and therefore possess vibrational and rotational energy states that are absent in monatomic gases. The transitions between the vibrational and rotational states usually provide the main contribution to the absorption coefficient in the important thermal radiation regions of the spectrum at moderate temperatures. As the temperature is raised, dissociation, electron transitions, and ionization become more probable, and the contributions of these additional processes to the absorption coefficient must be included.

When the absorption coefficient of a gas is determined experimentally, the contributions of all the line and continuum processes are superimposed. In computing such coefficients, each absorption process must be analyzed and then the complete coefficient obtained by combining the contributions from the various processes. In figure 4-3, the contributions to the spectral absorption coefficient as given by reference 9 are shown for air at a pressure of 1 atm and a range of temperatures. The ordinate is the fractional contribution of any of the transitions to the entire absorption process; hence, the ordinates of all curves sum to unity at each temperature. At low temperatures the entire absorption results from transitions of the oxygen between molecular states. As the temperature is increased, there is some formation of NO which provides additional bound-bound transitions. At high temperatures the continuous absorption processes discussed in sections 4.6.3 and 1.3 are dominating. These are bound-free (photodissociation) and free-free transitions.

The vibration-rotation bands are usually the most important absorbing and emitting spectral regions in engineering radiation calculations. The structure of such a band will now be examined in more detail and this will reveal the difficulty of computing band absorption coefficients from basic principles. Some of the simplified models of a band will then be discussed by means of which some band absorption features can be analyzed. The correlation of experimental band absorptance data will

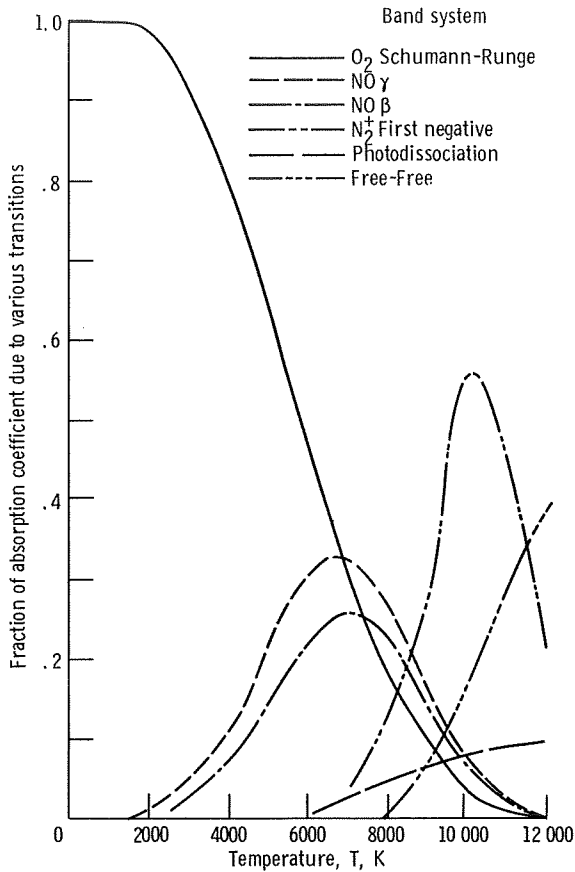


FIGURE 4-3.—Contributions of energy transitions in bands of various species to absorption coefficient of air at 1 atm (ref. 9).

then be considered to show how gas properties can be presented in a manner that is useful for engineering applications where band radiation quantities are required. Often in engineering heat-transfer problems, a reasonable approximation to the total radiation will suffice. It is then not necessary to go into the details of the radiation from the individual bands. For total radiation calculations, charts of gas total emittance have been developed from total radiation measurements. These charts will be discussed in chapter 5. Many of the functional dependencies of these charts had been developed empirically before the details of the radiation from the individual bands had been found. The information in the following sections will aid in understanding from a microscopic viewpoint how the physical variables influence gas radiation but is not intended to yield analytical predictions of the properties.

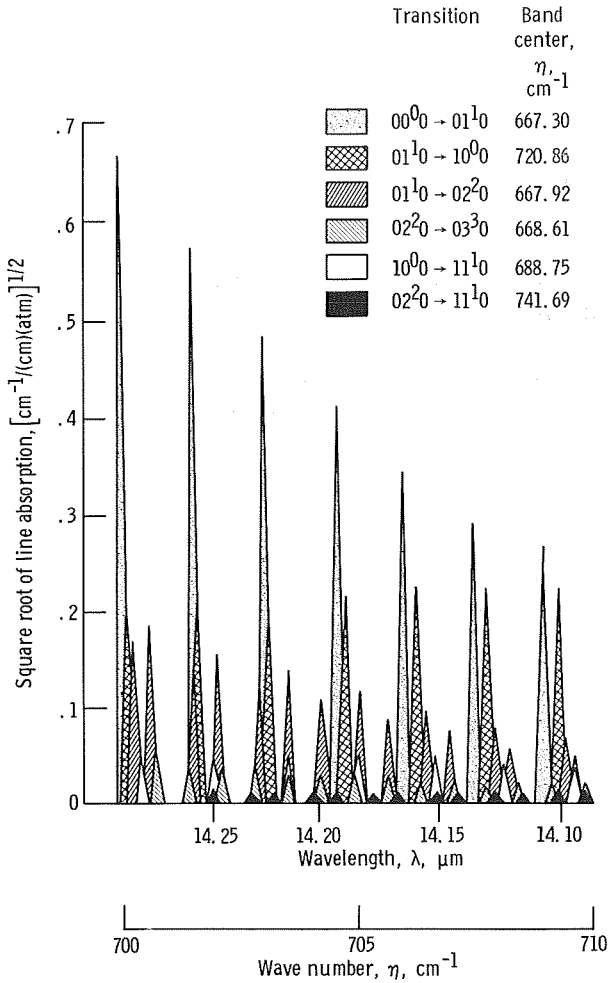


FIGURE 4-4.—A portion of high-resolution spectrum of carbon dioxide (ref. 10).

Let us now examine in more detail the vibration-rotation transitions governing the absorption coefficient of most polyatomic gases up to a temperature of about 3000 K. These transitions are strong functions of frequency, and consequently the absorption coefficient is also strongly spectrally dependent. The spectral absorption in a vibration-rotation band consists of groups of very closely spaced spectral lines resulting from transitions between vibrational and rotational energy states. An example is shown in figure 4-4 for a portion of the carbon dioxide spec-

trum.⁶ The absorption lines are so closely spaced in certain spectral regions that the individual lines are not resolved in most instances by experimental measurements. The lines appear to, or actually do, overlap as a consequence of broadening, and merge to form absorption bands. An example of absorption bands observed with low resolution are those for carbon dioxide that were shown in figure 1-2.

The large number of possible energy transitions that can produce an array of spectral lines as in figure 4-4 is illustrated by the many energy levels and transition arrows in figure 4-5. This figure shows the potential energy for a diatomic molecule as a function of the separation distance between its two atoms. The two curves are each for a different electronic energy state where the electron may be shared by the two atoms. The distance R_e is the mean interatomic distance corresponding to each of the electronic states. The long-dashed horizontal lines denote vibrational energy levels, while the short-dashed lines are rotational states superimposed on the vibrational states. Transitions between rotational levels of the *same* vibrational state involve small values of $E_j - E_i$. Hence from equation (4-33) these transitions give lines in band structures located at low frequencies; that is, in the far infrared. Transitions between rotational levels in *different* vibrational states give vibration-rotation bands at frequencies in the near infrared. If transitions occur from a rotational level of an electronic and vibrational state to a rotational level in a different electronic and vibrational state, then large $E_j - E_i$ are involved and a band system can be formed in the high frequency visible and ultraviolet regions of the spectrum.

In a detailed radiation exchange calculation the absorbed and emitted energy will be needed in each band region, for example in the four main CO₂ bands of figure 1-2. These spectral bands are separated by spectral regions that are nearly transparent. A possible approach to correlating gas properties is to examine the absorption of each band separately and develop empirical correlations describing the behavior of each band. If the absorptance of the individual bands can be correlated in terms of the pressure, temperature, and path length through the gas, then energy interchange methods can be applied on a band-by-band basis to compute the total energy transfer through a real gas.

Equations (4-62) for absorbed and emitted energy both involve the same type of integral, the only difference being that the integral for energy absorbed contains the incident intensity, while that for the emitted energy contains the blackbody intensity. Since the absorption bands

⁶ The notation (01⁰), etc. in figure 4-4 is a designation used to show the quantum state of a harmonic oscillator. In the general case ($v_1 v_2 v_3$), the v_i are the vibrational quantum numbers and l is the quantum number for angular momentum. Transitions between two energy states, such as those denoted by (00⁰) → (01⁰) give rise to absorption lines. Certain selection rules govern the allowable transitions. A good introductory treatment is given in chapter 3 of Goody (ref. 10).

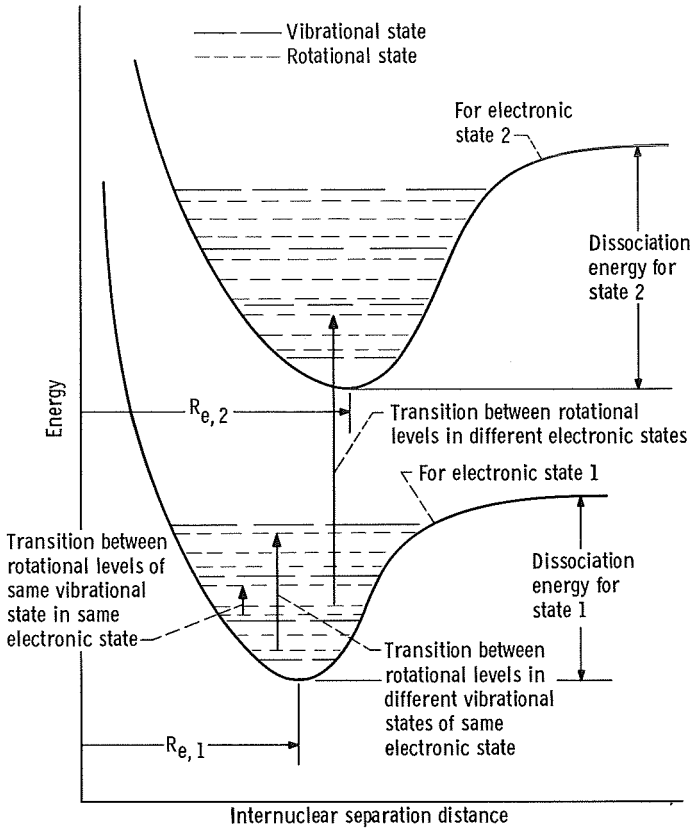


FIGURE 4-5. — Potential energy diagram and transitions for a diatomic molecule.

usually occupy a rather narrow spectral region, an average value of the $i'_{\Omega}(0)$ or $i'_{\Omega b}$ can be taken out of the integral for each band. Considering for example the total emitted energy, equation (4-62b) becomes

$$\frac{d^2 Q'_e}{dA_p d\omega} = \sum_l i'_{\Omega b, l} \int_l \{1 - \exp[-a_{\Omega}(\Omega)S]\} d\Omega \quad (4-72)$$

where the subscript l denotes a band, the integral is over each band, and the summation is over all the bands.

In similar fashion to the effective line width in equation (4-64) the integral in equation (4-72) is defined as the *effective band width* \bar{A}_l or

$$\bar{A}_l(S) \equiv \int_{\text{absorption band width}} \{1 - \exp[-a_{\Omega}(\Omega)S]\} d\Omega \quad (4-73)$$

The \bar{A}_l will have units of the spectral variable, which is Ω in the case of equation (4-73). More often in the literature \bar{A}_l is tabulated in terms of wave number so that it has units of cm^{-1} . The span of the absorption band that provides the upper and lower limits of the integral in equation (4-73) does not have a specific value that applies for all conditions. It can be defined as the spectral interval beyond which there is only a given small fractional contribution to \bar{A}_l . The width of this interval will increase slowly with path length as a result of proportionately more absorption taking place in the wings of the band.

By comparing equations (4-73) and (4-64) it is found that the \bar{A}_l for the band is the sum of the \bar{A}_{ij} for all the spectral lines that occupy the band if all the \bar{A}_{ij} act independently of each other. Generally, the spectral lines do overlap and as a consequence each line does not absorb as much energy as if it acted independently of adjacent lines.

As was observed in figure 4-4 an absorption band is typically composed of many broadened absorption lines. Hence the $a_\Omega(\Omega)$ in equation (4-73) is a complicated irregular function of frequency, and the integration for \bar{A}_l is difficult mathematically. The integration would also require that the detailed shape of all the broadened lines be known. It is evident that a simplified model for the form of $a_\Omega(\Omega)$ must be devised if integration over the lines to obtain band radiation properties is to be a fruitful analytical approach. Two common models are used which represent the extremes in specifying the individual line spacings and magnitudes.

Elsasser (ref. 11) has modeled the lines as all having the same Lorentz shape, equation (4-66), and being of equal heights and equal spacings. This gives a_Ω as a periodic function of Ω as shown in figure 4-6(a). The periodic function depends on the parameters governing the shape of the Lorentz line as well as on the spacing δ between them. The absorption coefficient at a particular frequency is found by summing the contributions from all the adjacent lines. The distance of the line centers from a position Ω are $|\Omega - 0|$, $|\Omega - \delta|$, $|\Omega - 2\delta|$, and so forth. Then summing all the contributions by use of the Lorentz shape in equation (4-66) gives (each line has integrated absorption coefficient S_c)

$$a_\Omega(\Omega) = \frac{S_c}{2\pi} \sum_{n=-\infty}^{\infty} \frac{\Delta_c}{\frac{\Delta_c^2}{4} + (\Omega - n\delta)^2}$$

This periodic function is inserted into equation (4-73) and after a simplifying transformation, the integral can be carried out numerically. Some of the results are given in reference 10. Analytical relations can

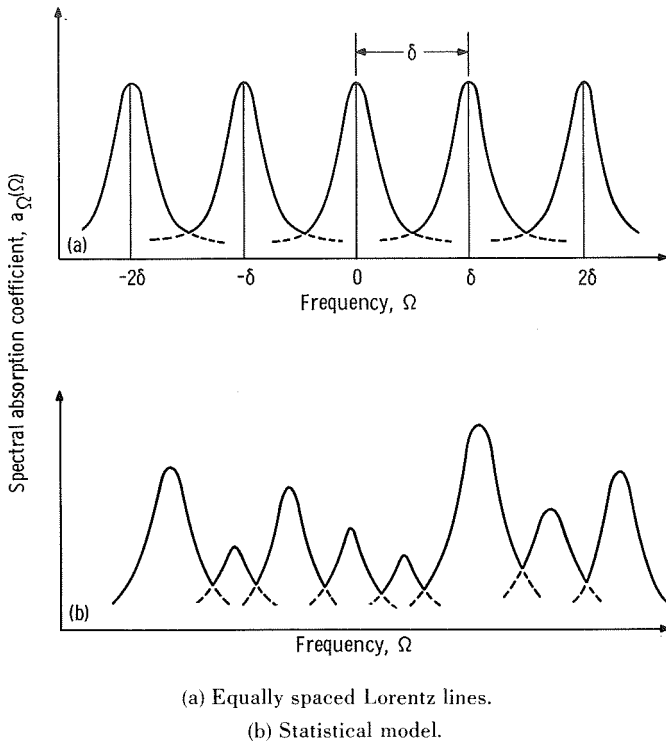


FIGURE 4-6.—Models of absorption lines forming an absorption band.

be obtained at the weak and strong absorption limits. These results have been used as a guide for experimental correlations and are discussed by Plass (ref. 12). Presenting the specific analytical results is more detailed than the treatment intended here so the reader is referred to references 10, 12, or 13 for further results.

Another band model is a statistical array of lines as shown in figure 4-6(b) and presented by Goody (ref. 10). There can be either a random spacing of identical lines or more generally the lines can also differ from each other. A spacing that is essentially random is typical of bands of polyatomic molecules such as CO_2 and water vapor. To apply the model, probability distributions of line strengths and positions must be assumed. These statistical assumptions remove the necessity of calculating the exact properties of the individual lines in the band.

Many other band models have been proposed, some of them of more utility in certain cases than the Elsasser or Goody models. Several of these band models are discussed by Goody (ref. 10) and Edwards and Menard (ref. 14). Modifications to the Elsasser model have been made recently by Kyle (ref. 15) and Golden (refs. 16 and 17) who treated evenly

spaced lines with a Doppler profile, and Golden (ref. 18) who treated the same case with a Voigt profile. The Voigt profile is a combination of the Doppler and Lorentz profiles, thus accounting for the presence in the gas of the both Doppler and collision broadening.

Once the line structure is specified that constitutes the band, the effective band width \bar{A}_l can be calculated from equation (4-73). It is evident that the \bar{A}_l will depend on the line spacing, the line half-width and the line integrated absorption, as well as other quantities when the random statistical model is used. To utilize these analytical results for radiative calculations involving a real gas mixture, it is necessary to know how all these factors are influenced by conditions such as the gas temperature, partial pressure of the absorbing gas, and the total pressure of the gas mixture. If the relations between these quantities are specified, then the correlation of experimental data based on the theoretically indicated dependencies of the band integration can be attempted. The background for these calculations is well charted by Goody (ref. 10). A few of the major functional relations indicated by the theory are examined in the remainder of this chapter. Edwards and coworkers (refs. 19 to 27) have assembled a large body of data on the common gases and have obtained correlations for many of the important band structures. References to these and other data are summarized in table 4-I and some of the results will be given later.

The radiative behavior of the absorption bands can be conveniently presented by correlating the effective band width \bar{A}_l for the various bands as a function of the path length, pressure, temperature, and so forth. As will be shown in section 5.7 the \bar{A}_l can be used in equation (5-74) to obtain the band absorptance for use in detailed spectral exchange calculations in enclosures. By using equation (1-43) the \bar{A}_l can also be used to calculate the total emittance of a uniform gas as

$$\begin{aligned} \epsilon'(T, P, S) &= \frac{\int_0^\infty \pi i'_{\Omega b} [1 - \exp(-a_\Omega S)] d\Omega}{\sigma T^4} \\ &= \frac{\pi}{\sigma T^4} \sum_l i'_{\Omega b, l} \int_l [1 - \exp(-a_\Omega S)] d\Omega \\ &= \frac{\pi}{\sigma T^4} \sum_l i'_{\Omega b, l} \bar{A}_l \end{aligned} \quad (4-74)$$

The ϵ' can be used, as described in section 5.6.1, for engineering calculations of radiation from an isothermal gas to an enclosure boundary.

TABLE 4-I.—AVAILABLE BAND ABSORPTANCE CORRELATIONS FOR ISOTHERMAL GASES

Gas	Bands	Reference	Comments	Type of correlation
CO ₂	All important	20, 30	$300 \leq T \leq 1400$ K	Equivalent band width
	2.7, 4.3, and 15 μm	^a 21, 29	$300 \leq T \leq 1400$ K, $0.1 \leq X \leq 23\ 000$ g/m ²	Exponential wide band
	9.4 and 10.4 μm	^a 22, 29	$300 \leq T \leq 1400$ K, $0.1 \leq X \leq 23\ 000$ g/m ²	Exponential wide band
	All important	31 to 34	$T \sim 300$ K	Equivalent band width
H ₂ O	All important	^a 23, 29	$300 \leq T \leq 1100$ K, $1 \leq X \leq 38\ 000$ g/m ²	Exponential wide band
	2.7 and 6.3 μm	26	$300 \leq T \leq 1100$ K, $1 \leq X \leq 21\ 000$ g/m ²	Equivalent line
	All important	31 to 34	$T \sim 300$ K	Equivalent band width
CH ₄	7.6 and 3.3 μm	^a 21, 29	$300 \leq T \leq 830$ K, $0.1 \leq X \leq 1200$ g/m ²	Exponential wide band
CO	2.35 and 4.67 μm	^a 24, 29	$300 \leq T \leq 1800$ K, $19 \leq X \leq 650$ g/m ²	Exponential wide band
HCl	35	Not correlated—presented in terms of spectral emittance
H ₂	36	Not correlated—presented in terms of spectral and total emittance
Atmospheric gases ^b	10	Discussion of literature up to 1960
Air	All important contributing bands	4 (Table 11-2)	References to literature up to 1965 for needed data to calculate band absorptance

^aCorrelations given in tables 4-II and 4-III.^bN₂, O₂, CO₂, O₃, H₂O, CH₄, and nitrogen oxides.

Let us now examine the behavior of \bar{A}_l for the limiting cases of weak and strong absorption which will provide some limits on which to base band correlations. For a single spectral line, it was found in equation (4-65) for a weak line and in equation (4-71) for a strong Lorentz line that the effective line width varied respectively as a linear and as a square root function of the product of path length S and integrated absorption coefficient S_{ij} . If it is assumed as a first approximation that within a band the effect of line overlap is small, then these trends would also apply to the effective band width and can be used as a basis for a first approximation in the correlation of experimental data. It follows that bands composed entirely of either weak lines or strong lines must be each correlated with a different path-length dependence. For weak lines, the use of equation (4-65) indicates that the correlation of the effective band width is expected to be for the l^{th} band,

$$\bar{A}_l(S) \propto S_l S \quad (4-75a)$$

For a strong collision broadened band, equation (4-71) indicates that

$$\bar{A}_l(S) \propto (S_l \Delta_c S)^{1/2} \quad (4-75b)$$

Considering a single gas, the integrated band absorption coefficient S_l depends on the number of molecules or atoms undergoing transitions and hence as a rough approximation is taken as proportional to the gas density. The collision "full" half-width Δ_c is given by equation (4-61) and because of the direct dependence on pressure the Δ_c is taken as being proportional to the density of the absorbing species. (The $T^{-1/2}$ in Δ_c would also have some influence.) Inserting these dependencies into equations (4-75) gives the weak and strong band approximations in terms of density and path length as

$$\bar{A}_l(S) \propto \rho S \quad (\text{weak band}) \quad (4-76a)$$

$$\bar{A}_l(S) \propto \rho S^{1/2} \quad (\text{strong band}) \quad (4-76b)$$

when the lines in the bands are all acting independently.

For a very strong band absorption, that is, for very long paths and many strong overlapping lines, the proportionality of equation (4-76b) does not hold. It is evident that with increasing S , the \bar{A}_l in equation (4-76b) would exceed its upper limit which from equation (4-73) would be the actual width of the absorption band. For very strong absorption there is some justification for taking the dependence of \bar{A}_l on ρ and S to be of the form

$$\bar{A}_l(S) \propto \ln \rho S \quad (4-77)$$

as discussed by Edwards and Menard (ref. 14).

A difficulty in the use of equations (4-75) and (4-76) is to know when the correlation for a given band will go from the linear to the square-root behavior. For intermediate absorption strengths these two limiting regimes do not join smoothly and an abrupt transition is not physically meaningful. An improvement was made by Edwards and Menard (ref. 14) who introduced a simplified correlation that transitions smoothly between the regions of differing dependency on ρ and S . The method has been used to successfully correlate experimental data (refs. 21 to 24). The basis of this correlation is the assumption that the rotation lines in the band are equally spaced and can be reordered in frequency so that they form an array with exponentially decreasing line intensities from the band center. For this reason, the model is called the *exponential wide band model*. Tien and Lowder (ref. 28) have presented band correlations with a single continuous correlation equation for all mass path lengths. The correlation is based on the construction of a function that meets all the mathematical requirements of the absorptance as a function of mass path length.

The exponential wide band model has been used to obtain correlation constants, and these have been gathered together by Edwards

TABLE 4-II.—EFFECTIVE BAND WIDTH CORRELATION EQUATIONS FOR ISOTHERMAL GAS^a

Pressure broadening parameter, $\beta = \frac{C_2^2 P_e}{4C_1 C_3}$	Lower limit of \bar{A} , η , cm^{-1}	Upper limit of \bar{A} , η , cm^{-1}	Effective band width, \bar{A} , η , cm^{-1}
$\beta \leq 1$	0	βC_3	$\bar{A} = C_1 X$
	βC_3	$C_3(2 - \beta)$	$\bar{A} = C_2 (X P_e)^{1/2} - \beta C_3$
	$C_3(2 - \beta)$	∞	$\bar{A} = C_3 \left(\ln \frac{C_2^2 X P_e}{4C_3} + 2 - \beta \right)$
$\beta > 1$	0	C_3	$\bar{A} = C_1 X$
	C_3	∞	$\bar{A} = C_3 \left(\ln \frac{C_1 X}{C_3} + 1 \right)$

^a C_1 , C_2 , C_3 , b , and n are in table 4-III. X is mass path length, ρS , g/m^2 . $P_e = [(p + b p_{N_2})/P_0]^n$ where $P_0 = 1$ atm, p is partial pressure of absorbing gas, and p_{N_2} is partial pressure of N_2 broadening gas in atmospheres.

et al. (ref. 29) from the references listed in table 4-I. The resulting effective band widths \bar{A}_l and upper and lower limits of the \bar{A}_l can be obtained from the relations in table 4-II. These results are given in units of wave number which is cm^{-1} . The quantities b , n , C_1 , C_2 , and C_3 needed to evaluate these relations are given in table 4-III for CO_2 , CH_4 , H_2O , and CO in a mixture with nitrogen. The method of using these band correlations will be shown by two example problems.

TABLE 4-III.—EXPONENTIAL BAND MODEL CORRELATION QUANTITIES^a

Gas	Band, μm	Band center, η , cm^{-1}	Pressure parameters		C_1 , $\text{cm}^{-1}/(\text{g})(\text{m}^{-2})$	C_2 , $\text{cm}^{-1}/[(\text{g})(\text{m}^{-2})]^{1/2}$ (b)	C_3 , cm^{-1} (b)
			b	n			
CO_2 ^c	15	667	1.3	0.7	19	$6.9(T/T_0)^{0.5}$	$12.9(T/T_0)^{0.5}$
	10.4	960	↓	.8	$0.76\varphi_1(T)$	$1.6(T/T_0)^{0.5}C_1^{0.5}$	$12.4(T/T_0)^{0.5}$
	9.4	1060	↓	.8	$0.76\varphi_1(T)$	$1.6(T/T_0)^{0.5}C_1^{0.5}$	$12.4(T/T_0)^{0.5}$
	4.3	2350	↓	.8	110	$31(T/T_0)^{0.5}$	$11.5(T/T_0)^{0.5}$
	2.7	3715	↓	.65	$4.0\varphi_2(T)$	$8.6\varphi_3(T)$	$24(T/T_0)^{0.5}$
CH_4	7.6	1310	1.3	0.8	28	$10(T/T_0)^{0.5}$	$23(T/T_0)^{0.5}$
	3.3	3020	1.3	.8	46	$14.5(T/T_0)^{0.5}$	$55(T/T_0)^{0.5}$
H_2O ^d	6.3	1600	5.0	1.0	41.2	44	$52(T/T_0)^{0.5}$
	2.7	3750	↓	↓	23.3	39	$65(T/T_0)^{0.5}$
	1.87	5350	↓	↓	$3.0\varphi_{011}(T)$	$6.0C_1^{0.5}$	$46(T/T_0)^{0.5}$
	1.38	7250	↓	↓	$2.5\varphi_{101}(T)$	$8.0C_1^{0.5}$	$46(T/T_0)^{0.5}$
CO ^e	4.7	2143	1.1	0.8	20.9	$\varphi_5(T)$	$22(T/T_0)^{0.5}$
	2.35	4260	1.0	.8	.14	$0.08\varphi_5(T)$	$22(T/T_0)^{0.5}$

^a For limits on T and X , see table 4-I.

^b T_0 is taken as 100 K for all cases.

^c For CO_2 ,

$$\varphi_1 = \left[1 - \exp\left(-\frac{hc}{kT}(\eta_3 - \eta_1)\right) \right] \left[\exp\left(-\frac{hc\eta_1}{kT}\right) - \frac{1}{2} \exp\left(-\frac{2hc\eta_1}{kT}\right) \right] \left[1 - \exp\left(-\frac{hc\eta_1}{kT}\right) \right]^{-1} \left[1 - \exp\left(-\frac{hc\eta_3}{kT}\right) \right]^{-1}$$

$$\varphi_2 = \left[1 - \exp\left(-\frac{hc}{kT}(\eta_1 + \eta_3)\right) \right] \left[1 - \exp\left(-\frac{hc\eta_1}{kT}\right) \right]^{-1} \left[1 - \exp\left(-\frac{hc\eta_3}{kT}\right) \right]^{-1}$$

$$\varphi_3 = \left[1 + 0.053 \left(\frac{T}{T_0}\right)^{3/2} \right]$$

where $\eta_1 = 1351 \text{ cm}^{-1}$, $\eta_2 = 667 \text{ cm}^{-1}$, and $\eta_3 = 2396 \text{ cm}^{-1}$.

^d For H_2O ,

$$\varphi_{\eta_1, \eta_2, \eta_3} = \left[1 - \exp\left(-\frac{hc}{kT} \sum_{i=1}^3 \nu_i \eta_i\right) \right] \prod_{i=1}^3 \left[1 - \exp\left(-\frac{hc\eta_i}{kT}\right) \right]^{-\nu_i}$$

where $\eta_1 = 3652 \text{ cm}^{-1}$, $\eta_2 = 1595 \text{ cm}^{-1}$, and $\eta_3 = 3756 \text{ cm}^{-1}$.

^e For CO ,

$$\varphi_5 = \left[15.15 + 0.22 \left(\frac{T}{T_0}\right)^{3/2} \right] \left[1 - \exp\left(-\frac{hc\eta}{kT}\right) \right]$$

where $\eta = 2143 \text{ cm}^{-1}$.

EXAMPLE 4-1: Find the effective band width \bar{A} of the 9.4- μm band of pure CO_2 at 1 atm and 500 K for a path length S of 0.364 m.

To obtain \bar{A} from the relations in table 4-II, the constant C_1 must be evaluated. From table 4-III at the 9.4- μm CO_2 band

$$C_1 = 0.76\varphi_1(T)$$

where

$$\begin{aligned} \varphi_1(T) = & \left\{ 1 - \exp\left[\frac{-hc(\eta_3 - \eta_1)}{kT}\right] \right\} \left[\exp\left(-\frac{hc\eta_1}{kT}\right) - \frac{1}{2}\exp\left(-\frac{2hc\eta_1}{kT}\right) \right] \\ & \times \left[1 - \exp\left(-\frac{hc\eta_1}{kT}\right) \right]^{-1} \left[1 - \exp\left(-\frac{hc\eta_3}{kT}\right) \right]^{-1} \end{aligned}$$

Substitute the values $\eta_1 = 1351 \text{ cm}^{-1}$, $\eta_2 = 667 \text{ cm}^{-1}$, $\eta_3 = 2396 \text{ cm}^{-1}$, $h = 6.625 \times 10^{-27} \text{ (erg) (sec)}$, $k = 1.380 \times 10^{-16} \text{ erg/K}$, $c = 2.998 \times 10^{10} \text{ cm/sec}$, and $T = 500 \text{ K}$. This gives $\varphi_1 = 0.0196$ so that $C_1 = 0.0149 \text{ m}^2/(\text{cm})(\text{g})$. Table 4-II gives the quantity β as $\beta = C_2^2 P_e / 4C_1 C_3$. For the 9.4- μm CO_2 band, table 4-III gives the C_2 and C_3 as

$$C_2 = 1.6 \left(\frac{T}{T_0} \right)^{0.5} C_1^{0.5}$$

and

$$C_3 = 12.4 \left(\frac{T}{T_0} \right)^{0.5}$$

so that

$$\beta = \frac{(1.6)^2 P_e \left(\frac{T}{T_0} \right)^{0.5}}{4 \times 12.4} = 0.0516 P_e \left(\frac{T}{T_0} \right)^{0.5}$$

From table 4-II, P_e for pure CO_2 at 1 atm is

$$P_e = \left(\frac{1+0}{1} \right)^n = 1$$

Then, since $T_0 = 100 \text{ K}$

$$\beta = 0.0516 \left(\frac{500}{100} \right)^{0.5} = 0.115$$

Also

$$C_3 = 12.4 \left(\frac{T}{T_0} \right)^{0.5} = 12.4 \left(\frac{500}{100} \right)^{0.5} = 27.7 \text{ cm}^{-1}$$

Because $\beta \leq 1$, the correlation equations for the specified conditions are the first set in table 4-II. The mass path length is given by

$$X = \rho S = 0.364 \rho \frac{\text{g}}{\text{m}^2}$$

The gas density is

$$\rho = \frac{1}{22.42 \frac{\text{liter}}{\text{g-mole}}} \left(\frac{44 \text{ g}}{\text{g-mole}} \right) \left(\frac{1000 \text{ liter}}{\text{m}^3} \right) \left(\frac{273}{500} \right) = 1.07 \times 10^3 \frac{\text{g}}{\text{m}^3}$$

so that the mass path length is

$$X = 390 \frac{\text{g}}{\text{m}^2}$$

The choice of correlation equation depends on the limits into which X causes \bar{A} to fall. The first equation in table 4-II gives

$$\bar{A} = C_1 X = 0.0149 \times 390 = 5.8 \text{ cm}^{-1}$$

but this falls well outside the prescribed upper limit of the band given by

$$\beta C_3 = 0.115 \times 27.7 = 3.2 \text{ cm}^{-1}$$

for the $\beta \leq 1$ part of the correlation. For intermediate X , the second line of table 4-II gives

$$\bar{A} = C_2 (XP_e)^{1/2} - \beta C_3$$

or

$$\bar{A} = \left[1.6 \left(\frac{500}{100} \right)^{1/2} (0.0149)^{1/2} \right] (390)^{1/2} - 3.2 = 5.4 \text{ cm}^{-1}$$

and this lies within the range

$$\beta C_3 \leq \bar{A} \leq C_3 (2 - \beta)$$

$$3.2 \leq \bar{A} \leq 52.2 \text{ cm}^{-1}$$

for this part of the correlation. The result for \bar{A} compares reasonably well with an experimental value of 5.9 cm^{-1} from reference 20 for similar conditions.

EXAMPLE 4-2: Determine the energy per unit area and solid angle of the 9.4- μm band emitted from the end of a thin column of CO_2 gas at 1 atm pressure and 500 K if the column is 0.364 m long.

Using equation (4-62b) and integrating only over the 9.4- μm band result in

$$\frac{d^2Q'_e}{dA_p d\omega} = \int_{\Delta\eta} i'_{\eta b}(\eta) [1 - \exp(-a\eta S)] d\eta \approx \bar{A} i'_{\eta b}(\eta_{\text{band center}})$$

where equation (4-73) has been substituted and $\eta_{\text{band center}}$ is the wave number of the band center. For this band table 4-III gives

$$\eta_{\text{band center}} = 1060 \text{ cm}^{-1}$$

Using equation (2-11c) of volume I for $i'_{\eta b}$ and \bar{A} from example 4-1 gives the result

$$\begin{aligned} \bar{A} i'_{\eta b}(\eta_{\text{band center}}) &= 5.4 \left(\frac{2C_1 \eta^3}{e^{C_2 \eta/T} - 1} \right)_{\text{band center}} \\ &= 5.4 \frac{1}{\text{cm}} \frac{2 \times 0.59544 \times 10^{-12} (\text{W})(\text{cm}^2)(1060)^3}{e^{1.4388 \times 1060/500} - 1} \frac{1}{\text{cm}^3} \\ \frac{d^2Q'_e}{dA_p d\omega} &= 3.8 \times 10^{-4} \frac{\text{W}}{\text{cm}^2} \end{aligned}$$

The preceding discussion has been for single component gases. If two gases are present and both absorb energy, then the band absorbance of each may overlap in some spectral regions. In this case, Hottel and Sarofim (ref. 30) show that, for two gases, a and b , in an overlapping band of width $\Delta\eta$, the following relation is valid:

$$\begin{aligned} \bar{A}_{a+b} &= \Delta\eta \left[1 - \left(1 - \frac{\bar{A}_a}{\Delta\eta} \right) \left(1 - \frac{\bar{A}_b}{\Delta\eta} \right) \right] \\ &= \bar{A}_a + \bar{A}_b - \frac{\bar{A}_a \bar{A}_b}{\Delta\eta} \end{aligned} \quad (4-78)$$

Thus the simple sum of the two \bar{A} is reduced by the quantity $\bar{A}_a \bar{A}_b / \Delta\eta$. Restriction is to wave number intervals over which both \bar{A}_a and \bar{A}_b are applicable average values, and in which there is no correlation between the positions of the individual lines of gases a and b .

Many additional complexities are introduced when a gas mixture is

considered. For example, the partial pressure p of absorbing gas in a multicomponent system varies with T and P , the populations of the energy states vary with T , and the overlapping of spectral lines changes with P . It is thus very complex to analytically formulate the dependence of \bar{A}_l on T , p , and P for a real gas mixture. Useful results must depend heavily on experiment while using theory as a guide.

Hottel and Sarofim (ref. 30) discuss in detail total absorptance curves of the type shown in figure 1-11. Such curves are available for a number of gases, and their accuracy has been confirmed by many recent measurements. The use of total absorptances and effective band widths for various engineering problems will be discussed in chapter 5.

4.7 CONCLUDING REMARKS

In this chapter, some consideration was given to microscopic absorption phenomena in gases. Derivations based on the microscopic ideas were related to some concepts already developed on the macroscopic basis—Planck's spectral distribution, induced emission, the equation of transfer, and the absorption coefficient. In addition, some framework was constructed concerning the radiative band absorption properties of polyatomic gases and their dependence on path length and density. The material on gas properties will be used in chapter 5 in conjunction with some engineering approaches for calculating radiative transfer in common gases.

REFERENCES

1. EINSTEIN, ALBERT: On the Quanta Theory of Radiation. *Phys. Zeits.*, vol. 18, Mar. 15, 1917, pp. 121-128.
2. EINSTEIN, ALBERT: Emission and Absorption of Radiation According to the Quantum Theory. *Verh. deut. phys. Ges.*, vol. 18, 1916, pp. 318-323.
3. HEITLER, WALTER: *The Quantum Theory of Radiation*. Third ed., Clarendon Press, Oxford, 1954, pp. 412-414.
4. BOND, JOHN W.; WATSON, KENNETH M.; AND WELCH, JASPER A., JR.: *Atomic Theory of Gas Dynamics*. Addison-Wesley Publ. Co., 1965.
5. WIESE, W. L.; SMITH, M. W.; AND GLENNON, B. M.: *Atomic Transition Probabilities. Vol. I: Hydrogen Through Neon—A Critical Data Compilation*. Rep. NSRDS-NBS-4, Vol. 1, National Bureau of Standards, May 20, 1966.
6. GRIEM, HANS R.: *Plasma Spectroscopy*. McGraw-Hill Book Co., Inc., 1964.
7. BREENE, ROBERT G.: *The Shift and Shape of Spectral Lines*. Pergamon Press, 1961.
8. PENNER, S. S.: *Quantitative Molecular Spectroscopy and Gas Emissivities*. Addison-Wesley Publ. Co., 1959.
9. ARMSTRONG, B. H.; ET AL.: *Radiative Properties of High Temperature Air*. *J. Quant. Spectrosc. Radiat. Transfer*, vol. 1, no. 2, 1961, pp. 143-162.
10. GOODY, R. M.: *Atmospheric Radiation. Vol. 1. Theoretical Basis*. Clarendon Press, Oxford, 1964.

11. ELSASSER, WALTER M.: Heat Transfer by Infrared Radiation in the Atmosphere. Harvard Meteorological Studies No. 6, Harvard University, 1942.
12. PLASS, GILBERT N.: Useful Representations for Measurements of Spectral Band Absorption. *J. Opt. Soc. Am.*, vol. 50, no. 9, Sept. 1960, pp. 868-875.
13. TIEN, C. L.: Thermal Radiation Properties of Gases. *Advances in Heat Transfer*. Vol. 5. T. F. Irvine, Jr., and J. P. Hartnett, eds., Academic Press, 1968, pp. 253-324.
14. EDWARDS, D. K.; AND MENARD, W. A.: Comparison of Models for Correlation of Total Band Absorption. *Appl. Opt.*, vol. 3, no. 5, May 1964, pp. 621-625.
15. KYLE, T. G.: Absorption of Radiation by Uniformly Spaced Doppler Lines. *Astrophys. J.*, vol. 148, no. 3, June 1967, pp. 845-848.
16. GOLDEN, S. A.: The Doppler Analog of the Elsasser Band Model. *J. Quant. Spectrosc. Radiat. Transfer*, vol. 7, no. 3, 1967, pp. 483-494.
17. GOLDEN, S. A.: The Doppler Analog of the Elsasser Band Model. II. *J. Quant. Spectrosc. Radiat. Transfer*, vol. 8, Mar. 1968, pp. 877-897.
18. GOLDEN, S. A.: The Voigt Analog of an Elsasser Band. *J. Quant. Spectrosc. Radiat. Transfer*, vol. 9, no. 8, Aug. 1969, pp. 1067-1081.
19. EDWARDS, D. K.: Radiant Interchange in a Nongray Enclosure Containing an Isothermal Carbon-Dioxide-Nitrogen Gas Mixture. *J. Heat Transfer*, vol. 84, no. 1, Feb. 1962, pp. 1-11.
20. EDWARDS, D. K.: Absorption of Infrared Bands of Carbon Dioxide Gas at Elevated Pressures and Temperatures. *J. Opt. Soc. Am.*, vol. 50, no. 6, June 1960, pp. 617-626.
21. EDWARDS, D. K.; AND MENARD, W. A.: Correlations for Absorption by Methane and Carbon Dioxide Gases. *Appl. Opt.*, vol. 3, no. 7, July 1964, pp. 847-852.
22. EDWARDS, D. K.; AND SUN, W.: Correlations for Absorption by the 9.4- μ and 10.4- μ CO₂ Bands. *Appl. Opt.*, vol. 3, no. 12, Dec. 1964, pp. 1501-1502.
23. EDWARDS, D. K.; FLORNES, B. J.; GLASSEN, L. K.; AND SUN, W.: Correlation of Absorption by Water Vapor at Temperatures from 300° K to 1100° K. *Appl. Opt.*, vol. 4, no. 6, June 1965, pp. 715-721.
24. EDWARDS, D. K.: Absorption of Radiation by Carbon Monoxide Gas According to the Exponential Wide-Band Model. *Appl. Opt.*, vol. 4, no. 10, Oct. 1965, pp. 1352-1353.
25. EDWARDS, D. K.; AND NELSON, K. E.: Rapid Calculation of Radiant Energy Transfer Between Nongray Walls and Isothermal H₂O or CO₂ Gas. *J. Heat Transfer*, vol. 84, no. 4, Nov. 1962, pp. 273-278.
26. WIENER, MICHAEL M.: Radiant Heat Transfer in Non-Isothermal Gases. Ph.D. Thesis, Univ. California at Los Angeles, 1966.
27. HINES, W. S.; AND EDWARDS, D. K.: Infrared Absorptivities of Mixtures of Carbon Dioxide and Water Vapor. *Chem. Eng. Progr. Symp. Ser.*, vol. 64, no. 82, 1968, pp. 173-180.
28. TIEN, C. L.; AND LOWDER, J. E.: A Correlation for Total Band Absorptance of Radiating Gases. *Int. J. Heat Mass Transfer*, vol. 9, no. 7, July 1966, pp. 698-701.
29. EDWARDS, D. K.; GLASSEN, L. K.; HAUSER, W. C.; AND TUCHSCHER, J. S.: Radiation Heat Transfer in Nonisothermal Nongray Gases. *J. Heat Transfer*, vol. 89, no. 3, Aug. 1967, pp. 219-229.
30. HOTTEL, HOYT C.; AND SAROFIM, ADEL F.: *Radiative Transfer*. McGraw-Hill Book Co., Inc., 1967.
31. HOWARD, JOHN N.; BURCH, DARRELL E.; AND WILLIAMS, DUDLEY: Near-Infrared Transmission Through Synthetic Atmospheres. *Geophys. Res. Papers No. 40, AFCRL-TR-55-213*, Air Force Cambridge Research Center, 1955.

32. HOWARD, J. N.; BURCH, D. E.; AND WILLIAMS, DUDLEY: Infrared Transmission of Synthetic Atmospheres. I. Instrumentation. *J. Opt. Soc. Am.*, vol. 46, no. 3, Mar. 1956, pp. 186-190.
33. HOWARD, J. N.; BURCH, D. E.; AND WILLIAMS, DUDLEY: Infrared Transmission of Synthetic Atmospheres. II. Absorption by Carbon Dioxide. *J. Opt. Soc. Am.*, vol. 46, no. 4, Apr. 1956, pp. 237-241.
34. HOWARD, J. N.; BURCH, D. E.; AND WILLIAMS, DUDLEY: Infrared Transmission of Synthetic Atmospheres. IV. Application of Theoretical Band Models. *J. Opt. Soc. Am.*, vol. 46, no. 5, May 1956, pp. 334-338.
35. STULL, V. ROBERT; AND PLASS, GILBERT N.: Spectral Emissivity of Hydrogen Chloride from 1000-3400 cm^{-1} . *J. Opt. Soc. Am.*, vol. 50, no. 12, Dec. 1960, pp. 1279-1285.
36. AROESTE, HENRY; AND BENTON, WILLIAM C.: Emissivity of Hydrogen Atoms at High Temperatures. *J. Appl. Phys.*, vol. 27, no. 2, Feb. 1956, pp. 117-121.

Chapter 5. The Engineering Treatment of Gas Radiation in Enclosures

5.1 INTRODUCTION

An extensive body of engineering literature exists dealing with radiation exchange between solid surfaces when no absorbing medium is present between them. The methods for treating such problems are highly developed, and have been examined at length in volumes I and II of this publication (refs. 1 and 2). The additional complication of having an intervening absorbing-emitting gas present in problems of energy exchange between surfaces can be accounted for by building upon the foundation established for the simpler problems. In this chapter, the relations developed in chapters 1 to 4 are used in the derivation of engineering methods for solving gas-radiation problems. These methods are a direct extension of the surface-surface energy exchange methods developed for enclosures in volume II. The engineer familiar with surface exchange analyses will then find that much of the nomenclature, and the physical intuition that he possesses, can be carried over to gas radiation problems.

Most of the material in this chapter will be concerned with an absorbing-emitting gas that is *isothermal*. As compared with the development in chapter 3, this provides the simplification that the gas temperature distribution need not be computed to obtain the radiative behavior of the gas. In section 5.8 some of the methods developed for the isothermal gas will be carried over to nonisothermal gas computations.

5.2 SYMBOLS

A	area
$AF\bar{\alpha}$	geometrical absorption factor
$AF\bar{\tau}$	geometrical transmission factor
\bar{A}	effective band width
a	absorption coefficient
a, b, c	dimensions in system of two rectangles
C	ratio $L_e/L_{e, o}$
C_{CO_2}	pressure correction coefficients
$C_{\text{H}_2\text{O}}$	
C_l	band coefficient in equation (5-76)
D	spacing between parallel plates; diameter
E_N	$(1 - \epsilon_N)/\epsilon_N$

E_n	exponential integral
e	emissive power
F	geometric configuration factor
\bar{F}	exchange factor
$\bar{g}\bar{g}$	gas-gas direct exchange area
$\bar{g}s$	gas-surface direct exchange area
h	height of cylinder
i	radiation intensity
L_e	mean beam length of gas volume
$L_{e,o}$	mean beam length for limiting case of small absorption
N	total number of surfaces in enclosure
P	total pressure of gas or gas mixture
p	partial pressure
Q	energy per unit time
q	energy flux; energy per unit area and time
R	radius of hemisphere, semicylinder, cylinder, or sphere
S	coordinate along path of radiation
\bar{S}	geometric mean beam length
$\bar{s}\bar{g}$	surface-gas direct exchange area
$\bar{s}\bar{s}$	surface-surface direct exchange area
T	absolute temperature
V	volume
W	width of plate
X	mass path length, ρS ; shortest dimension of rectangular parallelepiped
$\alpha(S)$	absorptance
$\bar{\alpha}(S)$	geometric mean absorptance
$\Delta\alpha, \Delta\epsilon$	correction for spectral overlap
β	cone angle, angle from normal of area
δ_{kj}	Kronecker delta
ϵ	emissivity of surface
$\epsilon(S)$	emittance of medium
η	wave number
κ	optical depth
λ	wavelength
ρ	reflectivity; density
σ	Stefan-Boltzmann constant
$\tau(S)$	transmittance
$\bar{\tau}(S)$	geometric mean transmittance
ω	solid angle

Subscripts:

b blackbody

CO_2	carbon dioxide
g	gas
H_2O	water vapor
i	incident, incoming
j, k	surfaces j or k
$j-k$	from surface j to surface k
l	absorption band l
o	outgoing
u	uniform
w	wall
λ	spectrally (wavelength) dependent
η	wave number dependent

Superscripts:

'	directional quantity
+	quantities defined after equation (5-67)
*, **	dummy variable of integration

5.3 NET RADIATION METHOD FOR ENCLOSURE FILLED WITH ISOTHERMAL GAS — SPECTRAL RELATIONS

In section 5.3 of volume II the radiation exchange equations were developed for an enclosure that did not contain an absorbing-emitting medium, and that had surfaces with spectrally dependent properties. Since the absorption properties of gases and other absorbing media are almost always strongly wavelength dependent, the present development will be carried out at a single wavelength. Then in a later section integrations will be performed over all wavelengths to obtain the total radiative behavior. As in most of the development of volume II it will be assumed that surface directional property effects are sufficiently unimportant that the surfaces can be treated as diffuse emitters and reflectors.

Often in a gas filled enclosure such as in an engine combustion chamber or industrial furnace, there is sufficient mixing so that the entire gas is essentially isothermal. In this instance the analysis is simplified by the fact that it is unnecessary to compute the gas temperature distribution. Even with this simplification, however, a detailed radiation exchange computation between the gas and bounding surfaces is quite involved.

Consider an enclosure composed of N surfaces, each at a uniform temperature as shown in figure 5-1. Typical surfaces are designated by k and j . The enclosure is filled with an absorbing emitting medium at uniform temperature T_g . The quantity Q_g is the amount of heat that

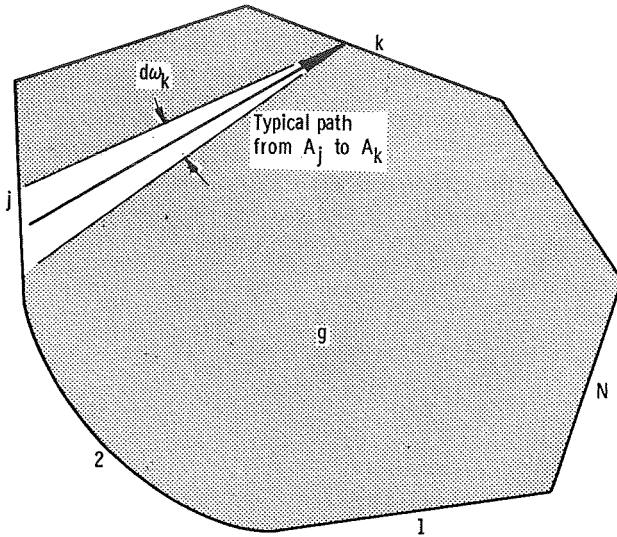


FIGURE 5-1.—Enclosure composed of N discrete surface areas and filled with uniform gas g (enclosure shown in cross section for simplicity).

it is necessary to *supply* by means other than radiation to the entire absorbing medium in order to maintain this temperature. A common source of the Q_g would be by combustion. If in the solution of a problem, Q_g comes out to be a negative number, the medium is gaining a net amount of radiative energy from the enclosure walls and the energy must be *removed* from the gas to maintain it at its steady temperature T_g . The Q_g is analogous to the Q_k in volume II which is the energy supplied by some external means to area A_k .

The enclosure theory will yield equations relating the Q_k and T_k for each surface and the Q_g and T_g of the gas or other absorbing isothermal medium filling the enclosure. Considering all the surfaces and the gas, if half of the Q 's and T 's are specified, then the radiative heat balance equations can be solved for the remaining unknown Q or T values. If the heat input to the gas from external sources Q_g is given, the analysis will yield the steady gas temperature T_g . Conversely, if T_g is given, the analysis will yield the energy that must be supplied to maintain this gas temperature.

The net radiation method as developed in chapters 3 and 5 of volume II will now be extended to include gas radiation terms. At the k^{th} surface of an enclosure as shown in figure 5-2 a heat balance gives

$$dQ_{\lambda, k} = dq_{\lambda, k} A_k = (dq_{\lambda 0, k} - dq_{\lambda i, k}) A_k \quad (5-1)$$

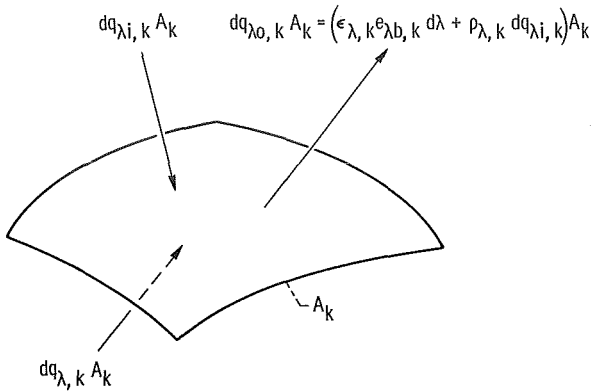


FIGURE 5-2.—Spectral energy quantities incident upon and leaving typical surface area of enclosure.

The $dq_{\lambda o, k}$ and $dq_{\lambda i, k}$ are respectively the outgoing and the incoming energy fluxes in a wavelength interval $d\lambda$. The $dQ_{\lambda, k}$ is the energy supplied to the surface in the wavelength region $d\lambda$. Note that as discussed in connection with equation (5-4) of volume II, the external energy supplied to A_k is

$$\int_{\lambda=0}^{\infty} dQ_{\lambda, k}$$

The outgoing spectral flux is composed of emitted and reflected energy

$$dq_{\lambda o, k} = \epsilon_{\lambda, k}(\lambda, T_k) e_{\lambda b, k}(\lambda, T_k) d\lambda + \rho_{\lambda, k}(\lambda, T_k) dq_{\lambda i, k} \quad (5-2)$$

The functional notation will usually be omitted in order to shorten the form of the equations that follow. The $e_{\lambda b, k} d\lambda$ is the blackbody spectral emission at T_k in the wavelength region $d\lambda$ about the wavelength λ .

The $dq_{\lambda i, k}$ in equation (5-1) is the incoming spectral flux to A_k . It is equal to the sum of the contributions from all the surfaces that reach the k^{th} surface after allowing for absorption by passing through the intervening gas, plus the contribution by emission from the gas. The equation of transfer allows for both attenuation and emission as radiation passes along a path through the gas. A typical path from A_j to A_k within an incident solid angle $d\omega_k$ is shown in figure 5-1. If all such paths and solid angles are accounted for by which radiation can pass from all the surfaces (including A_k if it is concave) to A_k , the solid angles $d\omega_k$ will encompass all of the gas region that can radiate to A_k . Thus, if the equation of transfer which includes the gas emission term is used to compute the energy transported along all paths between surfaces, the gas emission will automatically be included. The radiation passing from

one surface to another, including emission and absorption by the intervening gas, will now be considered.

A typical pair of surfaces is shown in figure 5-3. In the enclosure theory $dq_{\lambda o}$ is assumed uniform over each surface. Since the surfaces are assumed here to be diffuse, the spectral intensity leaving dA_j is $i'_{\lambda o, j} = dq_{\lambda o, j} / (\pi d\lambda)$. By use of the equation of transfer (eq. (2-10)), the intensity arriving at dA_k after traversing the path S is

$$i'_{\lambda i, j-k} = i'_{\lambda o, j} \exp(-\kappa_\lambda) + \int_0^{\kappa_\lambda} i'_{\lambda b, g}(\kappa_\lambda^*) \exp[-(\kappa_\lambda - \kappa_\lambda^*)] d\kappa_\lambda^* \quad (5-3)$$

where

$$\kappa_\lambda = \int_0^S a_\lambda(S^*) dS^*$$

is the optical depth along the path S . The gas is assumed to be at uniform temperature and to have a constant spectral absorption coefficient. Equation (5-3) then reduces to

$$i'_{\lambda i, j-k} = i'_{\lambda o, j} \exp(-a_\lambda S) + a_\lambda i'_{\lambda b, g} \int_0^S \exp[-a_\lambda(S-S^*)] dS^*$$

which can be further integrated to give

$$i'_{\lambda i, j-k} = i'_{\lambda o, j} \exp(-a_\lambda S) + i'_{\lambda b, g} [1 - \exp(-a_\lambda S)] \quad (5-4)$$

Now for convenience introduce the definitions that $\tau_\lambda(S) \equiv \exp(-a_\lambda S)$ is the spectral transmittance of the gas of path length S , and $\alpha_\lambda(S) \equiv 1 - \exp(-a_\lambda S)$ is the spectral absorptance along the path. Then equation (5-4) is written as

$$i'_{\lambda i, j-k} = i'_{\lambda o, j} \tau_\lambda(S) + i'_{\lambda b, g} (T_g) \alpha_\lambda(S) \quad (5-5)$$

This intensity arriving at dA_k in the solid angle $d\omega_k$ provides an arriving energy equal to $i'_{\lambda i, j-k} dA_k \cos \beta_k d\omega_k d\lambda$. But $d\omega_k = dA_j \cos \beta_j / S^2$ so that the arriving spectral energy is

$$\begin{aligned} d^3Q_{\lambda i, j-k} &= i'_{\lambda i, j-k} dA_k dA_j \frac{\cos \beta_k \cos \beta_j}{S^2} d\lambda \\ &= [i'_{\lambda o, j} \tau_\lambda(S) + i'_{\lambda b, g} (T_g) \alpha_\lambda(S)] \frac{dA_k dA_j \cos \beta_k \cos \beta_j}{S^2} d\lambda \quad (5-6) \end{aligned}$$

For a diffuse surface $dq_{\lambda o, j} = \pi i'_{\lambda o, j} d\lambda$, and also $e_{\lambda b, g} = \pi i'_{\lambda b, g}$, so that

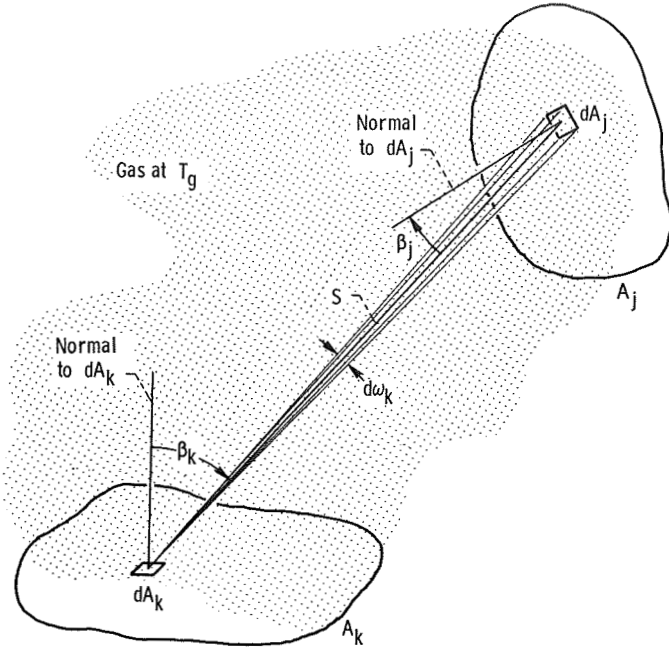


FIGURE 5-3.—Radiation between two surfaces with isothermal gas between them.

equation (5-6) can be written as

$$d^3Q_{\lambda i, j-k} = [dq_{\lambda o, j\tau\lambda}(S) + e_{\lambda b, g}(T_g)d\lambda\alpha_{\lambda}(S)] \frac{dA_k dA_j \cos \beta_k \cos \beta_j}{\pi S^2} \tag{5-7}$$

Equation (5-7) is now integrated over all of \$A_k\$ and \$A_j\$ to give the spectral energy along all paths from \$A_j\$ that is incident upon \$A_k\$,

$$dQ_{\lambda i, j-k} = \int_{A_k} \int_{A_j} [dq_{\lambda o, j\tau\lambda}(S) + e_{\lambda b, g}(T_g)d\lambda\alpha_{\lambda}(S)] \times \frac{\cos \beta_k \cos \beta_j}{\pi S^2} dA_j dA_k \tag{5-8}$$

The first term of the double integral is the spectral energy leaving \$A_j\$ that is transmitted to \$A_k\$. The second term is the spectral energy received at \$A_k\$ as a result of emission by the constant temperature gas in the envelope between \$A_j\$ and \$A_k\$. This envelope is the volume occupied by all straight paths between any part of \$A_j\$ and \$A_k\$.

5.3.1 Definitions of Spectral Transmission and Absorption Factors

The double integration in equation (5-8) has some similarity to the double integral in equation (2-22) of volume II for the configuration factor between two surfaces without an intervening gas. By analogy define the factor $\bar{\tau}_{\lambda, j-k}$ such that

$$F_{j-k} \bar{\tau}_{\lambda, j-k} \equiv \frac{1}{A_j} \int_{A_k} \int_{A_j} \frac{\tau_{\lambda}(S) \cos \beta_k \cos \beta_j}{\pi S^2} dA_j dA_k \quad (5-9)$$

where F_{j-k} is the geometric configuration factor with no absorbing medium as used in volume II. With no absorbing medium present, $\tau_{\lambda}(S) = 1$ and the right side of equation (5-9) becomes F_{j-k} . Hence, in this instance $\bar{\tau}_{j-k} = 1$. The $\bar{\tau}_{\lambda, j-k}$ is called the *geometric mean transmittance* from A_j to A_k . Similarly from the second quantity in the bracket of equation (5-8), a *geometric mean absorptance* $\bar{\alpha}_{\lambda, j-k}$ is defined as

$$F_{j-k} \bar{\alpha}_{\lambda, j-k} \equiv \frac{1}{A_j} \int_{A_k} \int_{A_j} \frac{\alpha_{\lambda}(S) \cos \beta_k \cos \beta_j}{\pi S^2} dA_j dA_k \quad (5-10)$$

For a nonabsorbing medium $\bar{\alpha}_{\lambda, j-k} = 0$, while for perfect absorption $\bar{\alpha}_{\lambda, j-k} = 1$. From the definitions of τ_{λ} and α_{λ} , and equations (5-9) and (5-10), the $\bar{\tau}_{\lambda}$ and $\bar{\alpha}_{\lambda}$ are related by

$$\bar{\alpha}_{\lambda, j-k} = 1 - \bar{\tau}_{\lambda, j-k} \quad (5-11)$$

An alternate terminology is also used wherein the entire quantity $A_j F_{j-k} \bar{\tau}_{\lambda, j-k}$ is called the *geometrical transmission factor*, and the quantity $A_j F_{j-k} \bar{\alpha}_{\lambda, j-k}$ is called the *geometrical absorption factor*. Equation (5-8) can now be written as

$$dQ_{\lambda i, j-k} = (A_j F_{j-k} \bar{\tau}_{\lambda, j-k}) dq_{\lambda 0, j} + (A_j F_{j-k} \bar{\alpha}_{\lambda, j-k}) e_{\lambda b, g}(T_g) d\lambda \quad (5-12)$$

When computing the heat exchange in an enclosure, it will be necessary to determine the $\bar{\tau}_{\lambda}$ and $\bar{\alpha}_{\lambda}$. This usually involves some difficult double integrations. In the present discussion the enclosure theory formulation will first be completed. Then the evaluation of $\bar{\tau}_{\lambda}$ and $\bar{\alpha}_{\lambda}$ will be considered. It is only necessary to perform one double integration to obtain both the $\bar{\tau}_{\lambda}$ and $\bar{\alpha}_{\lambda}$ because of the relation in equation (5-11).

5.3.2 Matrix of Enclosure Theory Equations

For an enclosure with N surfaces bounding an isothermal gas at T_g , the incident spectral energy on any surface A_k will equal that arriving from the directions of all surrounding surfaces, which gives

$$dQ_{\lambda i, k} = A_k dq_{\lambda i, k} = \sum_{j=1}^N (dq_{\lambda 0, j} A_j F_{j-k} \bar{\tau}_{\lambda, j-k} + e_{\lambda b, g} d\lambda A_j F_{j-k} \bar{\alpha}_{\lambda, j-k}) \quad (5-13)$$

From reciprocity (eq. (2-25) of vol. II) $A_j F_{j-k} = A_k F_{k-j}$ so that the A_k can be eliminated to give

$$dq_{\lambda i, k} = \sum_{j=1}^N (dq_{\lambda 0, j} F_{k-j} \bar{\tau}_{\lambda, j-k} + e_{\lambda b, g} d\lambda F_{k-j} \bar{\alpha}_{\lambda, j-k}) \quad (5-14)$$

Equations (5-1), (5-2), and (5-14) form a set of three equations in three unknowns $dq_{\lambda 0}$, $dq_{\lambda i}$, and dq_{λ} for each of the surfaces in the enclosure. The $dq_{\lambda i}$ is eliminated by combining equations (5-1) and (5-2) and also by substituting equation (5-14) into equation (5-1). This yields the set of two equations for each surface

$$dq_{\lambda, k} = \frac{\epsilon_{\lambda, k}}{1 - \epsilon_{\lambda, k}} (e_{\lambda b, k} d\lambda - dq_{\lambda 0, k}) \quad (5-15)$$

$$dq_{\lambda, k} = dq_{\lambda 0, k} - \sum_{j=1}^N (dq_{\lambda 0, j} F_{k-j} \bar{\tau}_{\lambda, j-k} + e_{\lambda b, g} d\lambda F_{k-j} \bar{\alpha}_{\lambda, j-k}) \quad (5-16)$$

Equation (5-15) is the same as for an enclosure without an absorbing gas (see eq. (5-8) of vol. II for example). Equations (5-15) and (5-16) are analogous to equations (3-6) and (3-7) of volume II for the simpler case of a gray enclosure without an absorbing gas. From the symmetry of the integrals in equations (5-9) and (5-10) and the reciprocity relation $A_j F_{j-k} = A_k F_{k-j}$, it is found that

$$\bar{\tau}_{\lambda, j-k} = \bar{\tau}_{\lambda, k-j} \quad (5-17)$$

and

$$\bar{\alpha}_{\lambda, j-k} = \bar{\alpha}_{\lambda, k-j} \quad (5-18)$$

Then equation (5-16) can also be written as

$$dq_{\lambda, k} = dq_{\lambda 0, k} - \sum_{j=1}^N (dq_{\lambda 0, j} F_{k-j} \bar{\tau}_{\lambda, k-j} + e_{\lambda b, g} d\lambda F_{k-j} \bar{\alpha}_{\lambda, k-j}) \quad (5-19)$$

As in section 3.3.1.1 of volume II, the set of equations (5-15) and (5-19) can be further reduced by solving equation (5-15) for $dq_{\lambda 0}$ and

inserting it into equation (5-19). This results in the relation

$$\sum_{j=1}^N \left(\frac{\delta_{kj}}{\epsilon_{\lambda,j}} - F_{k-j} \frac{1 - \epsilon_{\lambda,j}}{\epsilon_{\lambda,j}} \bar{\tau}_{\lambda,k-j} \right) dq_{\lambda,j} = \sum_{j=1}^N [(\delta_{kj} - F_{k-j} \bar{\tau}_{\lambda,k-j}) e_{\lambda b,j} d\lambda - F_{k-j} \bar{\alpha}_{\lambda,k-j} e_{\lambda b,g} d\lambda] \quad (5-20)$$

The Kronecker delta δ_{kj} has the values: $\delta_{kj}=1$ when $k=j$, and $\delta_{kj}=0$ when $k \neq j$. This equation is analogous to equation (3-19) of volume II. If equation (5-20) is written for each k from 1 to N , a set of N equations is obtained relating the $2N$ quantities dq_{λ} and $e_{\lambda b}$ for the surfaces, since the gas temperature and hence $e_{\lambda b,g}$ is assumed known. One-half of the dq_{λ} and $e_{\lambda b}$ values have to be specified and the equations can then be solved for the remaining unknowns. To determine the total energy quantities, this set of equations would have to be solved in a number of wavelength intervals and the integration of each quantity performed over wavelength.

5.3.3 Heat Balance on Gas

Before discussing the solution of the enclosure equations in more detail, there is an additional heat balance that is of interest. This is a heat balance on the gas, which will provide the energy required to maintain the gas at the specified temperature. From an energy balance on the entire enclosure, the energy that must be supplied to the gas by combustion, for example, is equal to the net quantity escaping from the boundaries. The total energy escaping from the enclosure at surface k is

$$-A_k \int_{\lambda=0}^{\infty} dq_{\lambda,k}$$

Then the energy added to the gas is found by summing over all surfaces; that is,

$$Q_g = - \sum_{k=1}^N A_k \int_{\lambda=0}^{\infty} dq_{\lambda,k} \quad (5-21)$$

This can be evaluated after the dq_{λ} are found for each surface in a sufficient number of wavelength intervals from the matrix of equation (5-20).

EXAMPLE 5-1: As an example of the net radiation method consider the heat transfer in a system of two infinite parallel plates at temperatures T_1 and T_2 ($T_1 > T_2$) separated by a gas at uniform temperature T_g .

Equation (5-20) applied to a two surface enclosure gives (note that $F_{1-1} = F_{2-2} = 0$) for $k=1$:

$$\frac{1}{\epsilon_{\lambda,1}} dq_{\lambda,1} - F_{1-2} \frac{1 - \epsilon_{\lambda,2}}{\epsilon_{\lambda,2}} \bar{\tau}_{\lambda,1-2} dq_{\lambda,2} = e_{\lambda b,1} d\lambda - F_{1-2} \bar{\tau}_{\lambda,1-2} e_{\lambda b,2} d\lambda - F_{1-2} \bar{\alpha}_{\lambda,1-2} e_{\lambda b,g} d\lambda \quad (5-22a)$$

and for $k=2$:

$$-F_{2-1} \frac{1 - \epsilon_{\lambda,1}}{\epsilon_{\lambda,1}} \bar{\tau}_{\lambda,2-1} dq_{\lambda,1} + \frac{1}{\epsilon_{\lambda,2}} dq_{\lambda,2} = -F_{2-1} \bar{\tau}_{\lambda,2-1} e_{\lambda b,1} d\lambda - F_{2-1} \bar{\alpha}_{\lambda,2-1} e_{\lambda b,g} d\lambda + e_{\lambda b,2} d\lambda \quad (5-22b)$$

For the infinite parallel plate geometry, $F_{1-2} = F_{2-1} = 1$, and from equations (5-17) and (5-18) $\bar{\tau}_{\lambda,2-1} = \bar{\tau}_{\lambda,1-2}$, and $\bar{\alpha}_{\lambda,2-1} = \bar{\alpha}_{\lambda,1-2}$. For simplicity the numerical subscripts on the $\bar{\tau}$ and $\bar{\alpha}$ will be omitted. Then equations (5-22a) and (5-22b) become

$$\frac{1}{\epsilon_{\lambda,1}} dq_{\lambda,1} - \frac{1 - \epsilon_{\lambda,2}}{\epsilon_{\lambda,2}} \bar{\tau}_{\lambda} dq_{\lambda,2} = (e_{\lambda b,1} - \bar{\tau}_{\lambda} e_{\lambda b,2} - \bar{\alpha}_{\lambda} e_{\lambda b,g}) d\lambda \quad (5-23a)$$

$$-\frac{1 - \epsilon_{\lambda,1}}{\epsilon_{\lambda,1}} \bar{\tau}_{\lambda} dq_{\lambda,1} + \frac{1}{\epsilon_{\lambda,2}} dq_{\lambda,2} = (-\bar{\tau}_{\lambda} e_{\lambda b,1} + e_{\lambda b,2} - \bar{\alpha}_{\lambda} e_{\lambda b,g}) d\lambda \quad (5-23b)$$

Equations (5-23a) and (5-23b) are solved simultaneously for $dq_{\lambda,1}$ and $dq_{\lambda,2}$. After rearrangement and using the relation $\bar{\alpha}_{\lambda} = 1 - \bar{\tau}_{\lambda}$, this yields

$$dq_{\lambda,1} = \frac{d\lambda}{1 - (1 - \epsilon_{\lambda,1})(1 - \epsilon_{\lambda,2})\bar{\tau}_{\lambda}^2} \{ \epsilon_{\lambda,1} \epsilon_{\lambda,2} \bar{\tau}_{\lambda} (e_{\lambda b,1} - e_{\lambda b,2}) + \epsilon_{\lambda,1} (1 - \bar{\tau}_{\lambda}) [1 + (1 - \epsilon_{\lambda,2}) \bar{\tau}_{\lambda}] (e_{\lambda b,1} - e_{\lambda b,g}) \} \quad (5-24a)$$

$$dq_{\lambda,2} = \frac{d\lambda}{1 - (1 - \epsilon_{\lambda,1})(1 - \epsilon_{\lambda,2})\bar{\tau}_{\lambda}^2} \{ \epsilon_{\lambda,1} \epsilon_{\lambda,2} \bar{\tau}_{\lambda} (e_{\lambda b,2} - e_{\lambda b,1}) + \epsilon_{\lambda,2} (1 - \bar{\tau}_{\lambda}) [1 + (1 - \epsilon_{\lambda,1}) \bar{\tau}_{\lambda}] (e_{\lambda b,2} - e_{\lambda b,g}) \} \quad (5-24b)$$

The total energy fluxes added to surfaces 1 and 2 are, respectively,

$$q_1 = \int_{\lambda=0}^{\infty} dq_{\lambda,1} \quad \text{and} \quad q_2 = \int_{\lambda=0}^{\infty} dq_{\lambda,2} \quad (5-25)$$

The total energy added to the gas in order to maintain its specified temperature is equal to the net energy removed from the plates. Hence, per unit area of the parallel plates

$$q_g = -(q_1 + q_2) \quad (5-26)$$

When the medium between the plates does not absorb or emit radiation,

then $\bar{\tau}_\lambda = 1$ and equations (5-24a) and (5-24b) reduce to equation (5-10) of volume II. With an absorbing-radiating gas present the numerical integration of equations (5-24a) and (5-24b) over all wavelengths to obtain the q_1 and q_2 is difficult because of the very irregular variations of the gas absorption coefficient with wavelength. The integration will be further discussed in section 5.7 by dividing the wavelength range into bands of finite width that are either absorbing or nonabsorbing.

5.4 EVALUATION OF SPECTRAL GEOMETRIC MEAN TRANSMITTANCE AND ABSORPTANCE FACTORS

To compute values from the exchange equations, the quantities $\bar{\tau}$ and $\bar{\alpha}$ or $(AF\bar{\tau})$ and $(AF\bar{\alpha})$ must be evaluated. By use of the definitions given in equations (5-9) and (5-10)

$$A_j F_{j-k} \bar{\tau}_{\lambda, j-k} = \int_{A_k} \int_{A_j} \frac{[\exp(-a_\lambda S)] \cos \beta_k \cos \beta_j}{\pi S^2} dA_j dA_k \quad (5-27)$$

$$\begin{aligned} A_j F_{j-k} \bar{\alpha}_{\lambda, j-k} &= \int_{A_k} \int_{A_j} \frac{[1 - \exp(-a_\lambda S)] \cos \beta_k \cos \beta_j}{\pi S^2} dA_j dA_k \\ &= A_j F_{j-k} (1 - \bar{\tau}_{\lambda, j-k}) \end{aligned} \quad (5-28)$$

It is evident that it is the double integral in equation (5-27) that must be carried out for various geometrical orientations of the surfaces A_j and A_k . The evaluation for some specific geometries will now be considered.

5.4.1 Hemisphere to Differential Area at Center of Its Base

As shown in figure 5-4, let A_j be the surface of a hemisphere of radius R , and dA_k be a differential area at the center of the hemisphere base.

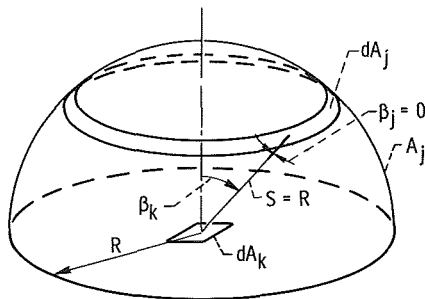


FIGURE 5-4. — Hemisphere filled with isothermal gas.

Then equation (5-27) becomes, since $S=R$ and $\beta_j=0$ (path R is normal to hemisphere surface),

$$A_j dF_{j-dk} \bar{\tau}_{\lambda, j-dk} = dA_k \int_{A_j} \frac{[\exp(-a_\lambda R)] \cos \beta_k \cos(0)}{\pi R^2} dA_j$$

The convenient dA_j is a ring element $dA_j = 2\pi R^2 \sin \beta_k d\beta_k$, and the factors involving R can be taken out of the integral as R is constant for the hemisphere geometry. This gives

$$\begin{aligned} A_j dF_{j-dk} \bar{\tau}_{\lambda, j-dk} &= dA_k \frac{\exp(-a_\lambda R) 2\pi R^2}{\pi R^2} \int_{\beta_k=0}^{\pi/2} \cos \beta_k \sin \beta_k d\beta_k \\ &= dA_k \exp(-a_\lambda R) \end{aligned}$$

By using $A_j dF_{j-dk} = dA_k F_{dk-j}$ and noting that $F_{dk-j} = 1$, this reduces to

$$\bar{\tau}_{\lambda, j-dk} = \exp(-a_\lambda R) \quad (5-29)$$

This especially simple relation will be used later in conjunction with the concept of mean beam length. This is an approximate technique wherein the radiation from an actual gas volume is replaced by that from an effective hemisphere of gas.

5.4.2 Top of Right Circular Cylinder to Center of Its Base

This geometry is shown in figure 5-5. Since $\beta_j = \beta_k = \beta$, the integral in equation (5-27) becomes for the top of the cylinder A_j radiating to the element at the center of its base dA_k

$$A_j dF_{j-dk} \bar{\tau}_{\lambda, j-dk} = dA_k \int_{A_j} \frac{[\exp(-a_\lambda S)] \cos^2 \beta}{\pi S^2} dA_j \quad (5-30)$$

A convenient change in the integral is made by noting that $dA_j \cos \beta / S^2$ is the solid angle by which the ring dA_j is viewed from dA_k . By considering the intersection of this solid angle with the surface of a unit hemisphere, it is found that this solid angle is also equal to $2\pi \sin \beta d\beta$. Making this substitution results in the integral in equation (5-30) being transformed so that

$$A_j dF_{j-dk} \bar{\tau}_{\lambda, j-dk} = dA_k \int_{A_j} [\exp(-a_\lambda S)] 2 \cos \beta \sin \beta d\beta \quad (5-31)$$

Now let $a_\lambda S = \kappa_\lambda$. Then from figure 5-5 $\cos \beta = h/S = ha_\lambda / \kappa_\lambda$, and $\sin \beta d\beta = -d(\cos \beta) = (ha_\lambda / \kappa_\lambda^2) d\kappa_\lambda$. As β goes from 0 to β_m the limits on the variable κ_λ are $\kappa_\lambda = a_\lambda h$ to $a_\lambda \sqrt{R^2 + h^2}$. Then equation (5-31) becomes

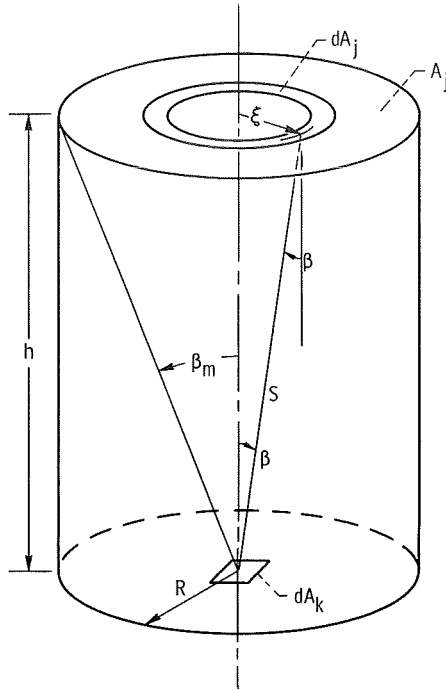


FIGURE 5-5.—Geometry for exchange from top of gas-filled cylinder to center of its base.

$$A_j dF_{j-ak} \bar{\tau}_{\lambda, j-ak} = dA_k 2h^2 a_\lambda^2 \int_{a_\lambda h}^{a_\lambda \sqrt{R^2+h^2}} \frac{\exp(-\kappa_\lambda)}{\kappa_\lambda^3} d\kappa_\lambda \quad (5-32)$$

This can be integrated by parts two times to yield

$$A_j dF_{j-ak} \bar{\tau}_{\lambda, j-ak} = (a_\lambda h)^2 dA_k \left(-\frac{e^{-\kappa_\lambda}}{\kappa_\lambda^2} + \frac{e^{-\kappa_\lambda}}{\kappa_\lambda} + \int \frac{e^{-\kappa_\lambda}}{\kappa_\lambda} d\kappa_\lambda \right) \frac{a_\lambda h \sqrt{(R/h)^2+1}}{a_\lambda h} \quad (5-33)$$

The last integral is a tabulated exponential integral function so the result can be evaluated without difficulty for various values of the parameters R/h and $a_\lambda h$.

The integral in equation (5-32) can also be found directly in terms of the exponential integral function defined in equation (2-45) by writing

$$\int_{a_\lambda h}^{a_\lambda \sqrt{R^2+h^2}} \frac{\exp(-\kappa_\lambda)}{\kappa_\lambda^3} d\kappa_\lambda = \int_{\infty}^{a_\lambda \sqrt{R^2+h^2}} \frac{\exp(-\kappa_\lambda)}{\kappa_\lambda^3} d\kappa_\lambda - \int_{\infty}^{a_\lambda h} \frac{\exp(-\kappa_\lambda)}{\kappa_\lambda^3} d\kappa_\lambda$$

By letting $\kappa_\lambda = (a_\lambda \sqrt{R^2 + h^2})/\mu$ and $a_\lambda h/\mu$, respectively, in the two integrals, they become

$$-\frac{1}{(a_\lambda \sqrt{R^2 + h^2})^2} \int_0^1 \mu \exp\left(-\frac{a_\lambda \sqrt{R^2 + h^2}}{\mu}\right) d\mu + \frac{1}{(a_\lambda h)^2} \int_0^1 \mu \exp\left(-\frac{a_\lambda h}{\mu}\right) d\mu$$

The integral in equation (5-32) can then be written in terms of the exponential integral function as

$$\int_{a_\lambda h}^{a_\lambda \sqrt{R^2 + h^2}} \frac{\exp(-\kappa_\lambda)}{\kappa_\lambda^3} d\kappa_\lambda = \frac{1}{(a_\lambda h)^2} E_3(a_\lambda h) - \frac{1}{\left[a_\lambda h \sqrt{\left(\frac{R}{h}\right)^2 + 1}\right]^2} E_3\left[a_\lambda h \sqrt{\left(\frac{R}{h}\right)^2 + 1}\right] \quad (5-34)$$

5.4.3 Side of Cylinder to Center of Its Base

Let dA_j be a ring around the wall of a cylinder as shown in figure 5-6, and note that $dA_j \cos \beta_j/S^2$ is the solid angle by which dA_j is viewed

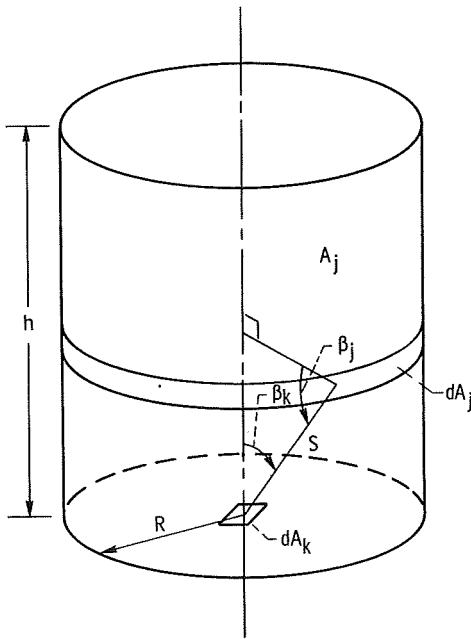


FIGURE 5-6.—Geometry for exchange from side of gas-filled cylinder to center of its base.

from dA_k . This solid angle is also equal to $2\pi \sin \beta_k d\beta_k$. Then equation (5-27) can be written for the side of the cylinder to dA_k as

$$A_j dF_{j-dk} \bar{\tau}_{\lambda, j-dk} = 2dA_k \int_{A_j} [\exp(-a_\lambda S)] \cos \beta_k \sin \beta_k d\beta_k \quad (5-35)$$

This is of the same form as equation (5-31). Let $a_\lambda S = \kappa_\lambda$; then $\sin \beta_k = R/S = Ra_\lambda/\kappa_\lambda$ and $\cos \beta_k d\beta_k = d(\sin \beta_k) = -(Ra_\lambda/\kappa_\lambda^2) d\kappa_\lambda$. Making these substitutions and integrating by parts as for equation (5-33) yield

$$\begin{aligned} A_j dF_{j-dk} \bar{\tau}_{\lambda, j-dk} &= 2dA_k R^2 a_\lambda^2 \int_{a_\lambda R}^{a_\lambda \sqrt{R^2+h^2}} \frac{\exp(-\kappa_\lambda)}{\kappa_\lambda^3} d\kappa_\lambda \\ &= dA_k \left(\frac{R}{h}\right)^2 (a_\lambda h)^2 \left(-\frac{e^{-\kappa_\lambda}}{\kappa_\lambda^2} + \frac{e^{-\kappa_\lambda}}{\kappa_\lambda} \right. \\ &\quad \left. + \int \frac{e^{-\kappa_\lambda}}{\kappa_\lambda} d\kappa_\lambda \right)_{a_\lambda h (R/h)}^{a_\lambda h \sqrt{(R/h)^2+1}} \quad (5-36a) \end{aligned}$$

Alternatively by use of equation (5-34)

$$\begin{aligned} A_j dF_{j-dk} \bar{\tau}_{\lambda, j-dk} &= 2dA_k \left(\frac{R}{h}\right)^2 (a_\lambda h)^2 \left\{ \frac{1}{\left[a_\lambda h \left(\frac{R}{h}\right) \right]^2} E_3 \left[a_\lambda h \left(\frac{R}{h}\right) \right] \right. \\ &\quad \left. - \frac{1}{\left[a_\lambda h \sqrt{\left(\frac{R}{h}\right)^2+1} \right]^2} E_3 \left[a_\lambda h \sqrt{\left(\frac{R}{h}\right)^2+1} \right] \right\} \quad (5-36b) \end{aligned}$$

As for equation (5-33) (or (5-34)), this result can be readily evaluated for various values of the parameters R/h and $a_\lambda h$.

5.4.4 Entire Sphere to Any Element on Its Surface or to Its Entire Surface

From figure 5-7 since $\beta_k = \beta_j$ let them both be simply β . Then $S = 2R \cos \beta$, and using the form in equation (5-31) gives

$$A_j dF_{j-dk} \bar{\tau}_{\lambda, j-dk} = \frac{2dA_k}{4R^2} \int_{S=0}^{2R} \exp(-a_\lambda S) S dS$$

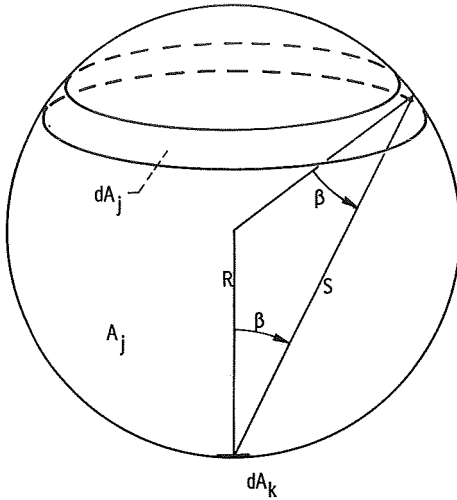


FIGURE 5-7.—Geometry for exchange of surface of gas-filled sphere to itself.

Integrating gives

$$A_j dF_{j-k} \bar{\tau}_{\lambda, j-k} = \frac{2dA_k}{(2a_\lambda R)^2} [1 - (2a_\lambda R + 1) \exp(-2a_\lambda R)] \quad (5-37)$$

which is in terms of only the single parameter $2a_\lambda R$.

Equation (5-37) can be integrated over any finite area A_k to give the $\bar{\tau}_\lambda$ from the entire sphere to A_k as

$$A_j F_{j-k} \bar{\tau}_{\lambda, j-k} = \frac{2A_k}{(2a_\lambda R)^2} [1 - (2a_\lambda R + 1) \exp(-2a_\lambda R)]$$

Since $F_{j-k} = A_k/A_j$ (from eq. (3-65) of vol. II),

$$\bar{\tau}_{\lambda, j-k} = \frac{2}{(2a_\lambda R)^2} [1 - (2a_\lambda R + 1) \exp(-2a_\lambda R)] \quad (5-38)$$

which also holds for the entire sphere to its entire surface.

5.4.5 Infinite Plate to Area on Parallel Plate

If there is considered on one plate an element dA_k (fig. 5-8) and on the other plate a concentric ring element dA_j centered about the normal to dA_k , the geometry is like that in figure 5-5 for a ring on the top of a cylinder to the center of its base. Then from equation (5-32)

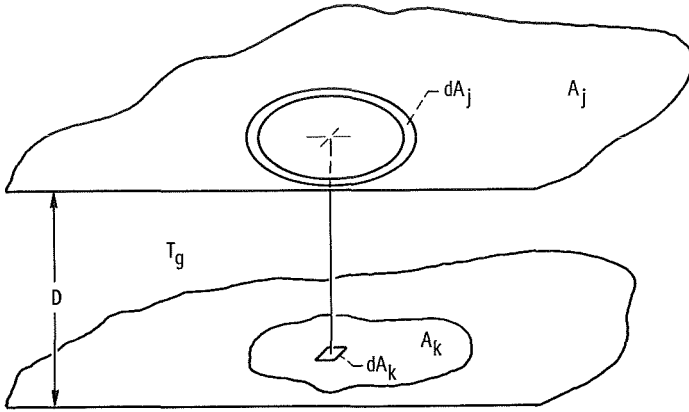


FIGURE 5-8.—Isothermal gas layer between infinite parallel plates.

$$A_j dF_{j-dk} \bar{\tau}_{\lambda, j-dk} = dA_k 2D^2 a_\lambda^2 \int_{a_\lambda D}^{\infty} \frac{\exp(-\kappa_\lambda)}{\kappa_\lambda^3} d\kappa_\lambda$$

where D is the spacing between the plates. By use of the procedure leading to equation (5-34), the integral is transformed to $E_3(a_\lambda D)/(a_\lambda D)^2$. Then integrating over any finite area A_k as shown in figure 5-8 gives

$$A_j F_{j-k} \bar{\tau}_{\lambda, j-k} = A_k 2E_3(a_\lambda D)$$

By using $A_j F_{j-k} = A_k F_{k-j}$ and noting that $F_{k-j} = 1$, this reduces to

$$\bar{\tau}_{\lambda, j-k} = 2E_3(a_\lambda D) \quad (5-39)$$

5.4.6 Rectangle to a Directly Opposed Parallel Rectangle

Consider as in figure 5-9 the exchange from a rectangle to an area element on a directly opposed parallel rectangle. The upper rectangle has been divided into a circular region and a series of partial rings of small width. The contribution from the circle of radius R to $A_j dF_{j-dk} \bar{\tau}_{\lambda, j-dk}$ can be found from equation (5-33) which is for the top of a cylinder to the center of its base. For the n th partial ring, let f_n be the fraction it occupies of a full circular ring. Then by use of equation (5-31), the contribution of all the partial rings to $A_j dF_{j-dk} \bar{\tau}_{\lambda, j-dk}$ is approximated by

$$dA_k \sum_n f_n \exp(-a_\lambda S_n) 2 \cos \beta_n \sin \beta_n \Delta \beta_n$$

This evaluation of $A_j dF_{j-dk} \bar{\tau}_{\lambda, j-dk}$ is carried out for several area

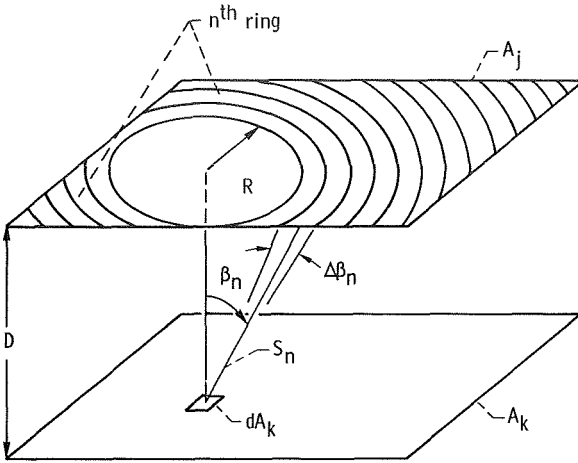


FIGURE 5-9.—Geometry for exchange between two directly opposed parallel rectangles with intervening gas.

patches on \$A_k\$. This is usually sufficient so that the integration over \$A_k\$ can be performed as indicated by equation (5-9) to yield

$$A_j F_{j-k} \bar{\tau}_{\lambda, j-k} = \int_{A_k} A_j dF_{j-dk} \bar{\tau}_{\lambda, j-dk}$$

5.5 THE MEAN BEAM LENGTH FOR RADIATION FROM AN ENTIRE GAS VOLUME TO ALL OR PART OF ITS BOUNDARY

In some practical situations it is desired to determine the radiant energy from a mass of isothermal gas to all or part of its boundaries, without considering emission and reflection from the boundaries. An example would be radiation from hot furnace gases to walls that are cool so that emission is small, and that are rough and contaminated with soot so that they are essentially nonreflecting. In equation (5-13) the \$dq_{\lambda o, j}\$, which is the spectral outgoing heat flux from a typical surface \$A_j\$, would then be zero. The spectral incoming energy at surface \$A_k\$ is then

$$A_k dq_{\lambda i, k} = \sum_{j=1}^N e_{\lambda b, g} d\lambda A_j F_{j-k} \bar{\alpha}_{\lambda, j-k} \tag{5-40}$$

If the geometry consists of a hemisphere of gas radiating to an area element \$dA_k\$ at the center of its base as shown in figure 5-4, equation (5-40) has an especially simple form. Since the hemispherical boundary is the only surface in view of \$dA_k\$, and \$dA_k\$ is a differential element, equation (5-40) reduces to

$$dA_k dq_{\lambda i, k} = e_{\lambda b, g} d\lambda A_j dF_{j-dk} \bar{\alpha}_{\lambda, j-dk} \quad (5-41)$$

From equation (5-29),

$$\bar{\alpha}_{\lambda, j-dk} = 1 - \bar{\tau}_{\lambda, j-dk} = 1 - \exp(-a_{\lambda}R)$$

Note also that for radiation between the surface of a hemisphere and the center of its base, $F_{dk-j} = 1$ so that from reciprocity $dF_{j-dk} = dA_k/A_j$. By combining these results, equation (5-41) reduces to the following simple expression giving the incident heat flux from a hemisphere of gas to the center of the hemisphere base,

$$dq_{\lambda i, k} = [1 - \exp(-a_{\lambda}R)] e_{\lambda b, g} d\lambda \quad (5-42)$$

From equation (5-42), $1 - \exp(-a_{\lambda}R)$ is the spectral emittance of the gas $\epsilon_{\lambda}(\lambda, T, P, R)$ for path length R .⁷ Then equation (5-42) becomes

$$dq_{\lambda i, k} = \epsilon_{\lambda}(a_{\lambda}R) e_{\lambda b, g} d\lambda \quad (5-43)$$

Thus a very simple form is obtained for the energy incident upon dA_k from the hemisphere of gas of radius R surrounding dA_k . The incident energy depends on the optical radius of the hemisphere $a_{\lambda}R$.

It would be most convenient if a relation having the simple form of equation (5-43) could be used to determine the value of $dq_{\lambda i, k}$ on A_k for any geometry of gas volume radiating to all or part of its boundary, rather than only for a hemisphere radiating to the center of its base. Because the geometry of the gas enters equation (5-43) only through $\epsilon_{\lambda}(a_{\lambda}R)$, it is possible to define a fictitious value of R , say L_e , that would give a value of $\epsilon_{\lambda}(a_{\lambda}L_e)$ such that equation (5-43) would give the correct $dq_{\lambda i}$ for another geometry. This fictitious length L_e is called the *mean beam length*. Then for an arbitrary geometry of gas let

$$dq_{\lambda i, k} = \epsilon_{\lambda}(a_{\lambda}L_e) e_{\lambda b, g} d\lambda = [1 - \exp(-a_{\lambda}L_e)] e_{\lambda b, g} d\lambda \quad (5-44)$$

The mean beam length is thus the required radius of a gas hemisphere such that it radiates a flux to the center of its base equal to the average flux radiated to the area of interest by the actual volume of gas.

⁷ For simplicity the prime notation used for a directional quantity will be omitted; in this instance the ϵ_{λ} is independent of direction.

5.5.1 Mean Beam Length for Gas Between Parallel Plates Radiating to Area on Plate

Consider for example the geometry of two black infinite parallel plates at zero absolute temperature separated by a distance D . The plates enclose a uniform gas at temperature T_g with absorption coefficient a_λ . The rate at which spectral energy is incident upon A_k on one plate (fig. 5-8) is from equations (5-40) and (5-39)

$$\begin{aligned} dQ_{\lambda i, k} &= A_k dq_{\lambda i, k} = e_{\lambda b, g} d\lambda A_j F_{j-k} \bar{\alpha}_{\lambda, j-k} \\ &= e_{\lambda b, g} d\lambda A_j F_{j-k} [1 - 2E_3(a_\lambda D)] \end{aligned} \quad (5-45)$$

Since the plates are infinite, $F_{k-j} = 1$. Then by reciprocity (eq. (2-25) of vol. II), $F_{j-k} = A_k/A_j$ and equation (5-45) reduces to

$$dq_{\lambda i, k} = [1 - 2E_3(a_\lambda D)] e_{\lambda b, g} d\lambda \quad (5-46)$$

Comparing equations (5-46) and (5-44) reveals the mean beam length to be

$$L_e = -\frac{1}{a_\lambda} \ln [2E_3(a_\lambda D)]$$

or in terms of the optical thickness $a_\lambda D$

$$\frac{L_e}{D} = -\frac{1}{a_\lambda D} \ln [2E_3(a_\lambda D)] \quad (5-47)$$

5.5.2 Mean Beam Length for Sphere of Gas Radiating to Any Area on Boundary

Consider gas in a nonreflecting sphere of radius R where the sphere boundary A_j is at $T_j = 0$. By use of equations (5-40) and (5-37) the radiation incident on an element dA_k is

$$\begin{aligned} dQ_{\lambda i, dk} &= e_{\lambda b, g} d\lambda A_j dF_{j-dk} \bar{\alpha}_{\lambda, j-dk} \\ &= e_{\lambda b, g} d\lambda A_j dF_{j-dk} \left\{ 1 - \frac{2dA_k}{(2a_\lambda R)^2 A_j dF_{j-dk}} \right. \\ &\quad \left. \times [1 - (2a_\lambda R + 1) \exp(-2a_\lambda R)] \right\} \end{aligned}$$

For a sphere $dF_{j-dk} = dA_k/A_j$ (by use of eq. (3-64) of vol. II). Then

$$\frac{dQ_{\lambda i, ak}}{dA_k} = dq_{\lambda i, ak} = e_{\lambda b, g} d\lambda \left\{ 1 - \frac{2}{(2a_\lambda R)^2} \times [1 - (2a_\lambda R + 1) \exp(-2a_\lambda R)] \right\}$$

Equate this to dq_λ from equation (5-44) to obtain

$$1 - \exp(-a_\lambda L_e) = 1 - \frac{2}{(2a_\lambda R)^2} [1 - (2a_\lambda R + 1) \exp(-2a_\lambda R)]$$

which gives

$$\frac{L_e}{2R} = -\frac{1}{2a_\lambda R} \ln \left\{ \frac{2}{(2a_\lambda R)^2} [1 - (2a_\lambda R + 1) \exp(-2a_\lambda R)] \right\} \quad (5-48)$$

In view of the general applicability of equation (5-38), equation (5-48) gives the correct mean beam length for the entire sphere radiating to any portion of its boundary.

5.5.3 Radiation from Entire Gas Volume to Its Entire Boundary in Limit When Gas Is Optically Thin

Because of the integrations involved, the mean beam length will usually be difficult to evaluate. It is fortunate that some practical approximations for the mean beam length can be found quite simply by looking at the limit when the gas is optically thin. In the optically thin limit, by expanding the exponential term in a series for small $a_\lambda S$, the transmittance $\tau_\lambda = \exp(-a_\lambda S)$ becomes

$$\lim_{a_\lambda S \rightarrow 0} \tau_\lambda = \lim_{a_\lambda S \rightarrow 0} \left[1 - a_\lambda S + \frac{(a_\lambda S)^2}{2!} - \dots \right] = 1$$

Any differential volume of the uniform temperature gas emits the spectral energy $4a_\lambda e_{\lambda b, g} d\lambda dV$. Since $\tau_\lambda = 1$, there is no attenuation of the emitted radiation and all of it reaches the enclosure boundary. For the entire radiating volume the energy reaching the boundary is $4a_\lambda e_{\lambda b, g} d\lambda V$ so that the *average* spectral flux received at the boundary of entire area A is

$$dq_{\lambda i} = 4a_\lambda e_{\lambda b, g} d\lambda \frac{V}{A} \quad (5-49)$$

By use of the mean beam length the average flux reaching the boundary is from equation (5-44),

$$dq_{\lambda i} = [1 - \exp(-a_{\lambda}L_e)]e_{\lambda b, g}d\lambda \quad (5-50)$$

For the special case of small absorption let L_e be designated by $L_{e, o}$. Then expand the exponential term in equation (5-50) in a series to obtain for small $a_{\lambda}L_{e, o}$

$$dq_{\lambda i} = \left\{ 1 - \left[1 - a_{\lambda}L_{e, o} + \frac{(a_{\lambda}L_{e, o})^2}{2!} - \dots \right] \right\} e_{\lambda b, g}d\lambda = a_{\lambda}L_{e, o}e_{\lambda b, g}d\lambda$$

Equating this to the $dq_{\lambda i}$ in equation (5-49) gives the desired result for the mean beam length of an optically thin gas radiating to its entire boundary,

$$L_{e, o} = \frac{4V}{A} \quad (5-51)$$

To give a few examples, for a sphere of diameter D

$$L_{e, o} = \frac{4 \frac{\pi D^3}{6}}{\pi D^2} = \frac{2}{3}D \quad (5-52)$$

For an infinitely long cylinder of diameter D

$$L_{e, o} = \frac{4 \frac{\pi D^2}{4}}{\pi D} = D \quad (5-53)$$

For gas between infinite parallel plates spaced D apart

$$L_{e, o} = \frac{4D}{2} = 2D \quad (5-54)$$

5.5.4 Correction for Mean Beam Length When Gas Is Not Optically Thin

For an optically thick gas it would be very convenient if L_e could be obtained by applying a simple correction factor to the $L_{e, o}$ computed from equation (5-51). It has been found that a useful technique is to introduce a correction coefficient C so that

$$L_e = CL_{e, o} \quad (5-55)$$

Then the incoming heat flux in equation (5-50) can be obtained as

$$dq_{\lambda i} = [1 - \exp(-a_{\lambda}CL_{e,o})]e_{\lambda b,g}d\lambda \quad (5-56)$$

The coefficient C will now be examined by considering the example of a radiating gas between infinite parallel plates spaced D apart. Using equation (5-54) in equation (5-56) gives

$$dq_{\lambda i} = [1 - \exp(-a_{\lambda}C2D)]e_{\lambda b,g}d\lambda$$

From equation (5-46) the actual flux received is

$$dq_{\lambda i} = [1 - 2E_3(a_{\lambda}D)]e_{\lambda b,g}d\lambda$$

To see how well these fluxes compare, the ratio

$$\frac{1 - 2E_3(a_{\lambda}D)}{1 - \exp(-2Ca_{\lambda}D)}$$

is plotted in figure 5-10 using a value of $C=0.9$ for a range of optical thicknesses $a_{\lambda}D$. This value of C was found by trial to yield a ratio close to unity for all $a_{\lambda}D$ and hence serves as a useful correction coefficient.

In table 5-1 the mean beam length $L_{e,o}$ is given for a number of geometries along with a value L_e that provides reasonably good radiative fluxes for nonzero optical thicknesses. The values of C are found to be in a range near 0.9 (refs. 3 to 5). Hence, it is recommended that for a geometry where L_e values have not already been calculated, the approximation can be used

$$L_e = 0.9L_{e,o} = 0.9 \frac{4V}{A} \quad (5-57)$$

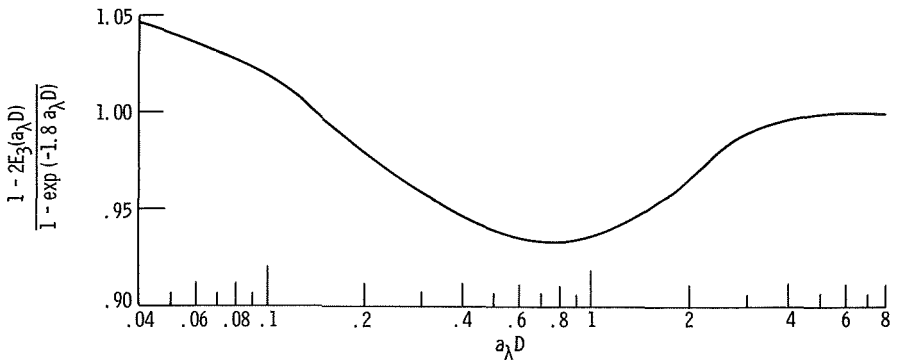



FIGURE 5-10.—Ratio of emission by gas layer to that calculated using a mean beam length $L_e = 1.8D$.

TABLE 5-I.—MEAN BEAM LENGTHS FOR RADIATION FROM ENTIRE GAS VOLUME

Geometry of gas volume	Characterizing dimension	Mean beam length for optical thickness, $a \times L_e \rightarrow 0$, $L_{e,0}$	Mean beam length corrected for finite optical thickness, ^a L_e	$C = L_e/L_{e,0}$
Hemisphere radiating to element at center of base	Radius R	R	R	1
Sphere radiating to its surface	Diameter D	$\frac{3}{2}D$	$0.65D$	0.97
Circular cylinder of height equal to diameter radiating to element at center of base	Diameter D	$0.77D$	$0.71D$	0.92
Circular cylinder of infinite height radiating to convex bounding surface	Diameter D	D	$0.95D$	0.95
Circular cylinder of semi-infinite height radiating to element at center of base	Diameter D	D	$0.90D$	0.90
Circular cylinder of semi-infinite height radiating to entire base	Diameter D	$0.81D$	$0.65D$	0.80
Circular cylinder of height equal to diameter radiating to entire surface	Diameter D	$\frac{3}{2}D$	$0.60D$	0.90
Cylinder of infinite height and semi-circular cross section radiating to element at center of plane rectangular face	Radius R	$1.26R$
Infinite slab of gas radiating to element on one face	Slab thickness D	$2D$	$1.8D$	0.90

^a Corrections are those suggested by Hottel et al. (refs. 3 and 4) or Eckert (ref. 5). Corrections were chosen to provide maximum L_e where these references disagree.

TABLE 5-1.—MEAN BEAM LENGTHS FOR RADIATION FROM ENTIRE GAS VOLUME—
concluded

Geometry of gas volume	Characterizing dimension	Mean beam length for optical thickness, $a_\lambda L_e \rightarrow 0$, $L_{e,0}$	Mean beam length corrected for finite optical thickness, ^a L_e	$C = L_e/L_{e,0}$	
Infinite slab of gas radiating to both bounding planes	Slab thickness D	$2D$	$1.8D$	0.90	
Cube radiating to a face	Edge X	$\frac{3}{2}X$	$0.6X$	0.90	
Rectangular parallelepipeds:	Shortest edge				
$1 \times 1 \times 4$ {	X 	radiating to 1×4 face	$0.90X$	$0.82X$	0.91
		radiating to 1×1 face	$.86X$	$.71X$.83
		radiating to all faces	$.89X$	$.81X$.91
$1 \times 2 \times 6$ {	radiating to 2×6 face	$1.18X$	
	radiating to 1×6 face	$1.24X$	
	radiating to 1×2 face	$1.18X$	
	radiating to all faces	$1.20X$	
Gas volume surrounding an infinite tube bundle and radiating to a single tube:	Tube diameter				
Equilateral triangular array:					
$S = 2D$	D ,	$3.4(S - D)$	$3.0(S - D)$	0.88	
$S = 3D$	and	$4.45(S - D)$	$3.8(S - D)$.85	
Square array:	spacing				
$S = 2D$	between tube centers S	$4.1(S - D)$	$3.5(S - D)$.85	

^a Corrections are those suggested by Hottel et al. (refs. 3 and 4) or Eckert (ref. 5). Corrections were chosen to provide maximum L_e where these references disagree.

5.6 TOTAL RADIATION EXCHANGE IN BLACK ENCLOSURE BETWEEN ENTIRE GAS VOLUME AND ENCLOSURE BOUNDARY BY USE OF MEAN BEAM LENGTH

In furnaces the walls are usually rough and soot covered so they act practically as black surfaces. An important industrial problem is the radiant exchange between the furnace gas and the walls. In this section the simplified case of a black enclosure will be considered. The total radiation exchange will be considered between the entire gas volume and the enclosure boundary. This development will be carried out by application of the mean beam length.

5.6.1 Radiation from Gas to All or Portion of Boundary

The mean beam length was found to be approximately independent of a_λ as evidenced by equation (5-57). This means that L_e can be used as a characteristic dimension of the gas volume and regarded as a constant while integrating over wavelength. The total heat flux from the gas incident on a surface is found by integrating equation (5-44) over λ

$$q_i = \int_0^\infty [1 - \exp(-a_\lambda L_e)] e_{\lambda b, g} d\lambda \quad (5-58)$$

where L_e is independent of λ . Now define a gas total emittance ϵ_g such that

$$q_i = \epsilon_g \sigma T_g^4 \quad (5-59)$$

Equating the last two relations results in

$$\epsilon_g = \frac{\int_{\lambda=0}^\infty e_{\lambda b, g} [1 - \exp(-a_\lambda L_e)] d\lambda}{\sigma T_g^4} \quad (5-60)$$

The ϵ_g is a convenient quantity which can be presented in graphical form for each gas in terms of the variables L_e and T_g . Then for a particular geometry and gas condition the ϵ_g can be found and applied by use of equation (5-59).

The ϵ_g charts that will be presented here have been developed by Hottel (ref. 3) from many experimental measurements. The gas pressure will enter as a parameter because of the dependence of a_λ on the gas density. If the gas is in a mixture, both the pressure of the mixture and the partial pressure of the radiating constituent under consideration will be parameters. A chart of ϵ_g was given for carbon dioxide (CO_2) in

figure 1-11. Charts are presented here in more detail for CO_2 and water vapor (figs. 5-11 and 5-13). Additional charts for sulfur dioxide, ammonia, carbon monoxide, methane, and a few other gases can be found in reference 4. The discussion here will be limited to radiation of CO_2 and water vapor.

When computing an average radiation to area A (a part or all of the bounding surface) by the relation from equation (5-59)

$$Q_i = q_i A = A \epsilon_g \sigma T_g^4 \quad (5-61)$$

the mean beam length for the gas geometry is first obtained from table 5-I or equation (5-57). Then, by knowing the partial pressure of the gas and its temperature, the gas emittance is found by using figures 5-11 to 5-15. Figure 5-11 gives the total emittance of CO_2 obtained experimentally using a mixture with air or other gases so that the total pressure of the mixture was at 1 atm while the partial pressure of the CO_2 was varied. The dotted lines are regions unsupported by experimental data. For a mixture total pressure other than 1 atm, there is a

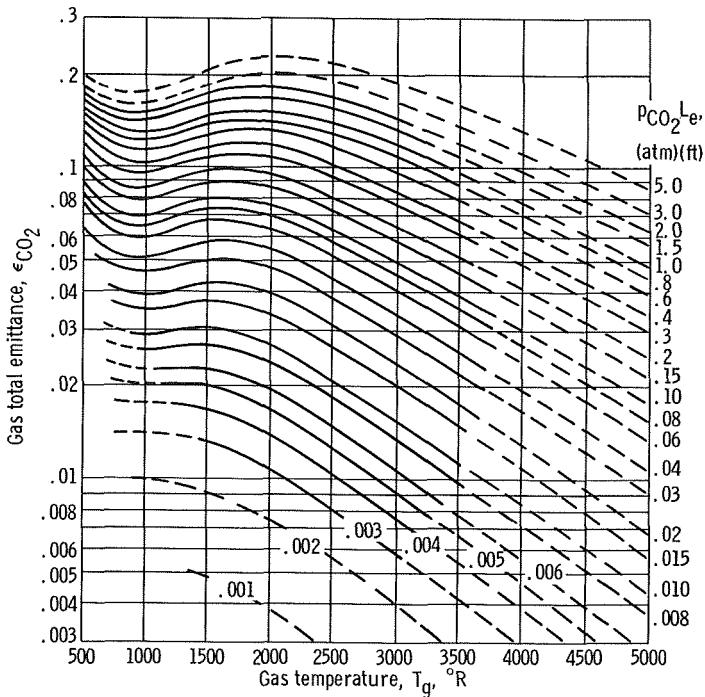


FIGURE 5-11.—Total emittance of carbon dioxide in a mixture having a total pressure of 1 atm (ref. 3).

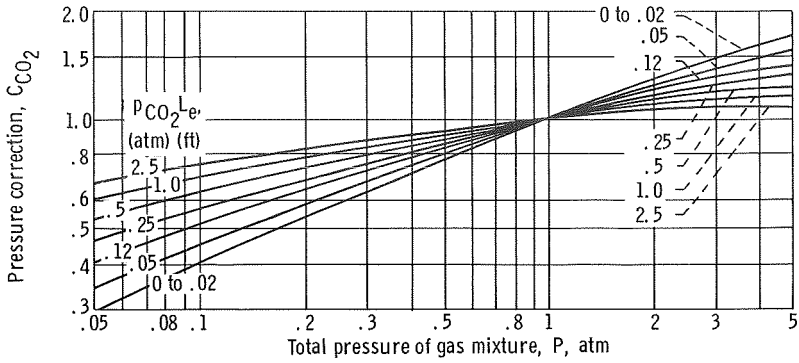


FIGURE 5-12.—Pressure correction for CO₂ total emittance for values of P other than 1 atm (ref. 3).

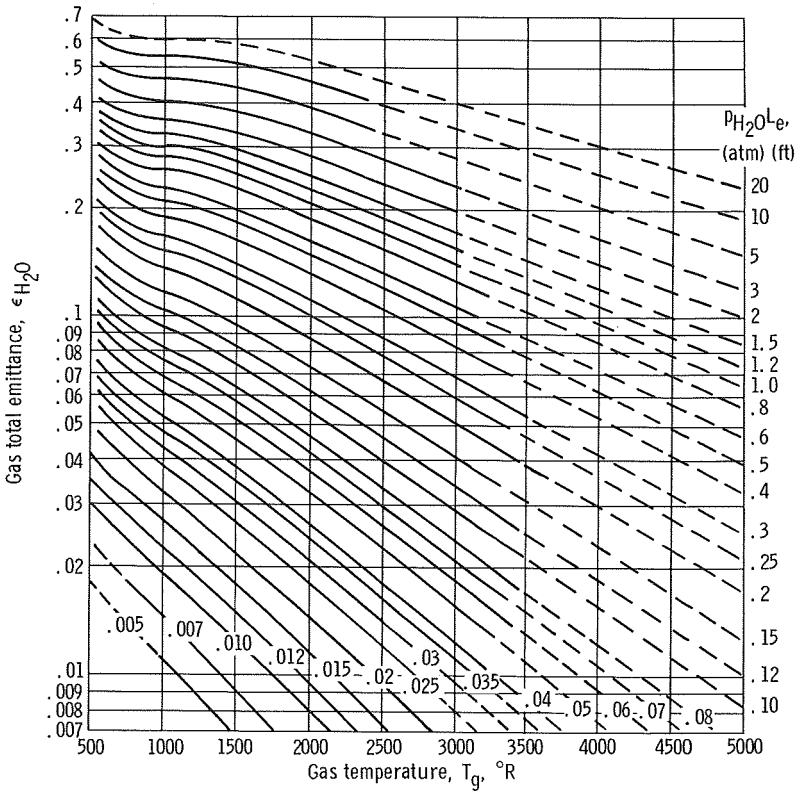


FIGURE 5-13.—Total emittance of water vapor in limit of zero partial pressure in a mixture having a total pressure of 1 atm (ref. 3).

pressure broadening correction that is to be applied (ref. 3). This is given as a multiplying coefficient, C_{CO_2} , in figure 5-12. In the case of water vapor the emittance is influenced in a slightly more complex manner by both the partial pressure of the water vapor and the total pressure of the gas mixture. For correlation purposes, the values in figure 5-13 are emittances that were "reduced," by using a factor depending on p_{H_2O} and $p_{H_2O}L_e$, to limiting values as the partial pressure p_{H_2O} approaches zero in a mixture having a total pressure $P = 1$ atm. A multiplying correction

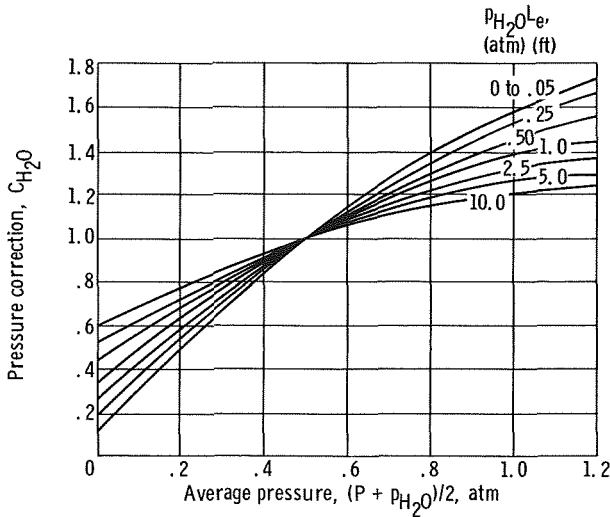


FIGURE 5-14.—Pressure correction for water vapor total emittance for values of p_{H_2O} and P other than 0 and 1 atm, respectively (ref. 3).

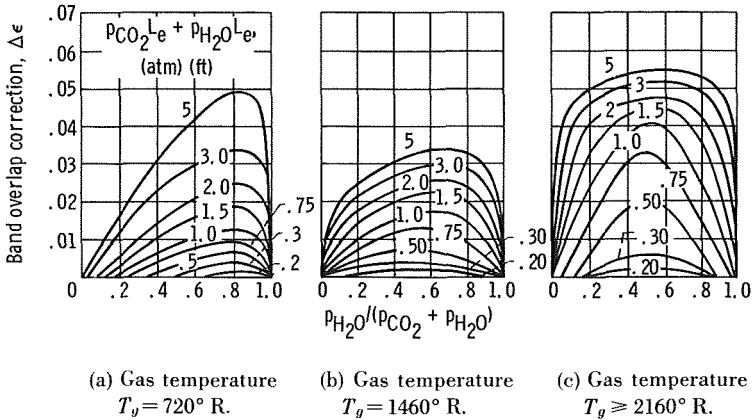


FIGURE 5-15.—Correction on total emittance for band overlap when both CO_2 and water vapor are present (ref. 3).

coefficient $C_{\text{H}_2\text{O}}$ is given in figure 5-14 to account for the actual partial and total pressures involved. If CO_2 and water vapor are both present in the gas mixture, an additional quantity $\Delta\epsilon$ must be included to account for an emittance reduction resulting from spectral overlap of the CO_2 and H_2O absorption bands. This correction is found from figure 5-15. For a mixture of CO_2 and water vapor in a nonabsorbing carrier gas the emittance is then given by

$$\epsilon_g = C_{\text{CO}_2}\epsilon_{\text{CO}_2} + C_{\text{H}_2\text{O}}\epsilon_{\text{H}_2\text{O}} - \Delta\epsilon \quad (5-62)$$

5.6.2 Exchange Between Entire Gas Volume and Boundary

Hottel (ref. 3) has provided a simple approximate procedure applicable when the cooled enclosure boundary is black and is at a temperature where it will emit appreciable radiation. The total energy removed at the wall must equal the energy being supplied by some external means such as combustion to the gas. Taking a heat balance on the gas then shows that the net *average* heat flux being *removed* at the wall is the gas emission minus the emission from the wall that is absorbed by the gas, that is,

$$\frac{Q}{A} = \sigma [\epsilon_g T_g^4 - \alpha_g(T_w) T_w^4] \quad (5-63)$$

The $\alpha_g(T_w)$ is the absorptance of the gas for radiation emitted from the wall at temperature T_w . The $\alpha_g(T_w)$ depends on T_w as this determines the spectral distribution of the radiation received by the gas. According to reference 3, the α_g can be found from

$$\alpha_g = \alpha_{\text{CO}_2} + \alpha_{\text{H}_2\text{O}} - \Delta\alpha \quad (5-64)$$

where

$$\alpha_{\text{CO}_2} = C_{\text{CO}_2}\epsilon_{\text{CO}_2}^+ \left(\frac{T_g}{T_w}\right)^{0.65} \quad (5-65)$$

$$\alpha_{\text{H}_2\text{O}} = C_{\text{H}_2\text{O}}\epsilon_{\text{H}_2\text{O}}^+ \left(\frac{T_g}{T_w}\right)^{0.45} \quad (5-66)$$

$$\Delta\alpha = (\Delta\epsilon)_{\text{at } T_w} \quad (5-67)$$

The $\epsilon_{\text{CO}_2}^+$ and $\epsilon_{\text{H}_2\text{O}}^+$ are respectively ϵ_{CO_2} and $\epsilon_{\text{H}_2\text{O}}$ obtained from figures 5-11 and 5-13 evaluated at the abscissa T_w and at the respective parameters $p_{\text{CO}_2}L_e(T_w/T_g)$ and $p_{\text{H}_2\text{O}}L_e(T_w/T_g)$. For further information the reader is referred to references 3 and 4.

EXAMPLE 5-2: A cooled right cylindrical tank 4 ft in diameter and 4 ft long is filled with hot gas at a total pressure of 1 atm. The interior surface of the tank is black. The gas is composed of two constituents; a transparent gas at a partial pressure of 0.75 atm, and the remainder carbon dioxide. The gas is uniformly mixed at a temperature of 2000° R. Compute how much energy must be removed from either end of the tank to keep it cool if the tank walls are all sufficiently cooled so that only radiation from the gas is significant.

The geometry is a finite circular cylinder of gas and the radiation to its base will be computed. Emission from the cooled walls is neglected. Using table 5-I, the corrected mean beam length for this geometry is $L_e = 0.60D = 2.4$ ft. The partial pressure of the CO_2 is 0.25 atm, so that

$$p_{\text{CO}_2} L_e = 0.25 \times 2.4 = 0.6 \text{ (atm)(ft)}$$

From figure 5-11, $\epsilon_{\text{CO}_2}(p_{\text{CO}_2} L_e, T_g) = 0.13$ and C_{CO_2} from figure 5-12 is 1.0 since the mixture total pressure is unity. Assuming the base of the tank to be sufficiently cool so that its emitted energy is negligible, the energy to be removed is from equation (5-61)

$$Q_i = \epsilon_{\text{CO}_2} \sigma T_g^4 A = 0.13 \times 0.173 \times 10^{-8} (2000)^4 \pi = 45,200 \frac{\text{Btu}}{\text{hr}}$$

5.7 TOTAL RADIATION EXCHANGE IN ENCLOSURE BY INTEGRATION OF SPECTRAL EQUATIONS

The mean beam length approach in the previous section was concerned with the radiation from a gas volume to all or a portion of a black enclosure boundary, or the average exchange between the gas and a black isothermal enclosure. For a more general analysis of radiation in an enclosure, the exchanges of total radiation must be considered between the various pairs of bounding surfaces having different temperatures. This involves integrating the exchange relations involving $\bar{\tau}_\lambda$ and $\bar{\alpha}_\lambda$ over all wavelengths. An example requiring such an integration was outlined in example 5-1 which considered a parallel plate geometry.

A form of the spectral equations was given by equation (5-20) that relates the gas blackbody emissive power and the spectral fluxes dq_λ supplied in a differential wavelength interval to each surface. In the solution accounting for spectral effects as described in section 5.3 of volume II for enclosures filled with nonabsorbing media, the set of enclosure equations is solved at each wavelength for the dq_λ (assume that the surface temperatures are specified) and the results then integrated over all wavelengths. For a gas radiation problem the gas properties vary so irregularly with wavelength that the detailed integration over λ

would be a practical impossibility. This leads to a consideration of using finite wavelength bands.

5.7.1 Band Equations

An approach that can be used to integrate over wavelength is developed by dividing the spectrum into absorbing and nonabsorbing bands. For a typical band of width $\Delta\lambda$, the integration of equation (5-20) gives

$$\int_{\Delta\lambda} \sum_{j=1}^N \left(\frac{\delta_{kj}}{\epsilon_{\lambda, j}} - F_{k-j} \frac{1 - \epsilon_{\lambda, j}}{\epsilon_{\lambda, j}} \bar{\tau}_{\lambda, k-j} \right) dq_{\lambda, j}$$

$$= \int_{\Delta\lambda} \sum_{j=1}^N [(\delta_{kj} - F_{k-j} \bar{\tau}_{\lambda, k-j}) e_{\lambda b, j} - F_{k-j} \bar{\alpha}_{\lambda, k-j} e_{\lambda b, g}] d\lambda \quad (5-68)$$

Now it is assumed that the bands are sufficiently narrow that $dq_{\lambda, j}$, $\epsilon_{\lambda, j}$, $\bar{\tau}_{\lambda, k-j}$, $\bar{\alpha}_{\lambda, k-j}$, $e_{\lambda b, j}$, and $e_{\lambda b, g}$ can be regarded as constants over the band width, being characteristic of some mean wavelength within the band or in the case of $\bar{\tau}$ and $\bar{\alpha}$ being averaged over the band as will be described in section 5.7.2. Then equation (5-68) can be written for band l as

$$\sum_{j=1}^N \left(\frac{\delta_{kj}}{\epsilon_{l, j}} - F_{k-j} \frac{1 - \epsilon_{l, j}}{\epsilon_{l, j}} \bar{\tau}_{l, k-j} \right) \Delta q_{l, j} = \sum_{j=1}^N [(\delta_{kj} - F_{k-j} \bar{\tau}_{l, k-j}) e_{l b, j}$$

$$- F_{k-j} \bar{\alpha}_{l, k-j} e_{l b, g}] \Delta\lambda \quad (5-69)$$

In a spectral region where the gas is essentially nonabsorbing, $\bar{\tau}_l = 1$ and $\bar{\alpha}_l = 0$ so that equation (5-69) reduces to

$$\sum_{j=1}^N \left(\frac{\delta_{kj}}{\epsilon_{l, j}} - F_{k-j} \frac{1 - \epsilon_{l, j}}{\epsilon_{l, j}} \right) \Delta q_{l, j} = \sum_{j=1}^N (\delta_{kj} - F_{k-j}) e_{l b, j} \Delta\lambda \quad (5-70)$$

which is of the form of equation (3-19) in volume II.

5.7.2 Transmission and Absorption Factors

The $\bar{\tau}_{l, k-j}$ in equation (5-69) is found from equation (5-27) by taking an integrated average over the band, that is,

$$\bar{\tau}_{l, k-j} = \frac{1}{A_k F_{k-j}} \int_{A_j} \int_{A_k} \left[\frac{1}{\Delta\lambda} \int_{\Delta\lambda} \tau_{\lambda}(S) d\lambda \right] \frac{\cos \beta_j \cos \beta_k}{\pi S^2} dA_k dA_j \quad (5-71)$$

Similarly the $\bar{\alpha}_{l,k-j}$ is obtained as

$$\bar{\alpha}_{l,k-j} = \frac{1}{A_k F_{k-j}} \int_{A_j} \int_{A_k} \left[\frac{1}{\Delta\lambda} \int_{\Delta\lambda} \alpha_\lambda(S) d\lambda \right] \frac{\cos \beta_j \cos \beta_k}{\pi S^2} dA_k dA_j \quad (5-72)$$

For each small band width

$$\bar{\alpha}_{l,k-j} = 1 - \bar{\tau}_{l,k-j}$$

and to evaluate $\bar{\alpha}_l$ and $\bar{\tau}_l$ only the single integral is needed

$$A_k F_{k-j} \bar{\alpha}_{l,k-j} = \int_{A_j} \int_{A_k} \frac{\alpha_l(S) \cos \beta_j \cos \beta_k}{\pi S^2} dA_k dA_j \quad (5-73)$$

where

$$\alpha_l(S) = \frac{1}{\Delta\lambda} \int_{\Delta\lambda} \alpha_\lambda(S) d\lambda = \frac{1}{\Delta\lambda} \int_{\Delta\lambda} [1 - \exp(-a_\lambda S)] d\lambda$$

From equation (4-73) the α_l can be expressed if desired in terms of the effective band width as

$$\alpha_l(S) = \frac{\bar{A}_l(S)}{\Delta\lambda} \quad (5-74)$$

To obtain $\bar{\tau}$ and $\bar{\alpha}$ for use in equation (5-69), the integral in equation (5-75) must be evaluated between pairs of finite surfaces in the various wavelength bands involved. It is evident that, when there are more than a few bands that absorb appreciably, the solution involves considerable computational effort. A simplification has been developed by Dunkle (ref. 6) that saves considerable labor and yields good accuracy. Dunkle assumes that the integrated band absorption is a linear function of path length. This has some physical basis as it holds exactly for a weak band as shown in equation (4-76a). Also it is the form of some of the effective band widths in table 4-II. As shown in reference 6 by means of a few examples, reasonable values of the energy exchange are obtained by use of this approximation. Hence let α_l in equation (5-73) have the linear form

$$\alpha_l(S) = C_l S \quad (5-76)$$

Now define a mean value of the path length S , called the *geometric*

mean beam length \bar{S}_{k-j} . This mean length is such that α_l evaluated from equation (5-76) by using $S=S_{k-j}$ will yield $\bar{\alpha}_{l, k-j}$ as found from the integral in equation (5-73). Substituting $\bar{\alpha}_{l, k-j}=C_l\bar{S}_{k-j}$ and $\alpha_l=C_lS$ into equation (5-73) gives

$$A_k F_{k-j} C_l \bar{S}_{k-j} = \int_{A_j} \int_{A_k} \frac{C_l S \cos \beta_j \cos \beta_k}{\pi S^2} dA_k dA_j$$

Hence the relation to obtain the geometric mean beam length \bar{S}_{k-j} is

$$\bar{S}_{k-j} = \frac{1}{A_k F_{k-j}} \int_{A_j} \int_{A_k} \frac{\cos \beta_j \cos \beta_k}{\pi S} dA_k dA_j \quad (5-77)$$

which is only dependent on geometry. Dunkle (ref. 6) has computed and tabulated values of \bar{S}_{k-j} for the geometries of parallel equal rectangles, rectangles at right angles, and between a differential sphere and a rectangle. Results for equal opposed parallel rectangles are shown in figure 5-16. Tabular values for parallel rectangles, and rectangles at right angles given in tables 5-II and 5-III. Other \bar{S}_{k-j} values are referenced by Hottel and Sarofim (ref. 4).

For a given gas at uniform conditions, the effective band width correla-

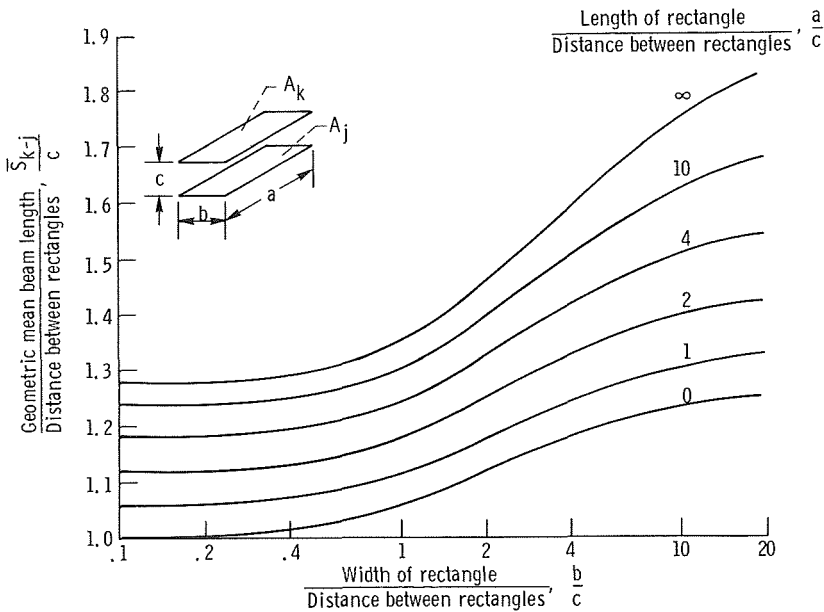
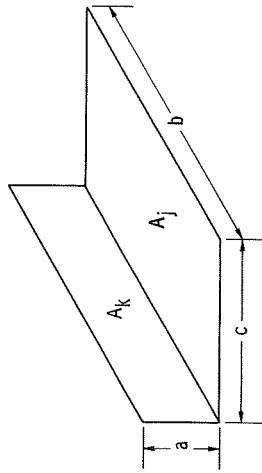


FIGURE 5-16. — Geometric mean beam lengths for equal parallel rectangles (ref. 6).

0.2	$\bar{S}_{k-j/c}$ F_{k-j}	1.003	1.004 .00626	1.006 .01240	1.015 .02391	1.028 .03398	1.058 .04941	1.120 .06971	1.182 .08353	1.210 .08859	1.235 .09272	1.256 .09586
0.4	$\bar{S}_{k-j/c}$ F_{k-j}	1.012	1.013 .01207	1.015 .02392	1.024 .04614	1.037 .06560	1.067 .09554	1.129 .13513	1.192 .16219	1.220 .17209	1.245 .18021	1.267 .18638
0.6	$\bar{S}_{k-j/c}$ F_{k-j}	1.025	1.026 .01715	1.028 .03398	1.037 .06560	1.050 .09336	1.080 .13627	1.143 .19341	1.206 .23271	1.235 .24712	1.261 .25896	1.282 .26795
1.0	$\bar{S}_{k-j/c}$ F_{k-j}	1.055	1.056 .02492	1.058 .04941	1.067 .09554	1.080 .13627	1.110 .19982	1.175 .28588	1.242 .34596	1.272 .36813	1.300 .38638	1.324 .40026
2.0	$\bar{S}_{k-j/c}$ F_{k-j}	1.116	1.117 .03514	1.120 .06971	1.129 .13513	1.143 .19342	1.175 .28588	1.246 .41525	1.323 .50899	1.359 .54421	1.393 .57338	1.421 .59563
4.0	$\bar{S}_{k-j/c}$ F_{k-j}	1.178	1.179 .04210	1.182 .08353	1.192 .16219	1.206 .23271	1.242 .34596	1.323 .50899	1.416 .63204	1.461 .67954	1.505 .71933	1.543 .74990
6.0	$\bar{S}_{k-j/c}$ F_{k-j}	1.205	1.207 .04463	1.210 .08859	1.220 .17209	1.235 .24712	1.272 .36813	1.359 .54421	1.461 .67954	1.513 .73258	1.564 .77741	1.609 .81204
10.0	$\bar{S}_{k-j/c}$ F_{k-j}	1.230	1.232 .04671	1.235 .09270	1.245 .18021	1.261 .25896	1.300 .38638	1.393 .57338	1.505 .71933	1.564 .77741	1.624 .82699	1.680 .86563
20.0	$\bar{S}_{k-j/c}$ F_{k-j}	1.251	1.253 .04829	1.256 .09586	1.267 .18638	1.282 .26795	1.324 .40026	1.421 .59563	1.543 .74990	1.609 .81204	1.680 .86563	1.748 .90785
∞	$\bar{S}_{k-j/c}$ F_{k-j}	1.272	1.274 .04988	1.277 .09902	1.289 .19258	1.306 .27698	1.349 .41421	1.452 .61803	1.584 .78078	1.660 .84713	1.745 .90499	1.832 .95125

TABLE 5-III. — CONFIGURATION FACTORS AND MEAN BEAM LENGTH FUNCTIONS FOR RECTANGLES AT RIGHT ANGLES

[From ref. 6]



a/b	c/b											
	0.05	0.10	0.20	0.4	0.6	1.0	2.0	4.0	6.0	10.0	20.0	∞
0.02	0.007982	0.008875	0.009323	0.009545	0.009589	0.009628	0.009648	0.009653	0.009655	0.009655	0.009655	0.009655
	.17840	.12903	.08298	.04995	.03587	.02291	.01263	.006364	.004288	.002594	.001305
	$A_k F_{k-j}/b^2$											
	$A_k F_{k-j} S_{k-j}/abc$											

0.05	$A_k F_{k-j} / b^2$ $A_k F_{k-j} / \bar{S}_{k-j} abc$	0.014369 .21146	0.018601 .18756	0.02117 .13834	0.02243 .08953	0.02279 .06627	0.02504 .04372	0.02316 .02364	0.02320 .01234	0.02321 .008342	0.02321 .002549	0.02321
0.10	$A_k F_{k-j} / b^2$ $A_k F_{k-j} / \bar{S}_{k-j} abc$		0.02819 .20379	0.03622 .17742	0.04086 .12737	0.04229 .09795	0.04325 .06659	0.04376 .03676	0.04390 .01944	0.04393 .013184	0.04394 .004049	0.04395
0.20	$A_k F_{k-j} / b^2$ $A_k F_{k-j} / \bar{S}_{k-j} abc$			0.05421 .18854	0.06859 .15900	0.07377 .13028	0.07744 .09337	0.07942 .05356	0.07999 .02890	0.08010 .01972	0.08015 .012047	0.08018
0.40	$A_k F_{k-j} / b^2$ $A_k F_{k-j} / \bar{S}_{k-j} abc$				0.10013 .16255	0.11524 .14686	0.12770 .11517	0.13514 .07088	0.13736 .03903	0.13779 .02666	0.13801 .01697	0.13814
0.60	$A_k F_{k-j} / b^2$ $A_k F_{k-j} / \bar{S}_{k-j} abc$					0.13888 .14164	0.16138 .11940	0.17657 .07830	0.18143 .04467	0.18239 .03109	0.18289 .02025	0.18318
1.0	$A_k F_{k-j} / b^2$ $A_k F_{k-j} / \bar{S}_{k-j} abc$						0.20004 .11121	0.23285 .08137	0.24522 .04985	0.24783 .03502	0.24921 .02196	0.25000
2.0	$A_k F_{k-j} / b^2$ $A_k F_{k-j} / \bar{S}_{k-j} abc$							0.29860 .07086	0.33462 .04924	0.34386 .03670	0.34916 .02401	0.35222
4.0	$A_k F_{k-j} / b^2$ $A_k F_{k-j} / \bar{S}_{k-j} abc$								0.40544 .04051	0.43104 .03284	0.44840 .02320	0.46020
6.0	$A_k F_{k-j} / b^2$ $A_k F_{k-j} / \bar{S}_{k-j} abc$									0.46982 .02882	0.49986 .02132	0.52368
10.0	$A_k F_{k-j} / b^2$ $A_k F_{k-j} / \bar{S}_{k-j} abc$										0.5502 .01759	0.6053
20.0	$A_k F_{k-j} / b^2$ $A_k F_{k-j} / \bar{S}_{k-j} abc$										0.6608 .008975	0.7156

tions discussed in chapter 4 can be used to obtain A_l . Using the $\Delta\lambda$ as described in the next paragraph fixes α_l from equation (5-74) and by fitting with a linear path length dependence determines C_l from equation (5-76). Corresponding to the geometric mean beam length between surfaces j and k , the $\bar{\alpha}$ can then be found as $C_l\bar{S}$ and the $\bar{\tau}$ as $1 - \bar{\alpha}$. Then equations (5-69) and (5-70) can be solved for each wavelength band l . The total energies at each surface k are found from

$$q_k = \sum_{\text{absorbing bands}} \Delta q_{l,k} + \sum_{\text{nonabsorbing bands}} \Delta q_{l,k} \quad (5-78)$$

The values of $\Delta\lambda$, the wavelength span of each band, must be specified in order to carry out the solution. As discussed after equation (4-73), this span can increase with path length. Edwards and Nelson (refs. 7 and 8) give recommended spans for CO_2 and H_2O vapor; these values are reproduced in table 5-IV for the parallel plate geometry. Note that these values are given in terms of wave number rather than wavelength. For other geometries, Edwards and Nelson give methods for choosing approximate spans for CO_2 and H_2O bands. Briefly, the method is to use approximate band spans based on the longest important mass path length in the geometry being studied. With this in mind, the limits of table 5-IV are probably adequate for problems involving CO_2 and H_2O vapor.

TABLE 5-IV.—APPROXIMATE BAND LIMITS FOR PARALLEL PLATE GEOMETRY

[From refs. 7, 8, and 11]

Gas	Band, λ , μm	Band, center, η , cm^{-1}	Band limits, η , cm^{-1} ^a	
			Lower	Upper
CO_2	15	667	$667 - (\bar{A}_{15}/1.78)$	$667 + (\bar{A}_{15}/1.78)$
	10.4	960	849	1013
	9.4	1060	1013	1141
	4.3	2350	$2350 - (\bar{A}_{4.3}/1.78)$	2430
	2.7	3715	$3715 - (\bar{A}_{2.7}/1.78)$	3750
H_2O	6.3	1600	$1600 - (\bar{A}_{6.3}/1.6)$	$1600 + (\bar{A}_{6.3}/1.6)$
	2.7	3750	$3750 - (\bar{A}_{2.7}/1.4)$	$3750 + (\bar{A}_{2.7}/1.4)$
	1.87	5350	4620	6200
	1.38	7250	6200	8100

^a \bar{A} are found for various bands from tables 4-II and 4-III. Terms such as $\bar{A}_{15}/1.78$ are $\bar{A}/2(1 - \tau_p)$ from eq. (17) and tables 1 and 2 of ref. 7.

If all surface temperatures are given in the problem at hand, the results found from equation (5-78) complete the solution. If q_k is given for n surfaces and T_k for the remaining $N-n$ surfaces, then the unknown surface temperatures are guessed and the calculated q_k are compared to the given values. If they do not agree, then new values of T_k for the n surfaces are assumed and the calculation is repeated. This procedure is continued until there is agreement between given and calculated q_k for all k . For the given T_g , equation (5-21) expressed as a sum over the wavelength bands gives the required energy input to the gas.

Two example problems will now be presented for an isothermal gas in an enclosure. Then the discussion will continue to consider removing the restriction of uniform conditions in the gas.

EXAMPLE 5-3: Two black parallel plates are separated by a distance of $D=1$ m. The plates are of width $W=1$ m and of effectively infinite length (fig. 5-17). The space between the plates is filled with carbon dioxide gas at a pressure of 1 atm and a temperature of 1000 K. If plate 1 is maintained at 2000 K and plate 2 is maintained at 500 K, find the energy flux that must be supplied to plate 2 to maintain its temperature.

As shown by figure 5-17 the geometry is a four boundary enclosure formed by the two plates and the two open bounding planes. The open

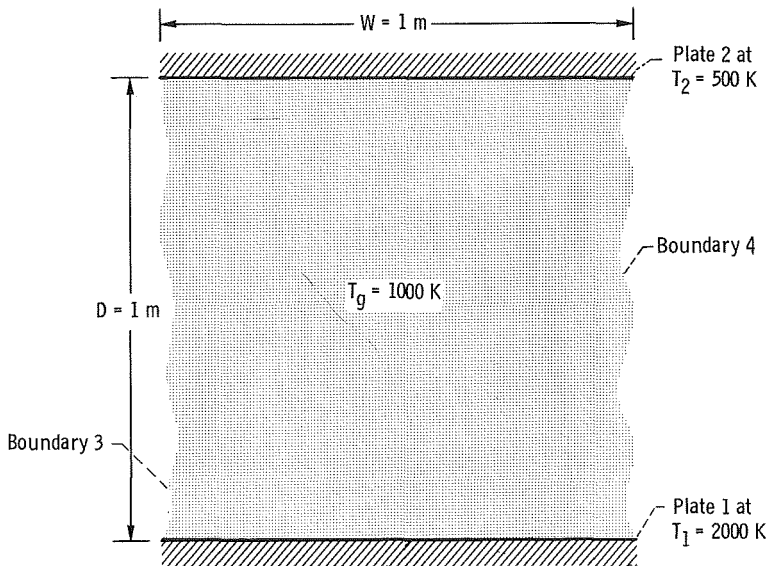


FIGURE 5-17.—Isothermal carbon dioxide contained between black plates (see example 5-3).

bounding planes are perfectly absorbing (i.e., nonreflecting) and radiate no significant energy for the present case as the temperature of the surrounding environment is assumed low. The energy flux added to surface 2 will be found by using the enclosure equation (5-20) where $k=2$ and $N=4$. Since all surfaces are black, $\epsilon_{\lambda,j}=1$ and equation (5-20) reduces to

$$\sum_{j=1}^4 \delta_{2j} dq_{\lambda,j} = \sum_{j=1}^4 [(\delta_{2j} - F_{2-j} \bar{\tau}_{\lambda,2-j}) e_{\lambda b,j} d\lambda - F_{2-j} \bar{\alpha}_{\lambda,2-j} e_{\lambda b,g} d\lambda]$$

The self-view factor $F_{2-2}=0$ in this case, and $e_{\lambda b,3}=e_{\lambda b,4}=0$, so the summations can be written out as

$$dq_{\lambda,2} = [-F_{2-1} \bar{\tau}_{\lambda,2-1} e_{\lambda b,1} + e_{\lambda b,2} - (F_{2-1} \bar{\alpha}_{\lambda,2-1} + F_{2-3} \bar{\alpha}_{\lambda,2-3} + F_{2-4} \bar{\alpha}_{\lambda,2-4}) e_{\lambda b,g}] d\lambda \quad (5-79)$$

To simplify the example, it will be carried out by considering the entire wavelength region as a single band. Then to obtain the total energy supplied to plate 2, integrate over all wavelengths to give

$$q_2 = -F_{2-1} \int_0^{\infty} \bar{\tau}_{\lambda,2-1} e_{\lambda b,1} d\lambda + \sigma T_2^4 - \int_0^{\infty} (F_{2-1} \bar{\alpha}_{\lambda,2-1} + F_{2-3} \bar{\alpha}_{\lambda,2-3} + F_{2-4} \bar{\alpha}_{\lambda,2-4}) e_{\lambda b,g} d\lambda$$

Using the definitions of total transmission and absorption factors which are

$$\bar{\tau}_{2-1} \sigma T_1^4 = \int_0^{\infty} \bar{\tau}_{\lambda,2-1} e_{\lambda b,1} d\lambda$$

$$\bar{\alpha}_{2-1} \sigma T_g^4 = \int_0^{\infty} \bar{\alpha}_{\lambda,2-1} e_{\lambda b,g} d\lambda$$

and so forth, the q_2 becomes

$$q_2 = \sigma T_2^4 - F_{2-1} \bar{\tau}_{2-1} \sigma T_1^4 - (F_{2-1} \bar{\alpha}_{2-1} + F_{2-3} \bar{\alpha}_{2-3} + F_{2-4} \bar{\alpha}_{2-4}) \sigma T_g^4 \quad (5-80)$$

To determine the $\bar{\tau}$ and $\bar{\alpha}$, the concept of geometric mean beam length will be used. For opposing rectangles, from figure 5-16 at an abscissa of 1.0 and on the curve for length to spacing ratio of ∞ , the $\bar{S}_{2-1}/D=1.34$ or $\bar{S}_{2-1}=1.34$ m. To determine $\bar{\alpha}_{2-1}$ which determines the emission of

the gas, use the emittance chart in figure 5-11 at a pressure of 1 atm, a beam length of 1.34 m (4.40 ft), and $T_g = 1000$ K (1800° R). This gives $\bar{\alpha}_{2-1} = 0.22$. When obtaining $\bar{\tau}_{2-1}$, note from equation (5-79) that the radiation in the τ_{2-1} term is $\epsilon_{\lambda b, 1}$ and is coming from wall 1. Therefore, it has a spectral distribution different from that of the gas radiation. To account for this nongray effect, equation (5-65) will be used with ϵ^+ evaluated at $p_{CO_2} \bar{S}_{2-1} (T_1/T_g) = 1.34 (2000/1000) = 2.78$ (atm) (m) = 9.11 (atm) (ft) and $T_1 = 2000$ K (3600° R). Then using figure 5-11 (extrapolated) and equation (5-65) results in

$$\bar{\tau}_{2-1} \approx 1 - 0.2 \left(\frac{1}{2} \right)^{0.65} = 1 - 0.13 = 0.87$$

From section 2.5.3.1 of volume II, the configuration factor F_{2-1} is given by

$$F_{2-1} = \frac{[(D^2 + W^2)^{1/2} - D]}{W} = \sqrt{2} - 1 = 0.414$$

Then $F_{2-3} = F_{2-4} = \frac{1}{2}(1 - 0.414) = 0.293$.

The $\bar{\alpha}_{2-3} = \bar{\alpha}_{2-4}$ remain to be found. For adjoint planes as in the geometry for table 5-III, the following expression from equation (12) of reference 6 can be used, obtained for the present case where $b \rightarrow \infty$, $a = 1$, and $c = 1$:

$$\bar{S}_{2-3} = \frac{1}{\pi F_{2-3}} (2 \ln \sqrt{2}) = \frac{2 \times 0.346}{\pi \times 0.293} = 0.752 \text{ m}$$

Using figure 5-11 at $p\bar{S} = 0.752$ (atm)(m) = 2.46 (atm)(ft) and $T_g = 1800^\circ$ R gives $\bar{\alpha}_{2-3} = \bar{\alpha}_{2-4} = 0.19$. Then

$$\begin{aligned} q_2 &= \sigma T_2^4 - 0.414(0.87)\sigma T_1^4 - (0.414 \times 0.22 + 2 \times 0.293 \times 0.19)\sigma T_g^4 \\ &= 5.73 \times 10^{-12} (500^4 - 0.36 \times 2000^4 - 0.20 \times 1000^4) \\ &= -33.8 \frac{\text{W}}{\text{cm}^2} \end{aligned}$$

The solution is now complete. Note that the largest contribution to q_2 is by energy leaving surface 1 and being absorbed by surface 2. Emission from the gas to surface 2 and emission from surface 2 are negligible.

EXAMPLE 5-4: Parallel nongray plates are 1 in. apart and are at temperatures of $T_1 = 2000^\circ$ R and $T_2 = 1000^\circ$ R. Pure CO_2 gas at 10-atm pressure and $T_g = 1000^\circ$ R is between the plates. The plate hemispherical

spectral emissivity as a function of wave number is approximated by the following table:

η, cm^{-1}	ϵ_η	η, cm^{-1}	ϵ_η
0 to 500	0.37	1150 to 2200	0.45
500 to 750	.26	2200 to 2500	.65
750 to 850	.32	2500 to 3600	.61
850 to 1000	.37	3600 to 3750	.69
1000 to 1150	.46	3750 to ∞	.73

Assume that only the 15-, 10.4-, 9.4-, 4.3-, and 2.7- μm CO_2 bands cause significant attenuation in the gas. Compute the total heat flux being added to plate 2.

In example 5-1 the spectral exchange was found for radiation between infinite parallel plates with a gas between them. The total energy added to plate 2 is found by integrating equation (5-24b) over all wave numbers

$$q_2 = \int_{\eta=0}^{\infty} \frac{\{\epsilon_{\eta,1}\epsilon_{\eta,2}\bar{\tau}_\eta(e_{\eta b,2} - e_{\eta b,1}) + \epsilon_{\eta,2}(1 - \bar{\tau}_\eta)[1 + (1 - \epsilon_{\eta,1})\bar{\tau}_\eta](e_{\eta b,2} - e_{\eta b,1})\}d\eta}{1 - (1 - \epsilon_{\eta,1})(1 - \epsilon_{\eta,2})\bar{\tau}_\eta^2}$$

In this example $\epsilon_{\eta,1} = \epsilon_{\eta,2}$ and $T_1 = T_2$ so the q_2 simplifies to

$$q_2 = - \int_0^{\infty} \frac{\epsilon_{\eta,1}^2 \bar{\tau}_\eta (e_{\eta b,1} - e_{\eta b,2})}{1 - (1 - \epsilon_{\eta,1})^2 \bar{\tau}_\eta^2} d\eta$$

The integration can be expressed in finite difference form as a sum over wave number bands. For the l^{th} band let $\epsilon_{\eta,1} = \epsilon_l$, $\bar{\tau}_\eta = \bar{\tau}_l$, and so forth. Then

$$q_2 = - \sum_l \frac{\epsilon_l^2 \bar{\tau}_l [e_b(T_1) - e_b(T_2)]_l \Delta\eta_l}{1 - (1 - \epsilon_l)^2 \bar{\tau}_l^2}$$

From equation (5-74) the $\bar{\tau}_l$ can be written as

$$\bar{\tau}_l = 1 - \bar{\alpha}_l = 1 - \frac{\bar{A}_l}{\Delta\eta_l}$$

where the \bar{A}_l is the integrated band width which includes the integrated path length variation for a parallel plate geometry. The q_2 now becomes

$$q_2 = - \sum_l \frac{\epsilon_l^2 \left(1 - \frac{\bar{A}_l}{\Delta\eta_l}\right) [e_b(T_1) - e_b(T_2)]_l \Delta\eta_l}{1 - (1 - \epsilon_l)^2 \left(1 - \frac{\bar{A}_l}{\Delta\eta_l}\right)^2}$$

The needed quantities and results for this problem are shown in the table. Values of \bar{A}_l were computed from the exponential wide band correlation data of tables 4-II and 4-III using the mean beam length from table 5-I as the effective path length. The wave number spans $\Delta\eta_l$ were computed from the data of table 5-IV, and values of

$$[e_b(T_1) - e_b(T_2)]_l \Delta\eta_l$$

for the nonabsorbing regions were computed using the $F_{0-\lambda T}$ factors from table V of the appendix to volume I. When the band correlations give $\bar{A}_l > \Delta\eta_l$, then $\bar{A}_l/\Delta\eta_l = 1.0$ is used since physically \bar{A}_l cannot exceed $\Delta\eta_l$.

Band, η , cm^{-1}	ϵ_l	\bar{A}_l , cm^{-1}	$\Delta\eta_l$, cm^{-1}	$[e_b(T_1) - e_b(T_2)]_l \Delta\eta_l$, Btu (hr)(ft ²)	$-q_{1,2}$, Btu (hr)(ft ²)
0 to 556	0.37	0	556	250	57
556 to 778 (15 μm)	.26	197	222	414	3
778 to 849	.32	0	71	158	30
849 to 1013 (10.4 μm)	.37	9.6	164	590	117
1013 to 1141 (9.4 μm)	.46	9.6	128	480	125
1141 to 2221	.45	0	1080	6758	1960
2221 to 2430 (4.3 μm)	.65	230	209	1550	0
2430 to 3573	.61	0	1143	7389	3240
3573 to 3750 (2.7 μm)	.69	253	177	955	0
3750 to ∞	.73	0	∞	7181	4110
					9642

The result for q_2 compares with a value of -9371 Btu/(hr)(ft²) found for the same problem by Edwards and Nelson (ref. 7).⁸ They use the network method of Oppenheim (ref. 9) in deriving the energy transfer equation, which, of course, gives the same result as that used here. Partial emittances were used in place of the band correlations for computing gas properties, and these led to slightly different wave number spans for the bands used in reference 7.

5.8 RADIATION THROUGH NONISOTHERMAL GASES

Edwards and coworkers (refs. 10 to 12) have further extended the band and geometric mean beam length approaches to account for non-isothermal gases. Removing the isothermal gas restriction introduces considerable additional complication. In a nonisothermal case, the band

⁸ The results of ref. 7 have an error in $q_{1,2}$ for the 2430- to 3590- cm^{-1} range. The comparison described here is after correction of that error.

absorption may vary strongly with position in the gas. Then, a linear absorption law may be valid in one portion of a gas, but a power law might be necessary in another portion. The Curtis-Godson technique that will be discussed in section 5.8.1 is the basis for one engineering treatment of nonisothermal gases (refs. 10 and 13 to 16). Another treatment, due chiefly to Hottel and coworkers (refs. 3, 4, and 17), is the zoning method discussed in section 5.8.2. The methods of chapter 3 can be used in simple geometries to treat radiation in nonisothermal gases. In connection with this, the exchange factor approximation is given in section 5.8.3. The methods in this chapter and the Monte Carlo techniques of chapter 6 are powerful enough to treat multidimensional problems.

5.8.1 The Curtis-Godson Approximation

An accurate and useful method for solving thermal radiation problems in nonuniform gases is the Curtis-Godson approximation (refs. 10 and 13 to 16). In this method, the transmittance of a given path through a nonisothermal gas is related to the transmittance through an equivalent isothermal gas. Then the solution can be obtained by using isothermal gas methods. The relation between the nonisothermal and the isothermal gas is carried out by assigning an equivalent amount of isothermal absorbing material to act in place of the nonisothermal gas. The amount is based on a scaling temperature and a mean density or pressure that is obtained in the analysis. These mean quantities are found by specifying that the transmittance of the uniform gas be equal to the transmittance of the nonuniform gas in the weak and strong absorption limits.

Goody (ref. 15), Krakow et al. (ref. 13), and Simmons (ref. 16) have discussed the Curtis-Godson method for the case of attenuation in a narrow vibration-rotation band. Excellent comparisons with exact numerical results were obtained. Weiner and Edwards (ref. 12) have applied the method for engineering environments, that is, for steep temperature gradients in gases with overlapping band structures. Comparison of the analysis with experimental data was again excellent. In the following development of the use of the method, spectral variations will be expressed in terms of wave number $\eta = 1/\lambda$ since the absorption band correlations are often expressed in terms of this variable. The Curtis-Godson technique is most useful when the temperature distribution in the gas is specified. If the gas temperature distribution is not known, an iterative procedure would have to be developed for its determination. This is not considered here as the method is not too practical for that type of calculation.

For a nonuniform gas the absorption coefficient a_η is variable along the path. An effective band width $\bar{A}_l(S)$ is defined in this instance analogous to equation (4-73) but using an integrated absorption coefficient

$$\begin{aligned}\bar{A}_l(S) &= \int_{\text{absorption}}^{\text{band width}} \left\{ 1 - \exp \left[- \int_0^S a_\eta(\eta, S^*) dS^* \right] \right\} d\eta \\ &= \Delta\eta_l - \int_l \left\{ \exp \left[- \int_0^S a_\eta(\eta, S^*) dS^* \right] \right\} d\eta\end{aligned}\quad (5-81)$$

Similarly for a path length extending from S^* to S , the effective band width is

$$\bar{A}_l(S - S^*) = \int_{\text{absorption}}^{\text{band width}} \left\{ 1 - \exp \left[- \int_{S^*}^S a_\eta(\eta, S^{**}) dS^{**} \right] \right\} d\eta \quad (5-82)$$

The equation of transfer will now be placed in a form utilizing $\bar{A}_l(S)$ and $\bar{A}_l(S - S^*)$.

The integrated form of the equation of transfer for intensity at S as a result of radiation traveling along a path from 0 to S is given from equation (3-1) by

$$\begin{aligned}i'_\eta(\eta, S) &= i'_\eta(\eta, 0) \exp \left[- \int_0^S a_\eta(\eta, S^*) dS^* \right] \\ &\quad + \int_0^S a_\eta(\eta, S^*) i'_{\eta b}(\eta, S^*) \exp \left[- \int_{S^*}^S a_\eta(\eta, S^{**}) dS^{**} \right] dS^*\end{aligned}\quad (5-83)$$

Now note that

$$\begin{aligned}-\frac{\partial}{\partial S^*} \left\{ 1 - \exp \left[- \int_{S^*}^S a_\eta(\eta, S^{**}) dS^{**} \right] \right\} \\ = a_\eta(\eta, S^*) \exp \left[- \int_{S^*}^S a_\eta(\eta, S^{**}) dS^{**} \right]\end{aligned}\quad (5-84)$$

Insert equation (5-84) into equation (5-83) to obtain

$$\begin{aligned}i'_\eta(\eta, S) &= i'_\eta(\eta, 0) \exp \left[- \int_0^S a_\eta(\eta, S^*) dS^* \right] \\ &\quad - \int_0^S i'_{\eta b}(\eta, S^*) \frac{\partial}{\partial S^*} \left\{ 1 - \exp \left[- \int_{S^*}^S a_\eta(\eta, S^{**}) dS^{**} \right] \right\} dS^*\end{aligned}\quad (5-85)$$

Equation (5-85) is now integrated over the band width $\Delta\eta_l$ of the l^{th} band, and the order of integration is changed on the last term. It is assumed that $i'_\eta(\eta, S)$, $i'_\eta(\eta, 0)$, and $i'_{\eta b}(\eta, S)$ can be approximated by average values within the band. Then

$$i'_l(S)\Delta\eta_l = i'_l(0) \int_l \left\{ \exp \left[- \int_0^S a_\eta(\eta, S^*) dS^* \right] \right\} d\eta \\ - \int_0^S i'_{l,b}(S^*) \frac{\partial}{\partial S^*} \int_l \left\{ 1 - \exp \left[- \int_{S^*}^S a_\eta(\eta, S^{**}) dS^{**} \right] \right\} d\eta dS^* \quad (5-86)$$

Equations (5-81) and (5-82) are substituted into equation (5-86) to obtain the equation of transfer in terms of the \bar{A}_l

$$i'_l(S)\Delta\eta_l = i'_l(0) [\Delta\eta_l - \bar{A}_l(S)] \\ - \int_0^S i'_{l,b}(S^*) \frac{\partial \bar{A}_l(S - S^*)}{\partial S^*} dS^* \quad (5-87)$$

An alternate form can be found by integrating equation (5-87) by parts to give

$$i'_l(S)\Delta\eta_l = i'_l(0) [\Delta\eta_l - \bar{A}_l(S)] + i'_{l,b}(0)\bar{A}_l(S) \\ + \int_0^S \bar{A}_l(S - S^*) \frac{di'_{l,b}(S^*)}{dS^*} dS^* \quad (5-88)$$

Equations (5-87) and (5-88) are nearly exact forms of the integrated equation of transfer in terms of the band properties. The only approximation is that the intensity in each term does not vary significantly across the wave number span of the band.

Note that, for a *uniform* gas, equation (5-88) gives, since $di'_{l,b}/dS = 0$,

$$i'_{l,u}(S)\Delta\eta_l = i'_l(0) [\Delta\eta_l - \bar{A}_{l,u}(S)] + i'_{l,b,u}\bar{A}_{l,u}(S) \quad (5-89)$$

where the u subscript denotes a uniform gas.

In order to compute $i'_l(S)$ or $i'_{l,u}(S)$ from equation (5-87), (5-88), or (5-89), expressions are needed for the effective band width \bar{A}_l for non-uniform and uniform gases. From equations (4-76a) and (4-76b), the limiting cases of \bar{A}_l for weak or strong absorption in a uniform gas have the form

$$\bar{A}_{l,u}(S) = C_{1,l} \rho_u S_u \quad (\text{weak}) \quad (5-90a)$$

$$\bar{A}_{l,u}(S) = C_{2,l} \rho_u S_u^{1/2} \quad (\text{strong}) \quad (5-90b)$$

where the $C_{1,l}$ and $C_{2,l}$ are coefficients of proportionality for the l th band.

For the nonuniform gas the effective band width will depend on the variation of properties along the path. The effective band widths are

then obtained by applying equations (5-90a) and (5-90b) locally along the path. This gives for a weak band

$$\bar{A}_l(S) = C_{1,l} \int_0^S \rho(S^*) dS^* \quad (\text{weak}) \quad (5-91a)$$

where the ρ is a function of position S^* along the path. Similarly for the strong band by first squaring equation (5-90b)

$$\bar{A}_l^2(S) = C_{2,l}^2 \int_0^S \rho^2(S^*) dS^*$$

so that

$$\bar{A}_l(S) = C_{2,l} \left[\int_0^S \rho^2(S^*) dS^* \right]^{1/2} \quad (\text{strong}) \quad (5-91b)$$

It has been assumed that the $C_{1,l}$ and $C_{2,l}$ do not vary along the path.

In the Curtis-Godson method the *nonuniform gas is replaced by an effective amount of uniform gas such that the correct intensity is obtained at the weak and strong absorption limits*. To have the uniform intensity equal the nonuniform intensity, equate the results from equations (5-89) and (5-88) to obtain

$$\begin{aligned} i'_i(0) [\Delta\eta_l - \bar{A}_{l,u}(S)] + i'_{i,b,u} \bar{A}_{l,u}(S) \\ = i'_i(0) [\Delta\eta_l - \bar{A}_l(S)] + i'_{i,b}(0) \bar{A}_l(S) + \int_0^S \bar{A}_l(S-S^*) \frac{di'_{i,b}(S^*)}{dS^*} dS^* \end{aligned}$$

which simplifies to

$$\begin{aligned} [i'_{i,b,u}(T_u) - i'_i(0)] \bar{A}_{l,u}(S) \\ = [i'_{i,b}(0) - i'_i(0)] \bar{A}_l(S) + \int_0^S \bar{A}_l(S-S^*) \frac{di'_{i,b}(S^*)}{dS^*} dS^* \quad (5-92) \end{aligned}$$

To have equation (5-92) valid at the weak absorption limit, substitute $\bar{A}_{l,u}$ from equation (5-90a) and \bar{A}_l from equation (5-91a) to obtain the following after canceling the $C_{1,l}$:

$$\begin{aligned} [i'_{i,b,u}(T_u) - i'_i(0)] \rho_u S_u = [i'_{i,b}(0) - i'_i(0)] \int_0^S \rho(S^*) dS^* \\ + \int_0^S \left[\int_{S^*}^S \rho(S^{**}) dS^{**} \right] \frac{di'_{i,b}(S^*)}{dS^*} dS^* \quad (5-93a) \end{aligned}$$

Similarly at the strong absorption limit, insert equations (5-90b) and (5-91b) into equation (5-92) to obtain

$$\begin{aligned}
 [i'_{l,b,u}(T_u) - i'_l(0)] \rho_u S_u^{1/2} &= [i'_{l,b}(0) - i'_l(0)] \left[\int_0^S \rho^2(S^*) dS^* \right]^{1/2} \\
 &+ \int_0^S \left[\int_{S^*}^S \rho^2(S^{**}) dS^{**} \right]^{1/2} \frac{di'_{l,b}(S^*)}{dS^*} dS^* \quad (5-93b)
 \end{aligned}$$

For a *known* distribution of temperature and density in a nonuniform gas, equations (5-93a) and (5-93b) can be solved simultaneously for ρ_u and S_u which are the equivalent uniform gas density and path length for that particular band. The $i'_{l,b,u}(T_u)$ is not an additional unknown since the temperature T_u corresponds to ρ_u . Then equation (5-89) can be used for any effective band width dependency on ρ_u and S_u (i.e., not at only the weak and strong limits) to solve for $i'_{l,u}(S)$. This will exactly equal the intensity $i'_l(S)$ in the nonuniform gas in the weak and strong limits and will usually be a good approximation for intermediate absorption values. Once the intensities are found, the heat transfer can be obtained by using the relations for a uniform gas. Almost invariably the evaluation of equations (5-93a) and (5-93b) will require numerical integration. Because the Curtis-Godson method requires evaluation of at least two integrals for each band along each path, it may in many cases be equally feasible to evaluate the exact equation (5-87) or (5-88). This is especially true if the problem is to be solved by electronic computer.

As originally formulated (see, for example, the discussion in Goody (ref. 15)), the Curtis-Godson approximation was limited to application over a small frequency span in an absorption band. The limitation was due to considerations of line overlapping, and the change in the spectral position of important lines with temperature. It has been shown, however (see, for example, Wiener and Edwards (ref. 12) and Plass (ref. 18)), that the method gives good results even when applied to situations with large temperature gradients while using fairly wide frequency spans. These references also account for overlapping absorption bands.

The Curtis-Godson technique appears to have application even in multidimensional problems, even though it was originally applied to one-dimensional atmospheric problems. Although no one has explicitly carried out such calculations, it should be possible to proceed as follows. For a known field of temperature and density, the medium and the boundaries are subdivided into convenient nearly isothermal zones. Between each two zones, an equivalent uniform path length and density are found for each important band by the use of equations (5-93a) and (5-93b). Based on these parameters, the values of \bar{A}_l can be obtained from one of the correlations of gas properties. The uniform gas analysis of section 5.7 can then be carried through to obtain intensities and heat flows.

5.8.2 The Zoning Method

The zoning method consists of subdividing nonisothermal enclosures filled with nonisothermal gas into areas and volumes that can be considered essentially isothermal. An energy balance is then written for each division of area and volume. This leads to a set of simultaneous equations for the unknown heat fluxes or temperatures in the same manner as the procedure discussed in section 5.3 for an isothermal gas. The method is not elegant in a formal mathematical sense but is practical and very powerful. Hottel and Sarofim (ref. 4) discuss the method at some length. Applications in multidimensional situations have been carried out by Hottel and Cohen (ref. 17) and Einstein (refs. 19 and 20). The discussion in this section is limited to cases when the energy exchange is only by radiation; extension to situations including conduction and convection is found in chapter 7 and reference 4.

The zoning method has an advantage over the Curtis-Godson method outlined in section 5.8.1 because unknown temperature distributions in the gas can be treated. The Curtis-Godson technique is most useful where the temperature distribution is known; if the distribution is not known, some method of iteration on the gas temperature must be developed.

The basic concepts of the zoning method will now be developed for a gas with a constant absorption coefficient. Consider a volume V_γ as in figure 5-18 and a surface A_k . From equation (1-33) the emissive power from a volume element dV_γ is $4\pi a_\lambda i'_{\lambda b} dV_\gamma d\lambda$ or per unit solid angle around dV_γ it is $a_\lambda i'_{\lambda b} dV_\gamma d\lambda$. The surface element dA_k subtends the solid angle $dA_k \cos \beta_k / S_{\gamma-k}^2$ when viewed from dV_γ . The fraction of radiation transmitted through the path length $S_{\gamma-k}$ is

$$\exp \left[- \int_{S_\gamma}^{S_k} a_\lambda(S^*) dS^* \right]$$

Multiplying these factors together and integrating over V_γ and A_k gives the spectral energy arriving at surface A_k from a gas volume V_γ as

$$dq_{\lambda i, \gamma-k} A_k = d\lambda \int_{V_\gamma} \int_{A_k} \frac{a_\lambda(\gamma) i'_{\lambda b}(\gamma) \cos \beta_k}{S_{\gamma-k}^2} \times \exp \left[- \int_{S_\gamma}^{S_k} a_\lambda(S^*) dS^* \right] dA_k dV_\gamma \quad (5-94)$$

If $a_\lambda(\gamma)$ is assumed uniform, then the exponential factor becomes

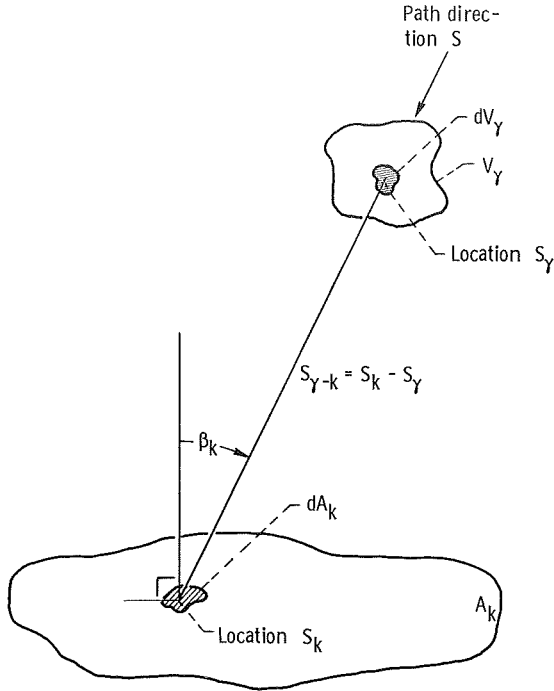


FIGURE 5-18. — Radiation from gas volume V_γ to area A_k .

$$\exp [-a_\lambda(S_k - S_\gamma)] = \tau_\lambda(S_{\gamma-k})$$

The entire gas volume has been divided into finite subvolumes V_γ and the assumption is made that conditions are uniform over each V_γ . Equation (5-94) then simplifies to

$$dq_{\lambda i, \gamma-k} A_k = d\lambda a_\lambda i'_{\lambda b}(\gamma) \int_{V_\gamma} \int_{A_k} \frac{\cos \beta_k}{S_{\gamma-k}^2} \tau_\lambda(S_{\gamma-k}) dA_k dV_\gamma \quad (5-95)$$

If the gas in addition is gray, then equation (5-95) can be integrated over all wavelengths to obtain the total incident energy on A_k as

$$q_{i, \gamma-k} A_k = a \frac{\sigma T_\gamma^4}{\pi} \int_{V_\gamma} \int_{A_k} \frac{\cos \beta_k}{S_{\gamma-k}^2} \tau(S_{\gamma-k}) dA_k dV_\gamma \quad (5-96)$$

Now define the *gas-surface direct exchange area* $\overline{g_\gamma s_k}$ as

$$\overline{g_\gamma s_k} \equiv \frac{a}{\pi} \int_{V_\gamma} \int_{A_k} \frac{\cos \beta_k}{S_{\gamma-k}^2} \tau(S_{\gamma-k}) dA_k dV_\gamma \quad (5-97)$$

Equation (5-96) then can be written as

$$q_{i, \gamma-k} A_k = \overline{g_{\gamma s_k}} \sigma T_{\gamma}^4 \tag{5-98}$$

Thus the energy arriving at A_k , $q_{i, \gamma-k} A_k$ is the blackbody emissive power of the gas in V_{γ} , σT_{γ}^4 radiated from an *effective* area $\overline{g_{\gamma s_k}}$.

Let the entire gas volume be divided into Γ finite regions. The energy flux incident upon surface element A_k from all Γ of the gas volume regions is then

$$(q_{i, k})_{from\ gas} = \frac{1}{A_k} \sum_{\gamma=1}^{\Gamma} \overline{g_{\gamma s_k}} \sigma T_{\gamma}^4 \tag{5-99}$$

Now consider the interchange between the bounding areas of the enclosure. The energy leaving surface area A_j and reaching A_k is, for a nonisothermal gas with uniform gray properties,

$$q_{i, j-k} A_k = \frac{q_{o, j}}{\pi} \int_{A_k} \int_{A_j} \tau(S_{j-k}) \frac{\cos \beta_j \cos \beta_k dA_j dA_k}{S_{j-k}^2} \tag{5-100}$$

where, as in the usual enclosure theory, $q_{o, j}$ is uniform over A_j . Now define the *surface-surface direct exchange area* as

$$\overline{s_j s_k} \equiv \int_{A_k} \int_{A_j} \tau(S_{j-k}) \frac{\cos \beta_j \cos \beta_k dA_j dA_k}{\pi S_{j-k}^2} \tag{5-101}$$

Equation (5-100) can then be written as

$$q_{i, j-k} A_k = \overline{s_j s_k} q_{o, j} \tag{5-102}$$

Thus the energy from A_j arriving at A_k , $q_{i, j-k} A_k$, is the energy flux leaving A_j times an *effective* area $\overline{s_j s_k}$. The energy flux incident upon area A_k as a result of the fluxes leaving all N surfaces of the enclosure is then

$$(q_{i, k})_{from\ surfaces} = \frac{1}{A_k} \sum_{j=1}^N \overline{s_j s_k} q_{o, j} \tag{5-103}$$

Now the total energy flux incident upon surface A_k can be obtained as

$$\begin{aligned} q_{i, k} &= (q_{i, k})_{from\ surfaces} + (q_{i, k})_{from\ gas} \\ &= \frac{1}{A_k} \left(\sum_{j=1}^N \overline{s_j s_k} q_{o, j} + \sum_{\gamma=1}^{\Gamma} \overline{g_{\gamma s_k}} \sigma T_{\gamma}^4 \right) \end{aligned} \tag{5-104}$$

The usual net radiation equations (eqs. (3-1) and (3-2) of vol. II) also

apply at surface A_k

$$q_k = q_{o, k} - q_{i, k} \quad (5-105)$$

$$q_{o, k} = \epsilon_k \sigma T_k^4 + (1 - \epsilon_k) q_{i, k} \quad (5-106)$$

For problems where T_γ is given for all gas volume elements V_γ , equations (5-104) to (5-106) are sufficient to solve for N unknown values of either T_k or q_k , or some combination of N values of T_k and q_k . The other N values of T_k and q_k must be provided as known boundary conditions. The methods of section 3.3 of volume II can be directly applied. Values of $\overline{s_j s_k}$ and $\overline{g_\gamma s_k}$ have been tabulated for cubical isothermal volumes and square isothermal boundary elements by Hottel and Cohen (ref. 17). Hottel and Sarofim (ref. 4) present a reference table to factors for eleven other geometries, and also an extensive tabulation of the factors for the cylindrical geometry.

When the T_γ of the Γ gas elements are unknowns, then Γ additional equations must be found. These are obtained by taking an energy balance on each gas zone. In radiative equilibrium, for each gas element V_γ the emission and absorption of energy are equal. Then for a gray gas with uniform properties a heat balance on the volume region V_γ gives

$$\begin{aligned} 4a\sigma T_\gamma^4 V_\gamma &= \sum_{\text{all } V_{\gamma^*}} \int_{V_\gamma} \int_{V_{\gamma^*}} \frac{4a\sigma T_{\gamma^*}^4 dV_{\gamma^*}}{4\pi} \tau(S_{\gamma^*-\gamma}) \frac{adV_\gamma}{S_{\gamma^*-\gamma}^2} \\ &\quad + \sum_{\text{all } A_k} \int_{V_\gamma} \int_{A_k} \frac{q_{o, k} \cos \beta_k}{\pi} dA_k \tau(S_{k-\gamma}) \frac{adV_\gamma}{S_{k-\gamma}^2} \\ &= a^2 \sum_{\gamma^*=1}^{\Gamma} \sigma T_{\gamma^*}^4 \int_{V_\gamma} \int_{V_{\gamma^*}} \frac{\tau(S_{\gamma^*-\gamma}) dV_{\gamma^*} dV_\gamma}{\pi S_{\gamma^*-\gamma}^2} \\ &\quad + a \sum_{k=1}^N q_{o, k} \int_{V_\gamma} \int_{A_k} \frac{\cos \beta_k}{\pi S_{k-\gamma}^2} \tau(S_{k-\gamma}) dA_k dV_\gamma \quad (5-107) \end{aligned}$$

It is assumed that a is uniform throughout the enclosure, and that V_γ and all the V_{γ^*} are each isothermal. As usual in the enclosure calculation methods, $q_{o, k}$ is taken as constant across A_k .

Define the *surface-gas direct exchange area* as

$$\overline{s_k g_\gamma} \equiv \frac{a}{\pi} \int_{V_\gamma} \int_{A_k} \frac{\cos \beta_k}{S_{k-\gamma}^2} \tau(S_{k-\gamma}) dA_k dV_\gamma \quad (5-108)$$

Comparing equation (5-108) with equation (5-97) shows that there is

reciprocity between the surface-gas and gas-surface direct exchange areas

$$\overline{s_k g_\gamma} = \overline{g_\gamma s_k} \quad (5-109)$$

Now define the *gas-gas direct exchange area* as

$$\overline{g_{\gamma*} g_\gamma} \equiv \frac{a^2}{\pi} \int_{V_\gamma} \int_{V_{\gamma*}} \frac{\tau(S_{\gamma*- \gamma}) dV_{\gamma*} dV_\gamma}{S_{\gamma*- \gamma}^2} \quad (5-110)$$

Substituting equations (5-108) to (5-110) into equation (5-107) gives

$$4a\sigma T_\gamma^4 V_\gamma = \sum_{\gamma*=1}^{\Gamma} \sigma T_{\gamma*}^4 \overline{g_{\gamma*} g_\gamma} + \sum_{k=1}^N q_{0,k} \overline{g_\gamma s_k} \quad (5-111)$$

The $\overline{g_{\gamma*} g_\gamma}$ have also been tabulated (ref. 17) so that equation (5-111) written for each V_γ provides the additional set of Γ equations required to obtain the gas temperature distribution.

The notation developed by Hottel and coworkers has been used in this section with only slight modification in developing the preceding equations. A comparison with the derivations of section 5.3 shows that, in terms of the notation used there (eq. (5-9)), the following identity exists:

$$F_{j-k} \bar{\tau}_{j-k} A_j = \overline{s_j s_k} \quad (5-112)$$

The gas-absorptance factor in equation (5-10), $F_{j-k} \bar{\alpha}_{j-k} A_j$ is generally not related in a useful way to $\overline{g_\gamma s_k}$. The latter quantity is derived for an element of gas volume, while $F_{j-k} \bar{\alpha}_{j-k} A_j$ is concerned with the entire gas volume.

Hottel and coworkers (refs. 3, 4, and 17) have developed the approach outlined in this section even further. Allowance for spectral variations in gas properties, done in an approximate but easily carried out manner, is possible. Variations in properties with position in the enclosure are handled by defining a suitable mean absorption coefficient between each set of zones. Einstein (refs. 19 and 20) modified the $\overline{g_s}$ and $\overline{g_g}$ factors to give better accuracy when strong gradients are present. All of these approximations become difficult to carry through if the absorption coefficient is a strong function of temperature.

5.8.3 The Exchange Factor Approximation

The specific situations discussed here are regions of *nonisothermal* gray gas between parallel plates, concentric cylinders, or concentric

spheres. These geometries have been considered in some detail in chapter 3. The purpose here is to reveal how the engineering concepts of exchange factors can be applied to extend the results for one of the previous solutions to more general cases. Specifically it will be shown how results for black bounding surfaces can be extended to the case where the surfaces are diffuse-gray. If the walls are diffuse-gray with hemispherical total emissivity $\epsilon(T)$, no great difficulty is involved in formulating the governing radiative integral equations as in chapter 3. The boundary condition for the solution of the equation of transfer is that the intensity leaving a diffuse wall is q_o/π where q_o is the outgoing radiation flux previously discussed in regard to enclosure theory. However, a better approach than solving the integral equations is that of Perlmutter and Howell (ref. 21) who have shown that, once the results are available for an analysis with black boundaries, the diffuse-gray wall results can be obtained from simple algebraic relations.

The theory follows the same general development as the net radiation method (section 3.3.1 of vol. II). A heat balance at surface A_k gives

$$Q_k = q_k A_k = (q_{o,k} - q_{i,k}) A_k \quad (5-113)$$

The energy flux leaving A_k is composed of emitted and reflected energy

$$q_{o,k} = \epsilon_k \sigma T_k^4 + (1 - \epsilon_k) q_{i,k} \quad (5-114)$$

If $q_{i,k}$ is eliminated from equations (5-113) and (5-114), the result is

$$Q_k = A_k \frac{\epsilon_k}{1 - \epsilon_k} (\sigma T_k^4 - q_{o,k}) \quad (5-115)$$

The $q_{i,k}$ in equation (5-114) can be found in terms of Hottel's exchange areas as in equation (5-104). However, here we choose to define a different quantity called the *exchange factor* \bar{F}_{j-k} . The exchange factor \bar{F}_{j-k} is defined as *the fraction of the energy leaving surface j that is incident on surface k when all boundaries are black and the intervening medium is in radiative equilibrium* (that is, the heat transfer in the gas is only by radiation without any heat sources or sinks). When the gas is transparent, \bar{F}_{j-k} becomes identical to the configuration factor F_{j-k} (section 2.4.3 of vol. II). Because the gas is in radiative equilibrium, energy conservation requires that energy leaving surface 1 must finally reach other enclosure surfaces or return to surface 1. Any energy absorbed in the gas must be reemitted by the gas to maintain equilibrium and the \bar{F}_{j-k} includes all interactions with the gas by means of which energy leaving A_j arrives at A_k .

For a general enclosure of N surfaces surrounding a gas in radiative equilibrium, the incident energy on surface k can be written in terms of exchange factors as

$$Q_{i,k} = \sum_{j=1}^N Q_{o,j} \bar{F}_{j-k} \tag{5-116}$$

Note that using exchange areas as in section 5.8.2 would require an additional term to account for energy emitted by the gas and reaching the wall. This term is included by definition within the \bar{F}_{j-k} .

If consideration is restricted to an enclosure having only two surfaces, equation (5-114) can be written by using equation (5-116) to eliminate $q_{i,k}$ as

$$\left. \begin{aligned} Q_{o,1} &= q_{o,1} A_1 = \epsilon_1 \sigma T_1^4 A_1 + (1 - \epsilon_1) (Q_{o,1} \bar{F}_{1-1} + Q_{o,2} \bar{F}_{2-1}) \\ Q_{o,2} &= q_{o,2} A_2 = \epsilon_2 \sigma T_2^4 A_2 + (1 - \epsilon_2) (Q_{o,1} \bar{F}_{1-2} + Q_{o,2} \bar{F}_{2-2}) \end{aligned} \right\} \tag{5-117}$$

Because the medium is in radiative equilibrium, all energy leaving a given surface must finally reach an enclosure surface. It follows that

$$\bar{F}_{1-1} + \bar{F}_{1-2} = 1 \tag{5-118a}$$

and

$$\bar{F}_{2-1} + \bar{F}_{2-2} = 1 \tag{5-118b}$$

Note that there is no energy being supplied to the gas by any external means such as combustion.

Because \bar{F}_{j-k} is defined as the fraction of energy leaving A_j that arrives at A_k for *black* boundaries enclosing a gas, it can be obtained from the black-walled solution, which it is assumed has already been found. Thus,

$$\bar{F}_{j-k} = \left(\frac{Q_{i,k}}{A_j \sigma T_j^4} \right)_{\text{black surfaces}} = \left(\frac{A_k \sigma T_k^4 - Q_k}{A_j \sigma T_j^4} \right)_{\text{black surfaces}} \equiv \psi_{j-k,b} \tag{5-119}$$

where the notation $\psi_{j-k,b}$ is used to emphasize that this is a quantity obtained from the black solution. For a transparent gas \bar{F}_{j-k} becomes equivalent to the usual geometric configuration factor F_{j-k} for interchange between two diffuse surfaces. The \bar{F} factors are found from equation (5-119) and by using the relations in equation (5-118). Then equations (5-117) are solved simultaneously for the Q_o 's and these are used in equation (5-115) to find Q_k . Thus the solution for gray walls can be found quite simply from the solution with black walls. The procedure will now be outlined for the infinite parallel plate case.

In the infinite parallel plate case and because the gas absorption

coefficient has been assumed constant, the fraction of energy leaving surface 1 that reaches surface 2 or \bar{F}_{1-2} must be equal to the fraction going from surface 2 to surface 1 or \bar{F}_{2-1} . This arises from the symmetry in radiation paths experienced by energy leaving either surface. In radiative equilibrium with no heat sources in the gas, the radiation absorbed at a position must be reemitted at that position. The radiation leaving either plate will undergo the same absorption-emission history while traveling to the other plate.

If \bar{F}_{1-2} is found from the black solution as

$$\bar{F}_{1-2} = \left(\frac{\sigma T_2^4 - q_2}{\sigma T_1^4} \right)_{\text{black surfaces}} = \psi_{1-2, b}$$

then $\bar{F}_{2-1} = \bar{F}_{1-2}$ and for simplicity call them ψ_b . From equation (5-118) $\bar{F}_{1-1} = \bar{F}_{2-2} = 1 - \psi_b$. Equations (5-117) then become

$$q_{o,1} = \epsilon_1 \sigma T_1^4 + (1 - \epsilon_1)(q_{o,1} - q_{o,1} \psi_b + q_{o,2} \psi_b)$$

$$q_{o,2} = \epsilon_2 \sigma T_2^4 + (1 - \epsilon_2)(q_{o,1} \psi_b + q_{o,2} - q_{o,2} \psi_b)$$

Solving simultaneously for $q_{o,1}$ and $q_{o,2}$ yields the symmetric relations,

$$q_{o,1} = \frac{\epsilon_1 \epsilon_2 \sigma T_1^4 + \epsilon_1 (1 - \epsilon_2) \psi_b \sigma T_1^4 + \epsilon_2 (1 - \epsilon_1) \psi_b \sigma T_2^4}{\psi_b (\epsilon_1 + \epsilon_2 - 2\epsilon_1 \epsilon_2) + \epsilon_1 \epsilon_2} \quad (5-120a)$$

$$q_{o,2} = \frac{\epsilon_1 \epsilon_2 \sigma T_2^4 + \epsilon_2 (1 - \epsilon_1) \psi_b \sigma T_2^4 + \epsilon_1 (1 - \epsilon_2) \psi_b \sigma T_1^4}{\psi_b (\epsilon_1 + \epsilon_2 - 2\epsilon_1 \epsilon_2) + \epsilon_1 \epsilon_2} \quad (5-120b)$$

The $q_{o,1}$ is substituted into equation (5-115) to yield after rearrangement

$$\frac{q_1}{\epsilon_1 \sigma (T_1^4 - T_2^4)} = \frac{\frac{1}{\epsilon_1} \psi_b}{\psi_b \left(\frac{1}{\epsilon_1} + \frac{1}{\epsilon_2} - 2 \right) + 1} \quad (5-121a)$$

Equation (5-121a) can be written in the alternate form

$$\frac{q_1}{\epsilon_1 \sigma (T_1^4 - T_2^4)} = \frac{(1 + E_1) \psi_b}{(E_2 + E_1) \psi_b + 1} \quad (5-121b)$$

where

$$E_1 = \frac{1 - \epsilon_1}{\epsilon_1}$$

$$E_2 = \frac{1 - \epsilon_2}{\epsilon_2}$$

Evaluating equation (5-121b) for the black case, $E_1 = E_2 = 0$ shows that

$$\psi_b = \frac{q_{1b}}{\sigma(T_1^4 - T_2^4)} \tag{5-121c}$$

Equation (5-121b) gives the energy supplied to surface 1 and removed from surface 2. If the gas absorption coefficient is independent of temperature, then energy leaving a boundary and reaching a given point in the gas will be attenuated by the same amount *regardless* of the gas temperature distribution. Further, any portion of the energy absorbed along the path is balanced by isotropic emission at each point. Using these facts, a synthesis of black-wall enclosure solutions and surface-gas element exchange factors can be used to find the temperature distribution in the gas for gray walls.

The energy emitted by a local volume element of gas of area A and thickness dx between the parallel plates (fig. 5-19) is given by

$$Q_e = 4a\sigma T^4(x)A dx$$

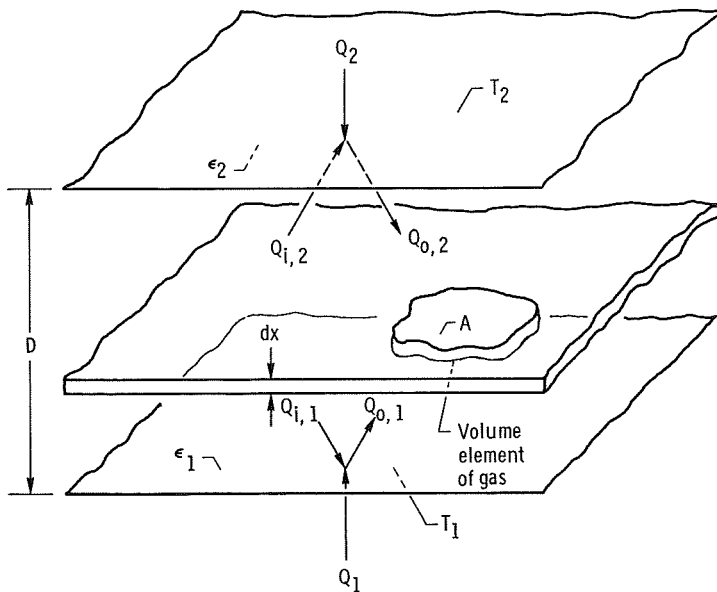


FIGURE 5-19.—Energy quantities for gas between infinite parallel gray plates.

For radiative equilibrium, this must equal the heat absorbed by the volume element which can be written as

$$4a\sigma T^4(x)A dx = Q_{o,1}d\bar{F}_{1-dx} + Q_{o,2}d\bar{F}_{2-dx} \quad (5-122)$$

or

$$\varphi = \frac{T^4(x) - T_2^4}{T_1^4 - T_2^4} = \frac{1}{4a\sigma(T_1^4 - T_2^4)} \left(\frac{q_{o,1}d\bar{F}_{1-dx}}{dx} + \frac{q_{o,2}d\bar{F}_{2-dx}}{dx} \right) - \frac{T_2^4}{T_1^4 - T_2^4} \quad (5-123)$$

Here $d\bar{F}_{j-dx}$ is the fraction of energy leaving boundary surface A_j that is *absorbed* in volume element $A dx$ when the boundaries are black. Again, the \bar{F} factors include the energy absorption and reemission from the gas as the energy travels from the surface to the volume element. Because radiative equilibrium is the condition being studied here, no energy is lost during these processes since all absorbed energy at a location must be re-emitted.

When the entire system is isothermal, equation (5-122) reduces to

$$4a dx = d\bar{F}_{1-dx} + d\bar{F}_{2-dx} \quad (5-124)$$

This relation is used to eliminate $d\bar{F}_{2-dx}$ from equation (5-123) written for the black surfaces. The resulting equation is solved for $d\bar{F}_{1-dx}$ giving

$$d\bar{F}_{1-dx} = 4a dx \varphi_b \quad (5-125)$$

where from equation (5-123)

$$\varphi_b = \frac{T_1^4 d\bar{F}_{1-dx} + T_2^4 d\bar{F}_{2-dx}}{4a dx (T_1^4 - T_2^4)} - \frac{T_2^4}{T_1^4 - T_2^4}$$

Then by substituting equation (5-125) into equation (5-124)

$$d\bar{F}_{2-dx} = 4a dx (1 - \varphi_b) \quad (5-126)$$

Substituting equations (5-125), (5-126), (5-120a), and (5-120b) to eliminate $d\bar{F}_{1-dx}$, $d\bar{F}_{2-dx}$, $q_{o,1}$, and $q_{o,2}$ from equation (5-123) results, after much manipulation, in the following gas temperature distribution:

$$\varphi = \frac{T^4(x) - T_2^4}{T_1^4 - T_2^4} = \frac{\varphi_b + E_2 \psi_b}{1 + \psi_b (E_1 + E_2)} \quad (5-127)$$

Equations (5-121) and (5-127) relate the energy transfer and fourth-power temperature distribution for the case of a gray gas between gray walls to the case of a gray gas between black walls for the geometry of infinite parallel plates. Similar relations for the geometry of infinitely long concentric cylinders are given in references 21 and 22, and these plus the relations for concentric spheres (refs. 23 to 25) are given in table 5-V.

EXAMPLE 5-5: A gray gas of absorption coefficient 0.5 cm^{-1} is contained between gray parallel plates spaced 2 cm apart. Plate 1 has temperature $T_1 = 1000 \text{ K}$, while plate 2 is at $T_2 = 840 \text{ K}$. The plates have emissivities of $\epsilon_1 = 0.1$ and $\epsilon_2 = 0.2$, respectively. What is the energy transfer between the plates and the temperature of the gas at a point 0.5 cm from surface 1?

If the walls were black, figure 2-6(b) gives, for $aD = 0.5 \times 2 = 1.0$,

$$\frac{q_1}{\sigma(T_1^4 - T_2^4)} = 0.56$$

so that from equation (5-121c)

$$\psi_b = 0.56$$

From table 5-V,

$$\psi = \frac{q_1}{\epsilon_1 \sigma (T_1^4 - T_2^4)} = \frac{(1 + E_1) \psi_b}{(E_2 + E_1) \psi_b + 1}$$

and, for this example,

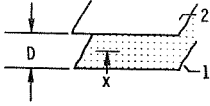
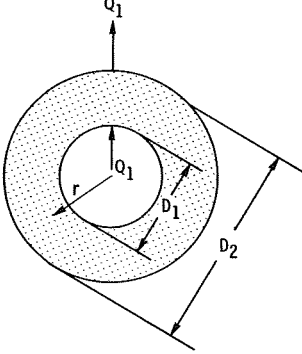
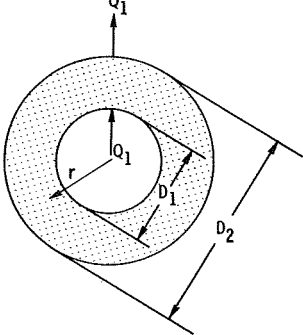
$$E_1 = \frac{1 - 0.1}{0.1} = 9$$

$$E_2 = \frac{1 - 0.2}{0.2} = 4$$

so that

$$\begin{aligned} q_1 &= \epsilon_1 \sigma (T_1^4 - T_2^4) \frac{(1 + 9) \times 0.56}{13 \times 0.56 + 1} \\ &= 0.1 \times 5.73 \times 10^{-12} (1 - 0.5) \times 10^{12} \times \frac{5.6}{8.28} = 0.194 \text{ W/cm}^2 \end{aligned}$$

TABLE 5-V.—RELATIONS BETWEEN GRAY AND BLACK-WALL SOLUTIONS FOR RADIATION BETWEEN SURFACES ENCLOSING A GRAY GAS IN RADIATIVE EQUILIBRIUM

Geometry	Relations ^a
<p data-bbox="314 282 479 305">Infinite parallel plates</p>  <p data-bbox="236 440 572 488">$(\psi_b$ and φ_b are given in ref. 3 of chapter 2 and figs. 2-6(a) and (b))</p>	$\psi = \frac{(1 + E_1)\psi_b}{(E_2 + E_1)\psi_b + 1}$ $\varphi(x) = \frac{\varphi_b(x) + E_2\psi_b}{(E_2 + E_1)\psi_b + 1}$
<p data-bbox="255 533 519 556">Infinitely long concentric cylinders</p>  <p data-bbox="250 938 561 967">$(\psi_b$ and φ_b are given in refs. 21 and 22)</p>	$\psi = \frac{(1 + E_1)\psi_b}{\left(\frac{D_1}{D_2} E_2 + E_1\right)\psi_b + 1}$ $\varphi(r) = \frac{\varphi_b(r) + E_2 \frac{D_1}{D_2} \psi_b}{\left(\frac{D_1}{D_2} E_2 + E_1\right)\psi_b + 1}$
<p data-bbox="329 1023 479 1047">Concentric spheres</p>  <p data-bbox="246 1429 549 1458">$(\psi_b$ and φ_b are given in refs. 23 to 25)</p>	$\psi = \frac{(1 + E_1)\psi_b}{\left[\left(\frac{D_1}{D_2}\right)^2 E_2 + E_1\right]\psi_b + 1}$ $\varphi(r) = \frac{\varphi_b(r) + E_2 \left(\frac{D_1}{D_2}\right)^2 \psi_b}{\left[\left(\frac{D_1}{D_2}\right)^2 E_2 + E_1\right]\psi_b + 1}$

^aDefinitions: $E_N = (1 - \epsilon_{wN})/\epsilon_{wN}$, $\psi = Q_1/[\epsilon_{w1} A_1 \sigma (T_{w1}^4 - T_{w2}^4)]$, $\psi_b = Q_{1b}/[A_1 \sigma (T_{w1}^4 - T_{w2}^4)]$,
 $\varphi(\xi) = [T^4(\xi) - T_{w2}^4]/(T_{w1}^4 - T_{w2}^4)$.

The temperature at the point $x=0.5$ cm can be calculated from the result in table V-5

$$\varphi(x) = \frac{T^4(x) - T_2^4}{T_1^4 - T_2^4} = \frac{\varphi_b(x) + E_2\psi_b}{(E_2 + E_1)\psi_b + 1}$$

From figure 2-6(a), at the abscissa $\kappa/\kappa_D = ax/aD = 0.25$ and on the curve for $\kappa_D = aD = 1$

$$\varphi_b = 0.62$$

so that

$$\varphi|_{x=0.5} = \frac{0.62 + 4 \times 0.56}{13 \times 0.56 + 1} = 0.345$$

Then

$$T^4(0.5) = T_2^4 + 0.345(T_1^4 - T_2^4) = [0.5 + 0.345(1 - 0.5)] \times 10^{12} = 0.673 \times 10^{12}$$

which gives

$$T(0.5) = 905 \text{ K}$$

Note that for gray walls a curve of φ against ax/aD will only have an antisymmetrical shape about $ax/aD = 0.5$ as in figure 2-6(a) when $\epsilon_1 = \epsilon_2$.

REFERENCES

1. SIEGEL, ROBERT; AND HOWELL, JOHN R.: Thermal Radiation Heat Transfer. I—The Blackbody, Electromagnetic Theory, and Material Properties. NASA SP-164, Vol. I, 1968.
2. HOWELL, JOHN R.; AND SIEGEL, ROBERT: Thermal Radiation Heat Transfer. II—Radiation Exchange Between Surfaces and in Enclosures. NASA SP-164, Vol. II, 1969.
3. HOTTEL, H. C.: Radiant-Heat Transmission. Heat Transmission. Third ed., William H. McAdams, McGraw-Hill Book Co., Inc., 1954, ch. 4.
4. HOTTEL, HOYT C.; AND SAROFIM, ADEL F.: Radiative Transfer. McGraw-Hill Book Co., Inc., 1967.
5. ECKERT, E. R. G.; AND DRAKE, ROBERT M., JR.: Heat and Mass Transfer. Second ed., McGraw-Hill Book Co., Inc., 1959.
6. DUNKLE, R. V.: Geometric Mean Beam Lengths for Radiant Heat-Transfer Calculations. J. Heat Transfer, vol. 86, no. 1, Feb. 1964, pp. 75-80.
7. EDWARDS, D. K.; AND NELSON, K. E.: Rapid Calculation of Radiant Energy Transfer between Nongray Walls and Isothermal H₂O and CO₂ Gas. J. Heat Transfer, vol. 84, no. 4, Nov. 1962, pp. 273-278.

8. EDWARDS, D. K.: Radiation Interchange in a Nongray Enclosure Containing an Isothermal Carbon-Dioxide-Nitrogen Gas Mixture. *J. Heat Transfer*, vol. 84, no. 1, Feb. 1962, pp. 1-11.
9. OPPENHEIM, A. K.: Radiation Analysis by the Network Method. *Trans. ASME*, vol. 78, no. 4, May 1956, pp. 725-735.
10. EDWARDS, D. K.; AND WEINER, M. M.: Comment on Radiative Transfer in Non-isothermal Gases. *Combustion and Flame*, vol. 10, no. 2, June 1966, pp. 202-203.
11. EDWARDS, D. K.; GLASSEN, L. K.; HAUSER, W. C.; AND TUCHSCHER, J. S.: Radiation Heat Transfer in Non-isothermal Nongray Gases. *J. Heat Transfer*, vol. 89, no. 3, Aug. 1967, pp. 219-229.
12. WEINER, M. M.; AND EDWARDS, D. K.: Non-isothermal Gas Radiation in Superposed Vibration-Rotation Bands. *J. Quant. Spectrosc. and Radiat. Transfer*, vol. 8, no. 5, May 1968, pp. 1171-1183.
13. KRAKOW, BURTON; BABROV, HAROLD J.; MACLAY, G. JORDAN; AND SHABOTT, ABRAHAM L.: Use of the Curtis-Godson Approximation in Calculations of Radiant Heating by Inhomogeneous Hot Gases. *Appl. Opt.*, vol. 5, no. 11, Nov. 1966, pp. 1791-1800.
14. SIMMONS, F. S.: Band Models for Non-isothermal Radiating Gases. *Appl. Opt.*, vol. 5, no. 11, Nov. 1966, pp. 1801-1811.
15. GOODY, R. M.: Atmospheric Radiation. Vol. I-Theoretical Basis. Clarendon Press, Oxford, 1964.
16. SIMMONS, F. S.: Application of Band Models to Inhomogeneous Gases. Molecular Radiation and its Application to Diagnostic Techniques. R. Goulard, ed., NASA TM X-53711, 1968, pp. 113-133.
17. HOTTEL, H. C.; AND COHEN, E. S.: Radiant Heat Exchange in a Gas-filled Enclosure: Allowance for Nonuniformity of Gas Temperature. *AIChE J.*, vol. 4, no. 1, Mar. 1958, pp. 3-14.
18. PLASS, GILBERT N.: Radiation from Nonisothermal Gases. *Appl. Opt.*, vol. 6, no. 11, Nov. 1967, pp. 1995-1999.
19. EINSTEIN, THOMAS H.: Radiant Heat Transfer to Absorbing Gases Enclosed between Parallel Flat Plates with Flow and Conduction. NASA TR R-154, 1963.
20. EINSTEIN, THOMAS H.: Radiant Heat Transfer to Absorbing Gases Enclosed in a Circular Pipe with Conduction, Gas Flow, and Internal Heat Generation. NASA TR R-156, 1963.
21. PERLMUTTER, M.; AND HOWELL, J. R.: Radiant Transfer Through a Gray Gas Between Concentric Cylinders Using Monte Carlo. *J. Heat Transfer*, vol. 86, no. 2, May 1964, pp. 169-179.
22. GREIF, RALPH; AND CLAPPER, GEAN P.: Radiant Heat Transfer Between Concentric Cylinders. *Appl. Sci. Res., Sec. A*, vol. 15, 1966, pp. 469-474.
23. RHYMING, R. L.: Radiative Transfer Between Two Concentric Spheres Separated by an Absorbing and Emitting Gas. *Int. J. Heat Mass Transfer*, vol. 9, no. 4, Apr. 1966, pp. 315-324.
24. SPARROW, E. M.; USISKIN, C. M.; AND HUBBARD, H. A.: Radiation Heat Transfer in a Spherical Enclosure Containing a Participating, Heat-Generating Gas. *J. Heat Transfer*, vol. 83, no. 2, May 1961, pp. 199-206.
25. VISKANTA, R.; AND MERRIAM, R. L.: Heat Transfer by Combined Conduction and Radiation between Concentric Spheres Separated by Radiating Medium. *J. Heat Transfer*, vol. 90, no. 2, May 1968, pp. 248-256.

Chapter 6. The Monte Carlo Technique

6.1 INTRODUCTION

The Monte Carlo technique is a method of statistical sampling of events to determine the average behavior of a system. In chapter 6 of volume II, the method was applied to radiative transfer between surfaces without an intervening medium. The information given in that chapter is a necessary prerequisite to that presented here. Based on the model of radiative transfer in volume II, extensions are made in this chapter to the cases of absorbing-emitting media. The model consists of following a finite number of energy bundles through their transport histories. The radiative behavior of the system is then determined from the average behavior of a number of these bundles.

Monte Carlo has more obvious utility in solving problems of radiative transfer through absorbing-emitting media than for surface radiation interchange problems. This is because a complete definition of the local radiation balance in a gas or other absorbing-emitting media requires an integration of the incoming radiation, not only from the surrounding surfaces, but from all volume elements of the surrounding medium. Such problems are difficult to solve analytically. As described in other chapters of this volume, much effort has been expended in attempting to develop standard analytical solution methods. This is often done by making as many assumptions, reasonable if possible, as are necessary to obtain an answer and philosophically accepting the resulting loss of accuracy, if not validity. Surfaces that are black, gray, diffuse, or specular, and gases that are optically dense, almost transparent, gray, or isothermal are typical assumptions that fall into this category. Few problems in radiative transfer are solved analytically without explicitly or implicitly making one or more of these assumptions, which may or may not apply to the problem under consideration.

By extending the Monte Carlo model of radiative energy exchange outlined for surface interaction problems in chapter 6 of volume II, it is possible to account for a large variety of effects in gas radiation problems. This can be done without resorting to the simplifying assumptions that are often necessary in the analytical approaches as typified by references 1 to 4.

6.2 SYMBOLS

a absorption coefficient

D	separation distance between parallel plates
e	emissive power
$F_{0-\lambda}$	fraction of total blackbody emission in spectral region $0-\lambda$
j	volume increment index
k	number of volume increments
L	dimensionless path length, l/D
l	path length to absorption
N	total number of Monte Carlo bundles per unit time
n	bundle index
P	probability density function
p	increment index
Q	energy per unit time
Q''	internal energy source rate per unit volume
q	energy flux; energy per unit area per unit time
R	randomly chosen number in range 0 to 1
r	radial coordinate
S	coordinate along path of radiation (will not have a subscript)
S	number of events at some position per unit time (will always have a subscript to avoid confusion with path length coordinate)
T	absolute temperature
V	volume
w	energy carried by sample Monte Carlo bundle
X	dimensionless distance, x/D
x	distance normal to surface
β	cone angle (measured from normal of area)
ϵ	emissivity
Θ	dimensionless temperature, T_j/T_1
θ	circumferential angle
κ_D	optical thickness, aD
λ	wavelength
σ	Stefan-Boltzmann constant

Subscripts:

b	blackbody
e	emitted
i	inner
j	volume increment j
l	path length
max	maximum
min	minimum
o	original, or outer
P	Planck mean value

- dV elemental volume dV
- w wall
- 1, 2 surface 1 or 2
- β for cone angle
- θ for circumferential angle
- λ spectrally dependent

Superscript:

- * dummy variable of integration

6.3 DISCUSSION OF THE METHOD

The additional factor introduced to the model previously discussed in volume II is the path length traveled by an individual energy bundle before it is absorbed or leaves the system. The required relations are given in table 6-I as related to a random number (see also example 6-1). It is possible to allow for variations in gas properties along the bundle path; indeed, it is in principle possible to account for variations in the refractive index of the medium by causing the bundles to travel curved paths.

TABLE 6-I.—USEFUL RELATIONS FOR MONTE CARLO SOLUTION OF GAS RADIATION PROBLEMS

Phenomenon	Variable	Relation
Emission from a volume element with absorption coefficient a_λ	Cone angle β	$\cos \beta = 1 - 2R_\beta$
	Circumferential angle θ	$\theta = 2\pi R_\theta$
	Wavelength λ Gray gas: Nongray gas:	$F_{0-\lambda} = R_\lambda$ $\frac{\int_0^\lambda a_\lambda i'_{\lambda b} d\lambda}{\int_0^\infty a_\lambda i'_{\lambda b} d\lambda} = R_\lambda$
Absorption by gas with absorption coefficient a_λ	Path length l Uniform gas properties: Nonuniform gas properties:	$l = -\frac{1}{a_\lambda} \ln R_l$ $-\int_0^l a_\lambda(S) dS = \ln R_l$

If a problem is solved in which radiative equilibrium can be assumed, then whenever a bundle is absorbed in the medium, a new bundle must be emitted from the same point in the medium to ensure no accumulation of energy. The functions required for determination of the angles and wavelengths of emission are shown in table 6-1. The new emitted bundle in the medium may be considered as merely the continuation of the history of the absorbed bundle, and the history is continued until the energy reaches a bounding surface.

Under conditions of radiative equilibrium, the total energy Q_e emitted by a volume element dV , is given by equation (1-34), integrated over all λ and not including induced emission

$$dQ_e = 4dV \int_0^\infty a_\lambda e_{\lambda b} d\lambda \quad (6-1)$$

For equilibrium the energy contained in the bundles emitted by the volume must be equal to the energy contained in the bundles absorbed, or

$$dQ_e = wS_{dV} \quad (6-2)$$

where w is the energy per bundle and S_{dV} is the number of bundles absorbed per unit time in dV . Then, if we note from equation (2-19) that

$$a_p \equiv \frac{\int_0^\infty a_\lambda e_{\lambda b} d\lambda}{\sigma T_{dV}^4} \quad (6-3)$$

where a_p is the Planck mean absorption coefficient, equation (6-3) can be substituted into equation (6-1) to eliminate the integral. Then equating equations (6-1) and (6-2) gives

$$T_{dV} = \left(\frac{wS_{dV}}{4a_p\sigma dV} \right)^{1/4} \quad (6-4)$$

This allows determination of the local temperature in the gas from the gas properties and the Monte Carlo quantities found in the solution. If a_p depends on local temperature T_{dV} , an iteration is required. A temperature distribution is assumed for a first iteration to obtain the bundle histories. These Monte Carlo quantities are used in equation (6-4) to obtain a new temperature distribution which is then used for the second iteration. The process is repeated until the temperatures converge.

There are so many variations possible on the Monte Carlo model,

many of which might lead to increased efficiency, that they cannot all be mentioned here. One of the most frequently suggested is the fractional absorption of energy when a bundle reaches a surface of known absorptivity. Using such a scheme, the bundle energy is reduced after each reflection. The bundle history is then followed until a sufficient number of reflections have occurred to reduce the bundle energy below some predetermined level. This level is chosen so that the effect of the bundle in succeeding reflections would be negligible. The history is then terminated. Such a procedure leads to better accuracy for many problems because a bundle history extends on the average through many more events, and a given number of bundles provides a larger number of events for compiling averages. Haji-Shiekh and Sparrow (ref. 5) have suggested some other shortcuts for reducing the programming difficulties of problems involving spectral and directional properties. The obvious rule of thumb is to use whatever shortcuts can be applied to the case in question and not be bound by cookbook rules.

EXAMPLE 6-1: A gray gas with constant absorption coefficient a is contained between infinite parallel black plates. Plate 1 is at temperature T_1 , and plate 2 is at temperature $T_2=0$. The plates are separated by a distance D . Construct a Monte Carlo flow chart for determining the energy transfer and the gas temperature distribution.

The emission per unit time and area from surface 1 is

$$q_{e,1} = \sigma T_1^4$$

If N energy bundles are to be emitted per unit time, then each one must carry an amount of energy w given by

$$w = \frac{q_{e,1}}{N} = \frac{\sigma T_1^4}{N}$$

The bundles are emitted at cone angles β given by the first line of table 6-I of volume II as

$$\sin \beta = \sqrt{R_\beta}$$

where R_β is a random number in the range 0 to 1. A typical bundle will travel a path length l after emission. The probability of traveling a given distance S before absorption in a medium of constant absorption coefficient a is

$$P(S) = \frac{e^{-aS}}{\int_0^{\infty} e^{-aS} dS} = ae^{-aS}$$

because of Bouguer's law, equation (1-12). Using equation (6-4) of chapter 6 in volume II, this is put in the form of a cumulative distribution to obtain

$$R_l = \frac{\int_0^l e^{-aS} dS}{\int_0^{\infty} e^{-aS} dS} = 1 - e^{-al}$$

or

$$l = -\frac{1}{a} \ln (1 - R_l)$$

However, because R_l is uniformly distributed between 0 and 1, this relation may as well be written as

$$l = -\frac{1}{a} \ln R_l$$

or

$$L = -\frac{1}{\kappa_D} \ln R_l$$

where $L = l/D$ and $\kappa_D = aD$.

The dimensionless distance normal to the plate $X = x/D$ that a bundle will travel when moving through a path length L is then

$$X = L \cos \beta = \frac{-\cos \beta}{\kappa_D} \ln R_l$$

Divide the distance D between the plates into k equal increments of dimensionless width $\Delta X = \Delta x/D$, and number the increments with an increment number j , where

$$j = 1, 2, 3, \dots, k$$

Then the increment number at which absorption occurs is

$$j = \text{TRUNC} \left(\frac{X}{\Delta X} \right) + 1$$

where TRUNC denotes the operation of truncating the value of $X/\Delta X$ to its integer. At each absorption, a tally is kept of the increment in which absorption occurs by increasing a counter S_j in the memory of the computer by one unit. This operation is denoted by

$$S_j = S_j + 1$$

If the bundle is absorbed in a gas element, it is immediately emitted from the same element to conserve energy in this steady-state problem. This is done by choosing an angle of emission β from the probability distribution for emission into all cone angles of a unit sphere surrounding dV

$$P(\beta) = \frac{\sin \beta \, d\beta}{\int_0^\pi \sin \beta \, d\beta}$$

Using the cumulative distribution function

$$R_\beta = \int_0^\beta P(\beta^*) \, d\beta^* = \frac{1 - \cos \beta}{2}$$

gives the emission angle in terms of a random number as

$$\beta = \cos^{-1}(1 - 2R_\beta)$$

The distance from the wall to the next absorption point is then given by

$$X = X_0 - \frac{\cos \beta}{\kappa_D} \ln R_t$$

where X_0 is the position of the previous absorption.

The process of absorptions and emissions is continued until the energy bundle reaches a black boundary. This occurs when $X \geq 1$ or $X \leq 0$, and a counter S_{w1} or S_{w2} is then increased by one unit to record the absorption at the black surface.

A new bundle is emitted, and the process is repeated until all N bundles have been emitted. The dimensionless net energy flux leaving surface 1 is then found from the total bundles emitted minus those reabsorbed

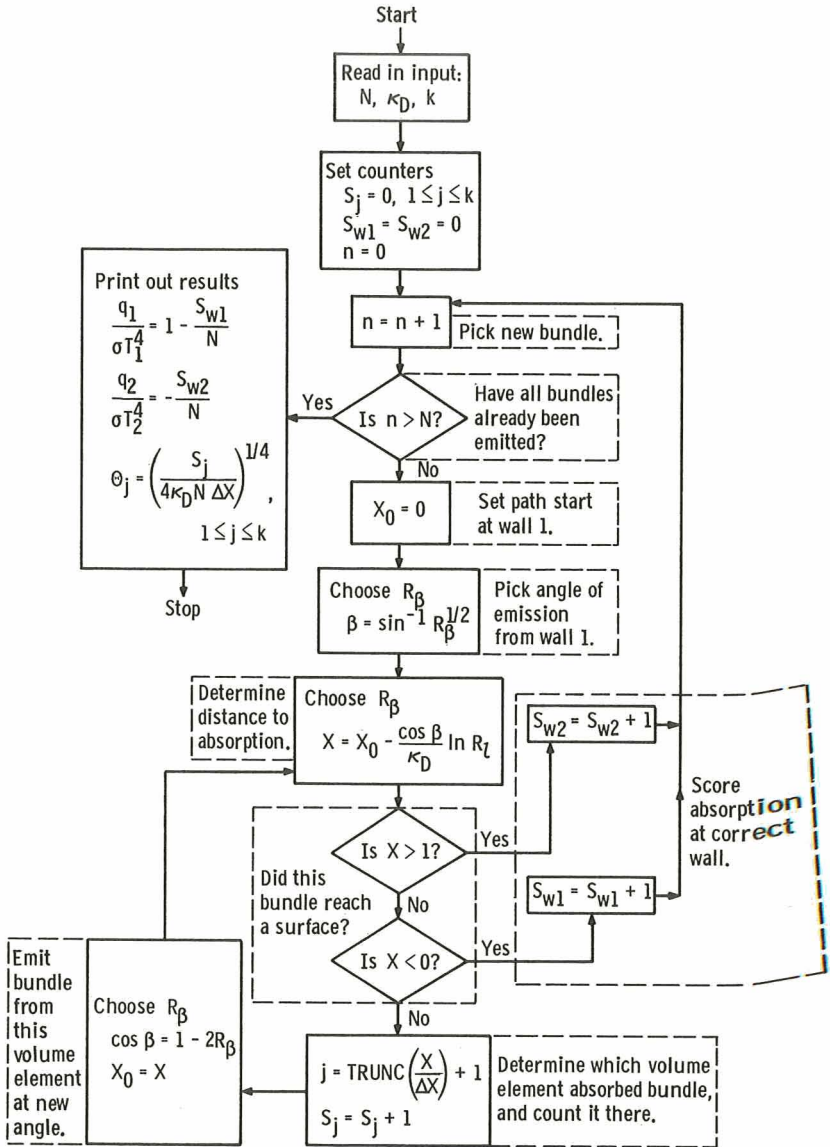


FIGURE 6-1.—Flow chart for Monte Carlo solution of radiant transfer between infinite parallel black plates.

at surface 1; that is,

$$\frac{q_1}{\sigma T_1^4} = \frac{q_{e,1} - wS_{w1}}{\sigma T_1^4} = \frac{w(N - S_{w1})}{\sigma T_1^4} = 1 - \frac{S_{w1}}{N}$$

The net energy flux *arriving* at surface 2 ($-q_2$) is given by

$$-\frac{q_2}{\sigma T_1^4} = \frac{wS_{w2}}{\sigma T_1^4} = \frac{S_{w2}}{N}$$

The temperature at each gas increment is found from equation (6-4) as

$$\Theta_j = \frac{T_j}{T_1} = \left(\frac{wS_j}{4\kappa_D \sigma \Delta X T_1^4} \right)^{1/4} = \left(\frac{S_j}{4\kappa_D N \Delta X} \right)^{1/4}$$

and the formulation is complete.

A flow chart is shown in figure 6-1. Note that, since $S_{w1} + S_{w2} = N$,

$$\frac{q_1}{\sigma T_1^4} = 1 - \frac{S_{w1}}{N} = -\frac{q_2}{\sigma T_1^4}$$

and, as expected, $q_1 = -q_2$; the only reason for printing out both quantities is to check on the results.

By noting the linearity with T^4 of this problem, it is possible to gain solutions for any combination of surface temperatures by use of this flow chart (ref. 6). Also, by use of the exchange factor relations of section 5.8.3, solutions can be obtained for any combination of gray surface emissivities.

Some results obtained by the Monte Carlo method will now be examined.

6.4 RADIATION THROUGH GRAY GASES

6.4.1 Infinite Parallel Planes

Because of the wealth of solutions available in the literature for a gray gas between infinite parallel plates, almost every new method of solution is tried in this configuration and then compared with the results of one or more of the analytical approaches typified by references 1 and 4.

The Monte Carlo method is no exception, and in reference 6 the

local gas emissive power and the net energy transfer between diffuse-gray plates is calculated in a manner quite similar to example 6-1. Parameters are the plate emissivity ϵ (taken equal for both plates) and various values of the gas layer optical thickness $\kappa_D = aD$ where a is constant. Two cases are examined, the first being a gas with no internal energy generation contained between plates at different temperatures. The second case is a gas with uniformly distributed energy sources between plates at equal temperatures. Figure 6-2 indicates the accuracy that can be obtained by Monte Carlo solutions in such idealized situations. The calculated energy transfer values have a 99.99 percent probability of lying within ± 5 percent of the midpoints shown.

In figure 6-3, the emissive power distribution within the gas is shown. Comparison with the exact solutions of references 1 and 4 is quite good; however, some trends common to all straightforward Monte Carlo solutions in gas radiation problems are as follows:

First, the calculated individual points in figure 6-3 reveal increasing error with decreasing optical thickness. This reflects the smaller fraction of energy bundles being absorbed in a given volume element as the optical thickness of the gas decreases. As the number of absorbed bundles decreases, the expected accuracy of the local emissive power becomes less, and more error naturally appears in the results. Conversely, as the optical thickness increases, error becomes less; and in figure 6-3, the curve of results for an optical thickness of ten is quite smooth.

A second effect mentioned in reference 6 is not evident from figure 6-3, and that is that the computing machine time required for solution of problems involving large optical thickness, say larger than ten, becomes quite large. This is simply because the free path of an energy bundle

$$L = -\frac{1}{\kappa_D} \ln R_l$$

becomes very short for large optical thickness; therefore, many absorptions occur during a typical bundle history.

Two limits are now obvious. For small optical thickness, accuracy becomes poor; for large optical thickness, computer running time becomes excessive. From a practical viewpoint, these are not serious limitations, as the transparent and diffusion approximations to the exact analytical formulation become valid in just those regions where the straightforward Monte Carlo approach begins to fail. In addition, the range of optical thickness over which a Monte Carlo solution can be effectively utilized can be extended by a variety of techniques, including those with the graphic names of "splitting," "Russian roulette,"

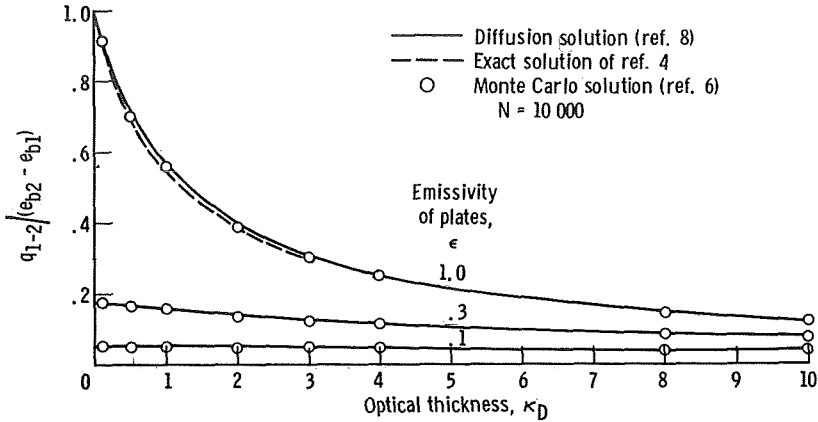


FIGURE 6-2. — Heat transfer between infinite parallel gray plates separated by gray gas.

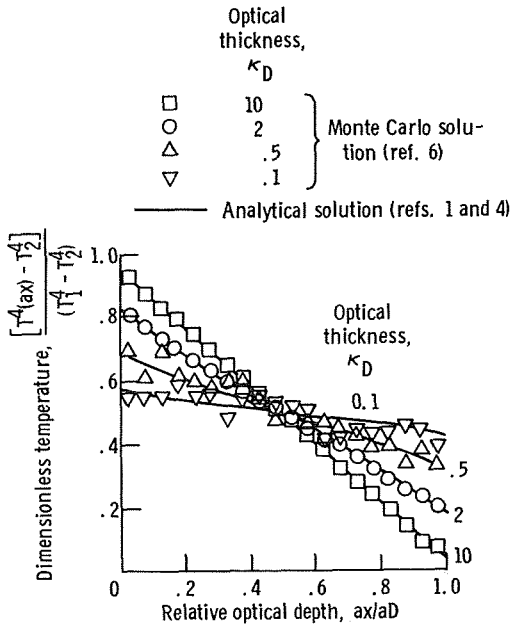


FIGURE 6-3. — Emissive power distribution in gray gas between infinite parallel black plates.

and a large number of specialized schemes for specific solutions. Many of these involve biasing the path length to increase the number of bundles absorbed in otherwise weakly absorbing regions.

6.4.2 Infinitely Long Concentric Cylinders

A more difficult problem to treat analytically than infinite parallel

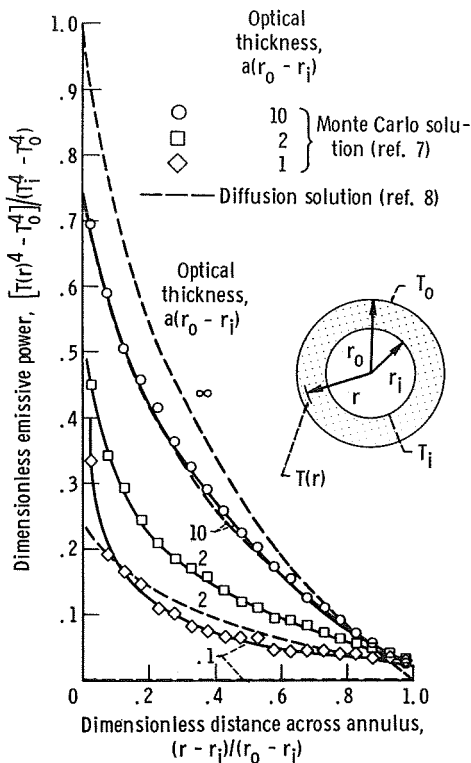


FIGURE 6-4.—Dimensionless emissive power distribution in gray gas in annulus between black concentric cylinders of radius ratio $r_i/r_o=0.1$.

plates is the determination of the emissive power distribution and local energy flux in a gray gas within the annulus between concentric cylinders. The energy equation for determining the emissive power at any radius involves an integral with the local radius appearing as one of the limits. When the energy equation is written for each incremental layer of gas, the resulting set of equations have integrals with limits that are different for every equation in the set. This set of integral equations must be solved simultaneously. The Monte Carlo approach, however, differs only slightly from that for parallel planes. The only additional complication is the determination of the bundle position in terms of cylindrical coordinates.

Some Monte Carlo results for an annular region are shown in figure 6-4 as taken from reference 7. Because of the analytical difficulties of this case, no exact formulation using integral techniques is available in the literature. Comparison of the results is therefore made with a modified diffusion solution (ref. 8). Trends in accuracy similar to those noted for the infinite plate case are evident.

6.4.3 Radiation Between Adjacent Gray Regions

A Monte Carlo formulation has also been applied to study the interaction of radiative energy between two regions, each of which has in-

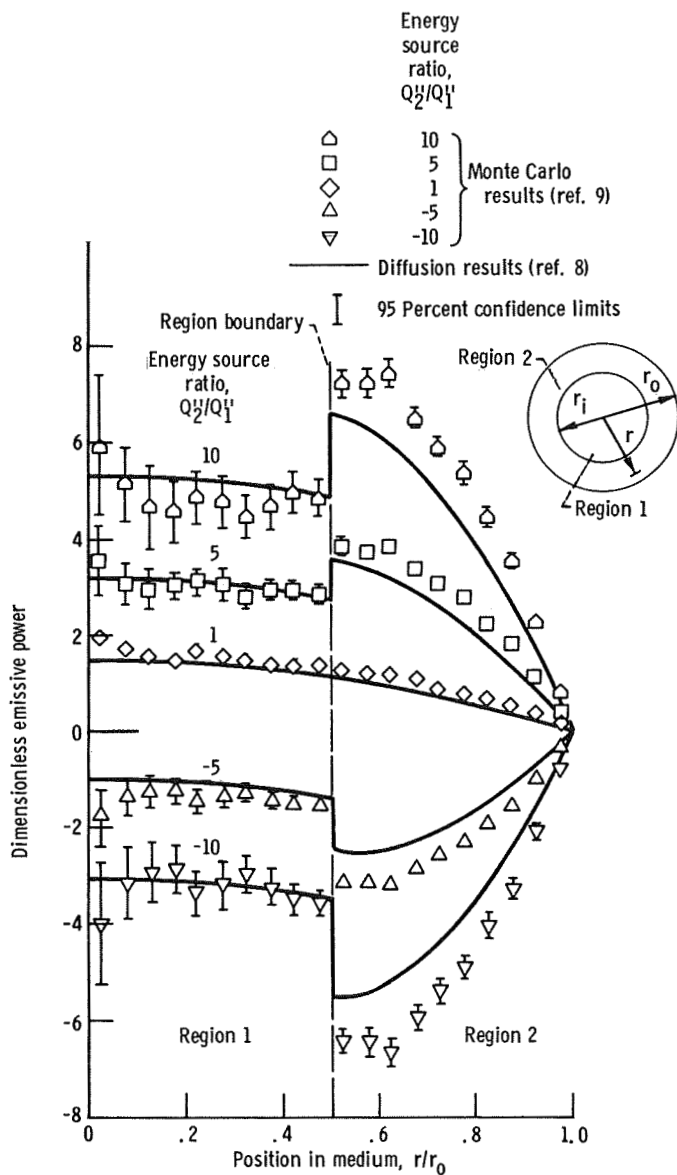


FIGURE 6-5.—Dimensionless emissive power distribution in coaxial gas regions with differing internal energy sources. Radius ratio $r_i/r_o=0.5$; optical thickness, 2 (in each region).

dividual gray radiative properties and internal energy generation rates (ref. 9). This is of interest here because it gives another insight into sources of error due to geometrical effects. Figure 6-5 shows the emissive power distribution in two concentric cylindrical regions of the same optical thickness but different rates of energy generation. The dimensionless emissive power shown in figure 6-5 has been adjusted for the wall slip (section 2.6.2) so that the curves all go to zero at the outer wall. The emissive power was made dimensionless by dividing by the local internal energy generation rate times the radius of the inner cylinder. The vertical bars give the 95 percent confidence limits on the Monte Carlo results.

The emissive power in the gas bears a direct proportionality to the number of energy bundles absorbed in a given volume element. The volume elements used in the calculation of the results shown in figure 6-5 are of equal radius and, therefore, of differing volumes. The elements near the center ($R \rightarrow 0$) have the smallest volume and, consequently, the smallest number of bundle absorptions. This is reflected in the increasing width of the 95 percent confidence limits at these points.

Taniguchi (ref. 10) has applied Monte Carlo to radiative transfer in a gray gas contained in rectangular parallelepipeds.

6.5 CONSIDERATION OF RADIATIVE PROPERTY VARIATIONS

The greatest criticism leveled against many methods for treating radiative transfer in gases is the inability to accurately account for the strong spectral, temperature, and pressure dependence of the radiative absorption coefficient. Such coefficients can sometimes be computed with reasonable accuracy by quantum-mechanical methods, but few analyses have been able to include the effect of all variables in the radiative transfer. Most treatments are limited to gray gases or use of various types of mean absorption coefficients.

Monte Carlo is well suited to consideration of property variations with many variables. It involves very little extra effort to assign wavelengths to individual energy bundles and to allow the paths of the bundles to depend on the local spectral absorption coefficient. The relations necessary to achieve this are given in table 6-I.

If property variations with temperature are considered, an iterative solution is usually necessary because the temperature distribution within the medium is not generally known *a priori*. Determination of the path length to absorption becomes more difficult also, because the absorption coefficient varies with position. By applying the formalism outlined in section 6.3.2 of volume II, the path length l is found to be given by

$$\ln R = - \int_0^l a_\lambda(S) dS \quad (6-5)$$

To evaluate this integral to determine l along a fixed line after choosing a random number R is time consuming but at least feasible. Howell and Perlmutter (ref. 11) used this approach, reducing the complexity somewhat by considering temperature and wavelength dependent absorption coefficients for hydrogen in the simple geometry of the gas contained between infinite parallel plates. They considered energy transfer through the gas between plates at different temperatures, and also the case of internal energy generation with a parabolic distribution of source strength in the gas. To evaluate the path length, equation (6-5) was approximated by dividing the gas into plane increments of thickness Δx . The path length through a given increment was then

$$\Delta l = \frac{\Delta x}{\cos \beta}$$

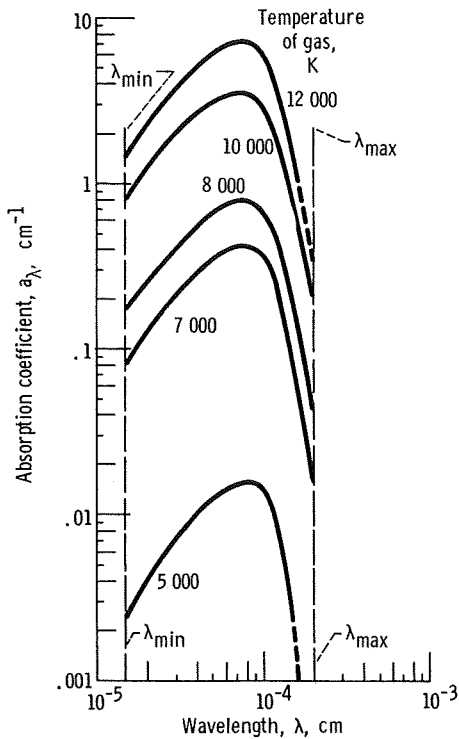


FIGURE 6-6.—Spectral absorption coefficient of hydrogen at 1000 atm (from ref. 11).

where β is the angle between the bundle path and the perpendicular to the plates. Equation (6-5) was then replaced by the computational form

$$\ln R + \Delta l \sum_{j=1}^p a_{\lambda,j} > 0 \tag{6-6}$$

and the summation was carried out until a value of the integer p was reached that satisfied the inequality. This value of p would be related to the increment number in which absorption occurs. The values of $a_{\lambda,j}$ were assumed for the first iteration and then recalculated in successive iterations on the basis of the newly computed local temperatures. This procedure was continued until convergence was obtained.

Figure 6-6 shows the property variations used, and figure 6-7 shows a set of emissive power distributions calculated as outlined. The accuracy becomes poorer, as evidenced by increased scatter, in the regions of low temperature because of the decrease with temperature of the absorption coefficient and, therefore, number of absorptions in the low temperature regions.

Taniguchi (ref. 12) used an incident mean absorption coefficient to account for property variations.

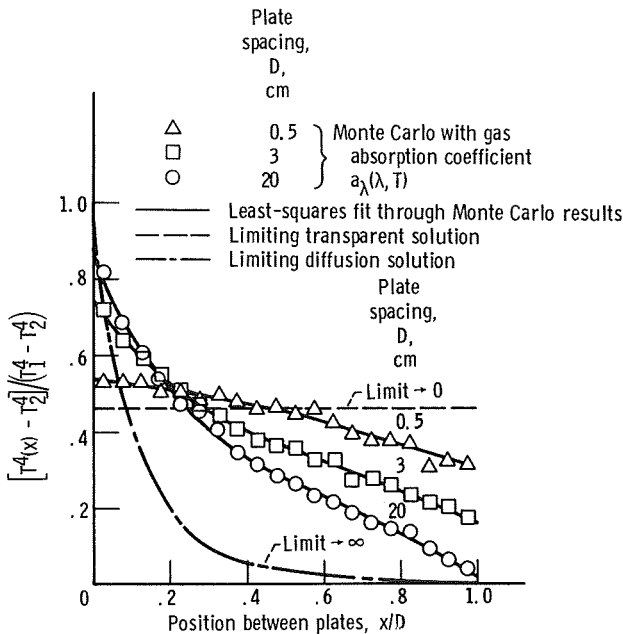


FIGURE 6-7.—Emissive power distribution in hydrogen between infinite parallel plates at temperatures $T_1=9500$ K and $T_2=4500$ K (from ref. 11).

6.6 COUPLING WITH OTHER HEAT TRANSFER MODES

When radiative transfer in a gas is coupled with conductive or convective energy transfer, solution becomes even more difficult. Combined energy transfer is occurring by radiation, where fourth power temperatures are governing, and by conduction and/or convection, where derivatives or differences of temperature to about the first power are governing. The radiative terms in the energy equation for such problems take the form of multiple integrals, while the conduction terms contain second derivatives. Further, the radiative surface properties which appear may be functions of wavelength, direction, and temperature. When gases are involved, these variables plus pressure can strongly affect the local gas radiation physical properties. The complete energy balance on each element of the system then takes the form of a nonlinear integrodifferential equation.

In the solution of coupled mode problems (refs. 13 to 16), the convective and conductive terms were treated as lumped energy sources or sinks, and Monte Carlo was used to evaluate the radiative terms on the basis of an assumed temperature distribution. With the radiative terms evaluated and substituted into the original equations, conventional numerical techniques were applied to the resulting differential equations and a local temperature distribution was generated. This was used as a basis for reevaluating the radiative integrals, and the procedure was continued until convergence.

An example of the power of the Monte Carlo approach in these problems is given in reference 16. Here the local temperature distribution as a function of length and radius, and the axial heat flux distribution in a conical rocket nozzle were determined under conditions expected in a gas-core nuclear propulsion system. Variations in physical properties with local temperature, pressure, and wavelength were examined, albeit not simultaneously, and coupled radiation and convection were considered. In addition, the ability was demonstrated of a layer of optically thick gas injected along the nozzle wall to attenuate the extreme predicted radiative fluxes to the wall.

6.7 TRANSIENT RADIATION PROBLEMS

The development of Monte Carlo techniques for radiative transfer under transient conditions has been done by Fleck (refs. 17 and 18) and Campbell (ref. 19). The model is essentially that outlined in previous sections, with the additional proviso that the flight times between events in the history of each bundle are computed, which adds considerable complexity to the problem. Energy bundles are followed along their paths, and their position at some time t is used to determine the distribution

of energy at that time. The bundles of course travel at the speed of light in the medium.

The review article by Fleck (ref. 17) gives a comprehensive discussion of applications, including the effects of scattering under transient conditions.

6.8 INCORPORATION OF SCATTERING PHENOMENA

Scattering of radiation is easily treated by Monte Carlo for any given distribution of scattering angles. It is analyzed exactly as absorption and nonisotropic reemission in a gas volume.

Collins and Wells (ref. 20) have used a modified Monte Carlo neutron diffusion code and other more specialized Monte Carlo codes to study the transmission of thermal radiation from a nuclear explosion. They examined the effects of Rayleigh scattering, and of Mie scattering (see chapter 8) from particles of a given size distribution. Multiple scattering within an atmosphere of arbitrarily described density distribution and effects due to ground and cloud reflections were included. Love et al. (ref. 21) and Stockham and Love (ref. 22) have studied problems with combined absorption and scattering by Monte Carlo.

6.9 CONCLUDING REMARKS

The Monte Carlo approach to radiation in attenuating media has been outlined. Perhaps a sufficient comment as to the power of the method is made by referring to example 6-1, or more specifically to figure 6-1. This figure gives a rather complete diagram of the logic required for programming the problem of energy transfer through a nonisothermal gray gas between infinite parallel black plates at different temperatures. A comparison of this diagram with the analyses of, say, references 1 to 4 or chapter 3 will show the simplifications in both concept and formulation that may be present in the Monte Carlo method.

REFERENCES

1. USISKIN, C. M.; AND SPARROW, E. M.: Thermal Radiation Between Parallel Plates Separated by an Absorbing-Emitting Nonisothermal Gas. *Int. J. Heat Mass Transfer*, vol. 1, no. 1, 1960, pp. 28-36.
2. HOTTEL, H. C.; AND COHEN, E. S.: Radiant Heat Exchange in a Gas-Filled Enclosure: Allowance for Nonuniformity of Gas Temperature. *AIChE J.*, vol. 4, no. 1, Mar. 1958, pp. 3-14.
3. VISKANTA, R.; AND GROSH, R. J.: Recent Advances in Radiant Heat Transfer. *Appl. Mech. Rev.*, vol. 17, no. 2, Feb. 1964, pp. 91-100.
4. HEASLET, MAX A.; AND WARMING, ROBERT F.: Radiative Transport and Wall Temperature Slip in an Absorbing Planar Medium. *Int. J. Heat Mass Transfer*, vol. 8, no. 7, July 1965, pp. 979-994.

5. HAJI-SHEIKH, A.; AND SPARROW, E. M.: Probability Distributions and Error Estimates for Monte Carlo Solutions of Radiation Problems. Progress in Heat and Mass Transfer, Vol. 2, Pergamon Press, 1969, pp. 1-12.
6. HOWELL, J. R.; AND PERLMUTTER, M.: Monte Carlo Solution of Thermal Transfer Through Radiant Media Between Gray Walls. J. Heat Transfer, vol. 86, no. 1, Feb. 1964, pp. 116-122.
7. PERLMUTTER, M.; AND HOWELL, J. R.: Radiant Transfer Through a Gray Gas Between Concentric Cylinders Using Monte Carlo. J. Heat Transfer, vol. 86, no. 2, May 1964, pp. 169-179.
8. DEISSLER, R. G.: Diffusion Approximation for Thermal Radiation in Gases with Jump Boundary Condition. J. Heat Transfer, vol. 86, no. 2, May 1964, pp. 240-246.
9. HOWELL, JOHN R.: Radiative Interactions Between Absorbing Emitting and Flowing Media with Internal Energy Generation. Paper 66-434, AIAA, June 1966. (See also NASA TN D-3614, 1966.)
10. TANIGUCHI, HIROSHI: The Radiative Heat Transfer of Gas in a Three Dimensional System Calculated by Monte Carlo Method. Bull. JSME, vol. 12, no. 49, Feb. 1969, pp. 67-78.
11. HOWELL, JOHN R.; AND PERLMUTTER, MORRIS: Monte Carlo Solution of Radiant Heat Transfer in a Nongrey Nonisothermal Gas with Temperature Dependent Properties. AIChE J., vol. 10, no. 4, July 1964, pp. 562-567.
12. TANIGUCHI, HIROSHI: Temperature Distributions of Radiant Gas Calculated by Monte Carlo Method. Bull. JSME, vol. 10, no. 42, Dec. 1967, pp. 975-988.
13. HOWELL, JOHN R.; STRITE, MARY K.; AND RENKEL, HAROLD: Heat-Transfer Analysis of Rocket Nozzles Using Very High Temperature Propellants. AIAA J., vol. 3, no. 4, Apr. 1965, pp. 669-673.
14. HOWELL, JOHN R.; AND STRITE, MARY KERN: Heat Transfer in Rocket Nozzles Using High-Temperature Hydrogen Propellant with Real Property Variations. J. Spacecraft Rockets, vol. 3, no. 7, July 1966, pp. 1063-1068.
15. HOWELL, JOHN R.; AND RENKEL, HAROLD E.: Analysis of the Effect of a Seeded Propellant Layer on Thermal Radiation in the Nozzle of a Gaseous-Core Nuclear Propulsion System. NASA TN D-3119, 1965.
16. HOWELL, JOHN R.; STRITE, MARY K.; AND RENKEL, HAROLD: Analysis of Heat-Transfer Effects in Rocket Nozzles Operating with Very High-Temperature Hydrogen. NASA TR R-220, 1965.
17. FLECK, JOSEPH A., JR.: The Calculation of Nonlinear Radiation Transport by a Monte Carlo Method. Statistical Physics. Vol. 1 of Methods in Computational Physics. Berni Alder, Sidney Fernbach and Manuel Rotenberg, eds., Academic Press, 1963, pp. 43-65.
18. FLECK, JOSEPH A., JR.: The Calculation of Nonlinear Radiation Transport by a Monte Carlo Method. Rep. UCRL-6698 (Del.), Lawrence Radiation Lab., Nov. 13, 1961.
19. CAMPBELL, PHILIP M.; AND NELSON, ROBERT G.: Numerical Methods for Nonlinear Radiation Transport Calculations. Rep. UCRL-7838, Lawrence Radiation Lab., Sept. 29, 1964.
20. COLLINS, DAVID G.; AND WELLS, MICHAEL B.: Monte Carlo Codes for Study of Light Transport in the Atmosphere. Volume I: Description of Codes. Rep. RRA-T54-1, Radiation Research Associates, Inc. (ECOM-00240-F, Vol. 1, DDC No. AD-625115), Aug. 1965.
21. LOVE, TOM J.; STOCKHAM, LEO W.; LEE, FU C.; MUNTER, WILLIAM A.; AND TSAI, YIH W.: Radiative Heat Transfer in Absorbing, Emitting and Scattering Media. Oklahoma Univ. (ARL-67-0210, DDC No. AD-666427), Dec. 1967.
22. STOCKHAM, LEO W.; AND LOVE, TOM J.: Radiative Heat Transfer from a Cylindrical Cloud of Particles. AIAA J., vol. 6, no. 10, Oct. 1968, pp. 1935-1940.

Chapter 7. Energy Transfer by Radiation Combined with Conduction and/or Convection

7.1 INTRODUCTION

When appreciable heat conduction and/or convection occur simultaneously with radiation in an absorbing-emitting medium, there are additional mathematical complications to those already discussed for radiation alone. Unless it can be shown that both the conduction and convection have a negligible effect compared with the radiation or vice versa, a nonlinear integrodifferential equation will result for the energy equation of the general problem having combined modes of heat transfer. Fortunately the formulation can be simplified for some circumstances when all modes must be included. For example, when the gas is optically thick the diffusion approximation can be applied. The radiation integrals are replaced by differential terms and a nonlinear differential equation will then result. Other approximations such as the transparent gas approximation (section 3.3.1) can be applied under suitable conditions to simplify the radiative terms.

Because the combined mode problems treated in this chapter are generally mathematically complex, it is not usually possible to obtain an analytical solution even for seemingly simple physical cases. Consequently, for each physical situation discussed here the analysis will be formulated and some of the intermediate steps in the solution outlined; then the results of a numerical solution are given and discussed. The situations considered will be a stationary conducting and radiating gas layer between two parallel planes, a boundary layer flow, and a channel flow of radiating and heat conducting gas.

7.2 SYMBOLS

A	area
a	absorption coefficient
c_p	heat capacity
D	distance between parallel planes; tube diameter
e	emissive power
\bar{F}	exchange factor
f	function of η in Blasius boundary layer solution: gas-to-gas exchange factor
g	surface-to-gas exchange factor

I	dimensionless intensity, $i/4\sigma T^4$
i	radiation intensity
K_v	function defined in eq. (7-27)
k	thermal conductivity
l	length
N_j	conduction-radiation parameter based on temperature, T_j
Pr	Prandtl number
Q	energy per unit time
q	energy flux, energy per unit area and time
q'''	heat generation per unit volume and time
r	radial coordinate
\vec{r}	position vector
S	surface area
T	absolute temperature
u, v	velocities in x -, y -directions
\bar{u}	mean velocity
V	volume
x, y	rectangular coordinates
α	thermal diffusivity
β	cone angle, angle from normal of area
δ	boundary layer thickness
ϵ	emissivity
η	Blasius similarity variable
Θ	dimensionless temperature, T/T_1
κ	optical depth
λ	wavelength
μ	$\cos \beta$
ν	kinematic viscosity
ρ	density of fluid
σ	Stefan-Boltzmann constant
τ	time
φ	dimensionless temperature group $(T^4 - T_2^4)/(T_1^4 - T_2^4)$
ψ	slip coefficient defined by eq. (7-25); boundary layer stream function
ω	solid angle

Subscripts:

b	blackbody
c	conduction
D	evaluated at $x = D$
e	emitted
i	incident; inlet

j	j^{th} surface
m	mean value
o	outlet
P	Planck mean value
R	Rosseland mean value
r	radiative
S	surface
V	volume
w	evaluated at wall
λ	spectrally dependent
0	free stream value
1, 2	surface 1 or 2
+	in direction of positive $\cos \beta$
-	in direction of negative $\cos \beta$

Superscripts:

'	directional quantity
*	dummy variable of integration

7.3 RADIATION AND CONDUCTION

There are a number of important practical situations where heat is transported within a medium by only the two modes of radiation and conduction. These usually involve solid or highly viscous media so that the movement of the medium and hence the convection is not important. In a liquid or gas, forced and/or free convection are usually of sufficient importance that they must be included. To develop the theory gradually, only the radiation and conduction terms are considered in this section; convection will be added later. The following are three practical situations where combined radiation-conduction transport is important.

One of the applications is in the glass industry. Although glass is often thought of as transparent, it can absorb a significant amount of radiation in certain wavelength regions (see fig. 5-27, vol. I). The absorbed radiation is then re-emitted within the glass thereby providing a radiative transport traveling layer by layer through the medium. The ordinary thermal conduction is thus augmented by a "radiative conduction." Radiative effects are quite important in influencing the temperature distribution within molten glass in a furnace. These effects have been analyzed by Kellett (ref. 1), Gardon (ref. 2), and Condon (ref. 3).

A second application is concerned with glassy materials that are sometimes used as an ablating coating to protect the interior of a body from high external temperatures by sacrificing the ablating surface. The

radiation-conduction process is important in regulating the temperature distribution within the ablating layer. The temperature distribution influences how the ablating material will soften, melt, or vaporize. These processes determine how efficiently the material will protect the surface. The radiative analysis of an ablating material has been considered by Kadanoff (ref. 4).

A third area of application that has arisen more recently is radiation within cryodeposits of solidified gas that form on a very cold surface. The cold surface may be on a space vehicle orbiting at the upper fringe of the atmosphere, or may be part of a cryopump which is a device used to produce a high vacuum by condensing the gas within a chamber. The cryodeposit coating changes the radiative properties of the cold surface and can thus significantly influence the radiative exchange with this surface. The radiative transfer in cryodeposits is considered in references 5 and 6.

In this section, some methods are examined for treating energy transfer by combined radiation and conduction. The conduction-radiation parameter will be introduced and the energy equation formulated. Then some approximations are considered, the most simple being the addition of separately computed radiation and conduction energy transfers to obtain the combined transfer. Any of the approximation methods to the equation of transfer presented in chapter 3 can be applied to simplify the radiation terms in these multimode problems, and the diffusion method will be applied here as an example. Also, the application in the literature of the Monte Carlo technique for combined mode problems has been mentioned in section 6.6.

7.3.1 The Conduction-Radiation Parameter

When conduction is present, a new dimensionless conduction-radiation

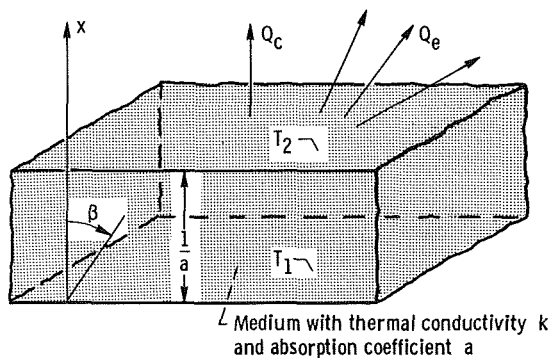


FIGURE 7-1.—Conduction through and radiation from plane volume element.

parameter N is introduced. The definition of N can be developed by analyzing the one-dimensional layer of material shown in figure 7-1. The material has thermal conductivity k , absorption coefficient a , and is one radiation mean free path thick. If it is assumed that the temperature profile within the slab is nearly linear, the conduction through the layer for area A is

$$Q_c = -kA \frac{T_2 - T_1}{\frac{1}{a}} \quad (7-1)$$

The total radiation emitted by the layer of area A can be written by using equation (1-34) as (not including induced emission)

$$Q_e = 4a\sigma T_m^4 A \left(\frac{1}{a} \right) \quad (7-2)$$

by suitably defining a mean temperature T_m and neglecting attenuation in the volume. The ratio of conducted to emitted flux is then

$$\frac{Q_c}{Q_e} = \frac{ka(T_1 - T_2)}{4\sigma T_m^4} \quad (7-3)$$

Dividing through by T_1 and letting $\Theta = T/T_1$ give

$$\frac{Q_c}{Q_e} = \frac{ka}{4\sigma T_1^3} \left(\frac{1 - \Theta_2}{\Theta_m^4} \right) = N_1 \left(\frac{1 - \Theta_2}{\Theta_m^4} \right) \quad (7-4)$$

The N_j is the *conduction-radiation parameter* based on the j^{th} temperature, defined by

$$N_j \equiv \frac{ka}{4\sigma T_j^3}$$

For the special case when $\Theta_m^4 = 1 - \Theta_2$ then $Q_c/Q_e = N_1$, and the parameter gives a measure of the relative energy amounts carried by conduction and emitted radiation for this layer of thickness $1/a$. Generally, however, N_j does *not* directly give the relative values of conduction to emission because the ratio of these values depends also upon both the temperature difference and temperature level in addition to N_j as shown by equation (7-4).

7.3.2 Energy Balance

To obtain an analytical solution for the combined conduction-radiation energy transfer in an absorbing-emitting medium, the general energy equation must be formulated. This is then solved subject to the boundary conditions to obtain the temperature distribution in the medium, and the heat flow can then be found. To formulate the energy equation, equation (2-16) is used for the total energy absorbed by a volume dV from the incident radiation intensity, and equation (2-17) gives the total energy emitted. In addition there will be a net energy gain per unit volume by heat conduction equal to $k\nabla^2 T$ for the case where k is a constant. Equating the net gain by conduction to the net loss by radiation gives

$$k\nabla^2 T = 4 \int_{\lambda=0}^{\infty} a_{\lambda} e_{\lambda b}(\lambda, T) d\lambda - \int_{\lambda=0}^{\infty} \int_{\omega=0}^{4\pi} a_{\lambda} i'_{\lambda}(\lambda, \omega) d\omega d\lambda \quad (7-5)$$

If there is internal heat generation in the medium, the heat thereby added per unit volume and time must be added to the left side of equation (7-5). The heat generation per unit time and volume will be designated as q''' and can be a function of position and time in the medium. This generation can be produced for example by electrical, chemical, or nuclear means.

For a transient problem some of the heat inflow to the volume element can be stored in the element. The energy storage per unit time and volume is $\rho c_p (\partial T / \partial \tau)$. Then for a transient situation with internal heat generation the energy equation becomes

$$k\nabla^2 T + q''' = 4 \int_{\lambda=0}^{\infty} a_{\lambda} e_{\lambda b}(\lambda, T) d\lambda - \int_{\lambda=0}^{\infty} \int_{\omega=0}^{4\pi} a_{\lambda} i'_{\lambda}(\lambda, \omega) d\omega d\lambda + \rho c_p \frac{\partial T}{\partial \tau} \quad (7-6)$$

The transient case for pure radiation problems is treated in section 9.6.

Since the radiation terms in equations (7-5) and (7-6) depend not only on the local temperature but on the entire surrounding radiation field, the energy equation is an integrodifferential equation for the temperature distribution in the medium. The conduction and heat storage terms depend on a different power of the temperature than the radiation terms and the energy equation is thus nonlinear.

Numerical solutions of the energy equation have been carried out by Gardon (see section 9.3.2), Viskanta and Grosh (refs. 7 and 8), and others. Most solutions have been for media in a plane-slab geometry, although some solutions have been carried out for other configurations (refs. 9 and

10). The following discussion will show how the energy equation is treated more specifically for a plane layer.

7.3.3 Plane Layer Geometry

Consider a layer of conducting-radiating material between parallel black plates as illustrated by figure 7-1. Plate 1 is at temperature T_1 , plate 2 is at T_2 , and the plates are a distance D apart. (The specific spacing of $1/a$ shown in the figure was used in section 7.3.1.) The medium between the plates has a constant thermal conductivity k and a gray absorption coefficient a . The integrodifferential equation governing the energy transfer will now be developed for this specific geometry.

For one-dimensional heat conduction, $\nabla^2 T$ in equation (7-5) is d^2T/dx^2 . Since the absorption coefficient does not depend on wavelength, it can be taken out of the integral signs. Then equation (7-5) reduces to

$$k \frac{d^2T}{dx^2} = 4a\sigma T^4(x) - a \int_{\omega=4\pi} i'(x) d\omega \quad (7-7)$$

As in equation (2-32), the incident intensity can be written in two parts traveling in directions having positive and negative $\cos \beta$, respectively,

$$k \frac{d^2T}{dx^2} = 4a\sigma T^4(x) - a \int_{\Delta} i'_+(x, \omega) d\omega - a \int_{\Sigma} i'_-(x, \omega) d\omega \quad (7-8)$$

The i'_+ and i'_- are given by equations (2-34) and (2-35) as

$$i'_+(x, \beta) = \frac{1}{\pi} \left\{ \sigma T_1^4 \exp\left(\frac{-ax}{\cos \beta}\right) + \frac{\sigma}{\cos \beta} \int_0^x T^4(x^*) \times \exp\left[\frac{a(x^* - x)}{\cos \beta}\right] adx^* \right\} \quad 0 \leq \beta \leq \frac{\pi}{2} \quad (7-9a)$$

$$i'_-(x, \beta) = \frac{1}{\pi} \left\{ \sigma T_2^4 \exp\left[\frac{a(D-x)}{\cos \beta}\right] - \frac{\sigma}{\cos \beta} \int_x^D T^4(x^*) \times \exp\left[\frac{a(x^* - x)}{\cos \beta}\right] adx^* \right\} \quad \frac{\pi}{2} \leq \beta \leq \pi \quad (7-9b)$$

Note that $\cos \beta$ is negative for the range of β in equation (7-9b). Equations (7-9a) and (7-9b) contain in them the boundary temperatures T_1 and T_2 . These are the two boundary conditions needed when solving equation (7-8) as this equation contains a second derivative

$$T(x) = T_1 \quad \text{at } x = 0$$

$$T(x) = T_2 \quad \text{at } x = D$$

By inserting equations (7-9a) and (7-9b) into equation (7-8), the i' is eliminated and an energy equation for $T(x)$ is obtained which can be solved numerically. However, some further simplifications in form are possible.

Define the nondimensional quantities $\mu = \cos \beta$, $\Theta = T/T_1$, $\Theta_2 = T_2/T_1$, $N_1 = ka/4\sigma T_1^3$, $\kappa = ax$, $\kappa_D = aD$, $I' = i'/4\sigma T_1^4$. Then by also using $d\omega = 2\pi \sin \beta d\beta = -2\pi d\mu$, equations (7-8) and (7-9) can be placed in the form

$$N_1 \frac{d^2\Theta(\kappa)}{d\kappa^2} = \Theta^4(\kappa) - 2\pi \int_0^1 I'_+(\kappa, \mu) d\mu - 2\pi \int_0^1 I'_-(\kappa, \mu) d\mu \quad (7-10)$$

where

$$I'_+(\kappa, \mu) = \frac{1}{4\pi} \left[\exp\left(\frac{-\kappa}{\mu}\right) + \int_0^\kappa \Theta^4(\kappa^*) \exp\left(\frac{\kappa^* - \kappa}{\mu}\right) \frac{d\kappa^*}{\mu} \right] \quad 0 \leq \mu \leq 1 \quad (7-11a)$$

$$I'_-(\kappa, \mu) = \frac{1}{4\pi} \left\{ \Theta_2^4 \exp\left[-\frac{(\kappa_D - \kappa)}{\mu}\right] + \int_\kappa^{\kappa_D} \Theta^4(\kappa^*) \exp\left(\frac{\kappa - \kappa^*}{\mu}\right) \frac{d\kappa^*}{\mu} \right\} \quad 0 \leq \mu \leq 1 \quad (7-11b)$$

Note that the signs have been changed by changing variables so that μ is positive throughout equations (7-10) and (7-11). Combining equations (7-10) and (7-11) to eliminate I' gives

$$N_1 \frac{d^2\Theta(\kappa)}{d\kappa^2} = \Theta^4(\kappa) - \frac{1}{2} \left(\int_0^1 \left\{ \exp\left(-\frac{\kappa}{\mu}\right) + \Theta_2^4 \exp\left[-\frac{(\kappa_D - \kappa)}{\mu}\right] \right\} d\mu + \int_0^{\kappa_D} \int_0^1 \frac{\Theta^4(\kappa^*)}{\mu} \exp\left(-\frac{|\kappa - \kappa^*|}{\mu}\right) d\mu d\kappa^* \right) \quad (7-12)$$

By using the exponential integral function defined in equation (2-45) and in the appendix, equation (7-12) can be written as

$$N_1 \frac{d^2 \Theta(\kappa)}{d\kappa^2} = \Theta^4(\kappa) - \frac{1}{2} \left[E_2(\kappa) + \Theta_2^4 E_2(\kappa_D - \kappa) + \int_0^{\kappa_D} \Theta^4(\kappa^*) E_1(|\kappa - \kappa^*|) d\kappa^* \right] \quad (7-13)$$

Equation (7-13) is the desired integrodifferential equation for the temperature distribution $\Theta(\kappa)$. It is a nonlinear equation since Θ is raised to the first power in the conduction term while it is raised to the fourth power in the radiation terms. The boundary conditions in dimensionless form are

$$\begin{aligned} \Theta &= 1 & \text{at } \kappa &= 0 \\ \Theta &= \Theta_2 & \text{at } \kappa &= \kappa_D \end{aligned} \quad (7-14)$$

Examining equations (7-13) and (7-14) shows that the solution depends on the parameters N_1 , κ_D , and Θ_2 .

In addition to the temperature distribution, the heat transfer across the layer from plate 1 to plate 2 is usually of interest. Equation (2-41) gave the net heat flux expression for radiation alone across a gray gas between black plates. This radiative flux equation was obtained for convenience at $x=0$. In addition at the same location there is now a conduction flux $-k(dT/dx)|_{x=0}$ so that the heat flux equation becomes (note that from energy conservation q will not depend on x for the situation being considered here)

$$q = -k \left. \frac{dT}{dx} \right|_{x=0} + \sigma T_1^4 - 2 \int_0^{\pi/2} \sin \beta \cos \beta \left[\sigma T_2^4 \exp\left(\frac{-\kappa_D}{\cos \beta}\right) + \frac{\sigma}{\cos \beta} \int_0^{\kappa_D} T^4(\kappa^*) \exp\left(-\frac{\kappa^*}{\cos \beta}\right) d\kappa^* \right] d\beta \quad (7-15)$$

On the right, the first term is the conduction away from wall 1, the second is the radiation leaving wall 1, the third is the radiation leaving wall 2 that is then attenuated by the medium and reaches wall 1, and the last term is the radiation from the medium to wall 1. By using the exponential integral function and the previously defined dimensionless variables, the heat flux can be written as

$$\frac{q}{\sigma T_1^4} = -4N_1 \left. \frac{d\Theta}{d\kappa} \right|_{\kappa=0} + 1 - 2 \left[\Theta_2^4 E_3(\kappa_D) + \int_0^{\kappa_D} \Theta^4(\kappa^*) E_2(\kappa^*) d\kappa^* \right] \quad (7-16)$$

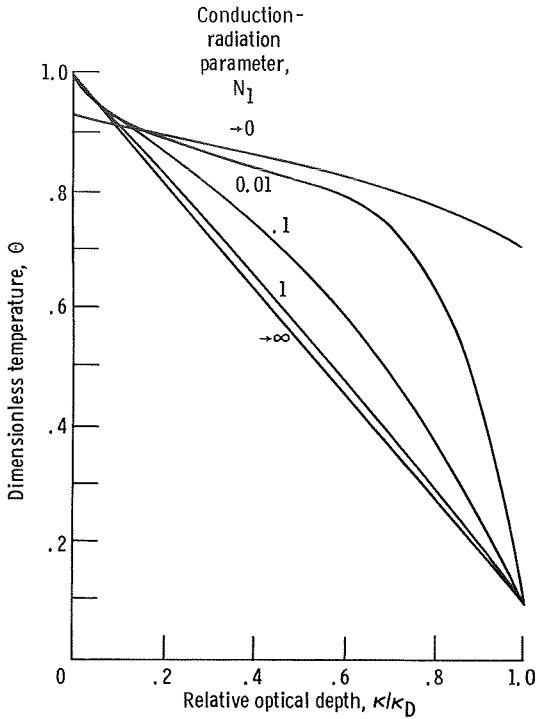


FIGURE 7-2.—Dimensionless temperature distribution in gray gas between infinite parallel black plates with conduction and radiation. Plate temperature ratio $\Theta_2=0.1$; optical spacing $\kappa_D=1.0$. (Data from ref. 7.)

Since there are no heat sources in the medium, this q computed at the lower wall is the same at all locations within the medium.

Viskanta and Grosh (refs. 7 and 8) obtained solutions of equation (7-13) by numerical integration and iteration. Some of their temperature distributions are shown in figure 7-2. For $N_1 \rightarrow \infty$ conduction dominates and the solution reduces to the linear profile for conduction through a plane layer. When $N_1=0$, the conduction term drops out and the temperature profile has a discontinuity (temperature slip) at each wall as discussed for the case of radiation alone in section 2.6.2. When conduction is present, there is no temperature slip. Some of the heat flux results from reference 8 as obtained from equation (7-16) are shown in table 7-I.

Timmons and Mingle (ref. 11) have carried out solutions for the same problem with specular, rather than diffuse, boundaries. Results are within a few percent of those for diffuse boundaries.

TABLE 7-I.—HEAT FLUX BETWEEN PARALLEL BLACK PLATES BY COMBINED RADIATION AND CONDUCTION THROUGH A GRAY MEDIUM

[From ref. 8]

Optical thickness, κ_D	Plate temperature ratio, Θ_2	Conduction-radiation parameter, N_1	Dimensionless energy flux, $q/\sigma T_1^4$
0.1	0.5	0	0.859
		.01	1.074
		.1	2.880
		1	20.88
		10	200.88
1.0	0.5	0	0.518
		.01	.596
		.1	.798
		1	2.600
		10	20.60
1.0	0.1	0	0.556
		.01	.658
		.1	.991
		1	4.218
		10	36.60
10	0.5	0	0.102
		.01	.114
		.1	.131
		1	.315
		10	2.114

7.3.4 Simple Addition of Radiation and Conduction Energy Transfers

A relatively simple idea to obtain the combined energy transfer by radiation and conduction is to assume that the interaction between the two transfer processes is so small that the processes can be considered to each act independently. Then the conduction and the radiation transfers are each formulated as if the other transfer mechanism were not present. Einstein⁹ (ref. 12) and Cess (ref. 13) have investigated this approximation for an absorbing-emitting gray medium between infinite parallel plates. When the plates were black, the results for the energy transfer were within 10 percent of the exact solution. Larger errors are

⁹ This is Thomas H. Einstein. Albert made his appearance in chapter 4.

possible if highly reflecting surfaces are present. Howell (ref. 14) shows that the additive solution is also fairly accurate for a gray gas between black concentric cylinders.

An additive solution cannot be used to predict temperature profiles. It is an effective and simple method of predicting energy transfer by combined modes, although the accuracy of the solutions so obtained becomes doubtful in some situations. The use of the additive method for problems where the accuracy has not been established by some comparisons with more exact solutions is not advisable.

EXAMPLE 7-1: By using the additive approximation, obtain a relation for the energy transfer from a gray infinite plate at temperature T_1 and emissivity ϵ_1 , to a parallel infinite gray plate at T_2 with emissivity ϵ_2 . The spacing between the plates is D , and the region between the plates is filled with a gray material with absorption coefficient a and thermal conductivity k . Use the diffusion approximation for the radiative transfer.

Without radiation, the energy flux from surface 1 to 2 by pure conduction to be used in the additive solution is

$$q_c = \frac{k(T_1 - T_2)}{D} \quad (7-17)$$

The diffusion solution for pure radiation from plate 1 to 2 can be found from table 3-II as

$$q_r = \frac{\sigma(T_1^4 - T_2^4)}{\frac{3aD}{4} + \frac{1}{\epsilon_1} + \frac{1}{\epsilon_2} - 1} \quad (7-18)$$

Since the two modes are assumed completely independent, the additive solution gives

$$q = q_c + q_r \quad (7-19)$$

After using the dimensionless variables defined in connection with equation (7-10), the expression for q becomes

$$\frac{q}{\sigma T_1^4} = \frac{4N_1(1 - \Theta_2)}{\kappa_D} + \frac{(1 - \Theta_2^4)}{\frac{3\kappa_D}{4} + \frac{1}{\epsilon_1} + \frac{1}{\epsilon_2} - 1} \quad (7-20)$$

Equation (7-20) must give correct results at $N_1 = 0$ (pure radiation) within the accuracy of the diffusion solution and at $N_1 \rightarrow \infty$ (pure con-

duction) because it simply adds these two limiting cases.

Comparison of $q/\sigma T_1^4$ from equation (7-20) with exact numerical solutions for $\epsilon_1 = \epsilon_2 = 1$ and $\Theta_2 = 0.5$ from the work of Viskanta and Grosh (refs. 7 and 8) is shown in figure 7-3. For this geometry and black surfaces, the results of the additive solution are very accurate. The additive method appears even better here because of the fortuitous benefit that the diffusion solution gives a pure radiation heat transfer that is slightly above the exact pure radiation solution (fig. 3-6) while the pure conduction result is too low. This is because the conduction solution is based on the linear gradient of T at the boundaries while the actual gradients are larger when radiation is present (see fig. 7-7(a) for example). The errors in the two solutions tend to cancel, thus giving a quite accurate combined solution for this geometry.

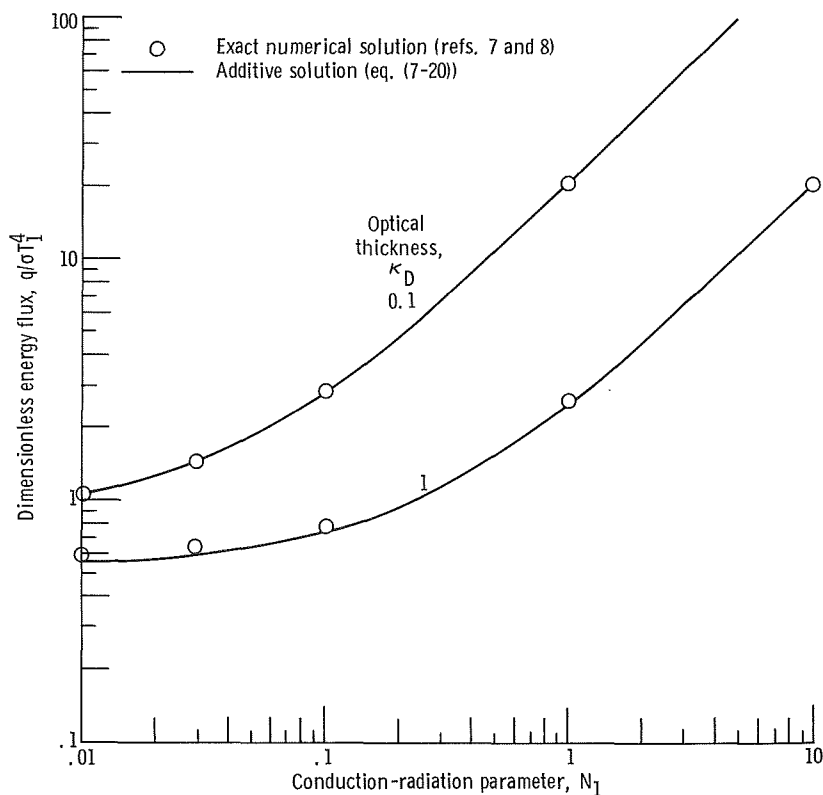


FIGURE 7-3.—Comparison of simple additive and exact numerical solutions of combined conduction-radiation energy transfer between black parallel plates. Plate temperature ratio $\Theta_2 = 0.5$.

7.3.5 The Diffusion Method

This method has the advantage over the additive method in that a solution is obtained to the coupled energy equation and this yields the temperature distribution in the medium. In section 3.4.2.1, it was shown that the diffusion heat flux for radiative transfer has the same form as the Fourier conduction law. By using the Rosseland mean absorption coefficient defined in equation (3-39), the radiative flux vector can be written as

$$\vec{q}_r = -\frac{4}{3a_R} \nabla e_b = -\frac{16\sigma T^3}{3a_R} \nabla T = -k_r \nabla T \quad (7-21)$$

where k_r is the *radiative conductivity* defined by

$$k_r \equiv \frac{16\sigma T^3}{3a_R} \quad (7-22)$$

Consequently, by use of the diffusion approximation, the energy flux vector by combined radiation and conduction at any position in the medium can be expressed as

$$\vec{q} = \vec{q}_r + \vec{q}_c = -(k_r + k) \nabla T = -\left(\frac{16\sigma T^3}{3a_R} + k\right) \nabla T \quad (7-23)$$

The local heat flux as given in equation (7-23) can be used as in the derivation of the heat conduction equation, to obtain an energy balance on a differential volume element within the absorbing-emitting medium. For example, in two-dimensional rectangular coordinates and with no internal heat sources, the energy equation is

$$\frac{\partial}{\partial x} \left[\left(\frac{16\sigma T^3}{3a_R} + k \right) \frac{\partial T}{\partial x} \right] + \frac{\partial}{\partial y} \left[\left(\frac{16\sigma T^3}{3a_R} + k \right) \frac{\partial T}{\partial y} \right] = 0 \quad (7-24)$$

The medium behaves like a conductor that has a thermal conductivity dependent on temperature.

To obtain the temperature distribution in the medium, an equation such as equation (7-24) must be integrated subject to the imposed boundary conditions. These conditions would often be the temperatures on the enclosure surfaces. However, near a boundary the diffusion approximation is not valid; consequently, the solution is incorrect near the wall and it cannot be matched directly to the wall boundary conditions. To overcome this difficulty, the boundary condition at the edge of the absorbing-emitting medium will be modified in such a way that the resulting solution to the diffusion equation will be correct in the region away from the boundaries where the diffusion approximation is valid.

In the pure radiation case, a temperature slip was introduced to overcome the difficulty of matching the diffusion solution in the medium to the wall temperature. For combined conduction-radiation problems, a similar slip concept was introduced by Goldstein and Howell (refs. 15 and 16). By using the method of matched asymptotic expansions, which in this case was used to match the linearized solutions for intensity, flux, and temperature near the wall with the diffusion solution for these quantities far from the wall, an effective slip condition was derived. As shown by figure 7-4, this slip gives the boundary condition $T(x \rightarrow 0)$ that the diffusion solution must have if it is to extend all the way to the wall. The slip is given in terms of the *slip coefficient* ψ which is a function only of the conduction-radiation parameter N . In terms of quantities at wall 1, ψ_1 is given by

$$\psi_1 = \frac{\sigma [T_1^4 - T^4(x \rightarrow 0)]}{q_{r,1}} \quad (7-25)$$

where q_r is the radiative energy flux at the boundary as evaluated by the diffusion approximation, T_1 is the wall temperature, and $T(x \rightarrow 0)$ is the extrapolated temperature in the medium at the wall (the effective slip temperature to be used in the diffusion solution). The ψ_1 is com-

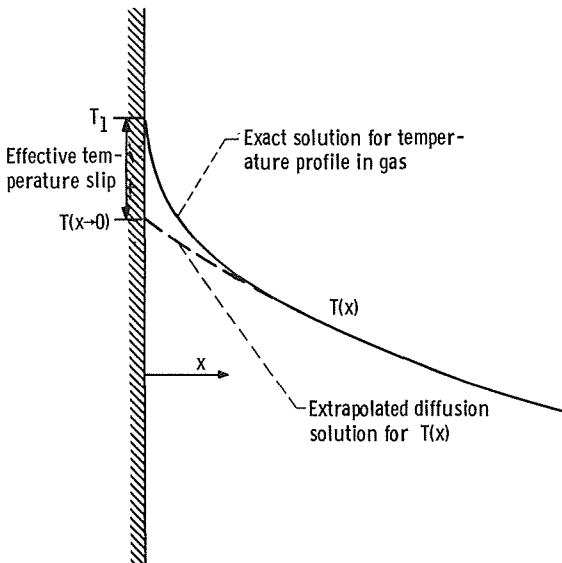


FIGURE 7-4.—Use of effective temperature slip as boundary condition for diffusion solution in combined conduction and radiation.

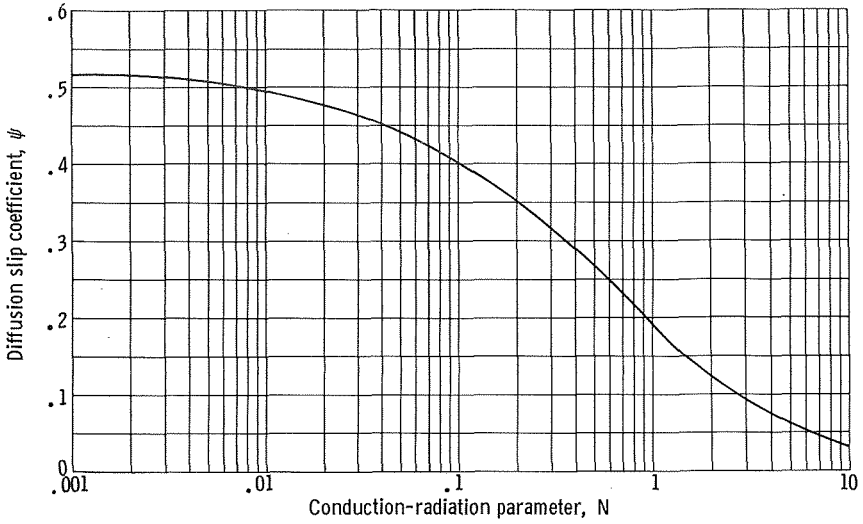


FIGURE 7-5.—Slip coefficient for combined conduction-radiation solutions by the diffusion approximation.

puted from the relations of reference 15 as

$$\psi_1 = \frac{3}{4\pi} \int_0^1 \tan^{-1} \left(\frac{1}{K_v} \right) dv \quad (7-26)$$

where K_v is the function

$$K_v = \frac{1}{\pi} \left[\frac{N_1}{2v^3} - \frac{2}{v} - \ln \left(\frac{1-v}{1+v} \right) \right] \quad (7-27)$$

A graph of ψ as a function of N that can be used for any geometry is shown in figure 7-5.

This type of solution should give accurate temperature distributions within the limits of the assumptions inherent in the diffusion approximation. Results can be obtained for both the energy transfer and the temperature profiles as will be shown by an example problem. Other solutions of this general type have been presented in references 17 and 18.

EXAMPLE 7-2: Using the diffusion method for combined conduction and radiation, find an equation for the temperature profile in a medium of constant absorption coefficient a and thermal conductivity k . The medium is contained between infinite parallel black plates at temperatures T_1 and T_2 spaced D apart with the lower plate 1 located at $x=0$.

Equation (7-23) in dimensionless form for this geometry becomes the following (note that $a_R = a$ in this case):

$$\frac{q}{\sigma T_1^4} = - \left(\frac{4}{3a} \frac{d\Theta^4}{dx} + \frac{k}{\sigma T_1^3} \frac{d\Theta}{dx} \right) = - \left(\frac{4}{3} \frac{d\Theta^4}{d\kappa} + 4N_1 \frac{d\Theta}{d\kappa} \right) \quad (7-28)$$

From energy conservation, since there are no internal heat sources the q is constant across the space between plates. Equation (7-28) can then be integrated from 0 to κ_D to yield

$$\frac{q}{\sigma T_1^4} \kappa_D = - \left\{ \frac{4}{3} [\Theta^4(\kappa_D) - \Theta^4(0)] + 4N_1 [\Theta(\kappa_D) - \Theta(0)] \right\} \quad (7-29)$$

where $\Theta(0)$ and $\Theta(\kappa_D)$ are *in the medium* at the lower and upper boundaries, respectively. These two temperatures must now be eliminated by using the slip boundary conditions to relate them to the specified wall temperatures T_1 and T_2 .

Consider first the boundary condition at wall 1. For the particular N_1 of the problem, the ψ_1 is found from figure 7-5 and set equal to

$$\psi_1 = \frac{\sigma [T_1^4 - T^4(0)]}{q_{r,1}}$$

From equation (7-23) the radiative flux at the wall $q_{r,1}$ can be written as

$$q_{r,1} = - \frac{16\sigma T_1^3}{3a} \left. \nabla T \right|_1 = \frac{16\sigma T_1^3}{3a} \frac{q}{\left(\frac{16\sigma T_1^3}{3a} + k \right)}$$

Then ψ_1 becomes

$$\psi_1 = \frac{\sigma [T_1^4 - T^4(0)]}{\left(\frac{\frac{4\sigma}{3a} q}{\frac{4\sigma}{3a} + \frac{k}{4T_1^3}} \right)}$$

This is rearranged into

$$\frac{4}{3a} q = \frac{1}{\psi_1} \left\{ \frac{4\sigma}{3a} [T_1^4 - T^4(0)] + \frac{k}{4T_1^3} [T_1^4 - T^4(0)] \right\} \quad (7-30)$$

As shown in derivation of ψ (ref. 15), the conditions where the diffusion solution is valid lead to the jump $T_1 - T(0)$ being small. For convenience a portion of equation (7-30) can then be linearized. With $T_1 - T(0) = \delta$ where δ is small, then

$$\frac{[T_1^4 - T^4(0)]}{4T_1^3} = \frac{[T_1^4 - (T_1 - \delta)^4]}{4T_1^3} \approx \frac{(T_1^4 - T_1^4 + 4T_1^3\delta)}{4T_1^3} = \delta = T_1 - T(0)$$

Then equation (7-30) becomes

$$\frac{4}{3} q \approx \frac{1}{\psi_1} \left\{ \frac{4\sigma}{3a} [T_1^4 - T^4(0)] + k[T_1 - T(0)] \right\}$$

or in dimensionless form

$$\frac{4}{3} \psi_1 \frac{q}{\sigma T_1^4} = \frac{4}{3} [1 - \Theta^4(0)] + 4N_1[1 - \Theta(0)] \quad (7-31)$$

Similarly at wall 2 (note that the value of ψ_2 corresponds to $N=N_2$ on fig. 7-5)

$$\frac{4}{3} \psi_2 \frac{q}{\sigma T_1^4} = \frac{4}{3} [\Theta^4(\kappa_D) - \Theta_2^4] + 4N_1[\Theta(\kappa_D) - \Theta_2] \quad (7-32)$$

Now add equations (7-29), (7-31), and (7-32) to eliminate the unknown temperatures in the medium $\Theta(0)$ and $\Theta(\kappa_D)$. This yields the nondimensional energy flux transferred across the layer as

$$\frac{q}{\sigma T_1^4} = \frac{(1 - \Theta_2^4) + 3N_1(1 - \Theta_2)}{\frac{3}{4} \kappa_D + \psi_1 + \psi_2} \quad (7-33)$$

The energy flux results of equation (7-33) are plotted in figure 7-6 and compared with the exact and additive solutions (the exchange factor approximation shown in the figure will be discussed in the next section). At $\kappa_D=1$, the results compare very well with the exact solution. For a small optical thickness $\kappa_D=0.1$, however, the diffusion-slip procedure breaks down for intermediate values of N_1 and the simple additive solution provides much better energy transfer values.

An advantage of the diffusion solution is that it will yield the temperature distribution in the medium. Temperature profiles can be predicted by integrating equation (7-28) from locations 0 to κ and then

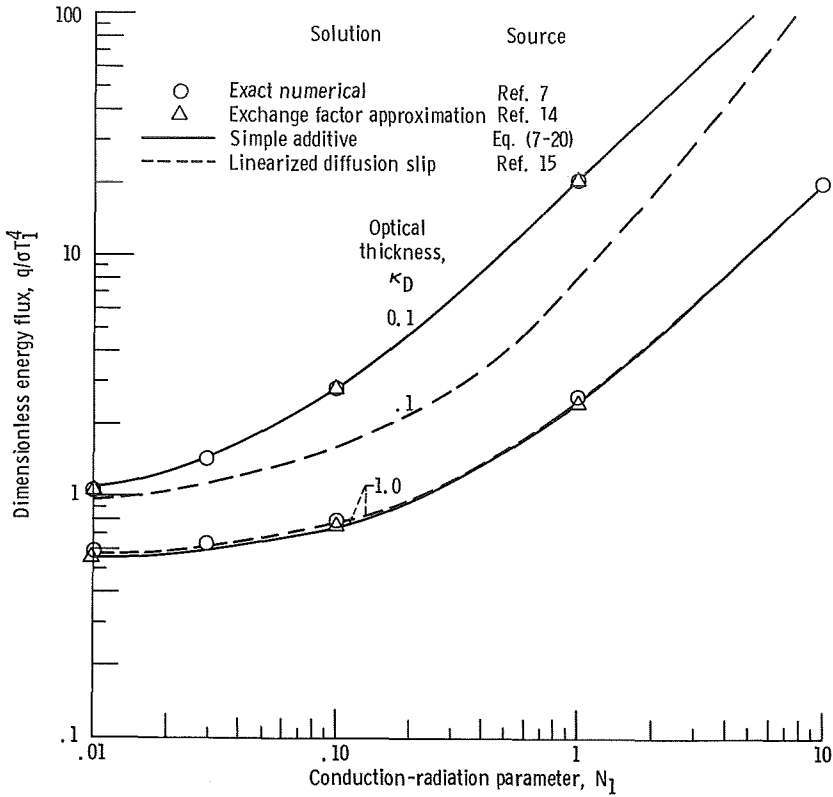


FIGURE 7-6.—Comparison of various methods for predicting energy transfer by conduction and radiation across a layer between parallel black plates. Plate temperature ratio $T_2/T_1 = \Theta_2 = 0.5$.

using equations (7-31) and (7-33) to eliminate $\Theta(0)$ and q . This yields

$$\frac{[1 - \Theta^4(\kappa)] + 3N_1[1 - \Theta(\kappa)]}{(1 - \Theta_2^4) + 3N_1(1 - \Theta_2)} = \frac{\frac{3\kappa}{4} + \psi_1}{\frac{3\kappa_D}{4} + \psi_1 + \psi_2} \tag{7-34}$$

Some temperature profiles are shown in figure 7-7. For $\kappa_D = 1$, figure 7-7(a), the profiles are poor except for the largest N_1 shown. Better results are obtained for all N_1 at larger κ_D because the assumptions in the diffusion solution become more valid. This is shown by figure 7-7(b), where results are compared for $\kappa_D = 10$. On the basis of the assumptions used in the diffusion slip analysis and the way in which the solutions compare with exact analytical solutions, good temperature distribution

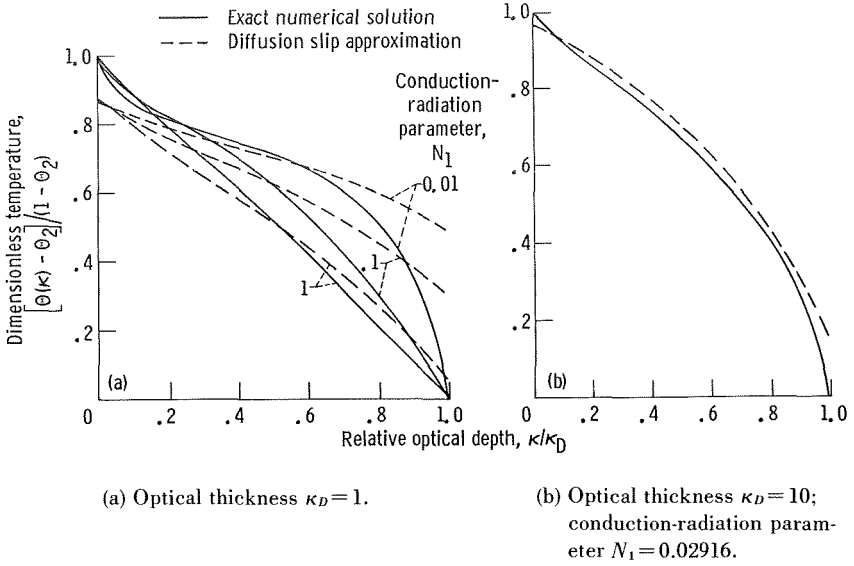


FIGURE 7-7.—Comparison of temperature profile by exact solution (ref. 7) with diffusion slip approximation. Plate temperature ratio $\Theta_2 = 0.5$; plate emissivities $\epsilon_1 = \epsilon_2 = 1.0$.

results are expected for $\kappa_D \gtrsim 2$. For $N_1 \rightarrow 0$ and $N_1 \rightarrow \infty$, the diffusion slip method goes to the correct limiting solutions.

Within their limits of applicability, diffusion methods provide a different interpretation of the conduction-radiation parameter from that presented in section 7.3.1. The ratio of the molecular conductivity k to the radiative conductivity k_r given by equation (7-22) is

$$\frac{k}{k_r} = \frac{k}{\frac{16\sigma T^3}{3a_R}} = \frac{3}{4} \left(\frac{ka_R}{4\sigma T^3} \right) = \frac{3}{4} N \tag{7-35}$$

Therefore, in the diffusion limit, N is a direct measure of the ratio of molecular to radiative conductivity. In consequence, N is in this case also a direct measure of the ratio of the energy transferred by the two modes.

7.3.6 The Exchange Factor Approximation

In section 5.8.3 the use of the exchange factor approximation was introduced in the context of pure radiation problems. In this section, these exchange factors are applied to combined mode problems, and it is shown that their use gives a convenient method of treating these problems. As stated in section 5.8.3, the exchange factor \bar{F}_{j-k} is defined as the fraction of the energy leaving surface j that is incident on surface

k when all boundaries are black and the intervening medium is in radiative equilibrium (i.e., when radiation is the only means of energy exchange). The \bar{F}_{j-k} includes the effect of absorption and re-emission of energy by the medium while the energy is in transit from A_j to A_k . A similar exchange factor between a surface area and volume element was also defined there. The reader may find it helpful to review section 5.8.3 before proceeding with the present material.

The total energy emitted by a volume element in the *presence* of heat conduction can be equated to three terms: (1) the energy that would be emitted in the absence of conduction, (2) the *net* energy supplied to the element by conduction (and thus must be radiated away), and (3) any additional energy dQ_{extra} added to the element by radiation over and above that given by the radiative equilibrium (zero conduction) case because of the change in temperature profile as a result of conduction being included. This can be written as

$$4a_p\sigma T^4 dV = 4a_p\sigma T_R^4 dV - (k\nabla^2 T) dV + dQ_{extra} \quad (7-36a)$$

The temperature T_R present in the radiative equilibrium case is conveniently written in terms of exchange factors as in equation (5-122) as

$$4a_p\sigma T_R^4 dV = \sum_j Q_{o,j} d\bar{F}_{j-av}$$

The $Q_{o,j}$ is the energy leaving the j^{th} surface of the enclosure surrounding the gas. The $d\bar{F}_{j-av}$ is the fraction of energy leaving the area A_j that is absorbed in dV for the case of radiative equilibrium in a black enclosure and includes the effects of gas absorption and emission while the energy is in transit from A_j to dV . Substituting this relation and assuming that dQ_{extra} is small reduce equation (7-36a) to

$$4a_p\sigma T^4 \approx \frac{1}{dV} \sum_j Q_{o,j} d\bar{F}_{j-av} - k\nabla^2 T \quad (7-36b)$$

Note that the exchange factors include the effect of gas-to-gas volume element radiant interchange based on the temperature profile for *no conduction* (radiative equilibrium). The approximation introduced in equation (7-36b) is that the gas-to-gas radiant exchange is not significantly affected by the new temperature profile that results because of the presence of gas conduction (i.e., $dQ_{extra} \approx 0$). The similar approximation is also made that the $Q_{o,j}$ can be used from the solution without conduction. If radiation predominates, then this is a good assumption; if radiation is small, then it will not matter that the radiative terms are somewhat inaccurate.

Equation (7-36b) is a nonlinear differential equation for T , the local gas temperature. Howell (ref. 14) has applied this approach to gray gases in annular enclosures and between infinite parallel plates. Accuracy is found to be comparable to the simple additive solution when computing the heat flux through the gas as shown in figure 7-6. The chief advantage of the method is that accurate temperature distributions can be obtained for combined-mode energy transfer problems with but little effort. The procedure will be demonstrated by the following example.

EXAMPLE 7-3: Find an expression that will yield the temperature profile in a gray gas contained between infinite parallel plates a distance D apart if the gas has absorption coefficient a , thermal conductivity k , and the plates are black at temperatures T_1 and T_2 . Use the exchange factor approximation.

Using a layer dx thick as the volume element results in governing energy equation (7-36b) becoming, in this geometry,

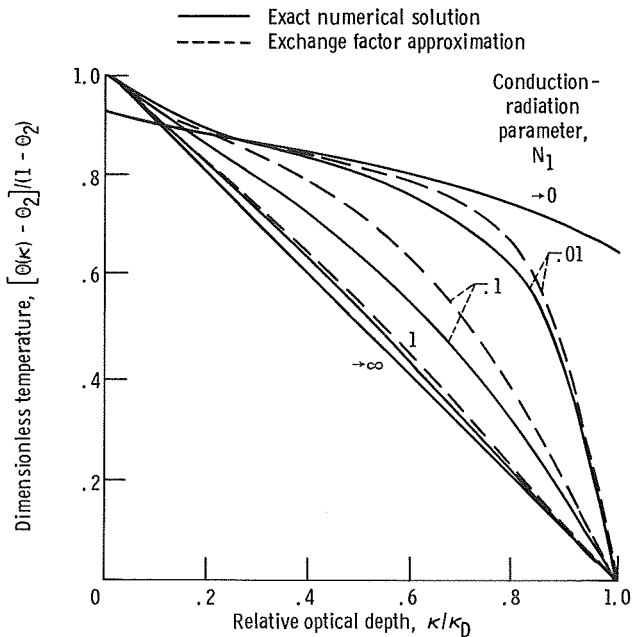


FIGURE 7-8.—Comparison of temperature profiles by exact solution with exchange factor approximation. Optical thickness $\kappa_D=1.0$; plate temperature ratio $\Theta_2=0.1$; plate emissivities $\epsilon_1=\epsilon_2=1.0$.

$$-k \frac{d^2 T(x)}{dx^2} dx + d\bar{F}_{1-dx} \sigma T_1^4 + d\bar{F}_{2-dx} \sigma T_2^4 = 4a\sigma T^4(x) dx \quad (7-37)$$

The exchange factors are given by equations (5-125) and (5-126) as

$$d\bar{F}_{1-dx} = 4adx \varphi_b(x)$$

and

$$d\bar{F}_{2-dx} = 4adx(1 - \varphi_b)$$

The φ_b can be obtained to good accuracy for this geometry by the diffusion relations, table 3-II, as

$$\varphi_b(\kappa) = \frac{\frac{3}{4}(\kappa_D - \kappa) + \frac{1}{2}}{\frac{3}{4}\kappa_D + 1}$$

Substituting these relations into equation (7-37) and using the usual nondimensional quantities give

$$\Theta^4(\kappa) + N_1 \frac{d^2 \Theta(\kappa)}{d\kappa^2} - \frac{1}{\left(\frac{3\kappa_D}{4} + 1\right)} \left[\frac{3}{4}(\kappa_D - \kappa) + \frac{1}{2} + \Theta_2^4 \left(\frac{3}{4}\kappa + \frac{1}{2} \right) \right] = 0 \quad (7-38)$$

which is to be solved subject to the boundary conditions $\Theta = 1$ at $\kappa = 0$ and $\Theta = \Theta_2$ at $\kappa = \kappa_D$. This relation gives the correct limiting diffusion solution for $N_1 \rightarrow 0$ and the correct conduction solution for $N_1 \rightarrow \infty$. Howell (ref. 14) has solved for $[\Theta(\kappa) - \Theta_2]/(1 - \Theta_2)$ numerically, using exchange factors from the numerical solutions of the pure radiation problem which are more accurate than the diffusion exchange factors used in equation (7-38). Agreement with the numerical solution of the coupled conduction-radiation problem is shown in figure 7-8.

The energy transfer by conduction was found by numerically evaluating $d\Theta/d\kappa|_{\kappa=0}$ and using this to evaluate the conduction flux at the boundary. The radiation flux was assumed to be unaffected by the conduction process in the spirit of the exchange factor approximation. The results obtained in this approximate way agree quite well with the numerical solution as shown in figure 7-6. Since $d\Theta/d\kappa$ varies with κ , while the radiative flux without conduction is constant with κ , evaluating $d\Theta/d\kappa$ at a location other than $\kappa = 0$ would give different results. For the most accurate

calculation of heat flux it was found (ref. 14) that the temperature gradient should be evaluated at the boundary with the highest temperature. Using the gradient at the coldest wall leads to a heat flux prediction that is always too large.

The exchange factor approximation is not limited to any range of geometry, surface emissivity, or optical thickness; it can be applied to any situation where the exchange factors have been previously obtained or where they can be obtained by some simplified pure radiation solution. The resulting nonlinear energy equation can usually be cast in the form of a matrix of nonlinear difference equations which are often easily solved by the numerical technique outlined by Ness (ref. 19). (See section 7.3.2, in vol. II.)

In situations where the boundaries are not the chief contributors to the radiant energy flux in the gas, then the gas temperature profile becomes important to the radiative flux distribution. In such a case the exchange factor approximation may become inaccurate; however, reference 14 does give results that compare well with exact numerical solutions for both energy transfer and temperature profiles in the geometries of parallel plates and concentric cylinders.

Lick (ref. 20) has also presented various approximations for solving conduction-radiation problems. He develops methods for treating gases with spectral and temperature-dependent properties. Goldstein and Howell (ref. 15) outline methods of treating temperature-dependent properties using the apparent slip technique.

Although numerical methods are the only way to obtain exact solutions to combined mode problems, the approximate methods outlined in this chapter should provide acceptable accuracy for most engineering problems. All the methods presented here can be applied to problems in two and three dimensions.

7.4 CONVECTION, CONDUCTION, AND RADIATION

The interaction of convection, conduction, and radiation in absorbing-emitting media occurs in many practical cases. Atmospheric phenomena, shock problems, rocket nozzles, industrial furnaces — all these and many more involve such interactions. As a consequence, a large amount of literature is available. Review articles and comprehensive books are given by references 13 and 21 to 25. In spite of this material, these problems remain difficult to solve. In this section, some of the methods used for these problems are outlined.

7.4.1 Boundary Layer Problems

A number of papers have appeared that deal with the effect of radiation on forced convection boundary layer heat transfer (refs. 26 to 30). Such boundary layer problems are approached by writing the usual continuity and momentum equations; these do not contain any radiation terms and are not influenced by heat transfer since constant fluid properties are assumed here. The energy equation is then written including an energy source term to account for the net thermal radiation gained by a volume element.

For a two-dimensional boundary layer flowing over a flat plate (fig. 7-9), assuming a gray fluid with constant properties, negligible viscous dissipation, and negligible radiative transport in the flow direction, the energy equation is

$$\rho c_p \left(u \frac{\partial T}{\partial x} + v \frac{\partial T}{\partial y} \right) = k \frac{\partial^2 T}{\partial y^2} - \frac{\partial q_r}{\partial y} \quad (7-39)$$

where q_r is the radiation flux in the positive y -direction shown in figure 7-9. The problem becomes one of introducing into equation (7-39) one of the formulations for q_r that have been developed, and then solving the resulting energy equation together with the momentum and continuity equations. In references 27 and 28, the diffusion solution is used for q_r and the last two terms in equation (7-39) can then be combined as was done in equation (7-23).

Various techniques can be used to solve the resulting energy equation. Novotny and Yang (ref. 26) used matched asymptotic expansions of the energy equation assuming a known flow field. A linearized energy equation near the surface was matched to an asymptotic solution far from the surface. Viskanta and Grosh (ref. 27) had earlier applied the diffusion approach; they assumed that the diffusion solution was valid all the way to the boundary.

Cess (ref. 28) and others have assumed the boundary layer to be optically thin, so that it emits but does not absorb radiation. By introducing some other assumptions, Cess was able to treat nongray gas effects. Neglecting absorbed radiation can be a useful approximation when the boundary layer is heated by frictional dissipation while surface and surrounding gas are cool.

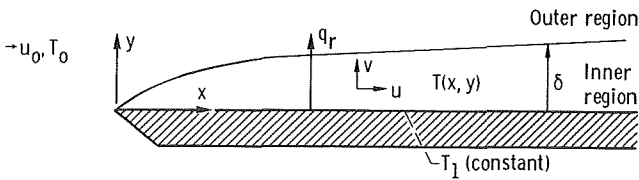


FIGURE 7-9.—Boundary layer flow over flat plate.

Fritsch, Grosh, and Wildin (ref. 29) studied the shielding of a body by a radiant absorbing layer. The boundary layer was assumed to absorb, but not to emit radiation. The effects of transpiration and an external radiation field were included. Howe (ref. 30) had treated a similar problem under somewhat different conditions of the external radiation field.

Novotny and Kelleher (ref. 31) and Cess (ref. 32) have examined the effect of radiation on the boundary layer development in free convection. An absorbing-emitting gas was treated and the radiation effects were linearized in both cases. Reference 31 treats the development of the boundary layer on a horizontal cylinder, while reference 32 examines the layer growth on a vertical plate. Gille and Goody (ref. 33) experimentally determined the onset of free convection in a gas exposed to thermal radiation.

7.4.1.1 *Optically thin thermal layer.*—Let us now consider in more detail the analysis for laminar forced flow on a flat plate. An expression is needed for the radiative source term $\partial q_r/\partial y$ in equation (7-39). Within the boundary layer type of assumptions it will be assumed that the thermal conditions are changing so slowly in the x -direction, as compared with the changes in the y -direction, that the region contributing to q_r at a specific x , say x^+ , are all at that x^+ and hence at temperatures $T(x^+, y)$. Then q_r can be evaluated from the one-dimensional relations derived previously as for equation (7-13). In equation (7-13) which is written for a region between two black walls and no convection, the conduction term is equal to the following (using y as the transverse coordinate):

$$k \frac{d^2 T}{dy^2} = 4a\sigma T^4 - 2a\sigma \left[T_1^4 E_2(\kappa) + T_2^4 E_2(\kappa_D - \kappa) + \int_0^{\kappa_D} T^4(\kappa^*) E_1(|\kappa - \kappa^*|) d\kappa^* \right] \quad (7-40)$$

The right side of equation (7-40) is thus the $\partial q_r/\partial y$ term when two walls are present. For one bounding wall, the T_2 term is not present and the upper limit of the integral is extended to infinity. Also the $T^4(\kappa^*)$ is replaced by $T^4(x, \kappa^*)$ to emphasize the approximation that, for the radiation term, the surroundings of position x are taken to be at $T(x, y)$. Then the boundary layer equation (7-39) becomes for the temperature $T(x, y)$

$$\rho c_p \left(u \frac{\partial T}{\partial x} + v \frac{\partial T}{\partial y} \right) = k \frac{\partial^2 T}{\partial y^2} - 4a\sigma T^4 + 2a\sigma \left[T_1^4 E_2(\kappa) + \int_0^{\infty} T^4(x, \kappa^*) E_1(|\kappa - \kappa^*|) d\kappa^* \right] \quad (7-41)$$

where $\kappa = ay$.

The temperature field can be considered as composed of two regions. Near the wall in the usual thermal boundary layer region of thickness δ that would be present in the absence of radiation, there are large temperature gradients and heat conduction is important. This region is usually of small thickness; hence, it can be assumed optically thin so that radiation will pass through it without attenuation. For larger y than this region, the temperature gradients are small and heat conduction is neglected compared with radiation transfer. The approximate analysis can now proceed, for example, along the path developed in reference 13.

In the outer region the velocity is the free stream value u_0 , and with the neglect of heat conduction the boundary layer equation reduces to

$$\rho c_p u_0 \frac{\partial T}{\partial x} = -4a\sigma T^4 + 2a\sigma \left[T_1^4 E_2(\kappa) + \int_0^\infty T^4(x, \kappa^*) E_1(|\kappa - \kappa^*|) d\kappa^* \right] \quad (7-42)$$

To obtain an approximate solution by iteration, substitute the incoming free stream temperature T_0 for the temperature on the right side as a first approximation and then carry out the integral to obtain a second approximation. This yields for the outer region to first-order terms

$$T(x, \kappa) = T_0 + \sigma(T_1^4 - T_0^4) E_2(\kappa) \left(\frac{2ax}{\rho c_p u_0} \right) + \dots \quad (7-43)$$

where at $x=0$, $T=T_0$.

At the edge of the thermal layer $\kappa = ay = a\delta$ which is small so that $E_2(a\delta) \approx E_2(0) = 1$. Hence, at $y = \delta$ equation (7-43) becomes

$$T(x, \delta) = T_0 + \sigma(T_1^4 - T_0^4) \left(\frac{2ax}{\rho c_p u_0} \right) + \dots \quad (7-44)$$

Equation (7-44) is the edge boundary condition that the outer radiation layer imposes on the inner thermal layer. The outer temperature is increasing linearly with x . This is the result of the flowing gas absorbing a net radiation from the plate in proportion to the difference $T_1^4 - T_0^4$ and the absorption coefficient a .

To solve the boundary layer equation in the inner thermal layer region, the last integral in equation (7-41) is divided into two parts, one from $\kappa=0$ to $a\delta$ and the second from $a\delta$ to ∞ . The first portion is neglected as the thermal layer is optically thin, and the second is evaluated by using the outer solution (eq. (7-43)). By retaining only first-order terms, the boundary layer equation reduces to

$$u \frac{\partial T}{\partial x} + v \frac{\partial T}{\partial y} = \alpha \frac{\partial^2 T}{\partial y^2} + \frac{2a\sigma}{\rho c_p} (T_1^4 + T_0^4 - 2T^4) \quad (7-45)$$

The boundary conditions are given by equation (7-44) at $y = \delta$, and the specified wall temperature $T = T_1$ at $y = 0$.

The solution becomes quite complex and will not be further developed here. The reader is referred to references 13 and 34 for additional information.

7.4.1.2 *Optically thick thermal layer.*—At the opposite extreme from the previous section, if the thermal layer has become very thick or the medium is highly absorbing, then the boundary layer would be optically thick. In this instance the analysis is considerably simplified as the diffusion approximation can be employed. Referring to equation (7-23) it is recalled that radiative diffusion adds a radiative conductivity to the ordinary thermal conductivity. Then the boundary layer energy equation (7-39) can be written as

$$\rho c_p \left(u \frac{\partial T}{\partial x} + v \frac{\partial T}{\partial y} \right) = \frac{\partial}{\partial y} \left[\left(\frac{16\sigma T^3}{3a_R} + k \right) \frac{\partial T}{\partial y} \right] \quad (7-46)$$

With the assumption of constant fluid properties, the boundary layer momentum equation and the continuity equation do not depend on temperature. Consequently, the flow is unchanged by the heat transfer, and velocity distribution is given by the Blasius solution (ref. 35). The Blasius solution is in terms of a similarity variable

$$\eta = y \sqrt{u_0/\nu x}$$

and the stream function and velocity components are given by

$$\begin{aligned} \psi &= \sqrt{\nu x u_0} f(\eta) \\ u &= \frac{\partial \psi}{\partial y} = u_0 \frac{df}{d\eta} \\ v &= -\frac{\partial \psi}{\partial x} = \frac{1}{2} \sqrt{\frac{\nu u_0}{x}} \left(\eta \frac{df}{d\eta} - f \right) \end{aligned}$$

These quantities are substituted into the energy equation which can then be placed in the form

$$-\frac{Pr}{2} \left(f \frac{dT}{d\eta} \right) = \frac{d}{d\eta} \left[\left(\frac{16\sigma T^3}{3a_R k} + 1 \right) \frac{dT}{d\eta} \right] \quad (7-47)$$

The boundary conditions that have been used are

$$T = T_1 \quad \text{at } \eta = 0$$

$$T = T_0 \quad \text{at } \eta = \infty$$

To be more precise, a diffusion-slip condition should be used at the wall but this has not been formulated for the combined radiation, convection, and conduction situation.

Let $\Theta = T/T_0$ and $N_0 = ka_R/4\sigma T_0^3$; then equation (7-47) becomes

$$-\frac{Pr}{2} \left(f \frac{d\Theta}{d\eta} \right) = \frac{d}{d\eta} \left[\left(\frac{4\Theta^3}{3N_0} + 1 \right) \frac{d\Theta}{d\eta} \right] \quad (7-48)$$

Numerical solutions were carried out in reference 27, and some typical temperature profiles are shown in figure 7-10. For $N_0 = 10$ the profile was found to be within 2 percent of that for conduction and convection alone (i.e., for $N_0 \rightarrow \infty$). The effect of radiation is found to thicken the thermal boundary layer similar to the effect of decreasing the Prandtl number. This would be expected since Prandtl number is the ratio of viscous to thermal diffusion ν/α . The radiation has supplied an additional means for thermal diffusion thereby effectively increasing the α .

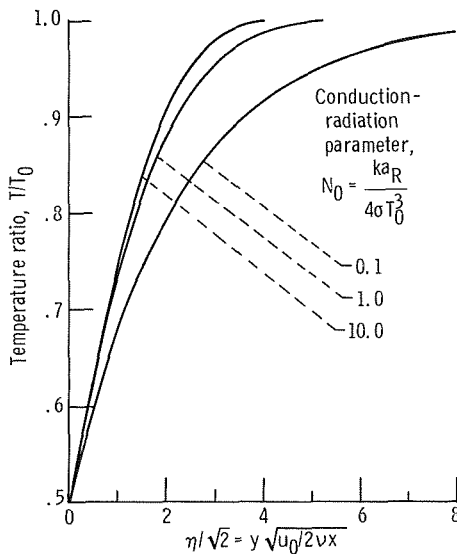


FIGURE 7-10.—Boundary layer temperature profiles for laminar flow on flat plate (ref. 27). Prandtl number $Pr = 1.0$; temperature ratio $T_1/T_0 = 0.5$.

7.4.2 Channel Flows

Of engineering interest in some high temperature heat exchange devices is the flow of an absorbing-emitting gas in a channel with radiative and convective energy transfer. The energy equation (7-39) (with $v=0$ for fully developed flow) still applies at all points in the flow. References 12 and 36 to 39 treat problems with varying degrees of approximation. Viskanta (ref. 36) gives approximate numerical solutions to the equations for laminar flow of a gray absorbing-emitting medium in a parallel plate channel. Temperature-independent properties are assumed. In addition to κ_D , N , and temperature ratios, a new parameter enters these problems. It is a Nusselt number which is defined in such a way as to include a radiative contribution and thus differs from the usual definition.

Einstein (refs. 12 and 37) has applied the gas-to-surface and gas-to-gas view factor methods of Hottel (section 5.8.2) to a solution of the energy equation in a parallel plate channel and in a circular tube. Both channels were of finite length, and internal heat generation in the gas was included. Comparison was made with the work of Adrianov and Shorin (ref. 38), who had used the cold material approximation (section 3.3.3) so that absorption but not emission from the gas was included. Chen (ref. 39) included scattering in his analysis of flow between parallel plates, but assumed a slug flow velocity profile.

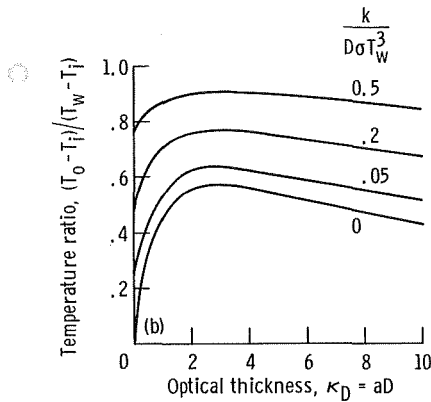
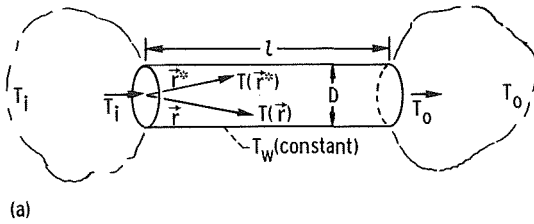
All the previous analyses mentioned in this section have been for gray gases flowing in channels with gray or black walls. All have assumed temperature-independent properties. However, deSoto and Edwards (ref. 40) have presented a tube flow heat transfer analysis that accounts for nongray gases with temperature-dependent properties. An exponential band model (section 4.6.4) was employed to account for the spectral effects. Entrance region flows were included.

Landram et al. (ref. 41) examined fully developed turbulent pipe flow of an optically thin gas, using Planck and incident mean absorption coefficients. The application of Monte Carlo methods to some channel flow problems was discussed in chapter 6.

To examine a specific situation, consider the analysis of Einstein (ref. 37) for flow in a tube of diameter D as shown in figure 7-11(a). Gas enters the tube at temperature T_i and leaves at T_o . The tube wall temperature is constant at T_w . The surrounding environments at the inlet and exit ends of the tube are assumed to be at the inlet and exit gas temperatures, respectively. The governing energy equation at position \bar{r} in the tube for laminar flow can be written as

$$\rho c_p u \frac{\partial T}{\partial x} \Big|_{\vec{r}} = \frac{k}{r} \left[\frac{\partial}{\partial r} \left(r \frac{\partial T}{\partial r} \right) \right] \Big|_{\vec{r}} - 4a\sigma T^4(\vec{r}) + a \left[\int \int \int_V \sigma T^4(\vec{r}^*) f(\vec{r}^* - \vec{r}) dV + \int \int_S \sigma T_s^4(\vec{r}^*) g(\vec{r}^* - \vec{r}) dS \right] \quad (7-49)$$

The triple integral is the radiation absorbed at \vec{r} as a result of emission from all the other gas in the tube. The $f(\vec{r}^* - \vec{r})$ is a gas-to-gas exchange factor from position \vec{r}^* to position \vec{r} . The double integral is the radiation absorbed at \vec{r} as a result of emission from the boundaries which include the tube wall and the end planes of the tube. The



(a) Tube geometry and boundary conditions.

(b) Exit temperature for $T_i/T_w = 0.4$, $l/D = 5$, and $\rho c_p u / \sigma T_w^3 = 33$.

FIGURE 7-11.— Combined radiation and convection for absorbing gas flowing in tube with constant wall temperature (ref. 37).

$g(\bar{r}^* - \bar{r})$ is a surface-to gas exchange factor, and the f and g are given in reference 37.

Some typical results of the numerical solution are given in figure 7-11(b) for a Poiseuille flow velocity profile. These results show how well the gas obtains energy from the wall since the ordinate is a measure of how close the exit gas approaches to the wall temperature. The results are given in terms of gas optical thickness based on tube diameter and a conduction-radiation parameter based on wall temperature. As the optical thickness is increased from zero, the amount of radiated energy from the wall that is absorbed by the gas increases to a maximum value. Then for a large κ_D the heat absorbed by the gas decreases. The decrease is caused by the self-shielding of the gas; for high κ_D most of the direct radiation from the tube wall is absorbed in a thin gas layer near the wall. Since the gas emission is isotropic, about one-half of the energy reemitted by this thin layer goes back toward the wall. Thus the gas in the center of the tube is shielded from the direct radiation and the heat transfer efficiency decreases.

7.4.3 Other Multimode Problems

Radiation effects in rocket exhaust plumes have been examined by deSoto (ref. 42). Kadanoff (ref. 4) treated radiation effects in ablating bodies. A very large body of literature exists that deals with reentry of bodies into the atmosphere (ref. 43) and radiation within and from hypersonic shocks. A rigorous treatment of these problems is difficult because of the nonequilibrium chemical reactions that are coupled with the radiation effects. References 43 and 22 to 25 give a good introduction and discussion of shock problems. Radiation interactions with a layer of gas including transpiration is treated in reference 44.

7.5 CONCLUDING REMARKS

The treatment of multimode problems in absorbing-emitting media can be viewed as solving conduction or convection problems with a distributed energy source (or sink) term present. This source (or sink) term is the local net radiation gain (or loss) within the medium. The radiative source term can be determined by either exact or whatever approximate methods can be applied in a given situation. Cases were mentioned in this chapter where exact, diffusion, additive, and optically thin formulations were used. As with almost all radiation problems, the basic equations describing the physical processes can usually be written. The difficulty is in solving these equations. It is not possible to discuss in detail the wide variety of physical situations and solution

methods that can be found in the literature. A number of references have been provided in this chapter to help guide the reader to some of the pertinent basic information.

REFERENCES

1. KELLETT, B. S.: Transmission of Radiation Through Glass in Tank Furnaces. *J. Soc. Glass Tech.*, vol. 36, 1952, pp. 115-123.
2. GARDON, ROBERT: The Emissivity of Transparent Materials. *J. Am. Cer. Soc.*, vol. 39, no. 8, Aug. 1956, pp. 278-287.
3. CONDON, EDWARD U.: Radiative Transport in Hot Glass. *J. Quant. Spectrosc. Radiat. Transfer*, vol. 8, no. 1, 1968, pp. 369-385.
4. KADANOFF, LEO P.: Radiative Transport Within an Ablating Body. *J. Heat Transfer*, vol. 83, no. 2, May 1961, pp. 215-225.
5. MERRIAM, R. L.; AND VISKANTA, R.: Radiative Characteristics of Cryodeposits for Room Temperature Black Body Radiation. Presented at the Cryogenic Engineering Conference, Case-Western Reserve Univ., Cleveland, Ohio, Aug. 1968.
6. MCCONNELL, DUDLEY G.: Radiant Energy Transport Within Cryogenic Condensates. Presented at the Institute of Environmental Sciences Annual Meeting and Equipment Exposition, San Diego, Calif., Apr. 11-13, 1966.
7. VISKANTA, R.; AND GROSH, R. J.: Heat Transfer by Simultaneous Conduction and Radiation in an Absorbing Medium. *J. Heat Transfer*, vol. 84, no. 1, Feb. 1962, pp. 63-72.
8. VISKANTA, R.; AND GROSH, R. J.: Effect of Surface Emissivity on Heat Transfer by Simultaneous Conduction and Radiation. *Int. J. Heat Mass Transfer*, vol. 5, Aug. 1962, pp. 729-734.
9. VISKANTA, R.; AND MERRIAM, R. L.: Heat Transfer by Combined Conduction and Radiation Between Concentric Spheres Separated by Radiating Medium. *J. Heat Transfer*, vol. 90, no. 2, May 1968, pp. 248-256.
10. GREIF, RALPH; AND CLAPPER, GEAN P.: Radiant Heat Transfer Between Concentric Cylinders. *Appl Sci. Res., Sec. A*, vol. 15, 1966, pp. 469-474.
11. TIMMONS, D. H.; AND MINGLE, J. O.: Simultaneous Radiation and Conduction with Specular Reflection. Paper 68-28, AIAA, Jan. 1968.
12. EINSTEIN, THOMAS H.: Radiant Heat Transfer to Absorbing Gases Enclosed Between Parallel Flat Plates with Flow and Conduction. NASA TR R-154, 1963.
13. CESS, R. D.: The Interaction of Thermal Radiation With Conduction and Convection Heat Transfer. *Advances in Heat Transfer*. Vol. I. Thomas F. Irvine, Jr., and James P. Hartnett, eds., Academic Press, 1964, pp. 1-50.
14. HOWELL, JOHN R.: Determination of Combined Conduction and Radiation of Heat Through Absorbing Media by the Exchange Factor Approximation. *Chem. Eng. Progr. Symp. Ser.*, vol. 61, no. 59, 1965, pp. 162-171.
15. GOLDSTEIN, MARVIN; AND HOWELL, JOHN R.: Boundary Conditions for the Diffusion Solution of Coupled Conduction-Radiation Problems. NASA TN D-4618, 1968.
16. HOWELL, J. R.; AND GOLDSTEIN, M. E.: Effective Slip Coefficients for Coupled Conduction-Radiation Problems. *J. Heat Transfer*, vol. 91, no. 1, Feb. 1969, pp. 165-166.
17. TAITEL, YEHUDA; AND HARTNETT, J. P.: Application of Rosseland Approximation and Solution Based on Series Expansion of the Emission Power to Radiation Problems. *AIAA J.*, vol. 6, no. 1, Jan. 1968, pp. 80-89.
18. WANG, L. S.; AND TIEN, C. L.: A Study of Various Limits in Radiation Heat-Transfer Problems. *Int. J. Heat Mass Transfer*, vol. 10, no. 10, Oct. 1967, pp. 1327-1338.

19. NESS, A. J.: Solution of Equations of a Thermal Network on a Digital Computer. *Solar Energy*, vol. 3, no. 2, 1959, p. 37.
20. LICK, WILBERT: Energy Transfer by Radiation and Conduction. Proceedings of the 1963 Heat Transfer and Fluid Mechanics Institute. Anatol Roshko, Bradford Sturtevant, and D. R. Bartz, eds., Stanford University Press, 1963, pp. 14-26.
21. VISKANTA, R.: Radiation Transfer and Interaction of Convection with Radiation Heat Transfer. *Advances in Heat Transfer*. Vol. 3. Thomas F. Irvine, Jr., and James P. Hartnett, eds., Academic Press, 1966, pp. 175-251.
22. PAI, SHIH-I: *Radiation Gas Dynamics*. Springer-Verlag, 1966.
23. BOND, JOHN W., JR.; WATSON, KENNETH M.; AND WELCH, JASPER A., JR.: *Atomic Theory of Gas Dynamics*. Addison-Wesley Publ. Co., 1965, chs. 10-13.
24. ZEL'DOVICH, YA. B.; AND RAIZER, YU. P.: *Physics of Shock Waves and High-Temperature Hydrodynamic Phenomena*. Vol. I, Academic Press, 1966, Pt. II.
25. VINCENTI, WALTER G.; AND KRUGER, CHARLES H., JR.: *Introduction to Physical Gas Dynamics*. John Wiley & Sons, Inc., 1965, chs. 11-12.
26. NOVOTNY, J. L.; AND YANG, KWANG-TZU: The Interaction of Thermal Radiation in Optically Thick Boundary Layers. *J. Heat Transfer*, vol. 89, no. 4, Nov. 1967, pp. 309-312.
27. VISKANTA, R.; AND GROSH, R. J.: Boundary Layer in Thermal Radiation Absorbing and Emitting Media. *Int. J. Heat Mass Transfer*, vol. 5, Sept. 1962, pp. 795-806.
28. CESS, R. D.: Radiation Effects Upon Boundary-Layer Flow of an Absorbing Gas. *J. Heat Transfer*, vol. 86, no. 4, Nov. 1964, pp. 469-475.
29. FRITSCH, C. A.; GROSH, R. J.; AND WILDIN, M. W.: Radiative Heat Transfer Through an Absorbing Boundary Layer. *J. Heat Transfer*, vol. 88, no. 3, Aug. 1966, pp. 296-304.
30. HOWE, JOHN T.: Radiation Shielding of the Stagnation Region by Transpiration of an Opaque Gas. NASA TN D-329, 1960.
31. NOVOTNY, J. L.; AND KELLEHER, M. D.: Free-Convection Stagnation Flow of an Absorbing-Emitting Gas. *Int. J. Heat Mass Transfer*, vol. 10, no. 9, Sept. 1967, pp. 1171-1178.
32. CESS, R. D.: The Interaction of Thermal Radiation with Free Convection Heat Transfer. *Int. J. Heat Mass Transfer*, vol. 9, no. 11, Nov. 1966, pp. 1269-1277.
33. GILLE, JOHN; AND GOODY, RICHARD: Convection in a Radiating Gas. *J. Fluid Mech.*, vol. 20, pt. 1, Sept. 1964, pp. 47-79.
34. CESS, ROBERT D.: The Interaction of Thermal Radiation in Boundary Layer Heat Transfer. Third International Heat Transfer Conference. Vol. 5. AIChE, 1966, pp. 154-163.
35. SCHLICHTING, HERMANN (J. KESTIN, TRANS.): *Boundary Layer Theory*. Fourth ed., McGraw-Hill Book Co., Inc., 1960, p. 116.
36. VISKANTA, R.: Interaction of Heat Transfer by Conduction, Convection, and Radiation in a Radiating Fluid. *J. Heat Transfer*, vol. 85, no. 4, Nov. 1963, pp. 318-328.
37. EINSTEIN, THOMAS H.: Radiant Heat Transfer to Absorbing Gases Enclosed in a Circular Pipe with Conduction, Gas Flow, and Internal Heat Generation. NASA TR R-156, 1963.
38. ADRIANOV, V. N.; AND SHORIN, S. N.: Radiative Transfer in the Flow of a Radiating Medium. *Trans. TT-1*, Purdue University, Feb. 1961.
39. CHEN, JOHN C.: Simultaneous Radiative and Convective Heat Transfer in an Absorbing, Emitting, and Scattering Medium in Slug Flow Between Parallel Plates. Rep. BNL-6876-R, Brookhaven National Lab., Mar. 18, 1963.

40. DESOTO, SIMON; AND EDWARDS, D. K.: Radiative Emission and Absorption in Nonisothermal Nongray Gases in Tubes. Proceedings of the Proc. 1965 Heat Transfer and Fluid Mechanics Institute. A. F. Charwat, ed., Stanford Univ. Press, 1965, pp. 358-372.
41. LANDRAM, C. S.; GREIF, R.; AND HABIB, I. S.: Heat Transfer in Turbulent Pipe Flow with Optically Thin Radiation. *J. Heat Transfer*, vol. 91, no. 3, Aug. 1969, pp. 330-336.
42. DESOTO, SIMON: The Radiation from an Axisymmetric, Real Gas System with a Nonisothermal Temperature Distribution. *Chem. Eng. Progr. Symp. Ser.*, vol. 61, no. 59, 1965, pp. 138-154.
43. PENNER, S. S.; AND OLFE, D. B.: *Radiation and Reentry*. Academic Press, 1968.
44. VISKANTA, R.; AND MERRIAM, R. L.: Shielding of Surfaces in Couette Flow Against Radiation by Transpiration of an Absorbing-Emitting Gas. *Int. J. Heat Mass Transfer*, vol. 10, no. 5, May 1967, pp. 641-653.

Chapter 8. Radiative Transfer in Scattering and Absorbing Media

8.1 INTRODUCTION

The extinction coefficient K for thermal radiation is composed of an absorption coefficient and a scattering coefficient as discussed in section 1.5.1. The equation of transfer when only absorption is present was treated in chapter 2. In this chapter extension is made to treating radiative transfer for cases where the scattering phenomenon becomes important. The elastic scattering processes are considered that are important insofar as radiative transfer calculations are concerned. Effects of polarization and the various inelastic scattering processes are only mentioned in passing. These processes along with other scattering effects are found in the more comprehensive treatments of scattering problems in references 1 to 6. The work of Van der Hulst (ref. 1) is especially valuable in giving a detailed discussion of elastic scattering from single particles.

When radiation impinges upon any substance, a part of the energy is removed by absorption, and another part is redirected by scattering. Scattering may occur from particles or objects of any size from electrons to planets, and scattering from particles or objects in each size range can be important in special situations. For elastic scattering the photon energy and therefore the frequency of the photon is unchanged by the scattering; for inelastic scattering the photon energy is changed.

In theoretical developments scattering is usually considered for a single particle. When a cloud of many particles is dealt with, the scattering intensities from the individual particles are usually added, thereby assuming that each particle scatters independently. This is a valid assumption if the particles are more than a few diameters apart. In most practical situations this assumption can be made as the particles are separated by much larger distances.

There are various phenomena that may occur when incident radiation strikes a particle. Some of the incident radiation may be reflected from the particle surface. The remaining portion of the radiation will penetrate into the particle where part of the radiation can be absorbed. If the particle is not a strong internal absorber, some of this radiation will pass back out. This may occur after traveling only a single path through the particle or the radiation may undergo multiple internal reflections and travel about within the particle before escaping. When interacting with the particle boundary, the radiation will be refracted and will also have

its direction changed by subsequent internal reflections. The redirection by these processes of the energy penetrating into the particle and then escaping is termed scattering by refraction. Additional scattering is caused by diffraction which produces, for example, the interference patterns observed when light passes through an aperture in a screen. Diffraction is the result of slight bending of the radiation propagation paths when passing near the edges of an obstruction.

The reflection, refraction, and diffraction depend on the optical properties (i.e., the complex refractive index $\bar{n}=n-i\kappa$) of the particle, and of the size of the particle relative to the wavelength of the incident radiation. An additional complication is the particle geometry. It is usually assumed that the medium surrounding the particles has a unity simple refractive index n and a zero extinction coefficient κ so that $\bar{n}=n-i0=1$. In this instance the surrounding medium does not enter into the optical behavior of the medium-particle system.

In principle the scattering behavior can be obtained from the solution of the Maxwell electromagnetic equations that govern the radiation field for the medium-particle system. However, the solution provides very complicated relations for even simple particle geometries. Hence in many instances a number of simplifications are made as will now be outlined.

One simplification is the geometric one of letting the scattering particles be spheres. This is not as restrictive an assumption as it might appear since, as discussed in reference 1, the results for spheres do have a wider geometric applicability. Consider an array of irregularly shaped particles, the surfaces of which are assumed composed of convex portions (no concave indentations). Because the particles are in a random orientation, an equal portion of surface elements will face each angular direction, which is the same angular distribution of surface elements as for a spherical particle. The net result is that the angular distribution of scattered radiation viewed at a distance from the actual particles will be the same as that scattered from spherical particles.

A second simplification is to consider the limiting solutions for scattering from large and from small spheres. A convenient parameter is $\pi D/\lambda$ where D is the sphere diameter. For large spheres ($\pi D/\lambda$ greater than about 5) the scattering is chiefly a reflection process and hence can be calculated from relatively simple geometrical reflection relations. There is also diffraction of the radiation passing near the sphere, but this is accounted for separately as will be discussed in section 8.4.4. For small spheres ($\pi D/\lambda$ less than about 0.6), the approximation of Rayleigh scattering can be used as will be discussed in section 8.4.5. For the intermediate range of $\pi D/\lambda$, the general Mie scattering results apply, but the results of this general solution of Maxwell's equations are quite complicated.

A third type of simplification is to look at limiting cases of the optical constants of the particle. For metals the n and κ are often large so the case can be considered where $\bar{n} = n - i\kappa \rightarrow \infty$. For a dielectric ($\kappa = 0$) a limiting case is where $n \approx 1$. In this instance the reflectivity of the particle surface will be small.

Limiting types of surface conditions are also considered (i.e., specular and diffuse surfaces). The particle surface can only act diffuse, however, if its dimensions are large compared with the wavelength of the incident radiation.

The theory and results will be discussed for several of the more useful scattering relations.

8.2 SYMBOLS

A	area
a	absorption coefficient
c	speed of light in medium
c_0	speed of light in vacuum
D	particle diameter
e	emissive power; electron charge
$G(\bar{n})$	function of \bar{n} in Rayleigh scattering relation, eq. (8-23)
H	distance defined in connection with eq. (8-54)
I	radiative source function, eq. (8-51)
i	radiation intensity
J_1	Bessel function of first kind of order one
K	extinction coefficient, $a + \sigma_s$
l_m	extinction mean free path
m_e	mass of electron
N	number density, particles per unit volume
n	simple refractive index
\bar{n}	complex refractive index, $n - i\kappa$
Q	energy per unit time
q	energy flux, energy per unit area and time
R	radius
r_0	classical electron radius
S	coordinate along path of radiation
s	scattering cross section
T	absolute temperature
V	volume
W	parameter in eq. (8-21)
x	coordinate direction normal to plane layer
α_p	polarizability
β	cone angle, angle from normal of area
θ	circumferential angle

κ	optical depth; extinction coefficient in complex refractive index
λ	wavelength
μ	$\cos \beta$
ν	frequency
ρ	reflectivity
σ_s	scattering coefficient
Φ	phase function for single scattering
φ	scattering angle measured from forward direction to direction to observer
ψ	spherical angle in fig. 8-4
Ω_0	albedo for single scattering, eq. (8-48)
ω	solid angle

Subscripts:

b	black
D	at position coordinate D
i	incident
p	particle; projected
s	scattered or scattering
λ	spectrally dependent
+	propagating in direction having positive $\cos \beta$
-	propagating in direction having negative $\cos \beta$
1, 2	refers to surfaces 1 or 2

Superscripts:

'	directionally dependent quantity
*	dummy variable of integration
(0), (1), (2)	zeroth-, first-, or second-order term or moment

8.3 SOME IMPORTANT QUANTITIES IN THE DESCRIPTION OF SCATTERING

8.3.1 The Scattering Cross Section

The extent of scattering to be expected is often measured in terms of the *scattering cross section* s . This is the apparent area that an object presents to an incident beam insofar as the ability of the object to deflect radiation from the beam is concerned. It is usually given in square centimeters for thermal radiation properties. This apparent area may be quite different from the physical cross-sectional area of the scatterers as can be seen from some of the approximate cross sections in table 8-1. In addition to depending on the particle size, the scattering cross section may depend upon the shape and material of the scattering body,

TABLE 8-I.—APPROXIMATE CROSS SECTIONS FOR VARIOUS BODIES EXPOSED TO INCIDENT PHOTONS

Body	Physical cross section, cm ²	Conditions	Type of scattering	Scattering cross section, cm ²	
Photon	Energy of incident photon small	$\sim 2 \times 10^{-36}$	
Free electron	Energy of photon \ll electron kinetic energy	Thomson	$\frac{8}{3} \pi r_0^2 = 6.65 \times 10^{-25} \equiv \sigma_T$	
		Energy of photon \gg electron kinetic energy	Compton	$\frac{3}{8} \sigma_T \frac{1}{\epsilon_p} \left(\frac{1}{2} + \ln 2\epsilon_p \right)$	
Atom or molecule	0.88×10^{-16} (first Bohr electron orbit)	Elastic, $\lambda \gg$ size of molecule or atom	Rayleigh	Proportional to $\sim 6.65 \times 10^{-25} / \lambda^4$	
		Inelastic	Energy of incident photon \gg electronic binding energy	Rayleigh, approaches Thomson	$\sim 6.65 \times 10^{-25}$
			Energy of incident photon \ll electronic binding energy	Raman	$\sim 6.65 \times 10^{-25}$
Particles of diameter D	$\frac{\pi D^2}{4}$	$\lambda \gg D$, single scattering	Approaches Compton	$\frac{3}{8} \sigma_T \frac{1}{\epsilon_p} \left(\frac{1}{2} + \ln 2\epsilon_p \right)$	
			Rayleigh	Proportional to V^2 / λ^4	
		$\lambda \approx D$	Mie	Varies widely	
		$\lambda \ll D$	Fraunhofer and Fresnel diffraction plus reflection	$\sim 2 \left(\frac{\pi D^2}{4} \right)$	

* r_0 = classical electron radius, 2.818×10^{-13} cm; $\epsilon_p = h\nu/m_e c^2$ where h is Planck's constant; σ_T = cross section for Thomson scattering; m_e = electron mass, 9.108×10^{-31} g.

and the wavelength, polarization, and coherence of the incident radiation.

The scattering cross section can be determined experimentally by measuring the amount of radiation in a beam that is able to penetrate through a cloud of scattering particles. One experimental difficulty is in separating the radiation that is scattered into the forward direction from the radiation that is transmitted without any particle interaction. This difficulty can be diminished by using an incident beam with a very small divergence angle. Then the forward direction of the transmitted radiation will encompass only a small solid angle which will include only a small portion of scattered radiation. The ratio of the scattered portion $di'_{\lambda, s}$ of the incident intensity to the intensity i'_λ of the incident beam is equal to the ratio of the apparent projected scattering area $dA_{s\lambda}$ occupied by all scattering particles, to the cross-sectional area of the incident beam dA . This gives the following for a beam traveling a differential distance within a medium in which it encounters the scattering area $dA_{s\lambda}$:

$$\frac{di'_{\lambda, s}}{i'_\lambda} = \frac{dA_{s\lambda}}{dA} \quad (8-1)$$

Note that the apparent projected scattering area of the particles can and usually will depend on wavelength.

The apparent scattering area presented by a group of the scattering particles is related to the average scattering areas of the individual particles by

$$dA_{s\lambda} = s_\lambda N_s dV = s_\lambda N_s dA dS \quad (8-2)$$

where N_s is the number density of the particles, s_λ is the average scattering cross section of the particles, and dV is a differential volume of the particle containing cloud as shown in figure 8-1. Inserting equation (8-2) into equation (8-1) gives the change di'_λ of the intensity as a result of scattering from the incident beam

$$-\frac{di'_\lambda}{i'_\lambda} = \frac{di'_{\lambda, s}}{i'_\lambda} = \frac{s_\lambda N_s dA dS}{dA} = s_\lambda N_s dS \quad (8-3)$$

There is also intensity scattered into the S direction which will contribute to di'_λ but this will be incorporated later.

By integrating equation (8-3) over a path from 0 to S , the intensity is found at S as a result of attenuation by scattering from the beam with original intensity $i'_\lambda(0)$,

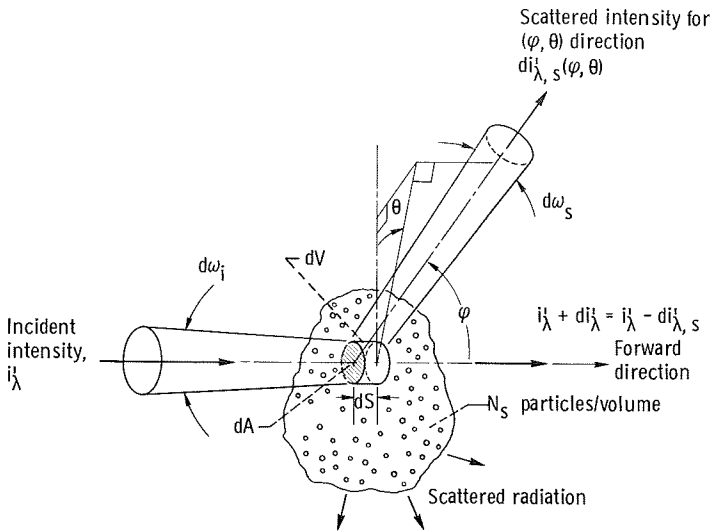


FIGURE 8-1.—Scattering of intensity into direction (φ, θ) from incident radiation within solid angle $d\omega_i$.

$$i'_\lambda(S) = i'_\lambda(0) \exp\left(-\int_0^S s_\lambda N_s dS^*\right) \tag{8-4a}$$

The portion of the incident intensity that was scattered away along the path is thus

$$i'_\lambda(0) - i'_\lambda(S) = i'_\lambda(0) \left[1 - \exp\left(-\int_0^S s_\lambda N_s dS^*\right)\right] \tag{8-4b}$$

The *scattering coefficient* $\sigma_{s\lambda}$ is now defined to be

$$\sigma_{s\lambda} \equiv s_\lambda N_s \tag{8-5}$$

so that equation (8-4a) becomes

$$i'_\lambda(S) = i'_\lambda(0) \exp\left[-\int_0^S \sigma_{s\lambda}(S^*) dS^*\right] \tag{8-6}$$

This is the pure scattering form of Bouguer's law (see section 1.5).

If there is a distribution of particle sizes to be considered in detail, the preceding analysis can be generalized. Let $N_s(R)dR$ be the number of particles per unit volume in the radius range from R to $R + dR$ and let $s_\lambda(R)$ be the scattering cross section for a particle of radius R . Then by

integrating over all the particles, the scattering coefficient is

$$\sigma_{s\lambda} = \int_{R=0}^{\infty} s_{\lambda}(R) N_s(R) dR \quad (8-7)$$

As in the interpretation of the extinction coefficient (section 1.5.2), the scattering coefficient $\sigma_{s\lambda}$ can be regarded as the reciprocal of the mean free path that the radiation will traverse before being scattered. The $\sigma_{s\lambda}$ is thus a reciprocal length, and can be regarded as a scattering area per volume along the path, $\sigma_{s\lambda} = dA_{s\lambda}/dV$ from equations (8-5) and (8-2). Since s_{λ} is $\sigma_{s\lambda}/N_s$, it is the effective scattering area per particle. The ratio of s_{λ} to the actual geometric projected area of the particle normal to the incident beam is termed the *efficiency factor*.

At particle densities near or below the molecular density of air at 1 atm ($N_s \approx 2.7 \times 10^{19}$ particles/cm³), it can be seen that for most of the processes listed in table 8-1 the scattering coefficient will be very small (and thus the scattering mean free path very long). This is especially true for photon-photon, Thomson, and Raman scattering, which may generally be ignored in engineering radiative transfer calculations.

The previous relations have been concerned with what portion of the intensity in an incident beam is lost as a result of being scattered away along a path. The additional information that will be required to formulate radiative transfer relations for scattering media is the directional distribution of the scattered radiation. This is given in terms of an angularly dependent phase function.

8.3.2 The Phase Function

Consider the radiation within solid angle $d\omega_i$ that is incident on area dA in figure 8-1. The entire portion of the incident intensity that is scattered away in the distance dS is given by equations (8-3) and (8-5) as

$$di'_{\lambda, s} = \sigma_{s\lambda} i'_{\lambda} dS \quad (8-8)$$

The $di'_{\lambda, s}$ is the spectral energy scattered within path dS per unit incident solid angle and area normal to the incident beam

$$di'_{\lambda, s} = \frac{d^4 Q'_{\lambda, s}}{d\omega_i dA d\lambda} \quad (8-9)$$

As shown by figure 8-1 the scattered energy produces an intensity distribution as a function of angles θ and φ measured relative to the forward

direction. A phase function $\Phi(\varphi, \theta)$ will be defined to describe the scattered angular distribution.

The scattered intensity in any direction (φ, θ) is defined as the energy scattered in that direction per unit solid angle of the scattered direction and per unit area and solid angle of the incident radiation; that is,

$$di'_{\lambda, s}(\varphi, \theta) = \frac{\text{spectral energy scattered in direction } (\varphi, \theta)}{d\omega_s dA d\omega_i d\lambda} = \frac{d^5 Q'_{\lambda, s}(\varphi, \theta)}{d\omega_s dA d\omega_i d\lambda} \quad (8-10)$$

The directional magnitude of $di'_{\lambda, s}(\varphi, \theta)$ is related to the entire intensity $di'_{\lambda, s}$ scattered away from the incident radiation by the phase function, such that

$$di'_{\lambda, s}(\varphi, \theta) = di'_{\lambda, s} \frac{\Phi(\varphi, \theta)}{4\pi} = \sigma_{\lambda s} i'_{\lambda} dS \frac{\Phi(\varphi, \theta)}{4\pi} \quad (8-11)$$

To better understand the phase function, note that the spectral energy per $d\lambda$ scattered into $d\omega_s$ per unit $d\omega_i$ and unit dA is $di'_{\lambda, s}(\varphi, \theta)d\omega_s$. Then the spectral energy per unit $d\omega_i$, unit dA and $d\lambda$ scattered into all $d\omega_s$ is $\int_{\omega_s=4\pi} di'_{\lambda, s}(\varphi, \theta)d\omega_s$. However, the scattered energy per unit $d\omega_i$, dA , and $d\lambda$ is $di'_{\lambda, s}$ so that

$$di'_{\lambda, s} = \int_{\omega_s=4\pi} di'_{\lambda, s}(\varphi, \theta)d\omega_s \quad (8-12)$$

Using equation (8-11) results in

$$di'_{\lambda, s}(\varphi, \theta) = \frac{\Phi(\varphi, \theta)}{4\pi} \int_{\omega_s=4\pi} di'_{\lambda, s}(\varphi, \theta)d\omega_s$$

which gives the phase function as

$$\Phi(\varphi, \theta) = \frac{di'_{\lambda, s}(\varphi, \theta)}{\frac{1}{4\pi} \int_{\omega_s=4\pi} di'_{\lambda, s}(\varphi, \theta)d\omega_s} \quad (8-13)$$

Thus, $\Phi(\varphi, \theta)$ has the physical interpretation of being the scattered intensity in a direction divided by the intensity that would be scattered in that direction if the scattering were isotropic. For isotropic

scattering then, $\Phi = 1$. By integrating equation (8-13) over all $d\omega_s$, it is evident that $\Phi(\varphi, \theta)$ is a normalized function such that

$$\frac{1}{4\pi} \int_{\omega_s=4\pi} \Phi(\varphi, \theta) d\omega_s = 1 \quad (8-14)$$

The phase function can be a complicated function of φ and θ as will be shown in subsequent sections.

8.4 SCATTERING FROM VARIOUS TYPES OF PARTICLES

8.4.1 A Cloud of Large Specularly Reflecting Spheres

One of the most simple scattering configurations is a cloud of large spherical particles ($\pi D/\lambda > \sim 5$) that have specularly reflecting surfaces. Figure 8-1 shows a differential volume element of the cloud with cross section dA normal to the incident radiation and with thickness dS . The incident energy intercepted by the volume element is $i'_\lambda d\omega_i dA$. It is assumed that the particle density is low enough so that each particle scatters independently and there is negligible shadowing of the particles by each other. Let the projected area of a particle normal to the direction of i'_λ be A_p so that the fraction of the incident energy on dA that strikes the particle is A_p/dA . Part of this energy will be absorbed and the remainder will be scattered by being reflected specularly.

The details of the reflection process are shown in figure 8-2. The energy intercepted by a band of cross section $Rd\beta$ on the surface of the sphere is equal to the energy intercepted by the particle multiplied by A_{band}/A_p , where A_{band} is the band area projected normal to i'_λ . This gives

$$\begin{aligned} \text{Energy intercepted by band} &= i'_\lambda d\omega_i d\lambda dA \frac{A_p}{dA} \frac{A_{band}}{A_p} \\ &= i'_\lambda d\omega_i d\lambda 2\pi R^2 \sin \beta \cos \beta d\beta \end{aligned}$$

The amount of reflected energy is $i'_\lambda d\omega_i d\lambda 2\pi R^2 \sin \beta \cos \beta d\beta \rho'_\lambda(\beta)$ where $\rho'_\lambda(\beta)$ is the directional specular reflectivity for incidence at angle β . The amount of energy reflected from the entire sphere is found by integrating over the sphere area, that is,

$$\text{Reflected energy} = i'_\lambda d\omega_i d\lambda \pi R^2 \int_0^{\pi/2} 2\rho'_\lambda(\beta) \sin \beta d(\sin \beta)$$

From equations (3-43a) and (3-17a) of volume I the integral is the hemispherical reflectivity ρ_λ . Hence the energy scattered by reflection

ularly reflected from the band of the sphere at angle β will be reflected into direction 2β and into a solid angle

$$d\omega_s = 2\pi \sin 2\beta d(2\beta) = 8\pi \sin \beta \cos \beta d\beta$$

The phase function is concerned only with the portion of the energy that is scattered. Since each particle is assumed to scatter independently, the scattered portion of the radiation emerging from a portion dV of the particle cloud when observed at a distance large compared with the individual particle diameter will have the same phase function as for a single particle. The energy incident on a single particle is $i'_\lambda d\omega_i d\lambda A_p$. Using the scattering cross section in equation (8-15), all the energy scattered away by a particle is $i'_\lambda d\omega_i d\lambda \pi K^2 \rho_\lambda$. Then the incident intensity that is scattered is from equation (8-9)

$$di'_{\lambda,s} = \frac{i'_\lambda d\omega_i d\lambda \pi R^2 \rho_\lambda}{d\omega_i A_p d\lambda} = i'_\lambda \rho_\lambda$$

The energy scattered away by a particle into $d\omega_s$ is

$$i'_\lambda d\omega_i d\lambda 2\pi R^2 \sin \beta \cos \beta d\beta \rho'_\lambda(\beta)$$

The scattered intensity into direction 2β (where this intensity is defined in eq. (8-10)) is

$$di'_{\lambda,s}(2\beta) = \frac{i'_\lambda d\omega_i d\lambda 2\pi R^2 \sin \beta \cos \beta d\beta \rho'_\lambda(\beta)}{d\omega_i A_p d\omega_s d\lambda} = \frac{i'_\lambda \rho'_\lambda(\beta)}{4\pi}$$

Inserting this into equation (8-11) gives

$$\Phi(2\beta) = \frac{\rho'_\lambda(\beta)}{\rho_\lambda} \quad (8-18)$$

The angle 2β is related to the angle φ in figure 8-2 by $\varphi = \pi - 2\beta$ so that relative to the forward scattering direction

$$\Phi(\varphi) = \frac{\rho'_\lambda\left(\frac{\pi - \varphi}{2}\right)}{\rho_\lambda} \quad (8-19)$$

For unpolarized incident radiation the reflectivity $\rho'_\lambda(\beta)$ for a dielectric sphere can be found from equation (4-61) of volume I. Also, the directional-hemispherical reflectivity is equal to unity minus the emissivity values in figure 4-5 of volume I. As shown by this figure, the $\rho'_\lambda(\beta)$ for

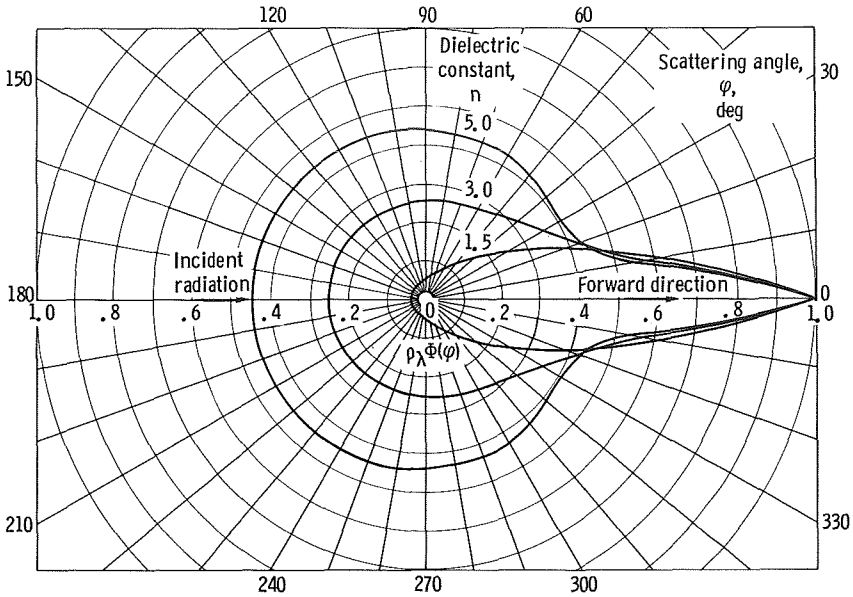


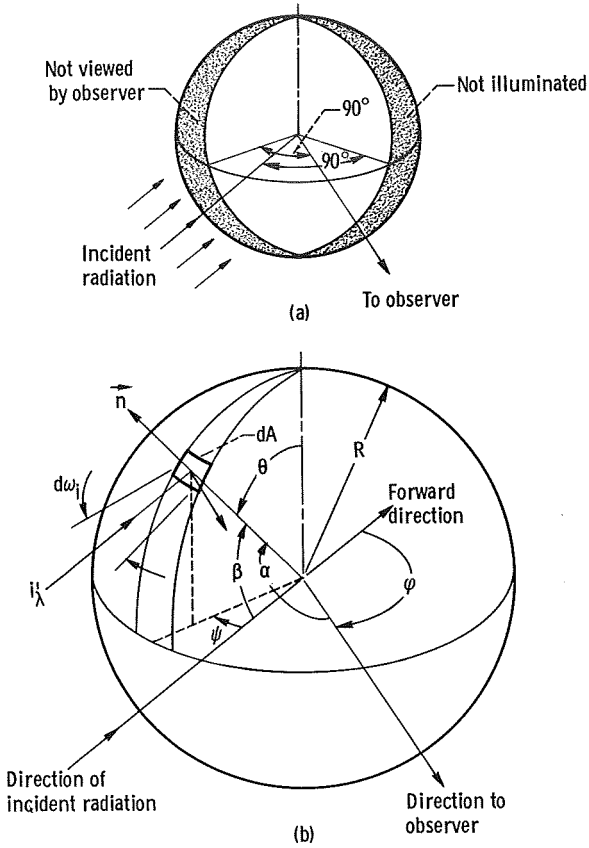
FIGURE 8-3.—Scattering diagram for specular reflecting sphere that is large compared with wavelength of incident radiation.

normal incidence is usually quite small compared with that at grazing angles ($\rho'_\lambda \rightarrow 1$ at $\beta = 90^\circ$). Consequently, the forward scatter from the sphere (at $\varphi = 0$) is unity, and the backward scatter (at $\varphi = \pi$) is small. By use of figure 4-5 of volume I, the quantity $\rho_\lambda \Phi(\varphi)$ can be plotted for various indices of refraction n as shown in figure 8-3. The ρ_λ for a dielectric can be found by use of figure 4-6 of volume I.

8.4.2 Reflection from a Diffuse Sphere

For the specularly reflecting sphere in figure 8-2 the energy scattered in each direction resulted from the reflection of energy at a single location on the sphere. If the sphere is diffuse, however, each surface element that intercepts incident radiation will reflect energy into the entire 2π solid angle above that element. Thus the radiation scattered into a specified direction will arise from the entire region of the sphere that receives radiation and is also visible from the specified direction. This is illustrated by figure 8-4(a). The shaded portion of the sphere will not contribute radiation in the direction of the observer because it either does not receive radiation or is hidden from the direction of observation.

Consider the sphere of radius R in figure 8-4(b). A typical surface area element dA is located at angles ψ and θ . The observer is at angle φ measured from the forward direction. The normal to dA is at angles



(a) Illuminated region visible to observer.
 (b) Geometry on sphere.

FIGURE 8-4.—Scattering by reflection from diffuse sphere.

β and α relative to the directions of incidence and observation. The incident spectral energy flux within the incident solid angle $d\omega_i$ is $i'_\lambda d\omega_i d\lambda$. The projected area of dA normal to the incident direction is $dA \cos \beta$, so the energy received by dA is $i'_\lambda d\omega_i d\lambda dA \cos \beta$. The amount of this energy that is reflected is $\rho'_\lambda i'_\lambda d\omega_i d\lambda dA \cos \beta$, where ρ'_λ is the diffuse directional-hemispherical spectral reflectivity. The ρ'_λ is assumed independent of incidence angle and hence is equal to the hemispherical reflectivity ρ_λ . Using the cosine law dependence for diffuse reflection gives the reflected energy per unit solid angle $d\omega_s$ in the direction of the observer as $\rho_\lambda i'_\lambda d\omega_i d\lambda dA \cos \beta \cos \alpha / \pi$. In order to integrate the reflected contributions that are received by the observer from all elements on the sphere surface, the dA , $\cos \beta$, and $\cos \alpha$ are expressed in terms of the spherical

coordinates R , ψ , and θ which gives $dA = R^2 \sin \theta d\theta d\psi$, $\cos \beta = \sin \theta \cos \psi$, and $\cos \alpha = \sin \theta \cos (\psi + \pi - \varphi)$. Then the energy scattered by reflection into the φ direction per unit solid angle $d\omega_s$ about that direction is

$$\frac{\rho_\lambda i'_\lambda d\omega_i d\lambda R^2}{\pi} \int_{\theta=0}^{\pi} \int_{\psi=-\pi/2}^{\varphi-(\pi/2)} \sin^3 \theta \cos \psi \cos (\psi + \pi - \varphi) d\psi d\theta$$

By integrating this becomes

$$\frac{\rho_\lambda i'_\lambda d\omega_i d\lambda R^2}{\pi} \frac{2}{3} (\sin \varphi - \varphi \cos \varphi)$$

The energy per unit $d\lambda$ scattered in direction φ per unit $d\omega_s$ and per unit area and solid angle of the incident radiation is obtained by dividing the scattered energy by $\pi R^2 d\omega_i d\lambda$ giving

$$di'_{\lambda,s}(\varphi) = \frac{\rho_\lambda i'_\lambda}{\pi^2} \frac{2}{3} (\sin \varphi - \varphi \cos \varphi)$$

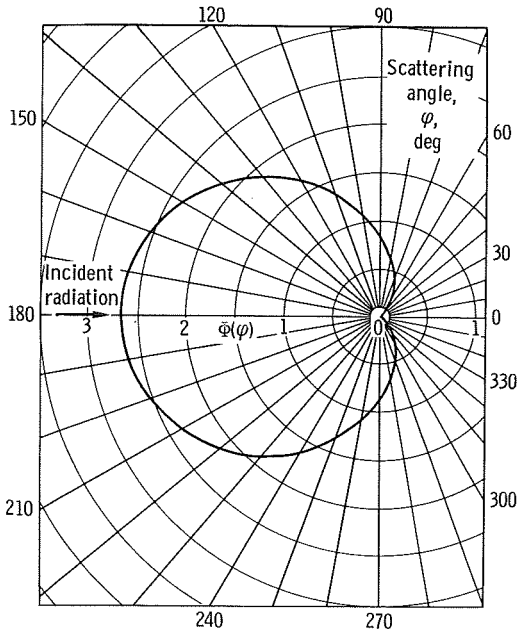


FIGURE 8-5.—Scattering phase function for diffuse reflecting sphere, large compared with wavelength of incident radiation and with constant reflectivity.

The entire amount of the incident intensity that is scattered is $di'_{\lambda, s} = \rho_{\lambda} i'_{\lambda}$. Then from equation (8-11), the directional magnitude of the scattered intensity is equal to the entire scattered intensity times the phase function

$$\frac{\rho_{\lambda} i'_{\lambda}}{\pi^2} \frac{2}{3} (\sin \varphi - \varphi \cos \varphi) = \rho_{\lambda} i'_{\lambda} \frac{\Phi(\varphi)}{4\pi}$$

so that the phase function for a diffuse sphere is

$$\Phi(\varphi) = \frac{8}{3\pi} (\sin \varphi - \varphi \cos \varphi) \quad (8-20)$$

The $\Phi(\varphi)$ from equation (8-20) is plotted in figure 8-5. The largest scattering is for $\varphi = 180^\circ$, that is, toward an observer back in the same direction as the origin of the incident radiation. In this instance, the entire illuminated surface of the sphere is observed.

8.4.3 Large Dielectric Sphere with Refractive Index Close to Unity

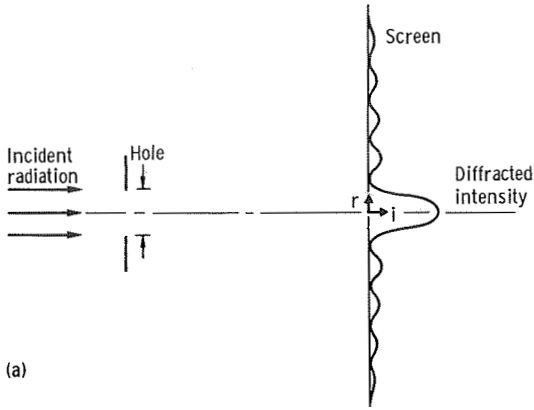
For a large dielectric ($\kappa=0$) sphere with refractive index $n \approx 1$ the reflectivity of the particle surface approaches zero. The incident radiation can thus pass with unchanged amplitude into the sphere and there is no scattering by reflection as in sections 8.4.1 and 8.4.2. With the extinction coefficient zero, the radiation will pass back out of the sphere with unchanged amplitude. However, the velocity $c = c_0/n$ inside the sphere medium is slightly less than that outside, so that radiation passing through different portions of the sphere and hence through different thicknesses will have different phase lags. The resulting interference of the waves passing out of the sphere yields a scattering cross section

$$s_{\lambda} = \frac{\pi D^2}{4} \left[2 - \frac{4}{W} \sin W + \frac{4}{W^2} (1 - \cos W) \right] \quad (8-21)$$

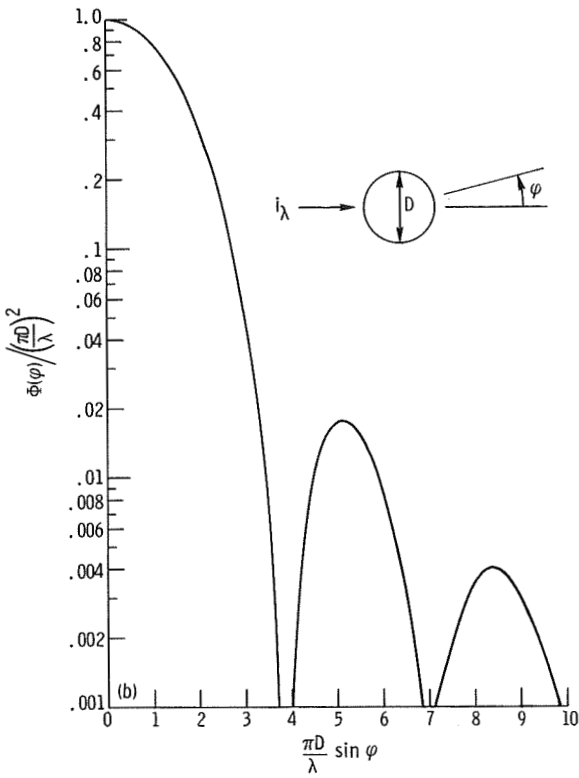
where $W = 2(\pi D/\lambda)(n-1)$. Additional information for this situation is given in reference 1.

8.4.4 Diffraction from a Large Sphere

For large spheres there is diffraction of the radiation passing in the vicinity of the particle. The effects of the diffraction and reflection must be added to obtain the total scattering behavior. Fortunately the diffraction is predominantly in the forward scattering direction. This means that the diffraction can be included in the radiative transfer



(a)



(a) Diffraction of radiation by hole.
 (b) Phase function for diffraction from large sphere.

FIGURE 8-6. — Diffraction by hole or large spherical particle.

as if it were part of the radiation transmitted past the particle without interacting with the particle. As a consequence, diffraction can often be neglected when considering the energy exchange within a scattering medium.

The most familiar form of diffraction is when light passes through a small hole or slit. As shown in figure 8-6(a) the result is a diffraction pattern of alternate illuminated and dark rings or strips. If a spherical particle is in the path of incident radiation, Babinet's principle states that the diffracted intensities are the same as for a hole. This is a consequence of fact that the hole and particle produce complementary disturbances in the amplitude of an incident electromagnetic wave. The energy diffracted by a spherical particle is thus the same as that diffracted by a hole of the same diameter. As a consequence, the entire projected area of the sphere takes part in the diffraction process, and the scattering cross section for diffraction is equal to the projected area $\pi D^2/4$. Since diffraction and reflection occur simultaneously, the total scattering cross section can approach $2(\pi D^2/4)$ when the sphere is highly reflecting.

The phase function for diffraction by a large sphere is given in terms of a Bessel function of the first kind of order one (ref. 1, pp. 107 and 108)

$$\Phi(\varphi) = \left(\frac{\pi D}{\lambda}\right)^2 \left[\frac{2J_1\left(\frac{\pi D}{\lambda} \sin \varphi\right)}{\frac{\pi D}{\lambda} \sin \varphi} \right]^2 \quad (8-22)$$

This function is plotted in figure 8-6(b). Since the abscissa is $(\pi D/\lambda) \sin \varphi$, for particles with large $\pi D/\lambda$ the diffracted radiation lies within a narrow angular region in the forward scattering direction. For small particles where $\pi D/\lambda$ is of order unity, the theory leading to equation (8-22) is invalid and the general Mie scattering theory must be applied. The integration to show that equation (8-22) satisfies equation (8-14) is discussed in reference 7 (p. 398); it is only necessary to integrate over small φ which simplifies the integration considerably.

8.4.5 Rayleigh Scattering

For many common situations, the scattering particles are considerably smaller in diameter than the wavelength of the incident radiation ($D \ll \lambda$). Scattering from such particles is termed Rayleigh scattering after Lord Rayleigh, who examined this situation. Rayleigh scattering is important in the atmosphere where the gas molecules are the scattering particles. The cross section for Rayleigh scattering can be derived from quantum theory or electromagnetic theory. Originally, Rayleigh

derived the functional dependence by dimensional analysis and arrived at the following result:

$$\frac{di'_{\lambda,s}}{i'_{\lambda}} \propto G^2(\bar{n}) \frac{V^2}{\lambda^4} \quad (8-23)$$

where V is the volume of a particle and $G(\bar{n})$ is an unknown function of the complex refractive index of the scattering material. The important result is that for Rayleigh scattering, *the scattered energy in any direction is proportional to the inverse fourth power of the wavelength of the incident radiation.* The inverse dependence upon the fourth power of wavelength shows that the shorter wavelengths will be Rayleigh scattered with a strong preference when the incident radiation covers a wavelength spectrum.

Rayleigh scattering by the molecules of the atmosphere accounts for the background of the sky being blue, and for the Sun becoming red in appearance at sunset. The blue portion of the incident sunlight is at the short wavelength end of the visible spectrum. Hence it undergoes strong Rayleigh scattering into all directions, giving the sky its overall blue background. Without molecular scattering, the sky would appear black except for the direct view of the Sun. As the Sun is setting, the path length for direct radiation through the atmosphere becomes much longer than during the middle of the day. In traversing this longer path more of the short wavelength portion of the spectrum is scattered away from the direct path of the Sun's rays. As a result, at sunset the Sun takes on a red color as the longer wavelength red rays are able to penetrate the atmosphere with less attenuation than the rest of the visible spectrum. If many dust particles are present, a deep red sunset may be seen.

If particles with a very limited range of sizes are present in the atmosphere, unusual scattering effects may be observed. Following the eruption of Krakatoa in 1883, the occurrence of blue and green Suns and Moons was noted over a period of many years. This effect was attributed to particles in the atmosphere of such a size range as to scatter only the red portion of the visible spectrum. On September 26 of 1950, a blue Sun and Moon were observed in Europe, a phenomenon believed due to finely dispersed smoke particles of uniform size carried from forest fires burning in Canada.

8.4.5.1 *Scattering cross sections for Rayleigh scattering.*—Equation (8-23) gives only the functional dependence of the scattered radiation on wavelength and particle volume, so that additional information is needed for the particle scattering cross section and the angular distribution of the scattered intensity. Consider first small nonabsorbing ($\kappa=0$) particles so that $\bar{n}=n$ and $D < \sim 0.2\lambda/n$ where λ is the wave-

length in the particle material. The Rayleigh scattering cross section for unpolarized incident radiation is found from more advanced theory to be

$$s_{\lambda} = \frac{24\pi^3 V^2}{\lambda^4} \left(\frac{n^2 - 1}{n^2 + 2} \right)^2 = \frac{8}{3} \frac{\pi D^2}{4} \left(\frac{\pi D}{\lambda} \right)^4 \left(\frac{n^2 - 1}{n^2 + 2} \right)^2 \quad (8-24)$$

Often Rayleigh scattering cross sections are given in terms of the polarizability α_p of the particles. This is a proportionality factor relating the forces induced in the molecules to the external electromagnetic field. Specifically it relates the dipole moment per unit volume (defined as the polarization) produced in the material to the external field. For the case under discussion here the polarizability is

$$\alpha_p = \frac{3}{4\pi} V \left(\frac{n^2 - 1}{n^2 + 2} \right) \quad (8-25)$$

so that equation (8-24) can be written

TABLE 8-II.—POLARIZABILITY FOR VARIOUS SCATTERING CONDITIONS

Scattering particles	Restrictions	Polarizability, α_p , length ³
Electrons (Thomson scattering)	Energy of incident photon is small, $h\nu \ll m_e c_0^2$	* $\frac{e^2}{m_e c_0^2} \left(\frac{\lambda}{2\pi} \right)^2$
Small dielectric particle	Particle diameter is small compared with wavelength in medium and in particle.	$\left(\frac{n^2 - 1}{n^2 + 2} \right) \left(\frac{D}{2} \right)^3$
Medium containing small particles (Lorentz-Lorentz)	Spacing between particles is small compared with wavelength ($< \lambda$). Particle diameter is very small ($D \ll \lambda$) compared with λ in both medium and particle. Spacing between particles $> D$.	$\frac{3}{4\pi N} \left \frac{\bar{n}^2 - 1}{\bar{n}^2 + 2} \right $
Medium containing small particles	Spacing between particles is large ($\gg \lambda$). Particle diameter is very small ($D \ll \lambda$).	$\frac{ \bar{n}^2 - 1 }{4\pi N}$
Medium containing small particles	Spacing between particles is large ($\gg \lambda$). Particle diameter is very small ($D \ll \lambda$). The \bar{n} is close to 1.	$\frac{ \bar{n} - 1 }{2\pi N}$

* $\frac{e^2}{m_e c_0^2}$ = classical electron radius, 2.818×10^{-13} cm.

$$s_{\lambda} = \frac{2^7 \pi^5 \alpha_p^2}{3 \lambda^4} \quad (8-26)$$

In this more general form, cross sections for various particles that follow the Rayleigh scattering relations can be introduced by substituting the requisite form for α_p into equation (8-26). Table 8-II gives some quantities for individual particles and particles in a nonparticipating medium.

The actual scattering cross section for particles in a medium may vary with λ in a manner somewhat different from a $1/\lambda^4$ dependence. In air at standard temperature and pressure, for example, the restrictions are satisfied such that Rayleigh scattering from the gas molecules should govern. However, the variation of refractive index with wavelength causes the variation of the scattering cross section to depart somewhat from the $1/\lambda^4$ dependence. This is shown in figure 8-7 where

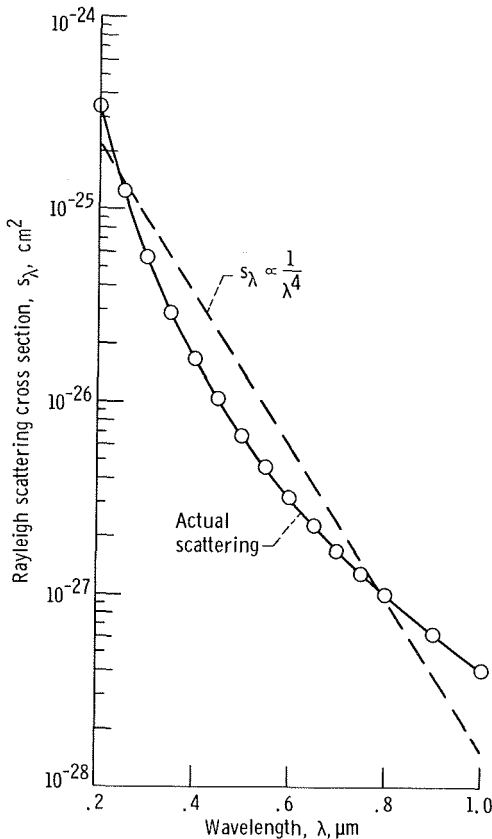


FIGURE 8-7.— Comparison of actual Rayleigh scattering cross section for air at standard temperature and pressure with $1/\lambda^4$ variation (from ref. 6).

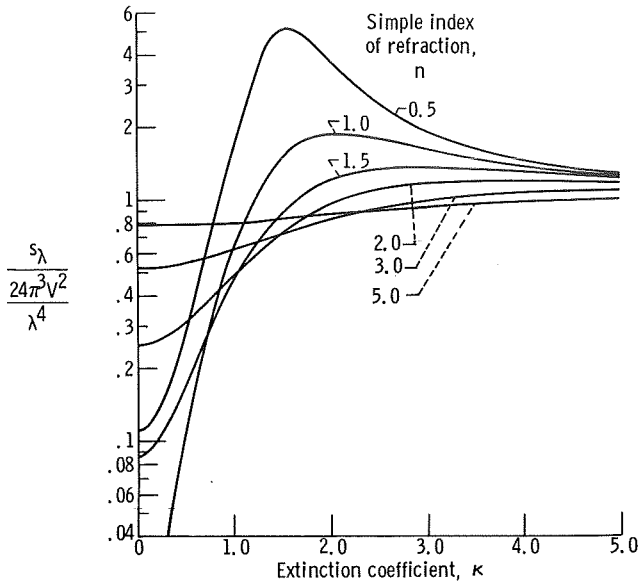


FIGURE 8-8.—Rayleigh scattering cross section as a function of simple index of refraction and extinction coefficient.

the actual scattering dependence on wavelength is compared with $1/\lambda^4$.

When the particles are of a conducting material with a complex index of refraction $\bar{n} = n - i\kappa$, the scattering cross section has the following form which is more general than that of equation (8-24)

$$s_\lambda = \frac{24\pi^3 V^2}{\lambda^4} \frac{|\bar{n}^2 - 1|^2}{|\bar{n}^2 + 2|^2} = \frac{8}{3} \frac{\pi D^2}{4} \left(\frac{\pi D}{\lambda} \right)^4 \frac{|\bar{n}^2 - 1|^2}{|\bar{n}^2 + 2|^2} \quad (8-27)$$

Inserting $\bar{n} = n - i\kappa$ and taking the square of the absolute value as indicated give

$$s_\lambda = \frac{24\pi^3 V^2}{\lambda^4} \frac{[(n^2 - \kappa^2 - 1)(n^2 - \kappa^2 + 2) + 4n^2\kappa^2]^2 + 36n^2\kappa^2}{[(n^2 - \kappa^2 + 2)^2 + 4n^2\kappa^2]^2} \quad (8-28)$$

For $\kappa = 0$ this reduces to equation (8-24). The quantity $s_\lambda / (24\pi^3 V^2 / \lambda^4)$ from equation (8-28) is given in figure 8-8 for various n and κ values.

8.4.5.2 *Phase function for Rayleigh scattering.*—For incident unpolarized radiation, electromagnetic theory gives for Rayleigh scattering

$$\Phi(\varphi, \theta) = \frac{3}{4}(1 + \cos^2 \varphi) \quad (8-29)$$

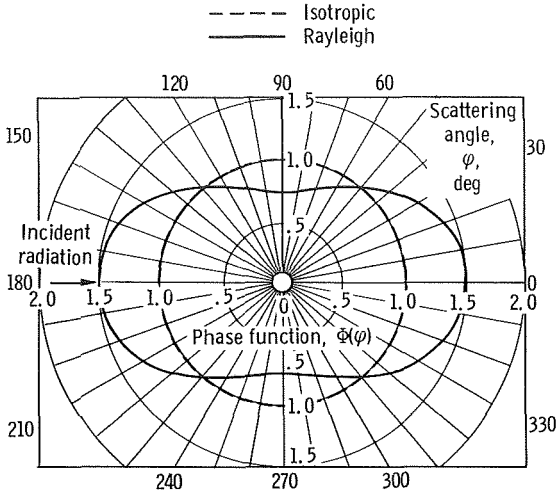


FIGURE 8-9.—Phase functions for Rayleigh and isotropic scattering.

This is independent of the circumferential angle θ .

A plot of the phase function for Rayleigh and for isotropic scattering is given in figure 8-9. For Rayleigh scattering, the scattered energy is directed preferentially along the forward direction of the incident radiation, and also strongly back toward the source of the radiation.

8.4.6 Mie Scattering Theory

When the particles that cause scattering are not large as treated in sections 8.4.1 to 8.4.3, and are not small enough to fall into the range that is adequately described by Rayleigh scattering relations, recourse must be taken to more complicated treatments. This is for the approximate range $(0.2/n) < (D/\lambda) < 1$ where λ is the wavelength inside the particle material. Gustav Mie (ref. 2) originally applied electromagnetic theory to derive the properties of the electromagnetic field that arises when a plane monochromatic wave is incident upon a spherical surface across which the optical properties n and κ change abruptly. As a consequence, the energy absorption by the medium, the absorption by the scattering particles, or both can be accounted for. The results of this theory apply over the entire range of particle diameters. As might be expected, strong polarization effects can be present. In certain cases, the phase function becomes very complicated as illustrated by figure 8-10.

Van der Hulst (ref. 1) gives an excellent detailed treatment of the Mie theory. The limiting cases of very small and very large particles are examined, and working formulae for all ranges of size are presented. The

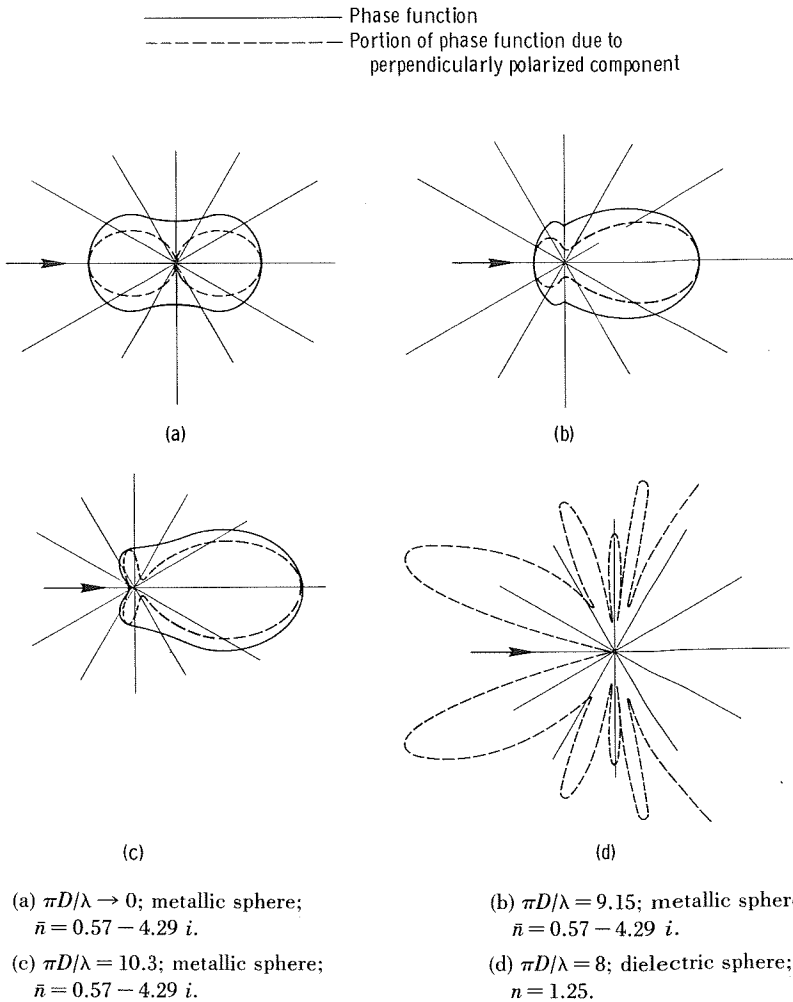


FIGURE 8-10.—Phase functions for Mie scattering from metallic and dielectric spheres (on arbitrary scales) from references 1 and 7.

cross sections and phase functions are discussed for dielectric and metallic particles of various shapes including spheres and cylinders. Some further work on absorbing particles, using detailed Mie scattering theory, has been done by Plass (ref. 3).

One of the simpler results from the Mie theory is for small spheres. The general Mie equations can be expanded into a power series in terms of the parameter $\pi D/\lambda$ giving the scattering cross section as

$$s_\lambda = \frac{8}{3} \frac{\pi D^2}{4} \left(\frac{\pi D}{\lambda} \right)^4 \left(\frac{\bar{n}^2 - 1}{\bar{n}^2 + 2} \right) \left[1 + \frac{3}{5} \frac{\bar{n}^2 - 2}{\bar{n}^2 + 2} \left(\frac{\pi D}{\lambda} \right)^2 + \dots \right]^2 \tag{8-30}$$

The second term in the square bracket is the first correction to the Rayleigh scattering relation which was valid for very small particles. When $\pi D/\lambda$ is very small, this term drops out and the relation becomes equation (8-27).

For small spheres the limit can also be considered where \bar{n} becomes very large. The scattering particles will then be very highly reflecting such as for a cloud of metallic particles. The result for this case cannot be obtained by letting \bar{n} in equation (8-30) approach infinity. As \bar{n} becomes large, the small part of the incident radiation that does penetrate the particle becomes almost totally internally reflected. This creates standing waves within the particle which provide resonance peaks in the scattering. The expansion used to obtain equation (8-30) did not account for this behavior. In the limit for $\bar{n} \rightarrow \infty$ the scattering cross section for small spheres is

$$s_\lambda = \frac{\pi D^2}{4} \left[\frac{10}{3} \left(\frac{\pi D}{\lambda} \right)^4 + \frac{4}{5} \left(\frac{\pi D}{\lambda} \right)^6 + \dots \right] \tag{8-31}$$

If, in addition to $\bar{n} \rightarrow \infty$, the particles are so small that only the first term in the bracket of equation (8-31) is significant, then for unpolarized incident radiation the phase function is given by

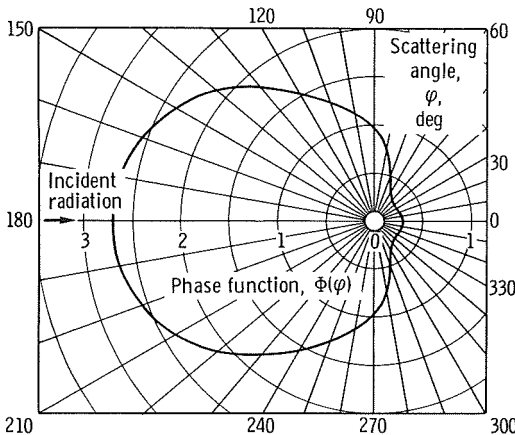


FIGURE 8-11.—Phase function for scattering of unpolarized incident radiation from small sphere with $\bar{n} \rightarrow \infty$.

$$\Phi(\varphi) = \frac{3}{5} \left[\left(1 - \frac{1}{2} \cos \varphi \right)^2 + \left(\cos \varphi - \frac{1}{2} \right)^2 \right] \quad (8-32)$$

A polar diagram of this function is given in figure 8-11. This shows that in contrast to Rayleigh scattering (fig. 8-9) the highly reflecting particles produce a very strong scattering back toward the source.

8.5 RADIATIVE TRANSFER IN SCATTERING MEDIA

Now that some of the fundamentals of scattering behavior have been examined, the methods of using this information in radiative transfer calculations can be treated. First, pure scattering problems are examined, and then the complete absorbing, emitting, and scattering case is considered.

8.5.1 The Equation of Transfer in a Pure Scattering Atmosphere

Let us consider first the situation of radiation transfer in a medium where there is scattering but no absorption or emission of radiation. The local intensity along a path will be attenuated by radiation scattered out into other directions, and will be enhanced by radiation scattered into the direction being considered. Figure 8-12 shows radiation with intensity i'_λ passing through a volume element $dAdS$ where dA is normal to the direction of i'_λ . While passing through the distance dS , a portion $di'_{\lambda,s}$ of the intensity will be scattered away. From equations (8-3) and (8-5) this is equal to

$$di'_{\lambda,s} = i'_\lambda(S) \sigma_{s\lambda} dS \quad (8-33)$$

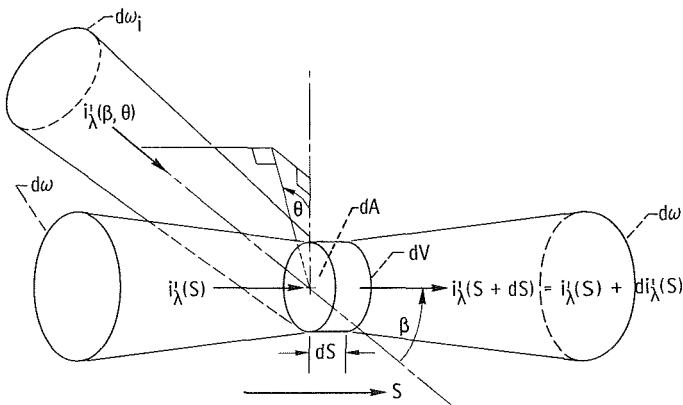


FIGURE 8-12.—Scattering of energy into S direction.

To compute the scattering from all directions into the direction of i'_λ , consider the radiation incident at angle (β, θ) as shown in figure 8-12. This radiation has intensity $i'_\lambda(\beta, \theta)$, and in the process of going through the volume element dV will pass through a path length $dS/\cos \beta$. From equation (8-11) oriented with respect to the present coordinate system, the intensity scattered from $i'_\lambda(\beta, \theta)$ into the direction of i'_λ is

$$di'_{\lambda, s} = \sigma_{s\lambda} i'_\lambda(\beta, \theta) \frac{dS}{\cos \beta} \frac{\Phi(\beta, \theta)}{4\pi} \quad (8-34)$$

However, from equation (8-10) $i'_{\lambda, s}$ is an intensity defined as energy in the scattered direction per unit $d\lambda$, per unit scattered solid angle, per unit incident solid angle $d\omega_i$, and per unit area normal to the incident intensity. This is the area normal to $i'_\lambda(\beta, \theta)$ which is $dA \cos \beta$. Then the spectral energy scattered into the S direction as a result of $i'_\lambda(\beta, \theta)$ is by use of equation (8-34)

$$\begin{aligned} d^4Q'_{\lambda, s} &= di'_{\lambda, s} d\omega d\omega_i d\lambda dA \cos \beta \\ &= \sigma_{s\lambda} i'_\lambda(\beta, \theta) \frac{dS}{\cos \beta} \frac{\Phi(\beta, \theta)}{4\pi} d\omega d\omega_i d\lambda dA \cos \beta \\ &= \sigma_{s\lambda} i'_\lambda(\beta, \theta) dS \frac{\Phi(\beta, \theta)}{4\pi} d\omega d\omega_i d\lambda dA \end{aligned}$$

The contribution of this scattered energy to the spectral intensity in the S direction is then

$$\frac{d^4Q'_{\lambda, s}}{dAd\omega d\lambda} = \sigma_{s\lambda} i'_\lambda(\beta, \theta) \frac{\Phi(\beta, \theta)}{4\pi} d\omega_i dS \quad (8-35)$$

To account for the scattering contributions from incident intensities from all directions, integrate over all $d\omega_i$ to obtain

$$\int_{\omega_i=4\pi} \frac{d^4Q'_{\lambda, s}}{dAd\omega d\lambda} = \frac{dS}{4\pi} \sigma_{s\lambda} \int_{\omega_i=4\pi} i'_\lambda(\beta, \theta) \Phi(\beta, \theta) d\omega_i \quad (8-36)$$

The scattering particles have been assumed randomly oriented so that the scattering cross section $\sigma_{s\lambda}$ is independent of the incidence direction.

By combining equations (8-33) and (8-36) the change of intensity in direction S is

$$\frac{di'_\lambda}{dS} = -\sigma_{s\lambda} i'_\lambda + \frac{\sigma_{s\lambda}}{4\pi} \int_{\omega_i=4\pi} i'_\lambda(\beta, \theta) \Phi(\beta, \theta) d\omega_i \quad (8-37)$$

As in equations (2-5) and (2-6) a *scattering optical thickness* $\kappa_{s\lambda}$ can be introduced such that

$$d\kappa_{s\lambda} \equiv \sigma_{s\lambda} dS \quad (8-38)$$

and

$$\kappa_{s\lambda}(S) = \int_0^S \sigma_{s\lambda}(S^*) dS^* \quad (8-39)$$

Then equation (8-37) becomes

$$\frac{di'_\lambda}{d\kappa_{s\lambda}} + i'_\lambda = \frac{1}{4\pi} \int_{\omega_i=4\pi} i'_\lambda(\beta, \theta) \Phi(\beta, \theta) d\omega_i \quad (8-40)$$

This has the same functional form as the equation for absorbing-emitting media (eq. (2-7)). As in equation (2-7), the term on the right side of equation (8-40) accounts for intensity added to the beam at each point along the path.

Equation (8-40) can be integrated along a scattering optical path from 0 to $\kappa_{s\lambda}$ in the same fashion as equation (2-10) was obtained. By analogy with equation (2-10) this gives

$$i'_\lambda(\kappa_{s\lambda}) = i'_\lambda(0) \exp(-\kappa_{s\lambda}) + \int_0^{\kappa_{s\lambda}} \left[\frac{1}{4\pi} \int_{\omega_i=4\pi} i'_\lambda(\beta, \theta) \Phi(\beta, \theta) d\omega_i \right]_{\kappa_{s\lambda}^*} \times \exp[-(\kappa_{s\lambda} - \kappa_{s\lambda}^*)] d\kappa_{s\lambda}^* \quad (8-41)$$

where $\kappa_{s\lambda}^*$ is a dummy integration variable, and the integral in the first square bracket is evaluated at $\kappa_{s\lambda}^*$. For an ideal scattering process where there is no absorption of photon energy by the scattering particles, there will be no exchange of energy with the medium. In this instance, there is only a directional redistribution of energy by the scattering. Then if $\sigma_{s\lambda}$ and Φ are independent of temperature, equation (8-41) applies regardless of the temperature distribution of the medium.

In situations such as a searchlight or laser beam, the **only** significant intensity source is that arising from the beam. Then the **energy** scattered from other sources into the direction of the beam will be **negligible** and equation (8-41) reduces to the simple exponential attenuation relation

$$i'_\lambda(\kappa_{s\lambda}) = i'_\lambda(0) \exp(-\kappa_{s\lambda}) \quad (8-42)$$

EXAMPLE 8-1: Derive the equations that describe the **local** intensity

and energy flux in a one-dimensional scattering layer. The layer is contained between infinite parallel black plates separated by a distance D . The lower and upper plates are maintained at temperatures T_1 and T_2 , respectively. The gas scatters isotropically, is nonconducting, and has an absorption coefficient of zero. The gas properties are assumed independent of wavelength.

Since the properties are assumed independent of wavelength, the λ subscripts can be omitted in what follows. The same relations will apply, however, for radiation at a single wavelength if the spectral emission from the walls is utilized. Note that for isotropic scattering the phase function is 1.

This example is the scattering counterpart of the development in section 2.6.2 which was concerned with a nonscattering, absorbing-emitting medium. If x is the distance measured normal from plate 1, the scattering optical distance from a point on the plate to a point in the medium is $\kappa_s/\cos \beta$ where it should be noted that this κ_s is based on the coordinate x , not on the actual path length of the radiation. Then by analogy with equations (2-34) and (2-35) the intensities in the directions having positive and negative $\cos \beta$ are respectively (see fig. 2-5)

$$i'_+(\kappa_s, \beta) = \frac{\sigma T_1^4}{\pi} \exp\left(\frac{-\kappa_s}{\cos \beta}\right) + \frac{1}{\cos \beta} \int_0^{\kappa_s} \left[\frac{1}{2} \int_{\beta^*=0}^{\pi} i'(\kappa_s^*, \beta^*) \sin \beta^* d\beta^* \right] \\ \times \exp\left[\frac{-(\kappa_s - \kappa_s^*)}{\cos \beta}\right] d\kappa_s^* \quad 0 \leq \beta \leq \frac{\pi}{2} \quad (8-43)$$

$$i'_-(\kappa_s, \beta) = \frac{\sigma T_2^4}{\pi} \exp\left(\frac{\kappa_{D,s} - \kappa_s}{\cos \beta}\right) \\ - \frac{1}{\cos \beta} \int_{\kappa_s}^{\kappa_{D,s}} \left[\frac{1}{2} \int_{\beta^*=0}^{\pi} i'(\kappa_s^*, \beta^*) \sin \beta^* d\beta^* \right] \\ \times \exp\left(\frac{\kappa_s^* - \kappa_s}{\cos \beta}\right) d\kappa_s^* \quad \frac{\pi}{2} \leq \beta \leq \pi \quad (8-44)$$

These relations for isotropic scattering can be solved in a manner analogous to that for an absorbing-emitting medium. Note that the integral in the last term on the right in equations (8-43) and (8-44) involves integrating over all β^* directions and hence includes the contributions from both i'_+ and i'_- . A β^* notation has been used to distinguish this integration variable over all directions from the β which has a restricted range for each of the equations.

The energy flux flowing from wall 1 to wall 2 can be found by analogy with equation (2-41) as

$$\begin{aligned}
 q = \sigma T_1^4 - 2 \int_0^{\pi/2} \sin \beta \cos \beta \left\{ \sigma T_2^4 \exp \left(-\frac{\kappa_{D,s}}{\cos \beta} \right) \right. \\
 \left. + \frac{\pi}{\cos \beta} \int_0^{\kappa_{D,s}} \left[\frac{1}{2} \int_{\beta^*=0}^{\pi} i'(\kappa_s^*, \beta^*) \sin \beta^* d\beta^* \right] \right. \\
 \left. \times \exp \left(-\frac{\kappa_s^*}{\cos \beta} \right) d\kappa_s^* \right\} d\beta \quad (8-45)
 \end{aligned}$$

In this equation the σT_1^4 is the energy flux leaving wall 1 by radiation. The second term is the flux incoming to wall 1 in two ways: (1) along direct paths from wall 2 along which the emitted radiation σT_2^4 is attenuated by scattering, and (2) by radiation scattered in at local positions between the plates and then attenuated before reaching wall 1.

8.5.2 Scattering in Absorbing-Emitting Media

If scattering, absorption, and emission are all of significance, then the equation of transfer as given by equation (2-4) is generalized by including the scattering terms of equation (8-37) to give

$$\frac{di'_\lambda}{dS} = \underbrace{-a_\lambda i'_\lambda(S)}_{\text{Loss by absorption (including the contribution by induced emission)}} + \underbrace{a_\lambda i'_{\lambda b}(S)}_{\text{Gain by emission (not including induced emission)}} - \underbrace{\sigma_{s\lambda} i'_\lambda(S)}_{\text{Loss by scattering}} + \underbrace{\frac{\sigma_{s\lambda}}{4\pi} \int_{\omega_i=4\pi} i'_\lambda(S, \omega_i) \Phi(\lambda, \omega, \omega_i) d\omega_i}_{\text{Gain by scattering into S-direction}}$$

(8-46)

The two terms representing losses by absorption and scattering can be combined. Then the equation of transfer for absorbing, emitting, and scattering media (for the case of elastic anisotropic scattering) is the following for the intensity in the solid angle ω about the S-direction:

$$\frac{di'_\lambda}{dS} = -(a_\lambda + \sigma_{s\lambda}) i'_\lambda(S) + a_\lambda i'_{\lambda b}(S) + \frac{\sigma_{s\lambda}}{4\pi} \int_{\omega_i=4\pi} i'_\lambda(S, \omega_i) \Phi(\lambda, \omega, \omega_i) d\omega_i \quad (8-47)$$

The sum $a_\lambda + \sigma_{s\lambda}$ is the extinction coefficient K_λ discussed in section 1.5.1.

The albedo for single scatter Ω_o is sometimes used which is defined

as the ratio of the scattering coefficient to the extinction coefficient, or

$$\Omega_{o\lambda} \equiv \frac{\sigma_{s\lambda}}{K_\lambda} = \frac{\sigma_{s\lambda}}{a_\lambda + \sigma_{s\lambda}} \quad (8-48)$$

The *optical depth* or *opacity* when both scattering and absorption are present is given by (this has been defined previously in eq. (1-17))

$$\kappa_\lambda(S) = \int_0^S K_\lambda(S^*) dS^* = \int_0^S (\sigma_{s\lambda} + a_\lambda) dS^* \quad (8-49)$$

where S^* is a dummy variable of integration. Equation (8-47) now becomes

$$\frac{di'_\lambda}{d\kappa_\lambda} = -i'_\lambda(\kappa_\lambda) + (1 - \Omega_{o\lambda})i'_{\lambda b}(\kappa_\lambda) + \frac{\Omega_{o\lambda}}{4\pi} \int_{\omega_i=4\pi} i'_\lambda(\kappa_\lambda, \omega_i) \Phi(\lambda, \omega, \omega_i) d\omega_i \quad (8-50)$$

Often, especially in the astrophysical literature, the final two terms in equation (8-50) are combined into *the source function* $I'_\lambda(\kappa_\lambda)$, defined as

$$I'_\lambda(\kappa_\lambda) \equiv (1 - \Omega_{o\lambda})i'_{\lambda b}(\kappa_\lambda) + \frac{\Omega_{o\lambda}}{4\pi} \int_{\omega_i=4\pi} i'_\lambda(\kappa_\lambda, \omega_i) \Phi(\lambda, \omega, \omega_i) d\omega_i \quad (8-51)$$

This is the source of intensity along the optical path from both emission and incoming scattering. The equation of transfer then becomes

$$\frac{di'_\lambda}{d\kappa_\lambda} = -i'_\lambda(\kappa_\lambda) + I'_\lambda(\kappa_\lambda) \quad (8-52)$$

The generalized equation of transfer including absorption, emission, and scatter is thus quite similar in form to the equation of transfer for pure absorption and emission that has been studied at length in chapters 2 and 3. Note that when $\Omega_{o\lambda} \rightarrow 0$ (no scattering), equation (8-52) does indeed reduce to the correct form for pure emission and absorption (eq. (2-7)). For $\Omega_{o\lambda} \rightarrow 1$ (pure scattering), equation (8-52) reduces to the pure scattering form (eq. (8-40)).

Because equation (8-52) is similar in form to equation (2-7), many of the mathematical approaches to solutions of the equation of transfer given in chapter 3 also apply when scattering is included. The texts by Chandrasekhar and Kourganoff (refs. 4 and 5) and the work of Goody (ref. 6) that deals with atmospheric effects treat at length scattering problems with and without absorption and emission for one-dimensional

atmospheres. A demonstration of the similarity with previous derivations given in chapter 3 will now be given by considering the diffusion approximation.

EXAMPLE 8-2: Derive a first-order diffusion relation for radiative transfer in a one-dimensional layer of absorbing-emitting isotropic medium with isotropic scattering.

Let x be the thickness coordinate normal to the layer boundaries. The equation of transfer for the general one-dimensional case including emission, absorption, and scattering is from equation (8-52) (as in eq. (3-17))

$$-\frac{\mu}{(\sigma_{s\lambda} + a_\lambda)} \frac{\partial i'_\lambda(x, \mu)}{\partial x} = i'_\lambda(x, \mu) - I'_\lambda(x, \mu) \quad (8-53)$$

where $\mu = \cos \beta$. For isotropic scattering the source function I'_λ is independent of direction and is given from equation (8-51) by

$$I'_\lambda(x) = (1 - \Omega_{o\lambda}) i'_{\lambda b}(x) + \frac{\Omega_{o\lambda}}{4\pi} \int_{\omega_i=4\pi} i'_\lambda(x, \omega_i) d\omega_i$$

In the diffusion approximation, the medium is optically dense. Consequently the radiation arriving at any location comes only from the immediate surroundings, as any other radiation would be absorbed or scattered before arriving at that location. Also in the diffusion approximation the radiant energy density changes slowly with position relative to distances for attenuation. This can be stated more rigorously by letting H be a path length over which the radiant energy density does change appreciably, and letting l_m be the extinction mean free path, $l_m = 1/(a_\lambda + \sigma_{s\lambda})$. Then for the diffusion approximation to apply $l_m/H \ll 1$. As in equation (3-19) the intensity is expanded in terms of powers of the small quantity

$$i'_\lambda = i'^{(0)}_\lambda + \frac{l_m}{H} i'^{(1)}_\lambda + \left(\frac{l_m}{H}\right)^2 i'^{(2)}_\lambda + \dots \quad (8-54)$$

Insert equation (8-54) into the equation of transfer to obtain

$$-\mu \frac{l_m}{H} \left[\frac{\partial i'^{(0)}_\lambda}{\partial \left(\frac{x}{H}\right)} + \frac{l_m}{H} \frac{\partial i'^{(1)}_\lambda}{\partial \left(\frac{x}{H}\right)} + \dots \right] = \left[i'^{(0)}_\lambda + \frac{l_m}{H} i'^{(1)}_\lambda + \dots \right] - i'_{\lambda b} + \frac{l_m}{l_{m,s}} \left\{ i'_{\lambda b} - \frac{1}{4\pi} \int_{\omega_i=4\pi} \left[i'^{(0)}_\lambda + \frac{l_m}{H} i'^{(1)}_\lambda + \dots \right] d\omega_i \right\} \quad (8-55)$$

where $l_{m,s} = 1/\sigma_{s\lambda}$. In addition to the expansion parameter l_m/H , there has appeared an additional quantity $l_m/l_{m,s}$ which gives the relation of the total extinction to that of scatter alone. For the diffusion approximation including absorption and scattering, this parameter will have to be of order one-half. For small $l_m/l_{m,s}$ the problem would degenerate to one of diffusion by absorption alone; this could be the situation in a dense gas containing a few scattering particles. For $l_m/l_{m,s}$ approaching 1 so $l_m \approx l_{m,s}$, there would be scattering alone as in a thin carrier gas with many scattering particles. Collect the terms in equation (8-55) of zeroth order in l_m/H to obtain

$$i'_{\lambda}(0) = i'_{\lambda b} - \frac{l_m}{l_{m,s}} \left[i'_{\lambda b} - \frac{1}{4\pi} \int_{\omega_i=4\pi} i'^{(0)}_{\lambda} d\omega_i \right] \tag{8-56}$$

The terms $i'_{\lambda b}$ and $\int_{\omega_i=4\pi} i'^{(0)}_{\lambda} d\omega_i$ on the right in equation (8-56) do not depend on the incidence angle $d\omega_i$. Hence $i'^{(0)}_{\lambda}$ on the left cannot depend on angle. By using this fact, equation (8-56) reduces to

$$i'_{\lambda}(0) = i'_{\lambda b} - \frac{l_m}{l_{m,s}} \left[i'_{\lambda b} - \frac{1}{4\pi} i'^{(0)}_{\lambda} 4\pi \right]$$

which further reduces to

$$i'^{(0)}_{\lambda} = i'_{\lambda b} \tag{8-57}$$

Now collect terms from equation (8-55) of first order in l_m/H to obtain

$$-\mu \frac{\partial i'^{(0)}_{\lambda}}{\partial \left(\frac{x}{H} \right)} = i'_{\lambda}(1) - \frac{l_m}{l_{m,s}} \frac{1}{4\pi} \int_{\omega_i=4\pi} i'^{(1)}_{\lambda} d\omega_i$$

Substitute equation (8-57) for $i'^{(0)}_{\lambda}$ to give

$$-\mu \frac{di'_{\lambda b}}{d \left(\frac{x}{H} \right)} = i'_{\lambda}(1) - \frac{l_m}{l_{m,s}} \frac{1}{4\pi} \int_{\omega_i=4\pi} i'^{(1)}_{\lambda} d\omega_i \tag{8-58}$$

To find $i'_{\lambda}(1)$, multiply by $d\omega_i = 2\pi \sin \beta d\beta = -2\pi d\mu$ and integrate over all solid angles

$$\frac{di'_{\lambda b}}{d\left(\frac{x}{H}\right)} \int_{\mu=-1}^{+1} \mu 2\pi d\mu = \int_{\omega_i=4\pi} i'_{\lambda}{}^{(1)} d\omega_i - \frac{l_m}{l_{m,s}} \left[\frac{1}{4\pi} \int_{\omega_i=4\pi} i'_{\lambda}{}^{(1)} d\omega_i \right] \int_{\omega_i=4\pi} d\omega_i$$

The integral on the left is zero so

$$0 = \int_{\omega_i=4\pi} i'_{\lambda}{}^{(1)} d\omega_i - \frac{l_m}{l_{m,s}} \int_{\omega_i=4\pi} i'_{\lambda}{}^{(1)} d\omega_i$$

Hence $\int_{4\pi} i'_{\lambda}{}^{(1)} d\omega_i = 0$ and equation (8-58) reduces to

$$i'_{\lambda}{}^{(1)} = -\mu \frac{di'_{\lambda b}}{d\left(\frac{x}{H}\right)} \quad (8-59)$$

Substitute equations (8-57) and (8-59) into equation (8-54) to obtain

$$i'_{\lambda} = i'_{\lambda b} - \frac{\mu}{(a_{\lambda} + \sigma_{s\lambda})} \frac{di'_{\lambda b}}{dx} \quad (8-60)$$

This is the same form as equation (3-23) for the nonscattering case, except that the extinction coefficient $a_{\lambda} + \sigma_{s\lambda}$ appears in place of the absorption coefficient. Then by analogy with equation (3-25) the energy flux in the x direction is given by the diffusion equation

$$\frac{dq_{\lambda}(x)}{dx} = \frac{-4}{3(a_{\lambda} + \sigma_{s\lambda})} \frac{de_{\lambda b}}{dx} \quad (8-61)$$

The net flux depends only on the emissive power gradient and the extinction coefficient when diffusion conditions apply.

Bobco (ref. 8) used a modified diffusion solution to find the directional emissivity for radiation from a semi-infinite slab of isothermal gray scattering-absorbing medium. The scattering was assumed isotropic. The directional emissivities of the slab were found to differ considerably from a diffuse distribution. Hsia and Love (ref. 9) treated energy transfer between parallel plates through an anisotropically scattering medium. Nonisothermal conditions in the medium were considered. Solutions were obtained by approximating the integral terms in the equation of transfer by a finite summation. The set of differential

equations that resulted were solved by a specialized matrix transformation technique.

Love et al. (ref. 10) studied plane and cylindrical boundaries with given reflectivities that enclose absorbing, emitting, and scattering gases. Both Monte Carlo and discrete ordinate methods were used for computing the energy transfer. Some experimentally determined values of the scattering phase functions for glass beads, and aluminum, carbon, iron, and silica particles were used for comparison of their effect in a variety of energy exchange cases. It is significant that little difference in energy transfer was found for the results using these experimental phase functions as compared with the results using either the Rayleigh or isotropic phase functions. It appears therefore that *the assumption of isotropic scattering is often justified in energy exchange calculations in enclosures.*

In figure 8-13, results from reference 10 are shown for the fraction

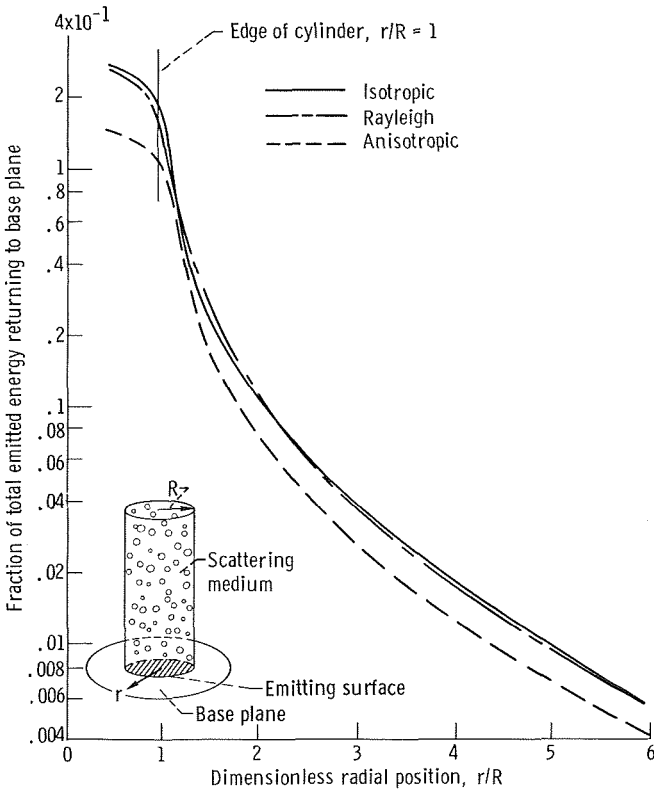


FIGURE 8-13.—Effect of scattering phase function on energy scattered back to base plane by cylinder of scattering medium. Optical diameter of cylinder, 2; height to diameter ratio, 5 (ref. 10).

of emitted energy from a black disk that is scattered back to the base plane from a cylinder of gas adjacent to the disk. The results for various scattering phase functions in the gas are in very good agreement. The various phase functions gave energy transfer results that had less variation in plane parallel geometries than in the cylindrical geometry. It should be emphasized that in some cases the insensitivity of results to the scattering phase function is probably not a valid assumption. Specifically the phase function will be important for beam transmission or other situations where strong sources transmit directionally into a scattering atmosphere.

REFERENCES

1. HULST, HENDRIK C. VAN DER: *Light Scattering by Small Particles*. John Wiley & Sons, Inc., 1957.
2. MIE, GUSTAV: *Optics of Turbid Media*. *Ann. d. Physik*, vol. 25, no. 3, Mar. 3, 1908, pp. 377-445.
3. PLASS, GILBERT N.: *Mie Scattering and Absorption Cross Sections for Absorbing Particles*. *Appl. Opt.*, vol. 5, no. 2, Feb. 1966, pp. 279-285.
4. CHANDRASEKHAR, SUBRAHMANYAN: *Radiative Transfer*. Dover Publ., 1960.
5. KOURGANOFF, VLADIMIR: *Basic Methods in Transfer Problems; Radiative Equilibrium and Neutron Diffusion*. Dover Publ., 1963.
6. GOODY, R. M.: *Atmospheric Radiation*. Vol. I. Theoretical Basis. Clarendon Press, Oxford, 1964.
7. BORN, MAX; AND WOLF, EMIL: *Principles of Optics*. Second ed., Pergamon Press, 1964.
8. BOBCO, R. P.: *Directional Emissivities from a Two-Dimensional, Absorbing-Scattering Medium: The Semi-Infinite Slab*. *J. Heat Transfer*, vol. 89, no. 4, Nov. 1967, pp. 313-320.
9. HSIA, H. M.; AND LOVE, T. J.: *Radiative Heat Transfer between Parallel Plates Separated by a Nonisothermal Medium with Anisotropic Scattering*. *J. Heat Transfer*, vol. 89, no. 3, Aug. 1967, pp. 197-204.
10. LOVE, TOM J.; ET AL.: *Radiative Heat Transfer in Absorbing, Emitting and Scattering Media*. Oklahoma Univ. (ARL-67-0210, DDC No. AD-666427), Dec. 1967.

Chapter 9. Some Specialized Effects in Absorbing-Radiating Media

9.1 INTRODUCTION

This chapter deals with four special radiation topics each of which has important applications, but in restricted areas. For this reason, some of the features of these topics are only briefly presented.

The first topic deals with media having a nonunity refractive index. This topic includes the radiation within, and penetrating into, materials such as glass and ice. When radiation from one material enters one of another refractive index, the bending and reflection of rays at the interface must be considered in the analysis. For closely spaced layers such as in cryogenic super insulation, there is an additional effect of radiation tunneling between layers.

The second topic is flames, both nonluminous and those containing luminous particles, mainly soot. A nonluminous hydrocarbon flame contains carbon dioxide and water vapor as its chief radiating constituents. Radiation by these gases is fairly well understood. When soot is present and the flame thereby becomes luminous, the radiation is dependent on the radiative properties of the soot and the soot concentration within the flame. There is some information available on soot radiative properties, but the amount is insufficient. In addition to the uncertainties in the soot properties, a serious difficulty in flame radiation computations is determining the soot concentration. The concentration depends on the particular fuel, the flame geometry, and the complicated mixing phenomena within the flame. At present there is no way of computing soot concentration from the basic parameters, such as the burner geometry, fuel-air ratio, and the particular fuel.

This chapter ends with brief discussions of two topics: luminescence and transient gas radiation problems. The recent limited interest in the latter stems chiefly from nuclear weapons calculations.

9.2 SYMBOLS

A	area
a	absorption coefficient
C	volume fraction of particles in medium
C_1, C_2	constants in Planck's spectral energy distribution
C_3	constant in Wien's displacement law

c	speed of light in medium
c_v	heat capacity at constant volume
\bar{c}_p	mean heat capacity
D	half thickness of slab; particle diameter
E	absorption efficiency factor for single particle
e	emissive power
$F(\lambda)$	function defined by eqs. (9-22) and (9-23)
H	enthalpy
i	radiation intensity
k, k_1, k_2	constants in equations for soot absorption
L_e	mean beam length
m	number of moles
N	number of particles per unit volume
n	simple refractive index (real part of $\bar{n} = n - i\kappa$)
p	partial pressure
Q	energy per unit time
q	energy flux, energy per unit area and time
S	coordinate along path of radiation
T	absolute temperature
t	time
t^*	dimensionless time, $(a\sigma T_o^3/\rho c_v)t$
V	volume
x	rectangular coordinate
α	exponent in eq. (9-18)
β	cone angle, angle from normal of area
β^*	angles giving total internal reflection
β_{max}	maximum angle where refraction occurs
ϵ	emittance
Θ	dimensionless temperature, T/T_o
θ	circumferential angle
κ	optical thickness, ax ; extinction coefficient in complex refractive index
λ	wavelength
ρ	density
σ	Stefan-Boltzmann constant
φ	scattering angle measured from forward direction to direction of observer (see fig. 8-1)
ω	solid angle

Subscripts:

b	blackbody
D	evaluated for length D
e	emitted

f	flame
g	green
i	input
m	medium
max	maximum value
o	no self-absorption; initial value
$prod$	products
r	red
ref	reference value
vac	in vacuum
λ	spectrally dependent
1, 2, 3	medium or boundary 1, 2, or 3

Superscript:

directionally dependent quantity

9.3 RADIATION PHENOMENA IN MEDIA WITH NONUNITY REFRACTIVE INDEX

Most of the discussion in this volume has been concerned with dielectric media that have a refractive index n of unity. This is not unduly restrictive, as the absorbing-emitting medium is usually a gas, and almost all gases have a refractive index that is very close to unity as shown by table 9-I (ref. 1). However, there are certain situations where the refractive index can be significantly different from unity or can be variable over a given path for radiation as a result of spatial temperature variations. Table 9-I lists some common materials that possess nonunity refractive indices. As discussed in section 2.4.12 of volume I, one effect of nonunity n is to increase the blackbody emission *within the medium* by a factor of n^2 . In this section, consideration is given to some situations where the effect of refractive index must be considered.

9.3.1 Media With Constant But Nonunity Refractive Index

Consider the case of radiation with intensity i'_1 in a dielectric medium of refractive index n_1 . Let the radiation in solid angle $d\omega_1$ pass into a dielectric medium of refractive index n_2 as pictured in figure 9-1. As a result of the differing indices of refraction, the rays will change direction as they pass into medium 2. The radiation in solid angle $d\omega_1$ at incidence angle β_1 will pass into solid angle $d\omega_2$ at an angle of refraction β_2 . If it is assumed that there is no reflection or scattering at the interface, the energy of the radiation is conserved when crossing the interface. From the definition of intensity this conservation of energy is given by

TABLE 9-1.—REFRACTIVE INDICES OF SOME COMMON SUBSTANCES

[From ref. 1]

Material	Refractive index, n
Gases	
Air	1.00029
Argon	1.00028
Carbon dioxide	1.00045
Chlorine	1.00077
Hydrogen	1.00014
Methane	1.00044
Nitrogen	1.00030
Oxygen	1.00027
Water vapor	1.00026
Liquids	
Chlorine	1.385
Ethyl alcohol	1.36 to 1.34 (16° to 76° C)
Oxygen	1.221
Water	1.33 to 1.32 (14° to 100° C)
Solids	
Glass	
Crown	1.50 to 1.55
Flint	1.55 to 1.95
Ice	1.31
Quartz	1.52 to 1.69
Rock salt	1.5 to 1.9

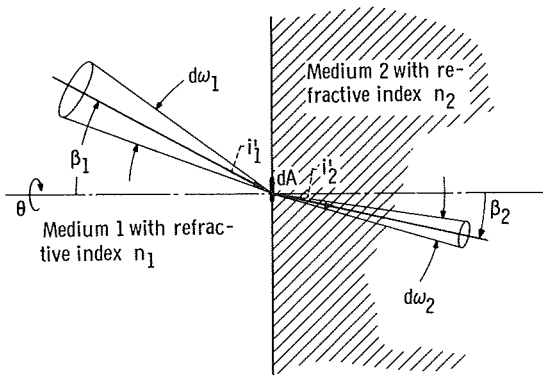


FIGURE 9-1.—Beam with initial intensity i_1' crossing interface between two dielectric media with unequal refractive indices.

$$i'_1 \cos \beta_1 dA d\omega_1 = i'_2 \cos \beta_2 dA d\omega_2 \quad (9-1)$$

where dA is an area element in the plane of the interface. Using the relation for solid angle

$$d\omega = \sin \beta d\beta d\theta \quad (9-2)$$

results in equation (9-1) becoming (noting that the increment of circumferential angle $d\theta$ is not changed in crossing the interface)

$$i'_1 \sin \beta_1 \cos \beta_1 d\beta_1 = i'_2 \sin \beta_2 \cos \beta_2 d\beta_2 \quad (9-3)$$

From equation (4-43) of volume I, Snell's law relates the indices of refraction to the angles of incidence and refraction by

$$\frac{n_1}{n_2} = \frac{\sin \beta_2}{\sin \beta_1} \quad (9-4)$$

Then by differentiation

$$n_1 \cos \beta_1 d\beta_1 = n_2 \cos \beta_2 d\beta_2 \quad (9-5)$$

Substituting equations (9-4) and (9-5) into equation (9-3) gives

$$\frac{i'_1}{n_1^2} = \frac{i'_2}{n_2^2} \quad (9-6)$$

Although equation (9-6) was derived for radiation crossing the interface of two media, the equation also holds for intensity at any point in a transparent medium with variable refractive index so long as the local properties of the medium are independent of direction, that is, are isotropic. This isotropy will be the case except in certain plasma physics applications. Thus, in general in a transparent isotropic medium, for either the spectral intensity, or the total intensity in a medium with spectrally independent refractive index

$$\frac{i'}{n^2} = \text{constant} \quad (9-7)$$

9.3.2 The Effect of Brewster's Angle

Consider a volume element dV inside a semi-infinite region of refractive index n_2 as shown in figure 9-2. Suppose that diffuse radiation of

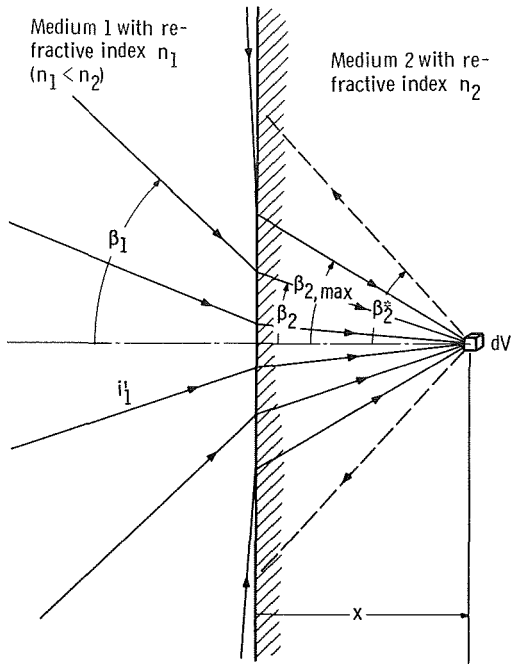


FIGURE 9-2.—Effect of refraction on radiation transport in media with nonunity refractive index.

intensity i_1' is incident upon the boundary of this region from a region having refractive index n_1 where $n_1 < n_2$. Radiation incident at grazing angles to the interface ($\beta_1 \approx 90^\circ$) will be refracted into medium 2 at a maximum value of β_2 given by

$$\sin \beta_{2, \max} = \frac{n_1}{n_2} \sin 90^\circ = \frac{n_1}{n_2} \quad (9-8)$$

Hence the volume element in medium 2 will receive direct radiation from medium 1 only at angular directions within the range

$$0 \leq \beta_2 \leq \beta_{2, \max} \left(= \sin^{-1} \frac{n_1}{n_2} \right) \quad (9-9)$$

Now consider emission from dV . The portion of this emission that enters region 1 will be along paths found by reversing the arrows on the solid lines in figure 9-2. However, there is also radiation from dV along paths such as those shown by the dashed lines in figure 9-2 that are incident on the interface at angles β_2^* , where

$$\sin \beta_2^* > \frac{n_1}{n_2} \quad (9-10)$$

From equation (9-4), this means that such a ray would enter medium 1 at an angle given by

$$\sin \beta_1 = \frac{n_2}{n_1} \sin \beta_2^* > \frac{n_2 n_1}{n_1 n_2} (=1) \quad (9-11)$$

But $\sin \beta_1$ cannot be greater than unity for real values of β_1 . This result is interpreted to mean that any ray incident upon the interface from medium 2 at any angle greater than that given by

$$\beta_{2, \max} = \sin^{-1} \frac{n_1}{n_2} \quad (9-12)$$

cannot enter medium 1, and must be totally reflected at the interface. The angle defined by equation (9-12) is called Brewster's angle.

From section 2.4.12 of volume I, the blackbody emission inside a dielectric medium with refractive index that is constant but not unity, has an intensity given by

$$i'_{b, m} = n^2 i'_b \quad (9-13)$$

Consequently, for an absorbing-emitting gray medium with absorption coefficient a , the total energy emitted by a volume element is

$$dQ_e = 4n^2 a \sigma T^4 dV \quad (9-14)$$

If spectral variations of n are known to be important, then an integration over wavelength must be included, provided of course that the data for n as a function of wavelength is known.

From equation (9-13) it might appear that because $n > 1$, the intensity radiated from a dielectric medium into air could be larger than the usual blackbody radiation i'_b . This is not the case as some of the energy emitted within the medium is reflected back into the emitting body at the medium-air interface. Consider a thick dielectric medium ($\kappa=0$) at uniform temperature and with refractive index n . The maximum intensity received at an element dA on the interface from all directions within the medium is $n^2 i'_b$. Only the energy within a cone having a vertex angle β_{\max} relative to the normal of dA will penetrate through the interface; for incidence angles larger than β_{\max} the energy will be reflected back into the medium. Hence, the energy received at dA that leaves the medium is

$$\int_{\beta=0}^{\beta_{max}} n^2 i'_b dA \cos \beta \, 2\pi \sin \beta \, d\beta = 2\pi n^2 i'_b dA \frac{\sin^2 \beta_{max}}{2}$$

From equation (9-8) with $n_1 = 1$ and $n_2 = n$ in this case, $\sin \beta_{max} = 1/n$ so that the total hemispherical emissive power leaving the interface is

$$2\pi n^2 i'_b dA \frac{1}{2n^2} = \pi i'_b dA$$

Dividing by πdA gives i'_b as the maximum diffuse intensity leaving the interface which is the expected blackbody radiation.

EXAMPLE 9-1: An elemental volume dV is located at $x = 1$ cm into a glass plate from the plate interface with air (as in fig. 9-2). Diffuse-gray radiation of intensity $10 \text{ W}/(\text{cm}^2)(\text{sr})$ in the air is entering the glass (note this intensity is entering the glass so the reflectivity of the interface has already been accounted for). If the absorption coefficient of the glass is 0.005 cm^{-1} and its refractive index is $n = 1.75$, determine the temperature at dV as a result of only this incident intensity. Assume the radiation absorbed from the surrounding glass is small, and neglect heat conduction.

An energy balance on dV states that the emitted energy will equal the incident energy that is transmitted through the glass and absorbed by dV , that is,

$$4n^2 a \sigma T^4(x) dV = a dV \int_{\omega=4\pi} i'(x, \beta) d\omega$$

From equation (9-7) the intensity $i'_{glass}(0, \beta)$ in the glass at the glass surface is related to the entering intensity in air $i'_{air}(0)$ by $i'_{glass}(0, \beta) = n^2 i'_{air}(0)$. Since the path length from the glass surface to dV is $x/\cos \beta$, the intensity $i'_{glass}(x, \beta)$ at dV is given by Bouguer's law as

$$i'_{glass}(x, \beta) = i'_{glass}(0, \beta) \exp\left(-\frac{ax}{\cos \beta}\right) = n^2 i'_{air}(0) \exp\left(-\frac{ax}{\cos \beta}\right)$$

Substituting into the energy balance and solving for T^4 gives

$$T^4 = \frac{i'_{air}(0)}{4\sigma} \int_{\omega=4\pi} \exp\left(-\frac{ax}{\cos \beta}\right) d\omega$$

Over part of the 4π solid angle surrounding dV there will be no energy incident on dV , so that the integration limits on β must be derived by

considering the restriction of equation (9-8). This gives

$$T^4 = \frac{2\pi i'_{air}(0)}{4\sigma} \int_0^{\beta_{max} = \sin^{-1}(1/1.75)} \exp\left(-\frac{ax}{\cos \beta}\right) \sin \beta d\beta$$

Let $\mu = \cos \beta$ to obtain

$$T^4 = \frac{2\pi i'_{air}(0)}{4\sigma} \int_{\cos \beta_{max}}^1 \exp\left(-\frac{ax}{\mu}\right) d\mu$$

From equation (2-45) this becomes

$$T^4 = \frac{2\pi i'_{air}(0)}{4\sigma} \left[E_2(ax) - \int_0^{\cos \beta_{max}} \exp\left(-\frac{ax}{\mu}\right) d\mu \right]$$

Now let $\gamma = \mu/\cos \beta_{max}$ to obtain

$$T^4 = \frac{2\pi i'_{air}(0)}{4\sigma} \left[E_2(ax) - \cos \beta_{max} E_2\left(\frac{ax}{\cos \beta_{max}}\right) \right]$$

Substituting numerical values gives

$$T^4 = \frac{2\pi 10 \text{ W/cm}^2}{4 \times 5.729 \times 10^{-12} \text{ W/(cm}^2)(\text{K}^4)} \left[E_2(0.005) - 0.821 E_2\left(\frac{0.005}{0.821}\right) \right]$$

The E_2 values can be found from table II in the appendix to give

$$T^4 = \frac{5\pi \times 10^{12}}{5.729} (0.18) \text{K}^4$$

$$T = 840 \text{ K}$$

In this example, the effect of the surface reflectivity in determining the intensity of the radiation that is able to cross the interface and enter the material was not explicitly treated. It can be introduced for optically smooth surfaces by using the electromagnetic theory relations for reflectivity from chapter 4 of volume I.

Gardon (refs. 2 to 5) has treated problems of thermal radiation in glass, where effects of the refractive index are substantial. Reference 2 includes some analysis of perpendicular and parallel polarization contributions; in references 3 and 4, a comprehensive analysis of the heat treatment of glass is given. This analysis of heat treatment includes the

effects of conduction within the glass and convection at the surface. In reference 5, a review of radiant heat transfer as studied by researchers in the glass industry is given, and a digest of much of the literature on the subject up to 1961 is presented. Condon (ref. 6) has given a more recent review of radiation problems in the glass industry from the viewpoint of the astrophysicist.

As mentioned in section 7.3, McConnell (ref. 7) has studied the radiation effects on a space vehicle that has a layer of frost deposited on its surface. An external source of radiation (the Sun or a diffuse source) is assumed to radiate to the frost layer, and the resulting temperature profile in the frost is analyzed as modified by sublimation of the frost at its free surface. The refractive index of the frost must be accounted for because of the modification of the usual radiation equations as outlined in example 9-1.

9.3.3 Radiative Transfer Between Dielectrics Spaced Closely Together

A highly effective insulation can be constructed from many layers of radiation reflecting films separated by vacuum to provide a series of alternate radiation and conduction barriers. One construction is to deposit highly reflecting metallic films on both sides of thin sheets of plastic. The sheets are then spaced apart by placing between them a cloth net with large open area between the fibers. Typically a stacking of 50 radiation shields per inch of thickness can be obtained in this manner. An important use of multilayer insulation is in low temperature applications such as insulation of cryogenic storage tanks.

The multilayer insulation can be quite effective. A conventional analysis of radiation between surfaces in vacuum shows that if two gray parallel plates with surface emissivity ϵ are separated by one radiation shield also having emissivity ϵ on both sides, the heat radiated between the plates will be reduced to one-half its value without the shield. The use of n shields all of emissivity ϵ will reduce the heat flow to $1/(n+1)$ of the uninsulated value. The additional effect to be discussed here arises because the reflecting layers are spaced very close to each other; the question is whether such small spacings can have any influence on the radiative transfer.

The situation of transfer between closely spaced surfaces was examined by Cravalho, Tien, and Caren (ref. 8) who considered the geometry shown in figure 9-3. The geometry consists of two semi-infinite dielectric media having refractive indices n_1 and n_3 , separated by a vacuum gap. In the usual analysis for radiative transfer between two surfaces (e.g., 1 and 3), as given by equation (5-11) of volume II, the heat flux transferred across the gap is given by

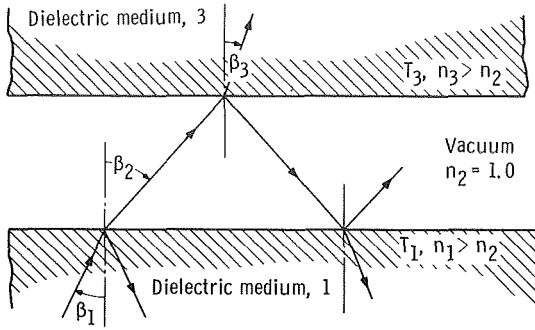


FIGURE 9-3.—Reflection and transmission of electromagnetic wave in gap between two dielectrics; $T_3 < T_1$.

$$q_1 = \int_0^{\infty} \left[\frac{e_{\lambda b, 1}(\lambda, T_1) - e_{\lambda b, 3}(\lambda, T_3)}{\frac{1}{\epsilon_{\lambda, 1}(\lambda, T_1)} + \frac{1}{\epsilon_{\lambda, 3}(\lambda, T_3)} - 1} \right] d\lambda$$

and the spacing between the plates does not appear. When the spacing between the surfaces is very small, however, there are two effects that enter which are a function of spacing. The first effect is wave interference, in which a wave reflecting back and forth in a gap between two dielectrics may undergo cancellation or reinforcement.

The second effect is radiation tunneling. Figure 9-3 reveals that for ordinary behavior at an interface as discussed in section 9.3.2 some of the radiation in medium 1 traveling toward region 2 can undergo total internal reflection at the interface when $n_1 > n_2$. For ordinary radiative behavior this would occur when the incidence angle β_1 is equal to or larger than Brewster's angle given by equation (9-12), that is, $\beta_1 \geq \sin^{-1}(n_2/n_1)$. When region 2 in figure 9-3 is sufficiently thin, however, electromagnetic theory predicts that, even for an intensity incident at β_1 greater than Brewster's angle total internal reflection will not occur. Rather, part of the incident intensity will propagate across the thin region 2 and enter medium 3. This effect is radiation tunneling as viewed classically.

As shown in reference 8, both tunneling and interference can become important only when the spacing between radiating bodies separated by vacuum is less than about $\lambda_{max, vac}(T_3)$ which is the wavelength in vacuum at maximum blackbody emissive power from a surface at the sink temperature T_3 . The $\lambda_{max, vac}(T_3)$ is found from Wien's displacement law as C_3/T_3 (eq. (2-17) of vol. I). The tunneling and interference effects also depend on temperature. Even for very small spacings on the order

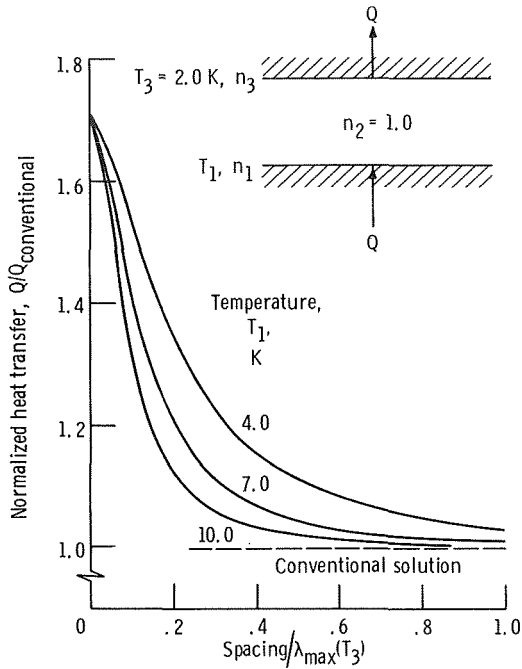


FIGURE 9-4.—Effects of wave interference and radiation tunneling on radiative transfer between two dielectric surfaces; $n_1 = n_3 = 1.25$; $\lambda_{max}(T_3) = 0.28978/n_3 T_3$ cm. (From ref. 8.)

of $\lambda_{max,vac}(T_3)$, the effects become very small at normal temperatures, and hence are only important in certain cryogenic applications where temperatures of a few degrees absolute are encountered. Figure 9-4 shows some representative results under conditions giving maximum effects and illustrates the influence of temperature T_1 . Note that $\lambda_{max}(T_3)$ in figure 9-4 is the wavelength in medium 3 and hence is given by $C_3/n_3 T_3$ from equation (2-33) of volume I. The conventional solution referred to in the figure is obtained when wave interference and radiation tunneling are neglected in the analysis.

9.4 FLAMES, LUMINOUS FLAMES, AND PARTICLE RADIATION

Under certain conditions, gases emit much more radiation in the visible region of the spectrum than would be expected from the absorption coefficients of the gas species that are present in chemical equilibrium. For example, the typical almost transparent blue flame of a bunsen burner can be made into a smoky yellow-orange flame by changing only the fuel-air ratio. Such luminous emission is usually ascribed to hot

carbon (soot) particles that are formed because of incomplete combustion in hydrocarbon flames. There is room for argument even here. Echigo, Nishiwaki, and Hirata (ref. 9) and others have advanced the hypothesis, supported by some experimental facts, that the luminous emission from some flames is due to the emission from vibration-rotation bands of chemical species that appear during the combustion process *prior* to the formation of soot particles. Since the formation of soot is the most widely accepted view, the radiation from soot will be emphasized here when discussing luminous flames.

Combustion in the general case is a very complicated chemical process often consisting of a system of chemical reactions occurring in series and parallel. The combustion process involves a variety of intermediate chemical species. The composition and concentration of these intermediate species cannot be predicted very well unless complete knowledge is available of the reaction kinetics of the flame, and this knowledge will not usually be at hand. Because the radiation properties of the flame depend on the distributions of species and the temperature variations within the flame, a detailed prediction of radiation from flames is not often possible by knowing only the original combustible constituents and the flame geometry. Because of these difficulties, it is usually necessary to resort to empirical methods for predicting radiation from systems involving combustion.

In order to facilitate the present discussion, let us separately examine two facets of predicting radiation from flames: (1) The calculation of a theoretical flame temperature by considering the chemical energy release and without accounting for heat loss by radiation, and (2) the more complex problem of radiation from a gas containing solid particles which will alter the theoretical flame temperature.

9.4.1 Theoretical Flame Temperature

To present empirical correlations of radiation from flames, a characteristic parameter is the average temperature of a well-mixed flame as a result of the addition of chemical energy. Fortunately, well-developed methods exist (refs. 10 to 12) for computing the theoretical flame temperature of a given combustion system from available thermodynamic data. The effect of preheating either the fuel or oxidizer or both can be included. Such calculations assume complete combustion of the fuel and no heat losses. The process of flame temperature computation can be conveniently shown by an example.

EXAMPLE 9-2: Using the mean heat capacity data of figure 9-5 (adapted from ref. 10) and the heat of combustion from table 9-II, calculate the theoretical temperature of an ethane flame burning with 100

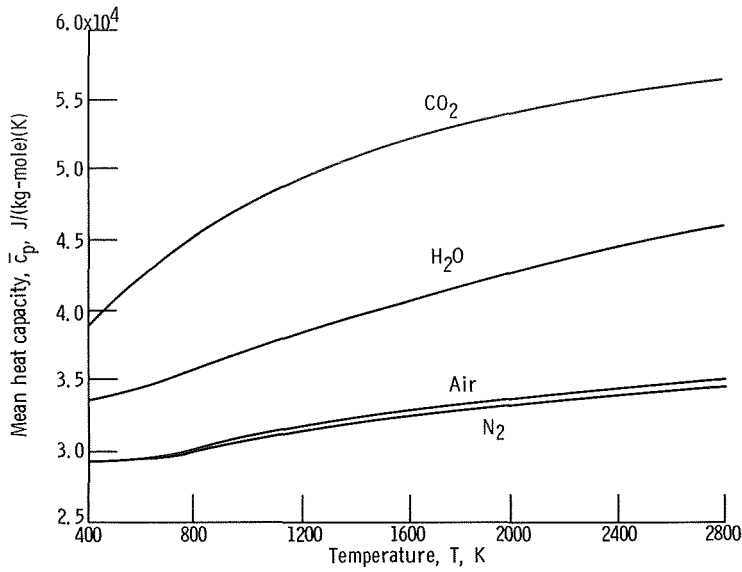
FIGURE 9-5.—Mean heat capacity of various gases averaged between T and 298 K.

TABLE 9-II.—HEAT OF COMBUSTION AND FLAME TEMPERATURE FOR HYDROCARBON FUELS

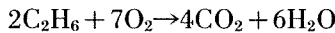
Fuel	Heat of combustion, J/kg	Maximum flame temperature, K (combustion with dry air at 298 K)		
		Theoretical (complete combustion)	Theoretical (with dissociation and ionization)	Experimental
Carbon monoxide (CO)	4.83×10^7	2615
Hydrogen (H ₂)	12.0	2490
Methane (CH ₄)	5.0	2285	2191	2158
Ethane (C ₂ H ₆)	4.74	2338	2222	2173
Propane (C ₃ H ₈)	4.64	2629	2240	2203
<i>n</i> -Butane (C ₄ H ₁₀)	4.56	2357	2246	2178
<i>n</i> -Pentane (C ₅ H ₁₂)	4.53	2360
Ethylene (C ₂ H ₄)	4.72	2523	2345	2253
Propylene (C ₃ H ₆)	4.57	2453	2323	2213
Butylene (C ₄ H ₈)	4.53	2431	2306	2208
Amylene (C ₅ H ₁₀)	4.50	2477
Acetylene (C ₂ H ₂)	4.82	2859
Benzene (C ₆ H ₆)	4.06	2484
Toluene (C ₆ H ₅ CH ₃)	4.09	2460

percent excess air (by volume). The ethane is supplied at room temperature (25° C) and the air feed is preheated to 500° C. The flame is burning in an environment at a pressure of 1 atm.

The theoretical flame temperature T is computed by using energy conservation and assuming no heat losses. The energy in the combustion constituents plus the energy of combustion is equated to the energy of the combustion products. This gives

$$T - T_{ref} = \frac{\left(\begin{array}{c} \text{energy in feed air and} \\ \text{fuel above } T_{ref} \end{array} \right) + \left(\begin{array}{c} \text{energy released} \\ \text{by combustion} \end{array} \right)}{\left(\begin{array}{c} \text{total mass of} \\ \text{products} \end{array} \right) \times \left(\begin{array}{c} \text{mean heat capacity} \\ \text{of products} \end{array} \right)} \quad (9-15)$$

For ethane, assuming complete combustion, the reaction is



Let us assume that 2 kilogram-moles of ethane are burned. Then 7 moles of oxygen are consumed during combustion. Since there is 100 percent excess air, only one-half of the feed air contributes oxygen to the combustion process, so a total of 14 moles of oxygen are introduced in the feed air. Oxygen makes up 21 percent by volume of the feed air, and since mole fraction is equal to part by volume, the moles of air used are

$$m_{air} = \frac{14}{0.21} = 66.67$$

Thus, the total input to the combustion process consists of 2 moles of ethane fuel and 66.67 moles of air. The sensible heat in the feed components above a reference temperature is

$$H_i = \sum_k [m\bar{c}_p(T_i - T_{ref})]_k$$

where \bar{c}_p is the mean heat capacity between the reference temperature and the input temperature T_i . Using data from figure 9-5, which has a reference temperature of 298 K (25° C), gives

$$\begin{aligned} H_i &= [m\bar{c}_p(T_i - T_{ref})]_{ethane} + [m\bar{c}_p(T_i - T_{ref})]_{air} \\ &= 0 + 66.67 \times 2.93 \times 10^4 (773 - 298) = 9.28 \times 10^8 \text{ joules (J)} \end{aligned}$$

where the ethane contributes nothing as it is supplied at T_{ref} . The heat

released by combustion ΔH is found by using the heat of combustion from table 9-II and the fact that the molecular weight of ethane is 30; that is,

$$\Delta H = 2 \text{ moles} \times 30 \frac{\text{kg}}{\text{mole}} \times 4.74 \times 10^7 \frac{\text{J}}{\text{kg}} = 28.4 \times 10^8 \text{ J}$$

The numerator of equation (9-15) is then

$$H_i + \Delta H = 37.7 \times 10^8 \text{ J}$$

Nitrogen, which makes up about 79 percent by volume of air, remains from that portion of the feed air that supplied the oxygen for combustion. The amount of nitrogen in the combustion products is then

$$33.3 \times 0.79 = 26.3 \text{ moles}$$

The total quantity of products after combustion is (in moles)

Carbon dioxide (CO ₂)	4
Water vapor (H ₂ O)	6
Air	33.3 (half of feed air)
Nitrogen (N ₂)	26.3

To find the denominator of equation (9-15), the individual quantities are summed

$$H_{prod} = \sum_j m_j \bar{c}_{p,j}$$

However, \bar{c}_p depends on the product temperature T , which is the flame temperature and is not yet known. We must estimate T to determine the $\bar{c}_{p,j}$ values and then substitute the quantities into equation (9-15). If the calculated flame temperature agrees with the assumed value, the solution is finished. Otherwise, a new temperature is estimated, H_{prod} is recalculated and substituted into equation (9-15), and this procedure is continued until the assumed and calculated flame temperatures agree. A table of calculations is as follows:

Assumed flame temperature, K	Mean heat capacity, \bar{c}_p , J/(kg)(mole)(K)				Product enthalpy, H_{prod} , J	Calculated temperature, K
	H ₂ O	CO ₂	Air	N ₂		
2400	4.44×10^4	5.51×10^4	3.35×10^4	3.30×10^4	2.47×10^6	1825
2000	4.25	5.36	3.33	3.28	2.44	1845

Because a 400 K change in the assumed flame temperature produced only about a 20 K change in the calculated flame temperature, a value of 1853 K is estimated as within a few degrees of the converged result.

In this example, it was assumed that the combustion process is complete and that no dissociations of the combustion products occur. In addition, no consideration has been given to energy loss from the flame by radiation, which would lower the flame temperature. Methods for including these effects are discussed in reference 12. A list of theoretical flame temperatures (no radiation included) is shown in table 9-II for various hydrocarbon flames. Results for complete combustion with dry air are shown, followed by calculated results modified to allow for dissociation and ionization of products. The latter are compared with experimental results. In addition, the heats of combustion of the substances are shown. All data are from references 12 and 13. Extensive tabulations of similar data for over 200 hydrocarbons are given in references 10 and 13.

Let us proceed to a consideration of the radiation emitted by a nonluminous flame now that its average temperature is known.

9.4.2 Radiation From Nonluminous Flames

The phenomena involved in radiation from the nonluminous portion of the combustion products are fairly well understood. The complexities of the chemical reaction are not too important here since it is the gaseous end products situated above the active burning region that are being considered. During combustion, chemical potential energy is released by the reaction of the fuel and oxidant atoms. This results in radiation in spectral lines and bands produced by the various types of transitions between energy states. In most instances a hydrocarbon combustion is being considered and the radiation is from the CO_2 and H_2O bands in the infrared. For flames a few or more feet thick as in commercial furnaces, the emission leaving the flame within the CO_2 and H_2O vibration-rotation bands can be close to blackbody emission.

The gaseous radiation properties and methods of chapter 5 can be used to compute the radiative heat transfer from the flame. The analysis is greatly simplified if the gas is well mixed so that it can be assumed isothermal. For a nonisothermal condition the gas can be divided into approximately isothermal zones, and the convection within the gas can also be included if the circulation pattern within the combustion chamber is known. A nonisothermal analysis with convection was carried out in reference 14 for cylindrical flames.

EXAMPLE 9-3: In example 9-2, the combustion products were 4 moles of CO_2 , 6 moles of H_2O vapor, 33.3 moles of air, and 26.3 moles of N_2 . Assume these gaseous products are in a cylindrical region 4 ft high and 2 ft in diameter and are uniformly mixed at the theoretical flame temperature 1853 K. The pressure is 1 atm. Compute the radiation leaving the gaseous region using the methods in sections 5.5 and 5.6.

The partial pressure of each constituent is equal to its mole fraction of the mixture. Then for the CO_2 and H_2O the partial pressures are

$$p_{\text{CO}_2} = \left(\frac{4}{69.6} \right) (1 \text{ atm}) = 0.0574 \text{ atm}$$

$$p_{\text{H}_2\text{O}} = \left(\frac{6}{69.6} \right) (1 \text{ atm}) = 0.0861 \text{ atm}$$

The mean beam length of the gas for negligible self-absorption can be computed from equation (5-51) as

$$L_{e,0} = \frac{4V}{A} = \frac{4 \left(\pi \frac{2^2}{4} \right) 4}{(2\pi \times 4) + 2\pi \frac{2^2}{4}} = \frac{16\pi}{10\pi} = 1.6 \text{ ft}$$

To include self-absorption, a correction factor of 0.9 is applied so the mean beam length becomes

$$L_e = 0.9(1.6) = 1.44 \text{ ft}$$

Then

$$p_{\text{CO}_2} L_e = 0.0574 \times 1.44 = 0.0825 \text{ (atm)(ft)}$$

$$p_{\text{H}_2\text{O}} L_e = 0.0861 \times 1.44 = 0.124 \text{ (atm)(ft)}$$

Using the gas emittance charts (figs. 5-11 to 5-15) at the flame temperature (3340 °R) results in

$$\epsilon_{\text{CO}_2} = 0.039$$

and

$$\epsilon_{\text{H}_2\text{O}} = 0.029 \times 1.08 = 0.031$$

The 1.08 factor in $\epsilon_{\text{H}_2\text{O}}$ is a correction for the partial pressure of the water

vapor not being zero. In addition, there is a negative correction resulting from spectral overlap of the CO_2 and H_2O radiation bands. This is obtained from figure 5-15 at the values of the parameters

$$\frac{p_{\text{H}_2\text{O}}}{p_{\text{CO}_2} + p_{\text{H}_2\text{O}}} = \frac{0.0861}{0.0574 + 0.0861} = 0.60$$

$$p_{\text{CO}_2}L_e + p_{\text{H}_2\text{O}}L_e = 0.0825 + 0.124 = 0.207 \text{ (atm)(ft)}$$

The correction is $\Delta\epsilon = 0.002$. Then the gas emittance is

$$\epsilon_g = \epsilon_{\text{CO}_2} + \epsilon_{\text{H}_2\text{O}} - \Delta\epsilon = 0.039 + 0.031 - 0.002 = 0.068$$

The radiation from the gas region is then computed as

$$Q = \epsilon_g A \sigma T_g^4 = 0.068(10\pi)0.173 \times 10^{-8} (3340)^4 = 0.46 \times 10^6 \frac{\text{Btu}}{\text{hr}}$$

9.4.3 Radiation From and Through Luminous Flames

In the region of the flame that is actively burning, there are several factors that complicate the radiative transfer. The simultaneous production and loss of energy produces a temperature variation and thus a variation of properties and emission within the flame. The intermediate combustion products resulting from the complex reaction chemistry can significantly alter the radiation characteristics from those of the final products. Soot is the most important radiating product formed when burning hydrocarbons. The soot emits in a continuous spectrum in the visible and infrared regions, and as a result of the visible radiation the flame is called luminous. The soot is quite important as it can often double or triple the heat that would be radiated by the gaseous products alone. A method for increasing the flame emission if desired is to promote slow initial mixing of the oxygen with the fuel so that large amounts of soot will form at the base of the flame.

Determining the effect soot has on the flame radiation resolves into two requirements. One of these is to somehow obtain the soot distribution in the flame. This depends on the type of fuel, the mixing of fuel and oxidant, and the flame temperature. The soot distribution is too complicated to calculate from basic principles, so some experimental knowledge of a given combustion system is needed. The second requirement is to know the radiative properties of the soot. Then if the soot concentration and distribution are known, a radiation computation can be attempted. At present the radiant properties of soot are only known to a first approximation.

If the flames found in both the laboratory and in industry are included, the individual soot particles produced in hydrocarbon flames generally range in size from a diameter of 50 angstroms (\AA) to greater than 3000 \AA . The soot can be in the form of spherical particles, agglomerated masses, or is sometimes in long filaments. The experimental determination of the physical form of the soot is most difficult, as any type of probe that is used to gather the soot for photomicrographic analysis may cause agglomeration of particles or otherwise alter the soot characteristics. The nucleation and growth of the soot particles is not well understood. Some of the soot can be nucleated in less than a millisecond after the fuel enters the flame, and the rate at which soot continues to form does not seem influenced much by the residence time of the fuel in the flame. It is an unknown precipitation mechanism that must govern the soot production.

Stull and Plass (ref. 15) and Siddall and McGrath (ref. 16) have computed the spectral emittance of luminous flames as a function of the volume fraction of soot particles present. This was done by the use of Mie theory (section 8.4.6), which is a direct application of electromagnetic theory, to obtain the radiation characteristics of the assumed spherical soot particles (the Mie result will be given in equation (9-22)). The calculations were carried out using optical properties of a baked electrode carbon at 2250 K as the assumed n and κ for soot carbon. The results should be valid over a range of temperatures because Howarth, Foster, and Thring (ref. 17) have shown that the absorption coefficient for carbon particles is at most a weak function of temperature.

For a beam of radiation passing through a gas containing suspended soot particles, it has been found experimentally that the attenuation obeys Bouguer's law, that is,

$$i'_\lambda(S) = i'_\lambda(0) \exp(-a_\lambda S) \quad (9-16)$$

For small particles such that $\pi D/\lambda < 0.25$ (where D is particle diameter), the Mie theory gives in equation (8-30) that the scattering cross section depends on $(\pi D/\lambda)^4$. The Mie theory also shows that, for the same conditions, the absorption cross section depends on $\pi D/\lambda$ to the first power (see eq. (9-22)). Thus the scattering is negligible compared with absorption, and a_λ in equation (9-16) is actually the absorption coefficient rather than the extinction coefficient of equation (1-13). Then as a consequence of equation (5-44), the spectral emittance of an isothermal luminous gas volume is written as

$$\epsilon_\lambda = 1 - \exp(-a_\lambda L_e) \quad (9-17)$$

where L_e is the mean beam length for the volume.

9.4.3.1 *Experimental correlation of soot spectral absorption.*—A relatively simple empirical relation for a_λ that has been found experimentally in some instances has the form

$$a_\lambda = Ck\lambda^{-\alpha} \quad (9-18)$$

where C is the soot volume concentration (average volume of particles per unit volume of cloud) and k is a constant. The λ will always be in microns for the numerical results given here. Hottel (ref. 18) recommends the use of

$$a_\lambda = \frac{Ck_1}{\lambda^{0.95}} \quad (9-19)$$

in the infrared region down to $\lambda = 0.8 \mu\text{m}$. In some more recent experiments, Siddall and McGrath (ref. 16) also found the functional relation of equation (9-19) to hold approximately. They give in the range from $\lambda = 1$ to $7 \mu\text{m}$ the following mean values of α :

Source of soot	Mean α for $\lambda = 1$ to $7 \mu\text{m}$
Amyl acetate	0.89, 1.04
Avtur kerosene	0.77
Benzene	0.94, 0.95
Candle	0.93
Furnace samples	0.96, 1.14, 1.25
Petrotherm	1.06
Propane	1.00

Thus the 0.95 exponent recommended by Hottel appears reasonable.

In reference 16 the data were also inspected in more detail to see if α had a functional variation with λ that would provide a more accurate correlation than using a constant α . In some instances α took the form

$$\alpha = a + b \ln \lambda$$

where a and b are positive constants. Examples are shown in figure 9-6. In other cases, as in figure 9-7, a more general polynomial was required to express α as a function of λ . Thus, as a generalization of equation (9-19), for the infrared region

$$a_\lambda = \frac{Ck_1}{\lambda^{\alpha(\lambda)}} \quad (9-19a)$$

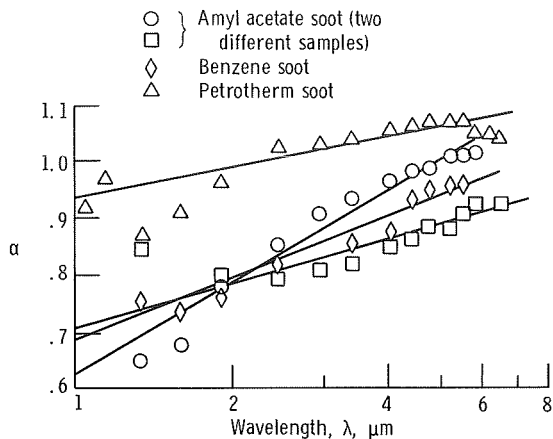


FIGURE 9-6.—Experimental values of α plotted against λ for cases where α varies approximately linearly in $\ln \lambda$ (ref. 16).

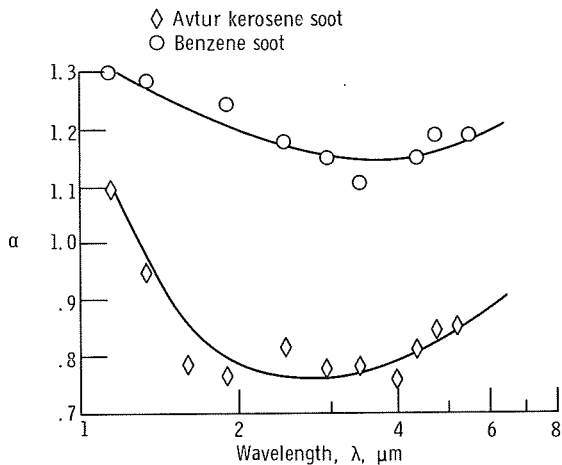


FIGURE 9-7.—Experimental values of α as a function of λ where α does not vary linearly with $\ln \lambda$ (ref. 16).

and letting α be a constant is only an approximation.

In the visible range an inspection by Hottel (ref. 18) of experimental data led to the recommended form

$$a_{\lambda} = \frac{Ck_2}{\lambda^{1.39}} \quad (9-20)$$

for the wavelength region around $\lambda = 0.6 \mu\text{m}$ (say $\lambda \approx 0.3$ to $0.8 \mu\text{m}$).

9.4.3.2 *Electromagnetic theory prediction of soot spectral absorption.*—To try to understand the absorption coefficient of a soot cloud from a more fundamental basis, electromagnetic theory can be employed (refs. 15, 16, 19, and 20). The absorption coefficient is written as

$$a_\lambda = E_\lambda AN \quad (9-21)$$

The product $E_\lambda A$ is the spectral absorption cross section, defined in the same manner as the scattering cross section s_λ used in equation (8-5). The N is the number of particles per unit volume, and A is the projected area of a particle ($A = \pi D^2/4$, as particles are assumed spherical). The E_λ by itself is the spectral absorption efficiency factor which is the ratio of the spectral absorption cross section to the actual physical cross section of the particle. For the limit of small particles the Mie equations give the E_λ for a small absorbing sphere as

$$E_\lambda = \frac{24\pi D}{\lambda} \frac{n\kappa}{[(n^2 - \kappa^2) + 2]^2 + 4n^2\kappa^2} \quad (9-22)$$

where n and κ are the simple index of refraction and the extinction coefficient of the sphere material when the complex index of refraction is expressed in the form $\bar{n} = n - i\kappa$. Since the optical quantities n and κ are functions of λ , equation (9-22) can be written as

$$E_\lambda = \frac{24\pi D}{\lambda} F(\lambda) \quad (9-23)$$

Then from equation (9-21)

$$a_\lambda = \frac{24\pi D}{\lambda} F(\lambda) AN = \frac{36\pi C}{\lambda} F(\lambda) \quad (9-24)$$

where $C = N\pi D^3/6$ is the volume of the particles per unit volume of the cloud. The ratio

$$\frac{a_\lambda}{C} = \frac{36\pi}{\lambda} F(\lambda) = \frac{36\pi}{\lambda} \frac{n\kappa}{[(n^2 - \kappa^2) + 2]^2 + 4n^2\kappa^2} \quad (9-25)$$

is then a function of wavelength and can be evaluated if the optical properties of soot are known as a function of λ .

In reference 20 the optical properties n and κ of propane soot were measured by collecting the soot and then compressing it on a brass plate.

The values obtained were as follows:

Wavelength, λ , μm	Simple refrac- tive index, n	Extinction coefficient, κ
0.4358	1.57	0.46
.4500	1.56	.50
.5500	1.57	.53
.6500	1.56	.52
.8065	1.57	.49
2.5	2.04	1.15
3.0	2.21	1.23
4.0	2.38	1.44
5.0	2.07	1.72
6.0	2.62	1.67
7.0	3.05	1.91
8.5	3.26	2.10
10.0	3.48	2.46

By using these values the a_λ/C was evaluated from equation (9-25) yielding figure 9-8. Although the a_λ/C decreases with λ as expected from the form of equation (9-18), it is evident that an approximate curve fit by straight lines (on the logarithmic plot) would yield exponents on λ somewhat different than those of equations (9-19) and (9-20).

The predicted form by Mie theory of $\alpha(\lambda)$ as used in equation (9-19a) can now be examined in more detail in the infrared region by equating the expressions in equations (9-19a) and (9-24). This gives

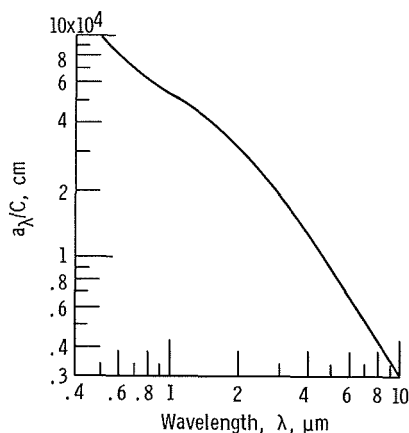


FIGURE 9-8.—Spectral absorption coefficient divided by volume concentration for propane soot (ref. 20).

$$\frac{k_1}{\lambda^{\alpha(\lambda)}} = \frac{36\pi}{\lambda} F(\lambda) \quad (9-26)$$

By evaluating this relation at $\lambda = 1$, the constant k_1 applicable to the infra-red region is found as

$$k_1 = 36\pi F(1) \quad (9-27)$$

Then

$$\lambda^{\alpha(\lambda)} = \lambda \frac{F(1)}{F(\lambda)}$$

Taking the logarithm of both sides and solving for $\alpha(\lambda)$ give

$$\alpha(\lambda) = 1 + \frac{\ln \left[\frac{F(1)}{F(\lambda)} \right]}{\ln \lambda} \quad (9-28)$$

The optical properties of the soot can then be used in $F(1)$ and $F(\lambda)$ as defined in equation (9-25), and $\alpha(\lambda)$ can be found. This was done in reference 16 using the properties of a baked electrode carbon at 2250 K. The results are shown in figure 9-9. The trend is the same as the experimental curves of figure 9-6, but the α values are larger than the experimental values. They are also larger than the average value recommended

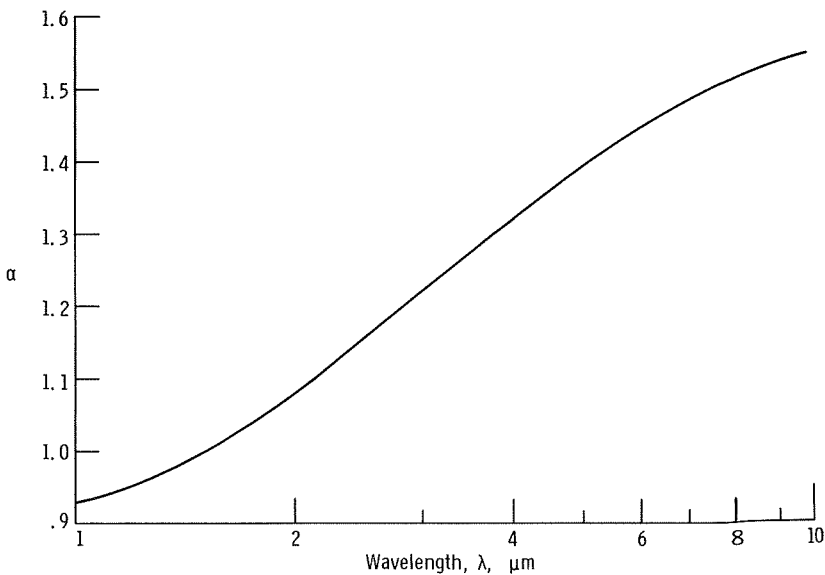


FIGURE 9-9.— Calculated variation of α with wavelength using properties of baked electrode carbon at 2250 K (ref. 16).

in equation (9-19). The discrepancy is probably partly due to the optical properties for the baked electrode carbon being different from that of soot.

9.4.3.3 *Total emittance of soot cloud.*—If a path S is now considered through an isothermal cloud of suspended soot having a uniform concentration, a total emittance can be found. This is the emittance accounting for the soot absorptance alone and does not include the emission from the suspending gas. The total emittance is found from equation (1-43) as

$$\epsilon(T, S) = \frac{\int_0^{\infty} e_{\lambda b} [1 - \exp(-a_{\lambda} S)] d\lambda}{\sigma T^4}$$

which can also be written as

$$\epsilon(T, CS) = \frac{\int_0^{\infty} e_{\lambda b} \left[1 - \exp\left(-\frac{a_{\lambda}}{C} CS\right) \right] d\lambda}{\sigma T^4} \quad (9-29)$$

By using a_{λ}/C from equation (9-25) or figure 9-8, the ϵ can be evaluated numerically and will be a function of the cloud temperature and the product of concentration and path length CS . This is shown in figure 9-10 for propane soot. By integrating over a distribution of particle sizes, it was found in reference 16 that the individual particle sizes were unimportant and thus at a fixed T and S the ϵ only depends on the soot volume concentration in the cloud.

Stull and Plass (ref. 15) also give results for the scattering coefficient

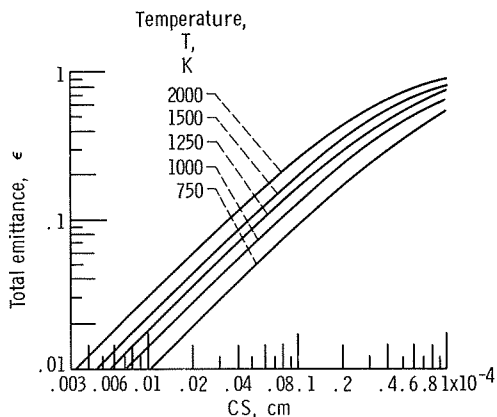


FIGURE 9-10.—Total emittance of soot suspensions as a function of temperature and volume fraction path-length product for propane soot (ref. 20).

of soot. Their results show that in most instances scattering has little effect on the emittance in the wavelength range that contains significant energy at hydrocarbon combustion temperatures. Erickson, Williams, and Hottel (ref. 21) have experimentally studied scattering from a luminous benzene-air flame. Their experimental results were found to agree with the predictions of Stull and Plass if the soot particles were taken to be of two predominant diameters. This indicated that small particles on the order of 250 \AA in diameter are formed along with agglomerated particles with an equivalent diameter of 1850 \AA . These sizes were observed by gathering soot with a probe and using electron microscopy. A comparison of some of the experimental results of reference 21 with the analysis of reference 15 is shown in figure 9-11.

Thring, Beer, and Foster (ref. 22) have put some of the results of Stull and Plass (ref. 15) along with their own extensive experimental results into useful graphs of emittance, extinction coefficient, and soot concentration for flames applicable in industrial practice. They note, however, that predictions of soot concentration can only be done for flames geometrically similar and with the same control variables as those which have already been studied. Their paper contains a useful review of the world-wide efforts to gather information and give methods for the prediction of radiation from luminous industrial flames. Other such information is found in references 23 to 26.

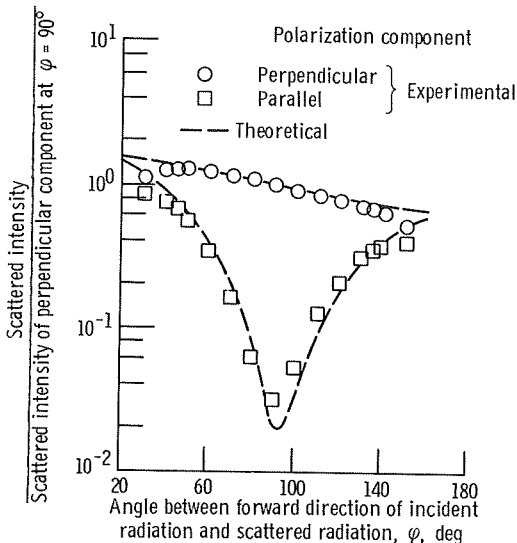


FIGURE 9-11.—Comparison of experiment with Mie scattering theory for radiation scattered from benzene-air flame at wavelength $\lambda = 5461 \text{ \AA}$. Theoretical curves based on spheres of diameter 250 \AA with 0.002 percent spheres of diameter 1850 \AA , all with complex refractive index ($n - i\kappa = 1.79 - 0.79 i$). (From ref. 21.)

In addition to the uncertainties in the optical properties and hence in the a_λ and ϵ of soot, it is noted that a_λ and ϵ are in terms of the soot concentration. To use equation (9-18), the Ck is needed. To use figure 9-10 to determine ϵ for a given flame size, the C in the abscissa must be known. At present there is no way to compute C from first principles knowing the fuel and burner geometry. Hence some indication of C or Ck must be obtained by examining flames experimentally. It may be possible to extrapolate performance for a particular application by examining a similar flame.

One technique that can be used to obtain information on the soot concentration quantity Ck_2 (as in eq. (9-20)) is to sight through the flame onto a cold black background with a pyrometer and match the brightness of the pyrometer filament to that of the flame while using first a red filter and then a green filter. With each of the filters, the pyrometer is also sighted on a blackbody source, and the source temperatures are obtained that produce the same brightness as when the flame was viewed. As a convenient simplification at the small λT for red and green wavelengths when considering typical flame temperatures, the blackbody intensity can be approximated very well by Wien's formula (eq. (2-13) of vol. I),

$$i'_{\lambda b} = \frac{2C_1}{\lambda^5 e^{C_2/\lambda T}} \quad (9-30)$$

Then if T_r is the blackbody temperature producing the same brightness as the flame did when using the red filter, this intensity is

$$i'_{\lambda b, r} = \frac{2C_1}{\lambda_r^5 e^{C_2/\lambda_r T_r}} \quad (9-31)$$

where λ_r is the red wavelength, 0.665 μm . This intensity can also be written as a spectral emittance of the flame times the blackbody intensity at the flame temperature which gives

$$\frac{2C_1}{\lambda_r^5 e^{C_2/\lambda_r T_r}} = \epsilon_{\lambda_r} \frac{2C_1}{\lambda_r^5 e^{C_2/\lambda_r T_f}} \quad (9-32)$$

By grouping the exponential terms and then taking the logarithm, the result can be rearranged into

$$\frac{1}{T_f} - \frac{1}{T_r} = \frac{\lambda_r}{C_2} \ln \epsilon_{\lambda_r} \quad (9-33)$$

Similarly by using a green filter

$$\frac{1}{T_f} - \frac{1}{T_g} = \frac{\lambda_r}{C_2} \ln \epsilon_{\lambda_g} \quad (9-34)$$

where the green wavelength λ_g is $0.555 \mu\text{m}$.

Now as a simple approximation, equation (9-20) is used for a_λ in the visible region. Then ϵ_λ from equation (9-17) is

$$\epsilon_\lambda = 1 - \exp\left(-\frac{Ck_2S}{\lambda^{1.39}}\right) \quad (9-35)$$

where S is the path length sighted through the flame. Substitute equation (9-35) into equations (9-33) and (9-34) to obtain

$$\frac{1}{T_f} - \frac{1}{T_r} = \frac{\lambda_r}{C_2} \ln \left[1 - \exp\left(-\frac{Ck_2S}{\lambda_r^{1.39}}\right) \right] \quad (9-36)$$

$$\frac{1}{T_f} - \frac{1}{T_g} = \frac{\lambda_g}{C_2} \ln \left[1 - \exp\left(-\frac{Ck_2S}{\lambda_g^{1.39}}\right) \right] \quad (9-37)$$

These two equations are solved for T_f and Ck_2 thereby yielding the needed measure of the soot concentration as well as the flame temperature.

As an approximation, the Ck_2 is assumed independent of wavelength and is used in equations (9-17), (9-19), and (9-20) to yield for a path length S

$$\epsilon_\lambda = 1 - \exp\left(-\frac{Ck_2S}{\lambda^{1.39}}\right) \quad \text{visible, } \lambda < 0.8 \mu\text{m} \quad (9-38)$$

$$\epsilon_\lambda = 1 - \exp\left(-\frac{Ck_2S}{\lambda^{0.95}}\right) \quad \text{infrared, } \lambda > 0.8 \mu\text{m} \quad (9-39)$$

Then with these spectral emittances the definition in equation (9-29) can be used to evaluate the total emittance of the flame as

$$\epsilon(T_f, S) = \frac{\int_0^\infty e_{\lambda b}(T_f) \epsilon_\lambda(\lambda, T_f, S) d\lambda}{\sigma T_f^4} \quad (9-40)$$

Some convenient graphs for use in this procedure are given in reference 18. The hope is that the Ck_2 obtained in this way can be applied to "simi-

lar” flames. This is a very rough approximation; there are so many variables affecting the flow and mixing in the flame that it is difficult to know when the flames will have a similar character. The detailed nature of flames is a continuing area of active research.

9.4.4 Radiation From Gases Containing Luminous Particles

In addition to the work on hydrocarbon luminous flames in the field of combustion, other fields involve consideration of radiation from luminous gases. A common example is the luminosity in the exhaust plume of solid fueled and some liquid fueled rockets. For a solid fuel the luminosity may be caused by particles of metal that are added to promote combustion stability. The metal particles are heated to high temperatures and may undergo oxidation, thereby becoming luminous.

The presence of particles in an otherwise weakly absorbing medium can cause the mixture to be strongly absorbing. “Seeding” of a gas with particles, such as finely divided carbon, has been proposed in order to increase the gas absorption (ref. 27), or as a means of shielding a surface from incident radiation (ref. 28). These techniques have possible application in connection with advanced propulsion systems.

Another use for seeding is in the direct determination of flame temperatures for a nonluminous flame by the *line reversal technique*. In this method, a seeding material such as a sodium or cadmium salt is introduced into an otherwise transparent flame. These materials produce a strong line in the visible spectrum because of an electronic transition. The cadmium gives a red line and the sodium a bright yellow line. A continuous source such as a tungsten lamp is placed so that it may be viewed *through* the seeded flame with a spectroscope. The intensity seen in the spectroscope at the line wavelength is, from the integrated equation of transfer, equation (2-10),

$$i'_{\lambda, scope} = i'_{\lambda, cont. source} \exp(-\kappa_{\lambda}) + \int_0^{\kappa_{\lambda}} i'_{\lambda b}(\kappa_{\lambda}^*) \exp[-(\kappa_{\lambda} - \kappa_{\lambda}^*)] d\kappa_{\lambda}^* \quad (9-41)$$

If the flame is assumed isothermal and of diameter D and no attenuation occurs along the remainder of the path between the continuous source and the spectroscope, equation (9-41) becomes

$$i'_{\lambda, scope} = i'_{\lambda, cont. source} \exp(-\kappa_{\lambda, D}) + i'_{\lambda b, flame} [1 - \exp(-\kappa_{\lambda, D})] \quad (9-42)$$

where

$$\kappa_{\lambda,D} = \int_0^D a_{\lambda}(S^*) dS^*$$

In the wavelength region adjacent to the absorbing and emitting spectral line, the flame is essentially transparent so the background radiation observed adjacent to the line is $i'_{\lambda,cont.source}$. Hence, by subtracting $i'_{\lambda,cont.source}$ from equation (9-42) the line intensity relative to the adjacent background is

$$i'_{\lambda,scope} - i'_{\lambda,cont.source} = (i'_{\lambda b, flame} - i'_{\lambda,cont.source}) \times [1 - \exp(-\kappa_{\lambda,D})] \quad (9-43)$$

If the flame is at a higher temperature than the continuous source, equation (9-43) shows that the line intensity in the spectroscopy will be greater than the continuous background intensity. The line will then appear as a bright line imposed upon a less bright continuous spectrum in the spectroscopy. By increasing the temperature of the continuous source, the source term will override. The line then appears as a dark line on a brighter continuous spectrum. If the continuous source is a blackbody and its temperature is made *equal* to the flame temperature, then

$$i'_{\lambda b, flame} = i'_{\lambda,cont.source}$$

and equation (9-43) reduces to $i'_{\lambda,scope} = i'_{\lambda,cont.source}$. The line will then disappear into the continuum in the spectroscopy. This is because the absorption by the flame and the flame emission exactly compensate. If the continuous source is a tungsten lamp, the source temperature measurement is usually made with an optical pyrometer.

It is noted that in the derivation of equation (9-43) it was assumed that the flame is transparent except within the spectral line produced by the cadmium or sodium seeding. If soot is in the flame, the soot particles absorb, emit, and scatter radiation in a continuous spectrum along the path of the incident beam. The line reversal technique is of less practical utility in this instance as it then depends on the soot behavior. The effect of soot is analyzed in reference 29.

Another instance of radiation attenuation by means of particles is found in the effect of dust or so-called "grains" that are believed to exist in the interstellar space and cause reductions in the observed intensity of radiation from stars (refs. 30 and 31).

9.5 LUMINESCENCE

The phenomenon of luminescence in its various forms is a fairly common one. The name covers a broad range of mechanisms that result

in emission of radiant energy by the transition of electrons from an excited state to a lower energy state, where the original excitation took place by means other than thermal agitation. This is an example of a process that is not in local thermodynamic equilibrium (section 1.8). Because the electronic transitions are between discrete energy states, the span of wavelengths over which the emission occurs is quite small. Luminescence, therefore, does not add significant energy to the spectrum of emission in engineering situations and can almost invariably be neglected in engineering calculations. However, there are some situations in which effects other than total energy transport are of interest. For that reason a very brief mention of luminescence is included here.

Luminescence is categorized in various ways. A common classification is by duration of the effect. Luminescence that persists over a relatively long¹⁰ period is called "phosphorescence," a word derived from the luminescence of white phosphorus.¹¹ Luminescence that persists only during the influence of some external exciting agent such as an ultraviolet lamp is called "fluorescence," a name arising from the strong luminescence shown by flourspar when so irradiated.

Another categorization is by description of the excitation agent. Thus, luminescence arising from a chemical reaction such as the oxidation of white phosphorus is called "chemiluminescence"; luminescence caused by a beam of incident electrons as on a color TV screen is "cathodoluminescence"; a biochemical reaction producing luminosity, as in fireflies and some marine animals, is called "bioluminescence"; luminous emission by the presence of an electric field as in certain commercial panel lamps is "electroluminescence"; and luminescence due to photon bombardment is often called "photoluminescence." The latter effect is caused by the same mechanism that causes the laser to function. Other mechanisms can cause luminescence in materials, but descriptive terms have not yet been coined. Examples are proton bombardment, which is believed to be responsible for the luminous red patches observed on the surface of the Moon, and nuclear reactions that cause luminous emission of radiation.

Because luminescence is common to materials at room temperature, it obviously cannot be predicted by the usual laws that govern thermal radiation as these would predict no visible radiation at such temperatures. This is the origin of the term *cold light* for fluorescent lamp emission. Rather, the quantum mechanical properties of such luminescent materials must be examined to explain their behavior. Some detailed material on luminescence is contained in references 32 and 33. The

¹⁰ Meaning in comparison with relatively short, to speak precisely.

¹¹ Phosphorus itself is named for the Greek word meaning "light carrying."

calculation of luminescence effects is outside the scope of this work and will not be treated further here.

9.6 TRANSIENT RADIATION PROBLEMS

The treatment of transient phenomena when radiation is present has been sparsely treated in the literature. Some problems dealing with the effects of nuclear weapons and some situations in astrophysics require inclusion of transient effects.

The equation of transfer as derived in chapter 2 neglected changes in radiation intensity with time. The equation of transfer is written for a beam of radiation of intensity i'_λ traveling in the S direction. As the radiation travels through the differential length from S to $S + dS$, its intensity is increased by emission and decreased by absorption. Also during the residence of the radiation within dS , the intensity can change with time. The residence time is $dt = dS/c$ where c is the speed of propagation in the medium. Hence, the change in i'_λ can be written as

$$di'_\lambda = \frac{\partial i'_\lambda}{\partial t} \frac{dS}{c} + \frac{\partial i'_\lambda}{\partial S} dS$$

By substituting for di'_λ , the equation of transfer (2-4) becomes

$$\frac{1}{c} \frac{\partial i'_\lambda(t, S)}{\partial t} + \frac{\partial i'_\lambda(t, S)}{\partial S} = a_\lambda(t, S) [i'_{\lambda b}(t, S) - i'_\lambda(t, S)] \quad (9-44)$$

Since the conditions such as temperature within the medium are changing with time, the absorption coefficient is a function of time as well as position.

Because the speed of light is usually very large compared with the other quantities in the transient term, the transient term is usually very small, and the equation of transfer reverts to the steady-state form that has been given throughout this work. In some analyses directed towards the study of nuclear weapons (refs. 17 and 18 of chapter 6), the transient term is included. To better understand the transient term, consider as a simple illustration what the radiative behavior would be if a thick uniform medium at temperature T_1 instantaneously had its temperature increased to a higher uniform value T_2 . The medium would then be at T_2 but the intensity within the medium would have to change from $i'_{\lambda b}(T_1)$ to $i'_{\lambda b}(T_2)$. During this process, the radiation would not be in equilibrium. The equation of transfer reduces to (assuming as an approximation that a_λ can be used in the emission term, which is an equilibrium assumption),

$$\frac{1}{c} \frac{\partial i'_{\lambda}(t)}{\partial t} = a_{\lambda}(T_2) [i'_{\lambda b}(T_2) - i'_{\lambda}(t)] \quad (9-45)$$

After integrating with the condition $i'_{\lambda} = i'_{\lambda b}(T_1)$ at $t=0$, the result is

$$\frac{i'_{\lambda b}(T_2) - i'_{\lambda}(t)}{i'_{\lambda b}(T_2) - i'_{\lambda b}(T_1)} = e^{-ca_{\lambda}(T_2)t} \quad (9-46)$$

The radiation relaxation time (time to change by a factor of e) for equilibrium to be reestablished is thus $1/ca_{\lambda}(T_2)$ which is usually very short for reasonable values of a_{λ} in view of the large value of the propagation velocity c in the medium.

In the preceding illustration, it was assumed that the medium temperature could be instantaneously raised so that at the beginning of the transient the radiation intensity was not in equilibrium at the black radiation value corresponding to T_2 . Generally the temperature change of a medium would be governed by the heat capacity of the medium, and consequently transient temperature changes would be much slower than the radiation relaxation time. Hence, when coupled with the transient energy conservation equation, which contains a heat capacity term, the unsteady term in the equation of transfer would be negligible. This is why the steady form of the equation of transfer, as derived in chapter 2, can be instantaneously applied during almost all transient heat transfer processes.

EXAMPLE 9-4: A gray medium is in a slab configuration originally at a uniform temperature T_o . The absorption coefficient is a , and the slab half thickness is D . The heat capacity of the medium at constant volume is c_v and its density is ρ . At time $t=0$, the slab is placed in surroundings at zero temperature. Neglecting conduction and convection, discuss the solutions for the temperature profiles for radiative cooling when a is very large and when a is very small.

At the slab center which is located at $x=0$, the condition of symmetry provides the relation for any time,

$$\frac{\partial T}{\partial x} = 0; \quad t, x = 0$$

At time $t=0$ there is the condition

$$T = T_o; \quad t = 0, x$$

As discussed in section 2.6.2 for radiation only being included, there will be a temperature slip at the boundaries $x = \pm D$, so that the temperature at the boundaries will be finite rather than being equal to the zero outside temperature. If heat conduction were present, the temperature slip would not exist.

For a large a the diffusion approximation can be employed and from equation (3-25) the heat flux in the x direction is

$$q(x, t) = -\frac{4}{3a} \frac{\partial e_b(x, t)}{\partial x} = -\frac{4\sigma}{3a} \frac{\partial T^4(x, t)}{\partial x}$$

By conservation of energy

$$-\frac{\partial q(x, t)}{\partial x} = \rho c_v \frac{\partial T}{\partial t}$$

Combining these two equations to eliminate q gives the transient energy diffusion equation for the temperature distribution in the slab

$$\rho c_v \frac{\partial T}{\partial t} = \frac{4\sigma}{3a} \frac{\partial^2 T^4(x, t)}{\partial x^2}$$

Defining dimensionless variables as follows:

$$t^* = \frac{a\sigma T_0^3 t}{\rho c_v} \quad \kappa = ax \quad \Theta = \frac{T}{T_0}$$

gives

$$\frac{\partial \Theta}{\partial t^*} = \frac{4}{3} \frac{\partial^2 \Theta^4(\kappa, t^*)}{\partial \kappa^2}$$

The initial condition and the boundary condition at $x = 0$ become, respectively,

$$\Theta(\kappa, 0) = 1$$

$$\frac{\partial \Theta}{\partial \kappa}(0, t^*) = 0$$

At the boundary $\kappa = aD$, a slip condition must be used. Using equation (3-45), when the surroundings are empty space at zero temperature, the $e_{bw} = 0$, and the $\epsilon_w = 1$, so that at the exposed boundary of the medium for any time

$$\sigma T^4 \Big|_{x=D} = \frac{1}{2} \left(-\frac{4}{3} \frac{\sigma}{a} \frac{\partial T^4}{\partial x} \right)_{x=D} - \frac{\sigma}{2a^2} \frac{\partial^2 T^4}{\partial x^2} \Big|_{x=D}$$

or

$$0 = \left(2\Theta^4 + \frac{4}{3} \frac{\partial \Theta^4}{\partial \kappa} + \frac{\partial^2 \Theta^4}{\partial \kappa^2} \right)_{\kappa = aD}$$

Similar relations apply at $x = -D$. For these conditions solution by numerical techniques is probably necessary.

For a small absorption coefficient, and since there are no enclosing radiating boundaries present, the emission approximation (section 3.3.2) can be applied. For very small a the medium is optically so thin that it is at uniform temperature throughout its thickness at any instant. From the results of example 3-2, the heat flux emerging from each boundary of the layer is

$$q = 4a\sigma T^4 D$$

then becomes

$$\rho c_v \frac{dT}{dt} = -4a\sigma T^4$$

or, in dimensionless terms,

$$\frac{d\Theta}{dt^*} = -4\Theta^4$$

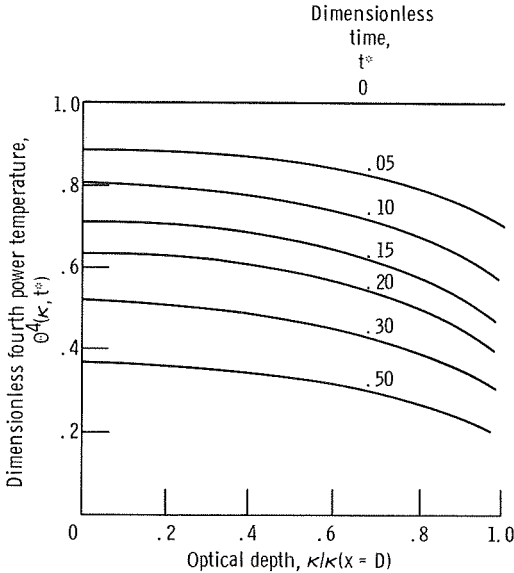


FIGURE 9-12.—Dimensionless temperature profiles as a function of time for radiative cooling of a gray slab; optical thickness $\kappa(x = D) = 1.0$. (From ref. 34.)

Integrating with the condition that $\Theta = 1$ at $t^* = 0$, the transient temperature throughout the slab is then given by

$$\Theta = \frac{1}{(1 + 12t^*)^{1/3}}$$

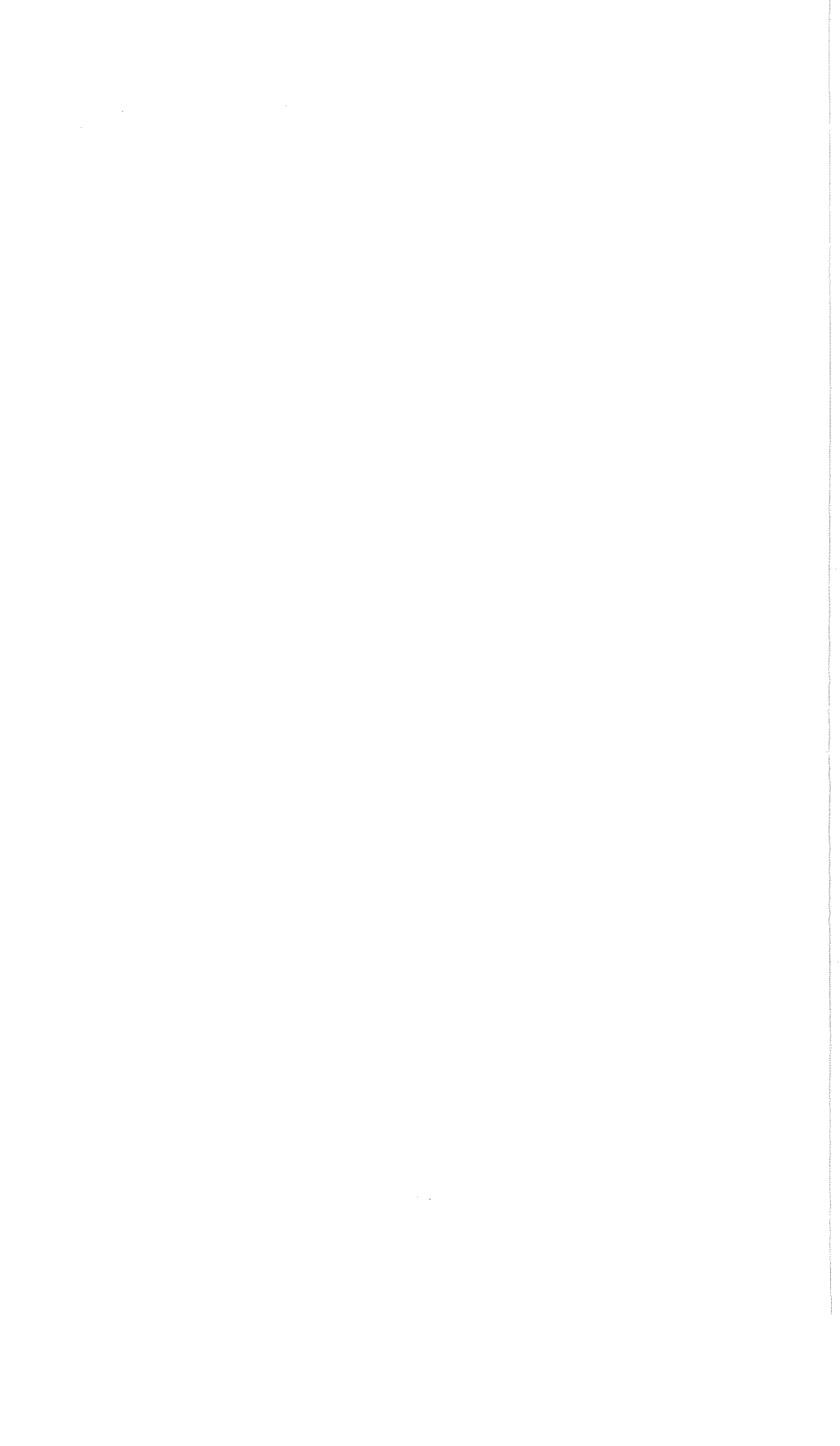
Viskanta and Bathla (ref. 34) have obtained numerical solutions to the transient form of the complete equation of transfer, along with the limiting solutions derived here. Some of their results for intermediate optical thickness are shown in figure 9–12. Numerical solutions for spherical geometries are found in references 35 and 36. Solutions to more involved transient problems by use of Monte Carlo are mentioned in section 6.7.

REFERENCES

1. HODGMAN, CHARLES D., ED.: Handbook of Chemistry and Physics. 38th ed., Chemical Rubber Publ. Co., 1956–1957.
2. GARDON, ROBERT: The Emissivity of Transparent Materials. *J. Am. Cer. Soc.*, vol. 39, no. 8, Aug. 1956, pp. 278–287.
3. GARDON, ROBERT: Calculation of Temperature Distributions in Glass Plates Undergoing Heat-Treatment. *J. Am. Cer. Soc.*, vol. 41, no. 6, June 1958, pp. 200–209.
4. GARDON, ROBERT: Appendix to Calculation of Temperature Distributions in Glass Plates Undergoing Heat Treatment (ref. 3). Mellon Inst., Pittsburgh, 1958.
5. GARDON, ROBERT: A Review of Radiant Heat Transfer in Glass. *J. Am. Cer. Soc.*, vol. 44, no. 7, July 1961, pp. 305–312.
6. CONDON, EDWARD U.: Radiative Transport in Hot Glass. *J. Quant. Spectrosc. Radiat. Transfer*, vol. 8, no. 1, 1968, pp. 369–385.
7. MCCONNELL, DUDLEY G.: Radiant Energy Transport in Cryogenic Condensates. Paper presented at Engineering Colloquium, Kentucky University, Lexington, Ky., Nov. 30, 1967.
8. CRAVALHO, E. G.; TIEN, C. L.; AND CAREN, R. P.: Effect of Small Spacings on Radiative Transfer Between Two Dielectrics. *J. Heat Transfer*, vol. 89, no. 4, Nov. 1967, pp. 351–358.
9. ECHIGO, R.; NISHIWAKI, N.; AND HIRATA, M.: A Study on the Radiation of Luminous Flames. Eleventh Symposium (International) On Combustion. The Combustion Institute, 1967, pp. 381–389.
10. PERRY, ROBERT H.; CHILTON, CECIL H.; AND KIRKPATRICK, SIDNEY D., EDs.: *Chemical Engineers' Handbook*. Fourth ed., McGraw-Hill Book Co., Inc., 1963.
11. HOUGEN, OLAF A.; WATSON, KENNETH M.; AND RAGATZ, ROLAND A.: *Material and Energy Balance*. Vol. 1 of *Chemical Process Principles*. Second ed., John Wiley & Sons, Inc., 1954.
12. GAYDON, A. G.; AND WOLFARD, H. G.: *Flames, Their Structure, Radiation, and Temperature*. Second ed., Macmillan and Co., 1960.
13. BARNETT, HENRY C.; AND HIBBARD, ROBERT R., EDs.: *Basic Considerations in the Combustion of Hydrocarbon Fuels with Air*. NACA Rep. 1300, 1957.
14. HOTTEL, H. C.; AND SAROFIM, A. F.: The Effect of Gas Flow Patterns on Radiative Transfer in Cylindrical Furnaces. *Int. J. Heat Mass Transfer*, vol. 8, no. 8, Aug. 1965, pp. 1153–1169.

15. STULL, V. ROBERT; AND PLASS, GILBERT N.: Emissivity of Dispersed Carbon Particles. *J. Opt. Soc. Am.*, vol. 50, no. 2, Feb. 1960, pp. 121-129.
16. SIDDALL, R. G.; AND MCGRATH, I. A.: The Emissivity of Luminous Flames. Ninth Symposium (International) on Combustion. W. G. Berl, ed., Academic Press, 1963, pp. 102-110.
17. HOWARTH, C. R.; FOSTER, P. J.; AND THRING, M. W.: The Effect of Temperature on the Extinction of Radiation by Soot Particles. Third International Heat Transfer Conference. Vol. 5, AIChE, 1966, pp. 122-128.
18. HOTTEL, H. C.: Radiant Heat Transmission. Heat Transmission. Third ed., William H. McAdams, McGraw-Hill Book Co., Inc., 1954, ch. 4.
19. HAWKSLEY, P. G. W.: The Methods of Particle Size Measurements. Part II. Optical Methods and Light Scattering. *Brit. Coal Utilization Res. Assoc. Monthly Bull.*, vol. 16, nos. 4 and 5, 1952, pp. 134-209.
20. DALZELL, W. H.; AND SAROFIM, A. F.: Optical Constants of Soot and Their Application to Heat-Flux Calculations. *J. Heat Transfer*, vol. 91, No. 1, Feb. 1969, pp. 100-104.
21. ERICKSON, W. D.; WILLIAMS, G. C.; AND HOTTEL, H. C.: Light Scattering Measurements on Soot in a Benzene-Air Flame. *Combustion and Flame*, vol. 8, no. 2, June 1964, pp. 127-132.
22. THRING, M. W.; BEER, J. M.; AND FOSTER, P. J.: The Radiative Properties of Luminous Flames. Third International Heat Transfer Conference. Vol. 5, AIChE, 1966, pp. 101-111.
23. THRING, M. W.; FOSTER, P. J.; MCGRATH, I. A.; AND ASHTON, J. S.: Prediction of the Emissivity of Hydrocarbon Flames. *International Developments in Heat Transfer*. ASME, 1963, pp. 796-803.
24. SATO, TAKASHI; AND MATSUMOTO, RYUICHI: Radiant Heat Transfer from Luminous Flame. *International Developments in Heat Transfer*. ASME, 1963, pp. 804-811.
25. YAGI, S.; AND INOUE, H.: Radiation from Soot Particles in Luminous Flames. Eighth Symposium (International) On Combustion. Williams and Wilkins, 1962, pp. 288-293.
26. BONE, WILLIAM A.; AND TOWNEND, DONALD T. A.: *Flame and Combustion in Gases*. Longmans, Green and Co., Ltd., 1927.
27. LANZO, CHESTER D.; AND RAGSDALE, ROBERT G.: Heat Transfer to a Seeded Flowing Gas from an Arc Enclosed by a Quartz Tube. *Proceedings of the 1964 Heat Transfer and Fluid Mechanics Institute*. Warren H. Giedt and Salomon Levy, eds., Stanford Univ. Press, 1964, pp. 226-244.
28. HOWELL, JOHN R.; AND RENKEL, HAROLD E.: Analysis of the Effect of a Seeded Propellant Layer on Thermal Radiation in the Nozzle of a Gaseous-Core Nuclear Propulsion System. NASA TN D-3119, 1965.
29. THOMAS, D. LYDDON: Problems in Applying the Line Reversal Method of Temperature Measurement to Flames. *Combustion and Flame*, vol. 12, no. 6, Dec. 1968, pp. 541-549.
30. GREENBERG, J. MAYO; AND ROARK, T. P., EDS.: *Interstellar Grains*. NASA SP-140, 1967.
31. DONN, B.; AND KRISHNA SWAMY, K. S.: Extinction by Interstellar Grains, Mie Particles and Polycyclic Aromatic Molecules. *Physica*, vol. 41, no. 1, Feb. 21, 1969, pp. 144-150.
32. CURIE, DANIEL (G. F. J. GARLICK, TRANS.): *Luminescence in Crystals*. John Wiley & Sons, Inc., 1963.
33. PRINGSHEIM, PETER: *Fluorescence and Phosphorescence*. Interscience Publ., 1949.
34. VISKANTA, RAYMOND; AND BATHLA, PRITAM S.: Unsteady Energy Transfer in a Layer of Gray Gas by Thermal Radiation. *Zeit. f. Angew. Math. Phys.*, vol. 18, no. 3, 1967, pp. 353-367.

35. VISKANTA, R.; AND LALL, P. S.: Transient Cooling of a Spherical Mass of High-Temperature Gas by Thermal Radiation. *J. Appl. Mech.*, vol. 32, no. 4, Dec. 1965, pp. 740-746.
36. VISKANTA, R.; AND LALL, P. S.: Transient Heating and Cooling of a Spherical Mass of Gray Gas by Thermal Radiation. *Proceedings of the Heat and Transfer Fluid Mechanics Institute*. M. A. Saad and J. A. Miller, eds., Stanford Univ. Press, 1966, pp. 181-197.



Appendix

RADIATION CONSTANTS

For the convenience of the reader, some of the important constants used in radiative transfer theory are gathered here in table I.

TABLE I.—FUNDAMENTAL NUMERICAL VALUES

First Bohr electron radius	$a_0 = \hbar^2/m_e e^2 = 0.5292 \times 10^{-8}$ cm
Speed of light in vacuum	$c_0 = 2.9979 \times 10^{10}$ cm/sec
Electron charge	$e = 4.803 \times 10^{-10}$ esu
Planck's constant	$h = 6.625 \times 10^{-27}$ (erg)(sec) $\hbar = h/2\pi = 1.054 \times 10^{-27}$ (erg)(sec)
Boltzmann constant	$k = 1.3804 \times 10^{-16}$ erg/K
Electron mass	$m_e = 9.108 \times 10^{-28}$ g
Classical electron radius	$r_0 = e^2/m_e c_0^2 = 2.818 \times 10^{-13}$ cm
Atomic unit cross section	$\pi a_0^2 = 0.880 \times 10^{-16}$ cm ²
Thomson cross section	$\sigma_T = 8\pi r_0^2/3 = 6.652 \times 10^{-25}$ cm ²
Electron volt	1 eV = 1.602 $\times 10^{-12}$ erg
Temperature associated with 1 eV	1 eV/k = 11 605 K
Rest energy of electron	$m_e c_0^2 = 8.186 \times 10^{-7}$ erg
Ionization potential of hydrogen atom	$e^2/2a_0 = 2\pi^2 e^4 m_e / h^2 = 13.60$ eV

EXPONENTIAL INTEGRAL RELATIONS

A summary of some useful exponential integral relations is presented here. Additional relations are given in references 1 to 3.

For positive real arguments, the n th exponential integral is defined as

$$E_n(x) \equiv \int_0^1 \mu^{n-2} \exp\left(\frac{-x}{\mu}\right) d\mu \quad (A1)$$

and only positive integral values of n will be considered here. An alternate form is

$$E_n(x) = \int_1^\infty \frac{1}{t^n} \exp(-xt) dt \quad (A2)$$

By differentiating equation (A1) under the integral sign, the recurrence relation is obtained

$$\left. \begin{aligned} \frac{d}{dx} E_n(x) &= -E_{n-1}(x) & n \geq 2 \\ \frac{d}{dx} E_1(x) &= -\frac{1}{x} \exp(-x) \end{aligned} \right\} \quad (\text{A3})$$

Another recurrence relation obtained by integration is

$$nE_{n+1}(x) = \exp(-x) - xE_n(x) \quad n \geq 1 \quad (\text{A4})$$

Also integration results in

$$\int E_n(x) dx = -E_{n+1}(x) \quad (\text{A5})$$

By use of equation (A4), all exponential integrals can be reduced to the first exponential integral given by

$$E_1(x) = \int_0^1 \mu^{-1} \exp\left(\frac{-x}{\mu}\right) d\mu \quad (\text{A6})$$

Alternate forms of $E_1(x)$ are

$$E_1(x) = \int_1^\infty t^{-1} \exp(-xt) dt = \int_x^\infty t^{-1} \exp(-t) dt \quad (\text{A7})$$

For $x=0$ the exponential integrals are equal to

$$\left. \begin{aligned} E_n(0) &= \frac{1}{n-1} & n \geq 2 \\ E_1(0) &= +\infty \end{aligned} \right\} \quad (\text{A8})$$

For large values of x there is the asymptotic expansion

$$E_n(x) = \frac{\exp(-x)}{x} \left[1 - \frac{n}{x} + \frac{n(n+1)}{x^2} - \frac{n(n+1)(n+2)}{x^3} + \dots \right] \quad (\text{A9})$$

Series expansions are of the form

$$\left. \begin{aligned}
 E_1(x) &= -\gamma - \ln x + x - \frac{x^2}{2 \cdot 2!} + \frac{x^3}{3 \cdot 3!} - \dots \\
 E_2(x) &= 1 + (\gamma - 1 + \ln x)x - \frac{x^2}{1 \cdot 2!} + \frac{x^3}{2 \cdot 3!} - \dots \\
 E_3(x) &= \frac{1}{2} - x + \frac{1}{2} \left(-\gamma + \frac{3}{2} - \ln x \right) x^2 + \frac{x^3}{1 \cdot 3!} - \dots
 \end{aligned} \right\} \quad (A10)$$

where $\gamma = 0.577216$ is Euler's constant. The general series expansion given in reference 3 is

$$E_n(x) = \frac{(-x)^{n-1}}{(n-1)!} [-\ln x + \psi(n)] - \sum_{\substack{m=0 \\ (m \neq n-1)}}^{\infty} \frac{(-x)^m}{(m-n+1)m!} \quad (A11)$$

where

$$\psi(1) = -\gamma$$

and

$$\psi(n) = -\gamma + \sum_{m=1}^{n-1} \frac{1}{m} \quad n \geq 2$$

Tabulations of $E_n(x)$ are given in references 2 and 3. An abridged listing given in table II is included here for convenience.

TABLE II.—VALUES OF EXPONENTIAL INTEGRALS $E_n(x)$

[From ref. 2]

x	$E_1(x)$	$E_2(x)$	$E_3(x)$	$E_4(x)$	$E_5(x)$
0	∞	1.0000	0.5000	0.3333	0.2500
.01	4.0379	.9497	.4903	.3284	.2467
.02	3.3547	.9131	.4810	.3235	.2434
.03	2.9591	.8817	.4720	.3188	.2402
.04	2.6813	.8535	.4633	.3141	.2371
.05	2.4679	.8278	.4549	.3095	.2339
.06	2.2953	.8040	.4468	.3050	.2309
.07	2.1508	.7818	.4388	.3006	.2278
.08	2.0269	.7610	.4311	.2962	.2249
.09	1.9187	.7412	.4236	.2919	.2219
.10	1.8229	.7225	.4163	.2877	.2190
.20	1.2227	.5742	.3519	.2494	.1922
.30	.9057	.4691	.3000	.2169	.1689
.40	.7024	.3894	.2573	.1891	.1487
.50	.5598	.3266	.2216	.1652	.1310
.60	.4544	.2762	.1916	.1446	.1155
.70	.3738	.2349	.1661	.1268	.1020
.80	.3106	.2009	.1443	.1113	.0901
.90	.2602	.1724	.1257	.0978	.0796
1.00	.2194	.1485	.1097	.0861	.0705
1.25	.1464	.1035	.0786	.0628	.0520
1.50	.1000	.0731	.0567	.0460	.0385
1.75	.0695	.0522	.0412	.0339	.0286
2.00	.0489	.0375	.0301	.0250	.0213
2.25	.0348	.0272	.0221	.0185	.0159
2.50	.0249	.0198	.0163	.0138	.0119
2.75	.0180	.0145	.0120	.0103	.0089
3.00	.0130	.0106	.0089	.0077	.0067
3.25	.0095	.0078	.0066	.0057	.0050
3.50	.0070	.0058	.0049	.0043	.0038

REFERENCES

1. CHANDRASEKHAR, SUBRAHMANYAN: Radiative Transfer. Dover Publications, Inc., 1960.
2. KOURGANOFF, VLADIMIR: Basic Methods in Transfer Problems. Dover Publications, Inc., 1963.
3. ABRAMOWITZ, MILTON; AND STEGUN, IRENE A., EDS.: Handbook of Mathematical Functions with Formulas, Graphs, and Mathematical Tables. Appl. Math. Ser. 55, Nat. Bur. Standards, 1964.

Index

- Absorptance, 24
- Absorption, 4
 - band correlations, 138, 146
 - band overlap, 152, 187
 - bound-bound, 7, 128
 - bound-free, 8, 137
 - free-free, 8, 137, 138
 - line, 7, 16, 128, 134
- Absorption coefficient,
 - definition, 13, 15
 - effective mean, 96
 - incident mean, 46, 93
 - mass, 13
 - Planck mean, 45, 66, 67, 93, 224
 - Rosseland mean, 78, 93
 - true, 19
- Absorption factors,
 - geometric mean, 164
 - geometrical, 164
- Addition of radiation and conduction, 251
- Angular frequency, 113
- Attenuation, 12
 - atmospheric, 1
 - Bouguer's law, 13, 16
- Band absorptance, 138
- Band models,
 - Elsasser, 143
 - exponential wide, 148
 - statistical, 144
- Band width,
 - correlations, 138, 148
 - effective, 142
 - limits, 196
 - tables, 146, 148, 149
- Bohr model of atom, 115
- Boltzmann distribution, 123, 132
- Bouguer, Pierre, 13
- Bouguer's law, 13, 16
- Boundary layer with radiation, 265
 - optically thin layer, 266
 - optically thick layer, 268
- Bremsstrahlung, 8
- Brewster's angle, 317
- Broadening, line,
 - collision, 129, 132
 - Doppler, 129, 131
 - natural, 129, 131
 - Stark, 129, 134
- Carbon dioxide radiation, 2
 - band, 5, 149
 - charts, 184, 185
 - mixture with water vapor, 186
- Carbon monoxide band radiation, 149
- Channel flows with radiation, 270
- Closely spaced dielectrics, 322
- Coefficient,
 - absorption, 13, 15, 19
 - emission, 23
 - extinction, 12
 - scattering, 13, 20, 283
- Cold medium approximation, 62, 70
- Collision broadening, 129, 132
- Conduction-radiation parameter, 244
- Coupled problems, 241, 264
 - additive solution, 251
 - boundary layer, 265
 - channel flows, 270
 - diffusion method, 254
 - Monte Carlo, 237
 - radiation and conduction, 237, 241, 243, 246, 247, 251
 - radiation, conduction and convection, 237, 241, 264
- Cross section,
 - absorption, 335
 - scatter, 280
- Curtis-Godson approximation, 202
- de Broglie, Louis, 117
- Degenerate states, 121
- Detailed balancing, 123
- Differential approximation, 102
 - boundary conditions, 106
 - equation of transfer, 106
 - solutions for simple geometries, table, 109
- Diffraction from sphere, 292

- Diffusion method, 62, 71, 74, 254
 - jump between two absorbing-emitting regions, 82, 86
 - jump boundary condition, 79
 - radiation and conduction, 254
 - Rosseland diffusion equation, 74, 75, 78
 - scattering, 308
- Diffusion solutions,
 - concentric cylinders, 89
 - concentric spheres, 89, 90
 - parallel plates, 83
 - table, 89
- Direct exchange area,
 - gas-gas, 211
 - gas-surface, 208
 - surface-gas, 210
 - surface-surface, 209
- Doppler broadening, 129, 131
- Effective line width, 135
- Effective band width, 142
- Efficiency factor, 284
- Einstein coefficients, 122
- Elsasser model, 143
- Emission, 4, 21
 - from volume, 23
 - induced, 19, 121, 122
 - line, 134
 - medium with nonunity refractive index, 315
 - spontaneous, 19, 122
- Emission approximation, 62, 67
- Emission coefficient, 23
- Emittance of gases,
 - carbon dioxide, 5, 149, 184
 - definition, 25, 145
 - water vapor, 149, 185
- Energy conservation, 43, 166, 246
- Energy density, 56
- Energy levels, 5, 128
- Enclosure theory, 159
 - band equations, 189
 - matrix of equations, 164
- Equation of transfer, 37, 38, 125
 - approximations to, table, 62
 - differential form, 40
 - integral form, 41
 - plane layer, 46, 49
 - photon model, 56, 125
- Equilibrium
 - local thermodynamic, 32
 - radiative, 45
- Exchange factor approximation, 211, 218, 260
- Exponential integrals,
 - definition, 56
 - in equation of transfer, 55, 248
 - relations between, 353
 - table of values, 356
- Exponential wide band model, 148, 149
- Extinction coefficient, 12
- Flames, 324
 - luminous, 331
 - nonluminous, 329
 - theoretical temperature, 325
- Flux vector, 58
- Gaunt factor, 128
- Geometric mean beam length, 191, 192, 194
- Gray gas, 83, 95, 229
 - definition, 47
 - transfer equations, 48
- Half width of line, 130
- Induced emission, 19, 121
- Intensity, 8
 - definition in medium, 9, 57
 - invariance along path in vacuum, 11
- Ionization potential, 6, 117
- Jump boundary condition, 72, 79, 82, 86, 88
- Kirchhoff's law, 26
- Krakatoa, 295
- Langley, Samuel P., 1
- Laser, 33
- Line,
 - broadening, 128
 - shape parameter, 129
 - strong, 137
 - weak, 136
 - width, 130, 132, 133, 135
- Line reversal technique, 342
- Local thermodynamic equilibrium, 32
- Lorentz profile, 131
- Luminous flames, 331
- Luminous particles, 342
- Luminescence, 343
- Mean absorption coefficient,
 - incident, 46, 93
 - Planck, 45, 66, 67, 93, 224
 - Rosseland, 78, 93
- Mean beam length, 175
 - gas not optically thin, 176, 179
 - geometric, 191, 192, 194
 - optically thin limit, 178
 - table of values, 181, 192
- Methane band radiation, 149

- Mie scattering, 278, 299
- Milne-Eddington approximation, 100
- Monte Carlo, 221, 223
 - adjacent gray regions, 233
 - concentric cylinders, 231
 - parallel plates, 225, 229
- Natural broadening, 129, 131
- Net radiation method, 159
- Nonluminous flames, 329
- Optical thickness, 15, 40, 47, 304, 307
- Optically thin limit, 53, 67, 178
- Oscillator strength, 127
- Parallel plates, 166, 196, 199
 - black with gray gas between, 49
 - diffusion solution, 83
 - Monte Carlo solution, 225, 229, 231
 - radiation and conduction, 247
- Particle radiation, 342
- Penetration distance, 14
- Phase function for scattering, 284
- Photon, 6, 56
 - momentum, 117
- Planck distribution, 121
- Planck mean absorption coefficient, 45, 66, 67, 93, 224
- Polarizability,
 - definition, 296
 - table for types of scattering, 296
- Population inversion, 34
- Radiative equilibrium, 45
- Rayleigh scattering, 294
 - cross section, 295
 - phase function, 298
- Refractive index,
 - nonunity, 315
- Rosseland diffusion equation, 74, 75, 78
- Rosseland mean absorption coefficient, 78, 93
- Rydberg constant, 117
- Scattering, 238, 277
 - anisotropic, 20
 - elastic, 20, 277
 - equation of transfer, 302, 306
 - inelastic, 7, 20, 277
 - isotropic, 20
- Scattering coefficient, 13, 20, 283
- Scattering cross section, 280
- Scattering from particles,
 - diffraction from sphere, 292
 - large dielectric sphere with refractive index near unity, 292
 - large diffuse sphere, 289
 - large specular sphere, 286
 - Mie scattering, 278, 299
 - Rayleigh scattering, 294
- Scattering optical thickness, 304
- Schuster-Schwarzschild approximation, 97
- Schrödinger wave equation, 117
- Seeding with particles, 342
- Slip, 53, 72
 - coefficient, 255
- Soot,
 - absorption coefficient, 333
 - concentration, 340
 - electromagnetic theory predictions, 335
 - optical properties, 336
 - total emittance, 338
- Source function, 307
- Spheres,
 - concentric, 89, 109
- Spontaneous emission, 19, 122
- Stark broadening, 129, 134
- Statistical weight, 121
- Stimulated emission, 19
- Strong line, 137
- Theoretical flame temperature, 325
- Thermodynamic equilibrium, local, 32
- Transfer equation, 38, 40, 125, 302, 306
- Transient problems, 237, 246, 345
- Transmittance, 29
- Transmittance factors,
 - geometric mean, 164, 168
 - geometrical, 164
- Transparent gas approximation, 62, 64
- True absorption coefficient, 19, 40, 127
- Uniform gas, 15, 159, 205
- Vibration-rotation band, 7
- Water vapor radiation,
 - band radiation, 149
 - charts, 185, 186
 - mixture with CO₂, 186
- Wave function, 118
- Weak line, 136
- Wien distribution, 125
- Zoning method, 207

NATIONAL AERONAUTICS AND SPACE ADMINISTRATION
WASHINGTON, D. C. 20546

OFFICIAL BUSINESS

POSTAGE AND FEES PAID
NATIONAL AERONAUTICS AND
SPACE ADMINISTRATION

FIRST CLASS MAIL

POSTMASTER: If Undeliverable (Section 158
Postal Manual) Do Not Return

"The aeronautical and space activities of the United States shall be conducted so as to contribute . . . to the expansion of human knowledge of phenomena in the atmosphere and space. The Administration shall provide for the widest practicable and appropriate dissemination of information concerning its activities and the results thereof."

— NATIONAL AERONAUTICS AND SPACE ACT OF 1958

NASA SCIENTIFIC AND TECHNICAL PUBLICATIONS

TECHNICAL REPORTS: Scientific and technical information considered important, complete, and a lasting contribution to existing knowledge.

TECHNICAL NOTES: Information less broad in scope but nevertheless of importance as a contribution to existing knowledge.

TECHNICAL MEMORANDUMS: Information receiving limited distribution because of preliminary data, security classification, or other reasons.

CONTRACTOR REPORTS: Scientific and technical information generated under a NASA contract or grant and considered an important contribution to existing knowledge.

TECHNICAL TRANSLATIONS: Information published in a foreign language considered to merit NASA distribution in English.

SPECIAL PUBLICATIONS: Information derived from or of value to NASA activities. Publications include conference proceedings, monographs, data compilations, handbooks, sourcebooks, and special bibliographies.

TECHNOLOGY UTILIZATION PUBLICATIONS: Information on technology used by NASA that may be of particular interest in commercial and other non-aerospace applications. Publications include Tech Briefs, Technology Utilization Reports and Notes, and Technology Surveys.

Details on the availability of these publications may be obtained from:

SCIENTIFIC AND TECHNICAL INFORMATION OFFICE
NATIONAL AERONAUTICS AND SPACE ADMINISTRATION

Washington, D.C. 20546